David G. Capco
Yongsheng Chen   *Editors*

Nanomaterial

Impacts on Cell Biology and Medicine

Springer

Advances in Experimental Medicine and Biology

Series Editors
Irun R. Cohen • Abel Lajtha • Rodolfo Paoletti • John D. Lambris

For further volumes:
http://www.springer.com/series/5584

David G. Capco • Yongsheng Chen
Editors

Nanomaterial

Impacts on Cell Biology and
Medicine

Springer

Editors
David G. Capco
Arizona State University
Tempe, Arizona
USA

Yongsheng Chen
Georgia Institute of Technology
Atlanta, Georgia
USA

Preface

The rapidly developing field of engineered nanomaterial has expanded in many commercial areas. More recent studies have begun to provide a foundation for understanding how nanomaterials influence cells and how they also can serve as methodological tools for studies in medicine and cell biology. At the cellular level, recent investigations have shown the effects of nanomaterials on specific subcellular structures, such as the actin-based brush border network in cells with an increasing emphasis on the barrier function of epithelial tissues, while other studies have shown involvement of nanomaterials in specific cytoplasmic signal transduction events such as the rise in intracellular free calcium, a signaling event known to regulate many changes in cell architecture and function. In parallel, nanomaterials are increasingly used in medicine for drug delivery, treatment of cancer, and an increasing number of new applications. In this regard the subject of nanomaterial crosses disciplinary boundaries between medicine, biology, and engineering, and this has resulted in some of the advances and implications being over overlooked. One of the intentions of this book is to bring this diverse area into sharper focus.

Nanomaterials are used in medicine in a variety of ways including cancer targeting and ablation. They can also target cells through modification of their surface chemistry, and because of this are used as tools for drug delivery. They have been used for tissue contrast enhancement and as wavelength-specific probes for fluorescent imaging. Nanomaterials have also been employed to track stem cells as well as to alter their state of commitment. The usage of nanomaterials has become so common that they are present in a number of consumer products. This book presents chapters, from a variety of experts, in areas relevant to cell biology and medicine in order to demonstrate the breadth of applications.

This book was written for advanced undergraduates in cell biology, engineering, and medical professionals. Most chapters have different but relevant methods sections that explain key technological manipulations. Every attempt was made to make these sections practical and understandable, but with enough information in each chapter to be of interest to researchers as well.

Tempe, AZ, USA   David G. Capco
Atlanta, GA, USA   Yongsheng Chen

Contents

Contributors

Anup Abraham Molecular and Cellular Biosciences, School of Life Sciences, Arizona State University, Tempe, AZ, USA

Isaac M. Adjei Department of Molecular Medicine, Cleveland Clinic Lerner College of Medicine of Case Western Reserve University, Cleveland, OH, USA
Department of Biomedical Engineering/ND20, Lerner Research Institute, Cleveland Clinic, Cleveland, OH, USA

Shariq Ali Department of Obstetrics and Gynecology, University of Texas Medical Branch, Galveston, TX, USA

Sergio Anguissola Centre for BioNano Interactions, School of Chemistry and Chemical Biology, University College Dublin, Belfield, Dublin 4, Republic of Ireland

Armelle Baeza-Squiban Unit of Functional and Adaptive Biology (BFA) CNRS EAC 4413, Laboratory of Molecular and Cellular Responses to Xenobiotics (RMCX), University Paris Diderot, Sorbonne Paris Cité, Paris, France

Moritz Beck-Broichsitter, PhD Faculté de Pharmacie, Institut Galien, Université Paris-Sud, Châtenay-Malabry, France

Adam Bohr, PhD Faculté de Pharmacie, Institut Galien, Université Paris-Sud, Châtenay-Malabry, France

Sonja Boland Unit of Functional and Adaptive Biology (BFA) CNRS EAC 4413, Laboratory of Molecular and Cellular Responses to Xenobiotics (RMCX), University Paris Diderot, Sorbonne Paris Cité, Paris, France

David G. Capco Molecular and Cellular Biosciences, School of Life Sciences, Arizona State University, Tempe, AZ, USA

Yongsheng Chen School of Civil and Environmental Engineering, Georgia Institute of Technology, Atlanta, GA, USA

Giuseppe Chichiriccò Department of Life, Health and Environmental Sciences, University of L'Aquila, L'Aquila, Italy

Sabrina Colafarina Department of Life, Health and Environmental Sciences, University of L'Aquila, L'Aquila, Italy

Zhengrong Cui, PhD Pharmaceutics Division, College of Pharmacy, The University of Texas at Austin, Dell Pediatric Research Institute, Austin, TX, USA

Kenneth A. Dawson Centre for BioNano Interactions, School of Chemistry and Chemical Biology, University College Dublin, Belfield, Dublin 4, Republic of Ireland

Songyan Du School of Civil and Environmental Engineering, Georgia Institute of Technology, Atlanta, GA, USA

Jean-Marie Dupret Unit of Functional and Adaptive Biology (BFA) CNRS EAC 4413, Laboratory of Molecular and Cellular Responses to Xenobiotics (RMCX), University Paris Diderot, Sorbonne Paris Cité, Paris, France

James J. Faust Molecular and Cellular Biosciences, School of Life Sciences, Arizona State University, Tempe, AZ, USA

Gabriella Fontecchio Department of Life, Health and Environmental Sciences, University of L'Aquila, L'Aquila, Italy

Stavros Garantziotis Clinical Research Program, National Institute of Environmental Health Sciences (NIEHS), National Institute of Health (NIH), Research Triangle Park, NC, USA

David Garry Centre for BioNano Interactions, School of Chemistry and Chemical Biology, University College Dublin, Belfield, Dublin 4, Republic of Ireland

Taraka Sai Pavan Grandhi Biomedical Engineering, School of Biological and Health Systems Engineering, Arizona State University, Tempe, AZ, USA

Marie-Claude Hofmann, PhD Department of Endocrine Neoplasia and Hormonal Disorders, University of Texas MD Anderson Cancer Center, Houston, TX, USA

Salik Hussain Clinical Research Program, National Institute of Environmental Health Sciences (NIEHS), National Institute of Health (NIH), Research Triangle Park, NC, USA

Philip M. Kelly Centre for BioNano Interactions, School of Chemistry and Chemical Biology, University College Dublin, Belfield, Dublin 4, Republic of Ireland

Željka Krpetić Centre for BioNano Interactions, School of Chemistry and Chemical Biology, University College Dublin, Belfield, Dublin 4, Republic of Ireland

Vinod Labhasetwar, PhD Department of Molecular Medicine, Cleveland Clinic Lerner College of Medicine of Case Western Reserve University, Cleveland, OH, USA

Department of Biomedical Engineering/ND20, Lerner Research Institute, Cleveland Clinic, Cleveland, OH, USA

Taussig Cancer Institute, Cleveland Clinic, Cleveland, OH, USA

Kungang Li School of Civil and Environmental Engineering, Georgia Institute of Technology, Atlanta, GA, USA

Benjamin M. Masserano Molecular and Cellular Biosciences, School of Life Sciences, Arizona State University, Tempe, AZ, USA

Adam H. Mielke Molecular and Cellular Biosciences, School of Life Sciences, Arizona State University, Tempe, AZ, USA

Youssef W. Naguib Pharmaceutics Division, College of Pharmacy, The University of Texas at Austin, Austin, TX, USA

Anna Poma Department of Life, Health and Environmental Sciences, University of L'Aquila, L'Aquila, Italy

Kaushal Rege Biomedical Engineering, School of Biological and Health Systems Engineering, Tempe, AZ, USA

Chemical Engineering, School of Engineering of Matter, Transport and Energy, Arizona State University, Tempe, AZ, USA

Fernando Rodrigues-Lima Unit of Functional and Adaptive Biology (BFA) CNRS EAC 4413, Laboratory of Molecular and Cellular Responses to Xenobiotics (RMCX), University Paris Diderot, Sorbonne Paris Cité, Paris, France

Christian A. Ruge, PhD Faculté de Pharmacie, Institut Galien, Université Paris-Sud, Châtenay-Malabry, France

Erik Rytting Department of Obstetrics and Gynecology, University of Texas Medical Branch, Galveston, TX, USA

Blanka Sharma Department of Biomedical Engineering/ND20, Lerner Research Institute, Cleveland Clinic, Cleveland, OH, USA

Steven Van Ginkel School of Civil and Environmental Engineering, Georgia Institute of Technology, Atlanta, GA, USA

Paul Westerhoff School of Sustainable Engineering and the Built Environment, Arizona State University, Tempe, AZ, USA

Yu Yang School of Sustainable Engineering and the Built Environment, Arizona State University, Tempe, AZ, USA

Wen Zhang, PhD John A. Reif, Jr. Department of Civil and Environmental Engineering, New Jersey Institute of Technology, Newark, NJ, USA

Presence in, and Release of, Nanomaterials from Consumer Products

1

Yu Yang and Paul Westerhoff

Contents

Y. Yang (✉) • P. Westerhoff
Civil, Environmental and Sustainable Engineering,
School of Sustainable Engineering and the Built
Environment, Arizona State University,
Tempe, AZ 85287-5306, USA
e-mail: yu.yang.2@asu.edu

Abstract

Widespread use of engineered nanomaterials (ENMs) in consumer products has led to concerns about their potential impact on humans and the environment. In order to fully assess the impacts and release of ENMs from consumer products, this chapter provides an overview of the types of consumer products that contain nanomaterials, the potential release mechanisms of these ENMs from consumer products, and the associated human exposure. Information from two large datasets on consumer goods associated with ENMs, namely, the U.S.-based Project for Emerging Nanotechnologies from the Woodrow Wilson International Center, and the European-based National Institute for Public Health and the Environment of Netherlands, have been summarized. These databases reveal that silver, titanium, carbon-based ENMs are the major nanomaterials associated with consumer products. The presence and potential release of silver, titanium, carbon-based, and other nanomaterials from consumer goods available in published literature are also summarized, as well as the potential human exposure scenarios of inhalation, ingestion, dermal, and combination of all means. The prospecting of nanomaterial in water and biosolids provides further evidence of ENM occurrence, which could be linked to the use of nanomaterials containing consumer goods. Finally, this overview provides guidelines on toxicity studies, which calls for further efforts to analyze the

biological effects of ENMs on human beings and their exposure pathways in consumer products.

1.1   Introduction

Nanomaterials are typically defined as having "internal or surface structures in one or more dimensions in the size range 1–100 nm" [1]. Metallic and carbon-based nanomaterials, in particular, are comprised of novel physicochemical properties, and because of their small size and high surface-area-to-volume ratio are viewed differently than their bulk material. Over the past two decades, the clear advantages in using nanomaterials for consumer products have led to a new stage in nanotechnology development [2]. This, in turn, has fueled a dramatic growth in the nanotechnology industry, from a $10 billion enterprise in 2012 to an anticipated up to $1 trillion by 2015 [3]. As these industries continue to create products with unique elements and geometries, the human and ecological risks stemming from engineered nanomaterials (ENMs) may increase as a result of potential hazards [4]. Evaluating these risks, therefore, necessitates development of new tools and models that are better able to assess both exposure levels and toxicity of nanomaterials. This chapter focuses on strategies to quantify the presence of major classes of ENMs in consumer products and their release into water or air after use. ENMs include nano-silver, titanium dioxide, and carbon based nanomaterials.

Nanotechnology advances that have taken place in different disciplines over the years have led to widespread ENM applications in many everyday products. Nano silver (nano Ag), for instance, has been used in pesticide, medicine, socks, fabrics, or disinfectant sprays [5–7]. Colloidal silver is known to have been employed by industry for over 100 years [6]. In fact, the earliest example of nanosilver use can be traced to the Roman Lycurgus Cup, which is a bronze and glass cup created in the fourth century AD [8]. The glass material in the cup, which is able to scatter green light and transmit red light, contains particles that are 70 nm in diameter composed of silver (70 %) and gold (30 %). Nano titanium dioxide (nano TiO_2) is used in personal care products, such as sunscreens or toothpaste, food for coloring and texture, paints, and self-cleaning industry cleansers [9, 10]. Multi-walled carbon nanotubes have been used both in the electronic industry, and the textile industry, where it appears in the form of flame retardants in plastics, polymers, and fabrics [11–13]. Clearly, nanomaterials are prevalent in many consumer products, and exposure to humans potentially exists in physical forms, such as dermal, ingestion, and inhalation.

While the release of ENMs from consumer goods is an inevitable outcome of human activity, such release is often intentional (e.g., disposal of used toothpaste down the drain, dissolution of nano Ag into sweat), which leads to not only human exposure, but also to discharge into the environment [10, 14]. Sewage has been identified as a major conveyor of ENMs from consumer products and industrial processing [15]. The occurrence of ENMs in sewage can provide us one measure of the amount of human exposure that takes place. Therefore, proper sewage treatment becomes a critical intervention strategy in order to prevent ENM release to the environment, and thus limit ecosystem/human exposure to ENMs. ENMs can enter into wastewater treatment plants (WWTPs) through washing and other recreational activities [5, 16]. Nano Ag released from silver containing plastics and textiles from daily washing enters drains and sewers and ends up in WWTPs [5, 17, 18]. Similarly, Nano TiO_2 enters water caused by washing, bathing, and swimming [19, 20]. Both macro- and nano-scale TiO_2 have been detected in WWTP effluents, with the majority of the Ti accumulated in biosolids. Nanosilver can be absorbed to biosolids and converted into nano- Ag_2S under anaerobic conditions [21–24]. Recent work has shown that many ENMs can be removed from sewage water, and concentrated into biosolids ([5, 25–27].

In the U.S., 40 % of biosolids end up in land applications [28]. Land amendment, which occurs as a result of these biosolids, leads to the transport of ENMs into soils [22, 28]. Sanitary landfill sites, which receive used textiles (clothes, socks) and other consumer products, are another repository of ENM containing solid wastes [24, 29, 30]. Life cycle analyses have suggested that over 50 % of ENMs produced globally ends up in landfills [15]. Thus, the use of ENMs in consumer products can potentially affect solid waste treatment, and once again, landfills may emerge as a location to assess retrospectively changes in use patterns of products incorporating nanotechnology.

The rapid rise in nanotechnology application in consumer products means that a more comprehensive investigation is needed into the exposure risks posed by ENMs to humans and the environment. David Warheit, who chaired the committee on health and environmental safety of nanomaterials for the European Centre for Ecotoxicology and Toxicology of Chemicals, has aptly remarked: "The number of implication studies has not caught up with the number of application studies" [31]. Therefore, the need for more studies of ENM implication continues to grow.

To understand both the implication and application aspects of ENMs, we provide here a comprehensive summary of consumer products that contain nanomaterials, potential paths for ENM release from consumer products, and the range of associated human exposure. Prospecting the presence of ENMs in water and sewer biosolids provides us with information and guidelines on toxicity tests, while addressing important questions: At what concentration levels do ENMs exist in the environment? Which chemical form of ENMs (e.g., oxidation state) should be tested for dose-response experiments?

1.2 Categorization of Consumer Products with Nanomaterials from Databases

In 2005, The Woodrow Wilson International Center for Scholars initiated the Project for Emerging Nanotechnologies (PEN), which aimed to provide an inventory of nanotechnology-based consumer products (either containing nanomaterials or production processes incorporating nanotechnology). For simplicity, all the information obtained from this project is cited as the Woodrow Wilson database in this chapter [32]. Originally, the inventory cited 54 different products in 2005; in 2011, the number of products increased to 1,317, representing a 24-fold increase during a 6-year period [32]. Of the total number of 1,317 products in 2011, 45 % (587), 28 % (367), and 20 % (261) originated in the U.S., Europe, and East Asia, respectively [32]. The number of nanotechnology-based products was projected to continue as advances in nanotechnology were further applied to consumer products. This inventory provides information such as product name, company, manufacturer or supplier, country of origin, category and subcategory, product description, and date of update [32]. Updates to this inventory were halted in 2011, as funding and priorities changed. More recently, Virginia Polytechnic Institute and State University's Center for Sustainable Nanotechnology (VT SuN) and the Woodrow Wilson International Center for Scholars have been partnering on a new effort to compile the Nano Consumer Products Inventory (NCPI), which incorporates the PEN dataset (http://www.nanotechproject.org/cpi/).

In 2010, an inventory of consumer products containing nanomaterials published by the National Institute for Public Health and the Environment (RIVM) of Netherlands was made available in the European market. The RIVM, based on advertisements of manufacturers, cited 858 products in 2010, showing a six-fold increase of 143 products that contained ENMs in 2007 [33]. Similar to the database maintained by the Woodrow Wilson center, the RIVM stated the following: "No verification of the actual presence of nanomaterials via measurements in claimed consumer products has been made" [33].

We re-categorized product information in the RIVM database to be consistent with those used in Woodrow Wilson database. Figure 1.1 provides a comparison of the Woodrow Wilson and RIVM databases. The quantity of each product depicted here is based on this re-arrangement.
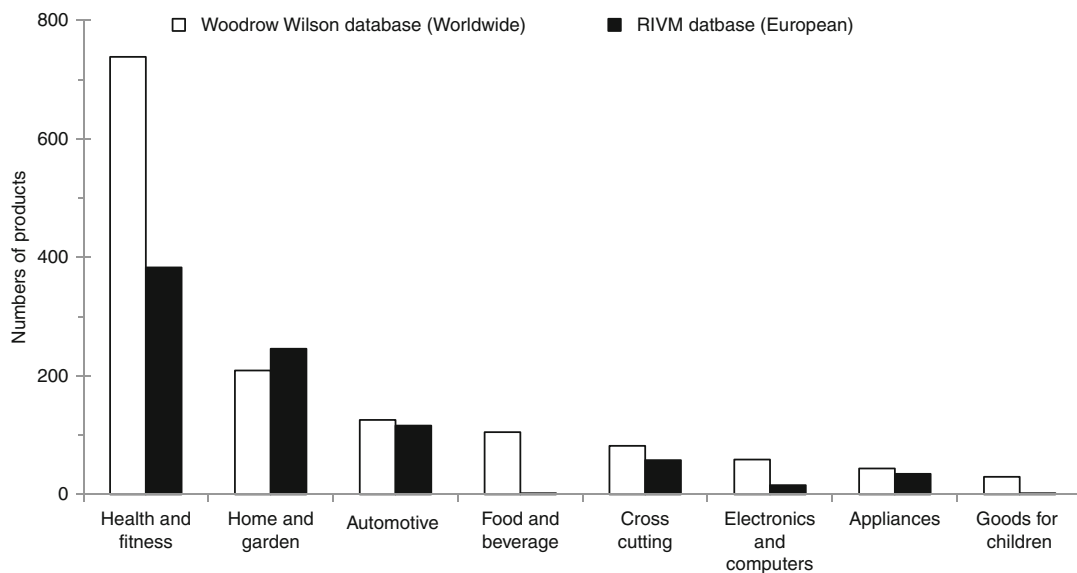
Fig. 1.1 Numbers of products in each category (The worldwide data is from Woodrow Wilson database [32], and the European data is from RIVM database [33])

Both databases show a similar dominant status of products, i.e., the number of health and fitness products is greater than the number of home and garden products, which in turn, is greater than the number of automotive products (Fig. 1.1). This trend indicates that the potential release of nanomaterials would come from three major categories: health and fitness, home and garden, and automotive.

Under the category of food and beverage, the two datasets show a marked difference in the numbers of products. The Woodrow Wilson database contained 105 products under food and beverage, whereas the RIVM database showed only 2 products in this category. Further analysis shows that in the 105 products listed in the food and beverage category from the Woodrow Wilson database, 63 (60 % of products), 17 (16 %), and 15 (14 %) were made in the U.S., China, and Japan, respectively [32]. Only four products listed in the Woodrow Wilson database were manufactured in Europe [32]. The much less number of available food and beverages tagged with nanomaterials in Europe may indicate that the European market is more conservative in application of nanomaterials and or nanotechnology in the food and beverage category.

The Woodrow Wilson and RIVM databases also provided descriptions of products, indicating nano silver, titanium dioxide, carbon based nanomaterials, gold, and zinc/iron to be the major nanomaterials associated with consumer products (Fig. 1.2; only products tagged with certain nanomaterial were counted). Nanosilver dominated among all the nanomaterials, which comprised 55 and 75 % of all products with a nanomaterial tag in the Woodrow Wilson and RIVM databases, respectively. The products associated with nano TiO_2 and carbon-based nanomaterials were the secondary and tertiary dominant consumer goods. The gold, carbon/iron based nanomaterials were the major ENMs incorporated with consumer products in the European market. According to the descriptions of both datasets, information of products summarized was based on product descriptions provided by the merchants, because information about actual contents and forms of nanomaterials in consumer products is rarely available. Thus, the screening of nanomaterial concentration and physicochemical properties should be assessed prior to studying the effects of nanomaterials on biological systems (or humans).
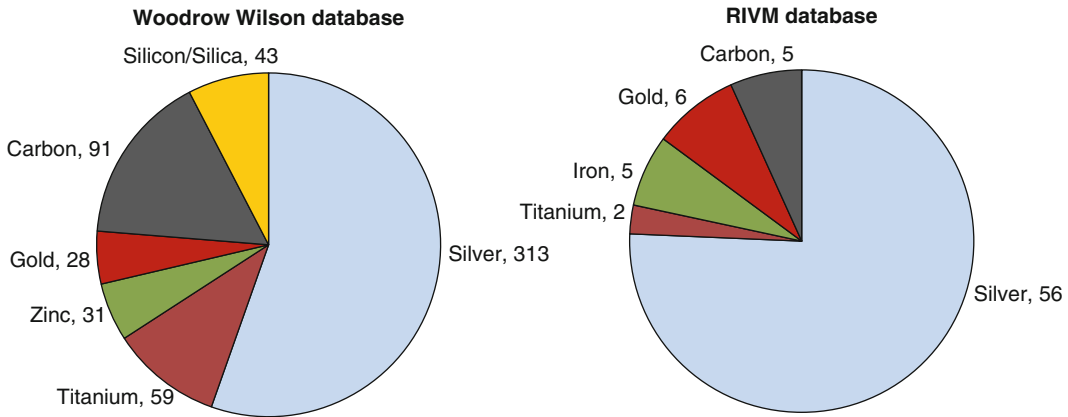
Fig. 1.2 Distribution of major nanomaterials associated with consumer products (Figure was synthesized upon open-source data from Woodrow Wilson and RIVM databases [32, 33])

1.3 Occurrence and Potential Exposure of Major Nanomaterials in Consumer Goods

As summarized in both databases, metallic nanomaterials are the major nanomaterials incorporated into consumer goods. The presence of metallic nanomaterials in consumer goods can be grouped into three categories based on the location where they are placed: (1) dispersed in bulk of products; (2) coated on the surface; (3) bound in products [34]. For example, nanosilver can be coated on textile surfaces, such as socks and shirts, dispersed in supplements such as MesoSilver®, or bounded on surfaces in make-up instruments (e.g., hair straightener) and tableware [32]. The different functions of consumer products, therefore, determine where nanomaterials exist, thus impacting ENM exposure pathways for humans. Other factors, such as concentration, shape, and chemical entities of nanomaterials also contribute to exposure assessment on humans and the environment [33].

Exposure to ENMs in consumer products may be direct, during human use of the product, or indirect as ENMs are released into the air or residuals passed on from prior uses [33]. The application routes contribute to the extent of exposure, which include inhalation, ingestion, dermal, and combination of all means [33]. Since health and fitness products have the highest content of nanomaterials compared to all other products, human exposure to nanomaterials should be carefully evaluated, particularly with the anticipated increased availability of nanoproducts in the future. Other direct exposure scenarios of ENMs exist in the manufacturing industry, including workplaces that produce paints, coatings, cosmetics, catalysts, and polymer composites with significant quantities of nanoparticles [35]. The application of silica nanoparticles as abrasives in chemical mechanical polishing (CMP) processes exposes workers to slurries. Further exposure to these byproducts occur when they are released into wastewater [36, 37].

The general flow of nanomaterial use and potential exposure is presented in Fig. 1.3. To better illustrate the occurrence and potential exposure of nanomaterials in consumer goods, we use nanosilver, carbon based nanomaterials, and titanium dioxide as representative nanomaterials. Moreover, according to recent U.S. EPA case studies [7, 9, 12, 13], these three types of ENMs are the dominant nanomaterials currently being used, as shown in Fig. 1.2.

1.3.1 Presence and Release of Nanosilver in Consumer Products

In 2011, the Woodrow Wilson database showed that about 24 % of 1,317 products claimed to
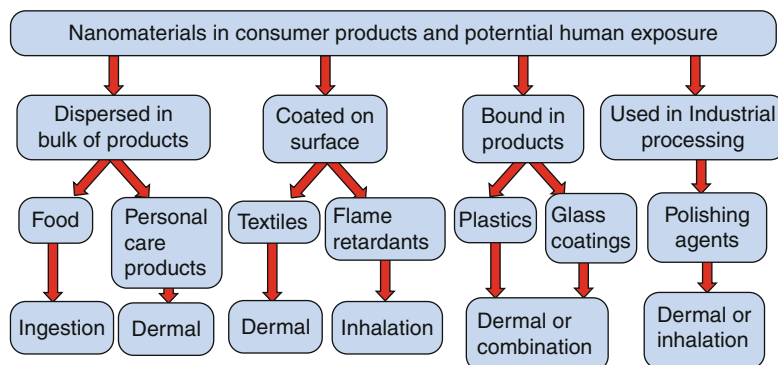
Fig. 1.3 Nanomaterials used in consumer goods and potential exposure to human beings

contain nanosilver [32]. These branded products included utensils, shoe soles, detergent, toothpaste, and even dietary supplements [32]. Products, such as toothpaste and dietary supplements led to direct dermal and ingestion exposure to humans. Recent estimates for production volume of raw nanosilver is in the range of 2.8–20 tons per year in the U.S. [38]. The inherent uncertainty in these estimates emerge because of the use of proxy parameters (e.g., size of company, using number of employees, and annual revenue of a company), but more generally show the expanding use of nanosilver in consumer goods will inevitably increase the potential for human exposure [12, 38]. One piece of evidence could be the growing number of patented consumer goods associated with nano Ag between 1980 and 2010 [39].

The release of nanosilver from consumer products varies based on the way in which nanosilver is employed in these products. One of the first experimental studies on nanosilver release was conducted by Westerhoff et al. [5], which tested six brands of socks, and found that they contained up to a maximum of 1,360 µg-Ag/g-sock; in a simulated 1-h wash test, approximately 650 µg of silver was leached into 500 mL of distilled water. Transmission electron microscopy (TEM) verified the presence of silver nanoparticles in the range of 10–500 nm in the sock material and related wash water. In another experimental study, an expanded screening test of silver release was conducted on commonly used consumer products, including a shirt, a medical mask and cloth, toothpaste, shampoo, detergent,

a towel, a toy teddy bear, and two humidifiers [40]. The released silver concentrations ranged from 1.4 to 270,000 µg Ag/g product in 500 mL of tap water, and the presence of silver micron- and nano- particles was confirmed in the released solution by TEM. The release of nanosilver via washing indicates the potential exposure of nanosilver to sewage systems and WWTPs from socks or textiles that have silver nanoparticles coated on their surface.

Another comprehensive study was carried out by Quadros et al. [14] to determine the release of silver from products incorporated with nanotechnology that commonly come into contact with children [14]. The consumer products tested included plush toys, fabric products, breast milk storage bags, sippy cups, cleaning products, humidifiers, and humidifier accessories. The release of silver was tested in a variety of liquids including tap water, orange juice, milk formula, synthetic saliva, sweat, and urine. The potential transport of silver into air and onto dermal wipes was examined as well. Among all the tested liquids, synthetic sweat and urine revealed the highest release of silver up to 38 % of the silver mass in products, while release of silver in tap water was less than 1.5 %. Silver could be transferred from products to wipes in a range of 0.3–2.3 µg/m^2. No significant release of silver to aerosol occurred. This comprehensive test showed the potential for dermal exposure of silver to children.

In addition to dermal exposure of nanosilver by washing or wiping of nanosilver-containing consumer products, researchers have demonstrated

that inhalation exposure can occur from emitted airborne particles from a surface disinfectant, an anti-odor spray, and a throat spray [41]. Each spray action released 0.24–56 ng of silver in aerosols and the continuous use of these products may lead to as high as 70 ng of silver deposition in the respiratory tract upon exposure modeling. The majority of silver identified in aerosols was in the range of 1–2.5 μm in diameter and associated with chlorine. The existence of silver nanoparticles was proved by using TEM. The emission of aerosols containing silver nanoparticles provides quantitative data and viable exposure scenarios to conduct risk assessment of nanosilver in consumer products.

Comprehensive assessments of nanosilver exposure to human beings require that we have more detailed information about the presence of nanosilver in consumer products. While toxicity evaluations of nanosilver are advancing rapidly, and producing large amounts of data, ranging from in vitro studies on cell lines and rodent experiments to ecological evaluations [42–44], the shapes of nanosilver ENMs are still largely ignored in toxicity studies, and only a limited number of actual release exposure studies have been conducted [43]. Therefore, there exists a need for more analytical studies that assess the exposure pathways of nanosilver in consumer products, as well as their biological effects on human beings.

1.3.2 Use and Release of Carbon-Based Nanomaterials in Consumer Goods

Carbon-based nanomaterials, the second most widely used nanomaterials according to the 2011 Woodrow Wilson database, account for 7 % of all listed nanoproducts [32]. They include, (but are not limited to) carbon nanotubes (CNTs), fullerenes (C60 and C70), and graphene [25, 45–48]. Though actual production of carbon-based nanomaterials is not available, the estimated production volumes of CNTs and fullerene are in the range of 55–1,101 and 2–80 tons per year, respectively [38]. Other estimates suggest that the global production of carbon nanotubes and fullerenes are in the range of 11–1,000 and ≤10 tons per year, respectively [49]. These anticipated values show the dominance of CNTs among carbon-based nanomaterials.

Commercial products associated with CNTs include sporting goods, such as tennis rackets, road forks, and bike seats [32]. Most CNTs produced are multiwall carbon nanotubes (MWCNTs) that consist of at least two more CNTs which concentrically telescoped [50]. The major applications of MWCNTs are in electrodes, electronic components, batteries, and synthetic textiles [50, 51]. The use of MWCNTs as flame-retardant coatings is estimated to be very low [13, 52]. Because of their unique properties, in which they offer both thermal stability and mechanical strength, CNTs are widely used as fillers in food packing materials [53], and therefore have received considerable scrutiny. In addition to human exposure through consumer products, another potential area of concern is workplace exposure to CNTs during the manufacturing process of these nanomaterials [35].

Dermal exposure via cosmetics containing CNTs has been researched extensively. Several commercial products employing fullerene, for example, are currently widely available in the market [25]. The actual presence of fullerene in cosmetics has been confirmed by TEM. The content of C60 was quantified in four cosmetics with a range of 0.04–1.1 μg/g, and C70 was qualitatively verified in two samples. A single-use of a cosmetic of 0.5 g may contain up to 0.6 μg of C60, indicating a potential pathway for human dermal exposure to fullerene. Pristine fullerenes may have low toxicity and thus the non-risk for human exposure is expected in workplaces with good hygiene conditions [54]. However, these results prove the immediate exposure of fullerenes to consumers via direct dermal application, and this is a major concern for long-term use of these cosmetics [54].

The application of graphene nano-platelets into polymers can produce a heat-resistant nanocomposite, which can be used in food-packaging applications [53]. Researchers have demonstrated that the dispersion of graphene nano-platelets in poly methyl methacrylate (PMMA) at 1–5 %

loading rate could increase the glass transition temperature for PMMA by 30 °C [46]. Though commercial products with graphene nanoplatelets are not available yet, these products are expected to eventually make it to the market due to their unique heat resistance capabilities [53]. A number of comprehensive toxicity and exposure tests are needed, however, to mitigate public concerns of these products before they are deployed on a large scale.

1.3.3 Occurrence of Titanium Dioxide Nanoparticles in Food and Personal Care Products

Since many applications of TiO_2 would benefit more from smaller primary particle sizes, the nanosized TiO_2 is expected to increase exponentially [55]. The Woodrow Wilson database has shown that about 5 % of 1,317 products was incorporated with nano TiO_2 in 2011 [32]. They include health and fitness products and personal care products, such as sunscreens and cosmetics that protect the skin against harmful ultraviolet (UV) rays [9]. The annual production of nano TiO_2 is estimated to be in the range of 7,800–38,000 tons in the U.S. [38]. TiO_2 nanoparticles incorporated in consumer products are synthesized to be amorphous and or to be a mixture of three different crystal structures: anatase, rutile, and brookite [56]. For example, five over-the-counter sunscreen products were found to have contained nano TiO_2, among which one was pure rutile and the remaining four were mixtures of anatase/rutile [57].

Titanium dioxide is used as a whitening agent in foods such as salad dressing, gum, icing, cookies, and candies [9, 32], since it is chemically stable under illumination, oxygen, and pH changes that can occur during food processing [58]. Titanium dioxide in the form of color additives may lead to a maximum ingestion of 112 mg of Ti per person per day [59]. Thus, the potential presence of TiO_2 nanoparticles as a food additive can result in human ingestion of nanomaterials. Examination of one sample of food grade TiO_2 powder shows that 36 % of particles are below

100 nm [10], which is a white food color additive, designated as E171 by the European Union. A screening of 89 foods reveals that titanium concentrations spanned from 0.00077 to 210 µg Ti/mg product [10]. Powdered donuts have the highest titanium concentration of 100 mg Ti per serving. Generally, foods with high concentration of titanium include sweets or candies, chocolate, chewing gum, and foods with white icing and or sugar toppings. Several dairy products with white color including milk, cheese, and yogurt have titanium concentrations comparable with non-dairy substitutes such as soy- and rice-based drinks, whose concentrations are in the range of 0.10–0.26 µg Ti/mL. Although 12 food products with the highest Ti concentrations are small enough to pass a 0.45 µm filter, additional research is needed to clarify the ultimate size fraction of Ti in foods.

The contents of Ti in personal care products have been examined on a sample pool of 8 toothpastes and 24 additional personal care products [10]. The titanium contents in all toothpastes are in the range of 0.7–5.6 µg/mg or from < 0.1 % to nearly 0.5 % by weight of the product. Several sunscreens that claim to contain TiO_2 have the highest contents of Ti, ranging from 14 to 90 µg/mg, while others not labeled as containing TiO_2 have Ti content of less than 0.01 µg/mg. White-colored shampoos, deodorants, and shaving creams have the lowest levels of titanium, below 0.01 µg/mg. Additional analysis reveals that the Ti content of 10.0 ± 0.63 µg Ti/mg on aspirin products, which is higher than in name-brand aspirin product containing 0.017 ± 0.005 µg Ti/mg. Several high-consumption pharmaceuticals contain titanium content that range from below detection limit (BDL, 0.0001 µg Ti/mg) to a high of 0.014 µg Ti/mg. Paints contain white pigments and thus could contain titanium as one of their ingredients. An analysis of titanium content has been conducted on two primary white paints, three primers, and two base paints [10]. The white paints, sealants, and base paints have titanium contents of ~110, 25–40, and 0.03–0.22 µg Ti/mg, respectively. Other nonwhite adhesives tested have not been found to have any detectable amounts of titanium.

The aforementioned results quantify the contents of titanium in food, personal care products, and

paints. The presence of nano TiO_2 particles as a food additive (E171) and in some consumer goods has been verified, which point to both dermal and ingestion exposure. As titanium in consumer products can also come from clays used in some foods and paints, the reported titanium contents can be the upper limit concentration of TiO_2 nanoparticles.

Washing of textiles modified by TiO_2 releases titanium into the environment [60]. Washing studies from six sun-protection clothes resulted in the release of TiO_2 particles, ranging from 0.01 to 3.4 % of total titanium in one wash cycle. TEM, coupled with energy dispersive x-ray diffraction (EDX) experiments, were able to identify the release TiO_2 particles, showing sizes in the range of 60–350 nm. Additional studies have investigated the potential transformation of nano TiO_2 particles formulated for sunscreens when placed in the media-simulating conditions of product use [61]. Though the remaining Al-based layer was still effective in preventing superoxide production, approximately 90 % wt/wt of coating constituents desorbed from the TiO_2 particle surfaces, thus demonstrating their transformations after entering into the environment.

1.3.4 The Use and Release of Other Nanomaterials

Other nanomaterials incorporated into foods and packing materials include silicate (clay) nanoparticles, starch nanocrystals, cellulose nanofibers, and nano chitin whiskers [62]. Polymer-nano composites can be promising food-packing materials, which are created by inserting nano scale fillers throughout a polymer matrix [63]. Filler materials contain starch nanocrystals [62], cellulose nano-fibers [64], and nano chitin whiskers [65]. Biodegradable starch/clay nanocomposite films can be used as food packaging as well, which can be produced by dispersing montmorillonite nanoparticles into starch based materials [66]. Additional examples and detailed descriptions are summarized in Table 1.1. With the advance in nanotechnology, more nanomaterials in consumer goods will appear in a variety of consumer goods.

1.4 Prospecting Nanomaterials in the Environment

The description provided thus far suggests the necessity to examine every product for uncovering contents of nanomaterials. Efforts have been made to examine the contents of ENMs in food and personal care products, verify the presence of ENMs (e.g. nano Ag, TiO_2, fullerene), and to explore the potential release/exposure to humans in some of them [10, 14, 25, 41]. However, we are still challenged in our in our ability to determine the fraction of nanomaterials in each product due to primarily to analytical constraints. An alternative approach to understanding potential exposure routes is to look at waste streams from society. Environmental exposure assessments require that nanomaterial concentration be examined in different surroundings. Accordingly, sewage wastewater and sludge, which convey wash-down from industry, scrubbers, food, and personal care products, have also been explored for the presence of nanomaterials.

1.4.1 Detection of ENMs in Water by Single Particle ICP-MS

Inductively coupled plasma-mass spectrometry (ICP-MS) is a standard analytical tool to measure metals in samples, which can determine total metal contents in aqueous or solid samples after acid digestion. Single particle ICP-MS (sp-ICP-MS) is an emerging analytical approach used for measuring nano-scale metal or metal oxide materials in water [71]. No acid digestion or complicated pretreatments are needed prior to injection. To prospect the concentration and size distribution of metallic nanomaterials in an aqueous environment, here sp-ICP-MS was applied to analyze filtrates of river, tap water, and effluent from WWTPs passing through 0.7 μm filters. Figures 1.4 and 1.5 convert the pulses from sp-ICP-MS into masses and equivalent number of particles using densities for TiO_2, CeO_2 or Ag, assuming all particles are spherical while following methods described elsewhere [72–75]. Therefore, sp-ICP-MS provides estimations of

Table 1.1 Occurrence of other nanomaterials in consumer goods

Food related materials	Types of ENMs	Application and advantages	References
Food packing materials	Nano SiO_2 and TiN	Applied as filler to increase abrasion resistance and mechanical strength	[67]
	Silicate nanoparticles	Used as filler in Durethan KU2-2601 packaging film (Bayer Polymer) to prevent contents from drying and oxidation	[68]
	Nano ZnO	Incorporated in plastic wrap with following functions: anti-UV, reflecting IR, sterilizing and anti-mold, temperature tolerance, and bearing grinding	[32]
	Clay nanocomposite	Imbued in plastic bottles such as beer container, which were less likely to shatter than glass bottles	[69]
	Clay nanoparticles	The layout of the nano clay particles is designed as a gas barrier to prevent the escape of CO_2 from the beverage and sneaking in of oxygen	[32]
	Starch nanocrystals, cellulose nanofibers, nano chitin whiskers	Fillers in polymer nanocomposites as food packing materials	[64], [62], [46]
	Montmorillonite nanoparticles	Fillers in biodegradable starch/clay nanocomposite films	[66]
Food and cookware	Carbon nanoparticles	In different carbohydrate based food caramels, such as bread, jaggery, sugar caramel, corn flakes and biscuits	[70]
	Selenium related NMs	In the tea	[32]
	Nano ceramic materials	Used in cookware/tea ware which are with high temperature tolerance and ultra-durable	[32]

the "maximum" number and size distributions of "equivalent" nanoparticles (Table 1.2). The minimum size detectable for TiO_2 is larger than for CeO_2 or Ag due to the aforementioned calculation methods and background signal. The concentrations of dissolved Ti, Ce, and Ag are included in Table 1.2, along with average equivalent nanoparticle sizes. Their concentrations show a trend of Ti > Ce > Ag, both in particle and dissolved concentrations, which reflects the natural abundance of three elements in earth's upper crust [76].

Assuming that all the Ti detected by sp-ICP-MS is in the form of TiO_2, we calculated the concentration of TiO_2-eqivalent particles (TiO_2-eq) from the mass of Ti. Tap water has the lowest TiO_2-eq particle concentration of 3.1 ng/L, while the concentration of TiO_2-eq in

the rest of waters ranges from 57 to 895 ng/L. The size distribution of TiO_2-eq particles demonstrates that there are few particles larger than 200 nm in tap water, and the rest of samples have a broader size distribution, in the range of 120–500 nm (Figs. 1.4 and 1.5). This reveals that drinking water treatment plants have efficiently removed larger Ti-bearing minerals (e.g., clays causing turbidity) from the source river water. The concentrations of TiO_2-eq particles in effluent of WWTPs are comparable to the river water, indicating the common presence of a combination of clays containing Ti and TiO_2 nanoparticles in aqueous environment. The occurrence of TiO_2 nanoparticles has been verified in WWTPs, which potentially may be from commercial products, such as sunscreen and industry processes [10, 27].
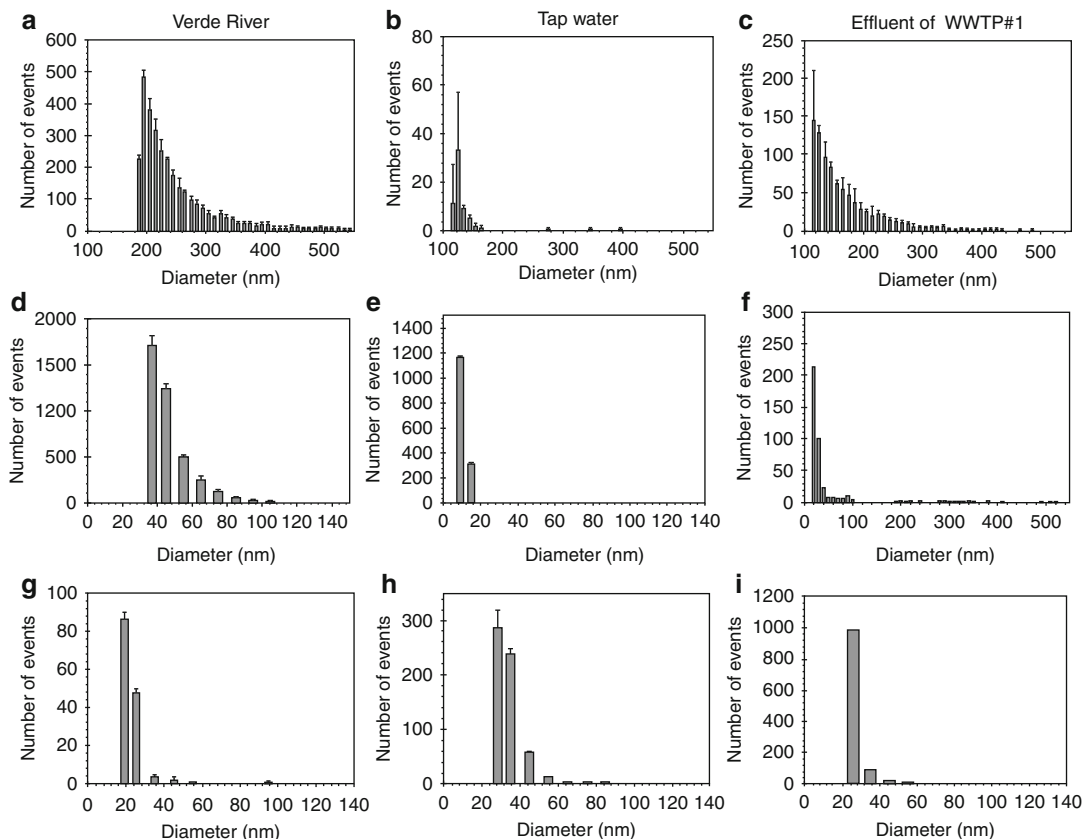
Fig. 1.4 Size distribution of nano- and larger particles as TiO$_2$-eq, CeO$_2$-eq and Ag-eq in Verde River, tab water, and effluent of WWTP #1: (**a**) TiO$_2$-eq in Verde River, (**b**) TiO$_2$-eq in tap water, (**c**) TiO$_2$-eq in effluent of WWTP #1, (**d**) CeO$_2$-eq in Verde River, (**e**) CeO$_2$-eq in tap water, (**f**) CeO$_2$-eq in effluent of WWTP #1, (**g**) Ag-eq in Verde River, (**h**) Ag-eq in tap water and (**i**) Ag-eq in effluent of WWTP #1. Error bars represents ±1 standard deviation of duplicate measurement

A similar assumption was made that all the Ce detected by sp-ICP-MS is in the form of CeO$_2$, and the concentration of CeO$_2$-eqivalent (CeO$_2$-eq) is from the mass of Ce. A similar trend exists for abundance and size ranges in tap water for CeO$_2$-eq particles, which has the lowest particle concentration of 0.1 ng/L and the shortest size range of 0–20 nm (Table 1.2 and Figs. 1.4 and 1.5). The size distributions of CeO$_2$-eq particles in other waters show the presence of nano-sized particles. Interestingly, the particle concentrations of CeO$_2$ in river water, tap water, and influent of WWTP are lower than in effluent of WWTPs (Table 1.2), the former of which were in the range of 0.1–18 ng/L and the latter of which ranges from 42 to 85 ng/L. Since cerium is a trace

element for microorganism, and it accumulates in bones of animals [77], the biodegradation of animal debris and microorganisms may release more cerium from the solid to water phases in WWTP. Thus WWTP could result in higher concentrations of cerium-containing nanoparticles detected by sp-ICP-MS.

The contents of silver determined by sp-ICP-MS exhibit a different profile compared to titanium and cerium. With an assumption that all the silver detected as particle is in the element form, the particulate concentrations of silver in all samples are calculated as low as 0.1–2.1 ng/L. The river water, influent and effluent of WWTPs have the total silver concentrations of 6.8–33 ng/L. However, the total silver concentration in tap water is 97 ng/L,
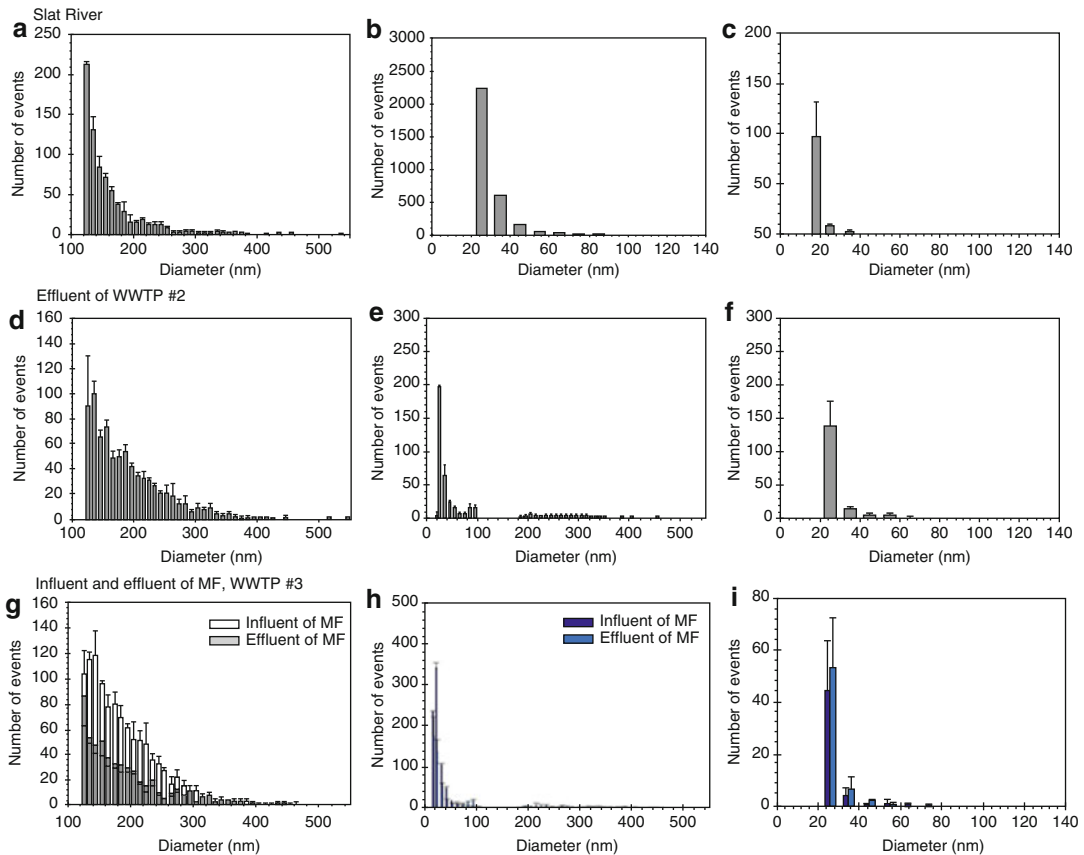
Fig. 1.5 Size distribution of nano- and larger particles as TiO_2-eq (**a**), CeO_2-eq (**b**) and Ag-eq (**c**) in Salt River, effluent of WWTP #2, influent of microfiltration (MF) in WWTP #3 and effluent of MF in WWTP #3

which is much higher than in other samples. Tap water has a higher dissolved silver concentration of 95 ng/L, while other samples show the dissolved silver concentrations in the range of 6.7–33 ng/L. The high content of total and dissolved silver may be associated with release from premise plumbing. The size profiles of silver in all water samples show the size range of 17–100 nm.

This work shows that nano-sized colloids already exist in the rivers, tap water, and sewers. Low levels of these nanomaterials in tap water are being ingested. They are the "background" of nanoparticles that we will be exposed to from consumer products. Since sp-ICP-MS only analyzed their size and mass concentrations, electron microscopy analysis would be required to provide additional information on the exact morphology and their likely sources.

1.4.2 Occurrence of ENMs in Biosolids of Wastewater Treatment Plants

Many ENMs used in consumer products will enter the sewer, and a large fraction of these (>90 %) appear to associate with biomass in WWTPs, which are removed (settled), dewatered, and processed into biosolids [26, 27, 78, 79]. Biosolids are a rich nutrient source of carbon, nitrogen, and phosphorous. Biosolids contains organic chemicals (flame retardants, personal care products, etc.) released from consumer products [80]; likewise, we speculate that they also contain nanomaterials from consumer products. For example, the presence of silver sulfide and titanium dioxide nanoparticles in biosolids was shown by scanning electron microscopy (SEM) and TEM [16, 22]. The authors' recent

Table 1.2 Size and concentration of TiO_2-eq, CeO_2-eq and Ag-eq in investigated samples

		Verde River	Salt River	Tap water	WWTP #1	WWTP #2	WWTP #3 Influent of MF	Effluent of MF
TiO_2-eq	D_{limit} (nm)	186	120	119	112	123	122	122
	D_{50} (nm)	225	144	124	143	174	174	167
	D_{80} (nm)	281	185	135	195	232	229	216
	Number concentration (ml^{-1})	3.53×10^4	8.92×10^3	7.54×10^2	1.22×10^4	1.05×10^4	1.46×10^4	5.61×10^3
	Particle mass concentration (ng/L) as Ti	895	67	3.1	95	124	169	57
	Dissolved concentration (ng/L) as Ti	4,812	1,775	1,837	1,277	3,151	2,965	3,035
	Total concentration (ng/L) as Ti	5,707	1,842	1,840	1,372	3,274	3,134	3,092
CeO_2-eq	D_{limit} (nm)	33	21	8.1	15	20	18	17
	D_{50} (nm)	41	25	9.3	19	31	23	25
	D_{80} (nm)	52	32	10.7	37	85	34	77
	Number concentration (ml^{-1})	4.83×10^4	3.85×10^4	1.76×10^4	5.56×10^3	5.53×10^3	1.07×10^4	6.95×10^3
	Particle mass concentration (ng/L) as Ce	18	6.9	0.1	42	65	16	85
	Dissolved concentration (ng/L) as Ce	45	8.5	0.1	5.4	26	14	8.8
	Total concentration (ng/L) as Ce	63	15	0.2	47	91	30	94
Ag-eq	D_{limit} (nm)	18	16	26	22	18	22	23
	D_{50} (nm)	19.2	17	31	25	19	24	24
	D_{80} (nm)	22.6	18	37	29	21	26	27
	Number concentration (ml^{-1})	1.83×10^3	1.42×10^3	7.89×10^3	1.04×10^4	1.02×10^4	7.81×10^2	9.29×10^2
	Particle mass concentration (ng/L) as Ag	0.2	0.1	1.9	2.1	0.4	0.1	0.1
	Dissolved concentration (ng/L) as Ag	13	6.7	95	23	15	30	33
	Total concentration (ng/L) as Ag	13	6.8	97	25	16	30	33

work reveals a broad range of metallic and metal oxide particles size ranges of <100–500 nm. Those particles have been characterized by scanning electron microscopy coupled with energy dispersive X-ray spectroscopy, showing the existence of precious metallic particles (e.g., silver and gold), catalytic residues (e.g., palladium), and other metallic particles (e.g., lead). New techniques are needed to quantify the exact contents of nanoparticles in biosolids for full exposure assessment.

1.5 Summary and Conclusions

This chapter provides an overview of current commercially-available consumer products associated with nanomaterials and nanotechnology. Information from two large datasets about consumer goods associated with nanomaterials has been summarized, including the U.S-based Project for Emerging Nanotechnologies from the Woodrow Wilson International Center, and the European-based national institute for public health and the environment (RIVM) in the Netherlands. Distribution and types of nanomaterials in consumer goods are presented. The presence and potential release of silver, titanium, carbon-based, and other nanomaterials from consumer goods have been summarized. The potential exposure scenarios have been discussed. The prospecting of nanomaterial in water and biosolids further showed their occurrence, which could be linked to the use of nanomaterials containing consumer goods. Further analytical methods are needed to extract and quantify the actual concentration of ENMs in consumer goods, water, and biosolids.

The risk associated with exposure to ENMs in consumer products is not only determined by the contents and physicochemical properties of ENMs, but also directly related to the application ways of consumer products with different exposure modes. For example, nanomaterials in textile leads to dermal exposure, and nanoparticle suspended in spray liquid could result in both dermal and inhalation risks. The application of consumer goods in different environments (e.g.,

cosmetics may come into swimming pool) differs in their potential release rate and transformation, and eventually their effects on human beings. Therefore, to understand impacts from ENMs in consumer products, better information is needed on exposure concentrations in different matrices (air, water, food) and modes of exposure (dermal, ingestion, inhalation, etc.). Such information can then be used to design appropriate toxicity testing. Exploring, or prospecting, for ENMs in products today or in the environment already (air, water, soil, food) may provide useful insights into how the chemical and physical properties of ENMs transformation throughout their life cycle from the point of synthesis, through incorporation into products, use of nano-enabled products, in release (e.g., sewage) into the environment.

References

1. Maynard AD (2011) Don't define nanomaterials. Nature 475(7354):31–31
2. Oberdorster G, Maynard A, Donaldson K, Castranova V, Fitzpatrick J, Ausman K, Carter J, Karn B, Kreyling W, Lai D, Olin S, Monteiro-Riviere N, Warheit D, Yang H, Group, A.r.f.t.I.R.F.R.S.I.N.T.S.W. (2005) Principles for characterizing the potential human health effects from exposure to nanomaterials: elements of a screening strategy. Part Fibre Toxicol 2(1):8
3. Gao J, Wang Y, Hovsepyan A, Bonzongo JCJ (2011) Effects of engineered nanomaterials on microbial catalyzed biogeochemical processes in sediments. J Hazard Mater 186(1):940–945
4. Wiesner MR, Lowry GV, Alvarez P, Dionysiou D, Biswas P (2006) Assessing the risks of manufactured nanomaterials. Environ Sci Technol 40(14):4336–4345
5. Benn TM, Westerhoff P (2008) Nanoparticle silver released into water from commercially available sock fabrics. Environ Sci Technol 42(11):4133–4139

6. Nowack B, Krug HF, Height M (2011) 120 years of nanosilver history: implications for policy makers. Environ Sci Tech 45(4):1177–1183

7. U.S.EPA (2012) Nanomaterial case study: nanoscale silver in disinfectant spray. National Center for Environmental Assessment, Office of Research and Development, U.S. Environmental Protection Agency, Research Triangle Park

8. Evanoff DD, Chumanov G (2005) Synthesis and optical properties of silver nanoparticles and arrays. ChemPhysChem 6(7):1221–1231

9. U.S.EPA (2010) Nanomaterial case studies: nanoscale titanium dioxide in water treatment and in topical sunscreen (final). U.S. Environmental Protection Agency, Washington, DC

10. Weir A, Westerhoff P, Fabricius L, Hristovski K, von Goetz N (2012) Titanium dioxide nanoparticles in food and personal care products. Environ Sci Technol 46(4):2242–2250

11. Binetruy C, Boussu F (2010) Recent advances in textile composites: 26–28 Oct 2010, Lille Grand Palais, Lille, France, DEStech Publications

12. U.S.EPA (2012) Nanomaterial case study: a comparison of multiwalled carbon nanotube and decabromodiphenyl ether flame-retardant coatings applied to upholstery textiles (external review draft). U.S. Environmental Protection Agency, Washington, DC

13. U.S.EPA (2013) Comprehensive environmental assessment applied to multiwalled carbon nanotube flame-retardant coatings in upholstery textiles: a case study presenting priority research gaps for future risk assessments (final report). U.S. Environmental Protection Agency, Washington, DC

14. Quadros ME, Pierson R, Tulve NS, Willis R, Rogers K, Thomas TA, Marr LC (2013) Release of silver from nanotechnology-based consumer products for children. Environ Sci Technol 47(15):8894–8901

15. Mueller NC, Nowack B (2008) Exposure modeling of engineered nanoparticles in the environment. Environ Sci Tech 42(12):4447–4453

16. Kiser MA, Westerhoff P, Benn T, Wang Y, Pérez-Rivera J, Hristovski K (2009) Titanium nanomaterial removal and release from wastewater treatment plants. Environ Sci Technol 43(17):6757–6763

17. Blaser SA, Scheringer M, MacLeod M, Hungerbuhler K (2008) Estimation of cumulative aquatic exposure and risk due to silver: contribution of nano-functionalized plastics and textiles. Sci Total Environ 390(2–3):396–409

18. Geranio L, Heuberger M, Nowack B (2009) The behavior of silver nanotextiles during washing. Environ Sci Tech 43(21):8113–8118

19. Giokas DL, Salvador A, Chisvert A (2007) UV filters: from sunscreens to human body and the environment. TrAC Trends Anal Chem 26(5):360–374

20. Wong SWY, Leung PTY, Djurišić A, Leung KMY (2010) Toxicities of nano zinc oxide to five marine organisms: influences of aggregate size and ion solubility. Anal Bioanal Chem 396(2):609–618

21. Kaegi R, Voegelin A, Sinnet B, Zuleeg S, Hagendorfer H, Burkhardt M, Siegrist H (2011) Behavior of metallic silver nanoparticles in a pilot wastewater treatment plant. Environ Sci Tech 45(9):3902–3908

22. Kim B, Park CS, Murayama M, Hochella MF (2010) Discovery and characterization of silver sulfide nanoparticles in final sewage sludge products. Environ Sci Tech 44(19):7509–7514

23. Yang Y, Chen Q, Wall JD, Hu Z (2012) Potential nanosilver impact on anaerobic digestion at moderate silver concentrations. Water Res 46(4):1176–1184

24. Yang Y, Zhang C, Hu Z (2013) Impact of metallic and metal oxide nanoparticles on wastewater treatment and anaerobic digestion. Environ Sci Process Impacts 15:39–48

25. Benn TM, Westerhoff P, Herckes P (2011) Detection of fullerenes (C60 and C70) in commercial cosmetics. Environ Pollut 159(5):1334–1342

26. Kiser MA, Ryu H, Jang H, Hristovski K, Westerhoff P (2010) Biosorption of nanoparticles to heterotrophic wastewater biomass. Water Res 44(14):4105–4114

27. Westerhoff P, Song G, Hristovski K, Kiser MA (2011) Occurrence and removal of titanium at full scale wastewater treatment plants: implications for TiO2 nanomaterials. J Environ Monitor 13(5):1195–1203

28. U.S.EPA (1999) Biosolids generation, use, and disposal in the United States. Environmental Protection Agency, Washington, DC

29. Reinhart DR, Berge ND, Santra S, Bolyard SC (2010) Emerging contaminants: nanomaterial fate in landfills. Waste Manag 30(11):2020–2021

30. Yang Y, Xu M, Wall JD, Hu Z (2012) Nanosilver impact on methanogenesis and biogas production from municipal solid waste. Waste Manag 32(5):816–825

31. Warheit DB (2010) Debunking some misconceptions about nanotoxicology. Nano Lett 10(12):4777–4782

32. PEN (2011) The project on emerging nanotechnologies. The Woodrow Wilson International Center for Scholars, Washington, DC

33. Wijnhoven SWP, Dekkers S, Kooi M, Jongeneel WP, de Jong WH (2010) Nanomaterials in consumer products. National Institute for Public Health and the Environment, Ministry of Health, Welfare and Sport, Bilthoven, Netherlands

34. Hansen SF, Larsen BH, Olsen SI, Baun A (2007) Categorization framework to aid hazard identification of nanomaterials. Nanotoxicology 1(3):243–250

35. Aitken RJ, Chaudhry MQ, Boxall ABA, Hull M (2006) Manufacture and use of nanomaterials: current status in the UK and global trends. Occup Med 56(5):300–306

36. Chin C-JM, Chen P-W, Wang L-J (2006) Removal of nanoparticles from CMP wastewater by magnetic seeding aggregation. Chemosphere 63(10):1809–1813

37. Lee S-H, Lu Z, Babu SV, Matijevic E (2002) Chemical mechanical polishing of thermal oxide films using silica particles coated with ceria. J Mater Res 17(10):2744–2749

38. Hendren CO, Mesnard X, Droge J, Wiesner MR (2011) Estimating production data for five engineered nanomaterials as a basis for exposure assessment. Environ Sci Technol 45(7):2562–2569

39. Lem KW, Choudhury A, Lakhani AA, Kuyate P, Haw JR, Lee DS, Iqbal Z, Brumlik CJ (2012) Use of nanosilver in consumer products. Recent Pat Nanotechnol 6(1):60–72

40. Benn T, Cavanagh B, Hristovski K, Posner JD, Westerhoff P (2010) The release of nanosilver from consumer products used in the home. J Environ Qual 39(6):1875–1882

41. Quadros ME, Marr LC (2011) Silver nanoparticles and total aerosols emitted by nanotechnology-related consumer spray products. Environ Sci Technol 45(24):10713–10719

42. Choi O, Hu Z (2008) Size dependent and reactive oxygen species related nanosilver toxicity to nitrifying bacteria. Environ Sci Tech 42(12):4583–4588

43. Schluesener J, Schluesener H (2013) Nanosilver: application and novel aspects of toxicology. Arch Toxicol 87(4):569–576

44. Yang Y, Gajaraj S, Wall JD, Hu Z (2013) A comparison of nanosilver and silver ion effects on bioreactor landfill operations and methanogenic population dynamics. Water Res 47(10):3422–3430

45. Bin Y, Mine M, Koganemaru A, Jiang X, Matsuo M (2006) Morphology and mechanical and electrical properties of oriented PVA–VGCF and PVA–MWNT composites. Polymer 47(4):1308–1317

46. Ramanathan T, Abdala AA, Stankovich S, Dikin DA, Herrera-Alonso M, Piner RD, Adamson DH, Schniepp HC, Chen X, Ruoff RS, Nguyen ST, Aksay IA, Prud'homme RK, Brinson LC (2008) Functionalized graphene sheets for polymer nanocomposites. Nat Nanotechnol 3(6):327–331

47. Wakabayashi K, Pierre C, Dikin DA, Ruoff RS, Ramanathan T, Brinson LC, Torkelson JM (2008) Polymer-graphite nanocomposites: effective dispersion and major property enhancement via solid-state shear pulverization. Macromolecules 41(6): 1905–1908

48. Zeng H, Gao C, Wang Y, Watts PCP, Kong H, Cui X, Yan D (2006) In situ polymerization approach to multiwalled carbon nanotubes-reinforced nylon 1010 composites: mechanical properties and crystallization behavior. Polymer 47(1):113–122

49. Piccinno F, Gottschalk F, Seeger S, Nowack B (2012) Industrial production quantities and uses of ten engineered nanomaterials in Europe and the world. J Nanopart Res C7-1109 14(9):1–11

50. Kohler AR, Som C, Helland A, Gottschalk F (2008) Studying the potential release of carbon nanotubes throughout the application life cycle. J Clean Prod 16(8–9):927–937

51. Schnorr JM, Swager TM (2011) Emerging applications of carbon nanotubes. Chem Mater 23(3): 646–657

52. Gonçalves AG, Jarrais B, Pereira C, Morgado J, Freire C, Pereira MFR (2012) Functionalization of textiles with multi-walled carbon nanotubes by a novel dyeing-like process. J Mater Sci 47(13):5263–5275

53. Arora A, Padua GW (2009) Review: nanocomposites in food packaging. J Food Sci 75(1):R43–R49

54. Aschberger K, Johnston HJ, Stone V, Aitken RJ, Tran CL, Hankin SM, Peters SAK, Christensen FM (2010) Review of fullerene toxicity and exposure—appraisal of a human health risk assessment, based on open literature. Regul Toxicol Pharmacol 58(3):455–473

55. Robichaud CO, Uyar AE, Darby MR, Zucker LG, Wiesner MR (2009) Estimates of upper bounds and trends in nano-TiO$_2$ production as a basis for exposure assessment. Environ Sci Technol 43(12):4227–4233

56. Macwan DP, Dave P, Chaturvedi S (2011) A review on nano-TiO$_2$ sol-gel type syntheses and its applications. J Mater Sci 46(11):3669–3686

57. Barker PJ, Branch A (2008) The interaction of modern sunscreen formulations with surface coatings. Prog Org Coat 62(3):313–320

58. Scotter MJ (2011) Methods for the determination of European Union-permitted added natural colours in foods: a review. Food Addit Contam A 28(5):527–596

59. Lomer MCE, Hutchinson C, Volkert S, Greenfield SM, Catterall A, Thompson RPH, Powell JJ (2004) Dietary sources of inorganic microparticles and their intake in healthy subjects and patients with Crohn's disease. Br J Nutr 92(06):947–955

60. Windler L, Lorenz C, von Goetz N, Hungerbuhler K, Amberg M, Heuberger M, Nowack B (2012) Release of titanium dioxide from textiles during washing. Environ Sci Technol 46(15):8181–8188

61. Auffan M, Pedeutour M, Rose J, Masion A, Ziarelli F, Borschneck D, Chaneac C, Botta C, Chaurand P, Labille J, Bottero J-Y (2010) Structural degradation at the surface of a TiO$_2$-based nanomaterial used in cosmetics. Environ Sci Technol 44(7):2689–2694

62. Chen Y, Cao X, Chang PR, Huneault MA (2008) Comparative study on the films of poly(vinyl alcohol)/pea starch nanocrystals and poly(vinyl alcohol)/native pea starch. Carbohydr Polym 73(1):8–17

63. Duncan TV (2011) Applications of nanotechnology in food packaging and food safety: barrier materials, antimicrobials and sensors. J Colloid Interface Sci 363(1):1–24

64. Azeredo HMC, Mattoso LHC, Wood D, Williams TG, Avena-Bustillos RJ, McHugh TH (2009) Nanocomposite edible films from mango puree reinforced with cellulose nanofibers. J Food Sci 74(5):N31–N35

65. Lu Y, Weng L, Zhang L (2004) Morphology and properties of soy protein isolate thermoplastics reinforced with chitin whiskers. Biomacromolecules 5(3):1046–1051

66. Avella M, De Vlieger JJ, Errico ME, Fischer S, Vacca P, Volpe MG (2005) Biodegradable starch/clay nanocomposite films for food packaging applications. Food Chem 93(3):467–474

67. Chaudhry Q, Castle L, Watkins R (2010) Nanotechnologies in food. Royal Society of Chemistry, Cambridge, UK

68. Joseph T, Morrison M (2006) Nanotechnology in agriculture and food. Institute of Nanotechnology. Nanoforum.org, European Nanotechnology Gateway.

69. Kusmono WMW, Mohd IZA (2013) Preparation and properties of clay-reinforced epoxy nanocomposites. Int J Poly Sci 7:690675

70. Sk MP, Jaiswal A, Paul A, Ghosh SS, Chattopadhyay A (2012) Presence of amorphous carbon nanoparticles in food caramels. Sci Rep 2. 1–5

71. Mitrano DM, Lesher EK, Bednar A, Monserud J, Higgins CP, Ranville JF (2011) Detecting nanoparticulate silver using single-particle inductively coupled plasma–mass spectrometry. Environ Toxicol Chem 31(1):115–121

72. Gray EP, Bruton TA, Higgins CP, Halden RU, Westerhoff P, Ranville JF (2012) Analysis of gold nanoparticle mixtures: a comparison of hydrodynamic chromatography (HDC) and asymmetrical flow field-flow fractionation (AF4) coupled to ICP-MS. J Anal Atom Spectrom 27(9):1532–1539

73. Mitrano DM, Barber A, Bednar A, Westerhoff P, Higgins CP, Ranville JF (2012) Silver nanoparticle characterization using single particle ICP-MS (SP-ICP-MS) and asymmetrical flow field flow fractionation ICP-MS (AF4-ICP-MS). J Anal Atom Spectrom 27(7):1131–1142

74. Reed RB, Higgins CP, Westerhoff P, Tadjiki S, Ranville JF (2012) Overcoming challenges in analysis of polydisperse metal-containing nanoparticles by single particle inductively coupled plasma mass spectrometry. J Anal Atom Spectrom 27(7): 1093–1100

75. Reed RB, Ladner DA, Higgins CP, Westerhoff P, Ranville JF (2012) Solubility of nano-zinc oxide in environmentally and biologically important matrices. Environ Toxicol Chem 31(1):93–99

76. Rudnick RL, Fountain DM (1995) Nature and composition of the continental-crust – a lower crustal perspective. Rev Geophys 33(3):267–309

77. Priest ND, Van de Vyver FL (1990) Trace metals and fluoride in bones and teeth. CRC Press, Boca Raton

78. Kiser MA, Ladner DA, Hristovski KD, Westerhoff PK (2012) Nanomaterial transformation and association with fresh and freeze-dried wastewater activated sludge: implications for testing protocol and environmental fate. Environ Sci Technol 46(13):7046–7053

79. Westerhoff PK, Kiser A, Hristovski K (2013) Nanomaterial removal and transformation during biological wastewater treatment. Environ Eng Sci 30(3):109–117

80. McClellan K, Halden RU (2010) Pharmaceuticals and personal care products in archived U.S. biosolids from the 2001 EPA national sewage sludge survey. Water Res 44(2):658–668

Nanoparticle Aggregation: Principles and Modeling

2

Wen Zhang

Contents

W. Zhang, PhD
John A. Reif, Jr. Department of Civil and Environmental Engineering, New Jersey Institute of Technology, Newark, NJ, USA
e-mail: wzhang81@njit.edu

Abstract

The high surface area to volume ratio of nanoparticles usually results in highly reactive and colloidal instability compared to their bulk counterparts. Aggregation as well as many other transformations (e.g., dissolution) in the environment may alter the physiochemical properties, reactivity, fate, transport, and biological interactions (e.g., bioavailability and uptake) of nanoparticles. The unique properties pertinent to nanoparticles, such as shape, size, surface characteristics, composition, and electronic structures, greatly challenge the ability of colloid science to understand nanoparticle aggregation and its environmental impacts. This review briefly introduces fundamentals about aggregation, fractal dimensions, classic and extended Derjaguin-Landau-Verwey-Overbeak (DLVO) theories, aggregation kinetic modeling, experimental measurements, followed by detailed discussions on the major factors on aggregation and subsequent effects on nanomaterial transport and reactivity.

2.1   Introduction

Aggregation of nanoparticles (NPs) in aqueous dispersions involves the formation and growth of clusters and is controlled by both interfacial chemical reactions and particle transport mechanisms. Many toxicological experiments have found it difficult to maintain real nano-sized materials in the media, largely because NPs in aqueous phase are subject to slow or fast aggregation depending on solution chemistries and particle characteristics. NPs may aggregate into clusters up to several microns in size, leaving them no longer in the nanometer range. The propensity of NPs to aggregate in aqueous environments determines their mobility, fate, and other environmental interactions [1–4].

Despite the advances in nanotechnology and colloidal science, theoretical principles remain elusive and demand continuing efforts on improving our understandings on the fundamental science that may regulate their potential for aggregation [5, 6]. Additionally, particles released to the environment undergo chemical and physical transformations and encounter a multitude of solution conditions important for aggregation, including solution pH, dissolved ions, naturally occurring organic matter, clays, and biocolloids.

This review focuses on the following topics: (1) colloid science principles that regulate the colloidal behavior of nanomaterials in the environment; (2) The effects of the intrinsic NP properties that challenge the theoretical understandings and affect the aggregation kinetics.

2.2   Colloid Science Behind Aggregation

Colloid science is defined as a branch of chemistry dealing with heterogeneous systems where dispersion (colloids) and dispersant are mixed. When particles are dispersed, sizes range between 1 nm and 1 μm in a continuous medium. Above this size range, particles likely begin to sediment out of suspension. By definition, the size range of

manufactured nanomaterials is within the size range of colloidal particles (i.e., <100 nm). Therefore, theories in colloid science should be applicable to manufactured nanomaterials.

Aggregation of colloidal particles occurs when physical processes bring particle surfaces in contact with each other and short-range thermodynamic interactions allow for particle–particle attachment to occur. There are two types of aggregation relevant to manufactured NPs in the environment: homoaggregation and heteroaggregation. Homoaggregation refers to aggregation of two particles of the same kind. Heteroaggregation refers to aggregation of dissimilar particles (e.g., nanoparticle–clay particle attachment). More frequently, heteroaggregation is referred to sorption or adsorption, deposition, or particle attachment toward a surrounding surface.

Most aggregation processes are fractal in nature [7]. The mass of a fractal aggregate, m(R), is proportional to its hydrodynamic radius, a_h, to a power d_F, the fractal dimension:

$$\mathrm{m}(R)\, \alpha\, a_h^{d_F} \qquad (2.1)$$

The fractal dimension depends on the aggregation rate. For instance, the lower the aggregation rate, the more particles have time to configure themselves into a more compact and denser structure, and the higher the fractal dimension. Typical diffusion-limited cluster aggregation (DLCA) aggregates possess a d_F of 1.7–1.8, while reaction-limited (RLCA) aggregates often exhibit a d_F value around 2.1. The concept of fractal dimension is thus used to describe aggregate structure (dendritic or compact). Homoaggregation under controlled laboratory conditions produces aggregates of reasonably predictable fractal dimension [5, 8], whereas heteroaggregation typically forms natural fractals (statistically self-similar over a limited range of length scales), making aggregation state more difficult to describe and predict. Figure 2.1 shows the comparison between monodisperse, dendritic, and compact clusters of aggregated NPs. The physical dimensions and density of the aggregates formed can significantly affect
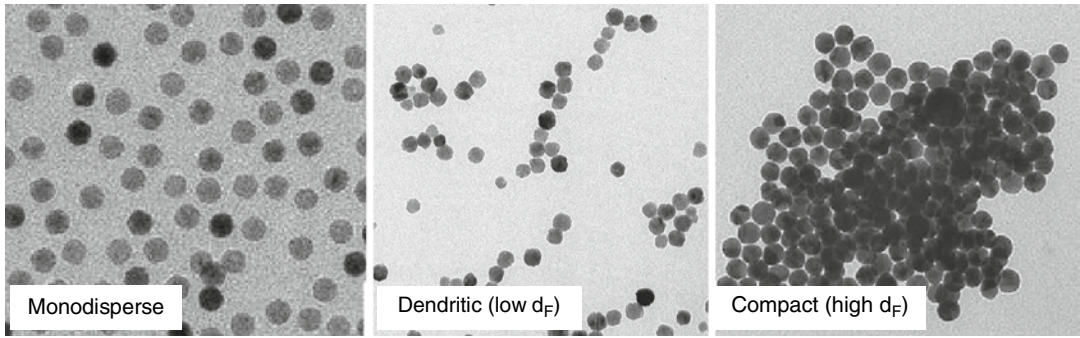
Fig. 2.1 Different aggregation states: monodisperse and polydisperse (dendritic and compact aggregates)

the reactive surface area, reactivity, bioavailability, and toxicity. Aggregate structure must therefore be determined and considered when interpreting fate, transport, and toxicity data.

The two types of aggregation processes (DLCA and RLCA) are differentiated by the collision efficiency (α), ranging from 0 to 1, which defines the probability that two particles attach successfully or irreversibly (also known as "sticking coefficient", "success rate" or "attachment efficiency"). When $\alpha = 1$, particle attachment occurs at the success rate of 100 %; When $\alpha = 0.5$, it means only half the collision results in the successful attachment. Particles attaching at first contact ($\alpha = 1$) form large dendritic aggregates, whereas particles sticking only after several collisions ($\alpha < 1$) form denser and less dendritic aggregates. DLCA occurs when the collision efficiency between particles is close to 1, whereas RLCA dominates when $\alpha < 1$ [9]. The aggregation behavior in these two regimes is fundamentally different in both kinetics and aggregate structures. In the RLCA regime, an increase in the electrolyte concentration screens the surface charge and reduces the energy barrier to aggregation, which leads to faster aggregation. At electrolyte concentrations above the critical coagulation concentration (CCC), the energy barrier is eliminated, and the DLCA regime (i.e., $\alpha = 1$) results. Thus, CCC is often used to distinguish the aggregation regimes of many nanoparticle systems [1–4].

2.3   DLVO Theory and Limitations

Although colloid science is fundamental to understanding and developing theories for nanomaterials systems, due to the novelty of nanomaterial properties, several studies have found that this is not always the case. Many recent studies have begun applying colloid science principles, based around Derjaguin-Landau-Verwey-Overbeak (DLVO) theory, to understand NP aggregation under various conditions. Manufactured NPs challenge the limits of colloid science, however, due to their small size, variable shape, structure, composition, roughness, and potential presence of adsorbed or grafted organic macromolecules. These local scale features on the nanoparticle surfaces add many complexities into the predictive work with DLVO theory.

Classic DLVO is based on a force (interaction energy) balance that comprises attractive van der Waals and repulsive electrostatic forces from the overlap between the electrical double layers of the interacting surfaces [10]. Under the Derjaguin integration approximation, the interaction energy between two spherical particles with radii of R_1 and R_2 is expressed as [11–13]:

$$U_{1w2}^{DLVO} = U_{1w2}^{vdW} + U_{1w2}^{EL} \tag{2.2}$$

$$U_{1w2}^{vdW}(h) = -\frac{A_H}{6}\left[\frac{8R_R^2}{h(8R_R+h)} + \frac{8R_R^2}{(4R_R+h)^2} + \ln\frac{h(8R_R+h)}{(4R_R+h)^2}\right] \quad (2.3)$$

$$U_{1w2}^{EL}(h) = 4\pi\varepsilon\varepsilon_0 R_R\left[\varphi_1\varphi_2\exp(-\kappa h) - \frac{1}{4}(\varphi_1^2+\varphi_2^2)\exp(-2\kappa h)\right] \quad (2.4)$$

$$\kappa^{-1} = \sqrt{\frac{\varepsilon\varepsilon_0 k_B T}{2N_A I e^2}} \quad (2.5)$$

where U_{1w2} is the total interaction energy between particle (1) and particle (2) in water (w) as a function of interaction distance (h). $U_{1w2}^{vdW}(D)$ is the van der Waals interaction energy; $U_{1w2}^{EL}(D)$ is the electrostatic interaction energy; and A_H is the particle (1) to particle (2) Hamaker constant in water (w) and is an intrinsic property of the two interacting materials, indicating the strength of the long-range mutual attraction between them [10]. R_R is the reduced particle radius, $R_R = R_1 R_2/(R_1 + R_2)$; for monodisperse NPs with a radius of R, R_R is equal to $1/2R$, and R is approximately equal to the measured hydrodynamic radius (r_H). z_i is the valency of the ith ion; e is unit charge, 1.602×10^{-19} C, and φ_1 and φ_2 are the surface potentials (mV) for the two interacting NP surfaces, which were approximately equal to their ζ potentials [14]. κ^{-1} is the Debye length (nm), indicative of the thickness of the electrical diffuse layer as a function of the ionic strength and electrolyte, ε_0 is the dielectric permittivity of a vacuum (8.854×10^{-12} C/(V·m)), ε is the dielectric constant of water (78.5), N_A is Avogadro's number (6.02×10^{23} mol^{-1}), and I is the ionic strength (M), $I = 0.5 \cdot \Sigma c_i Z_i^2$, where c_i is the molar concentration of one ionic species (i). The van der Waals interaction energy commonly indicates the attraction between two spherical particles; however, due to unique NPs shapes and compositions, expanded theoretical approaches may be needed [15]. The electrostatic interaction energy expresses the strength in the electrostatic attraction or repulsion between two interacting particles due to the formation of electric double layer (EDL) on the surface. An EDL is formed because the surface attracts counter-charged ions from the bulk solution as illustrated in Fig. 2.2a. Ionic strength, which is a measure of the amount of ions present in the bulk solution, determines the extent of the surface ionization and thickness of EDL. Low ionic strength means the EDL ion cloud extends far out from the particle (or a higher Debye length); high ionic strength conditions compress the EDL (a lower Debye length).

Classical DLVO simplifies thermodynamic surface interactions and predicts the probability of whether particles likely aggregate together by simply summing van der Waals and electric double-layer interaction energies to determine if the net interaction energy is negative (attractive) or positive (repulsive). If the net interaction energy has a positive peak (also known as interaction energy barrier; see Fig. 2.2b), aggregation will be unfavorable and successful particle attachment requires that the interacting particles overcome the energy barrier before they could contact each other. Figure 2.2b also demonstrates that particles can have a net attraction when they get close to proximity due to a negative energy trap or energy well (called primary energy minimum). There may or may not be a secondary minimum as shown by the black dotted line. Particles in the primary well are considered to be irreversibly aggregated whereas particles in the secondary well are reversibly aggregated (i.e., re-entrainment is possible if shear forces are exerted).

Despite considerable theoretical progress, there appears to be a sizable discrepancy between DLVO predications and instrumental force measurements in biotic and abiotic colloidal behavior [16, 17], such as colloid deposition and fouling [18, 19]. Specifically, these discrepancies are mainly including: DLVO only describes the short range interaction within 0.1–10 nm due to the exponential decay of the forces with distance [20–22], however, at short ranges less than, for instance, 0.1 nm, DLVO disagrees with
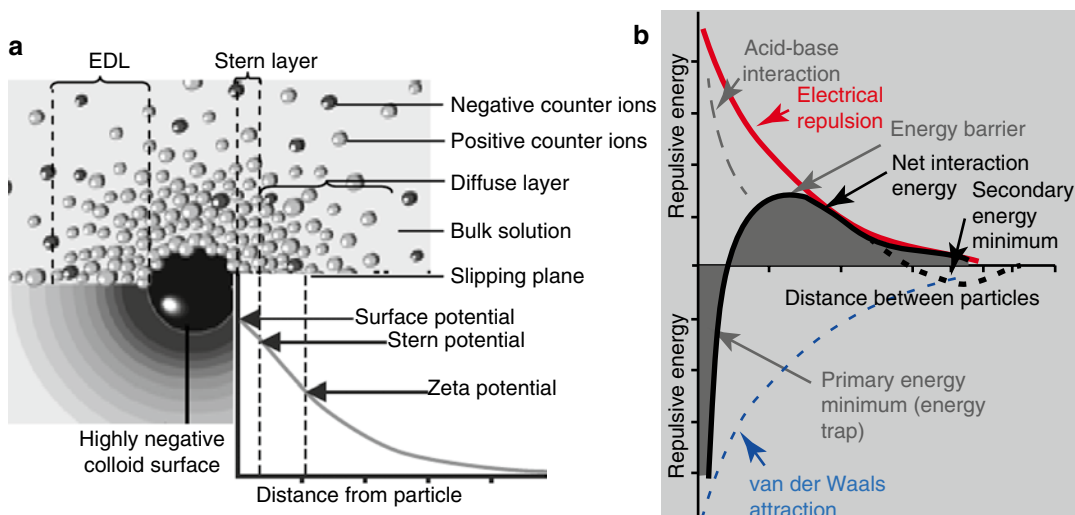
Fig. 2.2 (**a**) Schematic of double layer in a liquid at contact with a negatively-charged solid. (**b**) The net interaction energy as a function of the interacting distance. van der Waals interaction energy (*blue dashed line*), electrostatic interaction energy (*red line*), total Derjaguin-Landau-Verwey-Overbeak (DLVO) interaction energy (*solid black line*). The extended Derjaguin-Landau-Verwey-Overbeak (EDLVO) interaction energy considers non-DLVO forces such as acid-base interaction as indicated by the *black dashed line*

experiment and this is attributed to hydration forces [23, 24]; DLVO theory has preferably been used for monovalent salts at low salt concentrations of $<5 \times 10^{-2}$ M; Above 0.1 or 0.2 M (the regime of biological interest or physiological concentration), DLVO theory often loses all potency of predictability due to the shrinkage of electrostatic force and the rise of dispersion forces on charged particles [25, 26]; Similarly, London-van der Walls forces may also be retarded by the rise of dispersion forces but no single closed-form equation is available for calculating the influence of this retardation [27]. Such deviations have been ascribed to several predominant reasons, including surface roughness and the presence of other short range non-DLVO interactions [28–30]. Other researchers such as Ninham et al. proposed that the inconsistency of traditional DLVO in predicting the particle stability arise from the ab initio decomposition of forces into non-interacting van der Waals and Coulombic components [31].

Refinement of DLVO and Extended DLVO (EDLVO) models to include the effects of surface heterogeneity has led to model predictions that are more congruent to the measured results [21, 32, 33]. The so-called non-DLVO or extra-DLVO

forces invoke a suite of complex interfacial forces, probably including hydration force [34, 35], membrane fluctuations [25], hydrophobic [36], oscillatory [25], osmotic (depletion attraction) [37, 38], and steric, or Helfrich repulsion (effected by entropy effect) [39]. These classification of surface forces only distinguish them based on the effects since they are all electromagnetic in origin [40]. These additional non-classical DLVO interactions are evident in most cases of biological environments [25, 41] and accurate assessment of each force is often impossible due to the inadequate mathematical expressions and effective methods of quantitative measurement [22]. For example, the origin of hydrophobic and hydrophilic interactions is not completely understood yet and hydrophobic effect has been explained through the decrease in entropy of water molecules associated with cavity formation for dissolution of hydrophobic moieties [22]. Another example is that hydration forces that arise when two surface are within the distance of a few molecular diameters [42]. Atomic Force Microscope (AFM) study is unable to detect such short-ranged interaction because the absolute zero separation is difficult to determine [40].

In contrast to classical DLVO, extended DLVO or EDLVO is termed for the models considering Lewis acid-base interactions or other non-DLVO forces [11, 43]. Some research even used osmotic pressure or depletion attraction for the basis of EDLVO models [27, 44, 45]. In most cases of EDLVO model applications, Lewis acid-based interactions are considered as an important addition to DLVO theory and the predictions were found to be consistent with experiments in coagulations [27, 46]. In order to model the behavior and stability of NPs in aqueous environment with DLVO theory, appropriate simplifications, assumptions, and boundary conditions must be made to temper the results without the loss of generality.

2.4 Aggregation Kinetics Measurement and Modeling

2.4.1 Absolute Aggregation Rate Constant and Attachment Efficiency

The theory of colloid stability considers collision frequency (β) and efficiency (α) [47]. Collision frequency was theoretically solved by Smoluchowski [48, 49], while the basis for evaluation of the collision efficiency was given by Fuchs [50]. To use the Fuchs theory, the interaction energy as a function of the distance between interacting particles must be resolved by the classic DLVO theory. von Smoluchowski's population balance equation describes the irreversible aggregation kinetics of particles [51] and is expressed as

$$\frac{dn_k}{dt} = \frac{1}{2} \sum_{i+j=k} \alpha\left(r_i, r_j\right) \beta\left(r_i, r_j\right) n_i n_j - n_k \sum_{i=1}^{\infty} \alpha\left(r_i, r_k\right) \beta\left(r_i, r_k\right) n_i \tag{2.6}$$

where n_k (or n_i and n_j) is the number concentration of aggregates comprised of k (or i and j) primary particles (also called k-class or k-fold particles or aggregates), $\alpha\ (r_i, r_j)$ and $\beta\ (r_i, r_j)$ are the collision efficiency function and collision frequency function for class i and j particles, and r_i

and r_j are the radii of class i and j particles. Taking into account the van der Waals forces and hydrodynamic interactions, the collision frequency rate is then expressed as [52, 53]:

$$\beta\left(i, i\right) = \frac{8kT}{3\mu} \left[2\int_0^{\infty} \lambda\left(u\right) \frac{\exp\left(U_{iwi}^{vwd}\left(h\right) / kT\right)}{\left(2+u\right)^2} \, du \right]^{-1} \tag{2.7}$$

where $u = h/r$, and $\lambda\ (u)$ is the correction factor for the diffusion coefficient, which is related to the separation distance by the equation [54]:

$$\lambda\left(u\right) = \frac{6\left(u\right)^2 + 13\left(u\right) + 2}{6\left(u\right)^2 + 4\left(u\right)} \tag{2.8}$$

For microscale flocculation of heterodisperse particles with diameters, d_i and d_j, the collision frequency can be also expressed [55]:

$$\beta = \left(\frac{2k_B T}{3\mu} \right) \left(\frac{1}{d_i} + \frac{1}{d_j} \right) \left(d_i + d_j \right) \tag{2.9}$$

For monodisperse particles with the same diameters, $\beta = \dfrac{8k_B T}{3\mu}$, where μ is the viscosity of the solution (1×10^{-3} Pa$\cdot$s). Thus, the absolute aggregation rate can be simplified to:

$$\frac{dn_k}{dt} = -\frac{4}{3} \alpha \frac{k_B T}{\mu} n_i^2 \tag{2.10}$$

Early stage aggregation kinetics can be described by the rate of doublet formation, which apparently dominates compared to other higher-order aggregate formation. The loss in primary particles during the early stage of aggregation can be expressed as a second-order rate equation:

$$\left(\frac{dn_1}{dt} \right)_{t \to 0} = -k_{11} n_0^2 \tag{2.11}$$

where $n_1(t)$ is the concentration of primary particles as a function of time t, k_{11} is the absolute aggregation rate constant $\left(k_{11} = \dfrac{4}{3} \alpha \dfrac{k_B T}{\mu} \right)$, and

n_0 is the initial primary particle concentration, that is, $n_1(0) = n_0$. Within the Rayleigh-Gans-Debye (RGD) approximation, which is valid for primary particles that are relatively small compared to the incident wavelength [53, 56],

the absolute aggregation rate constant, k_{11}, can be determined through time-resolved DLS measurements conducted at a fixed scattering angle based on the relationship [53]:

$$\frac{1}{r_H(0,q)}\left(\frac{dr_H(t,q)}{dt}\right)_{t\to 0} = k_{11}n_0\left[1+\frac{\sin(2aq)}{2aq}\right]\left(1-\frac{1}{\delta}\right) \tag{2.12}$$

where q is the scattering vector defined by $(4\pi n/\lambda)\sin(\theta/2)$, with n being the refractive index of the medium, λ the wavelength of incident light, and θ the scattering angle; $r_H(t, q)$ is the hydrodynamic radius as a function of t and q; a is the primary particle radius; and δ is the relative hydrodynamic radius of the doublet, which is approximately 1.38 [53]. Usually DLS is run at a fixed angle, the only independent variable in Eq. (2.12) is t with r_H as the dependent variable. To obtain k_{11} through Eq. (2.12), KL Chen et al., proposed a linear least squares regression analysis for the increase in r_H with t [1]. The assumption for analysis is that the hydrodynamic radius for the doublet aggregate, $r_H(0)$, shall not be more than 3 nm in excess of the primary particle radius (a) and the final $r_H(t)$ to be equal to approximately 1.3a. The slope of the best fit line in the function of hydrodynamic radius (r_H) versus aggregation time (t) gives the estimation of the absolute aggregation rate con-

stant, k_{11}, for the early-stage aggregation of primary NPs [5, 6]:

$$\left[\frac{dr_H(t)}{dt}\right]_{t\to 0} \propto (k_{11})n_0 \tag{2.13}$$

The attachment efficiency, α, otherwise known as the inverse stability ratio, $1/W$, is used to represent the relative aggregation rate and also to divide the aggregation process into DLCA and RLCA as mentioned earlier. Attachment efficiencies are calculated by normalizing the measured k_{11} by the diffusion-limited aggregation rate constant $(k_{11})_{fast}$ determined under favorable aggregation conditions [57]:

$$\alpha = \frac{k_{11}}{(k_{11})_{fast}} \tag{2.14}$$

The attachment efficiency (α) is the reciprocal of the stability ratio W, which is defined as [3, 58]:

$$\alpha = 1/W \equiv \left[\int_0^\infty \lambda(u)\frac{\exp\left(U_{iwi}^{vdw}(h)/k_B T\right)}{(2+u)^2}du\right]\cdot\left[\int_0^\infty \lambda(u)\frac{\exp\left(U_{iwi}^{DLVO}(h)/k_B T\right)}{(2+u)^2}du\right]^{-1} \tag{2.15}$$

where U_{iwi}^{DLVO} is the total interaction energy between two interacting particles, which as shown in Eq. (2.2) is the sum of the van der Waals attractive energy U_{iwi}^{vdw} and the electrostatic interaction energy U_{iwi}^{EL}.

Equation (2.15) has been extensively used to study aggregation kinetics of various nanoparticle systems [59–65]. However, the theoretical calculation of the stability ratio ($1/W$) based on the

classic DLVO theory finds inconsistency with experimental observations due to the inherent limitations of the classic DLVO theory as discussed above [3, 66]. Despite the wide applications in many colloidal systems, the attachment efficiency calculation by Eq. (2.15) has some issues when applied to the nanoscale aggregation problems. For example, the calculated $1/W$ has been reported to be steeper than the experimental

value [3]. The discrepancy may arise from the assumption that van der Waals attraction is the sole driving force for particle aggregation, which could be true for colloidal particles. However, as we previously reported [3, 66], the nanoscale transport of NPs is governed by both interaction energy and random Brownian diffusion according to interfacial force boundary layer (IFBL) theory. For small NPs, the role of interaction energy should be discounted appreciably owing to its relatively small particle size, whereas random kinetic energy plays a dominant role in the transport mechanism. In contrast, for colloidal particles, the interfacial interaction plays a major role because the random kinetic motion (i.e., diffusivity) is substantially lower than that of NPs according to the Stokes-Einstein equation. On the other hand, the good fit between *1/W* and experimentally derived α is usually achieved by varying the Hamaker constant as a fitting parameter [67]. However, the Hamaker constant (A_H) reflects an intrinsic property of the material of the two interacting particles, which indicates the strength of long-range mutual attraction between two small volumes of the material [1–4, 59, 66]. In this sense, the Hamaker constant should thus be a fixed value for the pairwise interactions of NPs, or at least should not vary significantly. In fact, the Hamaker constant ($A_{H, 123}$) between particle 1 and particle 2 in solvent 3 can be calculated by the method of van Oss [3, 68, 69]. Moreover, from the assumption made for the derivation of Eq. (2.13), this experimental method for the determination of k_{11} or α should only be used to describe the early aggregation kinetics (e.g., hydrodynamic sizes of aggregates less than 30 % of the primary nanoparticle sizes). Thus, more experimental and theoretical work is needed to explicitly elucidate the fundamental mechanisms of nanoscale aggregation kinetics.

2.4.2 Experimental Measurement of Aggregation Kinetics

Aggregation process is commonly monitored using time resolved-dynamic light scattering (TR-DLS) on the commercial instruments such as Malvern Zetasizer and Coulter® Nano-sizer.

DLS is a non-invasive technique for measuring the size of NPs in a liquid dispersion. The technique measures the time-dependent fluctuations in the intensity of scattered light from a suspension of particles undergoing random Brownian motion. Analysis of these intensity fluctuations allows for the determination of the diffusion coefficients (*D*), which in turn yield the particle size through the Stokes-Einstein equation:

$$D = \frac{k_B T}{6\pi\mu r_H} \qquad (2.16)$$

In addition to hydrodynamic size, DLS is also commonly used to measure the electrophoretic mobility (EPM), which subsequently is converted to zeta potentials. As shown in Eq. (2.4), zeta potential is used to approximate the surface potential of colloidal particles and significantly affects the electrostatic interaction energy. the net electrophoretic mobility (μ_E, m/s/(V/m) or m²/ Vs) of the particles, which is then converted to the ζ potential using Henry's approximation [70]:

$$\mu_E = \frac{2\zeta\varepsilon\varepsilon_0 f(\kappa r)}{3\eta} \qquad (2.17)$$

where ε_0 is the dielectric permittivity of a vacuum (8.854×10^{-12} C/(V·m)), ε is the dielectric constant of water (78.5), *v* is the medium's dynamic viscosity (pa·s), κr is the ratio of particle radius to Debye double layer thickness, and $f(\kappa r)$ refers to Henry's function, which is 1.5 under the Smoluchowski approximation and 1 under the Hückel approximation. In aqueous media with moderate electrolyte concentrations, 1.5 is most commonly applied [71]. η is the viscosity of the liquid medium.

With the measurement of hydrodynamic sizes over time by DLS, the fractal dimension (*dF*) can be determined for particles with spherical primary particle shape. The aggregation curves could be fitted by a power-law relationship between r_H and the aggregation time (*t*) [72]:

$$r_H(t) = \left(1 + \frac{t}{t_a}\right)^{1/d_F} \qquad (2.18)$$

where t_a is the characteristic Brownian aggregation time for doublet formation and $t_a = 1/$

$(k_{11} \cdot n_0)$. The power-law growth is a characteristic feature of DLCA aggregation, while RLCA may exhibit both power-law or exponential growth [72].

2.4.3   Aggregation Kinetics Modeling

There is a pressing need for quantitative data on the aggregation kinetics of engineered NPs and a deeper understanding of the aggregation mechanisms operating at nanoscale, which are pivotal to assessment of their environmental fate, transport, and toxicity. For this reason, the stability and aggregation of NPs have been studied extensively over the past few years [5, 6, 64, 73]. Despite the advances in knowledge about the aggregation behavior of NPs, few studies have modeled aggregation kinetics (e.g., the growth rate of the hydrodynamic size) [74, 75]. Such models aid in understanding the general principles and mechanisms that govern stability and aggregation kinetics as well as in predicting nanoscale processes.

Because NPs are in a comparable dimension (e.g., 10–20 nm) with the electric double layer (EDL) surrounding their surface, aggregation can be viewed similar to two interacting ions, which is described by the Brønsted concept based on Transition State Theory [74–76]. Thus, some studies proposed that during the initial linear aggregation of primary NPs aggregation follows first- or second-order reaction kinetics [1–3, 5, 6], which is shown in Eq. (2.13). This is also supported by the examination of the evolution of the particle size frequency based on the DLS data. For instance, Fig. 2.3a shows the aggregation kinetics of CeO_2 NPs investigated by TR-DLS. The average hydrodynamic radius of CeO_2 NPs increased dramatically following the addition of salts and the width of PSD became broader and broader. The particle size frequency is evaluated by the power law distribution, which is usually used for colloids in natural waters [55]:

$$\frac{dN}{d(d_p)} = A(d_p)^{-B} = \frac{\Delta N}{\Delta(d_p)} \qquad (2.19)$$
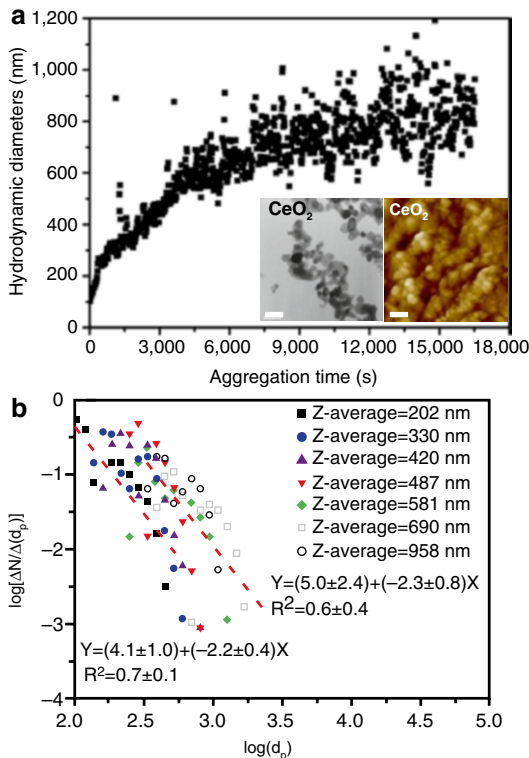
Fig. 2.3 (**a**) Aggregation kinetics of 10 mg/L CeO_2 NPs at an ionic strength of 20-mM KCl solution. The hydrodynamic diameters were Z-average data on the basis of the scattered light intensity. The insert shows the TEM and AFM images. (**b**) Evolution of the frequency distribution during aggregation of CeO_2 NPs at different measurement times (shown in the legend). The linear regression was conducted for the data of the Z-averages of 202 and 690 nm, and the fitting equations are shown next to the fitted curves (the *red dashed lines*) (This graph is produced by modification of the original one in Ref. [77])

where A is the power law density coefficient, d_p is the particle diameter, and B is the power law slope coefficient. Taking the logarithm of each side results in the expression gives: $\log\left[\dfrac{\Delta N}{\Delta(d_p)}\right] = \log A - B \cdot \log(d_p)$, which can be plotted to determine the coefficients A and B. On the basis of the data in Fig. 2.3a, the frequency distributions at different aggregation stages were derived in Fig. 2.3b. As the particles aggregated, $\log A$ increased, indicating that the total number of particles in each size range increased. B is a measure of the relative number of particles in

each size range [68]. Linear curve fitting in Fig. 2.3b reveals that the B values for CeO_2 NPs during aggregation range from 2.2 to 2.3, within the typical range (2–5) of B for most natural waters [78]. When B is greater than 1, small particles (primary NPs) dominate the evolution of particle size distribution (PSD) and aggregation kinetics [55]. Although many sophisticated models of aggregation kinetics have been developed, such as molecular dynamics [79] and Monte Carlo [80], aggregation kinetics rarely has been modeled using the concept of chemical reaction kinetics.

Aggregation kinetics is likely to be influenced more by particle interactions (namely, interaction energy) than by transport characteristics (e.g., mobility or diffusivity) [81]. Previously, we introduced the interfacial force boundary layer (IFBL) theory in modeling the adsorption kinetics of NPs onto the microbial surface and stressed the importance of particle interaction energy in the transport characteristics of NPs, in addition to the Ficker's Law or other conventional transport mechanisms (e.g., advection and dispersion) [67]. For small NPs, the role of interaction energy should be discounted appreciably owing to its relatively small particle size, whereas random kinetic energy plays a dominant role in the transport mechanism. In contrast, for colloidal particles, the interfacial interaction plays a major role because the random kinetic motion (i.e., diffusivity) is substantially lower than that of NPs according to the Stokes-Einstein equation. For instance, for particles <100 nm in size, Brownian diffusion was reported to control the long-range forces between individual NPs, causing collisions between particles. In this regard, Nikolakis et al. also proposed a transport model to account for the role of the energy barrier in the particle coagulation kinetics in addition to the dispersion term [81]:

$$\frac{\partial c}{\partial t} = \frac{1}{r_H^2} \frac{\partial}{\partial r} \left[D r_H^2 \frac{\partial c}{\partial r} + r_H^2 c \frac{D}{k_B T} \frac{\partial U}{\partial r_H} \right] \quad (2.20)$$

where c is the concentration of NPs, D is the diffusion coefficient of the NPs, k_B is the Boltzmann

constant, T is the absolute temperature, r is the transport distance, and U is the interaction energy between NPs. The first term $\left(D r_H^2 \frac{\partial c}{\partial r} \right)$ accounts for the effect of dispersion, which plays a role in

the initial stage of coagulation owing to the high concentration gradient and the high diffusion coefficient (D) for the primary NPs. On one hand, the effect of the dispersion term gradually diminishes as the primary particle concentration decreases and the aggregated particles concentration increases.

On the other hand, the magnitude of the interaction energy between small NPs is relatively low at the initial coagulation stage, and thus the second term $\left(r^2 c \frac{D}{k_B T} \frac{\partial U}{\partial r} \right)$ has no substantial

effect on the coagulation rate. Nevertheless, the energy barrier of large aggregated particles may be appreciably larger than that of primary NPs [67, 82]. Likewise, the diffusion coefficient for large aggregated particles is low, and thus the dispersion term is no longer rate limiting. Equation (2.20) agreed well with experimental observations of nanocrystal growth kinetics but has not been validated for use in nanoparticle aggregation kinetics. In fact, the coagulation rate derived from Eq. (2.20) has an Arrhenius form with the activation energy term (E_a) replaced by the interaction energy (U). The activation energy in the Arrhenius equation has a similar role as the energy barrier in the colloidal interactions because these two types of energy must be overcome before the reaction or aggregation occurs as illustrated in Fig. 2.4.

As indicated by the Maxwell approach, the primary and secondary energy minima could both be the deposition position for colloids due to the potential release of negative interaction energy [2–4]. However, the secondary energy minimum is only critical for particles greater than approximately 0.5 μm [83], whereas NPs generally will not significantly deposit or aggregate in the secondary energy minimum but more

Chemical reaction rate constant;*K*

$K \propto \exp\left(\dfrac{-E_a}{RT}\right)$

Activation energy;E_a

Reactants

Free-energy, ΔG

Products

Reaction themodynamics

Aggregation rate constant;*K*

$K \propto \exp\left(\dfrac{-E_b}{K_b T}\right)$

Repulsive energy

Net interaction energy

Energy barrier;E_b

Distance between particles

Primary energy minimum (energy trap)

Repulsive energy
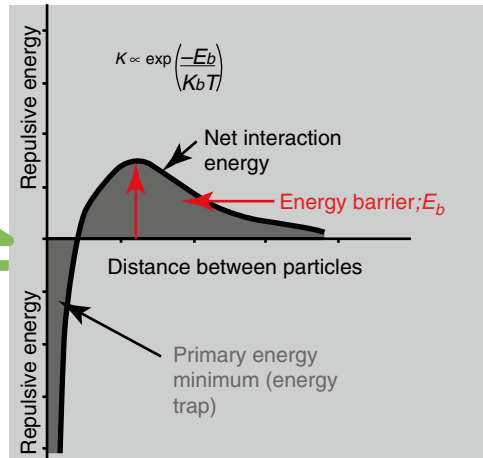
Interaction energestics

Fig. 2.4 Comparison between a typical reaction thermodynamics curve with the activation energy (E_a) required for the reaction to proceed and a total interaction energy

curve between two approaching particles with an energy barrier (E_b) that prevents two interacting particles from approaching each other

likely in the primary energy minimum [84, 85]. Thereby, Wen Zhang, et al. proposed to consider the role of E_b in aggregation kinetics and estimated the ratio of the number (ΔN) of particles with kinetic energy exceeding E_b to the total number (N) of particles with kinetic energy ranging from zero to infinity using the Maxwell-Boltzmann distribution and eventually derived a modified attachment efficiency (α_m) [77], which demonstrated the balanced consideration of interfacial energy and Brownian motion in evaluating the aggregation kinetics of nanoparticle dispersions when compared with the inverse stability ratio (1/W).

$$\frac{\Delta N_{E_b \to \infty}}{N_{0 \to \infty}} = \frac{\int_{v^C}^{\infty} 4\pi \left(\frac{m}{2\pi k_B T}\right)^{3/2} e^{-\frac{mv^2}{2k_B T}} v^2 dv}{\int_{0}^{\infty} 4\pi \left(\frac{m}{2\pi k_B T}\right)^{3/2} e^{-\frac{mv^2}{2k_B T}} v^2 dv} \quad (2.21)$$

$$= \frac{\int_{E_b}^{\infty} e^{-E} E^{1/2} dE}{\int_{0}^{\infty} e^{-E} E^{1/2} dE}$$

$$\alpha_m = \delta \cdot \frac{\Delta N}{N} = \delta \cdot \int_{E_b}^{\infty} e^{-E} E^{1/2} dE \quad (2.22)$$

where m is the molecular mass, k_B is the Boltzmann constant (1.38×10^{-23} J/K), T is temperature (K), v is the velocity of random motion (m/s), E_b can be obtained from the DLVO theory equations, and E is the random kinetic energy ($k_B T$) of NPs. Equation (2.21) thus yields the ratio of NPs with a minimum velocity of v (or a minimum kinetic energy of E_b) over the total number of NPs with the denominator constant (100 % of probability). δ is added to the Eq. (2.22) to physically account for the hydrodynamic damping effect (also called the drag effect) on the kinetic energy distribution of NPs as well as other potential discrepancies of the DLVO prediction. This is because the Boltzmann velocity distribution applies ideally to dilute systems of non-interacting gas molecules [6]. In aqueous phase, solvent molecules should dampen (or decrease) the kinetic motion of NPs, which is called velocity relaxation for Brownian particles [75]. Both the collision efficiency and frequency should be lower than those in dilute systems (e.g., air) [86]. Moreover, the particle concentration and the

medium viscosity may affect the kinetic energy distribution of NPs. To apply the Maxwell-Boltzmann distribution, the dispersed NPs are assumed to be Brownian particles (particles are moving continuously in Brownian motion with an average kinetic energy of $3k_BT/2$) in dilute systems [87, 88]. Since environmentally relevant concentrations of most engineered NPs in the environment are probably within the range of a few ng/L to μg/L [89, 90], the kinetic energy of NPs in aqueous phase should fit the Maxwell-Boltzmann distribution. In Zhang's study, aggregation experiments with a number of different metal oxides, metallic, and carbon-based nanomaterials were used to verify the new the

attachment efficiency for nanoparticle aggregation. The equation correctly interpreted the effects of ionic strength, natural organic matters (NOMs), and temperature on aggregation kinetics. Good agreements with experiment-derived attachment efficiency data for various other nanomaterial systems were also achieved. Overall, the new equation provides an alternative and complementary theoretical approach in addition to 1/W for predicting attachment efficiency.

In addition, based on the von Smoluchowski's population balance equation in Eq. (2.6) and the EDLVO theory, Kungang et al. established the DLA model to describe the aggregation kinetics of NPs in the DLA regime [91]:

$$\log r_H = \frac{1}{d_F} \log \left(1 + \frac{4k_B T}{3\mu} \left[2\int_0^\infty \lambda(u) \frac{\exp\left(U_{iwi}^{EDLVO}(h)/k_B T\right)}{(2+u)^2} du \right]^{-1} n_0 t \right) + \log a \qquad (2.23)$$

The aggregation kinetics in Eq. (2.23) seems to be capable of directly describing the growth of the aggregate radius over time. However, this equation is only limited in regimes where the collision efficiency is relatively high or close to unity (i.e., in the DLCA regime). In the RLCA regime and at other conditions with very low collision efficiencies, a rigorous expression does not exist because the collision efficiency is determined by the aggregate structure in addition to the interaction forces [9, 92]. In such regimes, a large number of collisions are required to achieve a successful aggregation, and the aggregates explore many possible mutual configurations before they stick together firmly. The aggregation rate coefficient in RLCA (K_{RLA}) is then directly proportional to the volume of the phase space (V_c), over which the center of one aggregate can be positioned to reach a bondable contact with another aggregate [92]. For two solid spheres with similar radii ($r_1 \approx r_2$ and both are equal to r), V_c is proportional to r^2. V_c is expected to be larger for fractal aggregates with similar radii than for solid spheres because the surfaces of the former are rough. In the RLA regime, it is proposed that $V_c \propto r^{dF}$ [92]. In the RLA regime, a rigorous

expression does not exist because the collision efficiency is determined by the aggregate structure in addition to the interaction forces [9, 92]. An empirical aggregation rate constant k_{RLA} was incorporated to the RLA model in order to describe the aggregation kinetics in the RLA regime:

$$\log r_H = \frac{2.303 k_{RLA}}{d_F} t + \log a \qquad (2.24)$$

2.5   Factors Affecting Aggregation Kinetics

While colloid science demonstrates that several forces with different natures and origins govern the kinetics and extent of particle aggregation, the following sections will elaborate the interplay of different factors presenting a combination of challenges to two predominant theories in colloid science, DLVO and EDLVO theories. These challenges include nanoparticle morphology (size or shape), surface characteristics (e.g., organic surface coating), composition or

crystallinity, solution chemistries such as pH, ionic strength, valence of electrolyte ions, and NOM, and environmental parameters (e.g., temperature and light irradiations), which have been reported to affect aggregation kinetics [1, 2, 5, 60, 68, 82, 93, 94].

2.5.1 Size and Shape Effect

Although there is no well-established rationale for cut-off size for NPs, the most common definition is that NPs have sizes less than 100 nm. The DLVO theory predicts that interaction energy barrier decrease as particle size decreases according to Eqs. (2.2), (2.3), and (2.4); Likewise, the attachment efficiency for small NPs will be high accordingly as the energy barrier (E_b) becomes small as shown in Eq. (2.22). This highlights that smaller particles are susceptible to aggregation at the same conditions, which is evidenced by many studies [82]. As particle decreases in size, a greater percentage of its atoms exist on the surface. Electronic structure, surface charge behavior, and surface reactivity can be altered as a result. For instance, a decrease in size will lead to a larger relative surface energy that would destabilize the system [95]. The smaller the particle, the higher the surface energy, thus smaller particles aggregate more readily than larger particles because aggregation will lower the free energy of the system. Furthermore, at the nanoscale, DLVO predications seem to have

more sizable discrepancies from experimental observations in colloidal behavior [16–19]. One of the potential reasons is that the DLVO theory treats interacting surfaces as infinite smooth and flat ones, which in reality does not exist, especially when material sizes decrease [10, 30, 96, 97]. Surface heterogeneity greatly challenges DLVO theory, which must be modified to account for the size-dependent effects, including hydration force [34, 35], surface roughness [11, 25], hydrophobic [36], oscillatory [25], osmotic (depletion attraction) [37, 38], and steric, or Helfrich repulsion (affected by entropy effect) [39].

In DLVO modeling, particles are modeled as spherical. However, in reality, NPs may come in a variety of irregular shapes, such as nanoplates, nanowire, nanotube, or nanorods. Both van der Waals and EDL forces are affected by changes in shape [56]. The attraction between spheres, rods (and cylinders), and platelets varies as h^{-1}, h^{-2}, and h^{-3}, respectively, where h is the separation distance [98]. EDL forces are theoretically a function of the interacting orientation for nonsperical particles that may exhibit different crystallographic orientations and thus different atomic arrangements on the surface. Nonconventional theories, such as surface element integration (SEI) [11, 99], may account for interfacial forces in irregular shapes (e.g., ellipsoids). With SEI, the particle-plate and plate-plate interaction energies of van der Waals and EDL are expressed in Eqs. (2.25), (2.26), (2.27), and (2.28), respectively [11]:

$$U^{vdW}\left(h\right) = -\frac{A_H}{12\pi h^2} \tag{2.25}$$

$$U^{EL}\left(h\right) = \kappa\varepsilon\varepsilon_0\varphi_1\varphi_2\left[\frac{\varphi_1^2 + \varphi_2^2}{2\varphi_1\varphi_2}\left(1 - \coth\kappa h\right) + \frac{1}{\sinh\kappa h}\right] \tag{2.26}$$

$$U^{vdW}\left(h\right) = -\frac{A_H R}{6h} \tag{2.27}$$

$$U^{EL}\left(h\right) = \pi\varepsilon\varepsilon_0 R\left[2\varphi_1\varphi_2 \ln\left(\frac{1 + \exp\left(-\kappa h\right)}{1 - \exp\left(-\kappa h\right)}\right) + \left(\varphi_1^2 + \varphi_2^2\right)\ln\left(1 - \exp\left(-2\kappa h\right)\right)\right] \tag{2.28}$$

where the parameters stand for the same physical meanings as in Eqs. (2.2), (2.3), and (2.5).

2.5.2 Surface Coating

NPs are typically stabilized with surface coatings to enhance the electrostatic, steric, or electrosteric repulsive force between NPs and thus to prevent aggregation or to provide other intended surface functionality [100–105]. Three classes of typical surface coatings are surfactants, polymers, and polyelectrolytes [106–109]. For instance, Sodium dodecyl sulfate (SDS) is widely used as a surfactant dispersant in many industries. The interplay between the universal Coulombic attraction and steric repulsion originating from the surface coating layers is expected to have a profound impact on aggregation kinetics as demonstrated in Fig. 2.5. Adsorbed or covalently bound surfactants prevent aggregation and enhance dispersion stability of NPs by increasing surface charge and electrostatic repulsion or by reducing interfacial energy between particle and solvent [110]. For example, compared with uncoated silver NPs, the critical coagulation concentrations of polyvinyl-pyrrolidone-silver NPs (PVP-AgNPs) and citrate-AgNPs are more than fourfold and two-fold higher, respectively [100]. Surfactant chain length, molecular weight, types of head groups, the affinity of coating molecules to the particle surface, repulsion from neighboring molecules, loss of chain entropy upon adsorption, and also nonspecific dipole interactions between the macromolecule, the solvent, and the surface significantly affect the adsorbed surfactant mass and layer conformation and hence the ability of a surfactant to stabilize NPs against aggregation [111, 112]. For example, Dederichs et al. found that the surfactant chain length is linearly related to the logarithm of the dispersion concentration, which defines the lowest concentration of a surfactant necessary to disperse hydrophobic particles [113]. Moore et al. reported that at similar molecular weight, cationic surfactants such as dodecyl-trimethylammonium bromide (MW = 308 g/mol)
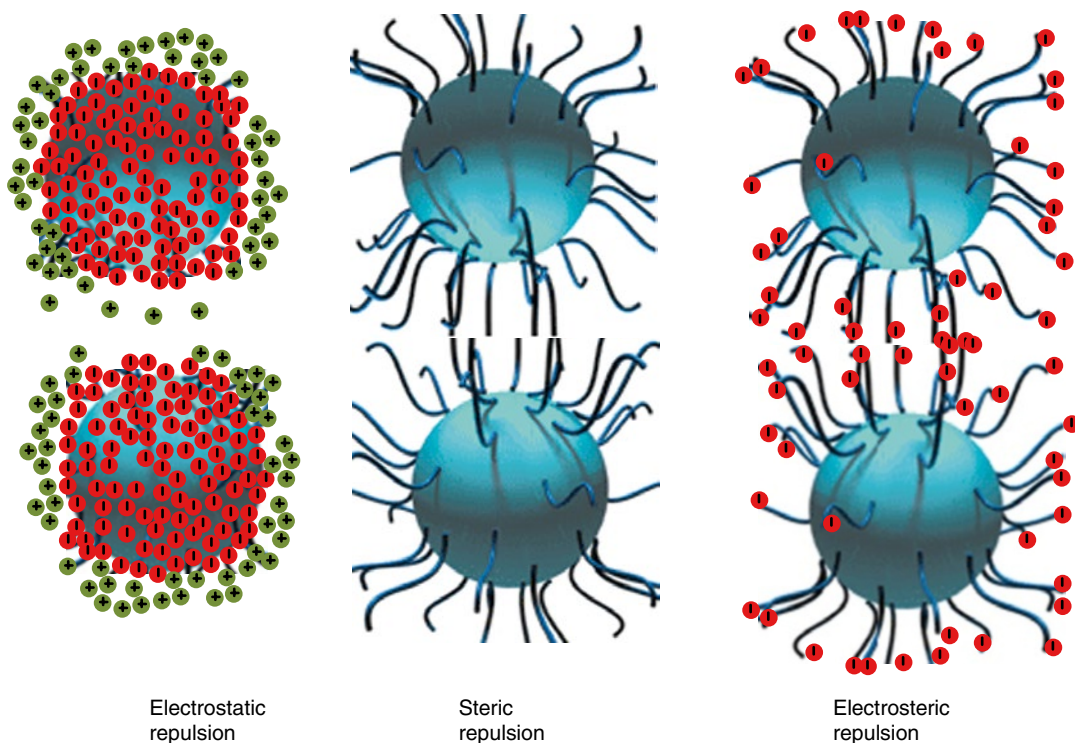

Electrostatic repulsion   **Steric repulsion**   **Electrosteric repulsion**

Fig. 2.5 Three typical interparticle repulsion mechanisms provided by the surface coating molecules

and cetyltrimethylammonium bromide (MW = 364 g/mol) were slightly more effective in stabilizing carbon nanotube than anionic sodium dodecylbenzenesulfonate (MW = 348 g/mol) [114].

Polymers are organic macromolecules consisting of repetitions of smaller monomer chemical units, which are generally of higher molecular weight than surfactants discussed previously. Synthetic (e.g., polyethylene glycol) or naturally occurring (e.g., biomacromolecules, such as proteins and polysaccharides) can be the surface active agents affecting the dispersion stability [4, 114]. Polyvinylpyrrolidone (PVP) is an environmentally friendly polymer that stabilizes NPs via steric repulsion [102, 103, 105]. Gold NPs (AuNPs) coated with bovine serum albumin (BSA) were stable as colloids at the pH of zero charge of bare AuNPs, suggesting steric stabilization due to adsorbed BSA layers [115].

Polyelectrolytes are charged polymers with ionizable groups built into the polymer structure (e.g., from $-COO^-$, $-SO_4^-$, or $-SO_3^-$ groups). These coatings can impart charge to the particles (positive or negative). poly(diallyldimethylammonium chloride) (PDDA) is a positively charged ionic polymer that acts as both a reducing and a stabilizing agent that prevents oxidation and agglomeration [116, 117]. Steric stabilization, composed of an osmotic contribution and an elastic contribution [118], is typically more robust than charge stabilization alone in preventing aggregation. The osmotic contribution is rooted in entropy reduction that occurs when hydrophilic polymer coating layers on two approaching surfaces interpenetrate. The adsorption of charged, high molecular weight species may provide electrosteric stabilization, which includes an additional repulsion due to the electrostatic interaction between the interpenetrating charged polymers.

Clearly surfactant–nanoparticle and polymer–nanoparticle interactions are extremely complex and the colloidal science describing or predicting adsorbed mass and adsorbed layer conformation is immature. Classical DLVO forces alone are not sufficient to accurately predict aggregation behavior. Understanding aggregation using a XDLVO theory presents potential promise by considering the additional forces like steric or acid-base forces [119, 120]. Natural aquatic environments contain monovalent and divalent salts as well as natural organic matter (humic and fulvic substances and polysaccharides). The aggregation state and fate and transport of nanomaterials in aquatic systems will be greatly influenced by their interaction with NOMs. NOMs have been shown to form a surface coating on colloids and NPs, enhances their stability via electrosteric stabilization mechanism [121]. For instance, humic acids prevent aggregation of NPs in solutions containing monovalent electrolytes (e.g., KCl and NaCl), whereas humic acids may prevent C_{60} NPs at low $CaCl_2$ concentrations but enhance C_{60} aggregation at high $CaCl_2$ concentrations due to the evolution of predominance of different interfacial forces from steric, bridging, van der Waals, EDL, and acid-base interactions [93].

2.5.3 Composition Effect

Chemical composition affects aggregation through changing the Hamaker constant, which governs van der Waals attraction, hydrophobicity, and surface charge. Particles with a high Hamaker constant have greater aggregation tendency compared with particles with a low Hamaker constant at the same solution and surface chemistry. The Hamaker constant for interaction between particle (*1*) and particle (*2*) in water (*w*) can be computed by the method of van Oss [27]:

$$A_{H,1w2} = \left(\sqrt{A_{11}} - \sqrt{A_{ww}} \right)\left(\sqrt{A_{22}} - \sqrt{A_{ww}} \right) \quad (2.29)$$

$$A_{ii} = 24\pi D_0^2 \cdot \gamma_i^{LW} \quad (2.30)$$

$$A_H = 24\pi D_0^2 \left(\sqrt{\gamma_1^{LW}} - \sqrt{\gamma_w^{LW}} \right)^2$$
$$\left(\textit{for the same type of } \mathrm{int}\,\textit{eracting particles}, 1 \right)$$
$$(2.31)$$

where γ_i^{LW} is the nonpolar Lifshitz-van der Waals component of the surface energy and D_0 is the

minimum equilibrium distance (0.157 nm). γ_i^{LW} for hematite (α-Fe$_2$O$_3$) NPs is 45.80 mJ/m^2 [122]; γ_i^{LW} for *E. coli* cells 27.92 mJ/m^2 [36]; γ_i^{LW} for water is 21.80 mJ/m^2 [123]. Therefore, the Hamaker constants of α-Fe$_2$O$_3$ NPs and *E. coli* cells are 8.2×10^{-18} J and 7.0×10^{-19} J, respectively. van der Waals attraction forces are approximately 12 times stronger for α-Fe$_2$O$_3$ NPs in comparison with *E. coli* bacterial cells.

Furthermore, chemical composition alters surface potential by establishing different ion adsorption with surface atoms. Particles with a high surface potential have low aggregation tendencies due to the electrostatic repulsion. Hydrophobic or hydrophilic interactions also depend significantly on surface atoms in aqueous environments. In XDLVO frameworks, hydrophobic Lewis acid–base interactions are quantified by the polar free energy $\Delta G_{HwE,D_0}^{AB}$ according to the Dupré equation [27]:

$$\Delta G_{HwE,D_0}^{AB} = 2\left[\left(\sqrt{\gamma_H^+} - \sqrt{\gamma_E^+}\right)\left(\sqrt{\gamma_H^-} - \sqrt{\gamma_E^-}\right)\right.$$
$$-\left(\sqrt{\gamma_H^+} - \sqrt{\gamma_w^+}\right)\left(\sqrt{\gamma_H^-} - \sqrt{\gamma_w^-}\right) \qquad (2.32)$$
$$\left.-\left(\sqrt{\gamma_E^+} - \sqrt{\gamma_w^+}\right)\left(\sqrt{\gamma_E^-} - \sqrt{\gamma_w^-}\right)\right]$$

where electron-acceptor (γ^+) and electron-donor (γ^-) are the polar surface tension components.

2.5.4 Crystal Structure Effect

Crystal structures like defect positions in the crystal lattice can alter surface charge. The surface charge of the same composition with different crystal structures may be different. For example, TiO$_2$, with three phases of crystallinity, has zeta potential of −35 mV for rutile and −20 mV for anatase, and brookite at pH 7.5. The origin of charge heterogeneities are commonly attributed to the existence of different crystallographic planes within each particle, which is reported to affect aggregation and deposition rates [68]. Different crystallographic planes, each with a different atomic density, will establish different extent of EDL and surface energy after interfacing with the aqueous phase and forming.

2.5.5 Effect of Solution pH and Ionic Solutes

pH and dissolved ionic species (quantified by ionic strength) affect nanoparticle stability in aqueous dispersion, primarily because these two parameters determine the surface charge (positive or negative; charge density and accumulation). Surface charge neutralization and EDL screening are the two primary modes that pH and ionic strength promote NP aggregation. Most NP surfaces have surface functional groups (e.g., hydroxide and oxide groups) that are exchangeable with aqueous H$^+$ or OH$^-$. Excess of H$^+$ (low pH) results in a positively charged particle surface, whereas excess of OH$^-$ (high pH) generally renders a negative surface charge. Thus, the solution pH shift can largely lead to the charge reversal and destabilization of NP dispersion due to the decrease of electrostatic repulsion at the pH of zero surface charge. Elevated concentrations of ionic species can compress the EDL and decrease the Debye length (κ^{-1}) as shown in Eq. (2.5). At when ionic strength reaches CCC, the repulsive energy barrier will be completely screened and rapid aggregation occurs. Electrostatic destabilization of is strongly influenced by valency (z) of ionic species and mostly independent of the individual cation (at constant z). The DVLO theory indicates that the CCC can be estimated when the potential energy of the system U=0 and dU/dh=0 [124, 125]:

$$CCC = \frac{9.85\times10^4 \varepsilon^3 k_B^5 T^5 \gamma^4}{N_A e^6 A_H^2 z^6} \qquad (2.33)$$

where γ is defined by:

$$\gamma = \frac{\exp\left[ze\psi_d / 2k_B T\right] - 1}{\exp\left[ze\psi_d / 2k_B T\right] + 1} \qquad (2.34)$$

where Ψ_d is Stern potential. The CCC is predicted to be inversely proportional to the sixth power of the valency of the metal ion [Eq. (2.33)]. This relationship, also known as the Shultz Hardy Rule, is valid for large values of the surface potential for which Eq. (2.34) approximately equals 1. At low potentials, CCC is proportional to ψ_d^4/z^2.
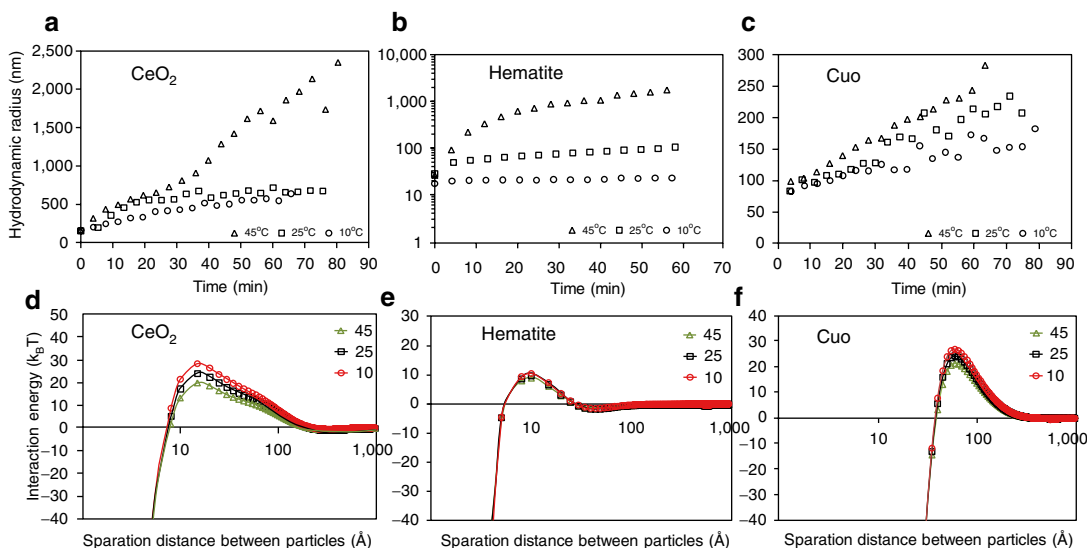
Fig. 2.6 (**a–c**) Aggregation kinetics of CeO$_2$, hematite, and CuO NPs at different temperatures. (**d–f**) The interaction energy profiles of these NPs. ζ potential (CeO$_2$)=21.5 mV, ζ potential (hematite)=10 mV, and ζ potential (CuO)=37 mV. Ionic strength is 0.002 M, pH=6, temperatures include 10, 25, and 45 °C

2.5.6 Temperature Effect

Although it is an important environmental factor, few studies have investigated the temperature dependence of NP aggregation kinetics [126, 127]. Temperatures influences aggregation kinetics through affecting the random Brownian motion of particles and the collision frequency [22, 128]. The high temperature increases the collision frequency between particles by increasing random kinetic energy of NPs [88, 89]. Thus, increasing the temperature substantially increases the aggregation rates. TR-DLS experiment results in Fig. 2.6a–c shows that the hydrodynamic diameters of CeO$_2$, hematite, and CuO NPs grew faster when the temperature increased from 15 to 45 °C. However, temperature may have complex impacts on attachment efficiency. At low ionic strength, temperature does not affect attachment efficiency. Conversely, at a higher ionic strength (25 mM), the attachment efficiency decreased significantly at 40 °C compared with 15 or 30 °C as computed by Eq. (2.22). Moreover, when the ionic strength was 50 mM, which is greater than the CCC for CeO$_2$ NPs, the experimentally derived attachment efficiencies do not vary at all with the temperatures as shown previously [77].

At elevated temperatures the interaction energy barrier (E_b) was found to decrease (Fig. 2.6d–f),

which should increase the aggregation rate exponentially [55]. Nevertheless, high temperatures also increase the potential disaggregation or the detachment, because the increased Brownian motion of water molecules could increase the hydrodynamic shear on the particle surface and possibly destabilize the aggregated clusters of NPs [129]. This may explain the decline in attachment efficiency with increasing temperature [77]. The other potential causes of temperature dependence of interaction energy is the surface charge of NPs that could vary with temperature as demonstrated elsewhere [130]. Some studies indicated that as the temperature increased, the zeta potential became less positive [131, 132]. The reason could be that increasing temperature favors proton desorption from the particle surface. The lower zeta potential of NPs implies that the electrostatic repulsion force or energy barrier between particles is lowered, and thus promotes the particle aggregation.

2.5.7 Gravity Force

It is also worth noting that despite of the broader size distribution, aggregation usually evolves to reach a quasi-steady state indicative of the deple-

tion of the primary NPs. In the quasi-steady state, aggregates continued to grow at a slower rate than the initial linear growth stage, and the aggregation progress was likely governed by aggregate–aggregate interactions, collisions, and sedimentation, which leads to a more randomly fluctuating PSD. Thus, differential sedimentation is often the result of the gravity effect, greatly accounting for the random fluctuations in PSD. One method to determine the role of sedimentation over random movement is the calculation of the Peclet number [133]:

$$Pe = \frac{2\pi\Delta\rho g r^4}{3k_B T} \qquad (2.35)$$

where $\Delta\rho$ is the density difference between dispersed NPs and dispersion medium, g is the acceleration due to gravity. When $Pe \ll 1$ Brownian motion dominates and aggregation is perikinetic, whereas when $Pe \gg 1$ aggregation is orthokinetic (differential sedimentation occurs). Equation (2.35) allows us to determine at what size of aggregated NPs could be the critical point where gravity may begin to play the dominant role compared to the Brownian motion and gravity should be taken into account.

Another alternative method is to estimate the sedimentation speed using the Stokes' equation and the average movement speed due to the thermal kinetic energy [134–136]:

$$u = \frac{\rho_g - \rho_y}{18\mu} g d^2 \qquad (2.36)$$

$$v = \sqrt{\frac{8k_B T}{\pi m \varsigma}} \qquad (2.37)$$

$$\zeta = \frac{2}{3} d^2 \rho_y \sqrt{\frac{2\pi k_B T}{m_m}} \left(1 + \frac{\pi\alpha}{8}\right) \qquad (2.38)$$

where u is the equilibrium settling velocity of particles in free sedimentation, ρ_g is the density of particles, ρ_y is the medium density (for water, 1 g/cm^3 at 25 °C), μ is the medium dynamic viscosity (Pa·s), d is the particle diameter, g is the gravity acceleration (9.8 N/kg), v is the average velocity of particles undergoing random kinetic movement according to the Maxwell velocity distribution [137, 138], ζ is friction coefficient, m_m is the molecular weight of water, and α is fraction of water molecules that are reflected diffusively and therefore leave the surface in equilibrium with surface (α is 0.1 for most cases) [139]. Figure 2.7 shows a comparative example
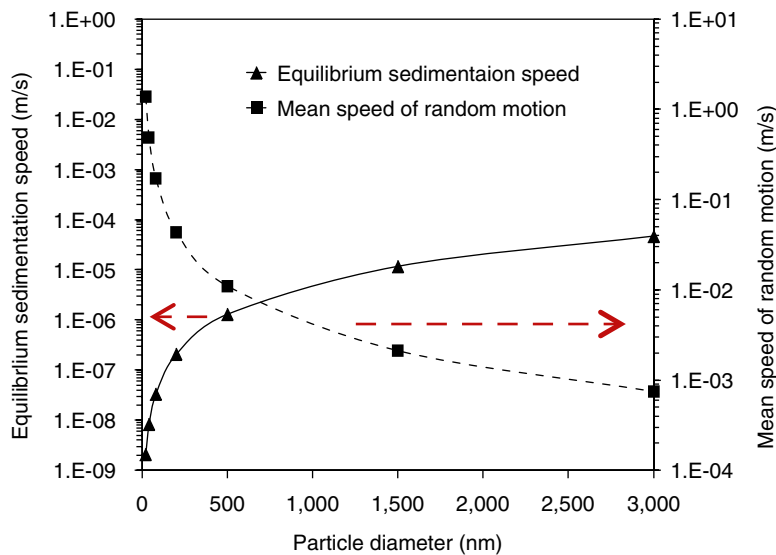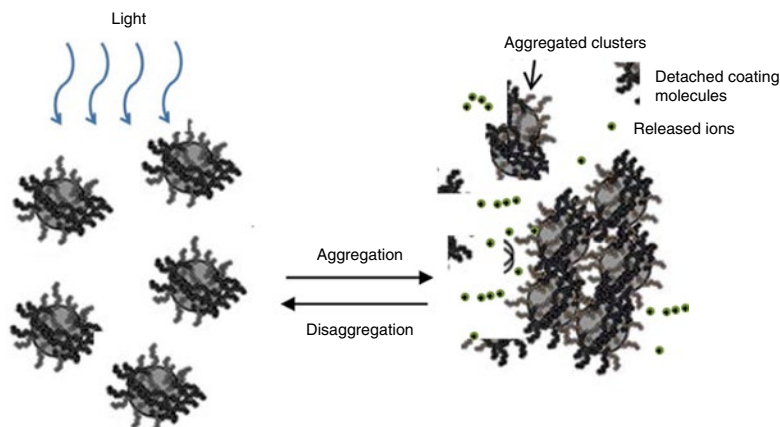

Fig. 2.7 Equilibrium speeds of sedimentation and random thermal motion for different sizes of AgNPs in water. ρ_g: 10.5 g/cm^3 (AgNPs), ρ_y: 1 g/cm^3 (water at 25 °C), μ: 1.0×10^{-3} Pa·s

Fig. 2.8 Light irradiation induced enhanced nanoparticle aggregation due to surface oxidation and detachment of surface coating [140, 144]

of NPs at different sizes. It is obvious that the sedimentation speed is far less than the random movement speed for the particle sizes up to 3,000 nm. Sedimentation is likely disturbed by the thermal motion of NPs.

2.5.8 Light Conditions

The light exposure is another important environmental factor affecting the physicochemical processes of NPs [104, 105, 140–143]. Light irradiation, such as UV, xenon lamp, solar, and even fluorescence light, has been shown to promote surface oxidation, dissolution into ionic species, and aggregation as shown in Fig. 2.8 [104, 141, 143, 145]. Metallic NPs exhibit the surface plasmon resonance (SPR) [146–148]. AgNPs and quantum dots (QDs) were both reported to have detachment of surface coatings under irradiation conditions [103, 143, 149], leading to simultaneous aggregation and dissolution. Among the three types of light irradiation conditions, the aggregation kinetics consistently followed the order UV-365 > xenon lamp > UV-254 for the same type of AgNPs, which indicated that the wavelength and photoenergy of the light irradiation influence the AgNP aggregation kinetics [144]. The aggregation of QDs is likely ascribed to oxygen radical generation and ion release, which promote homoaggregation of loosely coated QDs as demonstrated below [140].

2.5.9 Dissolved Oxygen

Dissolved oxygen (DO) in the aqueous environments tend to oxidize metallic NPs such as AgNPs and QDs [73, 140, 150, 151]. The oxidation invokes several complex physiochemical processes that may occur simultaneously (i.e., aggregation, oxidation of NPs, metallic cation release, complexation and speciation of metallic cations with aqueous components such as NOMs). The rapid surface oxidation has shown to affect aggregation processes [73, 140, 144]. The hydrodynamic sizes of AgNPs increased more drastically and randomly in the presence of DO probably due to the ion release and particle debris formation (see Fig. 2.8), whereas in the absence of DO the hydrodynamic sizes increased relatively slower and linearly. The destabilization of AgNPs and QDs was found to be related to the detachment of surface coating, compression of EDL and surface energy changes as illustrated in Fig. 2.8. In contrast, anoxic and anaerobic conditions exert low redox potentials, which inhibit oxidation and consequently lead to different aggregation kinetics.

It is presumable that the addition of strong oxidizers like H_2O_2 in the solution should
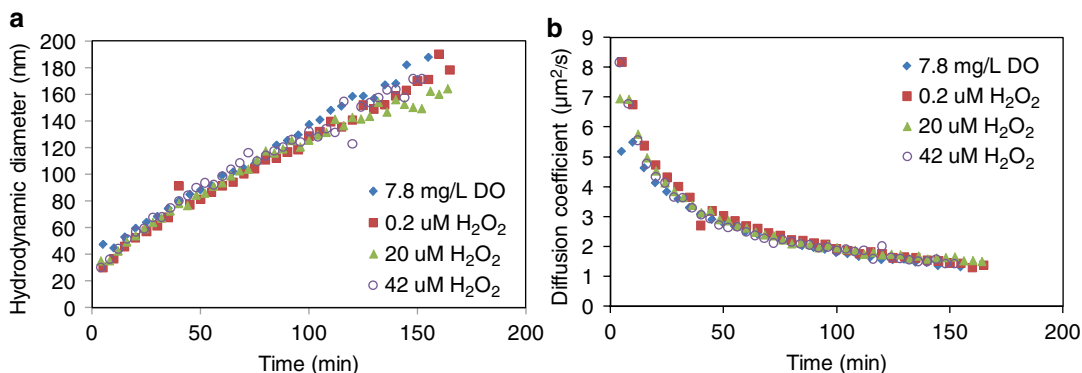
Fig. 2.9 Variations of hydrodynamic diameter and diffusion coefficient of 20-nm AgNPs in the medium with addition of different concentrations of H_2O_2 (This graph is cited from Ref. [73])

substantially increase the redox potential and increase the oxidation reaction rates as the oxidation reaction by H_2O_2 is more thermodynamically favorable than that with oxygen (see the following reaction energetics).

Net reactions	E^0 (V)
$1/4O_2 + H^+ + Ag_{(s)} = 1/2H_2O + Ag^+$	0.47
$1/2H_2O_2 + H^+ + Ag_{(s)} = Ag^+ + H_2O$	0.98

Accordingly, aggregation should proceed faster. However, Fig. 2.9a shows that aggregation kinetics of 20-nm AgNPs that apparently were unaffected by the increased concentrations of H_2O_2 compared to that in the presence of DO of 7.8 mg/L. Diffusion coefficients in Fig. 2.9b indicates that with H_2O_2 at the early stage of aggregation were lower than those with DO, suggesting that AgNPs formed larger aggregates under DO addition than they did in the presence of H_2O_2. Clearly, strong oxidizers could possibly promote oxidation reactions of metallic NPs but not definitely increase aggregation kinetics.

References

1. Chen KL, Mylon SE, Elimelech M (2006) Aggregation kinetics of alginate-coated hematite nanoparticles in monovalent and divalent electrolytes. Environ Sci Tech 40:1516–1523
2. Saleh NB, Pfefferle LD, Elimelech M (2008) Aggregation kinetics of multiwalled carbon nanotubes in aquatic systems: measurements and environmental implications. Environ Sci Technol 42:7963–7969
3. Chen KL, Elimelech M (2006) Aggregation and deposition kinetics of fullerene (C-60) nanoparticles. Langmuir 22:10994–11001
4. Saleh NB, Pfefferle LD, Elimelech M (2010) Influence of biomacromolecules and humic acid on the aggregation kinetics of single-walled carbon nanotubes. Environ Sci Tech 44:2412–2418
5. Keller AA, Wang H, Zhou D, Lenihan HS, Cherr G, Cardinale BJ et al (2010) Stability and aggregation of metal oxide nanoparticles in natural aqueous matrices. Environ Sci Technol 44:1962–1967
6. Petosa AR, Jaisi DP, Quevedo IR, Elimelech M, Tufenkji N (2010) Aggregation and deposition of engineered nanomaterials in aquatic environments: role of physicochemical interactions. Environ Sci Technol 44:6532–6549
7. Kim AY, Berg JC (1999) Fractal aggregation: scaling of fractal dimension with stability ratio. Langmuir 16:2101–2104
8. Barbot E, Dussouillez P, Bottero JY, Moulin P (2010) Coagulation of bentonite suspension by polyelectrolytes or ferric chloride: floc breakage and reformation. Chem Eng J 156:83–91
9. Runkana V, Somasundaran P, Kapur PC (2005) Reaction-limited aggregation in presence of short-range structural forces. AICHE J 51:1233–1245
10. Hermansson M (1999) The DLVO theory in microbial adhesion. Colloids Surf B Biointerfaces 14:105–119
11. Hoek EMV, Agarwal GK (2006) Extended DLVO interactions between spherical particles and rough surfaces. J Colloid Interface Sci 298:50–58
12. Gregory J (1975) Interaction of unequal double-layers at constant charge. J Colloid Interface Sci 51:44–51
13. Butt H-J, Kappl M (2010) Surface and interfacial force. Wiley-VCH Verlag GmbH & Co., Weinheim
14. Stumm W, Morgan JJ (1996) Aquatic chemistry, 3rd edn. Wiley, New York
15. Israelachvili JN (2011) Intermolecular and surface forces: revised 3rd edn. Academic Press, Elsevier Inc, Waltham, MA, USA
16. Hoek EMV, Bhattacharjee S, Elimelech M (2003) Effect of membrane surface roughness on colloid membrane DLVO interactions. Langmuir 19:4836–4847

17. Richard Bowen W, Doneva TA (2000) Atomic force microscopy studies of nanofiltration membranes: surface morphology, pore size distribution and adhesion. Desalination 129:163–172

18. Elimelech M, O'Melia CR (2002) Kinetics of deposition of colloidal particles in porous media. Environ Sci Tech 24:1528–1536

19. Elimelech M, Xiaohua Z, Childress AE, Seungkwan H (1997) Role of membrane surface morphology in colloidal fouling of cellulose acetate and composite aromatic polyamide reverse osmosis membranes. J Membr Sci 127:101–109

20. Zita A, Hermansson M (1994) Effects of ionic strength on bacterial adhesion and stability of flocs in a wastewater activated sludge system. Appl Environ Microbiol 60:3041–3048

21. Bhattacharjee S, Ko C-H, Elimelech M (1998) DLVO Interaction between rough surfaces. Langmuir 14:3365–3375

22. Grasso D, Subramaniam K, Butkus M, Strevett K, Bergendahl J (2002) A review of non-DLVO interactions in environmental colloidal systems. Rev Environ Sci Biotechnol 1:17–38

23. Butt H-J, Cappella B, Kappl M (2005) Force measurements with the atomic force microscope: technique, interpretation and applications. Surf Sci Rep 59:1–152

24. Pashley RM, McGuiggan PM, Ninham BW, Brady J, Evans DF (2002) Direct measurements of surface forces between bilayers of double-chained quaternary ammonium acetate and bromide surfactants. J Phys Chem 90:1637–1642

25. Bostrom M, Williams DRM, Ninham BW (2001) Specific ion effects: why DLVO theory fails for biology and colloid systems. Phys Rev Lett 87:168103

26. Kim HK, Tuite E, Nordén B, Ninham BW (2001) Co-ion dependence of DNA nuclease activity suggests hydrophobic cavitation as a potential source of activation energy. Eur Phys J E Soft Matter Biol Phys 4:411–417

27. von Oss CJ (2006) Interfacial forces in aqueous media, 2nd edn. Taylor & Francis Group, Boca Raton

28. Hirose M, Ito H, Kamiyama Y (1996) Effect of skin layer surface structures on the flux behaviour of RO membranes. J Membr Sci 121:209–215

29. Bhattacharjee S, Kim AS, Elimelech M (1999) Concentration polarization of interacting solute particles in cross-flow membrane filtration. J Colloid Interface Sci 212:81–99

30. Sun N, Walz JY (2001) A model for calculating electrostatic interactions between colloidal particles of arbitrary surface topology. J Colloid Interface Sci 234:90–105

31. Ninham BW (1999) On progress in forces since the DLVO theory. Adv Colloid Interface Sci 83:1–17

32. Elimelech M, O'Melia CR (1990) Effect of particle size on collision efficiency in the deposition of Brownian particles with electrostatic energy barriers. Langmuir 6:1153–1163

33. Walz JY (1998) The effect of surface heterogeneities on colloidal forces. Adv Colloid Interface Sci 74:119–168

34. Butt H-J (1991) Measuring electrostatic, van der Waals, and hydration forces in electrolyte solutions with an atomic force microscope. Biophys J 60:1438–1444

35. Chang Y-I, Chang P-K (2002) The role of hydration force on the stability of the suspension of Saccharomyces cerevisiae-application of the extended DLVO theory. Colloids Surf A Physicochem Eng Asp 211:67–77

36. Ong YL, Razatos A, Georgiou G, Sharma MM (1999) Adhesion forces between *E. coli* bacteria and biomaterial surfaces. Langmuir 15:2719–2725

37. Marenduzzo D, Finan K, Cook PR (2006) The depletion attraction: an underappreciated force driving cellular organization. J Cell Biol 175:681–686

38. Yodh AG, Lin K, Crocker JC, Dinsmore AD, Verma R, Kaplan PD (2001) Entropically driven self-assembly and interaction in suspension. Philos Trans R Soc Lond A Math Phys Eng Sci 359:921–937

39. Rijnaarts HHM, Norde W, Lyklema J, Zehnder AJB (1999) DLVO and steric contributions to bacterial deposition in media of different ionic strengths. Colloids Surf B Biointerfaces 14:179–195

40. Butt H-J, Jaschke M, Ducker W (1995) Measuring surface forces in aqueous electrolyte solution with the atomic force microscope. Bioelectrochem Bioenerg 38:191–201

41. Rijnaarts HHM, Norde W, Bouwer EJ, Lyklema J, Zehnder AJB (1995) Reversibility and mechanism of bacterial adhesion. Colloids Surf B Biointerfaces 4:5–22

42. Petsev DN, Vekilov PG (2000) Evidence for non-DLVO hydration interactions in solutions of the protein apoferritin. Phys Rev Lett 84:1339

43. Boström M, Deniz V, Franks GV, Ninham BW (2006) Extended DLVO theory: electrostatic and non-electrostatic forces in oxide suspensions. Adv Colloid Interface Sci 123–126:5–15

44. Bowen WR, Williams PM (1996) The osmotic pressure of electrostatically stabilized colloidal dispersions. J Colloid Interface Sci 184:241–250

45. Bowen WR, Williams PM (2001) Obtaining the osmotic pressure of electrostatically stabilized colloidal dispersions from frontal ultrafiltration experiments. J Colloid Interface Sci 233:159–163

46. Sposito G, Grasso D (1998) Electrical double layer structure, forces, and fields at the clay-water interface. In: Hsu JP (ed) Interfacial forces and fields: theory and applications. Marcel Dekker, New York

47. Verwey EJW (1947) Theory of the stability of lyophobic colloids. J Phys Colloid Chem 51:631–636

48. von Smoluchowski M (1916) Three lectures on diffusion, Brown's molecular movements and the coagulation of colloid parts. Physik Z 17:585–599

49. von Smoluchowski M (1916) Three presentations on diffusion, molecular movement according to Brown and coagulation of colloid particles. Physik Z 17:557–571

50. Fuchs N (1934) Theory of coagulation. Z Phys Chem Abt A Thermodynamik Kinetik Elektrochemie Eigenschaftslehre 171:199–208

51. von Smoluchowski M (1917) Versuch einer mathematischen Theorie der Koagulationskinetik kolloider Lösungen. Z Phys Chem 92:40

52. Elimelech M (1995) Particle deposition and aggregation: measurement, modelling, and simulation. Butterworth-Heinemann, Oxford/Boston

53. Holthoff H, Egelhaaf SU, Borkovec M, Schurtenberger P, Sticher H (1996) Coagulation rate measurements of colloidal particles by simultaneous static and dynamic light scattering. Langmuir 12:5541–5549

54. Honig EP, Roeberse G, Wiersema PH (1971) Effect of hydrodynamic interaction on coagulation rate of hydrophobic colloids. J Colloid Interface Sci 36:97

55. Crittenden J (2005) Water treatment: principles and design, 2nd edn. Wiley, Hoboken, NJ, USA

56. Elimelech M, Jia X, Gregory J, Williams R (1998) Particle deposition & aggregation: measurement, modelling and simulation. Butterworth-Heinemann, Woburn, MA, USA

57. Mylon SE, Chen KL, Elimelech M (2004) Influence of natural organic matter and ionic composition on the kinetics and structure of hematite colloid aggregation: implications to iron depletion in estuaries. Langmuir 20:9000–9006

58. Mcgown DNL, Parfitt GD (1967) Improved theoretical calculation of stability ratio for colloidal systems. J Phys Chem 71:449

59. Chen KL, Elimelech M (2009) Relating colloidal stability of fullerene (C-60) nanoparticles to nanoparticle charge and electrokinetic properties. Environ Sci Technol 43:7270–7276

60. French RA, Jacobson AR, Kim B, Isley SL, Penn RL, Baveye PC (2009) Influence of ionic strength, pH, and cation valence on aggregation kinetics of titanium dioxide nanoparticles. Environ Sci Technol 43:1354–1359

61. Gao J, Youn S, Hovsepyan A, Llaneza VL, Wang Y, Bitton G et al (2009) Dispersion and toxicity of selected manufactured nanomaterials in natural river water samples: effects of water chemical composition. Environ Sci Technol 43:3322–3328

62. Sharma VK (2009) Aggregation and toxicity of titanium dioxide nanoparticles in aquatic environment – a review. J Environ Sci Health A Tox Hazard Subst Environ Eng 44:1485–1495

63. El Badawy AM, Luxton TP, Silva RG, Scheckel KG, Suidan MT, Tolaymat TM (2010) Impact of environmental conditions (pH, ionic strength, and electrolyte type) on the surface charge and aggregation of silver nanoparticles suspensions. Environ Sci Technol 44:1260–1266

64. Li K, Zhang W, Huang Y, Chen Y (2011) Aggregation kinetics of CeO_2 nanoparticles in KCl and $CaCl_2$ solutions: measurements and modeling. J Nanopart Res 13:6483–6491

65. Yi P, Chen KL (2011) Influence of surface oxidation on the aggregation and deposition kinetics of multiwalled carbon nanotubes in monovalent and divalent electrolytes. Langmuir 27:3588–3599

66. Behrens SH, Christl DI, Emmerzael R, Schurtenberger P, Borkovec M (2000) Charging and aggregation properties of carboxyl latex particles: experiments versus DLVO theory. Langmuir 16:2566–2575

67. Zhang W, Rittmann B, Chen Y (2011) Size effects on adsorption of hematite nanoparticles on *E. coli* cells. Environ Sci Technol 45:2172–2178

68. Buettner KM, Rinciog CI, Mylon SE (2010) Aggregation kinetics of cerium oxide nanoparticles in monovalent and divalent electrolytes. Colloids Surf A Physicochem Eng Asp 366:74–79

69. Huynh KA, Chen KL (2011) Aggregation kinetics of citrate and polyvinylpyrrolidone coated silver nanoparticles in monovalent and divalent electrolyte solutions. Environ Sci Tech 45:5564–5571

70. Hunter RJ (2001) Foundations of colloid science, 2nd edn. Clarendon, Oxford

71. Elimelech M, Gregory J, Jia G, Williams R (1995) Surface interaction potentials. Butterworth-Heinemann, Woburn

72. Berka M, Rice JA (2005) Relation between aggregation kinetics and the structure of kaolinite aggregates. Langmuir 21:1223–1229

73. Zhang W, Yao Y, Li K, Huang Y, Chen Y (2011) Influence of dissolved oxygen on aggregation kinetics of citrate-coated silver nanoparticles. Environ Pollut 159:3757–3762

74. Kallay N, Zalac S (2002) Stability of nanodispersions: a model for kinetics of aggregation of nanoparticles. J Colloid Interface Sci 253:70–76

75. Penn RL (2004) Kinetics of oriented aggregation. J Phys Chem B 108:12707–12712

76. Ribeiro C, Lee EJH, Longo E, Leite ER (2005) A kinetic model to describe nanocrystal growth by the oriented attachment mechanism. Chemphyschem 6:690–696

77. Zhang W, Crittenden JC, Li K, Chen Y (2012) Attachment efficiency of nanoparticle aggregation in aqueous dispersions: modeling and experimental validation. Environ Sci Technol. doi:10.1021/es203623z

78. Trussell RR, Tate CH (1979) Measurement of particle size distribution in water treatment. In: Advances in laboratory techniques for water quality control. American Water Works Association, Philadelphia

79. Delhommelle J, Petravic J (2005) Shear thickening in a model colloidal suspension. J Chem Phys 123:074707

80. Charbonneau P, Reichman DR (2007) Systematic characterization of thermodynamic and dynamical phase behavior in systems with short-ranged attraction. Phys Rev E Stat Phys Plasmas Fluids 75:011507

81. Nikolakis V, Kokkoli E, Tirrell M, Tsapatsis M, Vlachos DG (2000) Zeolite growth by addition of subcolloidal particles: modeling and experimental validation. Chem Mater 12:845–853

82. He YT, Wan JM, Tokunaga T (2008) Kinetic stability of hematite nanoparticles: the effect of particle sizes. J Nanopart Res 10:321–332

83. Shen C, Li B, Huang Y, Jin Y (2007) Kinetics of coupled primary- and secondary-minimum deposition of colloids under unfavorable chemical conditions. Environ Sci Tech 41:6976–6982

84. Hahn MW, Abadzic D, O'Melia CR (2004) Aquasols: on the role of secondary minima. Environ Sci Tech 38:5915–5924

85. Tufenkji N, Elimelech M (2005) Breakdown of colloid filtration theory: role of the secondary energy minimum and surface charge heterogeneities. Langmuir 21:841–852

86. Rudyak VY, Krasnolutskii SL, Ivanov DA (2011) Molecular dynamics simulation of nanoparticle diffusion in dense fluids. Microfluid Nanofluidics 11:501–506

87. Laidler KJ (1997) Chemical kinetics. Chemical kinetics. McGraw-Hill, New Delhi

88. Houston PL (2006) Chemical kinetics and reaction dynamics, 2nd edn. Dover Publications, WCB/McGraw-Hill, New York, USA

89. Pierres A, Benoliel A-M, Zhu C, Bongrand P (2001) Diffusion of microspheres in shear flow near a wall: use to measure binding rates between attached molecules. Biophys J 81:25–42

90. Kendall K, Dhir A, Du SF (2009) A new measure of molecular attractions between nanoparticles near kT adhesion energy. Nanotechnology 20:275701–275704

91. Li K, Zhang W, Huang Y, Chen Y (2011) Aggregation kinetics of CeO_2 nanoparticles in KCl and $CaCl_2$ solutions: measurements and modeling. J Nanopart Res. doi:10.1007/s11051-011-0548-z

92. Ball RC, Weitz DA, Witten TA, Leyvraz F (1987) Universal kinetics in reaction-limited aggregation. Phys Rev Lett 58:274–277

93. Chen KL, Elimelech M (2007) Influence of humic acid on the aggregation kinetics of fullerene (C-60) nanoparticles in monovalent and divalent electrolyte solutions. J Colloid Interface Sci 309:126–134

94. Heidmann I, Christl I, Kretzschmar R (2005) Aggregation kinetics of kaolinite-fulvic acid colloids as affected by the sorption of Cu and Pb. Environ Sci Tech 39:807–813

95. Waychunas G, Kim C, Banfield J (2005) Nanoparticulate iron oxide minerals in soils and sediments: unique properties and contaminant scavenging mechanisms. J Nanopart Res 7:409–433

96. Bacchin P, Aimar P, Sanchez V (1996) Influence of surface interaction on transfer during colloid ultrafiltration. J Membr Sci 115:49–63

97. Pujar NS, Zydney AL (1998) Electrostatic effects on protein partitioning in size-exclusion chromatography and membrane ultrafiltration. J Chromatogr A 796:229–238

98. Vold MJ (1954) Van der Waals' attraction between anisometric particles. J Colloid Sci 9:451–459

99. Bhattacharjee S, Elimelech M (1997) Surface element integration: a novel technique for evaluation of DLVO interaction between a particle and a flat plate. J Colloid Interface Sci 193:273–285

100. Huynh KA, Chen KL (2011) Aggregation kinetics of citrate and polyvinylpyrrolidone coated silver nanoparticles in monovalent and divalent electrolyte solutions. Environ Sci Technol 45:5564–5571

101. Allen HJ, Impellitteri CA, Macke DA, Heckman JL, Poynton HC, Lazorchak JM et al (2010) Effects from filtration, capping agents, and presence/absence of food on the toxicity of silver nanoparticles to daphnia magna. Environ Toxicol Chem 29:2742–2750

102. Kittler S, Greulich C, Koeller M, Epple M (2009) Synthesis of PVP-coated silver nanoparticles and their biological activity towards human mesenchymal stem cells. Materialwiss Werkst 40:258–264

103. Levard C, Reinsch BC, Michel FM, Oumahi C, Lowry GV, Brown GE Jr (2011) Sulfidation processes of PVP-coated silver nanoparticles in aqueous solution: impact on dissolution rate. Environ Sci Technol 45:5260–5266

104. Li X, Lenhart JJ (2012) Aggregation and dissolution of silver nanoparticles in natural surface water. Environ Sci Technol 46:5378–5386

105. Ma R, Levard C, Marinakos SM, Cheng Y, Liu J, Michel FM et al (2012) Size-controlled dissolution of organic-coated silver nanoparticles. Environ Sci Technol 46:752–759

106. Hezinger AFE, Teßmar J, Göpferich A (2008) Polymer coating of quantum dots – a powerful tool toward diagnostics and sensorics. Eur J Pharm Biopharm 68:138–152

107. Hydutsky BW, Mack EJ, Beckerman BB, Skluzacek JM, Mallouk TE (2007) Optimization of nano- and microiron transport through sand columns using polyelectrolyte mixtures. Environ Sci Technol 41:6418–6424

108. Mayya KS, Schoeler B, Caruso F (2003) Preparation and organization of nanoscale polyelectrolyte-coated gold nanoparticles. Adv Funct Mater 13:183–188

109. Phenrat T, Saleh N, Sirk K, Kim H-J, Tilton R, Lowry G (2008) Stabilization of aqueous nanoscale zerovalent iron dispersions by anionic polyelectrolytes: adsorbed anionic polyelectrolyte layer properties and their effect on aggregation and sedimentation. J Nanopart Res 10:795–814

110. Rosen MJ, Kunjappu JT (2012) Surfactants and interfacial phenomena. Wiley, Hoboken, NJ, USA

111. Vaisman L, Wagner HD, Marom G (2006) The role of surfactants in dispersion of carbon nanotubes. Adv Colloid Interface Sci 128:37–46

112. Li X, Lenhart JJ, Walker HW (2011) Aggregation kinetics and dissolution of coated silver nanoparticles. Langmuir 28:1095–1104

113. Dederichs T, Möller M, Weichold O (2009) Colloidal stability of hydrophobic nanoparticles in ionic surfactant solutions: definition of the critical dispersion concentration. Langmuir 25:2007–2012

114. Moore VC, Strano MS, Haroz EH, Hauge RH, Smalley RE, Schmidt J et al (2003) Individually

suspended single-walled carbon nanotubes in various surfactants. Nano Lett 3:1379–1382

115. Brewer SH, Glomm WR, Johnson MC, Knag MK, Franzen S (2005) Probing BSA binding to citrate-coated gold nanoparticles and surfaces. Langmuir 21:9303–9307

116. Yang D, Rochette J, Sacher E (2005) Spectroscopic evidence for π-π interaction between poly (diallyl dimethylammonium) chloride and multiwalled carbon nanotubes. J Phys Chem B 109:4481–4484

117. Chen H, Wang Y, Dong S, Wang E (2006) One-step preparation and characterization of PDDA-protected gold nanoparticles. Polymer 47:763–766

118. Hiemenz PC, Rajagopalan R (1997) Principles of colloid and surface chemistry, revised and expanded. CRC Press, New York, USA

119. Li K, Chen Y (2012) Effect of natural organic matter on the aggregation kinetics of CeO_2 nanoparticles in KCl and $CaCl_2$ solutions: measurements and modeling. J Hazard Mater 209–210:264–270

120. Lin S, Cheng Y, Liu J, Wiesner MR (2012) Polymeric coatings on silver nanoparticles hinder autoaggregation but enhance attachment to uncoated surfaces. Langmuir 28:4178–4186

121. Hyung H, Fortner JD, Hughes JB, Kim J-H (2007) Natural organic matter stabilizes carbon nanotubes in the aqueous phase. Environ Sci Technol 41:179–184

122. Plaza RC, Zurita L, Duran JDG, Gonzalez-Caballero F, Delgado AV (1998) Surface thermodynamics of hematite yttrium oxide core-shell colloidal particles. Langmuir 14:6850–6854

123. Liu Y, Zhao Q (2005) Influence of surface energy of modified surfaces on bacterial adhesion. Biophys Chem 117:39–45

124. Shaw DJ, Costello B (1991) Introduction to colloid and surface chemistry. Butterworth-Heinemann, Oxford, 306 pp. ISBN 0 7506 1182 0, £ 14.95. Elsevier 1993

125. Lee R, Stack K, Richardson D, Lewis T, Garnier G (2012) Multi-salt coagulation of soft pitch colloids. Colloids Surf A Physicochem Eng Asp 409:74–80

126. García-García S, Wold S, Jonsson M (2009) Effects of temperature on the stability of colloidal montmorillonite particles at different pH and ionic strength. Appl Clay Sci 43:21–26

127. Garcia-Garcia S, Jonsson M, Wold S (2006) Temperature effect on the stability of bentonite colloids in water. J Colloid Interface Sci 298:694–705

128. Nel AE, Madler L, Velegol D, Xia T, Hoek EMV, Somasundaran P et al (2009) Understanding biophysicochemical interactions at the nano-bio interface. Nat Mater 8:543–557

129. Ryan JN, Elimelech M (1996) Colloid mobilization and transport in groundwater. Colloids Surf A Physicochem Eng Asp 107:1–56

130. Yongsheng C, Huang Y, Li K (2012) Temperature effect on the aggregation kinetics of CeO_2 nanopar-

ticles in monovalent and divalent electrolytes. J Environ Anal Toxicol 2:1–5

131. Datsko TY, Zelentsov VI (2009) Dependence of the surface charge and the fluorine adsorption by γ-aluminum oxide on the solution temperature. Surf Eng Appl Electrochem 45:404–410

132. Rodríguez K, Araujo M (2006) Temperature and pressure effects on zeta potential values of reservoir minerals. J Colloid Interface Sci 300:788–794

133. Kovalchuk NM, Starov VM (2011) Aggregation in colloidal suspensions: effect of colloidal forces and hydrodynamic interactions. Adv Colloid Interface Sci. doi:10.1016/j.cis.2011.05.009

134. Limbach LK, Li Y, Grass RN, Brunner TJ, Hintermann MA, Muller M et al (2005) Oxide nanoparticle uptake in human lung fibroblasts: effects of particle size, agglomeration, and diffusion at low concentrations. Environ Sci Technol 39:9370–9376

135. Prasher R, Bhattacharya P, Phelan PE (2006) Brownian-motion-based convective-conductive model for the effective thermal conductivity of nanofluids. J Heat Transfer 128:588–595

136. Ding G, Peng H, Jiang W, Gao Y (2009) The migration characteristics of nanoparticles in the pool boiling process of nanorefrigerant and nanorefrigerant-oil mixture. Int J Refrig 32:114–123

137. Rudyak VY, Kharlamov GV, Belkin AA (2000) Molecular dynamics simulation of nanoparticles diffusion in dense gases and liquids. J Aerosol Sci 31:432–433

138. Rudyak VY, Kharlamov GV, Belkin AA (2001) Diffusion of nanoparticles and macromolecules in dense gases and liquids. High Temp 39:264–271

139. Mädler L, Friedlander SK (2007) Transport of nanoparticles in gases: overview and recent advances. Aerosol Air Qual Res 7:304–342

140. Li Y, Zhang W, Li KG, Yao Y, Niu JF, Chen YS (2012) Oxidative dissolution of polymer-coated CdSe/ZnS quantum dots under UV irradiation: mechanisms and kinetics. Environ Pollut 164:259–266

141. Cheng Y, Yin L, Lin S, Wiesner M, Bernhardt E, Liu J (2011) Toxicity reduction of polymer-stabilized silver nanoparticles by sunlight. J Phys Chem C 115:4425–4432

142. Shi J-P, Ma C-Y, Xu B, Zhang H-W, Yu C-P (2012) Effect of light on toxicity of nanosilver to Tetrahymena pyriformis. Environ Toxicol Chem 31:1630–1638

143. Gorham JM, MacCuspie RI, Klein KL, Fairbrother DH, Holbrook RD (2012) UV-induced photochemical transformations of citrate-capped silver nanoparticle suspensions. J Nanopart Res 14:1–16

144. Li Y, Zhang W, Niu J, Chen Y (2013) Surface coating–dependent dissolution, aggregation, and ROS generation of silver nanoparticles under different irradiation conditions. Environ Sci Technol 47:10293–10301

145. Zarchi AAK, Mokhtari N, Arfan M, Rehman T, Ali M, Amini M et al (2011) A sunlight-induced method for rapid biosynthesis of silver nanoparticles using an Andrachnea chordifolia ethanol extract. Appl Phys A Mater Sci Process 103:349–353

146. Llansola Portoles MJ, David Gara PM, Kotler ML, Bertolotti S, San Roman E, Rodriguez HB et al (2010) Silicon nanoparticle photophysics and singlet oxygen generation. Langmuir 26:10953–10960

147. Misawa M, Takahashi J (2011) Generation of reactive oxygen species induced by gold nanoparticles under X-ray and UV irradiations. Nanomed Nanotechnol Biol Med 7:604–614

148. Ahamed M (2011) Toxic response of nickel nanoparticles in human lung epithelial A549 cells. Toxicol In Vitro 25:930–936

149. Lu W, Senapati D, Wang S, Tovmachenko O, Singh AK, Yu H et al (2010) Effect of surface coating on the toxicity of silver nanomaterials on human skin keratinocytes. Chem Phys Lett 487:92–96

150. Zhang W, Yao Y, Sullivan N, Chen Y (2011) Modeling the primary size effects of citrate-coated silver nanoparticles on their ion release kinetics. Environ Sci Technol 45:4422–4428

151. Liu JY, Hurt RH (2010) Ion release kinetics and particle persistence in aqueous nano-silver colloids. Environ Sci Technol 44:2169–2175

Influences of Nanomaterials on the Barrier Function of Epithelial Cells

3

Shariq Ali and Erik Rytting

Contents

Abstract

Recent advances in nanotechnology have led to exciting opportunities in medicine, energy, manufacturing, and other fields. Nevertheless, it is important to adequately assess the potential impacts of nanomaterial exposure. This chapter focuses on the interactions of nanomaterials with epithelial barriers in the lungs, intestine, kidneys, skin, and placenta. Methods for determining transepithelial electrical resistance and paracellular permeability are described. Effects on cell viability and barrier integrity depend on the chemical nature of the nanomaterial, nanoparticle size, surface coatings, and concentration. Disruption of tight junctions can affect permeability and interfere with normal regulatory processes of the epithelial barrier. Future research is needed to better understand the possibilities and the limits of novel approaches in nanotechnology.

Keywords

Nanomaterials • Nanoparticles • Epithelial cells • Tight junctions • Nanotoxicology

3.1   Introduction

En route to assist a man suffering from a heart attack, the driver of an ambulance failed to negotiate a curve, veered off the road, then crashed into a sign and three vehicles on display at a car

S. Ali • E. Rytting (✉)
Department of Obstetrics and Gynecology,
University of Texas Medical Branch,
301 University Boulevard, Galveston,
TX 77555-0587, USA
e-mail: sh2ali@utmb.edu; erik.rytting@utmb.edu

dealership [1]. Like this ambulance, nanoparticles may offer life-saving medical treatment, but it is important that they do not cause any structural damage along the way.

Due to their unique chemical and physical properties, nanomaterials are gaining an increasing presence and attention in the world. With applications in several areas, including aerospace, agriculture, cosmetics, energy, textiles, and medicine, engineered nanomaterials already constitute a trillion-dollar industry [2]. Concerns have been raised regarding potentially detrimental health effects upon occupational or environmental exposure to certain types of nanoparticles [3]. For particles intended for medical diagnostics or drug delivery in particular, the impact of nanomaterials on the human body needs to be studied in greater detail to assess any unintentional effects they may have on patients. This chapter will focus on the impact of nanomaterials on epithelial barrier functions in the intestines, lungs, kidneys, skin, and placenta.

Epithelia represent a diverse group of tissues that constitute a major functional structure in many organs of the human body. These tissues have a few common features, including cellular polarity (i.e. an apical and a basolateral surface), a supporting basement membrane, and specialized junctions between cells that may allow for communication between cells or transport between the lumenal and interstitial spaces. Typically only a few cells thick, these layers serve the critical purpose of separating body compartments from one another and from the outside world, as well as regulating their interaction [4].

Epithelial cells are distinct from other types of tissue (i.e., connective, muscle, nervous, and endothelial tissue) in structure and function. Connective tissue is generally considered to include cartilage, bone, and fibrous tissue, and is composed of cells and their corresponding extracellular matrix. Muscle tissue as well is distinct from epithelia in that its primary function is contraction in response to specific stimuli. In some instances, smooth muscle underlies epithelial layers and works with the epithelium to perform the function of the organ. For example, in the intestine, the epithelium selectively absorbs nutrients while smooth muscle layers help to mechanically break down food and move it along the length of the intestine [5]. Neurons are typically equipped with dendrites, from which electrical signals in the form of action potentials are received, and axons, through which the neuron can transmit its own signal based on electrical inputs [4]. Endothelial tissue refers to a layer of thin cells lining blood vessels and lymphatic vessels. These cells are responsible for regulating inflammation and inflammatory cell migration, and triggering cascades of hemostasis [6].

A number of proteins, including zonula occludens protein 1 (ZO-1), participate in the establishment of tight junctions, which are an important component of epithelial cell barrier function. The disruption of tight junctions can affect the permeability of substances across an epithelial barrier, and barrier dysfunction may contribute to disease progression [7]. Techniques to assess epithelial cell barrier function include measurements of transepithelial electrical resistance (TEER) and permeability of paracellular tracers, such as mannitol. TEER measurements quantify the transport of ions across cells, with paracellular ion transport representing the most substantial contribution to such readings [8]. An intact cellular barrier will display high TEER values and limit the permeability of paracellular markers. Loss of barrier integrity will lead to decreased TEER values and increased paracellular permeability. Just as a pocket with holes may result in lost coins, the consequences of a leaky epithelium could be costly.

## 3.2   Methodology

As TEER and paracellular transport measurements provide valuable information regarding the integrity of an epithelial cell layer, brief instructions regarding these experimental measurements are provided below:

3.2.1   TEER Measurements

1. Grow epithelial cells on permeable support inserts following the standard protocol for the cells of interest. TEER measurements are

Fig. 3.1 Illustration of transepithelial electrical resistance (TEER) measurement for a cell layer grown on a permeable support insert. This diagram depicts the placement of a chopsticks-style electrode to quantify the barrier integrity. TEER values are expressed as $\Omega \cdot cm^2$ by multiplying the resistance reading by the surface area of the cells
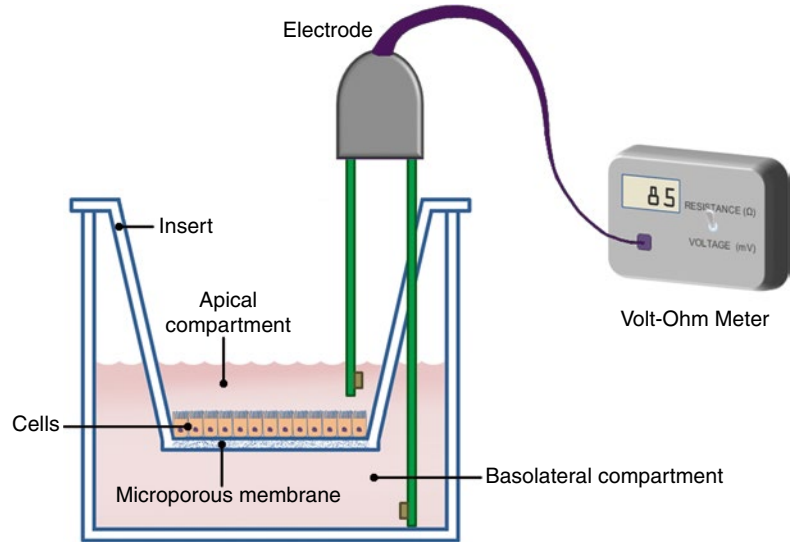
non-destructive, so multiple readings can be made on the same cell layer at various time points depending on the experimental plans.

2. The readings can be made with standard volumes of cell culture medium in the apical and basolateral compartments. Since TEER measurements are temperature-dependent, it is best to take the readings at room temperature so that there is no drift between the earliest and the latest readings. Take the inserts to be measured out of the incubator and set them in a sterile hood for about 15 min for equilibration to room temperature. If the electrodes will need to be rinsed between measurements of cells exposed to different experimental conditions, prepare a sufficient volume of cell culture medium to be equilibrated at room temperature for rinsing purposes.

3. Resistance measurements can be carried out using a chopsticks-style electrode pair or a specialized chamber. The chopsticks-style electrodes are of unequal lengths; the longer electrode should touch the bottom of the basolateral compartment while the shorter electrode is suspended in the apical fluid above the cells or the blank membrane. The specialized chambers are constructed with an electrode in the bottom of the chamber (contacting the basolateral fluid) and an electrode in the

chamber's removable lid which will contact the apical fluid (without touching the cells or membrane) when the lid is in place. An example of the placement of the chopsticks-style electrodes is shown in Fig. 3.1.

4. Set the volt-ohm meter to read resistance (ohms) and position the electrodes for the measurement.

5. Record the resistance of a blank insert (an insert without cells). This value is R_{blank}.

6. Record the resistance of an insert with cells (R_{total}). The resistance of the cells (R_{cells}) is calculated as follows: $R_{cells} = R_{total} - R_{blank}$.

7. These resistance values are in Ω. To convert to $\Omega \cdot cm^2$, multiply the R_{cell} value by the surface area (cell growth area) of the insert.

8. Return the cells to the incubator or proceed with the next steps of the experimental plan.

3.2.2 Paracellular Permeability Measurements

1. Select a paracellular marker. Radiolabeled mannitol is one of many options; this example will describe the use of Lucifer yellow CH lithium salt (a fluorescent compound).

2. The transport of Lucifer yellow will be determined across both blank inserts and inserts

with cells. Aspirate the cell culture medium from each insert (using care so as to not disturb the cell layer or damage the membrane) and wash the inserts once (both with and without cells) by adding standard volumes of warm (37 °C) transport medium (such as Hanks' balanced salt solution, HBSS) to the apical and basolateral compartments, and then aspirating. (The standard volumes depend on the type of insert used, and should be available from the commercial source of the inserts.)

3. Add the volumes of HBSS again to the inserts and allow the inserts to equilibrate in the HBSS for 30–45 min. In the meantime, prepare solutions of 60 μM Lucifer yellow in HBSS containing 1 % DMSO (dimethyl sulfoxide, which is added to help dissolve the Lucifer yellow). Prepare a sufficient volume of this solution to generate a standard curve for fluorescence detection.

4. Aspirate the HBSS from both sides of the inserts and add the standard volume of fresh, warm HBSS to the basolateral compartment. (In the case of Lucifer yellow, HBSS + 1 % DMSO should be used.)

5. At time zero, add the standard volume of the Lucifer yellow solution to the apical compartment.

6. At the desired time point (typically 15, 30, 60, or 120 min), remove a sample from the basolateral compartment and analyze it for fluorescence, together with a standard curve prepared from serial dilution of the same solution that was added to the apical compartment at time zero. (For Lucifer yellow, $\lambda_{ex} = 428$ nm, $\lambda_{em} = 540$ nm.)

7. Calculate the permeability of Lucifer yellow across the blank insert membranes (P_m) and across the cells on the inserts (P_t) using the following equation: $P = \frac{\Delta Q / \Delta t}{A \cdot C_0}$, where $\Delta Q / \Delta t$ is the mass flux, A is the surface area of the layer, and C_0 is the initial concentration on the apical side.

8. Calculate the apparent permeability across the cell layer itself (P_e) by the following equation:

$$P_e = \frac{1}{\frac{1}{P_t} - \frac{1}{P_m}}$$. P_e is usually expressed in cm/s [9].

3.3 Influences of Nanomaterials on Epithelial Barriers

3.3.1 Intestinal Epithelial Cells

The intestinal epithelium is the primary site of absorption for nutrients or medications administered orally. Nanoparticle uptake by M cells may also improve vaccine delivery, as M cells interact with lymphoid cells and are located around Peyer's patches [10]. All components of the intestinal epithelial barrier—including the mucus layer, intercellular junctions, follicle-associated epithelium, enterocytes, and efflux proteins within the epithelial cells—can be affected by nanomaterials.

Some nanoparticles cannot penetrate the intestinal mucus layer. For example, polymeric Eudragit® nanoparticles have been shown to become entrapped in a mucus plug and were unable to be taken up by the epithelium [11]. Mucus penetrating particles must have properties that prevent nonspecific adhesion to the mucus and are small enough to traverse its porous matrix. For example, Norwalk virus, a contagious diarrhea-causing agent, can cross the mucus layer because of its neutral charge and small size. Polymeric nanoparticles coated with polyethylene glycol (PEG, which is not considered to be mucoadhesive) have been shown to diffuse more readily through the mucus, and can even penetrate the more tightly adhered layer of mucus close to the epithelium [12]. Mucoadhesive polystryrene nanoparticles, on the other hand, can increase the pore size of mucus at certain concentrations, which may affect the protective properties of mucus [12, 13]. If the integrity of the mucus layer is compromised, substances such as bacteria can translocate more easily to the epithelial cells [11].

Tight junctions in the intestinal epithelial cell layer can be altered by a number of nanomaterials. For example, single-walled carbon nanotubes functionalized with carboxylic acid groups were shown to open tight junctions transiently, as confirmed by ZO-1 staining, TEER measurements, and permeability studies with Lucifer yellow, a paracellular marker [14]. Poly(amido amine)

(PAMAM) dendrimers can also open tight junctions, which can be blocked by endocytotic inhibitors, indicating an intracellular mechanism affecting the tight junctions [15]. Chitosan, a polysaccharide, chelates calcium and can interact with both F-actin and ZO-1, thus affecting tight junctions and increasing paracellular permeability [10, 16]. Although temporary disruption of tight junctions may increase the oral administration of therapeutic substances with limited bioavailability, such interference may affect the regulation of solute transport in the intestine [17, 18].

Nanomaterial effects upon efflux proteins and cell viability will also affect the barrier function of the intestinal epithelium. Carbon nanotubes functionalized with PEG and carboxylic acid groups have been shown to inhibit the activity of the efflux pump P-glycoprotein [14]. Cobalt ferrite nanoparticles reduced cell viability in Caco-2 cells, and PAMAM dendrimers may be cytotoxic, depending on the surface chemistry and concentration [15, 19]. As another example of the importance of surface modification, it has been shown that PEGylation of chitosan nanoparticles may reduce the cytotoxic effects of such particles [10]. Although silver nanoparticles did not affect membrane integrity nor cell viability in a co-culture of M cells and enterocytes, the nanoparticle exposure did result in the upregulation of a number of genes which are associated with oxidative stress [20].

3.3.2 Pulmonary Epithelial Cells

The epithelial barrier in the lungs includes cells in the upper airways which are lined with mucus all the way down to the cells in the alveolar sacs which are lined with surfactant. Type I alveolar epithelial cells make up the primary surface for gas exchange and Type II cells secrete surfactant [21]. The mucociliary escalator and clearance by macrophages represent additional components of the pulmonary barrier [22]. Nanomaterial properties determine their deposition within the lung, their interactions with mucus or surfactant, as well as their ability to induce an inflammatory response or cytotoxicity.

The deposition of nanoparticles in the lung is dictated in large part by the aerodynamic diameter, which depends on the size, shape, and density of a particle [23]. Although a large fraction of submicron particles will be exhaled, particles with aerodynamic diameters between 0.8 and 6 μm are capable of reaching the alveolar space [24]. It is important to acknowledge the difference between geometric diameter and aerodynamic diameter. For example, large porous particles having an average geometric diameter of 8 μm had a mean aerodynamic diameter of only 4 μm, and could therefore reach the central airways and the alveolar region [25, 26]. The chemical nature of particles, their size, and their surface coatings also affect interactions with mucus and the mucociliary transport rate [27, 28].

Pulmonary surfactant prevents alveolar collapse, so any effects of nanoparticles upon the surface tension of this fluid could have an impact on the alveolar barrier [24, 29]. High concentrations of polystyrene nanoparticles inhibited the surface activity of pulmonary surfactants in vitro, with negatively-charged particles having a more pronounced effect [29]. Carbon nanotubes can bind to surfactant proteins A and D, which may increase susceptibility to certain infections or disease states [30]. It has been suggested that precoating nanoparticles with surfactant components may reduce toxicity [31].

Several types of nanoparticles have been shown to cross the blood-air barrier, including metal, metal oxide, and organic nanoparticles [32]. Exposure to certain types of nanoparticles can also lead to cytotoxic effects to components of the pulmonary barrier. Cobalt ferrite nanoparticles display some cytotoxic effects on pulmonary cells, and aminated polystyrene nanoparticles caused holes in the membrane and reduced cell viability with evidence of an apoptotic pathway [19, 33]. Respiratory cytotoxic effects of carbon nanotubes include genotoxicity and oxidative stress [34].

Inflammatory effects can be measured by cytokine and chemokine release, as well as inflammatory cell migration and expression of cellular adhesion molecules. It is evident that nanomaterials may—by virtue of their size and

surface characteristics—initiate different types of inflammatory responses. For instance, aminated polystyrene nanoparticles caused interleukin-6 and interleukin-8 (IL-8) release in alveolar epithelial Type I-like cells, whereas unmodified polystyrene nanoparticles caused only IL-8 release [33]. Smaller polystyrene nanoparticles (60 nm) are more pro-inflammatory than larger (200-500 nm) particles [23]. Carbon nanotubes have been shown to cause elevations in TNF-α, various pro-inflammatory interleukins, and the chemokine CXCL-2. Carbon nanotube exposure in the lung has also been associated with granuloma formation and fibrosis [34]. In a co-culture model of the air-blood barrier employing human umbilical endothelial cells and A549 pulmonary epithelial cells, titanium dioxide nanoparticle exposure to the epithelium caused increased expression of E-selectin, intercellular adhesion molecule 1 (ICAM-1), platelet endothelial cell adhesion molecule (PECAM), vascular cell adhesion molecule (VCAM), and nitrous oxide on the endothelial side, and the increased adhesion of promonocytic cells on the endothelial side suggested inflammatory cell migration [35].

3.3.3 Renal Tubular Epithelial Cells

The kidney regulates fluid and electrolyte balance by glomerular filtration, tubular reabsorption, and tubular secretion. The renal tubules are lined with a single layer of epithelial cells which facilitate reabsorption of nutrients and ions, osmotic reabsorption of water, and active secretion of certain molecules and ions against a concentration gradient out of the blood and into the filtrate [36]. Due to effective pore size restrictions inherent in the process of glomerular filtration, proteins having hydrodynamic diameters greater than 6 nm are less likely to be filtered in the nephrons. A similar size threshold appears to exist for xenobiotic nanoparticles, as quantum dots only smaller than 5.5 nm were shown to be efficiently excreted by murine kidneys [37]. While renal tubular epithelial cells are likely to encounter only the smallest particles, it is important to note that the lack of renal excretion of

larger particles would result in longer circulation times and potential exposure times in other tissues.

Following evidence that carbon nanotubes can pass through the glomerulus and be excreted in the urine [38], the effects of carbon nanotubes and fullerene particles upon an in vitro model of distal tubule epithelial cells were investigated. Upon exposure to low concentrations of these carbon nanoparticles, reduced TEER values were observed. Such compromised barrier integrity could adversely affect normal renal function [39]. CdS nanoparticles (size range 2–12 nm) induced dose-dependent cell death in HK-2 proximal tubule epithelial cells. The exposure caused increases in reactive oxygen species and decreases in total GSH [40].

3.3.4 Skin Epithelial Cells

For a substance to be transdermally absorbed into the systemic circulation, it must first pass through the stratum corneum, with tightly packed dead cells in a lipid matrix that limits paracellular transport [36]. Beneath the stratum corneum lie the viable epidermis and the dermis, which is perfused by the skin's microvasculature. The transfollicular route is another means by which certain substances may reach the systemic circulation [41].

Many commercial sunscreen lotions contain TiO_2 nanoparticles, which led to recent concerns regarding the potential effects of systemic exposure to such particles following topical application. However, evidence suggests that TiO_2 nanoparticles do not penetrate human skin [42, 43]. In general, transdermal transport of nanoparticles greater than 10 nm in diameter is negligible unless the skin is damaged or disrupted. Nevertheless, larger nanoparticles can penetrate into hair follicles, and penetration of 40-nm nanoparticles into epidermal cells is possible if the hair sheath is removed [44]. The follicular barrier differs from the stratum corneum by the presence of intercellular tight junctions as opposed to a lipid matrix. Particles entering the follicles might remain there until they are cleared

by hair growth or sebum production [43]. It has been shown that TiO₂ nanoparticles can enter the follicles, but do not enter the dermis [45]. Other methods to disrupt the barrier to increase the dermal absorption of particles may include massage, flexed skin, dermabrasion, the use of chemical penetration enhancers, laserportation, dermatoportation, and sonophoresis [43, 45, 46].

The impact of nanoparticle exposure on cell viability in the skin epithelium depends on the nanomaterial. For instance, studies suggest no loss of cell viability following exposure to silver nanoparticles, TiO₂ nanoparticles, or ZnO nanoparticles [42, 47]. In fact, silver nanoparticles can enhance skin wound healing by accelerating re-epithelialization [47]. Carbon nanotubes, on the other hand, have been shown in HaCaT cells to reduce glutathione and vitamin E levels, which are protective against oxidative damage, and these nanotubes increase NF-κB activity and the release of IL-8 in human epidermal keratinocytes. Interestingly, multi-walled carbon nanotubes elicited an increase in IL-1β and a decrease in IL-6 levels, whereas single-walled carbon nanotubes caused an increase in IL-6 release but the release of IL-1β was not affected [48]. In separate studies, multi-walled carbon nanotubes induced cytotoxicity in human keratinocytes, but they did not affect TEER measurements across reconstructed human epidermis, thereby indicating no interference with intercellular junctions [49].

3.3.5 Placental Trophoblast Cells

The rate-limiting barrier of maternal-fetal exchange within the placenta is the trophoblast layer. On the fetal side of the placenta, fetal blood vessels branch out from the umbilical cord to form villous trees in functional units referred to as cotyledons, or placental lobes. These villous trees are bathed in maternal blood supplied from the maternal spiral arteries entering the maternal side of the placenta. The outer surface of the villi is surrounded by syncytiotrophoblast cells, which are multinucleated cells formed by the fusion of the precursor cytotrophoblast cells. Separating the maternal blood from the fetal circulation,

then, are the trophoblast layer, basal lamina, and the fetal vascular endothelium [50]. Human experimental models to predict any effects of nanomaterials upon the fetus in the womb include the ex vivo perfused human placenta, villous explants, isolated membrane vesicles, and cell culture models of trophoblast cells (e.g., BeWo cells and primary cultured cytotrophoblast cells) [9, 51].

Investigations regarding the potential transplacental transport of nanomaterials to date have included gold nanoparticles, PAMAM dendrimers, polystyrene nanoparticles, silica nanoparticles, TiO₂ nanoparticles, fullerenes, silicon nanoparticles, iron oxide nanoparticles, and poly(lactic-*co*-glycolic acid) (PLGA) nanoparticles [52–60]. The transport of these nanoparticles has been shown to depend upon size and nanomaterial. In like manner, the impacts of these particles upon trophoblast cell viability and barrier function also appear to be dependent upon the nature of the material. In placental perfusion experiments, PAMAM dendrimers did not affect placental endpoints measured throughout or after the perfusions (e.g., maternal-fetal oxygen transfer and the production of human chorionic gonadotropin) [55]. Polystyrene nanoparticles reduced BeWo b30 cell viability at high concentrations, likely due to pro-inflammatory effects [53]. BeWo cell exposure to iron oxide nanoparticles resulted in increased release of LDH, increased release of IL-6, and decreased cell viability [54]. PLGA nanoparticles, on the other hand, do not affect BeWo cell viability (unpublished results).

At high concentrations, silica nanoparticles reduced BeWo cell viability, which may be due to lipid peroxidation. However, at low concentrations, TEER values before and after a silica nanoparticle transport study did not change, suggesting that the barrier function remained intact [57]. When high concentrations of 70-nm silica nanoparticles were injected into pregnant mice, however, several effects upon the placental barrier were noted: spiral artery canal formation was altered, fetal vascular blood flow was reduced, the ratio of the spongiotrophoblast layer to the total placental area was reduced, apoptotic cell

death of spongiotrophoblasts was observed, and villous lengths in the labyrinth layer were reduced. Lower concentrations of the 70-nm silica nanoparticles did not exert these adverse responses. Larger silica nanoparticles and fullerene molecules also did not cause these same effects, but both the 70-nm silica particles and 35-nm TiO_2 particles resulted in smaller amnion sacs, smaller fetuses, and lower levels of soluble fms-like tyrosine kinase-1 (sFlt-1), which participates in the regulation of placental vasculature generation [60]. Changes to placental barrier function induced by certain types of nanomaterials could lead to serious consequences for fetal growth and development.

Conclusions

As advancements in nanotechnology continue to permeate a number of industries, it is important to recognize and plan for the potential impacts of human exposure to nanomaterials—whether that exposure is occupational, environmental, or intentional (e.g., medical diagnostics or therapy). Epithelial barriers play important roles in regulating the functions of various organs. Disruption of tight junctions and barrier integrity may lead to adverse effects, as outlined in several examples above. Although this discussion has focused on epithelial barriers in the lungs, intestines, kidneys, skin, and placenta, it is worth noting that this is not an exhaustive list of epithelial barriers within the body. Future research regarding the impacts of various nanomaterials on the barrier functions of epithelia is vital to better understand the possibilities and the limits of novel approaches in nanotechnology.

References

1. Bangor Daily News (1990) Ambulance damages 3 pickup trucks at Fort Kent on way to emergency call. Bangor Daily News, 24 January, p 6
2. Bohnsack JP, Assemi S, Miller JD et al (2012) The primacy of physicochemical characterization of nanomaterials for reliable toxicity assessment: a review of the zebrafish nanotoxicology model. Methods Mol Biol 926:261–316. doi:10.1007/978-1-62703-002-1_19.:261-316
3. Donaldson K, Stone V, Tran CL et al (2004) Nanotoxicology. Occup Environ Med 61:727–728
4. Kumar V, Robbins SL (eds) (2007) Robbins basic pathology. Saunders/Elsevier, Philadelphia
5. Yamada T (ed) (2009) Textbook of gastroenterology. Blackwell Publishing, West Sussex
6. Félétou M (2011) The endothelium: Part 1: multiple functions of the endothelial cells—focus on endothelium-derived vasoactive mediators. Morgan & Claypool Life Sciences, San Rafael
7. Marchiando AM, Graham WV, Turner JR (2010) Epithelial barriers in homeostasis and disease. Annu Rev Pathol 5:119–144
8. Blikslager AT, Moeser AJ, Gookin JL et al (2007) Restoration of barrier function in injured intestinal mucosa. Physiol Rev 87:545–564
9. Poulsen MS, Rytting E, Mose T et al (2009) Modeling placental transport: correlation of in vitro BeWo cell permeability and ex vivo human placental perfusion. Toxicol In Vitro 23:1380–1386
10. Rieux A, Fievez V, Garinot M et al (2006) Nanoparticles as potential oral delivery systems of proteins and vaccines: a mechanistic approach. J Control Release 116:1–27
11. Ensign LM, Cone R, Hanes J (2012) Oral drug delivery with polymeric nanoparticles: the gastrointestinal mucus barriers. Adv Drug Deliv Rev 64:557–570
12. Ensign LM, Schneider C, Suk JS et al (2012) Mucus penetrating nanoparticles: biophysical tool and method of drug and gene delivery. Adv Mater 24:3887–3894
13. Lai S, Wang YY, Cone R et al (2009) Altering mucus rheology to "solidify" human mucus at the nanoscale. PLoS ONE 4:e4294
14. Coyuco JC, Liu Y, Tan BJ et al (2011) Functionalized carbon nanomaterials: exploring the interactions with Caco-2 cells for potential oral drug delivery. Int J Nanomedicine 6:2253–2263
15. Sadekar S, Ghandehari H (2012) Transepithelial transport and toxicity of PAMAM dendrimers: implications for oral drug delivery. Adv Drug Deliv Rev 64:571–588
16. Yang Y, Pan D, Luo K et al (2013) Biodegradable and amphiphilic block copolymer-doxorubicin conjugate as polymeric nanoscale drug delivery vehicle for breast cancer therapy. Biomaterials 34:8430–8443
17. Bakhru SH, Furtado S, Morello AP et al (2013) Oral delivery of proteins by biodegradable nanoparticles. Adv Drug Deliv Rev 65:811–821
18. Shi L, Wang XL, Zhao F et al (2013) In vitro evaluation of 5-aminolevulinic acid (ALA) loaded PLGA nanoparticles. Int J Nanomedicine 8:2669–2676
19. Horev-Azaria L, Baldi G, Beno D et al (2013) Predictive toxicology of cobalt ferrite nanoparticles: comparative in-vitro study of different cellular models

using methods of knowledge discovery from data. Part Fibre Toxicol 10:32

20. Bouwmeester H, Poortman J, Peters R et al (2011) Characterization of translocation of silver nanoparticles and effects on whole-genome gene expression using an intestinal epithelium coculture model. ACS Nano 5:4091–4103

21. Ward HE, Nicholas TE (1984) Alveolar type I and type II cells. Aust N Z J Med 14:731–734

22. Rytting E, Nguyen J, Wang X et al (2008) Biodegradable polymeric nanocarriers for pulmonary drug delivery. Expert Opin Drug Deliv 5:629–639

23. Rabanel J, Aoun V, Elkin I et al (2012) Drug-loaded nanocarriers: passive targeting and crossing of biological barriers. Curr Med Chem 19:3070–3102

24. Kleinstreuer C, Zhang Z, Donohue JF (2008) Targeted drug-aerosol delivery in the human respiratory system. Annu Rev Biomed Eng 10:195–220

25. Tsapis N, Bennett D, Jackson B et al (2002) Trojan particles: large porous carriers of nanoparticles for drug delivery. Proc Natl Acad Sci U S A 99:12001–12005

26. Tsapis N, Bennett D, O'Driscoll K et al (2003) Direct lung delivery of para-aminosalicylic acid by aerosol particles. Tuberculosis (Edinb) 83:379–385

27. Henning A, Schneider M, Nafee N et al (2010) Influence of particle size and material properties on mucociliary clearance from the airways. J Aerosol Med Pulm Drug Deliv 23:233–241

28. Schuster BS, Suk JS, Woodworth GF et al (2013) Nanoparticle diffusion in respiratory mucus from humans without lung disease. Biomaterials 34:3439–3446

29. Beck-Broichsitter M, Ruppert C, Schmehl T et al (2014) Biophysical inhibition of synthetic vs. naturally-derived pulmonary surfactant preparations by polymeric nanoparticles. Biochim Biophys Acta 1838:474–481

30. Salvador-Morales C, Townsend P, Flahaut E et al (2007) Binding of pulmonary surfactant proteins to carbon nanotubes; potential for damage to lung immune defense mechanisms. Carbon 45:607–617

31. Schleh C, Hohlfeld J (2009) Interaction of nanoparticles with the pulmonary surfactant system. Inhal Toxicol 21(Suppl 1):97–103

32. Landsiedel R, Fabian E, Ma-Hock L et al (2012) Toxico-/biokinetics of nanomaterials. Arch Toxicol 86:1021–1060

33. Ruenraroengsak P, Novak P, Berhanu D et al (2012) Respiratory epithelial cytotoxicity and membrane damage (holes) caused by amine-modified nanoparticles. Nanotoxicology 6:94–108

34. Boczkowski J, Lanone S (2012) Respiratory toxicities of nanomaterials GÇö A focus on carbon nanotubes. Adv Drug Deliv Rev 64:1694–1699

35. Ramos-Godínez MP, González-Gómez BE, Montiel-Dávalos A et al (2013) TiO$_2$ nanoparticles induce endothelial cell activation in a pneumocyte-endothelial co-culture model. Toxicol In Vitro 27:774–781

36. Pandit NK (2007) Introduction to the pharmaceutical sciences. Lippincott Williams & Wilkins, Baltimore

37. Choi H, Liu W, Misra P et al (2007) Renal clearance of quantum dots. Nat Biotechnol 25:1165–1170

38. Lacerda L, Herrero MA, Venner K et al (2008) Carbon-nanotube shape and individualization critical for renal excretion. Small 4:1130–1132

39. Blazer-Yost BL, Banga A, Amos A et al (2011) Effect of carbon nanoparticles on renal epithelial cell structure, barrier function, and protein expression. Nanotoxicology 5:354–371

40. Pujalte I, Passagne I, Brouillaud B et al (2011) Cytotoxicity and oxidative stress induced by different metallic nanoparticles on human kidney cells. Part Fibre Toxicol 8:10. doi:10.1186/1743-8977-8-10.:10-18

41. Ramachandran C, Fleisher D (2000) Transdermal delivery of drugs for the treatment of bone diseases. Adv Drug Deliv Rev 42:197–223

42. Nohynek G, Dufour E (2012) Nano-sized cosmetic formulations or solid nanoparticles in sunscreens: a risk to human health? Arch Toxicol 86:1063–1075

43. Schneider M, Stracke F, Hansen S et al (2009) Nanoparticles and their interactions with the dermal barrier. Dermatoendocrinology 1:197–206

44. Prow TW, Grice JE, Lin LL et al (2011) Nanoparticles and microparticles for skin drug delivery. Adv Drug Deliv Rev 63:470–491

45. Labouta HI, Schneider M (2013) Interaction of inorganic nanoparticles with the skin barrier: current status and critical review. Nanomedicine 9:39–54

46. Scheiblhofer S, Thalhamer J, Weiss R (2013) Laser microporation of the skin: prospects for painless application of protective and therapeutic vaccines. Expert Opin Drug Deliv 10:761–773

47. Rigo C, Ferroni L, Tocco I et al (2013) Active silver nanoparticles for wound healing. Int J Mol Sci 14:4817–4840

48. Monteiro-Riviere N, Tran C (eds) (2007) Nanotoxicology: characterization, dosing and health effects. Informa Healthcare, New York

49. Vankoningsloo S, Piret JP, Saout C et al (2010) Cytotoxicity of multi-walled carbon nanotubes in three skin cellular models: effects of sonication, dispersive agents and corneous layer of reconstructed epidermis. Nanotoxicology 4:84–97

50. Rytting E, Ahmed MS (2013) Fetal drug therapy. In: Mattison DR (ed) Clinical pharmacology during pregnancy. Elsevier, Amsterdam

51. Saunders M (2009) Transplacental transport of nanomaterials. Wiley Interdiscip Rev Nanomed Nanobiotechnol 1:671–684

52. Ali H, Kalashnikova I, White MA et al (2013) Preparation, characterization, and transport of dexamethasone-loaded polymeric nanoparticles across a human placental in vitro model. Int J Pharm 454:149–157

53. Cartwright L, Poulsen MS, Nielsen HM et al (2012) In vitro placental model optimization for nanoparticle transport studies. Int J Nanomedicine 7:497–510

54. Correia Carreira S, Walker L, Paul K et al (2013) The toxicity, transport and uptake of nanoparticles in the in vitro BeWo b30 placental cell barrier model used within NanoTEST. Nanotoxicology. doi:10.3109/17435390.2013.833317

55. Menjoge AR, Rinderknecht AL, Navath RS et al (2011) Transfer of PAMAM dendrimers across human placenta: prospects of its use as drug carrier during pregnancy. J Control Release 150:326–338

56. Myllynen PK, Loughran MJ, Howard CV et al (2008) Kinetics of gold nanoparticles in the human placenta. Reprod Toxicol 26:130–137

57. Poulsen MS, Mose T, Maroun LL et al (2013) Kinetics of silica nanoparticles in the human placenta. Nanotoxicology. doi:10.3109/17435390.2013.812259

58. Refuerzo JS, Godin B, Bishop K et al (2011) Size of the nanovectors determines the transplacental passage in pregnancy: study in rats. Am J Obstet Gynecol 204:546–549

59. Wick P, Malek A, Manser P et al (2010) Barrier capacity of human placenta for nanosized materials. Environ Health Perspect 118:432–436

60. Yamashita K, Yoshioka Y, Higashisaka K et al (2011) Silica and titanium dioxide nanoparticles cause pregnancy complications in mice. Nat Nanotechnol 6:321–328

Engineered Nanoparticles Induced Brush Border Disruption in a Human Model of the Intestinal Epithelium

4

James J. Faust, Benjamin M. Masserano,
Adam H. Mielke, Anup Abraham,
and David G. Capco

Contents

J.J. Faust • B.M. Masserano • A.H. Mielke
A. Abraham • D.G. Capco (✉)
Molecular and Cellular Biosciences,
School of Life Sciences, Arizona State University,
Tempe, AZ 85287-4501, USA
e-mail: dcapco@asu.edu

Abstract

Nanoparticles hold great promise in cell biology and medicine due to the inherent physico-chemical properties when these materials are synthesized on the nanoscale. Moreover, their small size, and the ability to functionalize the outer nanoparticle surface makes them an ideal vector suited to traverse a number of physical barriers in the human body. While nanoparticles hold great promise for applications in cell biology and medicine, their downfall is the toxicity that accompanies exposure to biological systems. This chapter focuses on exposure via the oral route since nanomaterials are being engineered to act as carriers for drugs, contrast agents for specialized imaging techniques, as well as ingested pigments approved by regulatory agencies for human food products. After these nanomaterials are ingested they have the potential to interact with a number of biologically significant tissues, one of which is the epithelium of the small intestine. Within the small intestine exists enterocytes whose principal function is nutrient absorption. The absorptive process is

aided by microvilli that act to increase the surface area of the epithelium. Dense arrays of microvilli, referred to as the brush border, have recently been shown to undergo disruption as a consequence of exposure to nanomaterials. This chapter aims to set the stage for detailed mechanistic studies at the cell biology level concerning this newly emerging nanotoxicity research paradigm, as the underlying structural characterization responsible for the existence of microvilli have been elucidated.

Keywords

Nanoparticles • NPs • Brush border • Microvilli • Intestine • Methods • Caco-2 • Scanning electron microscopy • SEM • Transmission electron microscopy • TEM

4.1   Nanomaterials and Exposure to the Human Body

This chapter defines engineered nanomaterials as nanoparticles (NPs) deliberately constructed to exploit the unique characteristics of the material on the nanoscale (10^{-9} m in diameter), and not those NPs that exists due to natural environmental processes. Further, a nanoparticle is defined within this chapter as materials that have a diameter of 1–100 nm in any external dimension [1, 2]. In this chapter this definition includes NP agglomerates as the state of agglomeration can change depending on the location in the human body, and since the surface free-energy of individual NPs may still exist. Engineered NPs can take on a variety of geometries, crystal structures, or elemental composition(s) depending on their intended use. The excitement these NPs encourage is highlighted by the fact that the physicochemical parameters can be tailored if the surface of the nanomaterials is chemically functionalized through conjugation chemistry. That is, a number of physical interactions (e.g. covalent or noncovalent bonding) can be exploited at the NP surface to chemically "tailor" NPs. Examples for the use of engineered NPs include drug delivery [3], tissue contrast enhancement for MRI [4, 5], wavelength specific probes for fluorescence imaging [6, 7], cancer targeting [8] and ablation [9], environmental remediation of toxic compounds [10], and this list is by no means comprehensive. It is thus increasingly acknowledged that engineered NPs are an integral part of medical diagnostics, treatments, and consumer goods now and in the future.

While NPs have summoned considerable excitement within the scientific community because of the aforementioned characteristics, concern has been raised since some NPs act as a double-edged sword. Arguably the most widely known example of such a double-edged sword effect was exacted by the nanofiber, asbestos. Because of the material properties inherent to this nanofiber included tensile strength, and resistance to damage, it was ubiquitously used as components of construction materials. However, those human subjects chronically exposed to the nanofiber asbestos acquired respiratory pathologies such as mesothelioma. As a consequence of the aforementioned aftermath of human exposure to NPs, investigators have begun to characterize potential health-related effects of engineered NPs in a variety of in vitro cell culture models [11]. In such models, investigators employ cell systems that mimic the major site of tissue exposure for a given potential route of exposure, and this has lead to a number of insights concerning NPs in cell biology and medicine.

Due to the small size, three predominant routes by which NPs can intentionally or unintentionally enter the human body exist: These include inhalation, dermal, and exposure via the oral route. Concerning the latter, a great number of investigations have focused on understanding the uptake and subsequent transport of NPs through the gastrointestinal tract to improve bioavailability of pharmacological drugs, whereas few have investigated exposure in an effort to understand the response of individual cells in their social context. The remainder of this work will not address systemic transport of NPs from the gastrointestinal tract as systemic transport is beyond the scope of this chapter. Rather this work will flush out some of the unintended health effects NPs provoke as ingested components of consumer goods or as part of a medical application

with a focus on TiO$_2$ NPs. First, there is an extensive body of work, at the ultrastructural, biochemical, and molecular levels that set the foundation for understanding of effects of NPs on the cells of the gastrointestinal tract, and specifically, on the absorptive enterocytes that pass nutrients into the body. These components will be briefly reviewed as they provide key markers of assessing both gross and subtle effects of nanomaterials taken in by the oral route. Second, this chapter will describe an emerging nanotoxicity research paradigm; NP-induced brush border disruption. Finally, this chapter provides a detailed methods section which lays the basic framework for handling the principle model cell culture system for the absorptive cells of the gut including; (a) proper cell culture and technique, and; (b) scanning electron microscopy for the human brush border expressing cell line, Caco-2 BBe1. Inappropriate application of these techniques have resulted in several inconsistencies in results reported in the literature and have begun to confound the understanding of the system.

4.2 The Molecular Components of the Cytoskeletal Apparatus of the Intestinal Brush Border

4.2.1 Intestinal Microvilli and the Brush Border

When specimens are transversely sectioned through the long axis of the polarized enterocyte as part of the gut epithelium, the so-called microvilli appears as thin, "finger-like" projections emanating from the apical cell surface. While several different eukaryotic cells types assemble microvilli on their apical surface only those cells of the digestive tract and the kidney proximal tubule contain such an abundance of microvilli that early morphologists referred to these regions as brush borders (or striated borders). This cell specialization has captured the attention of investigators for decades, and its importance is underscored by the morphological and function redundancy found in mammals including

humans, to simple invertebrates such as the fruit fly, Drosophila (Fig. 4.1).

Depending on the location within the gut, the dimensions of microvilli can vary since an increase in the length and number of microvilli results in increased cell surface area. For example, absorptive cells of the small intestine have microvilli with a length of approximately 1–2 μm and a diameter of 100 nm. In contrast, those cells of the colon have fewer microvilli per cell, and the length of each microvillus is around 500–1,000 nm. Further, within the Crypts of the small intestine exist undifferentiated cells that contain a sparse number of microvilli at the cellular apex [12]. In light of the fact that microvilli on their luminal/apical surface contain integral membrane proteins responsible for absorption of complex macromolecules (e.g., carbohydrates, peptides, etc.) it is not surprising that the small intestine, acting as the principal site of nutrient absorption contains cells with a robust number of microvilli, while the colon functioning to reabsorb water contains relatively fewer. The story related to the morphometry of microvilli is complicated by the fact that dietary changes can result in a decreased length of the microvilli [13], and that some molecular components of the microvilli continuously undergo states of assembly and disassembly [14]. Since microvilli increase the cell surface area, it can be deduced that the cells of the small intestine have a greater surface area than cells of the large intestine. These facts indicate that studies related to NP-induced brush border disruption are complicated by both the anatomical location within the gastrointestinal tract, and the cell type employed, since these regions are variable.

Around the time the transmission electron microscope (TEM) became commercially available for biological samples, investigators captured the first detailed glances of the brush border with high spatial resolution [12, 15–18]. Later with improved technique in chemical fixation of biological samples McNabb and Sandborn [19] described filamentous structures at the core of the microvilli. In the early 1970 through the use of model organisms such as *Xenopus*, salamander, and chicken the formation and elongation of microvilli of the brush border was examined in
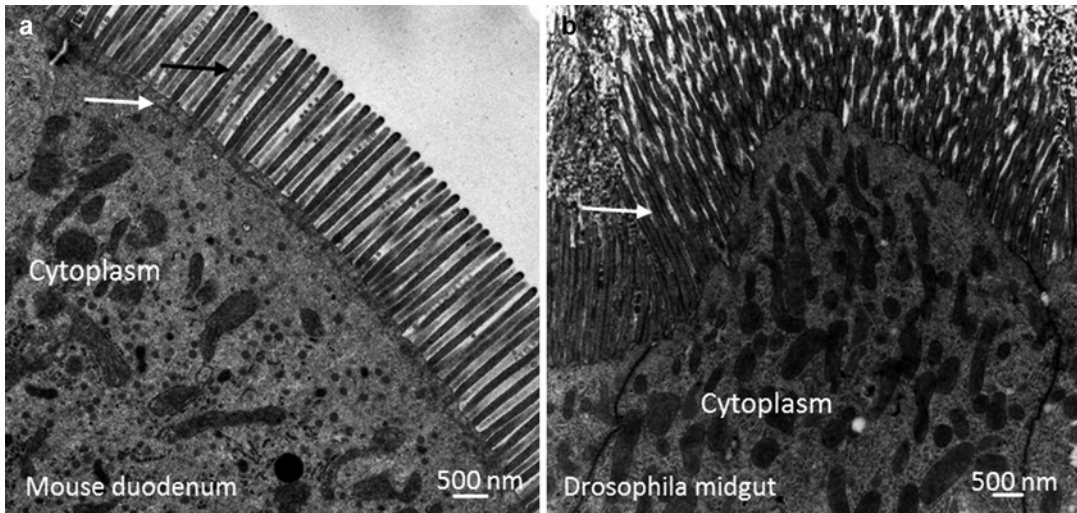
Fig. 4.1 Transmission electron micrographs comparing the morphology of the brush border from intestinal cells of mouse and cells of the midgut from Drosophila. (**a**) The micrographs were transversely sectioned through the long axis of the polarized enterocyte. Note the robust number of microvilli, each containing an electron-dense region at the apical tip of the microvillus. Furthermore, the individual microvilli are of uniform length and diameter despite constant turnover of the proteins within each microvillus. This indicates a high degree of organization and control of this cell specialization. The *black arrow* points to the center of a single microvillus, while the *white arrow* points to the electron-dense terminal web region that supports the microvilli. The scale bar is 500 nm. (**b**) In comparison to the mouse model, Drosophila cells of the midgut have a rounded curvature since undulating folds (i.e. plicae) do not exists in this model. However, microvilli contain similar structural proteins within the microvillus indicating a somewhat universal blueprint across species. The *arrow* (*white*) points to a single microvillus. The scale bar is 500 nm

detail, a process referred to as brush border morphogenesis. These model organisms were employed in part due to their ability to experimentally manipulate brush borders in vitro, and the gradual morphogenesis process unique to these models. Further, the ability to decorate actin filaments with heavy meromyosin (or the S-1 subfragment) enabled investigators to begin to identify the polarity of actin filaments in a variety of cell types [20]. In a hallmark study, Tilney and Mooseker isolated brush borders and imaged decorated filamentous components of the microvilli with heavy meromyosin. Biochemical analysis through the use of SDS-PAGE indicated that the most abundant protein of isolated brush borders migrated in a manner identical to purified chicken actin. Together these data were the first to indicate unambiguously that actin is the major (i.e. the most abundant) cytoskeletal protein component of microvilli [21]. These early studies spurred a flurry of subsequent investigations focused on identifying the molecular components underlying the process of brush border morphogenesis [22–27], which has been the focus of exhaustive reviews [28, 29].

4.2.2 The Microvillar Region

Anatomically the brush border is separated and historically defined as the microvilli and terminal web regions [29], see Fig. 4.2. Within the microvillus core exists ~20 actin filaments organized as parallel bundles in a hexagonal array that extend into, and are supported by, the terminal web region. The electron-dense tip is the site where the addition of actin monomers to F-actin occurs, and these filaments were found to have uniform polarity with minus ends enmeshed within the terminal web [25, 30, 31]. There are a number of proteins that secure F-actin bundles to one another. The first and most abundant is a 68-kDa protein known as fimbrin [32], which is also referred to in the literature as plastin 1, I-plastin,

or I-fimbrin. The second most abundant protein that bundles F-actin is the 95-kDa protein, villin which is stoichiometrically the minor to fimbrin [29, 33]. Finally the 30-kDa splice variant of espin acts to further crosslink axial bundles [34]. Each core bundle of actin filaments is laterally tethered in a helical arrangement to the plasma membrane by brush border myosin 1 (Myo1A), composed of a 110-kDa heavy chain and 4–5 calmodulin light chains [35–37]. Another protein that potentially fastens the core bundle to the plasma membrane is the 80-kDa protein ezrin, although this result has been questioned recently through the use of molecular modeling techniques [38–41]. In cultured LLC-PK1 cells ezrin was found to interact with the Rho-GEF, PLEKHG6, to promote apical rearrangement of the actin cytoskeleton via Rho-G [42]. Furthermore, in an impressive display of microscopy, Zwaenepoel and coworkers elucidated the role of novel ezrin-interacting partners of the Eps8 family responsible for proper brush border morphogenesis [43]. Through the

use of a yeast two-hybrid screen the authors found the novel protein Esp8L1a that interacts with phosphorylated ezrin and is a component of the brush border in LLC-PK1 cells. This novel component (Esp8L1a) of the porcine absorptive brush border was found to regulate microvilli length by capping F-actin at the plus tips [43].

4.2.3 The Terminal Web Region

The terminal web is a support structure within which the F-actin core rootlets terminate (Fig. 4.2). Structurally it is composed of the non-erythroid spectrins, fodrin and TW260/240 [44], and myosin II that link adjacent core bundles [25, 45]. The actin bundles are further stabilized along the length of core bundles by tropomyosin [46]. Within this meshwork α-actinin, a 95-kDa structural protein, associates with the microvillar rootlets and circumferential actin band [47]. Beneath the interconnecting fine fibrils within the terminal
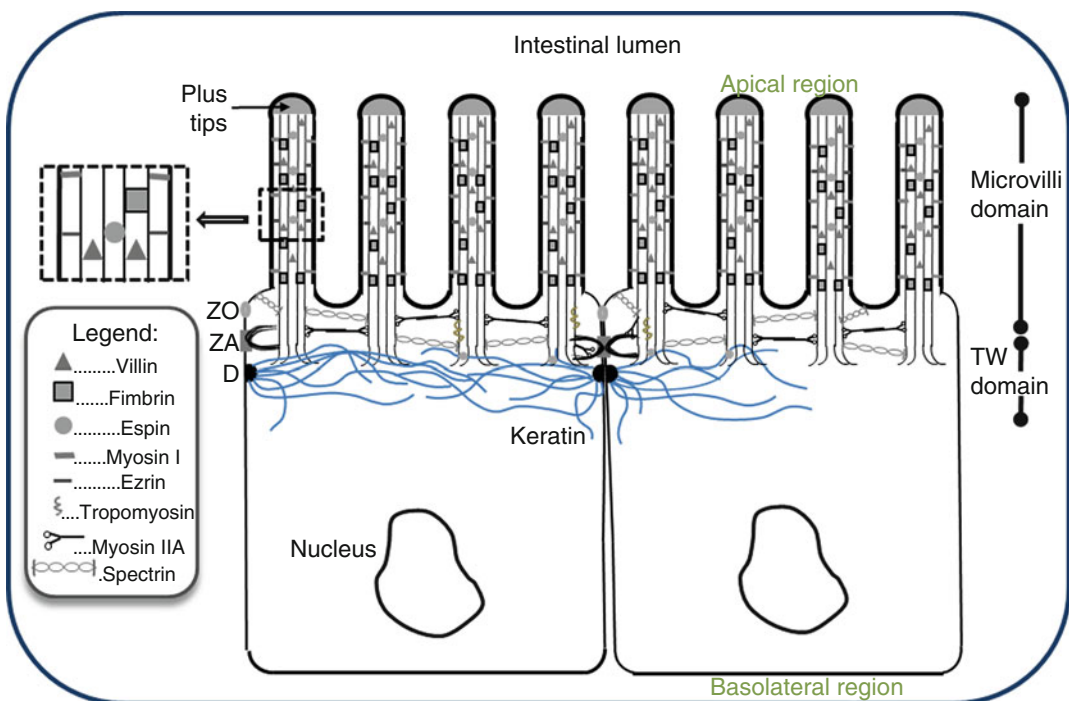

Fig. 4.2 Graphical representation of the molecular components of the brush border (The diagram was adapted from many of the sources cited in the text, and does not account for scale/molar ratios of individual proteins)

web region is the intermediate filament network, which extends from intercellular junctions [25, 31, 45]. Through immunohistochemical analysis fimbrin has also been shown to interact with cytokeratin 19, but not cytokeratin 8, in the terminal web. Further, in fimbrin knockout mouse model Grimm-Gunter et al. demonstrated a role for fimbrin in the terminal web [48]. Through the use of TEM the authors (Grimm-Gunter et al.) showed that these knockout mice have shorter microvilli with a disorganized and less densely packed terminal web region. The organelle-free zone, a region occupied, and extended by the terminal web, was significantly shorter in fimbrin deficient mice. For these reasons the authors suggest that fimbrin, aside from its classical role as a F-actin bundling protein in the microvillus core, is an essential component of the terminal web that may act to stabilize the core actin rootlets to the intermediate filament network [48]. In the differentiated enterocyte just beneath the intermediate filament network exists the microtubule network organized as parallel columns from the apical to the basolateral domain of the cell [49–51].

4.3　NP-Induced Brush Border Disruption

4.3.1　Molecular Targets Putatively Responsible for Brush Border Disruption

Several, as of yet, putative targets for the NP-induced disruption of the brush border exist. One mechanism is dependent on the inherent charge of the nanomaterial. The surface of any given nonfunctionalized (i.e. naked) NP contains large amounts of free energy due to the small size of the material. This free energy at the NP interface attracts oppositely charged components within its immediate environment. When naked (i.e. nonfunctionalized) NPs are in solution, this region is referred to as the electric double layer, and when the solution contains an abundance of proteins these layers are referred to as the hard and soft coronas (see Chap. 8). These corona proteins

bound to the NPs can elicit a number of biological responses [52] one of which is the ability of NPs to reorganize the lipid bilayer [53]. It is well known that under normal physiological conditions the concentration of intracellular-free calcium ($[Ca^{2+}]i$) in intestinal cells is at least five orders of magnitude lower than that of the extracellular environment. As a downstream consequence of a "leaky" plasma membrane a rapid increase in $[Ca^{2+}]i$ from the extracellular milieu could occur and activate the calcium-dependent enzyme, villin. Villin is a versatile protein that exists exclusively in cells that maintain a well-defined brush border. When $[Ca^{2+}]i$ levels are in the nanomolar concentrations, villin acts as a F-actin bundling protein. However, should the $[Ca^{2+}]i$ concentrations reach the micro-to millimolar range villin converts to an F-actin severing protein. Further, under certain circumstances villin assumes the role of capping F-actin. It was thus predicted by Koeneman and coworkers to be the causal agent responsible for the NP-induced brush border disruption accompanying exposure to a 70/30 % (anatase/rutile) mixture of TiO_2 NPs. This prediction was based on the fact that a dose-dependent disruption of the microvilli was observed as well as a dose-dependent increase in $[Ca^{2+}]i$. This prediction may be corroborated in part by siRNA disruption of villin; employing an antisense approach the authors (Beaulieu et al.) permanently down-regulated villin and observed what was referred to as "limp" microvilli. That is, the microvilli appeared to fall over and become parallel, and not perpendicular to the horizontal axis of the plasma membrane. This limp morphology was rescued by cDNA encoding a partial sense villin RNA [54] indicating that villin could play a role in the disruption observed by Koeneman and coworkers. The report [55] was notable in that it was the first to indicate that TiO_2 NPs, although classically considered to be relatively inert, have the ability to disrupt microvilli of the brush border after exposure to an in vitro model of the human intestine (the Caco-2 BBe1 cell model). This work has since prompted subsequent investigations into the potential effects TiO_2 NPs instigate after exposure in the Caco-2 cell model.

4.3.2 Brush Border Disruption as a Result of Exposure to NPs in Consumer Goods

There are number of benefits for the use of TiO₂ NPs in medicine and consumer goods. One example is the addition of TiO_2 NPs in sun screens, in part due to the fact that TiO_2 is highly reflective and acts as a protective physical barrier between human skin and the sun. However, under certain conditions ultraviolet light can interact with the TiO_2 NP surface and results in photocatalytic production of oxygen radicals. In an effort to reduce the photocatalytic effects, TiO_2 NPs that are components of sun screens can be encapsulated with aluminum oxide. After the aluminum oxide encasing, the NPs can be further functionalized to improve hydrophobicity. However, it has also become clear that NPs undergo changes thoughout, what is referred to as a "life cycle." The life cycle of NPs is defined as changes that can occur as the NP is modified by different conditions in the environment which can include different parts of the human body. The life cycle begins at the time NPs are manufactured and can be altered by temperature, pH, and light among other things, as their local physical environment is altered—for example, NPs in pure neutral water (pH 7.2) do not behave the same as they would in the acid conditions in the stomach (pH ~1–4). One study (Fisichella et al.) set out to investigate the life cycle of functionalized TiO_2 NPs that are components of these sun screens and subsequently the downstream effects in the Caco-2 cell model [56]. The authors treated the NPs with acid in an effort to mimic the effects of passage through the stomach as well as incubating replicate NPs in water while applying ultraviolet light, and assessed the physico-chemical changes accompanying these treatments. The study found that gastric or environmental conditions degraded the hydrophobic polydimethylsiloxane (PDMS) surface modification such that these NPs became hydrophilic and agglomerated over time. After degradation of the PMDS organic layer, the authors claimed that these TiO_2 NPs are not taken up by Caco-2 cells, and further, that they do not disrupt the brush border of Caco-2 cells at a concentration of 100 μg/mL after a 72 h exposure. However, other studies have clearly shown that nonfunctionalized TiO_2 NPs are internalized in the Caco-2 cell model, and this internalization was confirmed through the use of mass balance analysis [55]. Furthermore, recent studies suggest that a change in the NP life cycle from human skin to chlorine containing water sources such as swimming pools results in a rapid degradation of the protective aluminum shell [57].

While the study by Koeneman and colleagues was the first, it is not the only study to indicate a disruption of the brush border as a result of NP exposure. Employing a model iron oxide NP (hematite; α-Fe₂O₃) first Zhang et al., and later Kalive et al. demonstrated a NP-induced disruption of the brush border in Caco-2 cells [58, 59]. The study by Zhang and coworkers suggested that the interaction between the NP surface and plasma membrane resulted in adsorption of hematite to the cell surface. The authors hypothesized that movement of the brush border microvilli permitted access for the NPs to "wedge" between individual microvilli. The authors proposed that this wedging caused the arrays of microvilli to whorl around a central point at their microvillar tips when viewed by scanning electron microscopy (SEM) after NP exposure [59]. While individual microvilli do not oscillate to move materials in the gut under normal conditions, they do contain a number of molecular motors that act to stabilize both the microvillar and terminal web regions. Studies have shown that injection of antibodies directed against myosin II in a brush border expressing porcine cell line (LLC-PK1) result in microvilli that apparently became limp [60]. Through DNA microarray analysis it was found by Kalive et al. that a number of genes responsible for the production of intermediate filament proteins, some of which are components of the terminal web, are upregulated. Further regarding the microvillar region it was found that the gene responsible for the production of the actin capping protein CapZ (typed

in their publication as CAPZA) which is a known component of the plus tips of the microvilli was upregulated [58]. Unpublished data by Faust et al. corroborate upregulation of *CapZ* as a result of NP exposure, albeit in an established, brush border expressing model of the human placenta. Taken together these results suggest at least two independent mechanisms by which the NPs disrupt the archetypical organization of the brush border. First, structural components integral to terminal web continuity are altered at the gene level as a result of NP exposure. Since microvilli cannot exist without a supporting structure from which F-actin bundles exert force to deform the apical plasma membrane, it can be predicted that gross changes in the organization and composition of the terminal web at the protein level result in brush border disruption. Second, actin capping at the plus tips of the microvilli could induce a retraction of the brush border since the individual actin filaments continuously undergo a state of flux with addition of monomers at their plus tips.

More recently it has come to the attention of investigators that NPs are common additives to a number of ingested consumer goods [61]. The study by Weir et al. surveyed a number of food products and found P25 and E171 TiO_2 NPs in food. The latter is a pigment approved by the United State Food and Drug Administration in 1966 as a color additive for use in human food [62]. The authors (Weir et al.) found that 36 % of this pigment contained particles with one external dimension <100 nm in diameter. The study subsequently calculated dietary exposure and found that children under the age of 10 years in the United States and the United Kingdom are the greatest consumers of ingested TiO_2 NPs at concentrations of 1–2 mg TiO_2 per kilogram of body weight per day and 2–3 mg TiO_2 per kilogram of body weight per day, respectively [61]. These data highlight the need to assess the effects of food-grade NPs after exposure to models of the human gut, since studies indicate that TiO_2 NPs disrupt the human enterocyte brush border, and that food-grade pigments are being consumed as NPs.

4.4 Procedures to Procure Differentiated Brush Borders Using the Caco-2 BBe1 Cell Model

4.4.1 Introduction to Cell Culture and the Caco-2 BBe1 Cell Line

The procedures in the proceeding text describe routine maintenance of Caco-2 BBe1 cells from the date they are purchased, through cell culture, and conclude with a protocol to procure publication quality scanning electron micrographs of brush borders. While these methods seem straightforward, it is advised that only those investigators that have experience with cell culture and cell biology attempt to employ this model for studies related to materials science and engineering of nanomaterials as slight deviations from routine electron microscopy protocols or careless culture technique result in brush borders that appear in poor health. If untreated brush borders are in poor health then it becomes impossible to determine if NPs have an effect on the brush border. As a consequence, investigators have questioned whether or not these control brush borders are representative, and some have begun to show unhealthy epithelia as control specimens, albeit employing unorthodox cell culture or electron microscopy techniques. These differences highlight the need to standardize protocols to obtain accurate and comparable results between investigators.

In order to permit adequate resolution of brush borders and the subtle changes that may accompany brush border disruption, investigators commonly employ SEM and image at high magnification. The field of view in a scanning electron micrograph at high magnification can be the diameter of the average Caco-2 BBe1 cell after the 17–21 days of differentiation. The Fig. 4.3 is a representative scanning electron micrograph after the 17–21 days of proper aseptic technique and culture conditions required to permit brush border morphogenesis. When viewed as a
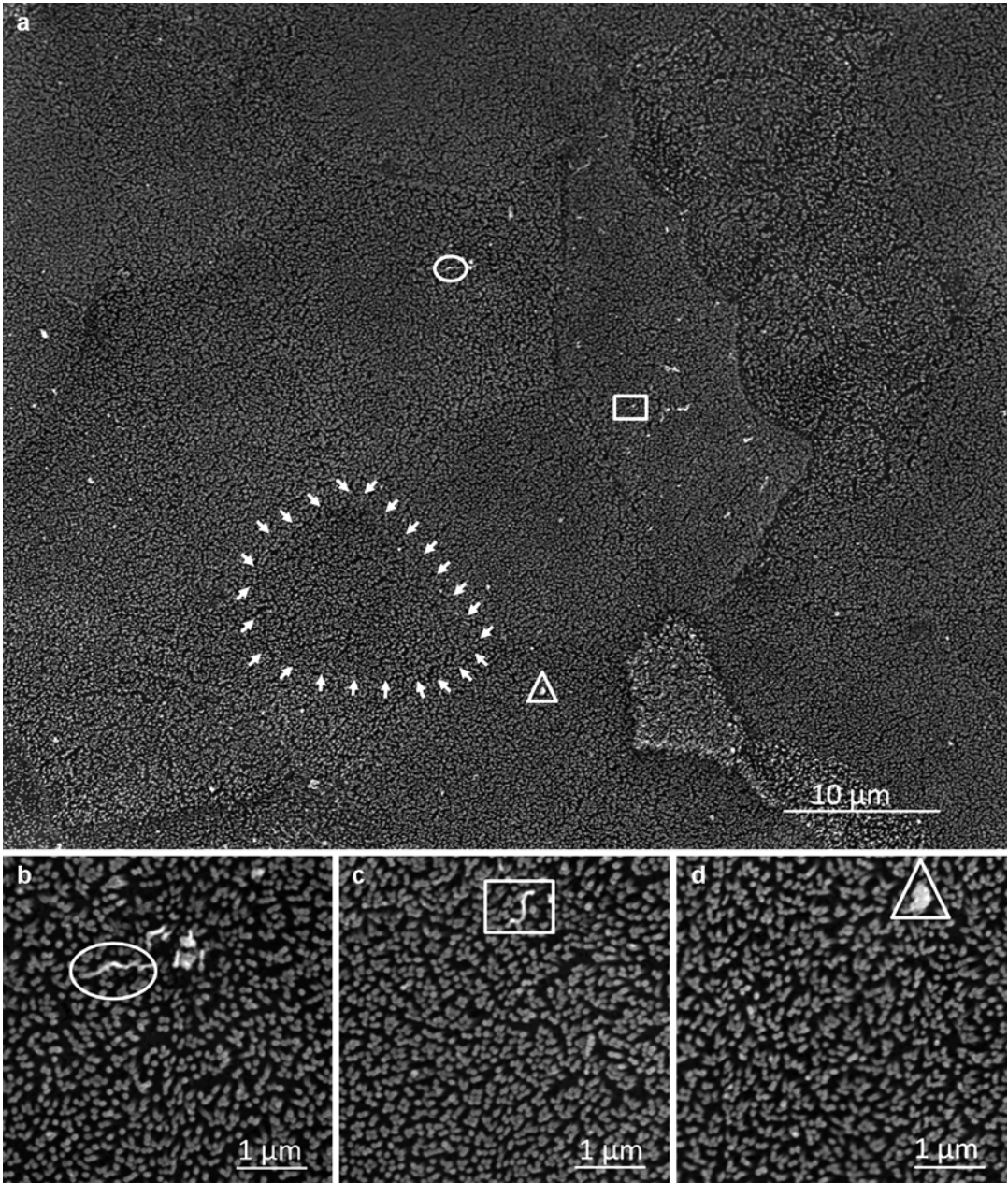
Fig. 4.3 The differentiated Caco-2 BBe1 epithelium, shown as a scanning electron micrograph demonstrates the classic archetypical organization of brush borders. (**a**) The low magnification view (originally captured at 1,500×) demonstrates a great number of cells with well defined brush borders. In this representative micrograph there are apparently 20+ cells within the field of view. The *white arrows* outline a single cell which was identified by the interdigitation of microvilli near the region of the intercellular junctions. The *oval*, *rectangle* and *triangle* serve as fiduciary markers for the high magnification views in (b–d). The scale bar is 10 μm. (**b–d**) Higher magnification views of three randomly chosen regions within the epithelium. Note the consistency in number and structure of the brush borders from these regions. The scale bar is 1 μm

scanning electron micrograph the apical surface of the Caco-2 BBe1 epithelium decorated with a well-ordered array of the finger-like projections known as microvilli (Fig. 4.3). The micrograph (Fig. 4.3a) was captured at a magnification of 1,500× in an attempt to balance resolution of individual microvilli with the number of cells in the field of view. At this magnification of 1,500× the intercellular borders become difficult to see. However, the telltale sign of the cell to cell interface is the slight interdigitation of microvilli outlined by white arrows (Fig. 4.3a). The micrographs shows three different regions directly surrounded by the oval, square, and triangle in Fig. 4.3a corresponding to three different cells imaged as higher (5,000×) magnification views (Fig. 4.3b–d) to illustrate in detail the archetypical organization of the human enterocyte brush border (Caco-2 BBe1 epithelia). It is important for the investigator to choose random areas when conducting morphometric analysis of brush borders. Further, the investigator must choose at least three random 1 μm^2 regions to count microvilli in order to procure statistical analysis from three independent experiments. Finally, if control specimens do not appear well organized as shown in Fig. 4.3, the entire experiment must be culled from analysis as the result from the experimental exposure would be ambiguous.

Details related to basic cell culture and aseptic technique are beyond the scope of this methods section. However, it is highly recommended that the investigator practice cell culture techniques as described in the Freshney text [63]. Historically, the parental Caco-2 cell line designated by American Type Culture Collection (ATCC) as HTB-37™ was employed to study the uptake and pharmacokinetics of novel drugs [64, 65]; for the first time a simplified model of the human gastrointestinal tract could be grown in culture and used in high throughput to screen materials. This cell line allured investigators as it could be propagated continuously in culture eliminating the expense and ethical concerns associated with procuring fresh human tissue. Further, a large number of cells can be grown for experimental analysis and used in standardized assays. While HTB-37™ sparked interest for its use as a predic-

tor of small molecule transport, it was limited in that epithelia formed from this cell line were found to be relatively heterogeneous, and some cells within this epithelium did not produce brush borders at all. In 1992 Peterson and Mooseker subcloned HTB-37™ and called these cell lines brush border expressing 1 and 2 (BBe1 and BBe2). This was, in part, first due to a need for a human cell line that faithfully mimicked the in vivo brush borders at the morphological and biochemical levels. And second, the need for an in vitro model that sustained gradual morphogenesis of the brush border in order to understand the molecular events accompanying brush border morphogenesis. Since that time there have been numerous investigators that have employed the Caco-2 BBe1 cell system to exploit the archetypical organization of the brush border in vitro [51, 66–69].

One benefit of in vitro cell systems is that the investigator can screen various NP diameters, concentrations, physico-chemical parameters, etc., for those NPs that result in relatively few toxic effects. For these reasons investigators have employed the Caco-2 BBe1 cell model in order to understand the effects NPs elicit after exposure via the oral route. The use of the Caco-2 cell model has been recommended by the International Life Science Institute Research Foundation/Risk Science Institute (ILSI RF/RSI) Nanomaterial Toxicity Screening Working Group as an attractive option to understand potential deleterious effects of NPs after exposure to the human gastrointestinal tract [70], However, recent studies indicate that care should be exercised concerning interpretation of experimental data procured from the use of Caco-2 (HTB-37™) for the aforementioned reasons [55, 56, 71]; First, it is essential that investigators clearly indicate which Caco-2 cell line was used during experimentation as many fail to report this critical piece of information; Second, and most disconcerting are control images shown by some that are not comparable to a plethora of reports in the literature dating back to 1992. Such results show the need for a standardize set of cell culture and microscopy preparation techniques, otherwise observations will become confounding.

The following text describes routine maintenance of the commercially available Caco-2 BBe1 cell line (ATCC, CRL-2102™) starting from thawing frozen, token ampules, to establishing user stocks. This methods section is concluded with a procedure that can be employed should the investigator wish to produce publication quality scanning electron micrographs of Caco-2 brush borders.

4.4.2   Procedure for Thawing Caco-2 BBe1 Cells from Frozen Cryogenic Ampules

1. Purchase 1–3 validated Caco-2 BBe1 cell lines from a geographically convenient cell repository at a low passage number. It was found that the archetypical structure of the brush border remains consistent until passage number 68 [72].

2. After placing the order for the cell line, begin by preparing sterile complete culture medium. The medium of choice for Caco-2 BBe1 cells is Dulbecco's Modification of Eagle's Medium (DMEM; Cellgro, 10-013), supplemented with 10 μg/mL human transferrin (Invitrogen; 0030124SA), 10,000 I.U./mL penicillin, 10,000 μg/mL streptomycin and 25 μg/mL amphotericin (Cellgro; 30-004-CI), and 10 % fetal bovine serum (Biosera; FBS2000). Cellgro supplies their medium in volumes of 500- or 1,000 mL. The Nalgene® plastic that contains the DMEM permits the additional volume of supplements. The complete culture medium is inverted in the Nalgene® plastic three to five times to make the mixture uniform and subsequently apportioned (100 mL each) into 125 mL Wheaton glass bottles. Under no circumstances should the medium come in contact with the tops of Wheaton glass bottles as the medium may become contaminated. These sterile, pre-labeled 125 mL glass bottles can be stored at 4 °C for up to 8 weeks.

3. Upon arrival of the cells immediately warm the complete culture medium to 37 °C in a recirculating water bath. This commonly takes 15 min to equilibrate the medium from 4 to 37 °C. Once equilibrated the closed bottle of complete culture medium is sprayed with 70 % ethanol and placed on the grating of the air curtain to dry. *Proceed to the next step immediately.*

4. Remove the cryogenic ampule containing the cells from the packaging, ensure that the cap is tightly sealed, and begin to thaw the contents by gently swirling the frozen ampule in a pre-equilibrated (37 °C) water bath. Inspect the ampule and continue to thaw with swirling until there appears a piece of ice that approximates the diameter of a pen tip. This thawing process takes about 2 min and should not be prolonged. It is advised that a trained member of the laboratory completes the thawing process. *Proceed to the next step immediately.*

5. Sterilize the external surface of the ampule with 70 % ethanol and it place on the grating of the air curtain. Situate all necessary materials within the working area of the biological safety cabinet only after the 70 % ethanol has air dried. *Proceed to the next step immediately.*

6. Transfer 9 mL of pre-equilibrated (37 °C) complete culture medium to a sterile 15 mL centrifuge tube, add the thawed cells, and centrifuge at 125 g for 5 min to pellet the cells. *Proceed to the next step immediately.*

7. Aspirate the supernatant, gently resuspend the cells in 1 mL of complete culture medium, and transfer 1 mL into a T-75 culture vessel. Add 9 mL of additional pre-equilibrated complete culture medium and gently rock the culture vessel five times to distribute the cells. Label the culture vessel with the investigator's name, the date, the cell type (Caco-2 BBe1), and the cell passage number. Quickly inspect the culture with an inverted phase-contrast microscope. The cells should appear as phase-bright spheres. *Proceed to the next step immediately.*

8. Transfer the culture vessels to a humidified cell culture incubator equilibrated to maintain a constant temperature of 37 °C with an atmosphere of 5 % CO_2 in air. The following day the cells should be inspected and the culture medium should be changed to remove nonviable cells.

4.4.3 Procedure for Feeding and Subculturing Caco-2 BBe1 Cells

For routine maintenance, complete culture medium should be replenished every 3 days with 10 mL per T-75 culture vessel. To remove cell culture medium aseptically, aspirate the old medium used by the cells and pipet fresh, pre-equilibrated, sterile medium.

1. Set the culture vessel and pre-equilibrated complete culture medium on the air grate of the biological safety cabinet while waiting for ethanol to dry from gloved hands, and the complete culture medium bottle. This typically takes 2 min.
2. Aseptically aspirate the used cell culture medium, and pipet fresh, pre-equilibrated complete culture medium. This typically takes 2 min.
3. Return the culture vessels to the cell culture incubator.

The number of cells that occupy the percent area of the culture vessel surface is defined as the "percent confluence." In other words, if 80 % of the culture vessel surface is occupied by cells, the culture is said to be 80 % confluent. Once 80 % confluence is reached the cells should be subcultured to prevent cell differentiation due to overcrowding of the cells.

4.4.4 Procedure for Subculturing Caco-2 BBe1 Cells

1. Place the following in a recirculating 37 °C water bath for 15 min: Ca^{2+}/Mg^{2+}-free phosphate buffered saline (PBS; Cellgro, 20-031-CV), complete culture medium, and 0.25 % trypsin/2.21 mM EDTA in Hanks Balanced Salt Solution (Cellgro, 25-050-Cl).
2. Place all materials including the cell culture vessels in the hood as described in the paragraphs in the text above.
3. Aspirate the complete growth medium from the culture vessel. *Proceed to the next step immediately.*
4. Rinse the cells once with Ca^{2+}/Mg^{2+}-free PBS (3 mL per T-75). Aspirate the PBS. *Proceed to the next step immediately.*

5. Apply 3 mL of 0.25 % trypsin/2.21 mM EDTA in Hanks Balanced Salt Solution, and return the T-75 culture vessel to the cell culture incubator for 5 min. *Proceed to the next step immediately.*
6. Pipet 3 mL of complete culture medium into the T-75 culture vessel to inactivate the trypsin, and transfer the entire volume (6 mL total) to a 15 mL centrifuge tube. *Proceed to the next step immediately.*
7. Centrifuge at 150 g for 5 min to pellet the cells. During this 5 min wait, label new sterile culture vessels with the appropriate information, and add complete growth medium to the new culture vessel. *Proceed to the next step immediately.*
8. Aspirate the supernatant to remove any residual trypsin, and resuspend the cell pellet in 1 mL of complete culture medium; gently mix to randomize the cells. Transfer 100 μL of the suspension to the new culture vessel and gentle agitate to distribute the cells. This results in a 1:10 dilution.
9. Return the cells to the cell culture incubator. The cells will become adherent within 12 h and will require additional subculturing after approximately 1 week in culture.

4.4.5 Procedure for Establishing User Caco-2 BBe1 Stocks

The procedures described up to this point detail the routine culture of Caco-2 cells starting from a newly purchased cell line. This newly purchased cell line is hereafter referred to as the "token stock," as it is the lowest passage, validated cell line. There are four stages of cell lines that should be maintained in a cell culture laboratory and those include, (1) token stocks, (2) seed stocks, (3) distribution stocks, and finally (4) user stocks. The fine details of each of these classifications are described in the Freshney text [63]. Under no circumstance should the casual user employ token, seed, or distribution stocks, as these are validated, and lowest in passage number required to maintain the cell line.

1. Acquire a new cell line (e.g., Caco-2 BBe1). Only an experienced laboratory member

should thaw and culture these cells as described in Sects. 4.4.2 and 4.4.3.

2. When this token stock is 80 % confluent, use this culture to establish three to five additional stocks. To do this subculture the cells as described in Sect. 4.4.3 in three to five different sterile culture vessels.

3. When these three to five stocks are 80 % confluent freeze the cell line (as described in Sect. 4.3), thaw one vial, and subsequently validate the cell line as described in the Freshney text before creating seed stocks.

4. To create seed stocks, thaw one to two token freeze stocks and generate 10–20 cryogenic ampules. Cryogenically preserve these ampoules (detailed in Sect. 4.3).

5. Create distribution stocks by thawing seed stocks to generate 20–100 cryogenic ampules. One of these seed ampules must be thawed and subsequently validated before user stocks are generated.

6. One seed stock ampules is given to each user in the laboratory and it is the responsibility of the user to generate additional backups as user stocks. User stocks should be generated at 10–20 ampules, and only the user that made these ampules should culture these cells. User ampules are discarded according to institutional biosafety protocols after the user has left the laboratory.

4.4.6   Cryogenically Preserving Caco-2 BBe1 Cells

There are a number of reasons why cell lines should be cryogenically preserved. For starters, after cells have been in culture for 2 months (approximately 10 subcultures) there is the potential of genetic drift and clone variation. Furthermore, transformation, dedifferentiation, contamination/cross-contamination, and cost all corroborate the utility of maintaining cryopreserved stocks.

As a basic outline for the procedure described in the text below the investigator will grow the cells to late log phase in the desired culture vessel, trypsinize the cells and centrifuge, and resuspend the entire cell volume in cryopreservation

medium. The cells are then immediately transferred to a cryogenic vial and heat is removed (i.e. the temperature is lowered) at 1 °C per minute. The cells are subsequently transferred to liquid nitrogen for long-term storage.

1. Only generate at maximum 10 late log phase cultures via aseptic technique at a time, as manipulating additional culture vessels at the same time is difficult, and will lead to errors.

2. Cryopreservation medium should be prepared the same day the cells are frozen. Cryopreservation medium contains 80 % complete culture medium supplemented with additional FBS at 10 % and DMSO at 10 %. Exercise caution as the addition of DMSO will result in an exothermic reaction, which raises the temperature beyond 37 °C. This rise in temperature will result in reduced viability if the cells are exposed to this increased temperature. DMSO should be cell culture tested, and can be purchased from sources such as ATCC, Sigma Aldrich, etc.

3. Label the cryopreservation vials with a solvent-resistant marker and include the following information: The investigators name, the date, the cell line, the passage number, and the surface area or type of culture vessel used to grow the cells.

4. Wash the cultures with PBS, trypsinize the cells, centrifuge the cells, and aspirate the supernatant as detailed in steps 1–8 of protocol 4.4.4. *Proceed to the next step immediately.*

5. Quickly resuspend the cell pellet(s) in cryopreservation medium, and transfer the contents of the centrifuge tube(s) to its own cryogenic ampule (Corning 2028). Completely tighten the threading of the cryogenic ampule. *Proceed to the next step immediately.*

6. Quickly place the cryogenic ampule(s) into a Nalgene® Mr. Frosty unit (Thermo Scientific, 5100-0001), gently tighten the lid of the Mr. Frosty unit, and place the entire unit into a −70 °C freezer.

7. After 12 h the cryogenic ampules are transferred to canes labeled for quick identification, and stored in a liquid nitrogen dewer. After 2 days, thaw one cryogenic ampule and determine cellular viability by the trypan blue exclusion assay.

4.5 Growing Caco-2 BBe1 Epithelia for Morphometric Analysis of Brush Borders, and a Protocol for Specimen Preparation for Scanning Electron Microscopy

The following text provides a protocol to prepare Caco-2 BBe1 epithelia for scanning electron microscopy. In this text the investigators employ a critical point drier to convert liquid CO_2 to a gaseous state. It is advised that the critical point drier, in the case described below, a Balzer CPD 020, contains a stirring apparatus to promote exchange between acetone and liquid CO_2. If the investigator does not have a Balzer CPD 020, the optimal chamber pressure, solvent exchanges, and times may need to be determined empirically. It is equally important to grow the epithelium on a suitable substrate. Non-compliant materials such as glass typically result in epithelia whose junctions appear non-continuous. Further, the extracellular matrix protein rat tail collagen I permits rapid cell adherence to the substrate, but other coating substrates (poly-D-lysine, fibronectin, etc.) should be used with caution as Caco-2 BBe1 may not adhere to these proteins. During this procedure heat is removed from the specimen chamber adiabatically and the specimens are slowly infiltrated with liquid CO_2. During the drying process the liquid is vented and vaporizes to its gaseous state. Caution: This amount of CO_2 gas can result in asphyxiation if the surrounding area is not properly ventilated. It is advised that the critical point drier has adequate ventilation aided by an exhaust system.

1. Caco-2 BBe1 cells are seeded at 2.35×10^5 cells/cm^2 on 6.5 mm (0.33 cm^2) Corning Transwell® inserts (Corning, 3495), and maintained for 17–21 days to promote differentiation of the epithelium [72]. This cell system permits optimal differentiation of the epithelium as both the apical and basal compartments are bathed with 300 μL and 1 mL of complete culture medium, respectively. The complete culture medium is replenished every 24–48 h. Any indication that the pH of the medium has changed results in brush borders that appear unhealthy (e.g. limp microvilli, few in numbers, etc.).

2. Only after 17–21 days of culture are the epithelia cytologically fixed. The primary fixative of choice is electron microscopy grade glutaraldehyde (Electron Microscopy Sciences, 16020) made 2 % in 100 mM sodium cacodylate buffer (pH 7.2). Specimens are fixed for 2 h at room temperature. *Proceed to the next step immediately.*

3. The specimens are washed 10 times each for 10 min in 100 mM sodium cacodylate buffer (pH 7.2). Copious amounts of buffer should be used during each incubation, and the specimens should be agitated gently at room temperature. *Proceed to the next step immediately.*

4. The epithelia are post-fixed in 1 % OsO_4 in sodium cacodylate buffer (pH 6.4) for 60 min at room temperature. During this time the specimens are protected from light. *Proceed to the next step immediately.*

5. The specimens are washed 10 times each for 10 min in Nanopure® water (18.2 MΩ/cm) at room temperature with gentle agitation. *Proceed to the next step immediately.*

6. The epithelia are dehydrated carefully by passing the specimens through an increasing graded ethanol series, and subsequently transitioning the specimens to acetone. It is advisable to use 100 % acetone that has been dried with molecular sieves for at least 2 days. *Proceed to the next step immediately.*

7. The only method that should be employed for drying specimens is with a critical point drier (e.g., Balzer CPD020), as all other methods will impart a number of structural artifacts. Fill the CDP chamber with enough anhydrous acetone to cover the specimens. The specimens are contained in a compartmentalized mesh basket, or solvent resistant container that permits infiltration of liquid CO_2 in exchange for acetone. Seal the chamber. *Proceed to the next step immediately.*

8. Cool the chamber to 4–6 °C by turning on the non-filtered liquid CO_2 cylinder to pass through the chamber walls. *Proceed to the next step immediately.*

9. Slowly begin to fill the chamber with filtered liquid CO_2. The investigator will note a rise in the chamber pressure. Rapidly adding liquid CO_2 will artifactually fracture intracellular junctions as shown elsewhere [73], and as a consequence, the epithelium will appear disrupted when viewed with a scanning electron microscope. Under no circumstance should the pressure exceed 50 bars when changing the liquid CO_2 as intercellular junctions will fracture. Turn on the stirring apparatus to mix the acetone and liquid CO_2. Wait 5 min for the acetone and the liquid CO_2 to mix. *Proceed to the next step immediately.*

10. Slowly vent the specimen chamber until the volume of the liquid mixture is just above the specimens. *Proceed to the next step immediately.*

11. Slowly fill the chamber with liquid CO_2. Once the chamber is filled, allow 5 min to mix the liquids. As indicated in step 9 the chamber pressure should not rapidly fluctuate. *Proceed to the next step immediately.*

12. Repeat step 11 for a total of 9 times. *Proceed to the next step immediately.*

13. Turn off the cooling and filling liquid CO_2 cylinders, the stirring apparatus, and change the temperature controller to 45 °C. It takes about 5–7 min (Balzer CPD 020) for the specimen chamber to approach the critical pressure and temperature of CO_2 as the temperature rises. *Proceed to the next step immediately.*

14. After the specimens have transitioned through the critical point of CO_2, and the temperature is above 42 °C, slowly begin to outgas (vent) the gaseous CO_2. This should take approximately 5–10 min at a rate of 5–10 bars of pressure released per minute. *Proceed to the next step immediately.*

15. Mount the specimens on an aluminum stub, and sputter coat the specimens with approximately 5 nm of vaporized metal (e.g., Pt/Au). After the specimens have been coated with metal they are stable for years when stored appropriately. The stubs can be housed in a small stub holder, and this entire box is stored desiccated in a vacuum sealed chamber.

Conclusions

At present there is a paucity of data regarding our understanding of the events that mediate disruption of the brush border in vitro. Several putative targets exist at a mechanistic level, and these clues pave the way to identify a potentially unifying mechanism that accounts for the disruption of the brush border after exposure to engineered nanomaterials. Since this nanotoxicity research paradigm is in its infancy it behooves investigators to adopt standardized cell models appropriate to the study of NP-induced brush border disruption. Indeed, accurate data that can be compared across laboratories encourages forward progress in the field.

How can engineered NPs whose elemental composition is different result in morphologically similar changes (disruption) to the brush border? Such a universal event after exposure to NPs suggests that a cellular response, and not necessarily an inherent physico-chemical property of the nanomaterial, may account for brush border disruption. It was proposed by Zhang and coworkers that adsorption of NPs to the cell surface resulted in disruption of the brush border [59]. If this is the case it could be predicted that sedimentation of agglomerated NPs onto the cell surface exacerbates disruption of the brush border. However, this hypothesis remains to be examined. The next mechanistic clue is derived from scanning electron microscopy and microarray data; both published [58] and unpublished results (Faust et al., in review) indicate that iron oxide (α-Fe_2O_3) nanoparticle exposure results in disruption of the brush border in Caco-2 and the B30 clone of BeWo, the latter is a human brush border expressing placenta cell model. Further, at the mRNA level the gene responsible for the actin filament capping protein, CapZ is upregulated in both cell systems. CapZ is a component of the plus tips of microvilli whose role is to "cap" the addition end of F-actin such that the filament cannot elongate. Upregulation of *CapZ* might suggest that the protein acts to reabsorb microvilli since additional actin monomers necessary to maintain the elongated

structure would be unable to nucleate at the plus ends. Finally, it is intriguing to speculate that alterations in the terminal web account for a NP-induced brush border disruption, as microarray data indicates changes to adhering junctions, which are known to be intimately connected with the terminal web.

References

1. Dunphy Guzman KA, Taylor MR, Banfield JF (2006) Environmental risks of nanotechnology: national nanotechnology initiative funding, 2000–2004. Environ Sci Technol 40:1401–1407

2. Foss Hansen S, Larsen BH, Olsen SI, Baun A (2007) Categorization framework to aid hazard identification of nanomaterials. Nanotoxicology 1:243–250

3. Arruebo M, Fernández-Pacheco R, Ibarra MR, Santamaría J (2007) Magnetic nanoparticles for drug delivery. Nano Today 2:22–32

4. Mahmoudi M, Sant S, Wang B, Laurent S, Sen T (2011) Superparamagnetic iron oxide nanoparticles (SPIONs): development, surface modification and applications in chemotherapy. Adv Drug Deliv Rev 63:24–46

5. Oh JK, Park JM (2011) Iron oxide-based superparamagnetic polymeric nanomaterials: design, preparation, and biomedical application. Prog Polym Sci 36:168–189

6. Howarth M, Takao K, Hayashi Y, Ting AY (2005) Targeting quantum dots to surface proteins in living cells with biotin ligase. Proc Natl Acad Sci U S A 102:7583–7588

7. Resch-Genger U, Grabolle M, Cavaliere-Jaricot S, Nitschke R, Nann T (2008) Quantum dots versus organic dyes as fluorescent labels. Nat Methods 5:763–775

8. Gao X, Cui Y, Levenson RM, Chung LW, Nie S (2004) In vivo cancer targeting and imaging with semiconductor quantum dots. Nat Biotechnol 22:969–976

9. Huang H-C, Rege K, Heys JJ (2010) Spatiotemporal temperature distribution and cancer cell death in response to extracellular hyperthermia induced by gold nanorods. ACS Nano 4:2892–2900

10. Sylvester P, Westerhoff P, Möller T, Badruzzaman M, Boyd O (2007) A hybrid sorbent utilizing nanoparticles of hydrous iron oxide for arsenic removal from drinking water. Environ Eng Sci 24:104–112

11. Donaldson K, Seaton A (2012) A short history of the toxicology of inhaled particles. Part Fibre Toxicol 9:13

12. Mukherjee T, Williams AW (1967) A comparative study of the ultrastructure of microvilli in the epithelium of small and large intestine of mice. J Cell Biol 34:447–461

13. Misch D, Giebel P, Faust R (1980) Intestinal microvilli: responses to feeding and fasting. Eur J Cell Biol 21:269–279

14. Stidwill RP, Wysolmerski T, Burgess DR (1984) The brush border cytoskeleton is not static: in vivo turnover of proteins. J Cell Biol 98:641–645

15. Granger B, Baker RF (1950) Electron microscope investigation of the striated border of intestinal epithelium. Anat Rec 107:423–441

16. Miller D, Crane RK (1961) The digestive function of the epithelium of the small intestine: II. Localization of disaccharide hydrolysis in the isolated brush border portion of intestinal epithelial cells. Biochim Biophys Acta 52:293–298

17. Palay SL, Karlin LJ (1959) An electron microscopic study of the intestinal villus. I. The fasting animal. J Biophys Biochem Cytol 5:363–371

18. Trier JS (1963) Studies on small intestinal crypt epithelium. I. The fine structure of the crypt epithelium of the proximal small intestine of fasting humans. J Cell Biol 18:599–620

19. McNabb J, Sandborn E (1964) Filaments in the microvillous border of intestinal cells. J Cell Biol 22:701–704

20. Ishikawa H, Bischoff R, Holtzer H (1969) Formation of arrowhead complexes with heavy meromyosin in a variety of cell types. J Cell Biol 43:312–328

21. Tilney LG, Mooseker M (1971) Actin in the brush-border of epithelial cells of the chicken intestine. Proc Natl Acad Sci U S A 68:2611–2615

22. Arpin M, Friederich E (1992) Cytoskeletal components in intestinal brush border morphogenesis: an evaluation of their function. In: Fleming TP (ed) Epithelial organization and development. Dordrecht, Springer

23. Bretscher A (1983) Microfilament organization in the cytoskeleton of the intestinal brush border. Cell Muscle Motil 4:239

24. Coudrier E, Kerjaschki D, Louvard D (1988) Cytoskeleton organization and submembranous interactions in intestinal and renal brush borders. Kidney Int 34:309

25. Hirokawa N, Tilney LG, Fujiwara K, Heuser JE (1982) Organization of actin, myosin, and intermediate filaments in the brush border of intestinal epithelial cells. J Cell Biol 94:425–443

26. Mooseker MS (1985) Organization, chemistry, and assembly of the cytoskeletal apparatus of the intestinal brush border. Annu Rev Cell Biol 1:209–241

27. Shibayama T, Carboni JM, Mooseker MS (1987) Assembly of the intestinal brush border: appearance and redistribution of microvillar core proteins in developing chick enterocytes. J Cell Biol 105:335–344

28. Bement WM, Mooseker MS (1996) The cytoskeleton of the intestinal epithelium: components, assembly, and dynamic rearrangements. In: Hesketh E, Pryme JF

(eds) The cytoskeleton: a multi-volume treatise, vol 3. JAI Press, Greenwich, pp 359–404

29. Heintzelman MB, Mooseker MS (1992) Assembly of the intestinal brush border cytoskeleton. Curr Top Dev Biol 26:93–122

30. Begg DA, Rodewald R, Rebhun LI (1978) The visualization of actin filament polarity in thin sections. Evidence for the uniform polarity of membrane-associated filaments. J Cell Biol 79:846–852

31. Hirokawa N, Heuser JE (1981) Quick-freeze, deep-etch visualization of the cytoskeleton beneath surface differentiations of intestinal epithelial cells. J Cell Biol 91:399–409

32. Bretscher A, Weber K (1980) Fimbrin, a new microfilament-associated protein present in microvilli and other cell surface structures. J Cell Biol 86:335–340

33. Bretscher A, Weber K (1980) Villin is a major protein of the microvillus cystoskeleton which binds both G and F actin in a calcium-dependent manner. Cell 20:839–847

34. Bartles JR, Zheng L, Li A, Wierda A, Chen B (1998) Small espin: a third actin-bundling protein and potential forked protein ortholog in brush border microvilli. J Cell Biol 143:107–119

35. Garcia A, Coudrier E, Carboni J, Anderson J, Vandekerkhove J, Mooseker M, Louvard D, Arpin M (1989) Partial deduced sequence of the 110-kD-calmodulin complex of the avian intestinal microvillus shows that this mechanoenzyme is a member of the myosin I family. J Cell Biol 109:2895–2903

36. Glenney JR, Osborn M, Weber K (1982) The intracellular localization of the microvillus 110 K protein, a component considered to be involved in side-on membrane attachment of F-actin. Exp Cell Res 138:199–205

37. Howe CL, Mooseker MS (1983) Characterization of the 110-kdalton actin-calmodulin-, and membrane-binding protein from microvilli of intestinal epithelial cells. J Cell Biol 97:974–985

38. Berryman M, Franck Z, Bretscher A (1993) Ezrin is concentrated in the apical microvilli of a wide variety of epithelial cells whereas moesin is found primarily in endothelial cells. J Cell Sci 105:1025–1043

39. Bretscher A (1983) Purification of an 80,000-dalton protein that is a component of the isolated microvillus cytoskeleton, and its localization in nonmuscle cells. J Cell Biol 97:425–432

40. Bretscher A, Reczek D, Berryman M (1997) Ezrin: a protein requiring conformational activation to link microfilaments to the plasma membrane in the assembly of cell surface structures. J Cell Sci 110:3011–3018

41. Brown JW, Mcknight CJ (2010) Molecular model of the microvillar cytoskeleton and organization of the brush border. PLoS One 5:e9406

42. D'Angelo R, Aresta S, Blangy A, del Maestro L, Louvard D, Arpin M (2007) Interaction of ezrin with the novel guanine nucleotide exchange factor PLEKHG6 promotes RhoG-dependent apical cytoskeleton rearrangements in epithelial cells. Mol Biol Cell 18:4780–4793

43. Zwaenepoel I, Naba A, da Cunha MML, del Maestro L, Formstecher E, Louvard D, Arpin M (2012) Ezrin regulates microvillus morphogenesis by promoting distinct activities of Eps8 proteins. Mol Biol Cell 23:1080–1095

44. Glenney JR, Glenney P, Weber K (1983) The spectrin-related molecule, TW-260/240, cross-links the actin bundles of the microvillus rootlets in the brush borders of intestinal epithelial cells. J Cell Biol 96:1491–1496

45. Hirokawa N, Cheney RE, Willard M (1983) Location of a protein of the fodrin-spectrin-TW260/240 family in the mouse intestinal brush border. Cell 32:953–965

46. Mooseker MS (1976) Brush border motility. Microvillar contraction in triton-treated brush borders isolated from intestinal epithelium. J Cell Biol 71:417–433

47. Bretscher A, Weber K (1978) Localization of actin and microfilament-associated proteins in the microvilli and terminal web of the intestinal brush border by immunofluorescence microscopy. J Cell Biol 79:839–845

48. Grimm-Günter E-MS, Revenu C, Ramos S, Hurbain I, Smyth N, Ferrary E, Louvard D, Robine S, Rivero F (2009) Plastin 1 binds to keratin and is required for terminal web assembly in the intestinal epithelium. Mol Biol Cell 20:2549–2562

49. Achler C, Filmer D, Merte C, Drenckhahn D (1989) Role of microtubules in polarized delivery of apical membrane proteins to the brush border of the intestinal epithelium. J Cell Biol 109:179–189

50. Gilbert T, le Bivic A, Quaroni A, Rodriguez-Boulan E (1991) Microtubular organization and its involvement in the biogenetic pathways of plasma membrane proteins in Caco-2 intestinal epithelial cells. J Cell Biol 113:275–288

51. Halbleib JM, Sääf AM, Brown PO, Nelson WJ (2007) Transcriptional modulation of genes encoding structural characteristics of differentiating enterocytes during development of a polarized epithelium in vitro. Mol Biol Cell 18:4261–4278

52. Monopoli MP, Åberg C, Salvati A, Dawson KA (2012) Biomolecular coronas provide the biological identity of nanosized materials. Nat Nanotechnol 7:779–786

53. Wang B, Zhang L, Bae SC, Granick S (2008) Nanoparticle-induced surface reconstruction of phospholipid membranes. Proc Natl Acad Sci U S A 105:18171–18175

54. de Beauregard MC, Pringault E, Robine S, Louvard D (1995) Suppression of villin expression by antisense RNA impairs brush border assembly in polarized epithelial intestinal cells. EMBO J 14:409

55. Koeneman BA, Zhang Y, Westerhoff P, Chen Y, Crittenden JC, Capco DG (2010) Toxicity and cellular responses of intestinal cells exposed to titanium dioxide. Cell Biol Toxicol 26:225–238

56. Fisichella M, Berenguer F, Steinmetz G, Auffan M, Rose J, Prat O (2012) Intestinal toxicity evaluation of TiO$_2$ degraded surface-treated nanoparticles:

a combined physico-chemical and toxicogenomics approach in Caco-2 cells. Part Fibre Toxicol 9:18

57. Virkutyte J, Al-Abed SR, Dionysiou DD (2012) Depletion of the protective aluminum hydroxide coating in TiO$_2$-based sunscreens by swimming pool water ingredients. Chem Eng J 191:95–103

58. Kalive M, Zhang W, Chen Y, Capco DG (2012) Human intestinal epithelial cells exhibit a cellular response indicating a potential toxicity upon exposure to hematite nanoparticles. Cell Biol Toxicol 28:343–368

59. Zhang W, Kalive M, Capco DG, Chen Y (2010) Adsorption of hematite nanoparticles onto Caco-2 cells and the cellular impairments: effect of particle size. Nanotechnology 21:355103

60. Temm-Grove C, Helbing D, Wiegand C, Honer B, Jockusch B (1992) The upright position of brush border-type microvilli depends on myosin filaments. J Cell Sci 101:599–610

61. Weir A, Westerhoff P, Fabricius L, Hristovski K, Von Goetz N (2012) Titanium dioxide nanoparticles in food and personal care products. Environ Sci Technol 46:2242–2250

62. FDA, U (2010) Summary of color additives listed for use in the United States in food, drugs, cosmetics, and medical devices. Color additives approved for use in cosmetics part 73, subpart C: Color additives exempt from batch certification, United States Food and Drug Administration

63. Freshney RI (2005) Culture of specific cell types. Wiley-Blackwell. http://bcs.wiley.com/he-bcs/Books?action=index&bcsId=5959&itemId=0470528125

64. Artursson P, Palm K, Luthman K (2001) Caco-2 monolayers in experimental and theoretical predictions of drug transport." Adv Drug Deliv Rev 46.1:27–43

65. Hidalgo IJ, Raub TJ, Borchardt RT (1989) Characterization of the human colon carcinoma cell line (Caco-2) as a model system for intestinal epithelial permeability. Gastroenterology 96:736–749

66. Bement WM, Forscher P, Mooseker MS (1993) A novel cytoskeletal structure involved in purse string wound closure and cell polarity maintenance. J Cell Biol 121:565–578

67. Faust J, Capco D (2012) Multifunctional scaffolds in eggs: sites for localization, signal transduction and meiotic spindle polarity. Front Biosci (Schol Ed) 5:496–506

68. Koeneman BA, Zhang Y, Hristovski K, Westerhoff P, Chen Y, Crittenden JC, Capco DG (2009) Experimental approach for an <i> in vitro </i> toxicity assay with non-aggregated quantum dots. Toxicol In Vitro 23:955–962

69. Peterson MD, Bement WM, Mooseker MS (1993) An in vitro model for the analysis of intestinal brush border assembly. II. Changes in expression and localization of brush border proteins during cell contact-induced brush border assembly in Caco-2BBe cells. J Cell Sci 105:461–472

70. Oberdörster G, Maynard A, Donaldson K, Castranova V, Fitzpatrick J, Ausman K, Carter J, Karn B, Kreyling W, Lai D (2005) Principles for characterizing the potential human health effects from exposure to nanomaterials: elements of a screening strategy. Part Fibre Toxicol 2:8

71. Faust JJ, Zhang W, Koeneman BA, Chen Y, Capco DG (2012) Commenting on the effects of surface treated- and non-surface treated TiO$_2$ in the Caco-2 cell model. Part Fibre Toxicol 9:42

72. Peterson MD, Mooseker MS (1993) An in vitro model for the analysis of intestinal brush border assembly. I. Ultrastructural analysis of cell contact-induced brush border assembly in Caco-2BBe cells. J Cell Sci 105:445–460

73. Passey S, Pellegrin S, Mellor H (2007) Scanning electron microscopy of cell surface morphology. Curr Protoc Cell Biol 4–17

Nanoparticles: Cellular Uptake and Cytotoxicity

5

Isaac M. Adjei, Blanka Sharma,
and Vinod Labhasetwar

Contents

I.M. Adjei
Department of Molecular Medicine, Cleveland Clinic
Lerner College of Medicine of Case Western Reserve
University, Cleveland, OH 44106, USA

Department of Biomedical Engineering/ND20,
Lerner Research Institute, Cleveland Clinic,
9500 Euclid Avenue, Cleveland, OH 44195, USA

B. Sharma
Department of Biomedical Engineering/ND20,
Lerner Research Institute, Cleveland Clinic,
9500 Euclid Avenue, Cleveland, OH 44195, USA

V. Labhasetwar, PhD (✉)
Department of Molecular Medicine, Cleveland Clinic
Lerner College of Medicine of Case Western Reserve
University, Cleveland, OH 44106, USA

Department of Biomedical Engineering/ND20,
Lerner Research Institute, Cleveland Clinic,
9500 Euclid Avenue, Cleveland, OH 44195, USA

Taussig Cancer Institute, Cleveland Clinic,
Cleveland, OH 44195, USA
e-mail: labhasv@ccf.org

Abstract

Understanding the interactions of nanoparticles (NPs) with cells and how these interactions influence their cellular uptake is essential to exploring the biomedical applications of NPs, particularly for drug delivery. Various factors, whether differences in physical properties of NPs or variations in cell-membrane characteristics, influence NP-cell interactions and uptake processes. NP-cell membrane interactions may also influence intracellular trafficking of NPs, their sorting into different intracellular compartments, cellular retention, and hence the efficacy of encapsulated therapeutics. A crucial consideration is whether such interactions might cause any toxicity,

starting with how NPs interact in transit with the biological environment prior to their interactions with targeted cells and tissues. Understanding the effects of various NP characteristics on cellular and biological processes could help in designing NPs that are efficient but also nontoxic.

Keywords

Polymers • Drug Delivery • Transport • Nanocarriers • Biocompatibility

Abbreviations

AFM	Atomic force microscopy
AR	Aspect ratio
CME	Clathrin-mediated endocytosis
CPP	Cell-penetrating peptides
CTAB	Cetyltrimethylammonium bromide
DMAB	Didodecyldimethylammonium bromide
DTAB	Dodecyltrimethylammonium bromide
HIV	Human immunodeficiency virus
MTs	Microtubules
NPs	Nanoparticles
PLGA	Poly (D, L-lactide co-glycolide)
RISC	RNA-induced silencing complex
RNAi	RNA-interference
siRNAs	Small interfering RNAs
SNPs	Silica NPs
TAT	*trans*-activating transcriptional activator

5.1 Introduction

Nanoparticles (NPs) with unique physical characteristics such as size, shape, and surface chemistry or that have been modified with different targeting ligands are designed and optimized to explore their use in various biomedical applications, particularly for drug delivery [1, 2] or imaging [3, 4]. The critical issue is to understand NP-cell interactions: for certain applications (e.g., gene therapy) [5], it may be desirable that NPs interact more efficiently with cells and more readily become internalized, whereas for other applications (e.g., vascular imaging agents), it may be necessary to minimize NP-cell interactions [6]. NP-cell interaction is a very dynamic process and depends on physical characteristics of NPs, as well as on cell-membrane properties [7, 8]. Physical characteristics of NPs such as shape, size, surface charge, or the presence of cell-penetrating peptides/targeting ligands on the NP's surface may influence NP-cell interactions. Similarly, cell-membrane properties such as membrane fluidity, type of receptors, receptor density, and recycling rate of receptors may influence NP-cell interactions and internalization [9]. Furthermore, NP-cell membrane interactions could determine the pathway by which uptake of NPs occurs, as well as their intracellular sorting into different cellular compartments and retention in the target area, which eventually could influence the efficacy of encapsulated therapeutics. In other cases, NPs are modified with hydrophilic polymers to minimize NP-cell interactions [10]. NP-cell membrane interactions are also being studied to understand NP-mediated toxicity. Therefore, it is timely to review parameters that influence NP-cell interactions, which could help in designing NPs that are efficient but nontoxic.

5.2 Mechanisms of Cellular Uptake

The mechanisms via which NPs enter cells are determined to a great extent by physical and interfacial characteristics of NPs, their interactions with the biological environment, and cell-membrane properties. NP size, shape, and surface characteristics (particularly charge and hydrophobicity) can influence the cellular uptake pathways [11, 12]. Furthermore, the interactions of NPs with cells may depend on conjugated ligands and cell-surface receptors for receptor-mediated uptake [13]. In addition, cell type and the nature of the cell's plasma membrane such as membrane fluidity, receptors, etc., can influence NP-cell membrane interactions and hence the uptake pathway. Several pathways for uptake may be used simultaneously, although with varying efficiency. Below we describe the common pathways by which NPs are internalized by cells.

5.2.1 Pinocytosis

Pinocytosis is the internalization of extracellular fluid and its content by cells and is subdivided into micro- or macropinocytosis, depending on the size of the cell-membrane invagination that traps the extracellular fluid. This pathway of cellular internalization of NPs can occur without direct interaction of NPs with the cell membrane because the bulk extracellular fluid is internalized [14]. However, NPs that interact with cell membranes have higher uptake through this mechanism than NPs that do not. Because of the small size of the cell membrane invaginations, pinocytosis is the predominant pathway for the uptake of large NPs and microparticles. Micropinocytosis occurs in almost all cells, whereas macropinocytosis occurs in specific cell types, e.g., immature dendritic cells [15, 16].

5.2.2 Clathrin-Mediated Endocytosis

Clathrin-mediated endocytosis (CME) is a cellular uptake mechanism that involves the formation of clathrin-coated endocytotic vesicles that are usually ~100 nm in diameter [17, 18]. Also known as receptor-mediated endocytosis, this uptake process is initiated by the binding of a ligand to its receptors on the cell membrane (Fig. 5.1). CME is the mechanism cells use to internalize ligand-conjugated NPs and it can be used to target NPs to specific cells [19, 20]. CME also becomes important when opsonins bind to NPs in a biological medium. An example is the opsonization of NPs by complement, that is, the group of proteins that are recognized by receptors on macrophages [21]. Another requirement to induce endocytosis is the size and amount of the cargo. It would take only a few large NPs to induce endocytosis, but cluster of many small NPs to induce CME [22].

5.2.3 Caveolae-Dependent Endocytosis

Caveolae are vesicles formed by cell-membrane invaginations that are 50–100 nm in diameter [23]. Caveolar vesicles enclose predominantly sphingolipids, cholesterol and caveolin (the predominant protein in caveolae) and bind to the associated protein to form microdomains, which dictate the cargo that is transported [24–26] (Fig. 5.1). These microdomains, which can con-

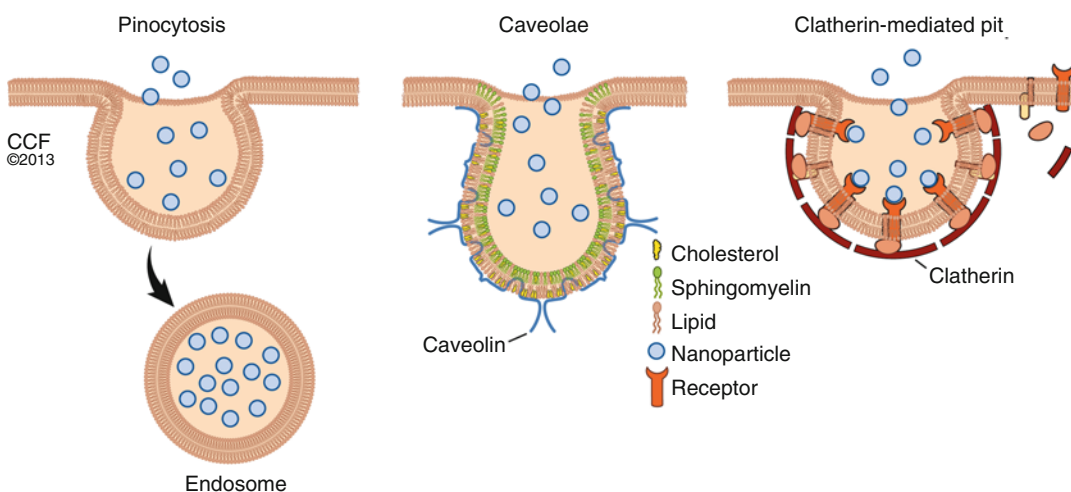**Fig. 5.1** Schematic of different cellular uptake mechanisms for NPs. The mechanisms of cellular uptake are determined by the physical characteristics of NPs. NPs with targeting ligands are generally internalized by clathrin-mediated endocytosis. Caveolae-mediated endocytosis is responsible for internalization of anionic NPs, whereas pinocytosis is the mechanism of choice for large NPs and microparticles

tain cationic lipids like sphingomyelin (whose polar domain contains an amine group), can interact with and mediate the endocytosis of anionic NPs like pegylated gold NPs where NP modified with polyethylene glycol [27, 28]. Caveolae-dependent endocytosis is the predominant pathway of uptake of NPs in endothelial and muscle cells [25, 29].

5.3   Interaction of NPs with Cells

5.3.1   Effect of Size and Shape of NPs on Cellular Uptake

The size of NPs influences their interaction with cell membranes and ultimately their intracellular uptake. NPs that are about 50 nm in diameter are generally taken up more rapidly by cells than larger NPs [30]. This preferential uptake of small NPs occurs because of the size of clathrin-coated pits and caveolar cell-membrane invaginations (50–200 nm in diameter) [31]. NPs smaller than 25 nm, on the other hand, may be too small, and hence large numbers are required to induce CME and caveolae-mediated endocytosis. For NPs smaller than 25 nm, pinocytosis is the preferred mechanism for uptake.

Although the size of NPs influences cellular uptake, this process is also influenced by cell type. Embryonic fibroblasts preferentially internalize single-walled nanotubes and gold NPs that are 25 nm rather than larger NPs. Epithelial cells, on the other hand, prefer 50 nm gold NPs over 25 nm or 70 nm gold NPs [27, 32]. These differences in cellular uptake are dependent on the predominant pathway for cellular uptake of each cell type. Cells in which cellular uptake is predominantly through macropinocytosis have a greater uptake of NPs >200 nm than cells processed via CME- or caveolae-dependent endocytosis.

Unlike inorganic NPs, which are relatively uniform in size, polymeric NPs, dendrimers and liposomes are polydisperse, which makes studying the impact of particle size on cellular uptake difficult [33]. This inherent polydispersity of polymeric NPs also affects our ability to predict the behavior of NPs interacting with cells.
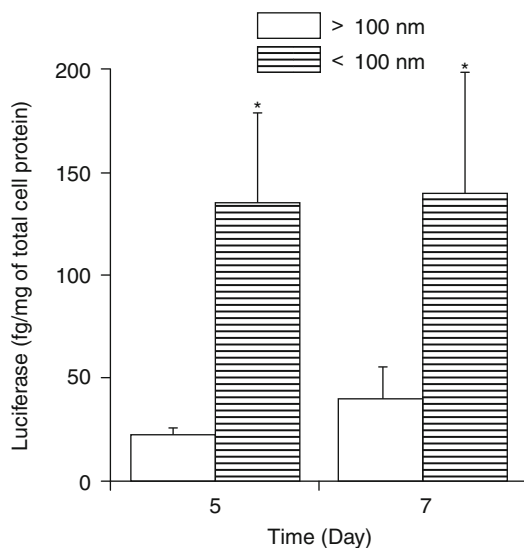

Fig. 5.2 Gene expression by small and large NPs fractionated from a single formulation in HEK-293 cells. The size of NPs influences the extent of gene expression. Cells transfected with NPs that are <100 nm in diameter have higher luciferase protein than cells transfected with NPs >100 nm (Reproduced with permission from Ref. [35]. Copyright 2002, Elsevier Ltd.)

However, even with these NPs, those with smaller mean particle size have a higher cellular uptake. An example is albumin NPs, where NPs with mean hydrodynamic diameters of 40 nm have greater cellular uptake than those with diameters of 100 nm [34]. Studies in our laboratory have also shown that NPs of <100 nm have greater transfection efficiency than larger (200 nm) NPs that were fractionated from the same formulation (Fig. 5.2). In this study, both NP populations showed similar uptake per weight, but the number of NPs internalized for the same weight would be greater for NPs of <100 nm than for NPs >200 nm, which could be the reason for higher gene expression with small NPs than with large ones [35]. The results thus suggest that NPs <100 nm are better for transfection than larger sized NPs.

When analyzing the cellular uptake of NPs on the basis of size, it is also important to determine the propensity of NPs to aggregate. Although most cellular uptake studies assume that cells interact with single NPs, some NP formulations (particularly those with a cationic surface charge)

aggregate in the presence of protein, making NP aggregation an important factor to consider when studying cellular uptake [36].

The shape of NPs influences how easily they are taken into cells, with rod-shaped gold NPs having a lower cellular uptake than spherical ones [37]. Among NPs of similar surface charge and diameters, the aspect ratio (AR), which defines the proportion between width and height of NPs, is more significant than size in predicting cellular uptake. NPs with an AR of 4 have been shown to have lower uptake by cells than those with ARs of 1 or 2 [27, 38]. These differences are explained by the kinetics of cellular uptake. It takes longer for the cell membrane to wrap around rod-shaped NPs than spherical NPs, and more rod-shaped NPs are required to induce endocytosis, in contrast to spherical NPs [7].

5.3.2 Effect of Surface Characteristics and Charge of NPs on Cellular Uptake

Surface characteristics of NPs can significantly influence their interactions with the cell membrane and hence their internalization pathways [39]. Surface characteristics and charge can influence (1) NP interactions with an anionic cell membrane [40] and (2) adsorption of proteins onto NPs, both of which affect NP-cell membrane interaction [3, 41–43]. A cell membrane is anionic because of the anionic head group of phospholipids and the presence of carbohydrates such as sialic acid [44, 45]. Even with their anionic surface charge, NPs interact with cell membranes and are taken up by different cells. This is because of interactions of anionic NPs with cationic lipid domains in the cell membrane [24, 46]. Because anionic NPs interact with lipid domains, their uptake usually involves caveolae-mediated endocytosis and not the classical CME pathway.

Much less studied aspects of cellular uptake of NPs are the roles of adsorbed proteins on anionic NPs and their role in cellular uptake. Opsonins such as complement and immunoglobulins adsorb onto anionic NPs and induce cellular uptake by CME instead of caveolae-mediated uptake [47]. The surface charge on NPs is conferred by the surface chemistry, and the nature of the chemical groups coating the NPs can influence NP-cell interaction [43]. Dimercaptosuccinic- and heparin-coated NPs both have anionic surface charges but show different interactions with cell membrane and subsequent uptake [48, 49].

Neutral NPs exhibit limited cellular uptake and are useful in applications where nonspecific interactions of NPs with cells and their subsequent cellular uptake is not desired. Modifying NPs with hydroxyl functional groups can attain a neutral surface charge [50]. The use of zwitterions can also impact neutral surface charge onto NPs [51]. These modifications decrease the interaction of NPs with plasma membrane and ultimately decrease cellular uptake.

Unlike anionic NPs, cationic NPs can directly bind to a cell's negatively charged plasma membrane [52]. This binding can be to the anionic head group of lipids or to other negatively charged groups on the cell membrane, such as monosaccharide sialic acid. Once they interact with the cell membrane, cationic NPs can induce internalization by CME. Because of their interaction with cell membranes and rapid endocytosis, cationic NPs serve as the basic platform for gene delivery and other applications that require rapid cellular internalization [50, 53, 54]. To obtain a cationic charge, positively charged polymers like chitosan and cationic emulsifiers like didodecyldimethylammonium bromide (DMAB) are being used in NP formulations [55, 56].

The molecular structure of surface modifiers also plays important roles in cellular interaction and uptake of NPs. A classic example is with cationic NPs; it is generally thought that it is the cationic surface charge of NPs that causes their interaction with the cell membrane. However, recent studies in our laboratory have shown that the molecular structure of the cationic surface modifier also influences interactions with the cell membrane and NP uptake. NPs modified with dichain cationic emulsifiers, DMAB, or single-chain cetyltrimethylammonium bromide (CTAB) and dodecyltrimethylammonium bromide (DTAB) showed different interactions with model
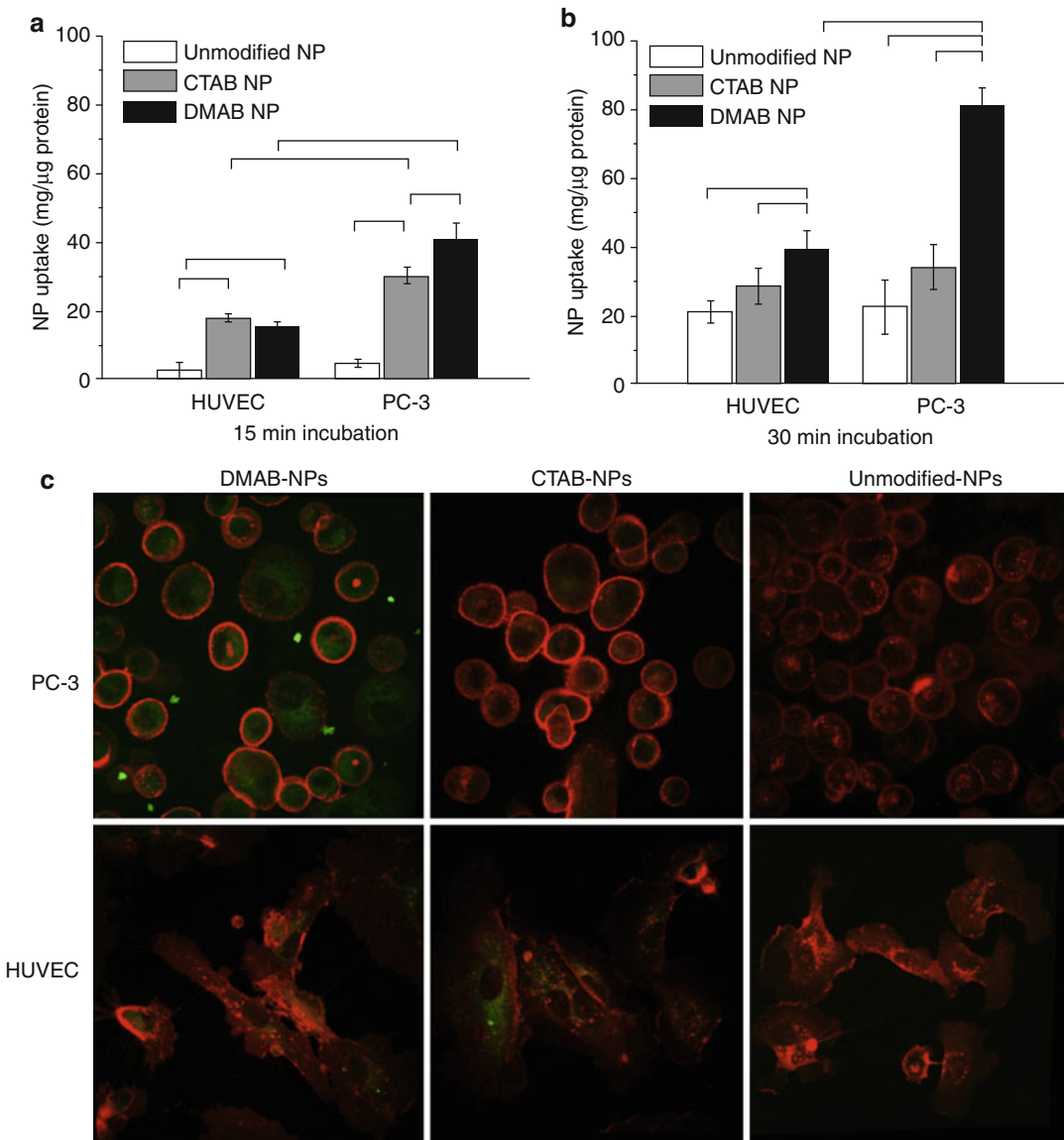
Fig. 5.3 The molecular structure of surfactants at the NP-cell interface influences cellular uptake of NPs, which is also cell-line dependent. Cellular uptake of unmodified, DMAB- and CTAB-modified NPs by human umbilical vascular endothelial cells and prostate cancer (PC-3) cells after 15 min (**a**) and 30 min (**b**) of incubation. (**c**) Confocal microscopy images of human umbilical vascular endothelial cells and PC-3 cells 30 min after incubation, with NPs with green and red representing NPs and cell membranes, respectively (Reproduced with permission from Ref. [59]. Copyright 2013, Elsevier Ltd.)

cell membranes. Dichain DMAB-modified NPs exhibited greater interaction and cellular uptake than single-chain, CTAB- or DTAB-modified NPs, although both formulations have a similar cationic zeta potential (Fig. 5.3). It has been proposed that DMAB, with its two hydrophobic chains, engages in greater interaction with the cell membrane than the single chains of CTAB and DTAB. Recently, we demonstrated that DMAB-modified NPs have greater biophysical interactions with prostate cancer cell-membrane lipids than normal human umbilical vascular

epithelial cell-membrane lipids. This selectivity of interaction leads to greater efficacy with p53 gene-loaded DMAB-modified NPs than unmodified NPs in tumor growth inhibition in a prostate cancer model [57–59].

5.3.3   Effect of Active Targeting on Cellular Uptake

To aid cellular internalization of NPs, particularly those with anionic and neutral surface charges, several targeting ligands have been used [60]. These ligands, e.g., transferrin, bind to receptors in the cell membrane and induce CME [61]. Because this method depends on the presence and number of target receptors, efficiency of targeted NPs is cell dependent and allows investigators to target specific cells in which receptors are overexpressed. In prostate cancer cells that overexpress transferrin receptors, transferrin-conjugated NPs demonstrate greater cellular uptake and are efficacious at inhibiting the growth of prostate tumors. In our studies, transferrin-conjugated NPs not only demonstrated greater cellular uptake but also showed sustained intracellular retention. Furthermore, direct intratumoral injection of paclitaxel-loaded transferrin-conjugated NPs demonstrated significantly greater tumor growth inhibition compared with unconjugated NPs, suggesting a greater degree of intratumoral retention of conjugated than unconjugated NPs, presumably due to interactions of conjugated NPs with transferrin receptors [62, 63] (Fig. 5.4).

Cell-penetrating peptides (CPPs), which facilitate cellular internalization of peptide-modified NPs, do not depend on receptors for cellular internalization. CPPs are rich in the positively charged amino acids arginine and histidine, which allows them to directly penetrate the cell membrane and become internalized [64]. However, because CPPs do not depend on receptors, they may not be cell specific [65]. An example of such CPPs is *trans*-activating transcriptional activator (TAT) peptide, derived from human immunodeficiency virus (HIV), which has shown efficacy in transporting NPs into different cells
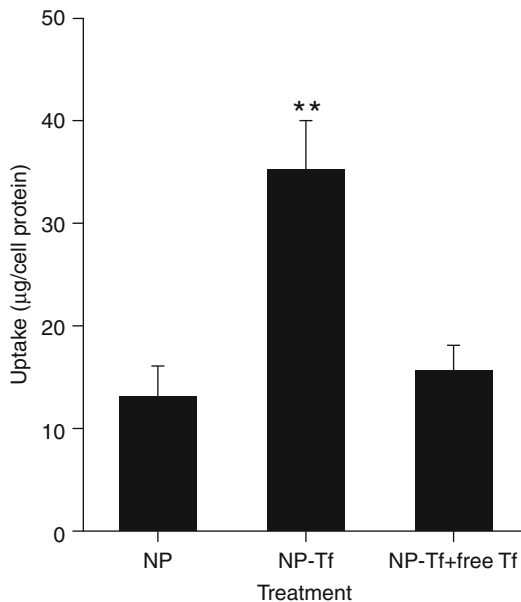

Fig. 5.4 Uptake of transferrin-conjugated and -unconjugated NPs by prostate cancer (PC-3) cells. Transferrin-conjugated NPs show greater cellular uptake than unconjugated NPs. Uptake of conjugated NPs is inhibited in the presence of an excess of free transferrin ligand, confirming uptake of transferrin-conjugated NPs is via receptor-mediated endocytosis brought about by transferrin receptors that are overexpressed on PC-3 cells (Reproduced with permission from Ref. [62]. Copyright 2004, John Wiley and Sons)

[66]. TAT-peptide-conjugated NPs have been particularly effective in transporting NPs into the brain, as they can cross the blood–brain barrier [67, 68].

In a similar manner as untargeted NPs, cellular uptake of conjugated NPs is affected by the size of NPs. Antibody-conjugated NPs of 25–50 nm in diameter have a higher cellular uptake than larger NPs [69]. For CPP-conjugated NPs, which directly penetrate the cell membrane, the effect of size becomes particularly significant as size increases [70]. This size limitation is due to the size of the clathrin-coated vesicles involved in their internalization.

Apart from NP size and the number of targeting ligands on NPs, the shape of NPs can influence their cellular uptake. In breast cancer cells that overexpress the *HER2/neu* receptor, nontargeted spherical NPs have been reported to show higher cellular uptake than rod- and

disk-shaped NPs, whereas when modified with antibodies to *HER2/neu*, nanodisks and nanorods show higher uptake than nanospheres [71]. This and other studies demonstrate that the shape of NPs can enhance cellular uptake of targeted NPs [72].

Despite the effectiveness of active targeting, NPs can be rendered ineffective when they are introduced into a biological medium. Depending on the physical characteristics of NPs, their surfaces (including conjugated ligands) can be covered with opsonins, making the ligand ineffective at initiating cellular internalization. This drawback can be overcome by using a linker to move the targeting ligand from the NP surface and away from the opsonins. The issue could also be overcome by designing NPs that are less opsonized [73].

5.4 Techniques for Studying NP-Cell Interaction and Cellular Uptake

5.4.1 Models for NP-Cell Interaction and Cellular Uptake

Understanding NP-cell interactions is important for designing NPs that either escape cellular uptake or are taken up efficiently by cells, depending on their applications. Studying this interaction is very difficult in whole-cell systems. Thus, different techniques using model cell membranes have been developed.

5.4.1.1 Lipid Monolayer
This method involves forming a lipid monolayer on an aqueous medium in a Langmuir-Blodgett instrument. Studies using this technique provide information about how strongly NPs interact with the head group of the lipids. Use of this method also helps determine if NPs will disrupt the cell membrane to enter the cell. When used in conjunction with atomic force microscopy (AFM), films from Langmuir-Blodgett interactions can identify interaction of NPs with lipid domains in the cell membrane [74, 75].

5.4.1.2 Supported Lipid Bilayers
A lipid bilayer can be formed with mica or silica wafers as a substrate or support to study interactions with NPs and drugs. The interaction between the lipid bilayer and drug/NP can be analyzed with AFM or other analytical techniques such as Fourier transform infrared resonance and X-ray photoelectron spectroscopy [76].

5.4.1.3 Liposomes
Liposomes are lipid vesicles formed to exclude the hydrophobic tails of lipids from aqueous phases and can be unilammelar or multilammelar. Multilammelar liposomes with two layers best mimic the cell membrane and are useful for studying the permeability of different NPs into the cell membrane. In conjunction with spectroscopic methods, the efficiency of NPs to cross lipid bilayers can be studied systematically [77].

5.4.2 Techniques for Studying Cellular Uptake

Several techniques are used to monitor the cellular uptake of NPs. Most of these are imaging or spectroscopic techniques that determine the cytoplasmic localization of NPs. To study the mechanism for uptake of NPs, various inhibitors of pathways of uptake have been used. These inhibitors help to elucidate different pathways cells use to internalize NPs and how the predominant pathway can change vis-à-vis the physical characteristics of NPs. A few of the commonly used inhibitors and the pathways/mechanisms they block are listed in Table 5.1. The NP uptake study is carried out at 4 °C or in the presence of metabolic inhibitors to determine if the uptake process is energy dependent, such as via endocytosis.

5.5 Intracellular Localization of NPs

Following cellular uptake of NPs, the next important question is where the NPs localize within cells. Where they finally localize affects the ther-

Table 5.1 Commonly used inhibitors to study mechanisms of NP uptake

| Name of inhibitor	Pathway inhibited	Uptake mechanism(s) affected
Nocodazole	Polymerization of microtubule	Clathrin-mediated endocytosis [78]
Cytochalasin A	Polymerization of actin	Caveolae-mediated endocytosis [79]
Chlorpromazine	Reversible translocation of clathrin from cell membrane	Clathrin-mediated endocytosis [80]
Genistein	Tyrosine kinase inhibitor	Caveolae-mediated endocytosis [81]
Lovastatin	Cholesterol synthesis	Clathrin- and caveolae-mediated endocytosis and macropinocytosis [22]

apeutic/medical function of NPs, as well as cytotoxicity. After endocytosis, NPs are typically contained within endosomal vesicles, which have an internal pH of ~5 [82]; these vesicles mature into late endosomes before fusing with lysosomes, at which point they are subjected to digestive enzymes and degradation. This process limits the effective delivery of many therapeutic agents to intracellular targets, other than the lysosomes. Therefore, endosomal escape is often a critical step in intracellular trafficking of NPs and subsequent targeting to appropriate subcellular compartment(s). Intracellular targets include the cytoplasm (to deliver, for example, small interfering RNAs [siRNAs] or glucocorticoids), the nucleus (for delivery of DNA and DNA-intercalating agents, such as doxorubicin), mitochondria (anti-oxidants or mitochondrial DNA), or other compartments.

5.5.1 Strategies for Endolysosomal Escape of NPs

Mechanisms of endolysosomal escape must be strategically designed into NPs. A widely used approach takes advantage of the "proton-sponge effect," which involves NPs having a high buffering capacity and the flexibility to swell when protonated. This is the typical mechanism via which cationic polymers, such as polyamines (polyethylenimine and polylysine are among the most common) escape the endosomal compartment [50, 54, 83]. These polymers have a strong buffering capacity, in the pH 5–7 range, and thereby prevent acidification of the endosomes by acting as "proton sponges." Protonation induces the flow of ions (protons and Cl⁻) and water (osmotic

swelling) into the endosome, which subsequently causes rupture of the endosomal membrane and release of the polymeric complexes/NPs.

An extension of the proton-sponge effect is the "umbrella effect," whereby the polymer unfolds from a collapsed to an extended state upon protonation at low pH (pH 5–6). The resulting increase in volume and space contributes to endosomal escape of the NP [83, 84]. NPs formulated from cationic lipids (lipoplexes) are able to escape from endosomes due to their interactions with the anionic phospholipids of endosome membranes. When lipoplexes are endocytosed, an electrostatic interaction occurs between the lipids of the lipoplex and the anionic lipids of endosomes facing the monolayer of the endosome, which consequently destabilizes the endosomal membrane by causing it to flip-flop. The cargo of the lipoplex is then released into the cytoplasm. This process can be controlled and enhanced based on the molecular structure of the lipids used in the lipoplex and the presence of lipids that facilitate the adoption of a nonbilayer structure (for example, dioleoylphosphatidylethanolamine and cholesterol) [83]. The use of cationic NPs is limited by their cytotoxicity, which relates to their mechanisms of entry into the cell as well as endosomal escape. Cationic NPs cause more pronounced disruption of the plasma membrane as well as mitochondrial and lysosomal damage compared with anionic NPs [50]. The strategy used by NPs formulated from cationic lipids is also employed by anionic NPs capable of charge reversal in the acidic endolysosome. In our study, we demonstrated that poly (D, L-lactide co-glycolide) (PLGA) NPs, which are anionic at physiologic pH (pH 7.4), undergo charge reversal in acidic pH of endosomes (pH ~5) and become
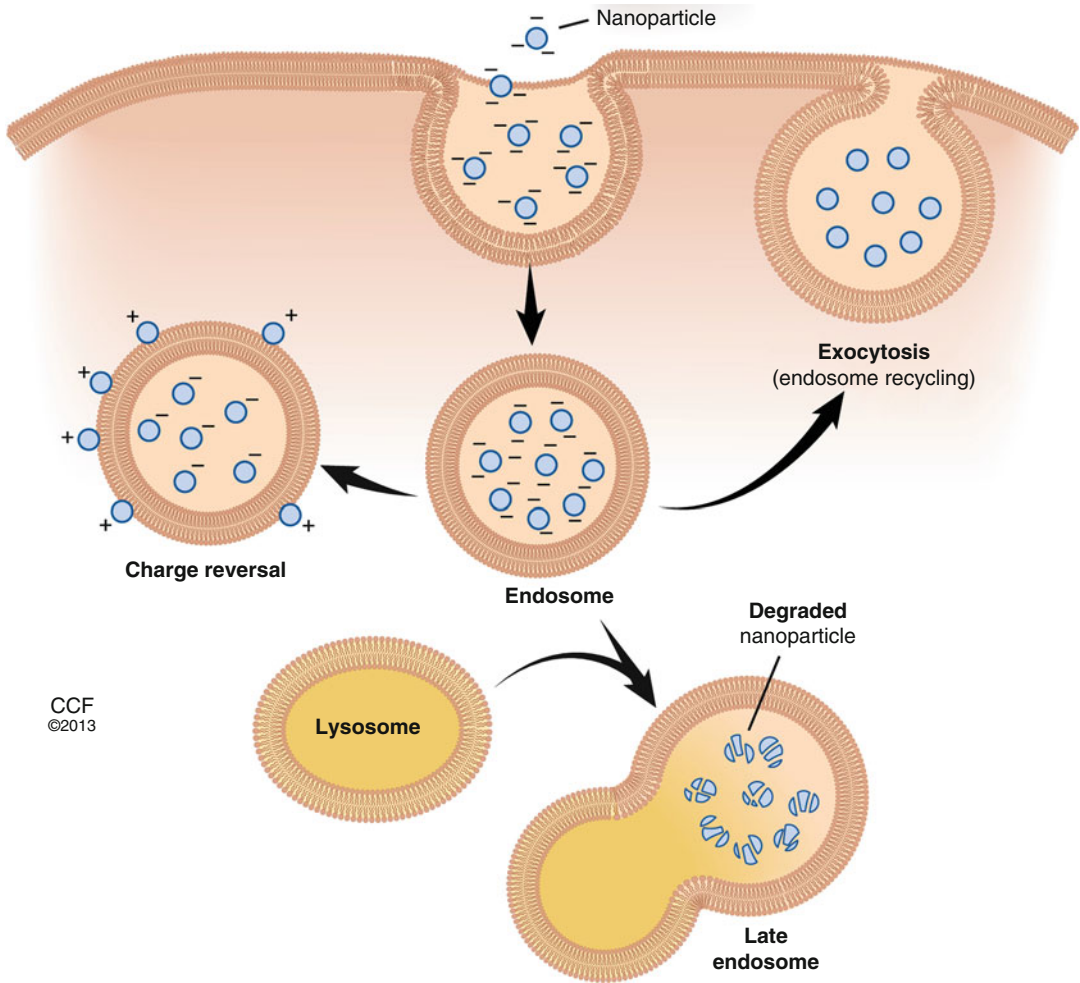
Fig. 5.5 Schematic of intracellular uptake and endo-somal escape of NPs, depicting charge reversal in acidic pH (pH ~5) of endosomes. NPs that exhibit a pH-dependent charge reversal, such as poly (D, L-lactide *co*-gly-colide) (PLGA) NPs, can escape the endosome by charge reversal. In the acidic condition of the secondary endosomes, anionic PLGA-NPs become cationic and interact with endosomal lipids, allowing their escape

cationic. This selective cationization of NPs in endosomes causes NPs to interact with the anionic endosomal membrane and escape into the cytoplasm. In that study, we demonstrated NP localization into the cytoplasmic compartment at as early as 10 min following incubation of cells with NPs, suggesting their rapid endosomal escape [85] (Fig. 5.5).

Agents that enhance endosomal escape, based on those employed by viruses and bacteria, have been used by researchers in the formulation of NPs. Fusogenic peptides have been incorporated onto NPs and used to destabilize the endosomal membrane. Membrane fusion plays an important role in cellular trafficking and endocytosis. Many viruses have membrane peptides, which undergo conformational change in response to a change in pH. These conformational changes allow the viral membrane to fuse with cellular membranes, including the lipid bilayer (for cell entry), as well as endosomal membranes (for endosomal escape). For example, fusogenic peptides derived from the influenza virus have been used to enhance endosomal escape of lipid and poly-meric carriers for delivery of nucleic acids [86–89].

Another mechanism inspired by viruses and bacteria involves the formation of pores in the endosomal membrane. Pore formation is based on the interplay between membrane tension, which enlarges the pore, and line tension, which closes the pore. Peptides that bind to the edges of pores loosen the internal membrane tension and stabilize pores in the membrane. This process can be induced by cationic amphiphilic peptides such as melittin and cecropin B [90–92]. HIV utilizes the transmembrane protein gp41 and the HIV-1 TAT gene product protein to facilitate endosomal escape, although the exact mechanisms are not well understood. The role of gp41 may be fusogenic or pore forming [83].

Photochemicals, either alone or incorporated into NPs, can be used to disrupt the endosomal membrane upon exposure to light. Photosensitizers, such as meso-tetra (4-sulfonatophenyl) porphine (TPPS4), disulfonated meso-tetraphenylporphine (TPPS2a), aluminum phthalocyanine disulfonate (AlPcS2a), and dendrimerphthalocyanine (Dpc), localize into the membranes of endosomes and lysosomes. After light exposure, these chemicals form short-lived reactive singlet oxygen, which destroys the endosomal/lysosomal membrane and enables the contents of the organelles to be delivered to the cytosol [93, 94].

5.5.2 Cytoplasmic Transport of NPs

The cell cytoplasm is a crowded molecular environment. It contains various macromolecules, the mesh-like cytoskeleton, and many embedded organelles. NPs and large macromolecules have limited diffusion within the cytoplasm. Endogenous proteins, organelles, and vesicles are actively transported along the cytoskeletal network, predominantly via microtubules (MTs) [95, 96]. The transport of endocytotic vesicles is organized by a network of MTs, which radiates from an MT organizing center (MTOC) near the nucleus toward the periphery of the cell. Transport along a MT is mediated by motor proteins such as dynein and kinesin. NPs that incorporate mechanisms to facilitate MT transport (for example, by using ligands with high affinity to dynein, a molecular motor protein responsible for transporting cargo along cytoskeletal microtubules) may be more successful in active transport through the cytoplasm.

5.5.3 Cytoplasmic Targeting of NPs

In some cases, the goal may be to deliver NPs to the cytoplasm itself because the site of action for a given therapeutic (e.g., glucorcorticoids, such as dexamethasone) is located there. Glucocorticoid receptors are located in the cytoplasm; therefore, by delivering the drug at/near its receptor site, a better therapeutic effect may be achieved while minimizing undesirable side effects. Previously, we have demonstrated a sustained antiproliferative effect of dexamethasone-loaded NPs in vascular smooth muscle cells compared with dexamethasone alone, which showed only a transitory effect. Dexamethasone-loaded NPs acted as an intracellular depot, sustaining the antiproliferative effect because of binding of the drug to glucocorticoid receptors present in the cytoplasm [97].

RNA interference (RNAi) also takes place in the cytoplasm. The delivery of siRNAs, for example, has been an area of active research for silencing the expression of genes associated with disease. RNAi oligonucleotides are introduced into cells, cleaved by dicer proteins into siRNAs, and incorporated into the RNA-induced silencing complex (RISC), which then mediates mRNA sequence-specific binding and cleavage to halt transcription of the mRNA into protein [98]. This process occurs within the cytoplasm, although the exact location of the RISC within the cytoplasm is not known. NPs, liposomes, lipoplexes, and polyplexes have been shown to improve the *in vivo* stability, target specificity, and cell and tissue uptake of encapsulated RNAi oligonucleotides [99]. After escaping the endosomes, the nanocarrier must release the siRNA into the cytosol, where it can then interact with the dicer and/or RISC. A better understanding of the location of the RISC within the cytoplasm may lead to further advancements in
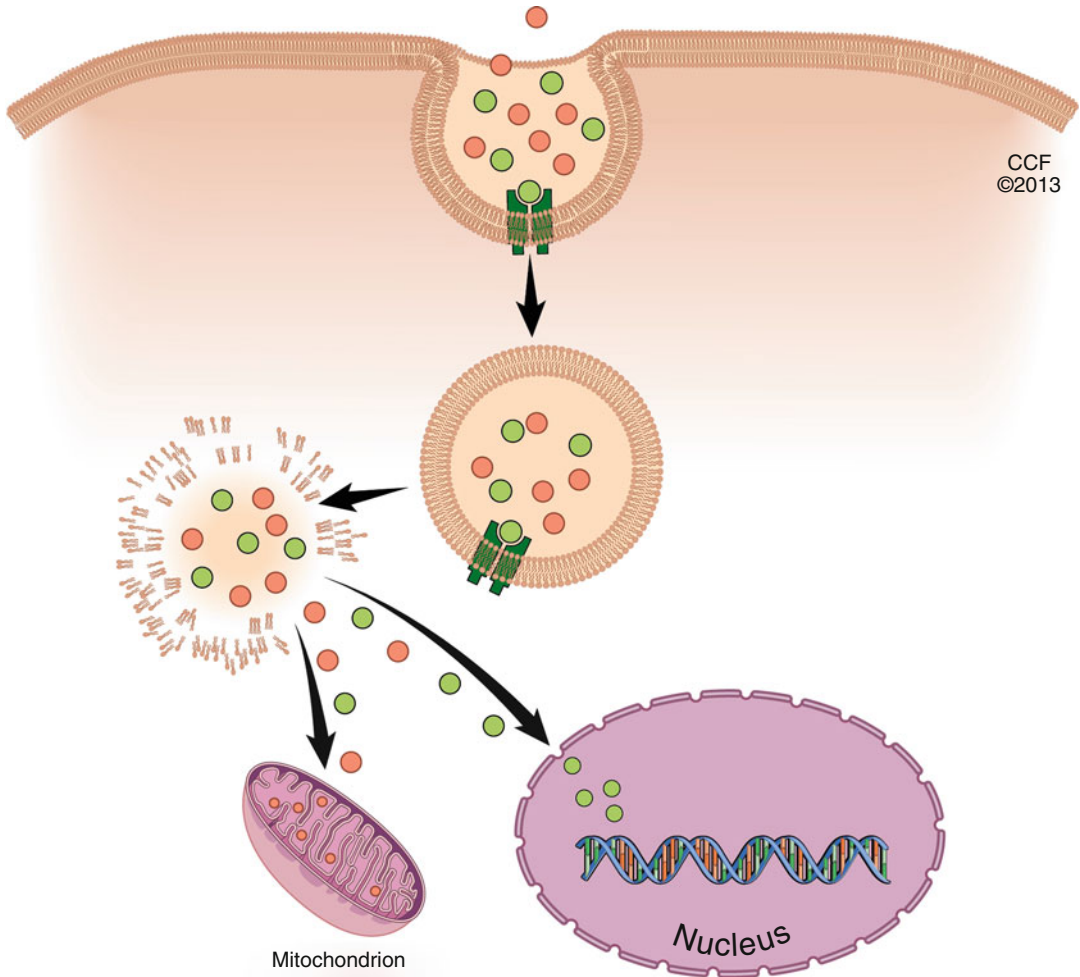
Fig. 5.6 Intracellular trafficking of NPs. Depending on the physical characteristics or presence of a targeting ligand, NPs target different intracellular organelles after endosomal escape into the cytoplasm. NPs that are modi-fied with mitochondriotropic agents localize in the mito-chondria, whereas NPs conjugated with nuclear localization signals are transported into the nucleus

intracellular targeting of nanocarriers for RNAi technology.

5.5.4 Nuclear Localization

Nuclear localization of NPs is important for the delivery of therapeutic genes or drugs whose target is the nucleus/DNA. NPs that localize in the perinuclear region have a greater chance of entering the nucleus or having the payload diffuse into the nucleus. Therefore, ideally, NPs must escape from the late endosomes before fusion with the lysosomes. NPs that escape from early endosomes, close to the cell membrane, have to travel the longest distance to get to the nucleus. The nuclear envelope acts as a barrier to the entry of molecules into the nucleus. Entry into the nucleus can occur either by passive or active transport through nuclear pore complexes (Fig. 5.6). Small molecules (<45 kDa) can diffuse freely through the nuclear membrane, whereas larger ones require a nuclear localization signal (NLS) peptide. NLSs are peptides with no general consensus sequence; they are mostly comprised of basic amino acids. Incorporation of NLSs onto NPs has been some-

what successful in improving delivery of NPs to the nucleus [100]. Several NP formulations have demonstrated the ability of NPs to localize in the perinuclear area [101, 102]. This ability may facilitate delivery of the payload to the nucleus, even if the NPs themselves do not actually enter the nucleus. In some cases, NPs have been visualized entering the nucleus [103], which may be more effective for delivery of nuclear targeted drugs/nucleic acids. Nuclear entry of nanocarriers may also be possible during mitosis, when the nuclear envelope temporarily becomes disassembled.

5.5.5   Mitochondria and Other Organelles

Targeting therapeutic agents to the mitochondria is a method that is gaining attention for the treatment of diseases such as diabetes, ischemia-reperfusion injury, cancer, and neurodegenerative diseases. The primary role of mitochondria is energy production for the cell via the electron transport chain, which is crucial for normal cell function and hence body function. Mitochondria also play key roles in regulating cell death and generating reactive oxygen species (ROS) [104]. Mitochondrial dysfunction contributes to a number of diseases, including those mentioned above [105]. As a result, there is increasing interest in drug/therapeutic targeting to the mitochondria for both cytoprotective and cytotoxic applications. Mitochondrial delivery is possible by exploiting some of the inherent characteristics of the organelle. The inner membrane of mitochondria is hydrophobic and anionic, with a high membrane potential (approximately −200 mV) [106]. As a result, lipophilic cations have a tendency to accumulate inside the mitochondrial membrane in response to the membrane potential and are referred to as mitochondriotropics (Fig. 5.6). Triphenylphosphonium (TTP) is one example of a mitochondriotropic moiety that has been incorporated onto the surface of NPs such as liposomes for enhancing mitochondrial accumulation [107, 108]. These systems are under investigation for mitochondrial gene therapy and for anticancer chemotherapy.

In the field of nanocarriers for mitochondrial drug targeting, the majority of approaches use cationic liposomes prepared from trimethylaminoethane carbamoyl cholesterol iodide (TMAEC-Chol) or dequalinium (DQAsomes), as well as branched polyethylenimine (PEI) to delivery peptide-DNA conjugates or micelles. Liposomes are able to fuse with the mitochondria membranes to deliver their cargo. Dequalinium liposomes have been used to bind or entrap drugs such as paclitaxel (a common chemotherapeutic agent) and DNA and transport them to the mitochondria.

Another inherent characteristic of mitochondria that may be used for targeting is their protein import machinery. Although mitochondria have their own DNA, the majority of proteins required by mitochondria are encoded by nuclear DNA. The proteins destined for mitochondria possess a mitochondrial localization signal or mitochondrial targeting signal, which enables them to be delivered to the mitochondria via mitochondrial protein import machinery. It is conceivable that MTS conjugated to nanocarriers could facilitate transport into the mitochondria; however, there are limits to the size of the cargo or carrier that could be delivered via this mechanism.

NP surface chemistry has been shown to affect intracellular localization of NPs. Carboxylate-functionalized polystyrene NPs were found to localize to the mitochondria, whereas plain polystyrene NPs and silica NPs accumulated at reticular and vesicular structures, as well as in the perinuclear region [109].

5.5.6   Methods for Studying Intracellular Tracking of NPs

Evaluating the intracellular location of NPs may be done via a number of microscopic techniques. NPs labeled with fluorescent dye can be visualized intracellularly (in live or fixed cells) using confocal microscopy [110]. Dyes can also be used to label intracellular structures to evaluate where the NPs are in relation to them. For example, LysoTracker Red dye emits red fluorescence in the acidic vesicles of the cell and therefore is

used as a marker of late endolysosomes. This dye process can therefore be a useful tool for distinguishing whether NPs colocalize within the endolysosome or whether they are able to escape the endolysosome into the cytoplasm [110]. Fluorescence recovery after photobleaching has been used to characterize NP transport and dynamics within the cell [111].

5.6   Cytotoxicity of NPs

NP size, charge, surface chemistry, shape, and structure (e.g., porosity, flexibility) can affect the manner in which NPs interact with biological environment and ultimately determine the potential for cytotoxicity. Numerous methods are used to evaluate cytotoxicity both *in vitro* and *in vivo*.

Advantages of the use of *in vitro* systems comprising cell lines for studying cytotoxicity include (1) the ability to determine the primary effects of NPs on target cells in the absence of secondary effects caused by inflammation; (2) the ability to identify primary mechanisms of toxicity in the absence of physiological and compensatory factors that may confound interpretation in whole animals; (3) efficiency, rapidity, and cost-effectiveness; and (4) facilitation/improvements in the design of subsequent whole-animal studies [112]. *In vitro* assays include the following: (1) Assays for cell viability/proliferation (e.g., thiazoylyl blue (3-[4,5-dimethylthiazol-2-yl]-2,5- diphenyltetrazolium bromide); (2) Mechanistic assays (generation of reactive oxygen species/oxidative stress, apoptosis, necrosis, DNA damage); (3) Microscopic evaluation of intracellular localization (scanning or transmission electron microscopy, video-enhanced differential interference contrast microscopy, AFM, fluorescence spectroscopy, magnetic resonance imaging); (4) Gene expression analysis (high-throughput systems); (5) Hemolysis (evaluates the impact of NPs on human red blood cells by quantifying the release of hemoglobin); and (6) Genotoxicity assays.

Although most cytotoxicity studies for NPs are conducted *in vitro*, they are limited in their ability to recapitulate the complexity of the *in vivo* environment. Acute toxicity studies are conducted to identify the "maximum tolerated dose" and "no observable effect level" of NP dosage. The following parameters are typically monitored in experimental rodent models:

- **Response to administered dose**: Shortly after administration of NPs (<30 min), hematological, cardiac, and neurological responses can occur.
- **Weight change**: This simple and feasible outcome measure is a sensitive indicator of overall animal health, although it is not specific. Further investigation of weight loss is required to determine cause of toxicity and target tissues/organs involved.
- **Clinical observation**: The functioning of organ systems may be evaluated based on clinical changes. For example, cardiovascular system function can be evaluated by the presence of cyanosis of tail, mouth, or footpads; vasodilation can be assessed by redness of skin and vasoconstriction by coldness of body. Respiratory effects manifest as dyspnea (shortness of breath). Gastrointestinal function may be assessed by amount of food consumed and quality of droppings. Imaging procedures, such as ultrasound, X-ray, computed tomography, and magnetic resonance imaging, may also be used to evaluate specific organ toxicity.
- **Mortality**: To ensure humane and ethical use of animals, animals should be euthanized if severe side effects are observed and the animal is not recovering.
- **Clinical pathology**: Analysis of blood and plasma to check blood counts and functioning of liver, kidney, heart, and the endocrine and exocrine systems.
- **Gross necropsy**: This step includes gross examination of each major organ and determination of organ weights, followed by histopathology for signs of toxicity.

Subacute toxicity studies are an extension of acute toxicity evaluation and are generally tailored to detect adverse effects that develop over 4–5 weeks (vs. 2 weeks for acute studies). NPs have distinct pharmacokinetic patterns compared with classic small-molecule drugs. NPs tend to

have longer blood circulation times and tend to localize in the liver and spleen. Understanding the pharmacokinetics of NPs is important to assessing toxicity. Quantification of NPs in organs of the reticuloendothelial system (liver, spleen, bone marrow, lymph nodes, and intestinal Peyer's patches) is of particular importance, due to the tendency of NPs to accumulate in these tissues. *In vivo* tracking of NPs is commonly done using radiolabelling, although other methods such as optical imaging are also used [6, 33, 113–115].

NPs that are not biodegradable, including metal oxides such as gold, carbon, and silica NPs, require longer periods of observation for subchronic (~13 weeks) and chronic toxicity (18–30 months). Such studies typically involve repeated exposures of the NPs under investigation. In addition to the parameters already discussed, ophthalmological examination, cardiac function, neurotoxicology, and immunotoxicology are also evaluated.

The following section describes the impact of NP properties on *in vivo* toxicity. Size and surface charge impact the cytotoxicity of NPs. Amine-terminated poly (amidoamine) dendrimers demonstrated greater *in vivo* toxicity (as determined by maximum tolerated dose) compared with carboxyl- and hydroxyl-terminated poly(amidoamine) dendrimers [116, 117]. The observed toxicity was related to an intravascular coagulation-like condition and hemolysis [118]. In addition, amine-terminated dendrimers were found to accumulate almost entirely in the liver, while carboxyl- and hydroxyl-terminated dendrimers demonstrated greater circulation time and renal clearance. Toxicity was not size dependent; therefore, it was likely related to increased protein opsonization. Size, however, did affect the toxicity of silica NPs (SNPs). For example, 50 nm SNPs were well tolerated *in vivo*; however, 200-nm SNPs with similar surface chemistry were six times less tolerated [116]. In this case, toxicity was determined to be due to embolization in the lungs, which occurred to a greater extent with larger SNPs. These studies indicate that the inherent material properties of the NPs used determine their size-related toxicity. Dendrimers are more flexible nanostructures with hollow spaces that offer less resistance to blood flow compared with silica NPs. This characteristic may also explain why mesoporous SNPs are better tolerated than nonporous SNPs. The response of the biological environment and protein interactions to NPs may vary greatly with the porosity of the NP, since pores allow for different molecular arrangements.

5.7 Concluding Statement

Making generalizations about NP-cell membrane interactions and their potential therapeutic impact or toxicity is difficult because of the use of different NPs, each one with unique features, and variations in cell membrane properties, which differ between tissues and depending on disease conditions. In addition, the same NPs could be used for different applications. It is quite clear that there cannot be a single NP formulation that would work for all applications or in many disease conditions. In this regard, computer simulation and models are being developed that can help in making certain predictions on NP-cell interactions and NP efficacy and potential toxicity. It is also important to correlate the *in vitro* findings to translation *in vivo*. With better understanding and background knowledge on NP-cell interactions, one could more confidently develop a strategy in designing effective NPs for biomedical applications.

References

1. Soppimath KS, Aminabhavi TM, Kulkarni AR, Rudzinski WE (2001) Biodegradable polymeric nanoparticles as drug delivery devices. J Control Release 70(1–2):1–20
2. Labhasetwar V, Song C, Levy RJ (1997) Nanoparticle drug delivery system for restenosis. Adv Drug Deliv Rev 24(1):63–85
3. Cognet L, Tardin C, Boyer D, Choquet D, Tamarat P, Lounis B (2003) Single metallic nanoparticle imaging for protein detection in cells. Proc Natl Acad Sci U S A 100(20):11350–11355
4. Hwang DW, Song IC, Lee DS, Kim S (2010) Smart magnetic fluorescent nanoparticle imaging probes to monitor microRNAs. Small 6(1):81–88
5. Sundaram S, Roy SK, Ambati BK, Kompella UB (2009) Surface-functionalized nanoparticles for tar-

geted gene delivery across nasal respiratory epithelium. FASEB J 23(11):3752–3765

6. Rabin O, Manuel Perez J, Grimm J, Wojtkiewicz G, Weissleder R (2006) An X-ray computed tomography imaging agent based on long-circulating bismuth sulphide nanoparticles. Nat Mater 5(2):118–122

7. Verma A, Stellacci F (2010) Effect of surface properties on nanoparticle–cell interactions. Small 6(1):12–21

8. Nel AE, Mädler L, Velegol D et al (2009) Understanding biophysicochemical interactions at the nano-bio interface. Nat Mater 8(7):543–557

9. MailäNder V, Landfester K (2009) Interaction of nanoparticles with cells. Biomacromolecules 10(9):2379–2400

10. Zhang Y, Kohler N, Zhang M (2002) Surface modification of superparamagnetic magnetite nanoparticles and their intracellular uptake. Biomaterials 23(7):1553–1561

11. Nativo P, Prior IA, Brust M (2008) Uptake and intracellular fate of surface-modified gold nanoparticles. ACS Nano 2(8):1639–1644

12. Slowing I, Trewyn BG, Lin VSY (2006) Effect of surface functionalization of MCM-41-type mesoporous silica nanoparticles on the endocytosis by human cancer cells. J Am Chem Soc 128(46): 14792–14793

13. Zhao F, Zhao Y, Liu Y, Chang X, Chen C, Zhao Y (2011) Cellular uptake, intracellular trafficking, and cytotoxicity of nanomaterials. Small 7(10):1322–1337

14. Buono C, Anzinger JJ, Amar M, Kruth HS (2009) Fluorescent pegylated nanoparticles demonstrate fluid-phase pinocytosis by macrophages in mouse atherosclerotic lesions. J Clin Invest 119(5): 1373–1381

15. Sallusto F, Cella M, Danieli C, Lanzavecchia A (1995) Dendritic cells use macropinocytosis and the mannose receptor to concentrate macromolecules in the major histocompatibility complex class II compartment: downregulation by cytokines and bacterial products. J Exp Med 182(2):389–400

16. Banchereau J, Steinman RM (1998) Dendritic cells and the control of immunity. Nature 392(6673):245–252

17. Brodsky FM, Chen C-Y, Knuehl C, Towler MC, Wakeham DE (2001) Biological basket weaving: formation and function of clathrin-coated vesicles. Annu Rev Cell Dev Biol 17(1):517–568

18. Ehrlich M, Boll W, Van Oijen A et al (2004) Endocytosis by random initiation and stabilization of clathrin-coated pits. Cell 118(5):591–605

19. Sorkin A (2004) Cargo recognition during clathrin-mediated endocytosis: a team effort. Curr Opin Cell Biol 16(4):392–399

20. Takei K, Haucke V (2001) Clathrin-mediated endocytosis: membrane factors pull the trigger. Trends Cell Biol 11(9):385–391

21. Perry DG, Daugherty GL, Martin WJ 2nd (1999) Clathrin-coated pit-associated proteins are required for alveolar macrophage phagocytosis. J Immunol 162(1):380–386

22. Rejman J, Oberle V, Zuhorn IS, Hoekstra D (2004) Size-dependent internalization of particles via the pathways of clathrin- and caveolae-mediated endocytosis. Biochem J 377(1):159–169

23. Nabi IR, Le PU (2003) Caveolae/raft-dependent endocytosis. J Cell Biol 161(4):673–677

24. Maxfield FR (2002) Plasma membrane microdomains. Curr Opin Cell Biol 14(4):483–487

25. Stan R-V (2002) Structure and function of endothelial caveolae. Microsc Res Tech 57(5):350–364

26. Bohdanowicz M, Grinstein S (2013) Role of phospholipids in endocytosis, phagocytosis, and macropinocytosis. Physiol Rev 93(1):69–106

27. Chithrani BD, Ghazani AA, Chan WC (2006) Determining the size and shape dependence of gold nanoparticle uptake into mammalian cells. Nano Lett 6(4):662–668

28. Anderson RG (1998) The caveolae membrane system. Annu Rev Biochem 67(1):199–225

29. Conner SD, Schmid SL (2003) Regulated portals of entry into the cell. Nature 422(6927):37–44

30. Kumari A, Yadav SK (2011) Cellular interactions of therapeutically delivered nanoparticles. Expert Opin Drug Deliv 8(2):141–151

31. Doherty GJ, Mcmahon HT (2009) Mechanisms of endocytosis. Annu Rev Biochem 78:857–902

32. Chithrani BD, Chan WC (2007) Elucidating the mechanism of cellular uptake and removal of protein-coated gold nanoparticles of different sizes and shapes. Nano Lett 7(6):1542–1550

33. Adjei IM, Peetla C, Labhasetwar V (2014) Heterogeneity in nanoparticles influences biodistribution and targeting. Nanomedicine (Lond) 9:267–278

34. Wang Z, Tiruppathi C, Minshall RD, Malik AB (2009) Size and dynamics of caveolae studied using nanoparticles in living endothelial cells. ACS Nano 3(12):4110–4116

35. Prabha S, Zhou W-Z, Panyam J, Labhasetwar V (2002) Size-dependency of nanoparticle-mediated gene transfection: studies with fractionated nanoparticles. Int J Pharm 244(1–2):105–115

36. Safi M, Courtois J, Seigneuret M, Conjeaud H, Berret JF (2011) The effects of aggregation and protein corona on the cellular internalization of iron oxide nanoparticles. Biomaterials 32(35):9353–9363

37. Zhang Y, Tekobo S, Tu Y et al (2012) Permission to enter cell by shape: nanodisk vs nanosphere. ACS Appl Mater Interfaces 4(8):4099–4105

38. Huang X, Teng X, Chen D, Tang F, He J (2010) The effect of the shape of mesoporous silica nanoparticles on cellular uptake and cell function. Biomaterials 31(3):438–448

39. Verma A, Uzun O, Hu Y et al (2008) Surface-structure-regulated cell-membrane penetration by monolayer-protected nanoparticles. Nat Mater 7(7):588–595

40. Harush-Frenkel O, Rozentur E, Benita S, Altschuler Y (2008) Surface charge of nanoparticles determines their endocytic and transcytotic pathway in polarized MDCK cells. Biomacromolecules 9(2):435–443

41. Gessner A, Lieske A, Paulke BR, Müller R (2002) Influence of surface charge density on protein adsorption on polymeric nanoparticles: analysis by two-dimensional electrophoresis. Eur J Pharm Biopharm 54(2):165–170

42. Ehrenberg MS, Friedman AE, Finkelstein JN, Oberdörster G, McGrath JL (2009) The influence of protein adsorption on nanoparticle association with cultured endothelial cells. Biomaterials 30(4):603–610

43. Cho WS, Thielbeer F, Duffin R et al (2014) Surface functionalization affects the zeta potential, coronal stability and membranolytic activity of polymeric nanoparticles. Nanotoxicology 8:202–211

44. Schauer R (2009) Sialic acids as regulators of molecular and cellular interactions. Curr Opin Struct Biol 19(5):507–514

45. Sampaio JL, Gerl MJ, Klose C et al (2011) Membrane lipidome of an epithelial cell line. Proc Natl Acad Sci U S A 108(5):1903–1907

46. Lingwood D, Simons K (2010) Lipid rafts as a membrane-organizing principle. Science 327(5961):46–50

47. Nagayama S, Ogawara K, Fukuoka Y, Higaki K, Kimura T (2007) Time-dependent changes in opsonin amount associated on nanoparticles alter their hepatic uptake characteristics. Int J Pharm 342(1–2):215–221

48. Bava A, Cappellini F, Pedretti E et al (2013) Heparin and carboxymethylchitosan metal nanoparticles: an evaluation of their cytotoxicity. Biomed Res Int 2013:1

49. Mejías R, Pérez-Yagüe S, Gutiérrez L et al (2011) Dimercaptosuccinic acid-coated magnetite nanoparticles for magnetically guided in vivo delivery of interferon gamma for cancer immunotherapy. Biomaterials 32(11):2938–2952

50. Fröhlich E (2012) The role of surface charge in cellular uptake and cytotoxicity of medical nanoparticles. Int J Nanomedicine 7:5577–5591

51. Arvizo RR, Miranda OR, Thompson MA et al (2010) Effect of nanoparticle surface charge at the plasma membrane and beyond. Nano Lett 10(7):2543–2548

52. Wang B, Zhang L, Bae SC, Granick S (2008) Nanoparticle-induced surface reconstruction of phospholipid membranes. Proc Natl Acad Sci U S A 105(47):18171–18175

53. Choi CH, Hao L, Narayan SP, Auyeung E, Mirkin CA (2013) Mechanism for the endocytosis of spherical nucleic acid nanoparticle conjugates. Proc Natl Acad Sci U S A 110(19):7625–7630

54. Shrestha R, Elsabahy M, Florez-Malaver S, Samarajeewa S, Wooley KL (2012) Endosomal escape and siRNA delivery with cationic shell cross-linked knedel-like nanoparticles with tunable buffering capacities. Biomaterials 33(33):8557–8568

55. Peetla C, Labhasetwar V (2008) Biophysical characterization of nanoparticle-endothelial model cell membrane interactions. Mol Pharm 5(3):418–429

56. Agnihotri SA, Mallikarjuna NN, Aminabhavi TM (2004) Recent advances on chitosan-based micro- and nanoparticles in drug delivery. J Control Release 100(1):5–28

57. Peetla C, Stine A, Labhasetwar V (2009) Biophysical interactions with model lipid membranes: applications in drug discovery and drug delivery. Mol Pharm 6(5):1264–1276

58. Peetla C, Rao KS, Labhasetwar V (2009) Relevance of biophysical interactions of nanoparticles with a model membrane in predicting cellular uptake: study with TAT peptide-conjugated nanoparticles. Mol Pharm 6(5):1311–1320

59. Sharma B, Peetla C, Adjei IM, Labhasetwar V (2013) Selective biophysical interactions of surface modified nanoparticles with cancer cell lipids improve tumor targeting and gene therapy. Cancer Lett 334(2):228–236

60. Byrne JD, Betancourt T, Brannon-Peppas L (2008) Active targeting schemes for nanoparticle systems in cancer therapeutics. Adv Drug Deliv Rev 60(15): 1615–1626

61. Yang PH, Sun X, Chiu JF, Sun H, He QY (2005) Transferrin-mediated gold nanoparticle cellular uptake. Bioconjug Chem 16(3):494–496

62. Sahoo SK, Ma W, Labhasetwar V (2004) Efficacy of transferrin conjugated paclitaxel loaded nanoparticles in a murine model of prostate cancer. Int J Cancer 112(2):335–340

63. Cho K, Wang X, Nie S, Chen ZG, Shin DM (2008) Therapeutic nanoparticles for drug delivery in cancer. Clin Cancer Res 14(5):1310–1316

64. Richard JP, Melikov K, Vives E et al (2003) Cell-penetrating peptides: a reevaluation of the mechanism of cellular uptake. J Biol Chem 278(1): 585–590

65. Duchardt F, Fotin-Mleczek M, Schwarz H, Fischer R, Brock R (2007) A comprehensive model for the cellular uptake of cationic cell-penetrating peptides. Traffic 8(7):848–866

66. Vivès E, Richard JP, Rispal C, Lebleu B (2003) TAT peptide internalization: seeking the mechanism of entry. Curr Protein Pept Sci 4(2):125–132

67. Santra S, Yang H, Stanley JT et al (2005) Rapid and effective labeling of brain tissue using TAT-conjugated CdS:Mn/ZnS quantum dots. Chem Commun 25:3144–3146

68. Rao KS, Reddy MK, Horning JL, Labhasetwar V (2008) TAT-conjugated nanoparticles for the CNS delivery of anti-HIV drugs. Biomaterials 29(33):4429–4438

69. Jiang W, Kimbetty YS, Rutka JT, Chanwarren CW (2008) Nanoparticle-mediated cellular response is size-dependent. Nat Nanotechnol 3(3):145–150

70. Oh E, Delehanty JB, Sapsford KE et al (2011) Cellular uptake and fate of pegylated gold nanopar-

ticles is dependent on both cell-penetration peptides and particle size. ACS Nano 5(8):6434–6448

71. Barua S, Yoo JW, Kolhar P, Wakankar A, Gokarn YR, Mitragotri S (2013) Particle shape enhances specificity of antibody-displaying nanoparticles. Proc Natl Acad Sci U S A 110(9):3270–3275

72. Kolhar P, Anselmo AC, Gupta V et al (2013) Using shape effects to target antibody-coated nanoparticles to lung and brain endothelium. Proc Natl Acad Sci U S A 110(26):10753–10758

73. Salvati A, Pitek AS, Monopoli MP et al (2013) Transferrin-functionalized nanoparticles lose their targeting capabilities when a biomolecule corona adsorbs on the surface. Nat Nanotechnol 8(2): 137–143

74. Brezesinski G, Möhwald H (2003) Langmuir monolayers to study interactions at model membrane surfaces. Adv Colloid Interface Sci 100–102:563–584

75. Peetla C, Bhave R, Vijayaraghavalu S, Stine A, Kooijman E, Labhasetwar V (2010) Drug resistance in breast cancer cells: biophysical characterization of and doxorubicin interactions with membrane lipids. Mol Pharm 7(6):2334–2348

76. Shaw JE, Slade A (2003) Yip CM: simultaneous in situ total internal reflectance fluorescence/atomic force microscopy studies of DPPC/dPOPC microdomains in supported planar lipid bilayers. J Am Chem Soc 125(39):11838–11839

77. Okumura Y, Zhang H, Sugiyama T, Iwata Y (2007) Electroformation of giant vesicles on a non-electroconductive substrate. J Am Chem Soc 129(6):1490–1491

78. Lakadamyali M, Rust MJ, Zhuang X (2006) Ligands for clathrin-mediated endocytosis are differentially sorted into distinct populations of early endosomes. Cell 124(5):997–1009

79. Gratton SE, Ropp PA, Pohlhaus PD et al (2008) The effect of particle design on cellular internalization pathways. Proc Natl Acad Sci U S A 105(33): 11613–11618

80. Rejman J, Bragonzi A, Conese M (2005) Role of clathrin- and caveolae-mediated endocytosis in gene transfer mediated by lipo- and polyplexes. Mol Ther 12(3):468–474

81. Parton RG, Richards AA (2003) Lipid rafts and caveolae as portals for endocytosis: new insights and common mechanisms. Traffic 4(11):724–738

82. Maxfield FR (1982) Weak bases and ionophores rapidly and reversibly raise the pH of endocytic vesicles in cultured mouse fibroblasts. J Cell Biol 95(2 Pt 1):676–681

83. Varkouhi AK, Scholte M, Storm G, Haisma HJ (2011) Endosomal escape pathways for delivery of biologicals. J Control Release 151(3):220–228

84. Jones RA, Cheung CY, Black FE et al (2003) Poly(2-alkylacrylic acid) polymers deliver molecules to the cytosol by pH-sensitive disruption of endosomal vesicles. Biochem J 372(Pt 1):65–75

85. Panyam J, Zhou WZ, Prabha S, Sahoo SK, Labhasetwar V (2002) Rapid endo-lysosomal escape

of poly(DL-lactide-co-glycolide) nanoparticles: implications for drug and gene delivery. FASEB J 16(10):1217–1226

86. Kwon EJ, Bergen JM, Pun SH (2008) Application of an HIV gp41-derived peptide for enhanced intracellular trafficking of synthetic gene and siRNA delivery vehicles. Bioconjug Chem 19(4):920–927

87. Kantchev EA, Chang CC, Chang DK (2006) Direct Fmoc/tert-Bu solid phase synthesis of octamannosyl polylysine dendrimer-peptide conjugates. Biopolymers 84(2):232–240

88. Hatakeyama H, Ito E, Akita H et al (2009) A pH-sensitive fusogenic peptide facilitates endosomal escape and greatly enhances the gene silencing of siRNA-containing nanoparticles in vitro and in vivo. J Control Release 139(2):127–132

89. Mok H, Park TG (2008) Self-crosslinked and reducible fusogenic peptides for intracellular delivery of siRNA. Biopolymers 89(10):881–888

90. Salomone F, Cardarelli F, Di Luca M et al (2012) A novel chimeric cell-penetrating peptide with membrane-disruptive properties for efficient endosomal escape. J Control Release 163(3):293–303

91. Ilker MF, Schule H, Coughlin EB (2004) Modular norbornene derivatives for the preparation of well-defined amphiphilic polymers: study of the lipid membrane disruption activities. Macromolecules 37(3):694–700

92. Ogris M, Carlisle RC, Bettinger T, Seymour LW (2001) Melittin enables efficient vesicular escape and enhanced nuclear access of nonviral gene delivery vectors. J Biol Chem 276(50):47550–47555

93. Selbo PK, Weyergang A, Høgset A et al (2010) Photochemical internalization provides time- and space-controlled endolysosomal escape of therapeutic molecules. J Control Release 148(1):2–12

94. Prasmickaite L, Hogset A, Selbo PK, Engesaeter BØ, Hellum M, Berg K (2002) Photochemical disruption of endocytic vesicles before delivery of drugs: a new strategy for cancer therapy. Br J Cancer 86(4):652–657

95. Pon LA (2011) Organelle transport: mitochondria hitch a ride on dynamic microtubules. Curr Biol 21(17):R654–R656

96. Barlan K, Rossow MJ, Gelfand VI (2013) The journey of the organelle: teamwork and regulation in intracellular transport. Curr Opin Cell Biol 25(4):483–488

97. Panyam J, Labhasetwar V (2003) Sustained cytoplasmic delivery of drugs with intracellular receptors using biodegradable nanoparticles. Mol Pharm 1(1):77–84

98. Pratt AJ, Macrae IJ (2009) The RNA-induced silencing complex: a versatile gene-silencing machine. J Biol Chem 284(27):17897–17901

99. Yuan X, Naguib S, Wu Z (2011) Recent advances of siRNA delivery by nanoparticles. Expert Opin Drug Deliv 8(4):521–536

100. Panyam J, Labhasetwar V (2004) Targeting intracellular targets. Curr Drug Deliv 1(3):235–247

101. Kim AJ, Boylan NJ, Suk JS, Lai SK, Hanes J (2012) Non-degradative intracellular trafficking of highly compacted polymeric DNA nanoparticles. J Control Release 158(1):102–107

102. Greulich C, Diendorf J, Simon T, Eggeler G, Epple M, Köller M (2011) Uptake and intracellular distribution of silver nanoparticles in human mesenchymal stem cells. Acta Biomater 7(1):347–354

103. Alkilany AM, Murphy CJ (2010) Toxicity and cellular uptake of gold nanoparticles: what we have learned so far? J Nanopart Res 12(7):2313–2333

104. Heller A, Brockhoff G, Goepferich A (2012) Targeting drugs to mitochondria. Eur J Pharm Biopharm 82(1):1–18

105. Malhi SS, Murthy RS (2012) Delivery to mitochondria: a narrower approach for broader therapeutics. Expert Opin Drug Deliv 9(8):909–935

106. Szabo I, Leanza L, Gulbins E, Zoratti M (2012) Physiology of potassium channels in the inner membrane of mitochondria. Pflugers Arch 463(2): 231–246

107. Wang X-H, Peng H-S, Yang L et al (2013) Poly-l-lysine assisted synthesis of core-shell nanoparticles and conjugation with triphenylphosphonium to target mitochondria. J Mater Chem B 1(38): 5143–5152

108. Theodossiou TA, Sideratou Z, Katsarou ME, Tsiourvas D (2013) Mitochondrial delivery of Doxorubicin by triphenylphosphonium-functionalized hyperbranched nanocarriers results in rapid and severe cytotoxicity. Pharm Res 30(11): 2832–2842

109. Johnston HJ, Semmler-Behnke M, Brown DM, Kreyling W, Tran L, Stone V (2010) Evaluating the uptake and intracellular fate of polystyrene nanoparticles by primary and hepatocyte cell lines in vitro. Toxicol Appl Pharmacol 242(1):66–78

110. Panyam J, Labhasetwar V (2003) Dynamics of endocytosis and exocytosis of poly(D, L-lactide-co-glycolide) nanoparticles in vascular smooth muscle cells. Pharm Res 20(2):212–220

111. Hemmerich PH, von Mikecz AH (2013) Defining the subcellular interface of nanoparticles by live-cell imaging. PLoS One 8(4):e62018

112. Arora S, Rajwade JM, Paknikar KM (2012) Nanotoxicology and in vitro studies: the need of the hour. Toxicol Appl Pharmacol 258(2):151–165

113. Lengyel JS, Milne JL, Subramaniam S (2008) Electron tomography in nanoparticle imaging and analysis. Nanomedicine (Lond) 3(1):125–131

114. Frangioni JV (2003) In vivo near-infrared fluorescence imaging. Curr Opin Chem Biol 7(5):626–634

115. Larson DR, Zipfel WR, Williams RM et al (2003) Water-soluble quantum dots for multiphoton fluorescence imaging in vivo. Science 300(5624): 1434–1436

116. Greish K, Thiagarajan G, Herd H et al (2012) Size and surface charge significantly influence the toxicity of silica and dendritic nanoparticles. Nanotoxicology 6(7):713–723

117. Yu T, Greish K, McGill LD, Ray A, Ghandehari H (2012) Influence of geometry, porosity, and surface characteristics of silica nanoparticles on acute toxicity: their vasculature effect and tolerance threshold. ACS Nano 6(3):2289–2301

118. Dobrovolskaia MA, Aggarwal P, Hall JB, McNeil SE (2008) Preclinical studies to understand nanoparticle interaction with the immune system and its potential effects on nanoparticle biodistribution. Mol Pharm 5(4):487–495

Atomic Force Microscopy Study of the Interaction of DNA and Nanoparticles

6

Kungang Li, Songyan Du, Steven Van Ginkel, and Yongsheng Chen

Contents

K. Li • S. Du • S. Van Ginkel • Y. Chen (✉)
School of Civil and Environmental Engineering,
Georgia Institute of Technology,
Atlanta, GA 30332, USA
e-mail: yongsheng.chen@ce.gatech.edu

Abstract

The interaction between nanoparticles (NPs) and DNA plays an important role in the genotoxicity of NPs, and it is imperative to characterize the nano/DNA interactions and explore the underlying chemical mechanisms. In this chapter, we demonstrated systematic experimental approaches based on atomic force microscope (AFM), coupled with modeling computation to probe the binding activity of NPs with DNA and the putative genotoxicity. Using quantum dots (QDs) as a model NP, we examined the binding kinetics, binding isotherm, binding specificity, and binding mechanisms of NPs to DNA with the application of AFM. We further assessed the binding affinity between NPs and DNA by calculating their interaction energy on the basis of Derjaguin-Landau-Verwey-Overbeek (DLVO) models. The modeling results of binding affinity were validated by the NPs/DNA binding images experimentally derived by AFM. The investigation of the relationship between the binding affinity of five NPs ((QDs (+), QDs (−), silver NPs, hematite NPs, and gold NPs) for DNA with their inhibition effects on DNA replication indicated that NPs with a high binding affinity for DNA molecules exhibited higher inhibition on DNA replication. The methodology employed in this study can be extended to study the interaction of other NPs with DNA, which is anticipated to benefit the future design of safe NPs, as well as the toxicological investigations of NPs.

6.1 Introduction

Rapid growth in nanotechnology has raised concerns of their environmental toxicity, as the same properties that make nanoparticles (NPs) useful in a variety of applications can potentially make them toxic and harmful to the environment. For instance, the extraordinarily small size of NPs not only contributes to their usefulness in industrial and biomedical applications, but also favors their entry into cells and may subsequently result in adverse effects for intracellular structures. Given their potential nanotoxicity such as DNA mutation, metabolism variation, gene regulation, and even population shift [1, 2], the interaction of NPs with biological systems should be carefully characterized.

At the interface between NPs and biological systems, the "nano-bio" interaction shaped by a variety of forces could determine key biophysiochemical processes such as particle wrapping at cell surfaces, endocytosis and intracellular biocatalysis [3]. Among the interaction of biomolecules (e.g., DNA, proteins, or polysaccharides) with engineered NPs, DNA-NP interactions through their molecular bindings and biochemical reactions can lead to significant impacts on DNA stability, DNA reactivity, gene regulation, and the activities of DNA-associated enzymes and metabolism in biological cells [2, 4]. The understanding of interactions between NPs and DNA not only contribute to the rational design of nanocomplexes in biomedical research, but also provide information for evaluating the toxic effects of NPs on intracellular DNA upon their entering into living biological cells. Therefore, it is imperative to develop experimental approaches to probe these nano-bio interface interactions by examining the structure of NPs-DNA bioconjugates and evaluating the particular response of DNA in the presence of NPs.

These bio/nano interactions can be addressed by atomic force microscopy (AFM) approaches. AFM is advantageous over many other sophisticated microscopy techniques in its capability to observe samples in liquid, which makes it exceptionally suitable for biological molecule imaging and thus it plays a major role in exploring nano-bio interactions. However, most of the recent AFM studies in this field focus on DNA-protein interactions [5–10], while very little research has been conducted using AFM to probe how NPs interact with DNA [2, 11–13]. DNA aggregation was observed when examining the DNA interaction with carbon nanoparticles (CNPs) [2]. Because DNA carries genetic information and regulates the synthesis of enzymes and other proteins, the deformation of DNA could potentially lead to the initiation of disease. Notwithstanding, the exploration of underlying mechanisms responsible for the observed binding activity are hindered by the fact that local identification of individual NPs and DNA molecules has not been achieved. Our group recently explored the use of Kelvin force microscopy (KFM), an electric mode of AFM, in characterizing the surface potential of NPs, which can serve as a complementary tool in revealing the interfacial biophysicochemical interactions between NPs and biological system at the nano scale. We hypothesized that different type of interactions with DNA from that of hydrophobic CNPs might occur on hydrophilic NPs such as QDs and metal oxide NPs. Hence, one of the research focuses in our group is to explore the use of AFM for direct imaging of NP-DNA interactions with a broad range of NPs, and the research results are purportedly to fill this knowledge gap in field.

The universal occurrence of aggregation of most NPs in aqueous media has raised concern about whether the observed toxicity and related mechanisms in those published studies are unequivocally associated with the real nanosized material, but not the aggregate/agglomerate. We are particularly interested in unaggregated NPs, i.e., monodisperse NPs, at the interface between NPs and biological systems, which is hypothesized to have unique local effects and might exert different toxicity mechanisms distinct from their

aggregates. To date, these mechanisms are not well documented yet.

The interaction of NPs with DNA has been mostly studied for the NPs commonly used in medical biotechnology such as gold, silver, and carbon nanotubes [1], and are rather limited compared with studies for the use of NPs in industrial applications and commercial products such as metal oxide nanomaterials. Therefore, a more comprehensive list of NPs is studied in our current research. The goal of our current research is to explore the nanotoxic mechanisms of "real" NPs, by developing systematic experimental approaches based on AFM to assess the effect of unaggregated NPs on single cells or biomolecules at the local scale. This chapter will discuss our research work in the application of AFM imaging techniques in characterizing nanoparticle-DNA binding and exploring its associated molecular interaction mechanisms as well.

6.2   Atomic Force Microscopy (AFM)

6.2.1   Overview of AFM

Atomic force microscopy (AFM), a force-based scanning probe microscopy, has emerged as a powerful technique for probing both physico-chemical and mechanical properties of bio-colloid surfaces on a sub-molecular scale [14–16]. In AFM, a sharp tip microfabricated from Si or Si_3N_4 with a radius of a few to 10's of nm, is scanned over the sample surface, which allows near-field interactions (physical, chemical, or biological) between the tip and the sample to be sensed and high-resolution images to be generated. Most AFMs use a laser beam deflection system, where a laser is reflected from the back of the reflective AFM cantilever and to a position-sensitive detector (photodiode) (Fig. 6.1). In detail, the AFM tip rasters in the x and y directions in the horizontal plane activated by the piezo scanner and scans the sample line by line. When the tip is brought into the proximity of a sample surface, forces between the tip and the
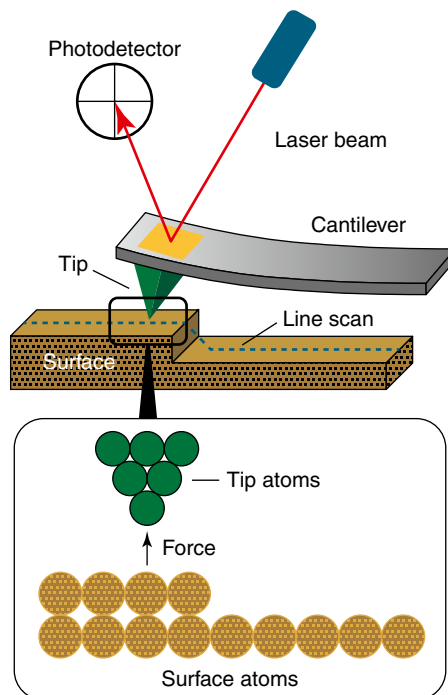

Fig. 6.1 Schematic illustration of AFM working principles (Ref. http://www.home.agilent.com)

sample lead to the cantilever deflection according to Hooke's law. The deflection is subsequently measured using a laser spot reflected from the top surface of the cantilever into an array of photodiodes. The position of the laser spot on the detector reflects angular deflections of the cantilever.

There are mainly two AFM-imaging modes in terms of the way the tip moves over the sample surface: contact mode and tapping mode. In contact mode, the cantilever is "dragged" across the surface of the sample and the contours of the surface are measured directly using the deflection of the cantilever. In tapping mode, the cantilever is externally oscillated near its resonance frequency and scanned over the sample surface. The oscillation amplitude and phase are modified by tip-sample interaction forces. These changes in oscillation with respect to the external reference oscillation provide information about the sample's characteristics.

AFM not only provides high-resolution topographic images, but also enables the interaction force measurement as a force spectroscopy
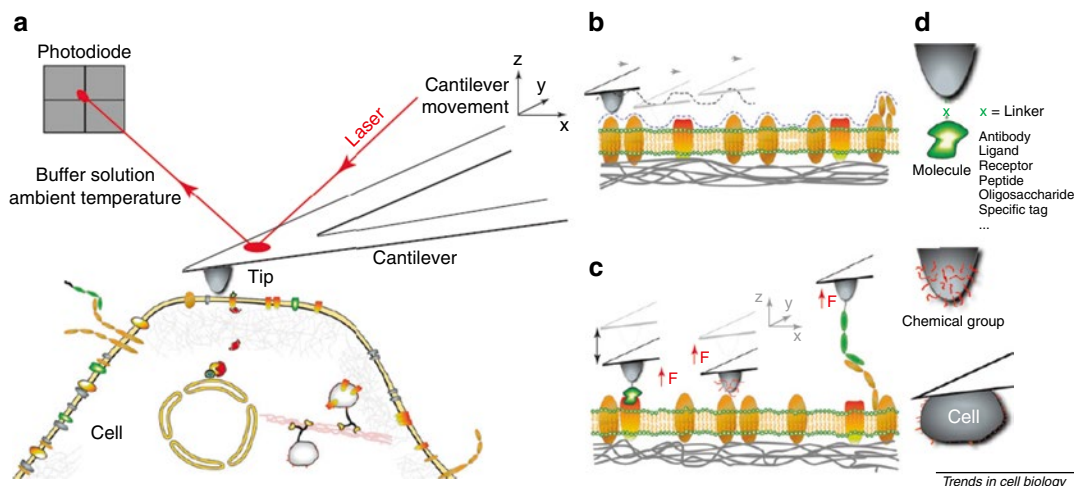
Fig. 6.2 AFM-based nanoscopy of living cells (**a**) Unlike other microscopy techniques, AFM works by sensing the tiny forces between a sharp tip and the cell surface. (**b**) In the (**a**) imaging mode, the AFM tip is scanned across the cell (*arrows*) to contour its surface topography (*dashed line*). (**c**) In force spectroscopy techniques, the AFM tip is used to measure cell-surface interactions to single-molecule resolution. Examples (from left to right) show a tip functionalized with a ligand to probe interactions with its cognate receptor, a tip coated with chemical groups to detect chemical interactions, and a tip carrying cell-adhesion molecules to probe homo- or heterophilic interactions towards other cell-adhesion molecules. (**d**) Most force-spectroscopy applications imply functionalizing the AFM tip or cantilever to specifically probe biological, chemical or cellular interactions [22]

(Fig. 6.2). By measuring the cell-surface interaction forces, AFM could assess the surface physical properties of a cell such as hardness, elasticity, and adhesiveness which are implicated in cellular motility, adhesion to surfaces, and stability. In the investigations of nano-bio interactions, the interaction between NPs and living cells were examined by AFM in contact mode and the interaction forces between immobilized *E. coli* cells and immobilized NPs was measured during the cycle of approach-contact-retract from the cell surface [17]. In addition, Kelvin force microscopy (KFM), the electric mode of AFM has been proven to be an effective tool in the investigation of interfacial nano-bio interactions. KFM is capable of characterizing nanomaterials by examining the nanoelectrical properties during their interfacial interaction with biomolecular matrices which is complementary to the topography and phase image generated by standard AFM. The measured surface potentials and electrostatic interactions with the application of KFM, are fundamental to biological processes at the molecular and cellular levels, and the improper generation or sensing of electric signals can indicate significant deviations in biological function [18]. The surface electrical properties

(e.g. surface heterogeneities and surface charge distribution) of *E. coli* cells and metallic NPs were quantified by KFM [19, 20], which can serve locally to identify and differentiate individual NPs and to map the surface heterogeneities of NPs and biological cells. Our research group has advanced the application of KFM in studying nano-bio interactions. Zhang et al. [13, 17] determined the morphological and electrical changes in DNA in *in vivo* and *in vitro* experiments after exposure to Quantum dots (QDs), and also successfully detected single QD-DNA binding for the first time [13]. Furthermore, Zhang et al. [21] also demonstrated the effectiveness of KPFM in imaging and quantifying the surface potentials of *E. coli* cells after being exposed to Hematite [21]. Taken together, AFM has demonstrated itself as an effective tool in understanding surface interactions of NPs with biological systems.

6.2.2 Comparison with Other Microscopic Techniques

A variety of methods are available for the characterization and imaging of nanoparticles, and the

Table 6.1 Comparison of AFM with SEM and TEM

Technique and Measurement principles	Application in nano-bio interaction study	Advantages	Limitations
AFM Deflection angle from cantilever probe	Characterizes surface morphology, surface potential, elasticity and other properties of NPs and biological components; measures forces at the nano-bio interfaces; probes the effect of NPs on the surface properties of biological components (e.g. cell penetrating processes of NPs)	High resolution (typical 1 nm to ~0.2 nm); capable of imaging in liquids; 3-D topographical images possible; non-destructive to samples; simple and cost-effective sample preparation; capable of probing mechanical and electrical properties of samples	Small field of view (2 μm); slow scanning speed; possible large image artifacts caused by types, sizes, and angles of probes, edge overshoot, and drift of scanners, errors during image processing, floor and acoustic vibrations, and other sources such as surface contamination
SEM Scattered electrons and X-rays	Determination of surface morphology of NPs and biological components; determination of the intermolecular and biological interactions of NPs (e.g., adsorption of NPs onto cell surface)	Large field of view (~20 μm); fast imaging speed; simple sample preparation; ability to image the cross-section of samples; compositional information can be obtained with energy dispersive spectroscopy (EDS)	Low resolution (typical 1–10 nm); conductive samples required; destructive to samples (particularly at high voltage); generally must be performed under vacuum
TEM Absorption and diffraction of electrons	Determines the nanoscale structure, crystallinity, and chemical components of NPs; elucidates interactions of NPs with biological components (e.g. cellular uptake of NPs)	High resolution (typical 1 nm~0.2 nm); fast imaging speed; compositional and crystallographic information can be obtained	Small field of view (~2 μm); expensive and complicated sample preparations; requires thin samples (<100 nm); destructive to samples; 2-D images only; must be performed under vacuum

most commonly used high-resolution imaging microscopes are scanning electron microscopy (SEM), transmission electron microscopy (TEM), and AFM. Different advantages and limitations are associated with each technique as summarized in Table 6.1. Electron microscopy is the simplest and widely used technique in determining the size and morphology of NPs, but one major drawback is that it requires samples to be present in a dry form and it fails to measure samples in dispersion, which restricts its use in imaging the biological molecules [23]. AFM can achieve atomic resolution of samples on flat surfaces with a high signal-to-noise ratio on a nanometer scale. Also, AFM does not require any additional sample pretreatment. Another distinctive attribute associated with AFM is it allows measurements in both gaseous and liquid environments, which makes AFM an ideal tool for biological imaging and has drawn some attention in the field of nano-bio interaction research.

6.2.3   AFM Imaging the Binding of NPs with DNA

The potential for binding between nanoparticles and DNA was probed by the application of AFM imaging. Using AFM, it is possible to determine extent of binding of NPs to DNA as well as to determine where the NPs are bound on DNA. AFM has been extensively used to study DNA-protein interactions, but its application in studying the interaction of DNA is relatively limited and the tested NPs are mostly biomedically used NPs such as gold, silver, and carbon nanotubes [2, 4, 24]. Our research has employed QDs as model NPs in the investigation of interfacial interactions of DNA with NPs. The associated unique photophysical properties and ultra-small sizes of QDs (similar to proteins and other biomacromolecules), not only allows versatile applications in biological sensing, imaging, and detection [25–28], but also renders a higher ten-

dency for nano-bio interactions which govern their cytotoxic and genotoxic effects. There is a lack of visualization of QD-DNA interactions though molecular dynamic modeling calculations indicate QDs could cause DNA damage and nick supercoiled DNA [29].

Our research group reported the outstanding performance of KFM in visualizing *in vitro* and *in vivo* binding between homopolymer DNA and QDs [13]. The binding of QDs caused the morphological change of two types of homopolymer DNAs from tangled networks to pearl-like particles, but no sequence-dependent binding was observed. Here, we report our recent work in the successful imaging of binding of QDs with DNA in air and liquids with AFM with our sample preparation method. This is the first study probing the interaction of NPs and DNA in liquids with AFM. In the subsequent section, the same sample preparation method and AFM imaging techniques were also applied to a DNA binding study with other class of NPs.

6.2.3.1 DNA

A *Sac*I-linearized plasmid DNA pGMEX-1 with 3,993 base pairs (Promega Corporation, Madison, WI) was diluted to 5 μg/mL with sterile Tris-EDTA buffer and with 10 mM 4-(2-hydroxyethyl)-1-piperazineethanesulfonic acid (HEPES) buffer for imaging in air and liquids, respectively.

6.2.3.2 Imaging Substrate

Mica is the commonly used substrate for DNA studies in liquids because DNA can retain its near-native conformation [30]. As both DNA and mica surfaces carry negative charges under physiological conditions, the binding of DNA onto mica was facilitated either with the aid of divalent ions (e.g. Mg^{2+} and Ni^{2+}) [31] or by modifying the mica surface (e.g. 3-aminopropyltriethoxysilane (APTES) modified mica) [32].

6.2.3.3 DNA Imaging

Slightly different sample preparations were applied for imaging the binding of NPs to DNA in air and liquid, respectively. For imaging in the air, DNA stock solution was diluted to 1 nM with sterile Tris-EDTA buffer. Mg^{2+} was added to a final concentration of 5 mM. 2.5 μL of the DNA

solution was deposited on a freshly cleaved mica substrate that was placed in a small covered petri dish, and incubated for 30 min. The mica surface was rinsed thoroughly with MilliQ water and then blown dry with ultrapure nitrogen gas. For imaging in the liquid, DNA stock was diluted to 0.1 nM with sterile 10 mM HEPES buffer (pH 7.4). $MgCl_2$ was added to a final concentration of 4 mM. 5 μL of the DNA solution was spotted onto a freshly cleaved mica substrate and incubated for 30 min. The sample was then rinsed with 1 mL of DNA imaging buffer (10 mM HEPES pH 7.4, 4 mM $MgCl_2$, 2 mM $NiCl_2$).

6.2.3.4 DNA and NP Binding Imaging

DNA of final concentrations of 0.2 and 0.1 nM for imaging in the air and in liquids, respectively, was mixed with NPs at a certain molar ratio and incubated for 1 h. The buffer solutions were the same as those used in the absence of NPs. 2.5 μL of the mixture was applied to mica substrates following the same procedures as the above-mentioned DNA immobilization methods, except that the incubation time on the substrate was 45 min to achieve an optimal imaging quality.

6.2.3.5 AFM Images

AFM images were collected at room temperature in the air or in liquid using the tapping mode. Rectangular silicon cantilevers and triangular silicon nitride cantilevers (BudgetSensors, Bulgaria) were used for imaging in the air and in the liquid, respectively [8]. The deflection amplitude was 2.5 V and the scanning speed was 1–2 μm/s.

A typical AFM topographical image of *Sac*I-*linearized* pGMEX-1 DNA molecules in air and water are shown in Fig. 6.3 and the single DNA molecules in contour shape are clearly visualized. The height of DNA molecules in liquid is higher than that in air, which is attributed to the mitigated compression of DNA in liquid by the tip. The binding of NPs onto DNA is indicated by the simultaneously obtained topography image and phase image, as shown in Fig. 6.4 with QDs as an example. When binding with DNA, the local heights of a DNA fragment along the surface of a substrate apparently varied. The binding activity is further corroborated by the phase image, which differentiate the NPs from the DNA based on their
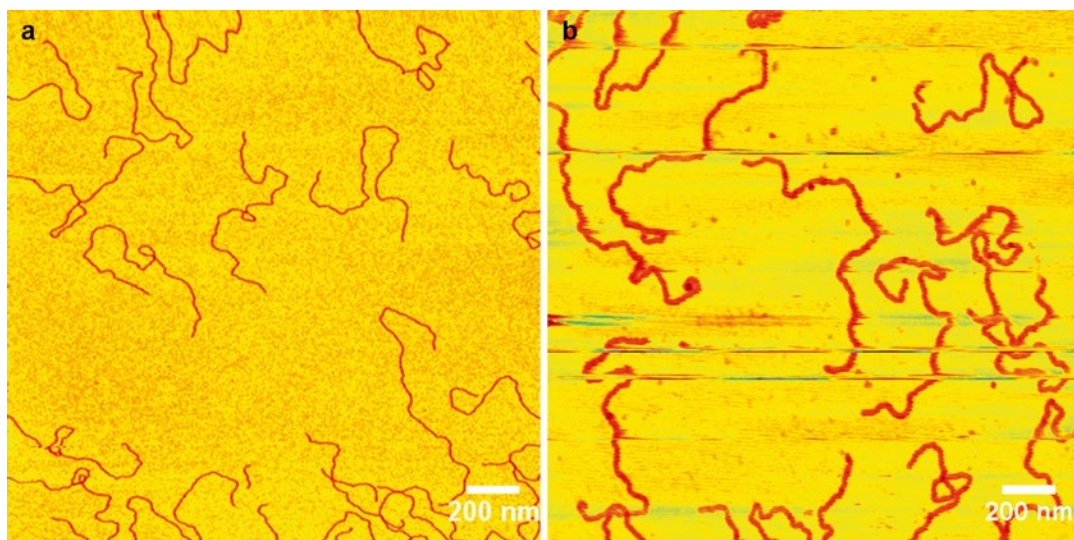
Fig. 6.3 AFM topographical images of DNA (**a**) in air, and (**b**) in liquid

different material properties even with a higher signal-to-noise ratio in comparison to topography images especially at a fast scanning rate [33]. DNA conformation also appeared to change, the details of which are discussed in later Section.

6.3   Quantifying the Binding Characteristics of NPs to DNA Using AFM

Association constants and binding specificities of NPs onto DNA are the primary thermodynamic properties for understanding DNA-NPs interactions. Several macroscopic methods, such as spectroscopic [34, 35] and electrochemical [36] techniques, were employed to investigate the thermodynamic equilibrium constants and binding specificities of NPs to DNA. Although powerful, these methods cannot determine the binding affinity of NPs for specific sites on DNA and are limited by assuming that the change in the instrumental signal like absorbance is directly proportional to the extent of binding [37]. However, the advantage of AFM (as will be described) is that it can overcome the limitations exhibited by conventional macroscopic methods by directly examining single molecules [6–9].

Using QDs as model NPs, we hereby demonstrated the methodology to determine the binding characteristics of NPs to DNA with AFM. We first developed theoretical modeling for characterizing the binding kinetics and binding isotherms of NPs with DNA, then fit the experimentally acquired QDs-DNA binding images into the developed models. Subsequently, the binding number and the binding positions of QDs on each DNA were counted and examined on a large number of single molecules, and the QDs-DNA binding constants and specificities were determined by conducting statistical analysis. This study is anticipated to benefit the future investigation of the interaction of NPs and DNA and thus the genotoxicity assessment of NPs as well as the rational design of NPs for medical and therapeutic applications.

6.3.1   Binding Kinetics and Binding Isotherms

Binding kinetics describe the average number of bound NPs per DNA molecule as a function of incubation time and is given in Eq. (6.1).

$$\frac{[NP_{bind}]}{[DNA]} = C_{eq}\left(1 - e^{-kt}\right) \tag{6.1}$$

where C_{eq} represents the average number of bound NPs per DNA at equilibrium, and k is the
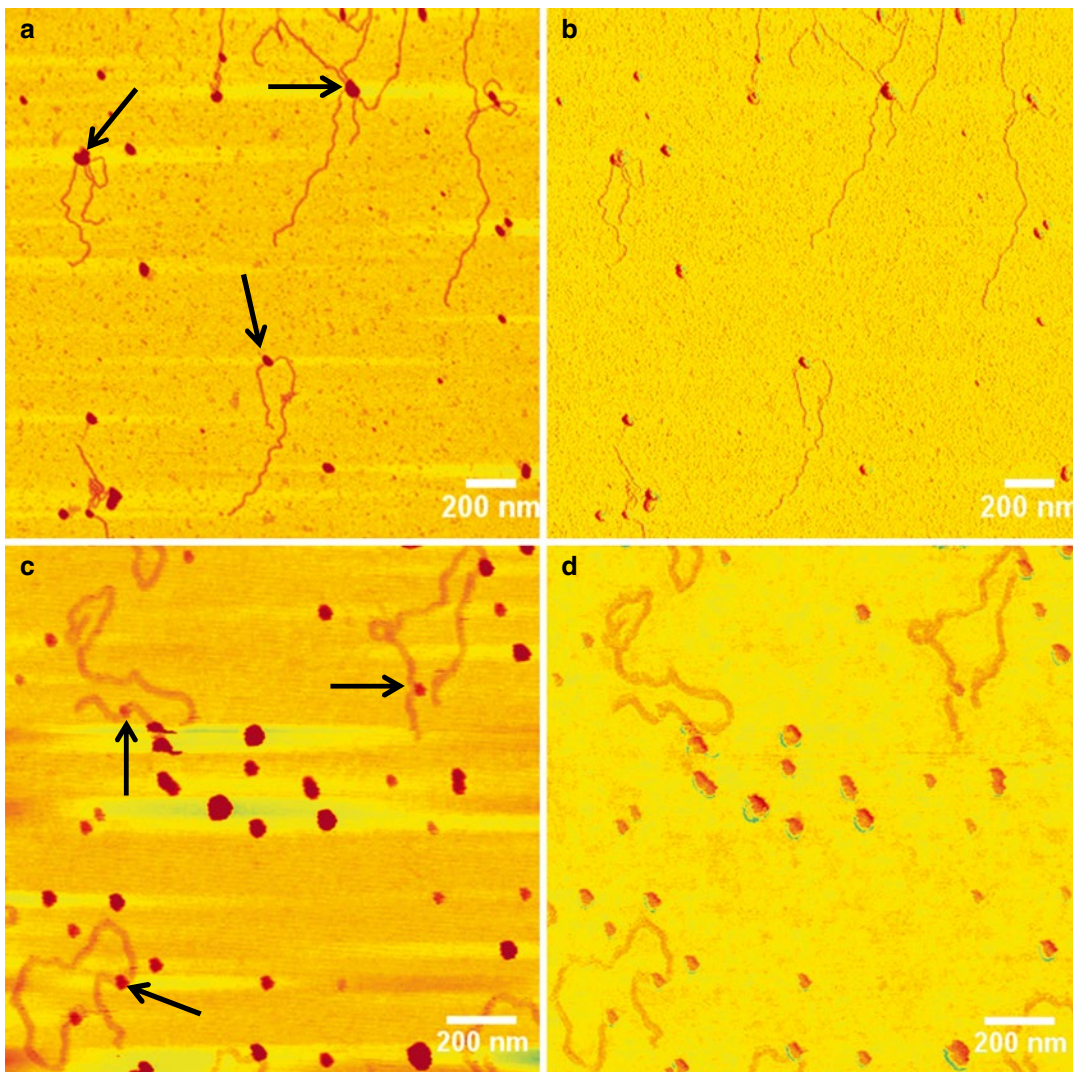
Fig. 6.4 (**a**, **b**) Are AFM topographical and corresponding phase images of QDs binding on DNA in the air, respectively. (**c**, **d**) Are AFM topographical and corresponding phase images of QDs binding on DNA in the liquid, respectively. *Black arrows* indicate representative binding sites of QDs on DNA

overall rate constant taking into account both adsorption and desorption.

Binding isotherms describe the equilibrium of the binding of NPs onto DNA. A Langmuir-type binding isotherm equation was derived and given in Eq. (6.2).

$$N = \frac{N_{\max} K [NP]}{1 + K [NP]} = \frac{N_{\max} [NP]}{1/K + [NP]} \quad (6.2)$$

where N and N_{max} are the binding number and the maximum binding number of NPs per DNA molecule, respectively; K is the equilibrium binding constant; $[NP]$ represents the number concentration of NPs.

The average number of bound QDs on DNA progressively increased as time elapsed, and finally reached a plateau (Fig. 6.5). The experimental observations fit the developed kinetics model very well with the least squared method. The average number of bound QDs is approximately five at equilibrium, and the rate constant is $0.40\,\mathrm{s}^{-1}$, which is comparable to a previous binding kinetic study on protein-DNA interactions [38].
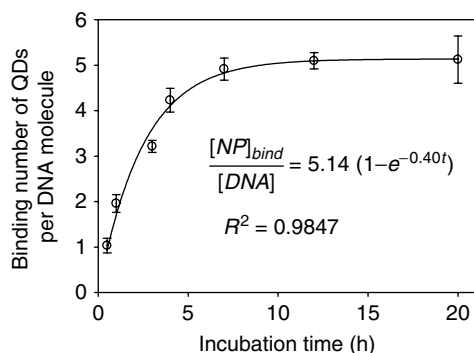
Fig. 6.5 Binding kinetics of QDs onto DNA molecules with a DNA-QDs molar ratio of 1:10. The line represents the model fit using Eq. (6.1)
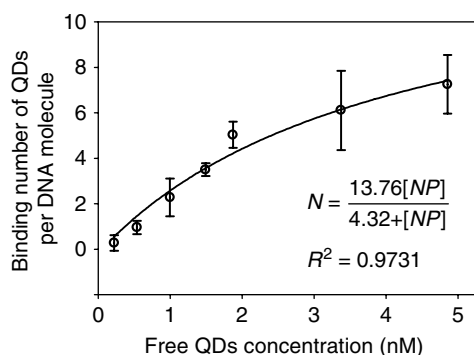

Fig. 6.7 Position histograms of QDs on DNA

Fig. 6.6 Binding isotherm of QDs onto DNA. The *line* represents the Langmuir-type fit using Eq. (6.2)

The binding isotherm (Fig. 6.6) characterizes the number of QDs per DNA molecule as a function of the free QDs concentration. As the DNA:QDs molar ratio increased from 1:1 to 1:20, the average binding number of QDs on DNA increased from approximately 0.4–7. The derived Langmuir-type equation fits the experimental data very well. The maximum binding number per DNA is approximately 14. The equilibrium binding constant K is approximately 0.23 nM^{-1}, which is close to previously reported binding constants of proteins onto DNA [39].

The binding specificities of QDs to DNA were determined by examining the binding positions of QDs on DNA. We defined the position of a QD as the ratio of the distance from its center to its closest DNA terminus to the contour length of DNA, as the two DNA ends are indistinguishable in AFM images. By examining a large number of QDs, the position histograms were plotted with
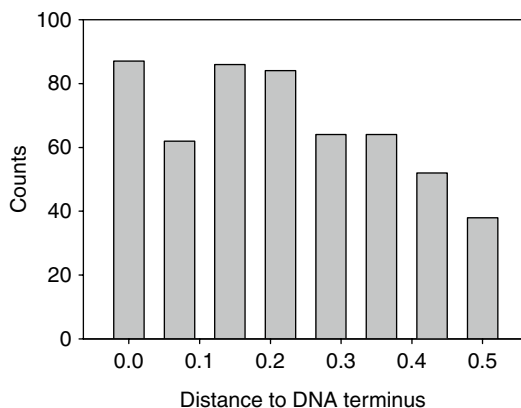
the position ranging from 0 to 0.5 (Fig. 6.7). We performed Kolmogorov-Smirnov tests to check whether the position distribution conforms to a uniform distribution or a Gaussian distribution. The results show the position distribution is generally uniform and no specific affinity of QDs to some sites were detected. Therefore, the specific binding cannot explain the existence of the maximum binding number of QDs on a DNA. We propose that the binding of a QD on DNA will prevent another QD from binding onto nearby positions because of the electrostatic repulsive force existing between two positively charged QDs.

In summary, using QDs as a model NP, a single-molecule imaging method based on AFM demonstrated its capability in examining the binding characteristics of NPs on DNA. We further proposed that a QD bound on DNA will prevent the binding of another QD onto its neighboring sites owing to the electrostatic repulsion between the two QDs. This single-molecule technique can be further extended to investigate the binding of other types of NPs on DNA, which potentially benefit research on the genotoxicity assessment of NPs as well as the design of functionalized NPs for biomedical applications.

6.4 Exploring the DNA-Binding Mechanisms of NPs

High-quality AFM imaging allows us to examine the fine conformation of QDs-DNA binding sites (Fig. 6.8a). By examining hundreds of DNA
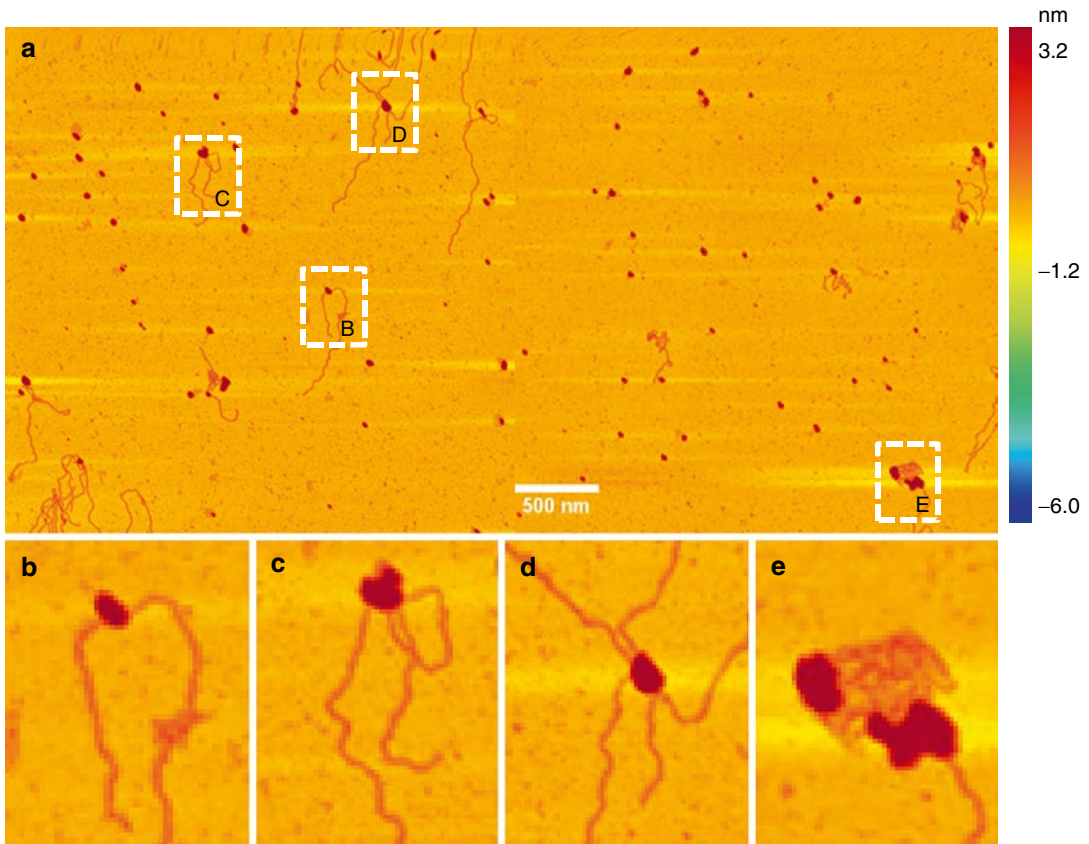
Fig. 6.8 Binding mechanisms of QDs to DNA observed by AFM. (**a**) AFM topographical images of DNA molecules binding with QDs. (**b**) QDs externally bind to the backbone of a single DNA and result in one binding site. (**c**) QDs induce DNA loops by simultaneously binding to two different sites on a DNA molecule. (**d**) QDs bridge two or more DNA molecules. (**e**) DNA wraps around QDs

molecules with AFM, four representative QDs-DNA binding mechanisms were suggested and are illustrated in Fig. 6.8b–e respectively: (1) QDs could externally bind to the DNA backbone via electrostatic interaction with the phosphate groups or through other interactions; (2) QDs likely generate DNA loops by simultaneously binding to two different sites on a DNA molecule; (3) QDs could bind to two or more DNA molecules and subsequently act as the intermolecular bridging agent; (4) DNA may wrap around the QDs, which play the similar role of histones in nucleosomes. This observation provides experimental validation about the NPs-DNA binding mechanisms proposed previously [12].

We statistically examined over 300 DNA molecules to count the frequency of each binding
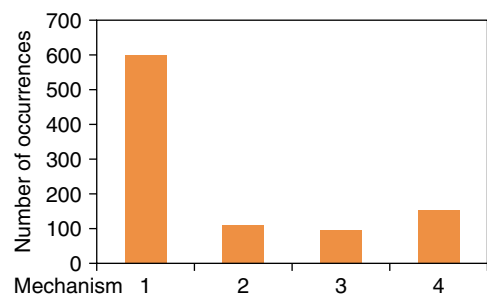

Fig. 6.9 Frequency of each binding mechanism

mechanism. As shown in Fig. 6.9, approximately 63 % of DNA-QDs interactions belong to mechanism (1), namely, QDs directly binding onto the DNA backbone. In addition, approximately 16 % of QDs binding to DNA would bridge two or
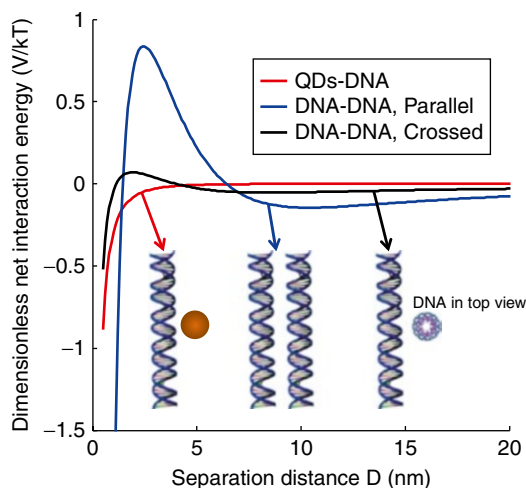
Fig. 6.10 Net interaction energy profiles for QDs and DNA, two parallel DNA molecules, and two crossed DNA molecules

more DNA molecules. The remaining 20 % almost equally belong to mechanisms (2) and (3).

To explore the underlying fundamentals on the unequal frequency of each binding mechanism, we further computed and analyzed the interaction energy between QDs and DNA molecules. The interaction between spherical NPs and DNA can be described with the Derjaguin-Landau-Verwey-Overbeek (DLVO) theory by treating the NP as a sphere and DNA as a uniformly charged cylinder because the dimension of the DNA is significantly larger than the separation distance between its neighboring charges (~0.17 nm) [40]. As shown in the net energy profiles (Fig. 6.10), no energy barrier exists for the interaction of QDs and DNA, indicating that the binding of QDs to the DNA backbone (i.e. mechanism (1)) was thermodynamically favourable. On the contrary, all of the other three mechanisms involve the approach of one section of DNA to another, which can be viewed as two negatively charged cylinders approaching each other, as the double-stranded DNA is a rigid polyelectrolyte with a persistent length of approximately 50 nm [41] remarkably larger than the separation distance between neighboring charges (~0.17 nm) [40]. The net interaction energy profiles for two parallel and crossed DNA molecules are presented in Fig. 6.10 from which

we can see that an energy barrier exists between two interacting DNA molecules regardless of their configuration. Hence the QDs-DNA configurations formed by mechanisms (2), (3) and (4) is less energetically favorable than by mechanism (1), which is consistent with the experimental observations that mechanism (1) dominated the QDs-DNA binding mechanisms.

6.5   Predicting the Binding Affinities of NPs for DNA and Comparison with AFM Observations

The binding affinities of NPs with DNA were predicted by computing the interaction energy between NPs and DNA molecules based on DLVO models, which describe the interfacial interactions between charged objects in liquid and is widely applicable in colloidal systems [42–44]. The interaction between spherical NPs and DNA can be described with the DLVO theory by treating the NP as a sphere and DNA as a uniformly charged cylinder and the total interactions were determined by the combination of van der Waals (vdW) and electrostatic double layer (EDL) interactions [45–48].

A number of parameters are required by the model including the size and the surface potential of both NPs and DNA molecules, and the Hamaker constant for NP-DNA interactions. The size of the five types of tested NPs was measured using AFM by examining at least 100 randomly picked particles. The determined radii of QDs (+), QDs (−), gold NPs, silver NPs, and hematite NPs are 8.54 ± 2.46, 7.80 ± 2.05, 2.76 ± 0.54, 6.41 ± 3.19, and 8.14 ± 1.44 nm, respectively. Here, the QDs (+) and QDs (−) refer to CdSe/ZnS core/shell QDs coated with polydiallydimethyl-ammonium chloride (PDDA) and poly (ethylene glycol) (PEG) with a carboxylic acid terminal end group, respectively, as the electrophoresis experiments showed the former carried positive surface charge while the latter carried negative charge. A high energy barrier suggests low binding affinity of the NP for DNA. The computed energy barriers between tested NPs and DNA are 0.18 kT for

QDs (−)-DNA, 0.08 kT for silver-DNA, 0.06 kT for gold-DNA, 0.02 kT for hematite-DNA, and 0 kT for QDs (+)-DNA. The results indicate that QDs (−) are least likely to bind to DNA compared with the other NPs, owing to the highest computed energy barrier between the QDs (−) and DNA molecules among the tested NPs. In contrast, the low determined energy barrier between QDs (+)-DNA will lead to the highest binding tendency. The modeling predictions on binding affinity are consistent with the experimental AFM imaging observations. As shown in Fig. 6.11, the QDs (+), silver NPs, hematite NPs, and gold NPs were observed to bind to DNA, while no binding was observed between the QDs (−) and DNA.

A number of databases have shown that nanoparticle binding to DNA has a significant impact on the bioactivities of DNA and DNA associated enzymes. Gold, silver, and carbon nanoparticles can enhance the specificity and sensitivity of the polymerase chain reaction (PCR), while at excess dosage these nanoparticles can inhibit DNA amplification [4, 49, 50]. Pre-occupation of DNA by NPs in the binding sites of proteins that are requisite for DNA replication, transcription, and repair processes (e.g. DNA polymerase/RNA polymerase and sigma factor) will likely disturb the biological activities in which these proteins are involved.

The AFM images in Fig. 6.11 have also indicated that the binding of NPs to DNA would dramatically change the DNA conformation, which may interfere with normal DNA functions. In contrast, DNA molecules incubated with QDs (−) did not show conformational changes, which supposedly maintained normal functions. Thereby, we employed the PCR method to probe the effect of NPs on DNA replication. The agarose gel electrophoresis results (Fig. 6.12) showed how the five types of NPs over a range of concentrations affected DNA replication. The quantity of PCR amplified DNA products were significantly reduced after silver NPs exposure at 0.03 nM. DNA replication was completely inhibited by silver NPs at 0.05 nM. QDs (+) completely inhibited DNA replication at 0.15 nM. Hematite NPs showed an obvious inhibition of DNA replication at 0.1 nM and a complete inhibition at 0.2 nM. Gold NPs affected DNA replication at 0.3 nM and completely impeded the replication process at the concentration of 0.5 nM. In contrast, QDs (−) did not show any inhibition at a concentration as high as 1.6 nM.

The relation between the concentration of tested NPs to inhibit DNA replication and the computed binding affinity of NPs with DNA was also investigated. As shown in Fig. 6.13, NPs that were predicted to have a high binding affinity (i.e., low energy barrier) for DNA molecules also had a high potential to inhibit DNA replication. Exceptionally, the Ag NPs have a higher inhibition ability compared with the model prediction. We speculate this could be attributed to Ag^+ released from Ag NPs which are documentarily detrimental to DNA replication [51]. Overall, the demonstrated relation between the inhibition ability of NPs toward DNA replication and their binding affinity with DNA implied that (1) the binding of NPs to DNA is likely an important mechanism for causing the genotoxicity of NPs, and (2) the DLVO model may act as a simple and effective tool for predicting the genotoxicity of NPs induced by the direct binding activity of NPs with DNA. It is worth noting that the measured size of all the tested DNA are no bigger than their nominal size, indicative of the absence of aggregation among the tested NPs. This validated the applicability of our developed predictive model for the genotoxicity of unaggregated NPs. Furthermore, the methodology in this study can help researchers screen NPs and prioritize their genotoxicological testing.

6.6 Summary and Future Perspectives

There are no simple ways of probing the interactions occurring in the nano-bio interface in real time or *in situ* provided the complexity of the biological system. Research findings acquired starting with DNA and/or proteins and then with cells will provide essential information for the development of eventually a comprehensive view of the environmental implications of NPs on biological systems.
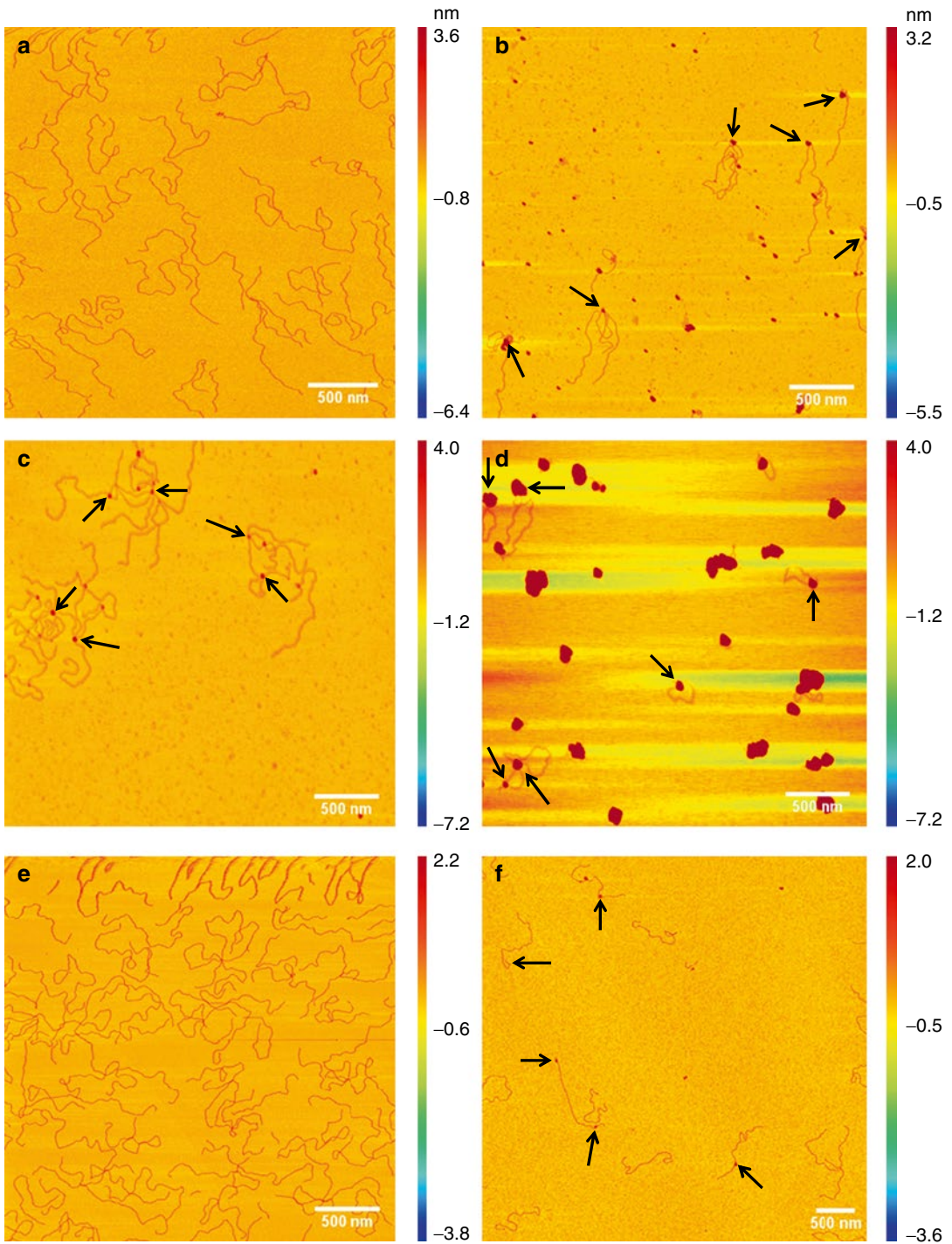
Fig. 6.11 AFM topographical images of (**a**) DNA molecules, (**b**) DNA binding with QDs (+), (**c**) DNA binding with silver NPs, (**d**) DNA binding with hematite NPs, (**e**) DNA incubated with QDs (−), and (**f**) DNA incubated with gold NPs. The *black arrows* indicate representative binding sites of NPs on DNA molecules. QDs (−) and gold NPs did not bind onto DNA molecules
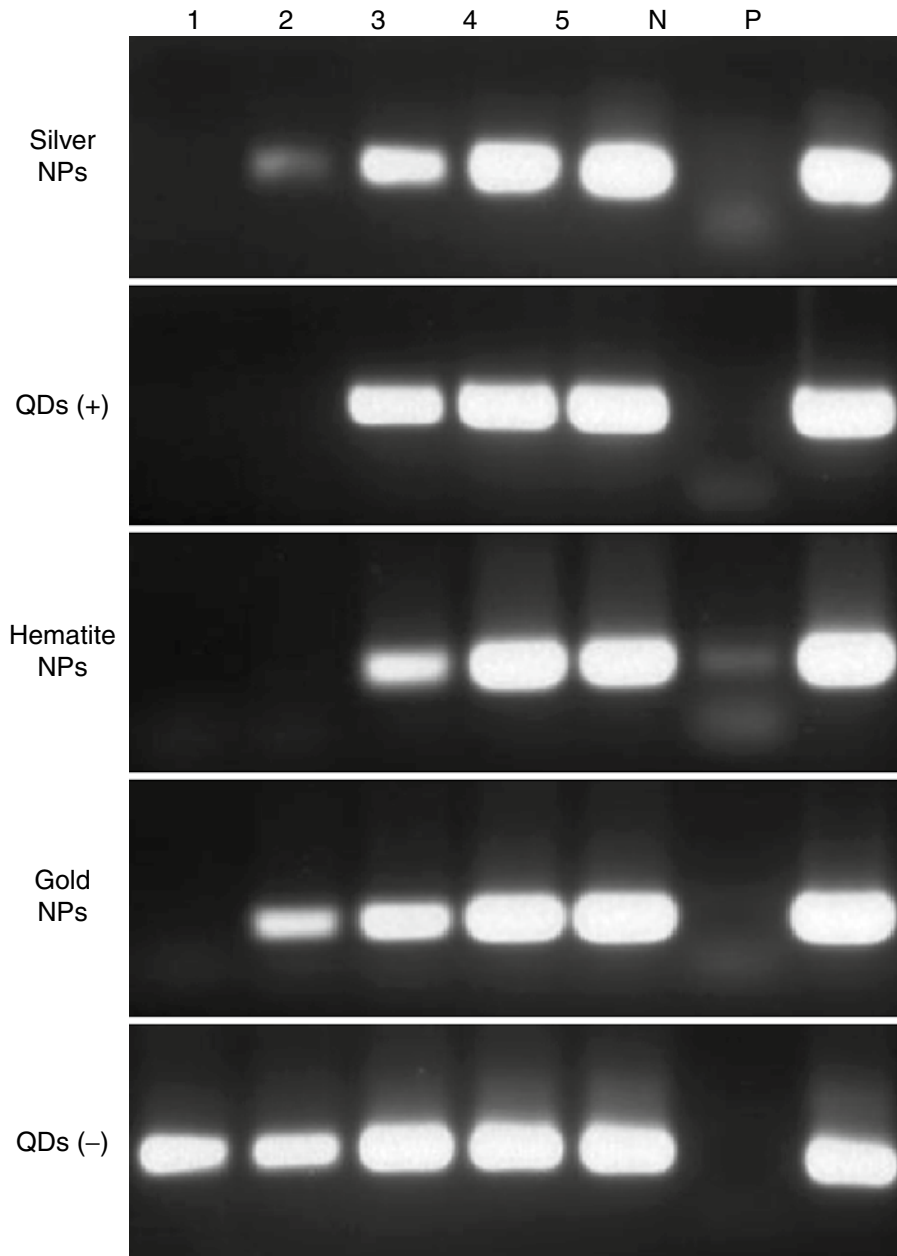
Fig. 6.12 Effects of NPs on DNA replication *in vitro* by quantification of PCR products. 50 ng of Linearized pGE-MEX-1 was used in each reaction to amplify a 180 bp PCR fragment except for negative control. Each type of NPs was tested under a range of concentrations. From lane 1–5, the final concentrations of silver NPs were 0.05, 0.03, 0.02, 0.01, 0.002 nM, QDs (+) were 0.2, 0.15, 0.1, 0.05, 0.01 nM, hematite NPs were 0.5, 0.2, 0.1, 0.05, 0.01 nM, gold NPs were 0.5, 0.03, 0.2, 0.01, 0.05 nM, and QDs (−) were 1.6, 0.8, 0.16, 0.08, 0.016 nM. N and P respectively represent the negative and positive controls for the PCR experiment. *N* negative control without DNA template and NPs, *P* positive control using 50 ng of DNA template without NPs

Research work from our lab together with others has proven the effectiveness of the AFM microscopic technique for both the quantitative and qualitative measurements in the exploration of nano-bio interactions. As being exemplified in our research work, the combination of experimental

Fig. 6.13 Relationship between the concentration of NPs to completely inhibit DNA replication *in vitro* and the height of the energy barrier between NPs and DNA. Data points represent individual replicates. A linear regression [y = 0.09 + 8.18x, r² = 0.9828] was performed for all data points except Ag NPs (the fitted line is not shown in the graph). Note that although QDs (−) did not inhibit DNA replication at the concentration even as high as 1.6 nM; we put that data point in the graph for comparison with other NPs
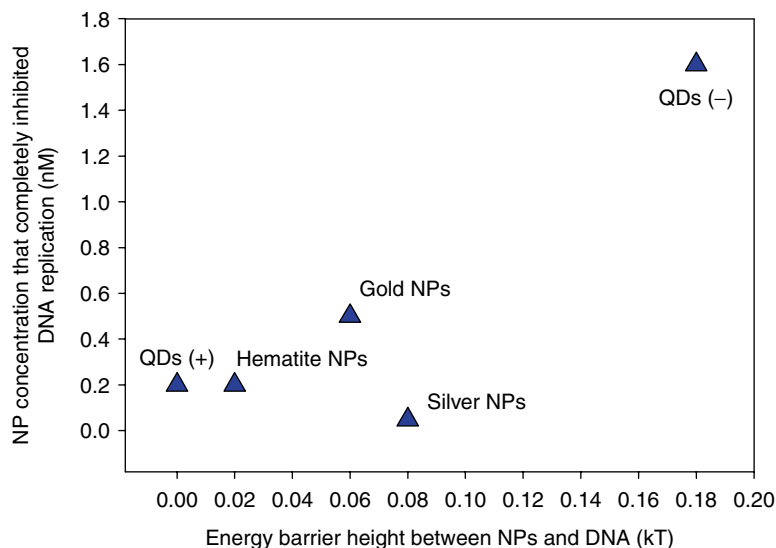
measurement mainly derived from AFM imaging techniques with the classic modeling computation of binding energy barrier extrapolated from colloid science, was proven to be a success in the development of predictive models for the genotoxicity of environmentally present NPs. Given the limitation of computation efficiency and the capacity of conventionally used computation simulation techniques such as molecular dynamic simulations, the methodologies developed in this study is considered to be a more practical alternative for this purpose. The methodology employed in this study with a short list of NPs can be extended to study the interaction of other NPs with DNA, which is anticipated to benefit the future investigation of the structure of NPs-DNA bioconjugates, and the toxicological perspectives of NPs-DNA interactions. Future studies may also include using AFM to investigate the NP-RNA interactions, and the effect of NPs on DNA transcription.

References

1. An HJ, Jin B (2012) Prospects of nanoparticle-DNA binding and its implications in medical biotechnology. Biotechnol Adv 30:1721–1732
2. An HJ, Liu QD, Ji QL, Jin B (2010) DNA binding and aggregation by carbon nanoparticles. Biochem Biophys Res Commun 393:571–576
3. Nel AE, Madler L, Velegol D, Xia T, Hoek EMV, Somasundaran P, Klaessig F, Castranova V, Thompson M (2009) Understanding biophysicochemical interactions at the nano-bio interface. Nat Mater 8:543–557
4. Yang WJ, Shen CC, Ji QL, An HJ, Wang JJ, Liu QD, Zhang ZZ (2009) Food storage material silver nanoparticles interfere with DNA replication fidelity and bind with DNA. Nanotechnology 20:0851-02
5. Allen MJ, Bradbury EM, Balhorn R (1997) AFM analysis of DNA-protamine complexes bound to mica. Nucleic Acids Res 25:2221–2226
6. Alonso-Sarduy L, Roduit C, Dietler G, Kasas S (2011) Human topoisomerase II-DNA interaction study by using atomic force microscopy. FEBS Lett 585:3139–3145
7. Hansma HG (2001) Surface biology of DNA by atomic force microscopy. Annu Rev Phys Chem 52:71–92
8. Lyubchenko YL, Shlyakhtenko LS (2009) AFM for analysis of structure and dynamics of DNA and protein-DNA complexes. Methods 47:206–213
9. Pastre D, Hamon L, Sorel I, Le Cam E, Curmi PA, Pietrement O (2010) Specific DNA-protein interactions on mica investigated by atomic force microscopy. Langmuir 26:2618–2623
10. Tessmer I, Moore T, Lloyd RG, Wilson A, Erie DA, Allen S, Tendler SJB (2005) AFM studies on the role of the protein RdgC in bacterial DNA recombination. J Mol Biol 350:254–262
11. An H, Jin B (2011) DNA exposure to buckminsterfullerene (C-60): toward DNA stability, reactivity, and replication. Environ Sci Tech 45:6608–6616
12. Li KG, Zhang W, Chen YS (2013) Quantum dot binding to DNA: single-molecule imaging with atomic force microscopy. Biotechnol J 8(1):110–116

13. Zhang W, Yao Y, Chen YS (2011) Imaging and quantifying the morphology and nanoelectrical properties of quantum dot nanoparticles interacting with DNA. J Phys Chem C 115:599–606
14. Butt H-J, Graf K, Kappl M (2003) Physics and chemistry of interfaces. Wiley-VCH, Weinheim
15. Butt HJ, Cappella B, Kappl M (2005) Force measurements with the atomic force microscope: technique, interpretation and applications. Surf Sci Rep 59: 1–152
16. Considine RF, Drummond CJ (2001) Surface roughness and surface force measurement: a comparison of electrostatic potentials derived from atomic force microscopy and electrophoretic mobility measurements. Langmuir 17:7777–7783
17. Zhang W, Stack AG, Chen YS (2011) Interaction force measurement between E. coli cells and nanoparticles immobilized surfaces by using AFM. Colloids Surf B Biointerfaces 82:316–324
18. Blanchard BJ, Thomas VL, Ingram VM (2002) Mechanism of membrane depolarization caused by the Alzheimer A beta 1–42 peptide. Biochem Biophys Res Commun 293:1197–1203
19. Oh YJ, Jo W, Yang Y, Park S (2007) Biofilm formation and local electrostatic force characteristics of Escherichia coli O157: H7 observed by electrostatic force microscopy. Applied Physics Letters 90:143901–143903
20. Sun L, Wang JJ, Bonaccurso E (2010) Nanoelectronic properties of a model system and of a conjugated polymer: a study by Kelvin probe force microscopy and scanning conductive torsion mode microscopy. J Phys Chem C 114:7161–7168
21. Zhang W, Hughes J, Chen YS (2012) Impacts of hematite nanoparticle exposure on biomechanical, adhesive, and surface electrical properties of Escherichia coli cells. Appl Environ Microbiol 78:3905–3915
22. Muller DJ, Dufrene YF (2011) Atomic force microscopy: a nanoscopic window on the cell surface. Trends in Biology 21:433–498
23. Dhawan A, Sharma V (2010) Toxicity assessment of nanomaterials: methods and challenges. Anal Bioanal Chem 398:589–605
24. Li HX, Rothberg L (2004) Colorimetric detection of DNA sequences based on electrostatic interactions with unmodified gold nanoparticles. Proc Natl Acad Sci U S A 101:14036–14039
25. Gill R, Zayats M, Willner I (2008) Semiconductor quantum dots for bioanalysis. Angew Chem Int Ed 47:7602–7625
26. Medintz IL, Uyeda HT, Goldman ER, Mattoussi H (2005) Quantum dot bioconjugates for imaging, labelling and sensing. Nat Mater 4:435–446
27. Michalet X, Pinaud FF, Bentolila LA, Tsay JM, Doose S, Li JJ, Sundaresan G, Wu AM, Gambhir SS, Weiss S (2005) Quantum dots for live cells, in vivo imaging, and diagnostics. Science 307:538–544
28. Qi LF, Gao XH (2008) Emerging application of quantum dots for drug delivery and therapy. Expert Opin Drug Deliv 5:263–267
29. Green M, Howman E (2005) Semiconductor quantum dots and free radical induced DNA nicking. Chem Commun (Camb) 1:121–123
30. Leung C, Maradan D, Kramer A, Howorka S, Mesquida P, Hoogenboom BW (2010) Improved Kelvin probe force microscopy for imaging individual DNA molecules on insulating surfaces. Appl Phys Lett 97:203703
31. Guthold M, Zhu XS, Rivetti C, Yang GL, Thomson NH, Kasas S, Hansma HG, Smith B, Hansma PK, Bustamante C (1999) Direct observation of one-dimensional diffusion and transcription by Escherichia coli RNA polymerase. Biophys J 77:2284–2294
32. Lyubchenko YL, Shlyakhtenko LS (1997) Visualization of supercoiled DNA with atomic force microscopy in situ. Proc Natl Acad Sci U S A 94:496–501
33. Stark M, Moller C, Muller DJ, Guckenberger R (2001) From images to interactions: high-resolution phase imaging in tapping-mode atomic force microscopy. Biophys J 80:3009–3018
34. Mahtab R, Harden HH, Murphy CJ (2000) Temperature- and salt-dependent binding of long DNA to protein-sized quantum dots: thermodynamics of "inorganic protein"-DNA interactions. J Am Chem Soc 122:14–17
35. Mahtab R, Sealey SM, Hunyadi SE, Kinard B, Ray T, Murphy CJ (2007) Influence of the nature of quantum dot surface cations on interactions with DNA. J Inorg Biochem 101:559–564
36. Zhao YD, Xu Q, Wang JH, Wang Z, Yin ZH, Yang Q (2008) Interaction of CdTe quantum dots with DNA. Electrochem Commun 10:1337–1339
37. Yang Y, Sass LE, Du CW, Hsieh P, Erie DA (2005) Determination of protein-DNA binding constants and specificities from statistical analyses of single molecules: MutS-DNA interactions. Nucleic Acids Res 33:4322–4334
38. Winter RB, Berg OG, Vonhippel PH (1981) Diffusion-driven mechanisms of protein translocation on nucleic-acids. 3. The Escherichia-coli-Lac repressor-operator interaction – kinetic measurements and conclusions. Biochemistry 20:6961–6977
39. Schofield MJ, Brownewell FE, Nayak S, Du CW, Kool ET, Hsieh P (2001) The Phe-X-Glu DNA binding motif of MutS – the role of hydrogen bonding in mismatch recognition. J Biol Chem 276: 45505–45508
40. Harries D (1998) Solving the Poisson-Boltzmann equation for two parallel cylinders. Langmuir 14: 3149–3152
41. Manning GS (2006) The persistence length of DNA is reached from the persistence length of its null isomer through an internal electrostatic stretching force. Biophys J 91:3607–3616

42. Derjaguin B, Sidorenkov G (1941) Thermoosmosis at ordinary temperatures and its analogy with the thermomechanical effect in helium II. C R Acad Sci De L Urss 32:622–626

43. Hoek EMV, Agarwal GK (2006) Extended DLVO interactions between spherical particles and rough surfaces. J Colloid Interface Sci 298:50–58

44. Verwey EJW, Overbeek JTG, van Nes K (1948) Theory of the stability of lyophobic colloids; the interaction of sol particles having an electric double layer. Elsevier Pub. Co., New York

45. Li KG, Chen YS (2012) Evaluation of DLVO interaction between a sphere and a cylinder. Colloids Surf A Physicochem Eng Asp 415:218–229

46. Schellman JA, Stigter D (1977) Electrical double-layer, zeta potential, and electrophoretic charge of double-stranded DNA. Biopolymers 16:1415–1434

47. Sharp KA, Honig B (1990) Electrostatic interactions in macromolecules – theory and applications. Annu Rev Biophys Biophys Chem 19:301–332

48. Stigter D (1977) Interactions of highly charged colloidal cylinders with applications to double-stranded DNA. Biopolymers 16:1435–1448

49. Li G, Levitus M, Bustamante C, Widom J (2005) Rapid spontaneous accessibility of nucleosomal DNA. Nat Struct Mol Biol 12:46–53

50. Mi LJ, Wen YQ, Pan D, Wang YH, Fan CH, Hu J (2009) Modulation of DNA polymerases with gold nanoparticles and their applications in hot-start PCR. Small 5:2597–2600

51. Chaloupka K, Malam Y, Seifalian AM (2010) Nanosilver as a new generation of nanoproduct in biomedical applications. Trends Biotechnol 28:580–588

Intracellular Signal Modulation by Nanomaterials

7

Salik Hussain, Stavros Garantziotis, Fernando Rodrigues-Lima, Jean-Marie Dupret, Armelle Baeza-Squiban, and Sonja Boland

Contents

S. Hussain (✉) • S. Garantziotis
Clinical Research Program, National Institute of Environmental Health Sciences (NIEHS),
National Institute of Health (NIH),
Research Triangle Park, NC, USA
e-mail: salik.hussain@nih.gov

F. Rodrigues-Lima • J.-M. Dupret
A. Baeza-Squiban • S. Boland
Unit of Functional and Adaptive Biology (BFA)
CNRS EAC 4413, Laboratory of Molecular and
Cellular Responses to Xenobiotics (RMCX),
University Paris Diderot, Sorbonne Paris Cité,
Paris, France
e-mail: boland@univ-paris-diderot.fr

Abstract

A thorough understanding of the interactions of nanomaterials with biological systems and the resulting activation of signal transduction pathways is essential for the development of safe and consumer friendly nanotechnology. Here we present an overview of signaling pathways induced by nanomaterial exposures and describe the possible correlation of their physicochemical characteristics with biological outcomes. In addition to the hierarchical oxidative stress model and a review of the intrinsic and cell-mediated mechanisms of reactive oxygen species (ROS) generating capacities of nanomaterials, we also discuss other oxidative stress dependent and independent cellular signaling pathways. Induction of the inflammasome, calcium signaling, and endoplasmic reticulum stress are reviewed. Furthermore, the uptake mechanisms can be of crucial importance for the cytotoxicity of nanomaterials and membrane-dependent signaling pathways have also been shown to be responsible for cellular effects of nanomaterials. Epigenetic regulation by nanomaterials, effects of nanoparticle-protein interactions on cell signaling pathways, and the induction of various cell death modalities by nanomaterials are described. We describe the common trigger mechanisms shared by various nanomaterials to induce cell death pathways and describe the interplay of different modalities in orchestrating the final outcome after nanomaterial exposures. A better understanding of signal modulations induced by nanomaterials is not only essential for the synthesis and design of safer nanomaterials but will also help to discover potential nanomedical applications of these materials. Several biomedical applications based on the different signaling pathways induced by nanomaterials are already proposed and will certainly gain a great deal of attraction in the near future.

Keywords

Signaling • Nanotoxicology • Nanomedicine • Oxidative stress • Protein interaction • Cell death • Physico-chemical characteristics

Abbreviations

AP-1	Activator protein 1
CB	Carbon black
CNT	Carbon nanotubes
LPS	Lipopolysacchrides
MWCNT	Multi-walled carbon nanotubes
NP	Nanoparticle
NADPH	Nicotinamide adenine dinucleotide phosphate
NF-κB	Nuclear factor-kappa B
Nrf-2	Nuclear factor (erythroid-derived-2)-related factor 2
QD	Quantum dots
ROS	Reactive oxygen species
SWCNT	Single walled carbon nanotubes
UPR	Unfolded protein response

7.1   Introduction

The increasing utilization of nanomaterials in consumer products, environmental sectors and nanomedicine has led to increased consumer, occupational and environmental exposures to these materials. The study of possible adverse health effects is thus warranted for the development of safe and consumer friendly nanotechnology. Many nanomaterials have indeed been shown to be toxic *in vitro* and *in vivo*, inducing inflammation, genotoxicity and cell death in various organ systems. Understanding the underlying cellular and molecular mechanisms is of crucial importance to design safer nanomaterials. Shvedova and colleagues have proposed that nanotoxicology must be defined as a discipline studying the interference of engineered nanomaterials with the function of cellular and extracellular nanomachineries [1]. This definition emphasizes not only the description of specific responses that are directly related to the nanomaterial size, but also the understanding of the underlying mechanisms. Furthermore it is important to analyze the consequences of nanomaterial-protein interactions on signal transduction. Finally, the establishment of common features of nanomaterials, which are responsible for the observed effects, is essential to predict possible

adverse health effects of new materials. A better understanding of signal modulations induced by nanomaterials will also help to discover potential biomedical applications of these materials.

This chapter reviews the current understanding of cellular effects (anti-oxidant defense, inflammation, apoptosis) induced by nanoparticles (NP) with focus on the underlying mechanisms and signal modulations. We discuss oxidative stress dependent mechanisms as well as signaling pathways which are independent of reactive oxygen species (ROS) production. We emphasize the role of NP-protein interactions in the effects induced and describe the physicochemical characteristics of nanomaterials responsible for the cellular effects.

7.2 Hierarchical Oxidative Stress Model

One of the major biological effects of nanomaterials is the production of ROS within the cells. Controlling the level of the cellular redox status is crucial for normal cell function and is a finely regulated process. The production of cellular oxidants is counterbalanced by the presence of antioxidants which allow maintaining a low level of ROS to prevent cell damage. An imbalance of this equilibrium leads to oxidative stress which at sustained high levels may result in an oxidative attack on cellular molecules including membrane constituents, proteins and the genomic DNA leading to cell death. On the other hand, during a transient induction of oxidative stress, ROS can act as second messengers in redox sensitive signaling pathways through reversible and transient protein oxidations, regulating their activity. Indeed, ROS can activate transcription factors such as NF-κB (nuclear factor-kappa B) which induces the expression of genes involved in pro-inflammatory responses and apoptosis whereas activation of the transcription factor AP-1 (activator protein 1) by ROS leads to proliferation and differentiation. At lower levels of oxidative stress, ROS induce an antioxidant defence by activating the nuclear factor (erythroid-derived-2)-related factor 2 (Nrf-2). This transcription factor binds to the antioxidant responsive elements (ARE) to induce the expression of phase II detoxifying and antioxidant enzymes such as glutathion *S* transferase (GST), γ glutamyl cysteine synthetase (GCS), nicotinamide adenine dinucleotide phosphate quinone oxidoreductase (NQO1), and heme oxygenase-1 (HO-1). A hierarchical cellular response to oxidative stress is thus observed, inducing an anti-oxidant defense at low levels, pro-inflammatory responses and proliferation at higher levels and finally cell death at very high oxidative stress levels. This three tiered oxidative stress model was proposed by Nel et al. to account for the toxicity of nanomaterials [2]. Several studies have since confirmed the central role of ROS production in the toxicity of numerous nanomaterials.

7.2.1 Mechanisms of Reactive Oxygen Species Production by Nanomaterials

Nanomaterials can generate and induce the production of ROS through different mechanisms (Fig. 7.1). The nanomaterial surface could present surface bound radicals such as $O_2^{\circ-}$, OH°, SiO° or TiO° which may react with O_2 to form $O_2^{\circ-}$ radicals which in turn could generate other ROS. Structural defects on the particle surface could also lead to the formation of reactive groups. Finally, the nanomaterial surface may also include transition metals which could generate ROS through Fenton-type and Haber-Weiss-type reactions. Furthermore, environmental oxidants such as ozone, semiquinones and NO could adsorb onto the nanomaterial surface and enter cells through the so called "Trojan Horse Effect". In addition to these inherent ROS generating properties, nanomaterials could also indirectly enable ROS production by triggering cellular mechanisms. Damage or activation of mitochondria could lead to the release of ROS produced by the mitochondrial electron transport chain. Another source of intracellular ROS is the nicotinamide adenine dinucleotide phosphate (NADPH) oxidase which could be activated by nanomaterials as shown for ZnO NPs [3]. This

Fig. 7.1 Overview of ROS production mechanisms by nanoparticles. Nanoparticles can induce ROS production either (1) through their intrinsic ability to catalyze oxidation reduction reactions through their surfaces or (2) through interaction with cellular components and normal ROS production mechanisms (e.g. mitochondria and NADPH oxidase system) or by decreasing the cellular anti-oxidant defense mechanisms (e.g. savaging/inactivation or decreased production of anti-oxidants)
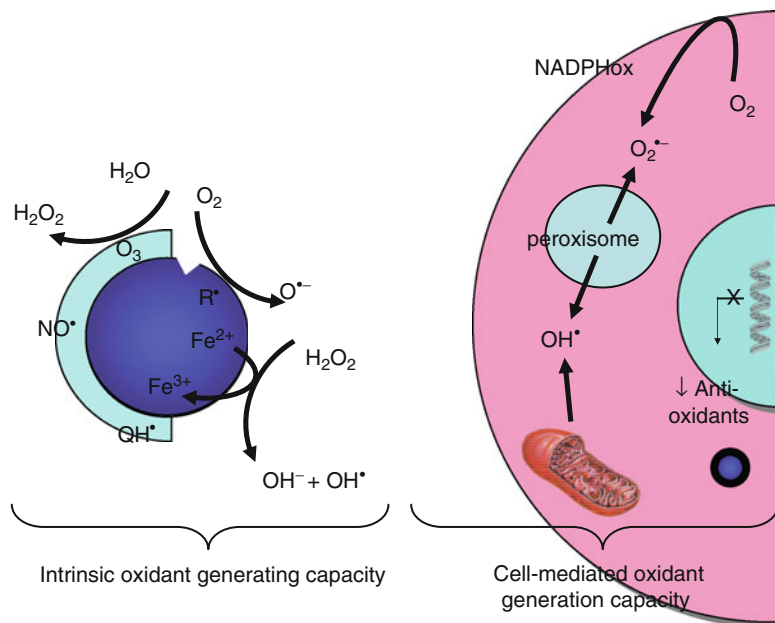
membrane bound enzyme is highly expressed in neutrophils and macrophages to ensure the respiratory burst for killing invading microorganisms through ROS production. Under physiological conditions this enzyme complex is latent in phagocytic cells. However, nanomaterials can activate the inflammatory cells inducing a respiratory burst in the absence of bacteria [4, 5]. NADPH oxidase is abundant in "professional" phagocytes but this protein is also present in non inflammatory cells where it contributes to cell signaling. Involvement of NADPH oxidase in CeO_2 and CoCr NP toxicity has for instance been demonstrated in fibroblasts [6, 7]. Other enzymes also generate ROS as by-products of their activity such as cytochrome P450, xanthine oxidase, lipoxygenase, cyclooxygenase as well as enzymes within the peroxisome complex. Activation of macrophages is an especially important mechanism of ROS production by high aspect ratio nanomaterials (HARN) as long, thin and biopersistent fibres could lead to "frustrated phagocytosis". This mechanism leads to the persistent release of oxidants and pro-inflammatory mediators and has been firstly described to account for the toxicity of asbestos but it has since been observed also for carbon nanotubes (CNT) [8]. A further indirect mechanism of

oxidative stress induction by nanomaterials is the depletion or inhibition of anti-oxidants leading to an imbalance of the redox homeostasis of the cell. Interference of nanomaterials with the scavenging properties of anti-oxidants and metalloproteins or inhibition of the synthesis of enzymatic or non enzymatic anti-oxidants by nanomaterials will indirectly trigger oxidative stress. For instance, Pl/Au nanorods have been shown to reduce the ability of ascorbic acid to scavenge radicals [9]. Nanomaterials may also inhibit repair mechanisms which eliminate molecules damaged by ROS potentiating their toxicity. On the other hand, some nanomaterials could also scavenge radicals on their surface or exert anti-oxidant properties (e.g. Au, Ag, CeO_2 and Pl NPs). CeO_2 NPs have oxygen buffering capacities which are attributed to the valence state of cerium and to defects in the crystal structure which are increased at the nano-scale. The anti-oxidant properties of CeO_2 NPs thus depend on the nanocrystal diameter [10] and the ratio of surface Ce^{3+}/Ce^{4+} [11]. This interesting anti-oxidant property of some nanomaterials is intended to be used in nanomedical applications [12, 13].

There are thus at least two major mechanisms of oxidative stress induction by nanomaterials. The cell mediated ROS production and ROS generation

in acellular conditions based on the intrinsic oxidant potential of the particles. Overall, nanomaterials with or without such oxidative properties may however also produce oxidants *via* cell-mediated mechanisms. It has for instance been shown that TiO$_2$ NPs have a low intrinsic capacity to produce oxidants compared to carbon black (CB) NPs but have been shown to induce the same level of intracellular ROS in bronchial epithelial cells [14] this implies that the oxidative stress potential of nanomaterials cannot solely be deduced by their cell-free oxidant generating properties.

7.2.2 Paradigm of the Graduated Oxidative Stress Responses Induced by Nanomaterials

ROS production induced by nanomaterials has been shown to orchestrate various cellular effects through different signaling pathways dependent on the level of oxidative stress induced. Many nanomaterials (CNT [15], Ag [16, 17], SiO$_2$ [18], CuO [19], and tungsten carbide Co [20]) have been shown to induce the activation of the transcription factor Nrf-2 leading to an increase of the expression of phase II detoxifying as well as antioxidant enzymes *in vitro*. The involvement of Nrf-2 in inducing an anti-oxidant defense to protect cells against nanomaterials was confirmed using Nrf-2 knockdown cells [19]. Activation of this signaling pathway and antioxidant defense has also been demonstrated *in vivo* for TiO$_2$ NPs [21]. ROS-dependent inflammatory responses are also very common nanomaterial effects induced through MAPK signaling and activation of NF-κB dependent inflammatory cytokine gene expression and have recently been reviewed [22]. The activation of the transcription factor AP-1 by nanomaterials has been reported less frequently but it has been shown to be induced *in vitro* and *in vivo* by CuO [19], CB [23], CNT [24], Co [25], WC-Co [26], Al$_2$O$_3$ [27] and iron oxide NPs [28]. High levels of oxidative stress may finally lead to cell death and nanomaterials have been shown to induce different apoptotic or necrotic signaling pathways which are discussed in Sect. 7.3.

Nanomaterials have thus been shown to induce different ROS dependent signaling pathways in accordance with the oxidative stress paradigm proposed by Nel et al. [2]. Activation of these signaling pathways by nanomaterials may thus induce an anti-oxidant defense at low levels of oxidative stress, proliferation and pro-inflammatory responses at higher oxidative stress levels and finally cell death at deleterious levels of ROS. High throughput analysis of signaling pathways, protein and gene expression have confirmed the induction of these cellular responses *in vitro* as well as *in vivo*. Gene expression profiles have shown that nanomaterials induce mostly expression of mRNAs associated with cell signaling, metabolism, and stress, but also cytoskeleton and vesicle trafficking or cell membrane proteins. Depending on the nanomaterials and concentrations the induced mRNAs or proteins were related to inflammation, cell cycle, apoptosis or DNA repair [21, 29–35]. High throughput screening of signaling pathways induced by several metal oxide NPs in macrophages have been performed and the use of Self Organizing Map (SOM) analysis revealed two cluster groups of sub-lethal pro-inflammatory responses and of lethal genotoxic responses [36] confirming the hierarchical cellular response to NPs. These approaches may also allow developing quantitative structure-activity relationships (QSAR). Some papers have compared the protein expression, gene expression and protein phosphorylation within the same study such as Ge and colleagues allowing the establishment of protein-interacting networks and upstream signaling pathways of toxicity responses but also detoxification pathways of TiO$_2$ in bronchial epithelial cells [37]. These cellular effects may have several pathophysiological consequences such as inflammation or fibrosis.

7.3 Other Cellular Mechanisms Induced by Nanomaterials

Beyond this graduated oxidative stress response paradigm other mechanisms could also induce cellular responses. Some of these effects are directly

or indirectly linked to oxidative stress but others are ROS-independent mechanisms. These mechanisms could however sometimes lead to intracellular ROS production and it is therefore often not easy to distinguish whether ROS are the cause or the consequence of cellular signaling pathways.

7.3.1 Oxidation of Biomolecules

The induction of high levels of oxidative stress by nanomaterials can lead to oxidation of cellular molecules. Oxidative DNA damage has been evidenced for many nanomaterials using several techniques such as the Fpg (formamidopyrimidine-DNA glycosylase) modified comet assay or detection of 8-hydroxydeoxyguanosine by immunohistochemistry or HPLC. This genotoxic insult can either be repaired or induce apoptosis but failure of these protection mechanisms could lead to mutagenesis. Protein oxidation could also be a consequence of oxidative stress which could lead to their inactivation as well as activation. The redox proteome (reversible and irreversible covalent protein modifications) links redox metabolism to biological structure and function. Lipid peroxidation on the other hand can induce lysosomal damage and this mechanism has been shown to be responsible for TiO_2 induced apoptosis [38] and can lead to inflammasome activation.

7.3.2 Inflammasome Activation

Inflammatory responses could not only be induced by NF-κB signaling but also through activation of the inflammasome. This multiprotein complex promotes the maturation of proinflammatory cytokines IL-1 beta and IL-18 and could be activated by ROS but also by other cellular mechanisms. For instance cathepsin B, which could be released after lysosome rupture induced by ROS dependent as well as ROS independent mechanisms can activate the inflammasome. A cathepsin B dependent activation of the inflammasome has been shown to be responsible for TiO_2 induced production of IL-1beta by macrophages [39]. TiO_2 NPs have also been shown to induce lipid peroxidation leading to lysosomal destabilisation with

subsequent release of cathepsin B in bronchial epithelial cells [38]. Conversely, amino-functionalized polystyrene NPs induced lysosomal destabilisation through a ROS independent mechanism due to proton accumulation within the lysosomes of macrophages due to the so-called "proton sponge" effect of these NPs [40]. Interestingly, iron oxide NPs induce lysosomal permeability but could suppress the lipopolysacchrides (LPS) induced production of IL-1 beta by decreasing the activity of cathepsin [41]. This inhibitory effect was however not observed for SiO_2 or TiO_2 NPs which increased the LPS induced inflammation through activation of the inflammasome [42, 43]. Mano et al. have also shown that TiO_2 NPs induce inflammatory responses by interaction of the NPs with Toll Like receptor 4 (TLR4) which is known to induce the inflammasome [44]. The cell death receptor P2X7 could also induce inflammasome activation through efflux of K^+ and SiO_2 and TiO_2 NPs have been shown to activate P2X7 leading to IL-1 beta secretion [45]. Others have also shown that NLRP3 inflammasome activation by TiO_2 involves K^+ efflux but did not require NP uptake leading to neutrophil recruitment *in vivo* through IL-1 alpha secretion [46]. The activation of the inflammasome could not only lead to inflammation but also to cell death through pyroptosis as observed for CB NPs [47] or induction of matrix metalloprotease 1 as shown for TiO_2 NPs in pulmonary fibroblasts [48]. Recent studies have shown that in synergy with toll-like receptor ligands, certain CB NPs could promote the activation of the NLRP3 inflammasome. This activation was shown to depend on the chemical surface functionalization [49]. However, it remains to be clearly determined which CB NP-dependent signals trigger this activation.

7.3.3 Calcium Signaling

Nanomaterials could also induce calcium signaling by increasing intracellular concentrations of Ca^{2+}. TiO_2 NPs have for instance been shown to induce the opening of L-type Ca^{2+} channels on mast cells as well as non specific influx of extracellular Ca^{2+} by permeation of the plasma membrane through an oxidative stress dependent mechanism [50].

A sustained elevation of Ca^{2+} was achieved by inducing the release of Ca^{2+} from the endoplasmic reticulum leading to histamine secretion. TiO_2 NPs also stimulate mucin secretion in epithelial cells by inducing extracellular Ca^{2+} influx and calcium release from the endoplasmic reticulum [51]. Intracellular Ca^{2+} increase is also involved in the inhibition of cell proliferation by Ag NPs [52].

7.3.4   Endoplasmic Reticulum Stress

Induction of endoplasmic reticulum stress and signaling by certain nanomaterials has recently attracted interest [53]. The endoplasmic reticulum fulfilld multiple cellular functions and many disturbances cause accumulation of unfolded proteins in the endoplasmic reticulum, triggering an evolutionarily conserved response, termed the unfolded protein response (UPR). The UPR is a signaling pathway, which is activated to regulate protein synthesis and restore normal equilibrium, in case of increased protein load or accumulation of unfolded or malformed proteins. The UPR leads to decreased protein synthesis and production of chaperons do facilitate protein folding. Once activated, UPR can either result in recovery or activate a cascade of reactions leading to inflammation through NF-κB and proeasome activation or ultimately to apoptosis. In a recent study, Christen and Fent have shown that Ag and silica NPs could induce the UPR pathway. Interestingly, induction of ER stress was not directly linked to the formation of ROS. This endoplasmic reticulum stress led to a subsequent decrease of cytochrome P450 1A activity, an important xenobiotic-metabolizing enzyme [54]. Co-exposure of these NPs with other pollutants such as the carcinogenic polycyclic aromatic hydrocarbons may thus lead to enhanced toxicity due to altered detoxification mechanisms.

7.3.5   Endocytic Pathways

Uptake mechanisms could also influence the toxicity of nanomaterials. Depending on the size, surface coating and their chemical nature, nanomaterials could enter cells by phagocytosis, macropinocytosis, clathrin-dependent endocytosis, caveolin dependent endocytosis or crossing of membranes by diffusion. The size dependent toxicity of TiO_2 NPs has thus been suggested to be due to the use of different endocytic pathways [55]. The cellular localization of nanomaterials may be particularly important in determining their toxicity. For instance, iron oxide NPs may exert catalase-like activities at cellular pH but in acidic environments like lysosomes they have peroxidase-like activity, resulting in the catalysis of H_2O_2 into hydroxyl radicals [56]. Furthermore, lysosomes present acidic pH conditions which could favor nanomaterial dissolution and even low-solubility NPs such as SiO_2 have been shown to dissolve over time within cells [57]. This solubilization is particularly important for nanomaterials releasing toxic ions such as Zn^{2+} or Ag^{2+} or transition metal ions, able to generate ROS through Fenton reactions. The effect of ZnO NPs has been shown to be greater than Zn^{2+} ions [58] which could be explained by the easy uptake of nanomaterials through classic endocytic mechanisms which facilitate the entry of toxic ions by the so-called "Trojan Horse Effect", circumventing the cellular protection mechanisms. Nanomaterials present within the lysosmes could also lead to their destabilization and release of lysosomal enzymes and cellular acidification. Lysosomal rupture by nanomaterials could for instance induce the release of the pro-apoptotic protein cathepsin (*see* Sect. 7.5) which could also activate the inflammasome. The uptake mechanism could thus have great importance for the toxicity of nanomaterials as it determines the capacity to enter the cells and the intracellular fate of the nanomaterial. As mentioned earlier, the use of classic phagocytic pathways by macrophages to capture CNT could also lead to frustrated phagocytosis due to the high-aspect ratio of these nanomaterials [8].

7.3.6   Membrane Dependent Signaling Pathways

Nanomaterials could increase lipid mediators such as leukotrienes and prostaglandins, which have pro- and anti-inflammatory effects as shown for

CB NPs in allergic animals [59]. Nanomaterials could also induce membrane receptor signaling such as shown for TiO$_2$ NPs which interact with toll-like receptors [44]. Furthermore, CB NPs activate the epidermal growth factor receptor (EGFR), due to ceramide accumulation in lipid rafts [60]. This lipid raft signaling induced by CB NPs has been shown to be dependent on oxidative stress induction. Interestingly, the compatible solute ectoine prevented efficiently the ceramide-EGFR signaling and the subsequent inflammation *in vivo* [60]. Lipid raft formation is also necessary for the induction of IL-1 beta secretion by TiO$_2$ [39] and CB NPs can induce integrin mediated signaling [61]. Ag, Au and iron oxide NPs on the other hand could disrupt EGFR signaling through mechanisms dependent on the NP type [62]. Nanomaterials could also alter receptor-ligand interactions. For instance, Pan et al. have shown recently that Au NPs can inhibit the interaction of VEGF165 (a splice variant of vascular endothelial growth factor A) with its receptor (VEGFR2), leading to decreased Akt phosphorylation and subsequently anti-angiogenic effects [63].

7.3.7 Epigenetic Regulations

MicroRNAs, small non-protein coding RNAs which regulate gene expression, have been shown to be upregulated by nanomaterials. Au NPs upregulated miR-155 leading to the downregulation of its target gene [64] and WC-Co NPs induced miR-21 signaling [65]. Citrullination of proteins was also reported for several nanomaterials [66]. This post-translational modification converts arginine residues into citrulline and is involved in gene expression modulation through histone modification.

7.4 Interaction of Nanomaterials with Proteins and Impact on Cell Signaling

In addition to the mechanisms described above, "alteration" (activation or inhibition) of cell signaling pathways by nanomaterials may also rely on NP-protein interactions [67]. It is now well known that when nanomaterials enter a physiological environment, they rapidly adsorb biomolecules [68]. In particular, proteins bind to the surface of nanomaterials to form a "biological coat" around the nanomaterial which is known as the protein corona [67, 69]. Several studies have been conducted to understand how nanomaterials can influence the structural properties of bound proteins and how "coated-proteins" influence the physical properties of the nanomaterials [68]. The protein corona is increasingly recognized as playing a major role in the biological effects of nanomaterials [70]. For instance, binding of proteins to nanomaterials may impair their functions by alteration of their structure [68]. More importantly, as the protein corona is what interfaces with the cell, surface-bound proteins can drive cell-specific uptake as well as activation/impairment of cell signaling events [68]. Recent studies with silica and polystyrene NPs confirm that a NP-corona forms rapidly and can drive NP uptake, thrombocyte activation and endothelial cell death [70].

As stated above, binding of proteins to nanomaterials can impair protein functions through alteration of their structures. In addition, changes in protein structure can lead to the exposure of amino acid regions that are normally buried within the folded protein. These newly exposed regions can interact with other macromolecules such as cell surface receptors and hence influence nanomaterial uptake, biodistribution, receptor activation and signaling. These mechanisms have been well exemplified by studies conducted by the Minchin group (Fig. 7.2) [71]. These authors have shown that certain negatively charged NPs (poly-acrylic acid-conjugated Au NPs) are able to bind and unfold plasma fibrinogen in a way that leads to the exposure of a cryptic sequence in the C-terminus of the α-chain of fibrinogen. This "new epitope" interacts specifically with Mac-1 receptor in human monocytic cells. Activation of the receptor induces the NF-κB signaling pathway with subsequent release of inflammatory cytokines. Interestingly, these effects were observed only with 5 nm NPs but not with 20 nm NPs. Whereas the pro-inflammatory properties of
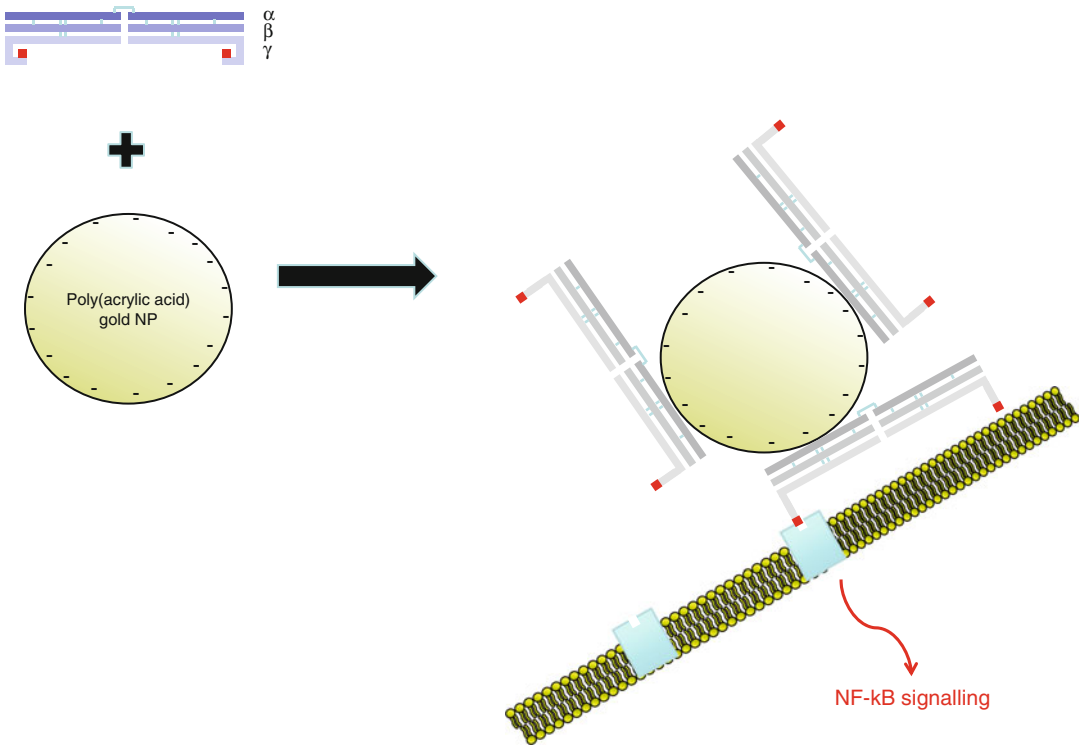
Fig. 7.2 Plasma fibrinogen is able to interact with negatively charged poly(acrylic acid) gold NP. With 5 nm NPs the binding of fibrinogen induces unfolding which exposes an amino acid sequences of the g chain. This new epitope interacts with MAC-1 receptor of monocytes, activates the NF-κB pathway which leads to pro-inflammatory cytokine release (Modified from Deng et al. [71])

different NPs have mostly been linked with their ability to induce oxidative stress, this study indicates that other mechanisms involving NP- protein interactions may also be at play [71].

Other studies have recently underlined that certain biological effects of nanomaterials can be driven by activation/inactivation of receptor-dependent signaling that in turn regulates cellular properties such as viability, proliferation, differentiation or cell cycle. Rosso et al. [72] have shown that plasma vitronectin bound to certain nanomaterials (maleic anhydride/alkyl vinyl ethers-based NPs) triggers activation of the vitronectin-integrin receptor. This activation leads to increased phosphorylation of ERK1/2 and FAK kinases and increased proliferation and cell cycle progression. In addition, the authors found that the NPs were internalized by cells through a direct interaction between the NPs and the vitronectin-integrin receptor [72].

Interactions of nanomaterials in cells with intracellular proteins with subsequent biological consequences have been reported previously [73]. Chen and von Mikecz have reported that SiO_2 NPs could enter the cell nucleus and contribute to the formation of nucleoplasmic protein aggregates similar to those found in certain neurodegenerative diseases. Such protein aggregation could be due to interaction of nanomaterials with intracellular/nuclear proteins, the nanomaterials acting as protein aggregation anchors [74]. More recently, it was suggested that alteration of cell cycle, DNA repair and inflammatory responses in human lung fibroblast cells by exposure to Ag NPs could also be due to the capability of these NPs to adsorb cytosolic proteins on their surface [75].

Overall, these studies underline the important role that protein-nanomaterial interactions and protein corona may play in the biological outcome of nanomaterial exposure.

7.5   Nanomaterials and Cell Death Signaling

Complex molecular mechanisms that govern the fate of cells are becoming increasingly well understood. It is now well established that the mode of cell death dictates the homeostasis and sometimes even fate of the organism. Studies have confirmed the important role of different cell death modalities in human diseases like sepsis, neurodegenerative disorders, stroke and cancer [76, 77] and therapeutic strategies based on the modulation of cell death signaling are currently being tested for treatment purposes. Nanomaterials can induce cell death through different modalities depending upon their physico-chemical characteristics. A detailed description of how changes in physico-chemical characteristics influence the toxicity of nanomaterials is discussed later in this chapter. Various nanomaterials can induce either programmed cell death pathways (apoptosis, autophagy, pyroptosis, and programmed necrosis) or non-programmed death pathways (accidental necrosis etc.).

7.5.1   Different Modes of Cell Death and Their Physiological and Pathological Significance

First definitions of different forms of cell death came from Schweichel and Merker in 1973 [78]. They classified cell death into type 1 cell death (heterophagy), type II cell death (autophagy), and type III cell death (not associated with any type of digestion), definitions that corresponds to the more modern concepts of apoptosis, autophagy, and necrosis, respectively. Since the first description of cell death mechanisms in 1960s, the most commonly used criteria to define different forms of cell death are based on morphological characteristics [78, 79]. However, the presence of particular morphology is not sufficient to establish a cause-effect link between given process and cell death [80]. The nomenclature Committee on Cell Death (NCCD) has published recommendations on defining various sub-routines of cell death and has encouraged the use of specific measureable

biochemical events [80–82]. Cell death can be defined either based on morphological criteria (apoptosis, necrosis, autophagy), enzymatic criteria (with or without involvement of nucleases and proteases), functional aspects (programmed vs. accidental, pathological vs. physiological) or immunological characteristics (immunogenic vs. non-immunogenic) [77].

Although there are more than 10 cell death modalities that can occur under physiological or pathological conditions, only few have been reported to occur after nanomaterial exposures. A brief description of cell death mechanisms induced by various nanomaterials with their physiological and pathological significance is given below.

Apoptosis was originally defined by Ker as a type of the cell death that occurs with rounding up of cell, reduction in cell volume (pyknosis), condensation of chromatin, fragmentation of nucleus (karyorhexis), plasma membrane blebbing, and maintenance of plasma membrane till late stages of the process [83]. Apoptosis can be broadly classified as extrinsic apoptosis (due to extracellular signals transmitted through transmembrane receptors) or intrinsic apoptosis (due to a plethora of intracellular events/damages). Intrinsic apoptosis is further divided into caspase dependent and caspase independent intrinsic apoptosis. Apoptosis refers to a controlled/programmed process of removal of individual cells inside the body without destruction or damage to the organism. During embryogenesis apoptosis serves an important function in organ and tissue development/ remodeling. Apoptosis of host cells occurs as a defense strategy in bacterial and viral infections to control the spread of infection. Moreover, apoptosis plays an important role in maintaining homeostasis and terminating an immune response (by removal of activated immune cells) [76]. Various pathological situations occur in case of deregulated apoptosis e.g. insufficient apoptosis occurs in cancers and autoimmune diseases while excessive apoptosis contributes to damage caused by neurodegenerative diseases, sepsis, stroke and myocardial infarction.

TiO$_2$ NPs induced apoptosis has been reported in a variety of cellular systems either through

extrinsic or intrinsic pathways. Hussain et al. reported the comparative toxicological mechanisms induced by titanium dioxide and CB NPs in human bronchial epithelial cells [38]. Authors dissected signaling events leading to similar outcome (apoptosis) and found a significant contribution of chemical composition in downstream signaling events. TiO_2 NPs were shown to induce cell death through ROS dependent extrinsic and intrinsic pathway in human lung fibroblast and breast epithelial cells [84]. Moreover, TiO_2 NPs induced cell death in BECs was shown to involve caspase 8/Bid pathway [85, 86]. Lipid peroxidation, p53 mediated DNA damage and caspase activation were observed after TiO_2 nanotubes exposure in neuronal stem cells at ≥ 150 µg/mL doses [85, 87]. This discrepancy in the observed mechanisms is most likely due to use of TiO_2 NPs of different crystal structure, differences in cell types and dose/duration of exposures. Other metal oxides like CeO_2, ZnO and NiO were also shown to induce apoptosis. Nano CeO_2 was shown to induce ROS and caspase independent apoptosis through the release of AIF in human peripheral blood monocytes at relatively realistic exposure concentrations (10 µg/mL) [88]. ZnO nanorods induced apoptosis in A549 cells through a p53 survivin, mitochondrial pathway through oxidative stress [89]. Nickel oxide NPs induce classic intrinsic apoptosis in human airway epithelial and breast cancer cells in contrast to Ni NPs which induce apoptosis through an extrinsic pathway [90, 91]. Various metal NPs have also shown abilities to induce apoptosis including Ag, Au, and Cu. Ag NPs induce ER stress dependent apoptosis [53] and Tsai et al. reported that Au NPs induce apoptosis in K562 through ER stress [92]. Nano copper induces both extrinsic and intrinsic apoptosis in mice kidney tissue [93].

Many biodegradable nanomaterials also induce apoptosis. Polyamidoamine (PMAM) dendrimer exposure leads to lysosomal damage induced apoptosis in KB cells [94]. Moreover, PMAM dendrimers induce mitochondrial toxicity in human lung cells [95] and polystyrene NPs (60 nm) exhibited charge dependent toxicity and lysosomal damage in RAW264.7 cells [96].

Many carbon based nanomaterials also induce apoptosis. CB NPs were shown to induce apoptosis through the mitochondrial pathway depending on ROS production and caspase activation [38]. Both single walled carbon nanotubes (SWCNT) and multi-walled carbon nanotubes (MWCNTs) have the ability to induce cell death. Multiple studies have shown apoptosis inducing properties of SWCNTs both *in vitro* and *in vivo* [1, 97, 98]. Recently, Fujita et al. reported that the toxicity of SWCNTs depends on size and length of the bundles of dispersed nanotubes resulting in differential responses even for the same bulk SWCNTs. They reported that SWCNT were not toxic to A549 cells and the residual metals may not be a definitive parameter for intracellular ROS generation [99].

Autophagy is an evolutionary conserved catabolic process, which is a slow and spatially restricted phenomenon. It involves sequestration of parts of cytoplasm in double membrane bound vesicles and digestion of these components by lysosomal hydrolases [82]. Autophagic cell death refers to cell death occurring with autophagy and should not be confused with cell death through autophagy [77]. Autophagy may either contribute to cell death or may constitute a cellular defense against nutrient or growth factor deprivation induced stress. Autophagy is characterized by lack of chromatin condensation and huge increase in the number of double membrane vacuoles (autophagic vacuoles) in the cytoplasm. It has been shown that autophagy not only plays an important physiological role in removal/recycling of damaged cellular organelles but also helps in defense against bacterial infections and in immune response against viruses (through antigen presentation) [100, 101]. The role of autophagy in cell death during ischemia/reperfusion injury and in HIV-1 induced CD4+ T lymphocyte cell death has also been demonstrated.

An excellent review about autophagy induction and lysosomal impairment by nanomaterials has been recently published [102]. Various mechanisms are described in this manuscript through which nanomaterials interact with the autophagy pathways and include overloading of lysosomes, inhibition of lysosomal enzymes and

disruption of cytoskeleton-mediated vesicular trafficking leading to a state of autophagy dysfunction. Bare-Fe NPs induce oxidative stress and activation of ERK pathway in association with autophagic vesicle accumulation in RAW264.7 cells [103]. Au, iron core-Au shell NPs and iron oxide NPs show cell death associated with autophagic vesicle accumulation [104–106]. Au NPs induce size dependent lysosomal impairment and autophagic vesicle formation [107]. ZnO NPs induce apoptosis and necrosis in RAW264.7 macrophages through p47phox- and Nrf2- independent manner [3]. CeO_2 NPs were shown to induce autophagy in human peripheral blood monocytes that contributed to the cytotoxic effects of nano ceria [88]. A highly purified form of MWCNTs (vapor-grown carbon fiber, HTT2800) was shown to induce LC3b expression in human bronchial epithelial cells [108]. Fullerenes were shown to induce concentration dependent toxicity and induced necrosis at high doses while autophagy was observed at low doses [109]. Quantum dots (QD) induce autophagy in human mesenchymal stem cells in a size dependent manner [110] and CdSe QDs were shown to induce autophagy in porcine kidney cells [111, 112]. PMAM dendrimers promote acute lung injury *in vivo* and autophagic cell death through Akt-TSC2-mTOR signaling [113]. The induction of autophagy by nanomaterials is also intended to be exploited for therapeutic purposes (review of [102]).

Pyroptosis is a caspase-1 dependent cell death leading to release of inflammatory mediators (IL-1β and IL-18). It can be effectively blocked by the use of specific inhibitors of caspase-1or its genetic knockout [80]. Pyroptosis protects from infection and induces pathological inflammation [114]. Pyroptosis occurs in various pathophysiological situations like stroke, bacterial and viral infections [115, 116]. This phenomenon can affect the homeostasis in multiple ways (local tissue damage and released inflammatory mediators cause the influx of inflammatory/immune cells) and contributes to the pathogenesis of different diseases like asthma and COPD. CeO_2 nanorods and wires, at lengths ≥200 nm and aspect ratio ≥22, have been shown to induce progressive

pro-inflammatory effects (IL-1β release) and cytotoxicity of THP-1 cells [117]. CB NPs were shown to induce inflammasome dependent pyroptosis in RAW274.6 cells. Cell death induction and inflammatory responses were shown to be effectively modulated by using caspase-1 inhibitor or pyroptosis inhibitor [47]. We have observed that MWCNT exposure leads to significant inflammasome dependent pyroptosis in primary human bronchial epithelial cells which in turn activates a pro-fibrotic response in human fibroblasts (Hussain, unpublished data).

Necrosis was originally defined as cell death which does not present characteristics of apoptosis and autophagy. For decades it was assumed that necrosis is an accidental form of cell death, however recently many researchers have confirmed the existence of programmed necrosis [118]. Nanomaterials that induce necrosis include Au, Ag, TiO_2, and fullerenes [109, 119, 120]. Unfortunately, no specific biochemical test exists for the confirmation of necrosis per se but another specific type of regulated necrosis (necroptosis) can be identified by the ability of RIP-1 kinase to inhibit it [121]. Nano graphene oxide was shown to induce Toll-like Receptor 4 (TLR4) dependent necrosis in macrophages [122]. Go induced macrophage cell death was partially attributed to RIP1-RIP3 complex-mediated programmed necrosis downstream of TNF-α induction.

7.5.2 Cell Type Specificity and Sensitivity

Cell type specificity/sensitivity has been observed in cell death mechanism induction by many different nanomaterials. Polystyrene NPs were shown to be toxic in RAW macrophages and BAES-2B epithelial cells but fail to induce a toxic response in endothelial cells at comparable doses [123]. Similarly, palladium NPs were shown to be toxic in bronchial epithelial cells but no toxicity was observed in case of A549 cells [124]. Au NPs demonstrate higher toxicity in K562 leukemia cells but are non-toxic in mononuclear cells [92]. Alili et al. [125] demonstrated that ceria NPs preferentially killed SCL-1

squamous carcinoma cells through ROS production and oxidation of proteins at the same concentrations (150 μM) which were not toxic to dermal fibroblasts [125]. Ceria NPs, which induce apoptosis and autophagy in human peripheral blood monocytes are non-toxic to primary human bronchial epithelial cells at comparable doses (Hussain, unpublished data). Moreover, we also observed cell differentiation stage dependence in the toxicity of nano ceria in human peripheral blood monocytes and monocyte-derived macrophages. This resistance appears to be related to the higher capacity of macrophages to resist mitochondrial damage (Hussain, unpublished data). The differential sensitivity of various cell types could also be attributed to the differences in uptake mechanisms and differences in the ability to handle with oxidative insult (total anti-oxidant capacity).

7.5.3   Shared Mechanisms and Identification of Key Triggers

A review of the literature indicates that the lysosomal compartment plays an important role in the toxicity of various groups of nanomaterials. This range from the pH dependent dissolution of soluble metal oxides (e.g. ZnO NPs) and physical damage to the lysosomal membrane by the nanomaterials (e.g. CNTs) to the ROS dependent damage to the lysosomal membrane (e.g. TiO_2 NPs). These events lead to the release of lysosomal proteases resulting in diverse outcomes ranging from inflammasome activation and pyroptosis to caspase activation and necrosis.

Another main pathway involves mitochondrial damage resulting in either caspase-dependent (through activation of caspase 3/7 and caspase 9) or caspase-independent apoptosis (through the release of apoptosis inducing factor, AIF). Mitochondrial damage can take place either due to ROS generated on the surface of nanomaterials or due to physical damage to the mitochondrial membrane. The disturbed oxidant balance can occur either through the increased ROS production or through a defec-

tive antioxidant defense in response to persistent nanomaterial exposure (as postulated in case of ceria NPs).

Taken together, these results indicate that nanomaterial induced cell death signaling occurs through the classical cell death pathways and any "nano specific" cell death modality has not yet been discovered.

7.5.4   Interplay Between Various Cell Death Modalities

Various nanomaterials can induce distinct cell death pathways in the same cell type depending upon their various physicochemical factors including chemical composition, size etc. [38, 120]. Some nanomaterials have been shown to induce multiple cell death modalities after single exposure [88, 126]. This question of interplay between different pathways is very complex as one mechanism might be the result of other mechanisms or a defense strategy of the body. One particular pathway that has both pro-survival and pro-death roles is autophagy. It has always been intriguing to establish the exact role of autophagy in a particular exposure. The most important question in case of autophagy is to clarify whether cells are dying due to autophagy, due to some process that induces autophagy in parallel, or is autophagy a pro-survival mechanism. Moreover, studies have shown that cell death with autophagic vesicle detection may be completely independent from autophagic vesicle accumulation in the cells [127]. For more details the reader is referred to an excellent publication that reviewed this topic [128]. Various biochemical and genetic approaches can help dissect this issue in detail.

7.6   Role of Physico-Chemical Characteristics in Nanomaterial Toxicity

Biological responses to nanomaterial exposure are determined by a large diversity of factors linked to the various physico-chemical character-

istics of the nanomaterials: size, surface area (taking into account the porosity and roughness of the particle), shape, bulk chemical composition (including the crystal structure), surface chemistry (including lipophilicity as well as surface charge or coatings) and surface reactivity which is linked to the two preceeding factors (surface area and surface chemistry). Various experimental studies have demonstrated the significance of these characteristics as determinants of nanomaterial biological activity/toxicity [14, 38, 129–131]. Some excellent reviews and expert opinion about this can be found elsewhere [132–135].

7.6.1 Size

It has been postulated that most nanomaterials have a critical size of 30 nm below which they show their typical nano characteristics as the number of atoms on the surface exponentially increases below this cutoff [136]. Studies have confirmed the higher toxic potentials of NPs compared to micrometer sized particles or larger size NPs [129, 137–139]. However, some studies demonstrate that an actual increase in size in the nanometer range is associated with higher toxicity. This stands particularly correct while studying the hemolytic potentials of nanomaterials (e.g. silica (both amorphous (2–335 nm) and mesoporous (100–600 nm)) [140, 141]. It was postulated that larger particles attach to the larger surface of the red blood cells leading to membrane damage and deformity. Coradeghini [142] demonstrated size dependent toxicity on mouse fibroblasts and degradation of clathrin heavy chain after exposure to Au NPs [142]. Size is also a determining factor for the mode of entry into the cells as it has been shown that smallest NPs enter the cells *via* caveola, clathrin coated pits or lipid raft mediated uptake [133, 143, 144]. Similarly, QDs show size dependence in co-localization with different organelles [145]. Size not only determines the uptake of nanomaterials but also the interaction with proteins and the translocation potential from the site of deposition. Indeed it has been shown that Au NPs show

size dependent translocation potentials (1.4 vs 18 nm) [146].

7.6.2 Surface Area and Porosity

The surface area of nanomaterials is not only dependent on the size but also on their porosity. It was shown that mesoporous Si NPs show higher biocompatibility and less hemolytic potentials as compared to the particles of same size but different porosity [147]. For the equal mass of particles with same chemical composition and crystalline structure, a greater toxicity was found for NPs than for larger particles. This led to the conclusion that inflammatory effects of nanomaterials depend upon the surface area [148]. A surface area dependent inflammatory response after inhalation or instillation has been shown for various nanomaterials including CB, TiO_2 or Ni [138, 149, 150]. It has been found that 21 nm TiO_2 was 43 fold more potent to induce pulmonary inflammation than 250 nm particles [150]. It was demonstrated that titanium dioxide NPs instilled at same surface dose but different mass exert similar toxic responses fitting the same response curve. Hussain et al. [14] showed a direct correlation between the particle surface area and potentials to induce pro-inflammatory and oxidative responses in bronchial epithelial cells exposed to CB or TiO_2 NPs. Some studies contradicted the significance of surface area dose metric [151, 152]. Wittmaack [152] analyzed the data already published by Stoeger et al. [131] and Oberdorster et al. [134] and suggested that particle number seemed to be the best dose metric rather than surface area. Furthermore, Warheit and colleagues concluded that smaller and larger NPs respond in a similar manner in cytotoxicity testing [151].

7.6.3 Crystalline Structure

Nanomaterials of same chemical composition can have different crystalline structures, which can potentially influence the toxicity of the material. The most widely used example to elaborate

such effects is TiO_2, which has many crystalline forms out of which anatase, rutile and brookite are most actively studied. Sayes et al. [153, 154] demonstrated that the anatase form of titanium dioxide is 100 times more toxic than the same mass of rutile form and that the ROS production after UV illumination follows a similar trend as the biological activity [154]. However, another literature report contradicted these results and demonstrated that the rutile TiO_2 induces oxidative DNA damage in the absence of light but anatase NPs of same size did not [155]. Jiang et al. [156] did a comprehensive study on model TiO_2 NPs. Different sizes (3–200 nm) of anatase, rutile or anatase/rutile mixtures of different ratios and amorphous TiO_2 were compared with regard to their ability to produce ROS in a cell-free phosphate buffer assay. Based on their experimentation they ranked NPs from highest to lowest reactivity as amorphous > anatase > anatase/rutile mixture > rutile [156]. Furthermore, they normalized the ROS-producing abilities to NP surface area and found striking size dependence. They observed that NPs between 3 and 10 nm have about the same ROS production abilities per unit surface area followed by a steep increase between 10 and 30 nm and a constant but still higher ROS production capacity per unit surface area between 50 and 200 nm. The authors suggested that this finding is due to higher number of defects per unit surface area in larger anatase NPs as compared to smaller ones.

7.6.4 Chemical Composition

Particle chemistry is critical for determining the toxic potential of nanomaterials. Although it was suggested that size is more important than chemical composition in the toxicity of nanomaterials, the extrapolation of the results showing similar extent of inflammation from different chemical compositions is not possible [157]. Hussain et al. [38] showed that chemical composition dictates the nature of intracellular cell death signaling as CB and TiO_2 NPs of comparable sizes induce distinct cell death pathways. Wang et al. showed that the toxicity of QD depend upon their composi-

tion as CdSe QD are more toxic than CdTe whereas ZnS-AgInS2 QD were much less toxic [158]. This cytotoxicity was attributed to the leakage of highly toxic cadmium ions. Indeed, the solubility of the nanomaterials is a critical feature for their toxicity. The biological effects could either be increased by insolubility leading to biopersistance of the material or in contrast by dissolution as also observed for ZnO and CuO NPs which toxicity could be attributed to leaching of Zn or Cu ions [159]. However, particle associated toxicity was also observed in other studies using ZnO NPs [160]. It is important to note that dissolution kinetic is size-dependent and therefore an important factor to be considered for nanomaterial toxicity though several other physico-chemical characteristics influence dissolution kinetics: particle surface characteristics such as roughness or curvature influence the kinetics of dissolution and adsorbed molecules could either slower solubility or serve to catalyse dissolution. The aggregation state of the particles needs also to be considered as a hindering factor of solubility [161]. It is interesting to note that acidity could favor dissolution and thus preferential uptake of nanomaterials into lysosomes or the less acidic caveolar compartment could thus influence the fate of the particles as shown for ZnO and CeO NPs [123].

7.6.5 Aggregation and Concentration

The concentration dependency of nanomaterial-induced effects is not clear enough. One important factor, which is usually ignored while interpreting these results is the state of aggregation of the nanomaterials, which is important in determining the extent of internalization and clearance of the nanomaterials. Indeed, aggregation is dependent on the concentration of the test substance and higher nanomaterial concentrations have been shown to promote aggregation [144, 155, 162]. This results in reduced toxicity as compared to that observed at lower concentrations [163]. It is postulated that aggregation depend upon surface charge, material type, size

etc. [148]. Most of the times the observed aggregates are larger than the threshold limit for the biological responses and thus result in no toxicity.

The agglomeration state not only increases the size of the nanomaterial influencing its lung penetration, deposition and cellular uptake but also the solubility of the material [161]. This factor also determines the extent of translocation across cellular barriers and biokinetics inside the body. The physico-chemical surface properties of the material such as charge and hydrophobicity are the main determinants for the degree of aggregation but characteristics of the suspending media (pH, viscosity, ionic strength etc.) also play a role. Thus coatings of derivative groups as well as dispersants may allow the stabilization of nanomaterials by preventing the formation of aggregates which has an effect on toxicity. For instance dispersion of SWCNT by the use of surfactant [164] or by adding functional groups [153] reduces effectively the cytotoxicity.

7.6.6 Aspect Ratio

A direct relationship exists between aspect ratio and toxicity. CNTs are classical examples of engineered long aspect ratio nanomaterials. These materials have many similarities with asbestos but untill now there is no agreement on the toxic potential of these nanomaterials. These materials exist in a multitude of morphologies, sizes and surface/end functionalizations which make their risk evaluation increasingly difficult. Typically CNTs have diameters between 0.4 and 100 nm and lengths from a few nanometers to several centimeters. It has been shown that when administered in similar doses, CNTs have higher toxic potentials as compared to spherical particles (CB, silica). In this study authors demonstrated that SWCNTs induce granuloma, alveolar wall thickening, acute inflammation and progressive fibrosis and these effects were attributed to their physicochemical properties and fibrous nature [165]. High aspect ratio nanomaterials (HARN) can indeed induce frustrated phagocytosis leading to inflammation [8]. CeO_2 nano-

rods and wires, at lengths ≥ 200 nm and aspect ratio ≥ 22, have been shown to induce progressive pro-inflammatory effects (IL-1β release) and cytotoxicity of THP-1 cells [117]. These findings suggested that both, length and diameter components of aspect ratio, should be considered while addressing the toxic effects of high aspect ratio nanomaterials.

7.6.7 Surface-Coating/ Modifications

As described earlier the surface of nanomaterials is an important determinant for their toxic potential. A thorough understanding of nanomaterial surface composition helps in defining the interactions of nanomaterials with biological systems. Such surface modifications can be either deliberate or unintended. Unintended surface modifications arise from the interaction of nanomaterials with their environment (air/liquid) resulting in the attachment of environmental components. Presence of oxygen, ozone, oxygen free radicals and metals on the surface of nanomaterials can lead to enhanced potentials to produces ROS. Absorption of LPS and bacterial endotoxins to nanomaterials is a common problem as these are ubiquitous in nature and can play an important role in the biological responses to nanomaterials [166]. Surface modifications of engineered nanomaterials during the production process lead to surface functionalization and influence their toxicity. Acid treatment of MWCNT leads to more carboxyl, carbonyl and hydroxyl groups and thus increases the cytotoxicity [167] but on the other hand functionalization that increases the water-solubility of SWCNT leads to decreased cytotoxicity [153]. Functionalization dependent decrease in toxicity of MWCNT was also observed [168]. It has been shown that surface oleic acid modifications influence iron oxide and nickel ferrite particle cytotoxicity [169]. Recently it has been shown that uptake and toxicity of sub-10 nm cerium oxide depend upon the surface coating with citrate coated NPs having higher potentials of internalization than polymer-coated NPs [170]. Moreover, it has been shown that toxicity of QD

can be mitigated by appropriate functionalization [171]. Agglomeration of the NPs occurring concomitant with ageing may be a contributing factor to this decrease in toxicity. Moreover, structural defects on the surface of MWCNT are mainly responsible for the pulmonary toxicity observed *in vivo* and *in vitro*. Indeed, annealing structural defects and elimination of metal contaminants by heating reduces the lung responses after intratracheal instillation but further grinding of the material restored their toxic potential [172].

7.6.8   Interplay

Beside these inherent properties of the nanomaterials the interaction between particles or molecules will also determine their toxicity. Interactions between particles of different composition could have unexpected biological consequences as seen for cobalt tungsten carbide particles known to induce hard metal lung disease. It is the contact between the particles which causes the release of ROS involved in the pathogenic response as pure cobalt or carbide particles are inert and soluble cobalt salts in contact with carbide particles have no effect [173]. Recently the same effect has been observed for co-exposure to CB and Fe_2O_3 NPs leading to oxidative effects whereas exposure to either particle type alone has no effect [174]. This synergistic effect is probably due to intracellular redox reactions between CB and Fe^{3+} solubilized within the lysosomal compartment leading to the generation of Fe^{2+}.

Conclusions

The diversity and complexity of the factors involved makes nanotoxicology a very challenging field. Several parameters could influence the final biological response to nanomaterials and it is thus difficult to predict the human health hazard after exposure. A thorough physicochemical characterization of the tested nanomaterial prior to *in vitro* or *in vivo* biological evaluation is needed to allow the comparison of data and to draw general or specific conclusions on toxicity of nanomaterials for public health

risk assessments. Nanomaterials have the ability to induce either oxidative stress dependent or independent mechanisms and acellular ROS production potentials may not accurately predict the biological activity of nanomaterials. The complex interactions of nanomaterials with proteins could also impact on signaling pathways. Nanomaterials have shown the ability to induce classical cell death signaling pathways in ROS dependent or independent manners and this ability can also be correlated to different physico-chemical characteristics of nanomaterials. Taken together it becomes evident that nanomaterials are capable of either inducing complex cellular signaling mechanisms or modifying existing signaling pathways resulting in adverse/unanticipated outcomes. It is therefore essential that a mechanistic approach with detailed elaboration of cellular signaling events is adopted for the safety evaluation of nanomaterials as well as for the development of safer and consumer friendly nanotechnology.

References

1. Shvedova AA, Kagan VE, Fadeel B (2010) Close encounters of the small kind: adverse effects of man-made materials interfacing with the nano-cosmos of biological systems. Annu Rev Pharmacol Toxicol 50:63–88
2. Nel A, Xia T, Madler L, Li N (2006) Toxic potential of materials at the nanolevel. Science 311:622–627
3. Wilhelmi V, Fischer U, Weighardt H, Schulze-Osthoff K, Nickel C, Stahlmecke B, Kuhlbusch TA, Scherbart AM, Esser C, Schins RP, Albrecht C (2013) Zinc oxide nanoparticles induce necrosis and apoptosis in macrophages in a p47phox- and Nrf2-independent manner. PLoS One 8:e65704
4. Abrikossova N, Skoglund C, Ahren M, Bengtsson T, Uvdal K (2012) Effects of gadolinium oxide nanoparticles on the oxidative burst from human neutrophil granulocytes. Nanotechnology 23:275101
5. Tulinska J, Kazimirova A, Kuricova M, Barancokova M, Liskova A, Neubauerova E, Drlickova M, Ciampor F, Vavra I, Bilanicova D, Pojana G, Staruchova M, Horvathova M, Jahnova E, Volkovova K, Bartusova M, Cagalinec M Dusinska M (2013) Immunotoxicity and genotoxicity testing of PLGA-PEO nanoparticles in human blood cell model. Nanotoxicology doi:10.3109/17435390.2013.816798
6. Culcasi M, Benameur L, Mercier A, Lucchesi C, Rahmouni H, Astean A, casano G, Botta A, Kovacic

H, Pietri S (2012) EPR spin trapping evaluation of ROS production in human fibroblasts exposed to cerium oxide nanoparticles: evidence for NADPH oxidase and mitochondrial stimulation. Chem Biol Interact 199:161–176

7. Raghunathan VK, Devey M, Hawkins S, Hails L, Davis SA, Mann S, Chang IT, Ingham E, Malhas A, Vaux DJ, Lane JD, Case CP (2013) Influence of particle size and reactive oxygen species on cobalt chrome nanoparticle-mediated genotoxicity. Biomaterials 34:3559–3570

8. Murphy FA, Schinwald A, Poland CA, Donaldson K (2012) The mechanism of pleural inflammation by long carbon nanotubes: interaction of long fibres with macrophages stimulates them to amplify pro-inflammatory responses in mesothelial cells. Part Fibre Toxicol 9:8

9. Zhou YT, He W, Wamer WG, Hu X, Wu X, Lo YM, Yin JJ (2013) Enzyme-mimetic effects of gold@ platinum nanorods on the antioxidant activity of ascorbic acid. Nanoscale 5:1583–1591

10. Lee SS, Song W, Cho M, Puppala HL, Nguyen P, Zhu H, Segatori L, Colvin VL (2013) Antioxidant properties of cerium oxide nanocrystals as a function of nanocrystal diameter and surface coating. ACS Nano 7:9693–9703

11. Das S, Singh S, Dowding JM, Oommen S, Kumar A, Sayle TX, Saraf S, Patra CR, Vlahakis NE, Sayle DC, Self WT, Seal S (2012) The induction of angiogenesis by cerium oxide nanoparticles through the modulation of oxygen in intracellular environments. Biomaterials 33:7746–7755

12. Colon J, Hsieh N, Ferguson A, Kupelian P, Seal S, Jenkins DW, Baker CH (2010) Cerium oxide nanoparticles protect gastrointestinal epithelium from radiation-induced damage by reduction of reactive oxygen species and upregulation of superoxide dismutase 2. Nanomedicine 6:698–705

13. Rehman MU, Yoshihisa Y, Miyamoto Y, Shimizu T (2012) The anti-inflammatory effects of platinum nanoparticles on the lipopolysaccharide-induced inflammatory response in RAW 264.7 macrophages. Inflamm Res 61:1177–1185

14. Hussain S, Boland S, Baeza-Squiban A, Hamel R, Thomassen LC, Martens JA, Billon-Galland MA, Fleury-Feith J, Moisan F, Pairon JC, Marano F (2009) Oxidative stress and proinflammatory effects of carbon black and titanium dioxide nanoparticles: role of particle surface area and internalized amount. Toxicology 260:142–149

15. Brown DM, Donaldson K, Stone V (2010) Nuclear translocation of Nrf2 and expression of antioxidant defence genes in THP-1 cells exposed to carbon nanotubes. J Biomed Nanotechnol 6:224–233

16. Kang SJ, Ryoo IG, Lee YJ, Kwak MK (2012) Role of the Nrf2-heme oxygenase-1 pathway in silver nanoparticle-mediated cytotoxicity. Toxicol Appl Pharmacol 258:89–98

17. Prasad RY, Mcgee JK, Killius MG, Suarez DA, Blackman CF, Demarini DM, Simmons SO (2013) Investigating oxidative stress and inflammatory responses elicited by silver nanoparticles using high-throughput reporter genes in HepG2 cells: effect of size, surface coating, and intracellular uptake. Toxicol In Vitro 27:2013–2021

18. Gehrke H, Fruhmesser A, Pelka J, Esselen M, Hecht LL, Blank H, Schuchmann HP, Gerthsen D, Marquardt C, Diabate S, Weiss C, Marko D (2013) In vitro toxicity of amorphous silica nanoparticles in human colon carcinoma cells. Nanotoxicology 7:274–293

19. Piret JP, Jacques D, Audinot JN, Mejia J, Boilan E, Noel F, Fransolet M, Demazy C, Lucas S, Saout C, Toussaint O (2012) Copper(II) oxide nanoparticles penetrate into HepG2 cells, exert cytotoxicity via oxidative stress and induce pro-inflammatory response. Nanoscale 4:7168–7184

20. Zhang XD, Zhao J, Bowman L, Shi X, Castranova V, Ding M (2010) Tungsten carbide-cobalt particles activate Nrf2 and its downstream target genes in JB6 cells possibly by ROS generation. J Environ Pathol Toxicol Oncol 29:31–40

21. Ze Y, Hu R, Wang X, Sang X, Ze X, Li B, Su J, Wang Y, Guan N, Zhao X, Gui S, Zhu L, Cheng Z, Cheng J, Sheng L, Sun Q, Wang L, Hong F (2014) Neurotoxicity and gene-expressed profile in brain-injured mice caused by exposure to titanium dioxide nanoparticles. J Biomed Mater Res A 102:470–478

22. Manke A, Wang L, Rojanasakul Y (2013) Mechanisms of nanoparticle-induced oxidative stress and toxicity. BioMed Res Int 2013:942916

23. Mroz RM, Schins RP, Li H, Drost EM, Macnee W, Donaldson K (2007) Nanoparticle carbon black driven DNA damage induces growth arrest and AP-1 and NFkappaB DNA binding in lung epithelial A549 cell line. J Physiol Pharmacol 58(Suppl 5):461–470

24. Pacurari M, Yin XJ, Zhao J, Ding M, Leonard SS, Schwegler-Berry D, Ducatman BS, Sbarra D, Hoover MD, Castranova V, Vallyathan V (2008) Raw single-wall carbon nanotubes induce oxidative stress and activate MAPKs, AP-1, NF-kappaB, and Akt in normal and malignant human mesothelial cells. Environ Health Perspect 116:1211–1217

25. Wan R, Mo Y, Zhang X, Chien S, Tollerud DJ, Zhang Q (2008) Matrix metalloproteinase-2 and -9 are induced differently by metal nanoparticles in human monocytes: the role of oxidative stress and protein tyrosine kinase activation. Toxicol Appl Pharmacol 233:276–285

26. Ding M, Kisin ER, Zhao J, Bowman L, Lu Y, Jiang B, Leonard S, Vallyathan V, Castranova V, Murray AR, Fadeel B, Shvedova AA (2009) Size-dependent effects of tungsten carbide-cobalt particles on oxygen radical production and activation of cell signaling pathways in murine epidermal cells. Toxicol Appl Pharmacol 241:260–268

27. Dey S, Bakthavatchalu V, Tseng MT, Wu P, Florence RL, Grulke EA, Yokel RA, Dhar SK, Yang HS, Chen Y, St Clair DK (2008) Interactions between SIRT1 and AP-1 reveal a mechanistic insight into the

growth promoting properties of alumina (Al2O3) nanoparticles in mouse skin epithelial cells. Carcinogenesis 29:1920–1929

28. Murray AR, Kisin ER, Tkach AV, Yanamala N, Mercer R, Young SH, Fadeel B, Kagan VE, shvedova AA (2012) Factoring-in agglomeration of carbon nanotubes and nanofibers for better prediction of their toxicity versus asbestos. Part Fibre Toxicol 9:10

29. Busch W, Kuhnel D, Schirmer K, scholz S (2010) Tungsten carbide cobalt nanoparticles exert hypoxialike effects on the gene expression level in human keratinocytes. BMC Genomics 11:65

30. Ganguly K, Upadhyay S, Irmler M, Takenaka S, Pukelsheim K, Beckers J, Hamelmann E, Schulz H, Stoeger T (2009) Pathway focused protein profiling indicates differential function for IL-1B, -18 and VEGF during initiation and resolution of lung inflammation evoked by carbon nanoparticle exposure in mice. Part Fibre Toxicol 6:31

31. Okoturo-Evans O, Dybowska A, Valsami-Jones E, Cupitt J, Gierula M, Boobis AR, Edwards RJ (2013) Elucidation of toxicity pathways in lung epithelial cells induced by silicon dioxide nanoparticles. PLoS One 8:e72363

32. Perkins TN, Shukla A, Peeters PM, Steinbacher JL, Landry CC, Lathrop SA, Steele C, Reynaert NL, Wouters EF, Mossman BT (2012) Differences in gene expression and cytokine production by crystalline vs. amorphous silica in human lung epithelial cells. Part Fibre Toxicol 9:6

33. Qu Y, Huang Y, Lu X (2013) Proteomic analysis of molecular biocompatibility of gold nanoparticles to human dermal fibroblasts-fetal. J Biomed Nanotechnol 9:40–52

34. Witzmann FA, Monteiro-Riviere NA (2006) Multi-walled carbon nanotube exposure alters protein expression in human keratinocytes. Nanomedicine 2:158–168

35. Yang B, Wang Q, lei R, Wu C, Shi C, Yuan Y, Wang Y, Luo Y, Hu Z, Ma H, Liao M (2010) Systems toxicology used in nanotoxicology: mechanistic insights into the hepatotoxicity of nano-copper particles from toxicogenomics. J Nanosci Nanotechnol 10:8527–8537

36. Rallo R, France B, Liu R, Nair S, George S, Damoiseaux R, Giralt F, Nel A, Bradley K, Cohen Y (2011) Self-organizing map analysis of toxicity-related cell signaling pathways for metal and metal oxide nanoparticles. Environ Sci Tech 45:1695–1702

37. Ge Y, Bruno M, Wallace K, Winnik W, Prasad RY (2011) Proteome profiling reveals potential toxicity and detoxification pathways following exposure of BEAS-2B cells to engineered nanoparticle titanium dioxide. Proteomics 11:2406–2422

38. Hussain S, Thomassen LC, Ferecatu I, Borot MC, Andreau K, Martens JA, Fleury J, Baeza-Squiban A, Marano F, Boland S (2010) Carbon black and titanium dioxide nanoparticles elicit distinct apoptotic pathways in bronchial epithelial cells. Part Fibre Toxicol 7:10

39. Morishige T, Yoshioka Y, Tanabe A, Yao X, Tsunoda S, Tsutsumi Y, Mukai Y, Okada N, Nakagawa S (2010) Titanium dioxide induces different levels of IL-1beta production dependent on its particle characteristics through caspase-1 activation mediated by reactive oxygen species and cathepsin B. Biochem Biophys Res Commun 392:160–165

40. Lunov O, Syrovets T, Loos C, Nienhaus GU, Mailander V, Landfester K, Rouis M, Simmet T (2011) Amino-functionalized polystyrene nanoparticles activate the NLRP3 inflammasome in human macrophages. ACS Nano 5:9648–9657

41. Wu HY, Chung MC, Wang CC, Huang CH, Liang HJ, Jan TR (2013) Iron oxide nanoparticles suppress the production of IL-1beta via the secretory lysosomal pathway in murine microglial cells. Part Fibre Toxicol 10:46

42. Sandberg WJ, Låg M, Holme JA, Friede B, Gualtieri M, Kruszewski M, Schwarze PE, Skuland T, Refsnes M (2012) Comparison of non-crystalline silica nanoparticles in IL-1β release from macrophages. Part Fibre Toxicol 9:32

43. Winter M, Beer HD, Hornung V, Kramer U, Schins RP, Forster I (2011) Activation of the inflammasome by amorphous silica and TiO2 nanoparticles in murine dendritic cells. Nanotoxicology 5:326–340

44. Mano SS, Kanehira K, Taniguchi A (2013) Comparison of cellular uptake and inflammatory response via toll-like receptor 4 to lipopolysaccharide and titanium dioxide nanoparticles. Int J Mol Sci 14:13154–13170

45. Dekali S, Divetain A, Kortulewski T, Vanbaelinghem J, Gamez C, Rogerieux F, Lacroix G, Rat P (2013) Cell cooperation and role of the P2X7 receptor in pulmonary inflammation induced by nanoparticles. Nanotoxicology 7:1302–1314

46. Yazdi AS, Guarda G, Riteau N, Drexler SK, Tardivel A, Couillin I, Tschopp J (2010) Nanoparticles activate the NLR pyrin domain containing 3 (Nlrp3) inflammasome and cause pulmonary inflammation through release of IL-1α and IL-1β. Proc Natl Acad Sci U S A 107:19449–19454

47. Reisetter AC, Stebounova LV, Baltrusaitis J, Powers L, Gupta A, Grassian VH, Monick MM (2011) Induction of inflammasome-dependent pyroptosis by carbon black nanoparticles. J Biol Chem 286:21844–21852

48. Armand L, Dagouassat M, Belade E, Simon-Deckers A, Le Gouvello S, Tharabat C, Duprez C, Andujar P, Pairon JC, Boczkowski J, Lanone S (2013) Titanium dioxide nanoparticles induce matrix metalloprotease 1 in human pulmonary fibroblasts partly via an interleukin-1β-dependent mechanism. Am J Respir Cell Mol Biol 48:354–363

49. Yang MI, Flavin K, Kopf I, Radics G, Hearnden CH, McManus GJ, Moran B, Villalta-Cerdas A, Echegoyen LA, Giordani S, Lavelle EC (2013) Functionalization of carbon nanoparticles modulates

inflammatory cell recruitment and NLRP3 inflammasome activation. Small 9:4194–4206

50. Chen Z, Yin JJ, Zhou YT, Zhang Y, Song L, Song M, Hu S, Gu N (2012) Dual enzyme-like activities of iron oxide nanoparticles and their implication for diminishing cytotoxicity. ACS Nano 6:4001–4012

51. Chen EY, Garnica M, Wang YC, Chen CS, Chin WC (2011) Mucin secretion induced by titanium dioxide nanoparticles. PLoS One 6:e16198

52. Asharani PV, Hande MP, Valiyaveettil S (2009) Anti-proliferative activity of silver nanoparticles. BMC Cell Biol 10:65

53. Zhang R, Piao MJ, Kim KC, Kim AD, Choi JY, Choi J, Hyun JW (2012) Endoplasmic reticulum stress signaling is involved in silver nanoparticles-induced apoptosis. Int J Biochem Cell Biol 44:224–232

54. Christen V, Fent K (2012) Silica nanoparticles and silver-doped silica nanoparticles induce endoplasmatic reticulum stress response and alter cytochrome P4501A activity. Chemosphere 87:423–434

55. Scherbart AM, Langer J, Bushmelev A, Van Berlo D, Haberzettl P, Van Schooten FJ, Schmidt AM, Rose CR, Schins RP, Albrecht C (2011) Contrasting macrophage activation by fine and ultrafine titanium dioxide particles is associated with different uptake mechanisms. Part Fibre Toxicol 8:31

56. Chen EY, Garnica M, Wang YC, Mintz AJ, Chen CS, Chin WC (2012) A mixture of anatase and rutile TiO(2) nanoparticles induces histamine secretion in mast cells. Part Fibre Toxicol 9:2

57. Quignard S, Mosser G, Boissiere M, Coradin T (2012) Long-term fate of silica nanoparticles interacting with human dermal fibroblasts. Biomaterials 33:4431–4442

58. Shen C, James SA, De Jonge MD, Turney TW, Wright PF, Feltis BN (2013) Relating cytotoxicity, zinc ions, and reactive oxygen in ZnO nanoparticle-exposed human immune cells. Toxicol Sci 136:120–130

59. Beck-Speier I, Karg E, Behrendt H, Stoeger T, Alessandrini F (2012) Ultrafine particles affect the balance of endogenous pro- and anti-inflammatory lipid mediators in the lung: in-vitro and in-vivo studies. Part Fibre Toxicol 9:27

60. Peuschel H, Sydlik U, Grether-Beck S, Felsner I, Stöckmann D, Jakob S, Kroker M, Haendeler J, Gotić M, Bieschke C, Krutmann J, Unfried K (2012) Carbon nanoparticles induce ceramide- and lipid raft-dependent signalling in lung epithelial cells: a target for a preventive strategy against environmentally-induced lung inflammation. Part Fibre Toxicol 9:48

61. Weissenberg A, Sydlik U, Peuschel H, Schroeder P, Schneider M, Schins RP, Abel J, Unfried K (2010) Reactive oxygen species as mediators of membrane-dependent signaling induced by ultrafine particles. Free Radic Biol Med 49:597–605

62. Comfort KK, Maurer EI, Braydich-Stolle LK, Hussain SM (2011) Interference of silver, gold, and iron oxide nanoparticles on epidermal growth factor signal transduction in epithelial cells. ACS Nano 5:10000–10008

63. Pan Y, Ding H, Qin L, Zhao X, Cai J, Du B (2013) Gold nanoparticles induce nanostructural reorganization of VEGFR2 to repress angiogenesis. J Biomed Nanotechnol 9:1746–1756

64. Ng CT, Dheen ST, Yip WC, Ong CN, Bay BH, Lanry Yung LY (2011) The induction of epigenetic regulation of PROS1 gene in lung fibroblasts by gold nanoparticles and implications for potential lung injury. Biomaterials 32:7609–7615

65. Hou L, Bowman L, Meighan TG, Shi X, Ding M (2013) Induction of miR-21-PDCD4 signaling by tungsten carbide-cobalt nanoparticles in JB6 cells involves ROS-mediated MAPK pathways. J Environ Pathol Toxicol Oncol 32:41–51

66. Mohamed BM, Verma NK, Davies AM, Mcgowan A, Crosbie-Staunton K, Prina-Mello A, Kelleher D, Botting CH, Causey CP, Thompson PR, Pruijn GJ, Kisin ER, Tkach AV, Shvedova AA, Volkov Y (2012) Citrullination of proteins: a common post-translational modification pathway induced by different nanoparticles in vitro and in vivo. Nanomedicine (Lond) 7:1181–1195

67. Monopoli MP, Aberg C, Salvati A, Dawson KA (2012) Biomolecular coronas provide the biological identity of nanosized materials. Nat Nanotechnol 7:779–786

68. Walkey CD, Chan WC (2012) Understanding and controlling the interaction of nanomaterials with proteins in a physiological environment. Chem Soc Rev 41:2780–2799

69. Walczyk D, Bombelli FB, Monopoli MP, Lynch I, Dawson KA (2010) What the cell "sees" in bionanoscience. J Am Chem Soc 132:5761–5768

70. Tenzer S, Docter D, Kuharev J, Musyanovych A, Fetz V, Hecht R, Schlenk F, Fischer D, Kiouptsi K, Reinhardt C, Landfester K, Schild H, Maskos M, Knauer SK, Stauber RH (2013) Rapid formation of plasma protein corona critically affects nanoparticle pathophysiology. Nat Nanotechnol 8:772–781

71. Deng ZJ, Liang M, Monteiro M, Toth I, Minchin RF (2011) Nanoparticle-induced unfolding of fibrinogen promotes Mac-1 receptor activation and inflammation. Nat Nanotechnol 6:39–44

72. Rosso F, Marino G, Grimaldi A, Cafiero G, Chiellini E, Chiellini F, Barbarisi M, Barbarisi A (2013) Vitronectin absorbed on nanoparticles mediate cell viability/proliferation and uptake by 3T3 swiss albino mouse fibroblasts: in vitro study. BioMed Res Int 2013:539348

73. Sanfins E, Dairou J, Hussain S, Busi F, Chaffotte AF, Rodrigues-Lima F, Dupret JM (2011) Carbon black nanoparticles impair acetylation of aromatic amine carcinogens through inactivation of arylamine N-acetyltransferase enzymes. ACS Nano 5:4504–4511

74. Chen M, Von Mikecz A (2005) Formation of nucleoplasmic protein aggregates impairs nuclear function in response to SiO2 nanoparticles. Exp Cell Res 305:51–62

75. Asharani P, Sethu S, Lim HK, Balaji G, Valiyaveettil S, Hande MP (2012) Differential regulation of intracellular factors mediating cell cycle, DNA repair and inflammation following exposure to silver nanoparticles in human cells. Genome Integrity 3:2

76. Duprez L, Wirawan E, Vanden Berghe T, Vandenabeele P (2009) Major cell death pathways at a glance. Microbes Infect 11:1050–1062

77. Galluzzi L, Maiuri MC, Vitale I, Zischka H, Castedo M, Zitvogel L, Kroemer G (2007) Cell death modalities: classification and pathophysiological implications. Cell Death Differ 14:1237–1243

78. Schweichel JU, Merker HJ (1973) The morphology of various types of cell death in prenatal tissues. Teratology 7:253–266

79. Kerr JF (1965) A histochemical study of hypertrophy and ischaemic injury of rat liver with special reference to changes in lysosomes. J Pathol Bacteriol 90:419–435

80. Galluzzi L, Vitale I, Abrams JM, Alnemri ES, Baehrecke EH, Blagosklonny MV, Dawson TM, Dawson VL, El-Deiry WS, Fulda S, Gottlieb E, Green DR, Hengartner MO, Kepp O, Knight RA, Kumar S, Lipton SA, Lu X, Madeo F, Malorni W, Mehlen P, Nunez G, Peter ME, Piacentini M, Rubinsztein DC, Shi Y, Simon HU, Vandenabeele P, White E, Yuan J, Zhivotovsky B, Melino G, Kroemer G (2012) Molecular definitions of cell death subroutines: recommendations of the Nomenclature Committee on Cell Death 2012. Cell Death Differ 19:107–120

81. Kroemer G, Galluzzi L, Vandenabeele P, Abrams J, Alnemri ES, Baehrecke EH, Blagosklonny MV, El-Deiry WS, Golstein P, Green DR, Hengartner M, Knight RA, Kumar S, Lipton SA, Malorni W, Nunez G, Peter ME, Tschopp J, Yuan J, Piacentini M, Zhivotovsky B, Melino G (2009) Classification of cell death: recommendations of the Nomenclature Committee on Cell Death 2009. Cell Death Differ 16:3–11

82. Kroemer G, Jaattela M (2005) Lysosomes and autophagy in cell death control. Nature reviews. Cancer 5:886–897

83. Kerr JF, Wyllie AH, Currie AR (1972) Apoptosis: a basic biological phenomenon with wide-ranging implications in tissue kinetics. Br J Cancer 26:239–257

84. Yoo KC, Yoon CH, Kwon D, Hyun KH, Woo SJ, Kim RK, Lim EJ, Suh Y, Kim MJ, Yoon TH, Lee SJ (2012) Titanium dioxide induces apoptotic cell death through reactive oxygen species-mediated Fas upregulation and Bax activation. Int J Nanomedicine 7:1203–1214

85. Kang SJ, Kim BM, Lee YJ, Hong SH, Chung HW (2009) Titanium dioxide nanoparticles induce apoptosis through the JNK/p38-caspase-8-Bid pathway in phytohemagglutinin-stimulated human lymphocytes. Biochem Biophys Res Commun 386:682–687

86. Shi Y, Wang F, He J, Yadav S, Wang H (2010) Titanium dioxide nanoparticles cause apoptosis in BEAS-2B cells through the caspase 8/t-Bid-independent mitochondrial pathway. Toxicol Lett 196:21–27

87. Park EJ, YI J, Chung KH, Ryu DY, Choi J, Park K (2008) Oxidative stress and apoptosis induced by titanium dioxide nanoparticles in cultured BEAS-2B cells. Toxicol Lett 180:222–229

88. Hussain S, Al-Nsour F, Rice AB, Marshburn J, Yingling B, Ji Z, Zink JI, Walker NJ, Garantziotis S (2012) Cerium dioxide nanoparticles induce apoptosis and autophagy in human peripheral blood monocytes. ACS Nano 6:5820–5829

89. Ahamed M, Akhtar MJ, Raja M, Ahmad I, Siddiqui MK, Alsalhi MS, Alrokayan SA (2011) ZnO nanorod-induced apoptosis in human alveolar adenocarcinoma cells via p53, survivin and bax/bcl-2 pathways: role of oxidative stress. Nanomedicine 7:904–913

90. Siddiqui MA, Ahamed M, Ahmad J, Majeed Khan MA, Musarrat J, Al-Khedhairy AA, Alrokayan SA (2012) Nickel oxide nanoparticles induce cytotoxicity, oxidative stress and apoptosis in cultured human cells that is abrogated by the dietary antioxidant curcumin. Food Chem Toxicol 50:641–647

91. Zhao J, Bowman L, Zhang X, Shi X, Jiang B, Castranova V, Ding M (2009) Metallic nickel nano- and fine particles induce JB6 cell apoptosis through a caspase-8/AIF mediated cytochrome c-independent pathway. J Nanobiotechnol 7:2

92. Tsai YY, Huang YH, Chao YL, Hu KY, Chin LT, Chou SH, Hour AL, Yao YD, Tu CS, Liang YJ, Tsai CY, Wu HY, Tan SW, Chen HM (2011) Identification of the nanogold particle-induced endoplasmic reticulum stress by omic techniques and systems biology analysis. ACS Nano 5:9354–9369

93. Sarkar A, Das J, Manna P, Sil PC (2011) Nano-copper induces oxidative stress and apoptosis in kidney via both extrinsic and intrinsic pathways. Toxicology 290:208–217

94. Thomas TP, Majoros I, Kotlyar A, Mullen D, Holl MM, Baker JR Jr (2009) Cationic poly(amidoamine) dendrimer induces lysosomal apoptotic pathway at therapeutically relevant concentrations. Biomacromolecules 10:3207–3214

95. Lee JH, Cha KE, Kim MS, Hong HW, Chung DJ, Ryu G, Myung H (2009) Nanosized polyamidoamine (PAMAM) dendrimer-induced apoptosis mediated by mitochondrial dysfunction. Toxicol Lett 190:202–207

96. Xia T, Kovochich M, Liong M, Zink JI, Nel AE (2008) Cationic polystyrene nanosphere toxicity depends on cell-specific endocytic and mitochondrial injury pathways. ACS Nano 2:85–96

97. Tyurina YY, Kisin ER, Murray A, Tyurin VA, Kapralova VI, Sparvero LJ, Amoscato AA, Samhanarias AK, Swedin L, Lahesmaa R, Fadeel B, Shvedova AA, Kagan VE (2011) Global phospholipidomics analysis reveals selective pulmonary peroxidation profiles upon inhalation of single-walled carbon nanotubes. ACS Nano 5:7342–7353

98. Wang L, Luanpitpong S, Castranova V, Tse W, Lu Y, Pongrakhananon V, Rojanasakul Y (2011) Carbon nanotubes induce malignant transformation and tumorigenesis of human lung epithelial cells. Nano Lett 11:2796–2803

99. Fujita K, Fukuda M, Endoh S, Kato H, Maru J, Nakamura A, Uchino K, Shinohara N, Obara S, Nagano R, Horie M, Kinugasa S, Hashimoto H, Kishimoto A (2013) Physical properties of single-wall carbon nanotubes in cell culture and their dispersal due to alveolar epithelial cell response. Toxicol Mech Methods 23:598–609

100. Nakagawa I, Amano A, Mizushima N, Yamamoto A, Yamaguchi H, Kamimoto T, Nara A, Funao J, Nakata M, Tsuda K, Hamada S, Yoshimori T (2004) Autophagy defends cells against invading group A Streptococcus. Science 306:1037–1040

101. Paludan C, Schmid D, Landthaler M, Vockerodt M, KUBE D, Tuschl T, Munz C (2005) Endogenous MHC class II processing of a viral nuclear antigen after autophagy. Science 307:593–596

102. Stern ST, Adiseshaiah PP, Crist RM (2012) Autophagy and lysosomal dysfunction as emerging mechanisms of nanomaterial toxicity. Part Fibre Toxicol 9:20

103. Park EJ, Umh HN, Kim SW, Cho MH, Kim JH, Kim Y (2014) ERK pathway is activated in bare-FeNPs-induced autophagy. Arch Toxicol 88:323–36

104. Khan MI, Mohammad A, Patil G, Naqvi SA, Chauhan LK, Ahmad I (2012) Induction of ROS, mitochondrial damage and autophagy in lung epithelial cancer cells by iron oxide nanoparticles. Biomaterials 33:1477–1488

105. Li JJ, Hartono D, Ong CN, Bay BH, Yung LY (2010) Autophagy and oxidative stress associated with gold nanoparticles. Biomaterials 31:5996–6003

106. Wu YN, Yang LX, Shi XY, Li IC, Biazik JM, Ratinac KR, Chen DH, Thordarson P, Shieh DB, Braet F (2011) The selective growth inhibition of oral cancer by iron core-gold shell nanoparticles through mito-chondria-mediated autophagy. Biomaterials 32:4565–4573

107. Ma X, Wu Y, Jin S, Tian Y, Zhang X, Zhao Y, Yu L, Liang XJ (2011) Gold nanoparticles induce autopha-gosome accumulation through size-dependent nanoparticle uptake and lysosome impairment. ACS Nano 5:8629–8639

108. Tsukahara T, Matsuda Y, Usui Y, Haniu H (2013) Highly purified, multi-wall carbon nanotubes induce light-chain 3B expression in human lung cells. Biochem Biophys Res Commun 440:348–353

109. Harhaji L, Isakovic A, Raicevic N, Markovic Z, Todorovic-Markovic B, Nikolic N, Vranjes-Djuric S, Markovic I, Trajkovic V (2007) Multiple mecha-nisms underlying the anticancer action of nanocrys-talline fullerene. Eur J Pharmacol 568:89–98

110. Seleverstov O, Zabirnyk O, Zscharnack M, Bulavina L, Nowicki M, Heinrich JM, Yezhelyev M, Emmrich F, O'Regan R, Bader A (2006) Quantum dots for human mesenchymal stem cells labeling. A size-dependent autophagy activation. Nano Lett 6:2826–2832

111. Johnson-Lyles DN, Peifley K, Lockett S, Neun BW, Hansen M, Clogston J, Stern ST, Mcneil SE (2010) Fullerenol cytotoxicity in kidney cells is associated with cytoskeleton disruption, autophagic vacuole accumulation, and mitochondrial dysfunction. Toxicol Appl Pharmacol 248:249–258

112. Stern ST, Zolnik BS, Mcleland CB, Clogston J, Zheng J, Mcneil SE (2008) Induction of autophagy in porcine kidney cells by quantum dots: a common cellular response to nanomaterials? Toxicol Sci 106:140–152

113. Liu HL, Zhang YL, Yang N, Zhang YX, Liu XQ, Li CG, Zhao Y, Wang YG, Zhang GG, Yang P, GUO F, Sun Y, Jiang CY (2011) A functionalized single-walled carbon nanotube-induced autophagic cell death in human lung cells through Akt-TSC2-mTOR signaling. Cell Death Dis 2:e159

114. Bergsbaken T, fink SL, cookson BT (2009) Pyroptosis: host cell death and inflammation. Nature reviews. Microbiology 7:99–109

115. Fink SL, Cookson BT (2005) Apoptosis, pyroptosis, and necrosis: mechanistic description of dead and dying eukaryotic cells. Infect Immun 73:1907–1916

116. Kepp O, Galluzzi L, Zitvogel L, Kroemer G (2010) Pyroptosis – a cell death modality of its kind? Eur J Immunol 40:627–630

117. Ji Z, Wang X, Zhang H, Lin S, Meng H, Sun B, George S, Xia T, Nel AE, Zink JI (2012) Designed synthesis of CeO2 nanorods and nanowires for studying toxicological effects of high aspect ratio nanomaterials. ACS Nano 6:5366–5380

118. Hitomi J, Christofferson DE, Ng A, Yao J, Degterev A, Xavier RJ, Yuan J (2008) Identification of a molecular signaling network that regulates a cellular necrotic cell death pathway. Cell 135:1311–1323

119. Kim TH, Kim M, Park HS, Shin US, gong MS, Kim HW (2012) Size-dependent cellular toxicity of silver nanoparticles. J Biomed Mater Res A 100:1033–1043

120. Pan Y, Leifert A, Ruau D, Neuss S, Bornemann J, Schmid G, Brandau W, Simon U, Jahnen-Dechent W (2009) Gold nanoparticles of diameter 1.4 nm trig-ger necrosis by oxidative stress and mitochondrial damage. Small 5:2067–2076

121. Vandenabeele P, Galluzzi L, Vanden Berghe T, Kroemer G (2010) Molecular mechanisms of necroptosis: an ordered cellular explosion. Nature reviews. Mol Cell Biol 11:700–714

122. Qu G, Liu S, Zhang S, Wang L, Wang X, Sun B, Yin N, Gao X, Xia T, Chen JJ, Jiang GB (2013) Graphene oxide induces toll-like receptor 4 (TLR4)-dependent necrosis in macrophages. ACS Nano 7:5732–5745

123. Xia T, Kovochich M, Liong M, Madler L, Gilbert B, Shi H, Yeh JI, Zink JI, Nel AE (2008) Comparison of the mechanism of toxicity of zinc oxide and cerium oxide nanoparticles based on dissolution and oxida-tive stress properties. ACS Nano 2:2121–2134

124. Wilkinson KE, Palmberg L, Witasp E, Kupczyk M, Feliu N, Gerde P, seisenbaeva GA, Fadeel B, Dahlen SE, Kessler VG (2011) Solution-engineered palla-dium nanoparticles: model for health effect studies of automotive particulate pollution. ACS Nano 5:5312–5324

125. Alili L, Sack M, Karakoti AS, Teuber S, Puschmann K, Hirst SM, Reilly CM, Zanger K, Stahl W, Das S, Seal s, Brenneisen P (2011) Combined cytotoxic and anti-invasive properties of redox-active nanoparticles in tumor-stroma interactions. Biomaterials 32:2918–2929

126. Hussain S, Garantziotis S (2013) Interplay between apoptotic and autophagy pathways after exposure to cerium dioxide nanoparticles in human monocytes. Autophagy 9:101–103

127. Fimia GM, Kroemer G, Piacentini M (2013) Molecular mechanisms of selective autophagy. Cell Death Differ 20:1–2

128. Kroemer G, Levine B (2008) Autophagic cell death: the story of a misnomer. Nature reviews. Mol Cell Biol 9:1004–1010

129. Napierska D, Thomassen LC, Rabolli V, Lison D, Gonzalez L, Kirsch-Volders M, Martens JA, Hoet PH (2009) Size-dependent cytotoxicity of monodisperse silica nanoparticles in human endothelial cells. Small 5:846–853

130. Pan Y, Neuss S, Leifert A, Fischler M, Wen F, Simon U, Schmid G, Brandau W, Jahnen-Dechent W (2007) Size-dependent cytotoxicity of gold nanoparticles. Small 3:1941–1949

131. Stoeger T, Reinhard C, Takenaka S, Schroeppel A, Karg E, Ritter B, Heyder J, Schulz H (2006) Instillation of six different ultrafine carbon particles indicates a surface area threshold dose for acute lung inflammation in mice. Environ Health Perspect 114:328–333

132. Bouwmeester H, lynch I, Marvin HJ, Dawson KA, Berges M, Braguer D, Byrne HJ, Casey A, Chambers G, Clift MJ, Elia G, Fernandes TF, Fjellsbo LB, Hatto P, Juillerat L, Klein C, Kreyling WG, Nickel C, Riediker M, Stone V (2011) Minimal analytical characterization of engineered nanomaterials needed for hazard assessment in biological matrices. Nanotoxicology 5:1–11

133. Oberdorster G (2010) Safety assessment for nanotechnology and nanomedicine: concepts of nanotoxicology. J Intern Med 267:89–105

134. Oberdorster G, Maynard A, Donaldson K, Castranova V, Fitzpatrick J, Ausman K, Carter J, Karn B, Kreyling W, Lai D, Olin S, Monteiroriviere N, Warheit D, Yang H (2005) Principles for characterizing the potential human health effects from exposure to nanomaterials: elements of a screening strategy. Part Fibre Toxicol 2:8

135. Rivera Gil P, Oberdorster G, Elder A, Puntes V, Parak WJ (2010) Correlating physico-chemical with toxicological properties of nanoparticles: the present and the future. ACS Nano 4:5527–5531

136. Auffan M, Rose J, Bottero JY, Lowry GV, Jolivet JP, Wiesner MR (2009) Towards a definition of inorganic nanoparticles from an environmental, health and safety perspective. Nat Nanotechnol 4:634–641

137. Carlson C, Hussain SM, Schrand AM, Braydich-Stolle LK, Hess KL, Jones RL, Schlager JJ (2008) Unique cellular interaction of silver nanoparticles: size-dependent generation of reactive oxygen species. J Phys Chem B 112:13608–13619

138. Oberdorster G, Finkelstein JN, Johnston C, Gelein R, Cox C, Baggs R, Elder AC (2000) Acute pulmonary effects of ultrafine particles in rats and mice. Res Rep Health Eff Inst 96:5–74; disc 75–86

139. Park J, Lim DH, Lim HJ, Kwon T, Choi JS, Jeong S, Choi IH, Cheon J (2011) Size dependent macrophage responses and toxicological effects of Ag nanoparticles. Chem Commun 47:4382–4384

140. Rabolli V, Thomassen LC, Princen C, Napierska D, Gonzalez L, Kirsch-Volders M, Hoet PH, Huaux F, Kirschhock CE, Martens JA, Lison D (2010) Influence of size, surface area and microporosity on the in vitro cytotoxic activity of amorphous silica nanoparticles in different cell types. Nanotoxicology 4:307–318

141. Zhao Y, Sun X, Zhang G, Trewyn BG, Slowing II, Lin VS (2011) Interaction of mesoporous silica nanoparticles with human red blood cell membranes: size and surface effects. ACS Nano 5:1366–1375

142. Coradeghini R, Gioria S, Garcia CP, Nativo P, Franchini F, Gilliland D, Ponti J, Rossi F (2013) Size-dependent toxicity and cell interaction mechanisms of gold nanoparticles on mouse fibroblasts. Toxicol Lett 217:205–216

143. Geiser M, Rothen-Rutishauser B, Kapp N, Schurch S, Kreyling W, Schulz H, Semmler M, Im Hof V, Heyder J, Gehr P (2005) Ultrafine particles cross cellular membranes by nonphagocytic mechanisms in lungs and in cultured cells. Environ Health Perspect 113:1555–1560

144. Nel AE, Madler L, Velegol D, Xia T, Hoek EM, Somasundaran P, Klaessig F, Castranova V, Thompson M (2009) Understanding biophysico-chemical interactions at the nano-bio interface. Nat Mater 8:543–557

145. Nabiev I, Mitchell S, davies A, Williams Y, Kelleher D, Moore R, Gun'ko YK, Byrne S, Rakovich YP, Donegan JF, Sukhanova A, Conroy J, Cottell D, Gaponik N, Rogach A, Volkov Y (2007) Nonfunctionalized nanocrystals can exploit a cell's active transport machinery delivering them to specific nuclear and cytoplasmic compartments. Nano Lett 7:3452–3461

146. Semmler-Behnke M, Kreyling WG, Lipka J, Fertsch S, Wenk A, Takenaka S, Schmid G, Brandau W (2008) Biodistribution of 1.4- and 18-nm gold particles in rats. Small 4:2108–2111

147. Lu J, Liong M, Zink JI, Tamanoi F (2007) Mesoporous silica nanoparticles as a delivery system for hydrophobic anticancer drugs. Small 3:1341–1346

148. Buzea C, Pacheco II, Robbie K (2007) Nanomaterials and nanoparticles: sources and toxicity. Biointerphases 2:MR17–MR71

149. Donaldson K, Brown D, Clouter A, Duffin R, Macnee W, Renwick L, Tran L, Stone V (2002) The pulmonary toxicology of ultrafine particles. J Aerosol Med 15:213–220

150. Oberdorster G, Ferin J, Lehnert BE (1994) Correlation between particle size, in vivo particle persistence, and lung injury. Environ Health Perspect 102(Suppl 5):173–179

151. Warheit DB, Webb TR, Sayes CM, Colvin VL, Reed KL (2006) Pulmonary instillation studies with nanoscale TiO2 rods and dots in rats: toxicity is not dependent upon particle size and surface area. Toxicol Sci 91:227–236

152. Wittmaack K (2007) In search of the most relevant parameter for quantifying lung inflammatory response to nanoparticle exposure: particle number, surface area, or what? Environ Health Perspect 115:187–194

153. Sayes CM, Liang F, Hudson JL, Mendez J, Guo W, Beach JM, Moore VC, Doyle CD, West JL, Billups WE, Ausman KD, Colvin VL (2006) Functionalization density dependence of single-walled carbon nanotubes cytotoxicity in vitro. Toxicol Lett 161:135–142

154. Sayes CM, Wahi R, Kurian PA, Liu Y, West JL, Ausman KD, Warheit DB, Colvin VL (2006) Correlating nanoscale titania structure with toxicity: a cytotoxicity and inflammatory response study with human dermal fibroblasts and human lung epithelial cells. Toxicol Sci 92:174–185

155. Gurr JR, wang AS, Chen CH, Jan KY (2005) Ultrafine titanium dioxide particles in the absence of photoactivation can induce oxidative damage to human bronchial epithelial cells. Toxicology 213:66–73

156. Jiang J, Oberdorster G, Elder A, gelein R, Mercer P, Biswas P (2008) Does nanoparticle activity depend upon size and crystal phase? Nanotoxicology 2:33–42

157. Risom L, Moller P, Loft S (2005) Oxidative stress-induced DNA damage by particulate air pollution. Mutat Res 592:119–137

158. Wang L, Zheng H, Long Y, Gao M, Hao J, Du J, Mao X, Zhou D (2010) Rapid determination of the toxicity of quantum dots with luminous bacteria. J Hazard Mater 177:1134–1137

159. Mortimer M, Kasemets K, Kahru A (2010) Toxicity of ZnO and CuO nanoparticles to ciliated protozoa Tetrahymena thermophila. Toxicology 269:182–189

160. Moos PJ, Chung K, Woessner D, Honeggar M, Cutler NS, Veranth JM (2010) ZnO particulate matter requires cell contact for toxicity in human colon cancer cells. Chem Res Toxicol 23:733–739

161. Borm P, Klaessig FC, Landry TD, Moudgil B, Pauluhn J, Thomas K, Trottier R, Wood S (2006) Research strategies for safety evaluation of nanomaterials, part V: role of dissolution in biological fate and effects of nanoscale particles. Toxicol Sci 90:23–32

162. Churg A, Stevens B, Wright JL (1998) Comparison of the uptake of fine and ultrafine TiO2 in a tracheal explant system. Am J Physiol 274:L81–L86

163. Takenaka S, Karg E, Roth C, Schulz H, Ziesenis A, Heinzmann U, Schramel P, Heyder J (2001) Pulmonary and systemic distribution of inhaled ultrafine silver particles in rats. Environ Health Perspect 109(Suppl 4):547–551

164. Wick P, Manser P, Limbach LK, Dettlaff-Weglikowska U, Krumeich F, Roth S, Stark WJ, Bruinink A (2007) The degree and kind of agglomeration affect carbon nanotube cytotoxicity. Toxicol Lett 168:121–131

165. Shvedova AA, Kisin ER, Murray AR, Gorelik O, Arepalli S, Castranova V, Young SH, Gao F, Tyurina YY, Oury TD, Kagan VE (2007) Vitamin E deficiency enhances pulmonary inflammatory response and oxidative stress induced by single-walled carbon nanotubes in C57BL/6 mice. Toxicol Appl Pharmacol 221:339–348

166. Vallhov H, Qin J, Johansson SM, Ahlborg N, Muhammed MA, Scheynius A, Gabrielsson S (2006) The importance of an endotoxin-free environment during the production of nanoparticles used in medical applications. Nano Lett 6:1682–1686

167. Magrez A, Kasas S, Salicio V, Pasquier N, Seo JW, Celio M, Catsicas S, Schwaller B, Forro L (2006) Cellular toxicity of carbon-based nanomaterials. Nano Lett 6:1121–1125

168. Li R, Wang X, Ji Z, Sun B, Zhang H, Chang CH, Lin S, Meng H, Liao YP, Wang M, Li Z, Hwang AA, Song TB, Xu R, Yang Y, Zink JI, Nel AE, Xia T (2013) Surface charge and cellular processing of covalently functionalized multiwall carbon nanotubes determine pulmonary toxicity. ACS Nano 7:2352–2368

169. Guadagnini R, Moreau K, Hussain S, Marano F, Boland S (2013) Toxicity evaluation of engineered nanoparticles for medical applications using pulmonary epithelial cells. Nanotoxicology doi:10.3109/17435390.2013.855830

170. Safi M, Sarrouj H, Sandre O, Mignet N, Berret JF (2010) Interactions between sub-10-nm iron and cerium oxide nanoparticles and 3T3 fibroblasts: the role of the coating and aggregation state. Nanotechnology 21:145103

171. Derfus AM, Chen AA, Min DH, Ruoslahti E, Bhatia SN (2007) Targeted quantum dot conjugates for siRNA delivery. Bioconjug Chem 18:1391–1396

172. Muller J, Delos M, Panin N, Rabolli V, Huaux F, Lison D (2009) Absence of carcinogenic response to multiwall carbon nanotubes in a 2-year bioassay in the peritoneal cavity of the rat. Toxicol Sci 110:442–448

173. Lison D, Carbonnelle P, Mollo L, lauwerys R, Fubini B (1995) Physicochemical mechanism of the interaction between cobalt metal and carbide particles to generate toxic activated oxygen species. Chem Res Toxicol 8:600–606

174. Guo B, Zebda R, Drake SJ, Sayes CM (2009) Synergistic effect of co-exposure to carbon black and Fe2O3 nanoparticles on oxidative stress in cultured lung epithelial cells. Part Fibre Toxicol 6:4

Nanomaterials: Impact on Cells and Cell Organelles

8

Željka Krpetić, Sergio Anguissola, David Garry,
Philip M. Kelly, and Kenneth A. Dawson

Contents

Ž. Krpetić • S. Anguissola • D. Garry • P.M. Kelly
K.A. Dawson (✉)
Centre for BioNano Interactions, School of
Chemistry and Chemical Biology, University College
Dublin, Belfield, Dublin 4, Republic of Ireland
e-mail: kenneth.a.dawson@cbni.ucd.ie

Abstract

Colloidal nanoparticles designed for the interactions with cells are very small, nanoscale objects usually consisting of inorganic cores and organic shells that are dispersed in a buffer or biological medium. By tuning the material properties of the nanoparticles a number of different biological applications of nanomaterials are enabled *i.e.* targeting, labelling, drug delivery, use as diagnostic tools or therapy. For all biological applications of nanoparticles, it is important to understand their interactions with the surrounding biological environment in order to predict their biological impact, in particular when designing the nanoparticles for diagnostic and therapeutic purpose. Due to the high surface-to-volume ratio, the surface of nanomaterials is very reactive. When exposed to biological fluids, the proteins and biomolecules present therein tend to associate with the nanoparticles' surface. This phenomenon is defined as biomolecular corona formation. The biomolecular corona plays a key role in the interaction between nanoparticles and biological systems, impacting on how these particles interact with biological systems on a

cellular and molecular level. This book chapter describes the nature of the interactions at the bio-nano interface, shows the design strategy of nanoparticles for nanomedicine, and defines the concepts of biomolecular corona and biological identity of nanoparticles. Moreover, it describes the interaction of functionalised nanomaterials with cell organelles and intracellular fate of nanoparticles and it shows therapeutic application of gold nanoparticles as dose enhancers in radiotherapy.

Keywords

Gold nanoparticles • Biomolecular corona • Bio-nano interactions • Radiotherapy dose enhancers

8.1   Introduction

Engineering nanoparticles for biomedical applications is one of the fastest growing fields of research nowadays. Due to their small size, at the nanoscale, materials behave differently than those present in bulk, which gives them unique physical and chemical properties that can be exploited for many different applications. Key applications of nanoparticles include cancer treatments such as hyperthermia or radiotherapy cancer treatments, using nanoparticles as drug carriers, and biolabeling through single particle detection by electron microscopy and resonance light scattering or photothermal microscopy. For all biological applications of nanoparticles, it is important to understand their interactions with the surrounding biological environment and target cells, in order to predict their biological impact; particularly when designing nanoparticles for diagnostic and therapeutic purposes. Understanding of the bio-nano interactions is key to maximising the particle's efficacy.

One example is the striking difference in colour between bulk gold and gold nanoparticles that testifies to the dramatic change in material properties. The colour change is due to a systematic shift to lower energy of the plasmon resonance of nanoparticles as the particle size decreases on the nanoscale. This property has

resulted in gold nanoparticles being used as visible/near infrared diagnostic tools in the rapidly emerging field of nanomedicine/diagnostics [1].

Nanomaterials possess specific intrinsic reactivity due to increased surface area, compared to bulk materials. The choice of materials for development of nanomedical tools is very important in order to advance the nanoparticle-based therapeutics as an alternative to the traditional ones [2]. In spite of fruitful on-going research in the recent years, hitherto only a few types of particles, e.g. liposomes and albumin nanoparticles have been FDA-approved as nanoparticle-based therapeutics and are present worldwide in clinical practices impacting the medicine and healthcare [3]. Because of their ease of preparation, surface modification, size and shape tuneability and unique optical properties there is a particular attention to research on metal nanoparticles. Metal nanoparticles, specifically the ones made of gold, have been proven versatile agents in diverse biomedical applications, *i.e.* diagnostic assays [4], delivery [5] of drugs and genes and radiotherapy enhancement [6, 7]. The number of properties associated with the particle size in addition to material related properties used in biological applications makes nanoparticles ideal platforms for the development of new biomedical tools.

Nanoparticles designed for biomedical applications are generally smaller than target biological entities, which gives them unique capability to interact with biomolecules present on the surface of the cells and those present inside the cell cytoplasm and in cell organelles. This makes nanoparticles an ideal class of nano-vehicles useful to target/detect diseases at an early stage of development [8, 9] or act as intracellular reporters [10].

Depending on their surface functionalities, particle size and shape, and state of aggregation, presence or absence of the biomolecular corona, nanomaterials can interact with biological systems in many ways, by impacting the cell integrity, utilising different uptake routes or targeting different organelles, depending on the cell type. Nanoparticle design may affect the interaction of particles within the human body in their ability to

overcome diverse biological barriers [3]. This process can often be very complex, as it involves direct interaction of nanomaterials with biological fluids that in many cases leads to the formation of a biomolecular corona and ultimately impacts the particle uptake route, biodistribution and fate of nanoparticles. There is increasing evidence of a range of possible interactions with biological systems and health effects of manufactured nanoparticles. All these effects depend on the nanoparticles' fate and distribution in the cell/organism. It is thus of great importance to keep in mind key properties while designing and manufacturing nanoparticles for biomedical applications, that is: extreme control of reproducibility, high monodispersity of colloidal systems, excellent stability in biological fluids and low toxicity to healthy cells.

This book chapter explores the interactions of engineered nanomaterials at the bio-nano interface. Moreover it shows the importance of the surface chemistry properties of nanoparticles in bio-nano interactions and biological impacts to cells. Herein we describe interactions of nanoparticles with the plasma membrane of cells, both specific and non-specific. Key features concerning the design of nanoparticles for nanomedicine are outlined. Moreover, we provide a comprehensive state of the art update of the biomolecular corona that in many cases confers the biological identity of nanoparticles and describe how the biomolecular corona impacts the nanoparticles. Following, we describe the effects and control of the biomolecular corona and interactions of functionalised nanoparticles with cell organelles. Particular attention is given to receptor-mediated endocytosis, as the primary route of cellular uptake of the nanoparticulate materials leading to accumulation in acidic compartments called lysosomes. Examples of lysosomal rupture depending on specific nanoparticle surface chemistry are described, as well as the effect of nanoparticle load dilution during cell division. Importantly, this book chapter shows successful examples of organelle targeting by engineered nanoparticles, gives examples of nanomaterials capable of crossing biological barriers and explores the intracellular fate of

nanoparticulate matter. The role of gold nanoparticles as dose enhancers in radiotherapy, resulting from specific organelle localisation is highlighted as an example of application in nanomedicine.

8.2   Interactions at the Bio-Nano Interface

In order to assess the impact of nanoparticles originated from industrial or consumer products, or when designing nanoparticles destined to be administered to an organism or a cell and fulfil specific diagnostic/therapeutic activity, it is important to know their interactions with biological systems. These interactions can often be predicted by their surface chemistry. Additionally it is also important to know how the cell machinery operates. One of the key criteria for assessing the nanoparticle toxicity and addressing the health and safety of nanomaterials is the ability to cross the cell membrane.

Nanoparticles interact with individual cells and living organisms in a fundamentally different manner than small molecules, *i.e.* drugs. Small neutral molecules, e.g. CO_2 and O_2 can freely pass through cell membranes [11, 12]. However, larger organic molecules such as sugars, amino acids, and ions similar to the nanoparticles require an energy dependent transport mechanism in order to gain access to the cell, and overcome the protective barrier, *i.e.* the cell membrane. Often, when presented to a cell in a biological medium non-functionalised nanoparticles have a dynamic biomolecular protective layer known as the biomolecular corona, in addition to absorbed surface ions, lipids and other stabilising ligand molecules [13]. More detailed description of the biomolecular corona and its effects can be found in Sect. 8.4 of this book chapter. In this section, we describe how in the case of particles bearing the biomolecule corona, the cell recognises this layer on the particle surface and establishes a number of specific or non-specific interactions [14].

Before we describe the mechanisms used by nanoparticles to cross the cell membrane, we first

need to take into account the concept of bio-nano interface. The term 'bio-nano interface' refers to the interface where the artificial engineered nanomaterials or nanoparticle systems, interact with biological systems at the nano-scale level. Here the organic and synthetic worlds merge into a new class of science concerned with the safe use of nanotechnology and design of nanomaterials for biomedical applications.

As nanotechnology products are increasing in the environment and consumer products so too is the likelihood of exposure of humans coming in contact with nanomaterials, which may lead to unknown effects on human health. At a bio-nano interface, nanoparticles can interact with components of biological fluids, such as proteins or phospholipids, components of cells such as membranes, nucleic acids, endocytotic vesicles and other organelles, to establish a number of interfaces that depend on colloidal forces as well as dynamic biophysicochemical interactions, kinetics and thermodynamic exchanges between nanomaterial surfaces and the biologically relevant surfaces. These interactions often lead to formation of biomolecular coronas, intracellular uptake and biocatalytic processes that can have either biocompatible or bioadverse outcomes. Biomolecules available in biological fluids may induce phase transformations, release of free energy, restructuring and dissolution at the nanoparticle surface. For the safe use of nanotechnology in nanomedicine, probing the diverse interfaces allows the investigator to develop and predict relationships between structure and activity that are determined by properties of nanomaterials such as size, shape, surface chemistry, roughness and surface coatings. However, it may be very difficult and perhaps impossible to describe all the biophysicochemical interactions happening at the bio-nano interface, but it is an area ripe for investigation and implementation of nanotechnology in nanomedicine.

Before a nanoparticle is presented to biological fluids, there is a need to first assess key nanoparticle characteristics such as the chemical composition, size, shape, porosity, surface functionalisation and hydrophilic/hydrophobic properties [15]. By understanding these fundamental

properties we can define the 'naked nanoparticles' surface properties in complex interactions at a bio-nano interface [16].

When unfunctionalised nanoparticles ('naked nanoparticles') are dispersed in a biological media, their surface is exposed to a very different environment than the one created by chemical synthesis. Some nanomaterials allow formation of stable colloids known as 'naked particles' (such as SiO_2, polystyrene, Fe_2O_3), *i.e.* particles that contain no foreign stabiliser at the surface other than the core particle material or water species and are presented as stable colloidal dispersions. These particles are important for the study of biological interactions between biomolecules and plain inorganic surfaces. When in contact with biological media or fluids, surface properties of these particles affect physicalchemical characteristics such as zeta potential, colloidal stability and particle agglomeration state, among others [17]. Therefore, the medium in which the nanoparticles are dispersed determines the stability of the nanoparticle dispersion according to parameters such as pH, ionic strength, detergents, temperature and importantly, protein concentration [18]. Moieties present on the particle's surface are responsible for the interactions between the nanoparticle and the surrounding medium, and influence the dispersion properties and adsorption/desorption of biomolecules.

After the bio-molecular corona has formed on the surface of 'naked' particles, it is considered a key feature in shaping nanoparticle-cell membrane interactions that may lead to either specific ligand-mediated nanoparticle uptake or non-specific nanoparticle uptake (Fig. 8.1) [13, 17, 19].

8.2.1 Nanoparticle Interactions with the Cell Surface Environment

The heterogeneous nature of the nanoparticle's bio-molecular corona is given by the presence of different surface ions, proteins, lipids that can influence interactions of cells when in contact with nanoparticles, but how is the cell surface contributing to the interactions? The cell

Fig. 8.1 Nanoparticle-cell membrane surface adhesion is dependent on the material and bio-molecular surface identity of the nanoparticle

Nanoparticle
Endosome
Lysosome
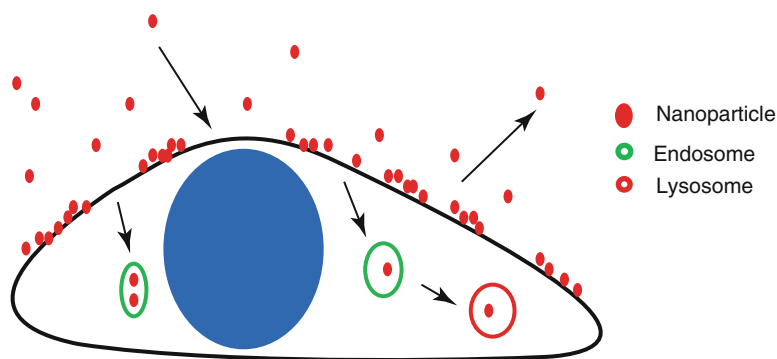
membrane represents a robust biological barrier to most molecules, allowing the cell to maintain homeostasis, *i.e.* conditions that are very different from those in the extracellular space. Naturally, the surface of cell membranes differs significantly from that of the surface of nanoparticles, *i.e.* it is a non-rigid compliant heterogeneous structure that can re-adjust due to its fluidity or thermodynamics of the membrane. However, even though the cell membrane surface is non-rigid, the same physical forces apply to the membrane as to the nanoparticle dispersions [20]. This non-rigid cell membrane provides intelligent and robust protection to the cell *via* rigorous selection of what molecules may gain access to the cell's interior [21].

In addition to its protective function, the plasma membrane accomplishes a regular exchange of ions, building blocks for proteins, lipids and signalling molecules with the surrounding environment and neighbouring cells, selectively allowing the transport of material across the membrane in both directions. This transport is generally regulated by a number of carrier proteins and ion channels existing within the membrane structure, which perform key roles in nanoparticle uptake mechanisms and cross membrane transport.

The cell membrane is made of glycerophospholipids, which are single molecules consisting of two main units, a hydrophilic head and a hydrophobic tail, forming a robust phospholipid bilayer [22]. This unique primary structure of individual glycerophospholipids allows for a self-organising, energy-free aggregation of these lipids into bilayers. The formation of a phospholipid bilayer

is a spontaneous process that results in the hydrophobic tails aligning inwards (inside the bilayer) and the hydrophilic heads facing both outside the cell and inside the cell's cytoplasm. Glycerophoslipids are the most abundant lipids present in the cell membrane. However, 20 % of the lipid content of cell membrane is made up of cholesterol [23]. Glycerophospholipids form the main structure of the cell's bilayer while cholesterol regulates and provides stiffness to the cell membrane. Other less abundant lipids play important roles in cell signalling pathways. In addition to the lipid structure, cell membranes are embedded with trans-membrane proteins which account for half the mass of the total membrane. These proteins contain hydrophobic domains that insert in the lipid bilayer linking the extracellular region to the cytoplasm and allowing highly regulated signal transduction across the plasma membrane; transmembrane proteins are very important for trafficking of nanoparticles through regulated mechanisms of endo- and exocytosis.

The plasma membrane or cell surface presented to nanoparticles and other macromolecules displays a heterogeneous distribution of proteins embedded in the lipid membrane. Such a distribution is very highly organised in functional clusters so that surface receptors do not function individually, but assemble into multimeric units to perform their function, e.g. clusters of growth factor receptors and adhesion molecules exist which form a pro-survival signalling platform [24] or clusters receptors can initiate the formation of endocytotic vesicles [25]. These membrane receptor clusters are reported to have a size of 10–50 nm in diameter, suggesting an important

relationship between size and uptake of nanoparticles by cells. Such relationship would imply that a single 50 nm nanoparticle with a favourable bio-molecular composition could interact with a receptor-rich region or patch and would be more favourably internalised; whereas, in the case of a 500 nm nanoparticle, it would have to interact with multiple surface receptor patches at the same time and therefore make nanoparticle-cell receptor interactions less favourable [26], Smaller nanoparticles have been reported to have higher uptake rates, which supports our hypothesis of a more favourable size for nanoparticle uptake [27–29]. They may not be able to recruit the necessary receptors in order to create a favourable invagination to perform nanoparticle-receptor mediated uptake resulting in lower nanoparticle uptake *via* this pathway but allowing alternative routes of uptake and as a consequence, unexpected intracellular localisation.

8.2.2 Specific and Non-specific Nanoparticle-Cell Membrane Interactions

As it will be described more extensively in the next section of this chapter, biomolecules that are adsorbed on the surface of nanoparticles have the potential to interact with their respective receptors on the plasma membrane of cells. This phenomenon can be exploited and controlled by functionalising the surface of nanoparticles with specific functional ligands capable of targeting specific cell receptors.

Nanoparticles functionalised with ligands such as an antibody, protein or aptamer specific to a cell membrane-bound receptor are capable of targeting cells of interest for diagnostic purposes [30, 31]. To enable the nanoparticle-ligand-receptor binding, nanoparticles are required to locate receptor-rich areas on the cell membrane and gain the correct adhesion interactions for internalisation [32]. After the primary contact has been made between the ligand located on the particle's surface and the receptor present on the cell membrane, more cell receptors are required to diffuse to the site of adhesion and aid in the

invagination of the receptor-bound nanoparticle [33]. This receptor patch interaction plays an important role in the kinetics of nanoparticle uptake, *i.e.* once a nanoparticle has overcome the resistive forces (electrostatic, steric repulsion and Van der Waal's forces) that prevent particle-cell membrane interactions, the nanoparticle must then recruit enough cell surface receptors in order to create sufficient thermodynamic energy to overcome the membrane elastic recoil force and therefore allow membrane wrapping to become favourable [33, 34]. Once membrane wrapping is favourable, the membrane forms a vessel *via* engulfing the site of adhesion for specific-ligand binding [35]. As implied, this process would result in receptor mediated endocytosis and thus the internalisation of the nanoparticulate material *via* the endocytosis mechanisms [35].

However common the route of internalisation of extracellular materials is *via* endocytosis and this is not a trivial process, as increasing the competition of a system by increasing the protein concentration to physiological-like levels can inhibit nanoparticle-ligand-receptor binding. For example, it has been demonstrated that nanoparticles with conformational linked transferrin proteins bound to the nanoparticle surface can specifically target a transferrin cell membrane receptor and perform receptor mediated nanoparticle uptake in A549 cells, in serum free conditions. However, when the protein concentration of the medium was increased to physiological-like levels, the ability of the transferrin-functionalised nanoparticles to bind the receptor was inhibited [36]. This suggests that in protein rich environments, with increased competition, the nanoparticle-receptor interaction may be masked, therefore preventing the nanoparticle from identifying its target molecule.

Nonspecific attractive forces, intrinsic to the nanoparticle surface characteristics, hydrophobicity and surface smoothness can also lead to nanoparticle-membrane interactions and nanoparticle uptake. The zeta potential values of nanoparticles' dispersions can create a favourable charge interaction with phosphate head groups on the membrane surface and even with the protein receptors to initiate nanoparticle-membrane adhesion [37]. Cationic nanoparticles [38],

interact more favourably with the cell membrane surface when compared to anionic nanoparticles [39]. Furthermore, the hydrophobicity of the nanoparticles plays a role in surface membrane adhesion and penetration. It has been suggested that nanoparticles that have more hydrophobic character than the cell membrane itself, can embed themselves in the membrane and therefore gain access to the cell interior through this alternative pathway. Additionally, less hydrophobic particles are less likely to be taken up by the cell *via* this nonspecific adhesion pathway, than more hydrophobic nanoparticles of the same size. Furthermore, nanoparticle-cell interactions may be more favourable if surface protrusions or blemishes are present as hydrophilic and electrostatic repulsive forces are greatly reduced, increasing the chances of surface adhesion. Therefore, a designed nanoparticle with a collection of attributes such as hydrophobicity, cationic nature and with surface protrusions would represent ideal candidates for non-specific-cell membrane interactions and uptake [32].

Specific and nonspecific nanoparticle-cell membrane interactions are both avenues for potential applications in future nanoparticle cell targeting as both harness different physicochemical properties in order to navigate across the cell membrane. Both specific and non-specific ligand binding in many cases would perform membrane wrapping and internalisation although *via* different nanoparticle-membrane surface interactions [33].

8.3   Design of Nanoparticles for Nanomedicine

There are many properties leading to the adoption of gold nanoparticles in medicine/life science applications which include their biocompatibility, ease of functionalization [40] and the related historical use in treating rheumatoid arthritis [41]. A key point regarding the development of stable biofunctional nanoparticles for applications in biomedicine is their potential for non-specific interactions with molecules in the biological environment [42].

Because of the potential disruption of the particle surface properties resulting from the formation of a biomolecular corona, biological and biomedical applications of nanoparticles notably require highly stable nanoparticles in physiological conditions while maintaining their physical and chemical properties. Importantly, the stability from a biological point of view means solubility/dispersion in physiological environments, as well as the absence of nonspecific interactions.

Stability of the particles can be successfully achieved by means of a formation of a ligand shell which passivates the surface energy of a particle. Recent strategies involved the use of thiol ligands with hydrophilic functional groups that are capable of forming a self-assembling monolayer (SAM) at the surface of gold nanoparticles [43–46] or using polymeric stabilisers, e.g. functionalised (amino/mercapto) dextrans [47]. Forming a self-assembling monolayer of ligand molecules on the surface of gold nanoparticles provide several advantages over using polymers for particle capping. The use of SAMs provides minimal changes in hydrodynamic diameter of particles that is of crucial importance for many biomedical applications. It avoids steric hindrance of nanoparticle probes that prevents molecular interactions as well as the proper penetration of the nano-objects in constrained biological spaces e.g. cell junctions or synapses. The most useful SAMs range from PEGylated alkanethiols to peptides.

The design of SAMs for gold particle stabilisation in aqueous solutions involves the following strategy starting at the surface of the gold nanoparticle and extending outward: a thiol (or dithiol) [48] group for covalent linkage to the metal core of the particle [49], followed by a hydrophobic region that allows robust close packing of the monolayer, and a hydrophilic terminus which is exposed to the surrounding aqueous solution that ensures excellent particle solubility and overall particle stability in physiological environments. Ideally, a specific functional group is available at the end of the ligand (e.g. –COOH, -OH, -NH$_2$, -NTA, -biotin, -N$_3$ etc.) to allow grafting of proteins, biomolecules,
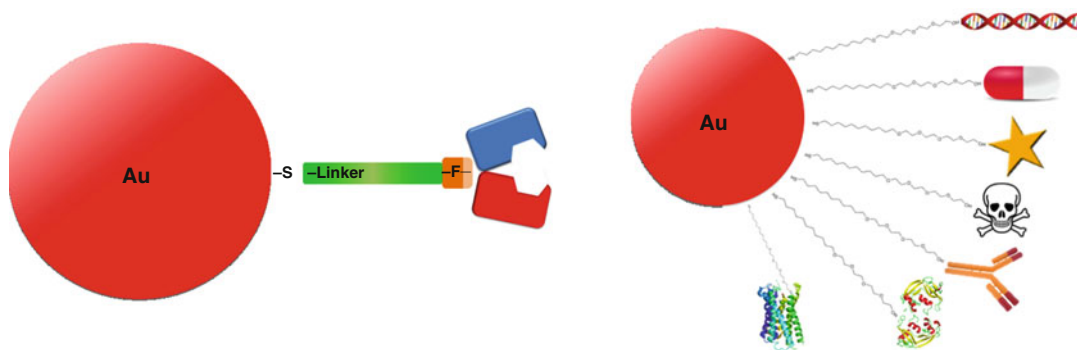
Fig. 8.2 Design strategy for manufacturing functionalised nanoparticles destined for interacting with biological systems. (*Left*) Monolayer ligand shells containing a functional ligand molecule on the surface of the gold nanoparticle that is providing covalent linkage through thiolated ligands, water soluble linker (e.g. PEG units), bearing diverse functional ends (*F*) to which a biomolecule can be readily attached *via* a number of grafting and click chemistry routes. (*Right*) Functional ligands are enabling attachment of potentially any kind of biomolecules and different applications: DNA for gene therapy, drugs for drug delivery, dyes for intracellular reporting and/or sensing, toxins for cancer therapy, antibodies/proteins/receptors for targeting and bio-nano interactions

antibodies, dyes creating a functional nanoparticle. This design strategy is represented schematically in Fig. 8.2.

The most successful example of SAMs are PEGylated alkanethiols, that can be used to form mixed monolayers, *i.e.* creating particles with diverse functionalities available on the surface in a desired ratio and peptides, such as CALNN [44]. The CALNN peptide is a very good example of a ligand capable of protecting silver nanoparticles from oxidation when dispersed in aqueous solutions containing electrolytes and generally prevent electrolyte-induced aggregation of both gold and silver nanoparticles [50]. Moreover, it can serve as a starting sequence (with function of binding to the particle core) in order to create extended peptide sequences bearing a specific biomolecular function, e.g. cell penetrating peptide TAT (CALNNAGRKKRRQRRR) Pntn (CALNNGRQIKIWFQNRRMKWKK) or nuclear localization sequences (NLS) (CALNNGGFSTSLRARKA) [51]. In particular, SAM of functional ligands can be designed to present biomolecular recognition functions that are readily accessible at the particle surface and that may be incorporated in a controlled valency [52]. As described, this artificial rationally designed pentapeptide system provides a simple means to produce nanoparticles carrying a single biomolecular recognition function [53].

In spite of progress in developing ligands that are able to form SAMs on nanoparticle surfaces, the general problem regarding the non-specific binding of nanoparticles has been often over looked. Indeed, complex biological environments contain high concentrations of biological macromolecules (typically 200–400 mg/mL nucleic acids, proteins, carbohydrates, lipids). These can often contain a variety of functional groups (e.g. amines, carbonyl, thiols) some of which can potentially bind to the metal nanoparticle itself or to the matrix protecting the particle. Thus, non-specific binding and/or subsequent exchange of ligands leading to the changes in the passivating particle ligand shell of the particles can cause loss of the particle recognition function, disabling the ability to recognize a specific target for labelling applications. Clearly, it is very important to prevent both non-specific interactions of the particles and ligand exchange, by creating robust ligand shells for nanoparticle stabilisation.

Summarising, while designing nanoparticles for biomedical applications, the following criteria should be followed: (i) providing a compact and robust protective monolayer of stabilizing ligands that ensures maximum surface coverage; (ii) provide high stability in physiological solutions (both in chemical and biological terms) and (iii) maintain control of the particle surface. Moreover, it is important to identify

a concentration of ligands that is sufficiently high to obtain a compact matrix. The stability of capped nanoparticles in complex biological environments can not be predicted solely on their resistance to electrolyte-induced aggregation. Indeed, biological environments are extremely complex, due to their dynamic contents, some of which will bind to metal nanoparticles in a non-specific way, if special attention is not taken to prevent this. Therefore, both non-specific interactions of the particles and subsequent exchange of ligands must be prevented, in order to engage the engineered nanoparticles as useful probes for biological and biomedical applications.

Gold nanoparticles are very versatile, easy to prepare in a range of sizes [54] and shapes [55] with a range of functionalising strategies available, thanks to the thiol chemistry. These strategies are important since they involve the addition of biologically relevant moieties to confer specific biological function(s) to the nanoparticles.

8.4 Biomolecular Corona and Biological Identity of Nanoparticles

The study of the effects of nanoparticles on complex biological systems is a constantly evolving field of research, where a number of parameters need to be considered involving both the physical and chemical properties of nanoparticles and also their biological counterparts. Focussing only on one of these aspects could be misleading and could generate scientific findings that are out of context. Because of their high surface-to-volume ratio, the surface of nanomaterials is very reactive. Such high reactivity translates into very complex and dynamic interactions with the surrounding environment, as the nanoparticle attempts to reduce its surface energy. In this section, the aim is to describe how nanoparticles dispersed in biological matrices containing complex mixtures of biomolecules settle to a low surface energy state, by adsorbing biomolecules from the surrounding environment. This process, which may appear relatively simple at first instance, is in fact very dynamic and complex, and dependent on specific properties of the nanoparticles examined, such as surface charge, shape, curvature and material, but also specific properties of the biological mixture, including the composition of the biomolecules and their relative concentrations.

8.4.1 The Concept of Biomolecular Corona

Owing to their size alongside other properties, nanoparticles have high surface energies. Whilst this is an important consideration when designing stable nanoparticle dispersions, capable of avoiding agglomeration, it also has a significant impact on their biological interactions. When nanoparticles are exposed to biological fluids (e.g. blood plasma, cerebrospinal fluid, lung lining fluid) the proteins and biomolecules present therein tend to associate with the nanoparticles' surfaces in order to passivate their high surface energy [17].

Biological fluids, by their very nature, are highly complex systems. For example, human blood plasma contains over 3,700 proteins [56] with a dynamic protein concentration range spanning 10 orders of magnitude. When 'naked' nanoparticles are exposed to biological fluids, a huge variety of biomolecules present therein will combine to form this "corona" on the particle surface. It has been established that the types of biomolecules that comprise this corona depend on relative concentration of protein species present in the exposed fluid and a range of different parameters describing the nature of the nanoparticles including material, size [57], surface curvature [58], and surface chemistry.

The significance of this paradigm is that the biological machinery, *i.e.* the cell, is not able to 'see' a bare particle surface, but instead interact with an arrangement of proteins and biomolecules present on the particle's surface with which it can interact [14]. The biomolecular corona therefore plays a key role in the interaction between nanoparticles and biological systems, impacting on how these particles interact with biological systems on a cellular and molecular level [59].
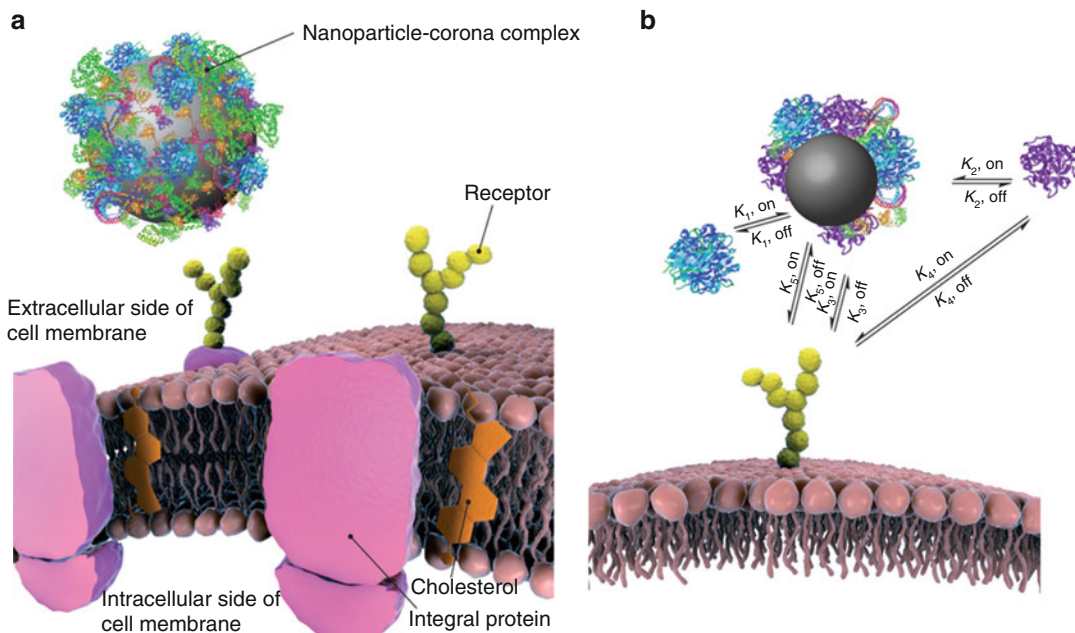
Fig. 8.3 Schematic showing the nanoparticle biomolecular corona and potential biological interaction (*left*); Exchange processes that occurs between the proteins on the nanoparticle surface, the proteins in solution and the cell membrane (*right*) (Reproduced with permission from Monopoli et al. [13])

Since the conceptualisation of the biomolecular corona a great deal of work has been performed to understand how it forms, evolves and subsequently impacts nanobiotechnology and nanomedicine [13]. Within the biomolecule corona, proteins and other biological species interact with the surface of nanoparticles with different affinity, where species with low affinity are dynamically exchanged from the surface this is referred to as the "dynamic corona". Species with higher affinities reside for longer times on the nanoparticle surface, this "hard corona" is typically stable for at least several hours (Fig. 8.3) [60, 61]. This means that due to the long term stability of some proteins, nanoparticles can retain a 'protein memory' of locations where they have been, and potentially transport and drag some biomolecules into compartments normally inaccessible.

The dynamic corona denotes proteins and biomolecules which are loosely associated with the nanoparticle. This layer is under constant renovation, where proteins and other biomolecules are free to exchange between the nanoparticle surface and the rest of the free biomolecules available in solution. As a result, the dynamic corona is not stable for long periods of time, and can be easily disturbed by dilution or removal of the biological fluid. This makes the dynamic corona experimentally difficult to study.

8.4.2 Impact of the Biomolecular Corona on the Dispersion and Biological Effects of Nanoparticles

The adsorption of biologically relevant molecules on the surface of nanoparticles may completely change the nature of the nanoparticles' surface properties. Not only does it increase the overall size of the particle, but it also alters the surface chemistry of the particle. In essence, this means that cells almost never see a naked nanoparticle surface, in fact cells exposed to nanoparticles in serum-free conditions, for example, with no proteins present, exhibit cell death as the high surface energy of the nanoparticle is able to interact

with the cell membrane essentially by punching holes in it while impacting the cell integrity in an attempt to lower its surface energy [62, 63]. The presence of a biomolecular corona protects the cell from this damage which would not reflect a real biological situation.

8.4.3   Effects and Control of the Biomolecular Corona

In many cases, the biomolecular corona is considered a side effect, which must be avoided. This is because, by covering the surface with a biomolecular layer the intrinsic functions of the nanoparticles are often masked. This is particularly important for functionalised nanoparticles, *i.e.* nanoparticles designed to carry specific functional groups and/or payload that is relevant for drug delivery [2]. If a biomolecular corona is formed around functionalised particles, or it impacts the particle stability, functional groups present therein are covered by a layer of biomolecules from the media, rendering the particles invisible for subsequent biological interactions.

To avoid this, several attempts have been made to control the composition of the biomolecular corona. One approach involves surface modification of the nanoparticles in order to render them less favourable for proteins to bind. The most widely used methods involve utilising the antifouling properties of hydrophilic polymers, most commonly polyethylene glycol (PEG) [64]. Depending on the amount and length of the polymer grafted onto the particle surface it is possible to create different conformations of PEG, most notably brush conformation (close packed) and mushroom (more mobile) [65]. It should be noted that the presence of these polymers drastically reduces the association of proteins and other biomolecules however, it does not impede it completely [66].

PEGylated particles [67] have an important effect on the enhanced permeability and retention (EPR) effect. This EPR effect, discovered by Maeda et al., is mostly observed in cancerous or inflamed tissues [68].

In targeted drug delivery, the surface of nanoparticles is modified and functionalised in such a way to cause particles to target and/or enter preferentially specific biological regions and locally treat exclusively the affected areas. The most common targets in nanomedicine are cancerous cells, whose targeting favourably reduce side effects and increase the efficacy of cancer treatment. One of the approaches to facilitate targeted treatment involves grafting or modifying the surface of the nanoparticle with molecules or biological ligands for plasma membrane receptors that are overexpressed on cancer cells compared to the normal tissue. Examples of this approach could include growth factors or antibodies for members of the Epidermal Growth Factor receptor family (Her2) in breast cancer or Hepatocyte Growth Factor Receptor in liver cancer.

When these modified nanoparticles are introduced into biological fluids there is a potential for other proteins to associate with them. In fact it has been shown that the presence of serum proteins can reduce targeted nanoparticle specificity, rendering certain targeting approaches ineffective [36].

On the other hand, the arrangement and orientation of the biomolecules on the surface of a nanoparticle can be quite different to what is seen typically by biological systems. For example, the surface of nanoparticles can cause unfolding or denaturation of the proteins, exposing portions of the specific amino acid sequence presented in a way that does not occur naturally. One instance of this shows how PAA (polyacrylic acid) coated gold nanoparticles of diameters smaller than 20 nm are able to unfold the protein fibrinogen, exposing a specific epitope involved in the recruitment of macrophages. This process causes activation of Mac-1 receptors, resulting in cytokine release and inflammation [69].

The biomolecular corona has negative implications for some applications however, for many others it provides a useful function. In one case the adsorption of proteins and controlled agglomeration of gold nanorods was used to trap drugs in a protein-particle matrix. The release of the drug could be achieved by local heating of the

nanoparticles, taking advantage of specific plasmonic properties of these particles, which involves irradiation of the nanorods with an infrared laser [70].

8.5 Interaction of Functionalised Nanomaterials with Cell Organelles

The complex and dynamic relationship between surface properties of nanomaterials and their interactions with biomolecules has the potential to generate novel and unexpected impacts on biological systems, some of which could be further exploited for diagnostic and therapeutic purposes. A systematic approach has been employed to investigate how nanoparticles interact with cells *in vitro*, which are the modalities used to cross the plasma membrane and utilise cell specific pathways to reach subcellular organelles. These pathways differ between nanoparticles with different surface chemistry and functionalisations, and the biological outcomes also are influenced by the subcellular localisation and the surface properties of nanoparticles. The formation of a biomolecular corona could be exploited to allow for highly toxic nanoparticles, which in absence of a protein corona would cause non-regulated necrotic cell death, to be delivered inside the cell and only release their toxic potential in form of controlled apoptotic cell death once the protein corona is degraded by the lysosomal enzymes. On the contrary, finely tuned custom engineering of the nanoparticle surface components is highly desired, if intended to deliver the nanoparticles to a specific target organelle or sub-cellular compartment by escaping the endo-lysosomal pathway.

8.5.1 Receptor Mediated Endocytosis Leading to Lysosomal Accumulation of Nanoparticles

It has been widely recognised that mammalian cells in culture can internalise large amounts of the cell membrane in an invagination pit to engulf and accept nanoparticles through a process called endocytosis [21]. Endocytosis is an umbrella term pertaining to clathrin-dependent and clathrin-independent receptor mediated endocytosis, pinocytosis and phagocytosis [71]. The best described nanoparticle-ligand-receptor mediated uptake is *via* a clathrin-dependent endocytosis mechanism by which a high density region of trans-membrane high affinity receptors bind to their complimentary ligand and form a invagination pit on the cell membrane surface using cytoplasmic membrane coating proteins called clathrin [72]. The newly formed clathrin coated vesicles, called early endosomes, and their contents are now completely engulfed inside the cell, and present in the cell's cytoplasm (Fig. 8.4). The nanoparticle containing endosome tends to follow the endo-lysosomal internalisation pathway, and further mature into acidic lysosomes, designed to degrade unwanted material for further use in protein synthesis, using lysosomal enzymes called cathepsins (Fig. 8.5). It has been suggested that lysosomes are the 'grave yard' of nanoparticles, as cells rarely show nanoparticle exocytosis or nanoparticle recycling back to the cell surface, which is common in the case of protein receptor recycling processes post endocytosis [73]. In rare cases, nanoparticles were shown to escape the lysosomal pathway and access recycling pathways of the endocytotic process [74]. Additionally, it has also been suggested that some nanoparticles irrespective of physical dimensions, shape and surface modifications can avoid this fate and be stored in non-lysosomal organelles [75].

8.5.2 Lysosomal Rupture as a Consequence of Nanoparticle Surface Chemistry

Nanoparticles, irrespective of specific or nonspecific uptake tend to accumulate in lysosomal compartments after navigating the endo-lysosomal pathways. However, it has been demonstrated that cationic nanoparticles can cause lysosomes to swell and eventually rupture following uptake [39]. It is believed that positively
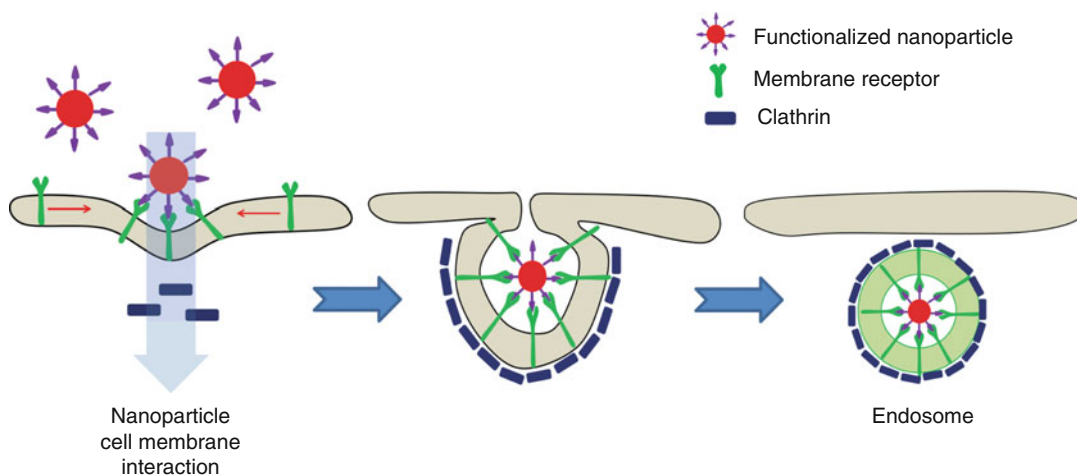
Fig. 8.4 Functionalised nanoparticles enter cells *via* specific nanoparticle-cell membrane interactions. This process is initiated by nanoparticles adhering specifically to the membrane receptors, forming a nanoparticle invagination pit and becoming internalised forming a clathrin-mediated endosome
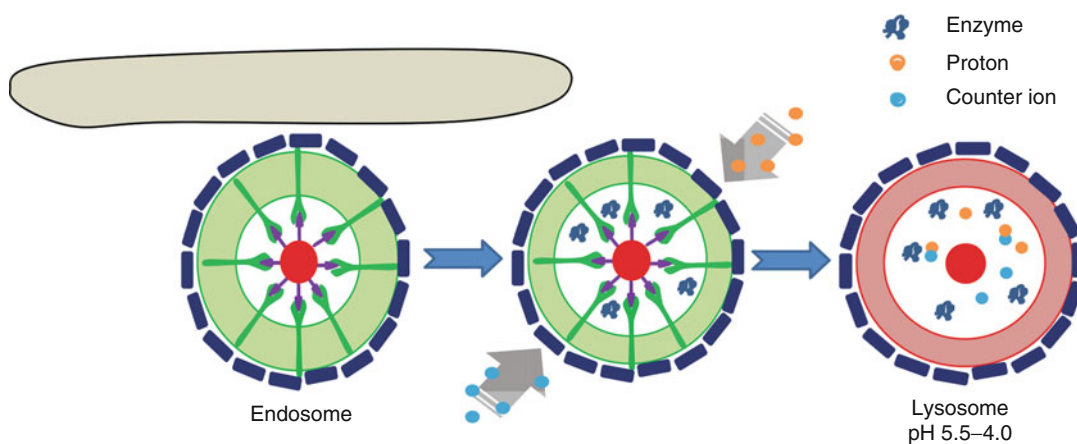

Fig. 8.5 During lysosomal degradation of unwanted material, lysosomes create the acidic environment necessary for enzymatic activity *via* pumping protons across their membrane using proton pumps. Additionally, chloride counter ions accompany each proton *via* chloride ion channels

charged amine groups on the surface of polystyrene nanoparticles are involved in this event. The swelling and rupture of lysosomes was shown by labelling the biomolecular corona on the surface of the cationic particles [76]. The fluorescently labelled corona was monitored in its evolution during uptake of nanoparticles and was observed to be colocalised with the nanoparticles once they reached the lysosomes. Over time, the intensity of the labelled corona decreased, consistently with observed increased cathepsin activity, suggesting that the lysosomal enzymes began to degrade the bio-molecular corona exposing the amino groups on the particle's surface.

This implies that highly positive polystyrene particles can enter cells by using the strongly bound protein corona biomolecules and can gain access to the lysosomal pathway, at which point the lysosomal enzymes degrade the bio-molecular protective layer uncovering the amino groups on the particle surface. The protonated amino groups on the surface of the nanoparticles, once exposed, result in lysosomal

compartment rupture which releases enzymes and other lysosomal contents in the cytoplasm, causing cell death by apoptosis [39, 77, 78].

8.5.3 Nanoparticle Load Dilution Due to Cell Division

Recent studies have investigated the relationships between nanoparticle internalisation and load volume with the different phases of the cell cycle [73]. The cell cycle consists of four consecutive phases, G1, S, G2 and M, each potentially contributing differently to nanoparticle uptake and carrying load. In the phase subsequent to cell division, known as G1 phase, cells have a high metabolic rate due to demand for structural proteins post mitosis. The G1 phase is followed by the S phase, where DNA synthesis occurs in order to replicate existing DNA previous to mitosis. The G2 phase is characterised by intense protein synthesis to allow the cell to prepare for mitosis or cell division and is characterised by high metabolic rate. In the final phase, the M phase, the cell divides into two daughter cells. Using fluorescently labelled carboxy-functionalised polystyrene nanoparticles, it was demonstrated that cells that had just performed mitosis had the lowest nanoparticle load, followed by cells in S phase and finally the cell population with the largest load of nanoparticles was in G2/M phase. The cell cycle phases have different duration, revealing that the uptake of nanoparticles is not influenced or affected by specific phases of the cell division. Furthermore, because exocytosis of carboxy-functionalised polystyrene nanoparticles in A549 cells was shown to be negligible, it was concluded that when the cell performs mitosis, the load of nanoparticles was divided between the newly formed daughter cells [73].

8.5.4 Organelle Targeting by Engineered Nanoparticles

One of the main goals when designing nanoparticles for drug delivery and therapeutic applications is the targeting of specific intracellular organelles. We have described so far how non-functionalised nanoparticles mainly follow the endocytotic cell uptake pathway and accumulate in the lysosomes, which may be a viable approach if the intention is to cause apoptosis in cells. However, this route of internalisation is not effective in the attempts to deliver a specific payload e.g. blocking peptides or siRNA directly to the cytoplasm or the nucleus. In order to maximise this effect, a targeting system needs to be tailored in order to deliver the nanoparticle to the desired sub-cellular compartment.

Targeting approaches are available to deliver nanoparticles to specific organelles by using functional ligands located on the nanoparticle surface, leading to delivery of the particles to a specific location. Current obstacles with utilising the lysosomal pathway for drug delivery reside on the fact that drugs entering the cell *via* the endo-lysosomal pathway remain trapped in lysosomal compartments and are degraded resulting in a fraction of the intended drug reaching the cells cytoplasm [79]. This lysosomal degradation renders drugs that show promising results *in vitro* to have poor bioavailability *in vivo*. It is now conceivable to perform drug delivery to specific organelles, enhancing the drug load delivery to the location of interest by potentially bypassing the lysosomal degradation pathway which nanoparticles tend to utilities as their main method of entry. Partially, this can be achieved by some alternative methods, e.g. electroporation, microinjection, laser irradiation, lysosomal rupture post uptake. The main target of gene therapy approaches is the cell nucleus, the organelle that stores and ensures correct transcription and replication of the genetic information.

The cell nucleus is surrounded by a membrane with different composition from the plasma membrane, *i.e.* the nuclear membrane contains pores of few nanometre in size that are utilised for the protein signalling involved in regulations of all the cellular processes. Additionally, the nuclear membrane only disassembles during the mitotic phase of the cell division. All these factors contribute to limited access of nanoparticles to the nucleus and therefore additional efforts are

required to direct the nano-vehicles to the cell nuclei.

One of the promising approaches utilises anticancer ligands targeting proteins such as nucleolin [80]. Nucleolin is a nuclear phosphoprotein that is abundant in the nucleus of healthy cells but is overexpressed and translocated to the plasma membrane in metastatic cells. By targeting the overexpressed nucleolin protein on the cell membrane, nanoparticles can be trafficked directly to the nucleus. Aptamers containing a peptide sequence specific to bind nucleolin were grafted onto the surface of gold nanostars and successfully shuttled directly to the cell nucleus avoiding the cells lysosomal degradation pathways. This pathway has potential to be used in drug delivery and gene therapy approaches by utilising nanoparticle's ability to transport high drug loads to the nucleus.

While nanoparticles can not directly be used in many cases to target the nucleus, they have a great potential for targeting of cancer cells. Nanoparticle can carry the anticancer drugs and high loads of pro-apoptotic drugs in order to target the mitochondria and deliver the drugs specifically to the site of activation, *i.e.* mitochondrial membrane. Polymeric particles with various surface modification have been shown to evade the endosomal compartment vesicles soon after invagination of the particle at the cell membrane, long before the vesicle has matured into a lysosome [81]. This example of endosomal escape enables the nanoparticle delivery of the drugs to the cytoplasm, while preventing the degradation in the acidic lysosome. A high dose of a pro-apoptotic drug released in the cytoplasm is capable of causing assembly of pro-apoptotic Bcl-2 proteins, formation of Permeability Transition Pores on the mitochondrial membrane and result in the release of cytochrome C, which activates the downstream caspase proteolytic cascade and leads to execution of apoptotic cell death [82].

Using the high dose bearing capabilities of nanoparticles to deliver drugs to specific tissues or cell compartments is vastly increasing the drug efficiency. Current drug delivery systems also rely on diffusion to deliver drugs into cells. It is important to note that these current systems do not allow the delivery of the intended drug in a targeted manner, causing side effects to the patient, in a lot of cases severe, resulting from healthy organs being exposed to the drug. Moreover, once the drug has diffused into cells, it may be metabolised or actively pumped out of the cell before it can exert its activity.

8.6 Intracellular Fate of Nanoparticles

Despite advancements in nanoscience, relatively little is known about the intracellular fate and function of nanoparticles post uptake. In general, the fate of any particulate matter taken up by a cell is the endo-lysosomal system, a number of vesicular bodies the content of which is physically and chemically isolated from the remainder of the cytoplasm, where it is either digested enzymatically or eventually removed from the cell by exocytosis [83].

Nanoparticle fate is related in some cases with the kinetics of nanoparticle–protein association and dissociation that has important roles in determining the particle's interactions with biological surfaces and in particular with the receptors. The main obstacle to be overcome in order to fully realise the potential of any of the exciting applications of nanoparticles in nanomedicine is that particles taken up by a cell *via* endocytosis usually remain confined to the endocytic vesicles and are thus not available to report on or even participate in metabolic events that take place outside this confinement. This imposes severe limitations to the usefulness of nanoparticles as intracellular agents and probes.

Advancement of bionanotechnology implies challenging this internalisation pathway in order to achieve the uptake routes that circumvent endocytotic mechanisms *via* the so-called direct uptake. Some reports on the attempt of direct uptake include the delivery of nanoparticles directly to the cytoplasm. The most effective of these is microinjection [84] where the particles are directly injected mechanically into individual cells. Other methods are either based on temporarily debilitating the cell membrane, e.g. by

application of electric fields (electroporation) [85], or on rapid mechanical expansion of the cells that leads to uptake of particles adsorbed to the outer cell membrane (osmotic shock treatment) [86]. Naturally, these approaches are limited to research applications *in vitro* and thus not suitable for upscaling to use in tissues or entire organisms *in vivo*.

To date, the most effective strategies in avoiding endocytosis include the modification of nanoparticle surface chemistry. Recent reports show how modification of the particle surface and specific surface chemistry design may play a role in circumventing endocytotic routes. This includes the use of cell penetrating peptides (CPPs) and specific peptides with nuclear localisation sequences (NLSs) to guide particles in the cell interior that may end up in diverse organelles, including the cell nuclei [87]. There are also other functional moieties or enzymes that may facilitate direct transfer of the cell membrane, or specific structures of the ligand shell as suggested by Stellacci and co-workers [88].

Other ways rely on the typical endocytotic uptake with subsequent release of the particles from the endosome into the cytoplasm. While this may also be possible by combinations of CPPs that lead to the disruption of the endosome [87] it can also be done by exploiting externally triggered photochemical or photothermal effects caused by laser irradiation that can be used to perforate the endosomal membrane, in particular, if the respective vesicle contains metal nanoparticles [89]. It was shown that laser-activated gold nanoparticles can kill a cell even when the laser energy is insufficient to trigger an increase in temperature causing the hyperthermia effects [90]. This photothermal therapy approach does not cause any thermal effects, but the photoemission of electrons from the gold generates damage inducing free radicals. Electron microscopy studies showed that the subcellular damage inflicted by the laser, following endocytotic uptake, released the particles from the endocytotic vesicles to the cytoplasm *via* specific endosomal damage; in particular, dissolution of the membrane of endosomes filled with fewer particles was observed while endosomes filled with more particles remained intact or suffered only minor damage. Another effect observed was the escape of nanoparticles into the cytoplasm after surgical rupture of the endosomal membrane.

Cell-penetrating peptides (CPPs) are a class of peptides capable of crossing the cell membrane and are widely used to transport cargo into cells. Importantly, depending on their particular amino acid sequence, they are capable of reaching different cell organelles in the cytoplasm, such as mitochondria and cell nuclei. Gold nanoparticles labelled with CPPs have the ability to cross the cell membrane, and can be found initially in the cytoplasm, but are then concentrated into vesicular structures [51]. Moreover, evidence was observed of intracellular membrane penetration occurring over time. It was found that the TAT peptide, originally extracted from the HIV virus, was best able to facilitate uptake of gold nanoparticles and subsequent particle roaming. In particular, after a 2 h incubation, nanoparticles were found dispersed in the cytoplasm. After 10 h, aggregation was observed, with evidence of membrane rupture occurring, presumably as part of the translocation process. After 24 h, very dense assemblies were observed, leading to exocytosis of the particles. Interestingly, nanoparticles were observed initially in the mitochondria and nucleus, but no particles were observed after 24 h, even after the cells were incubated with fresh particles. This behaviour could suggest that the cells are adapting to the presence of the nanomaterials and developing strategies to protect crucial regions from these particles.

Direct uptake, if substantiated, may become relevant to drug delivery, intracellular probes, some viral infections, transfection, protein trafficking and to the manifestation of the potential toxicity of engineered nanoparticulate objects. The latter, in particular, is very topical since the current implementation of nanoparticles in a broad range of applied technologies is expected to cause a significant increase in the exposure of humans and the environment to such materials.

8.7 Nanoparticles as Dose Enhancers in Radiotherapy

As outlined in Sect. 8.6 generally nanoparticles are taken up by cells *via* endocytosis. Broader application of nanotechnology in medicine strictly depends on the progress of the field of research dealing with the design of multimodal nanoparticles that can fulfil different tasks and in some cases overcome formation of the biomolecular corona.

One promising route of application of nanoparticles in radiotherapy cancer treatment is the novel use of gold nanoparticles as dose enhancers in radiation therapy. Radiotherapy is a widely utilised effective therapeutic tool in the treatment of forms of cancer refractive to chemotherapy.

In general, radiotherapy seeks to achieve local tumour control by delivering doses high enough to effectively kill all of the target cells in a tumour mass, preventing progression or recurrence. Typically, this involves the use of doses on the order of 50–100 Gy, depending on the tumour location. Moreover, this approach is aided by differences in the biology of healthy and cancerous cells. Cancerous cells are highly proliferative by their nature, dividing rapidly and often with lack of control. Thus they are genetically less stable, as they have less time to repair induced damage before their division, and tend to have less effective cell cycle regulation when compared to healthy cells. This makes cancerous cells more sensitive to the effects of ionising radiation.

However, the doses needed to effectively eradicate the tumour are still dramatically larger than those typically encountered from background radiation. Moreover, the radiation must be delivered with great care in order to balance the benefits of killing cancerous cells with the potential toxicity in the surrounding healthy ones. Several techniques are used to maximise the therapeutic benefit of radiation therapy. This includes fractionation and spatial conformation of radiation. To improve this treatment, modern radiation therapy is delivered using a diverse sophisticated techniques, e.g. 3D Conformal Radiotherapy (3DCRT), Intensity Modulated Radiotherapy (IMRT) and Volumetric Modulated Arc Therapy (VMAT) which are able to spare the healthy tissue by delivering multiple fields of radiation to the patient from different directions which only overlap within the target volume, while delivering lower doses to healthy tissue and only delivering full doses to the tumour volume. Despite the advancement of these techniques, toxicity of the healthy tissue remains a significant limiting factor for delivery of radiotherapy, due to the difficulties associated with delivering the dose solely to the target volume.

To address this problem and advance the radiotherapy cancer treatment, the use of heavy charged particle therapies have been developed involving beams of protons or heavy ions. In this way most of the energy of the particles is deposited at a characteristic depth, which can be tuned in order to target the tumour mass more precisely, reducing the dose to the healthy tissues.

8.7.1 Gold Nanoparticle Radiosensitisation

Development of improved modalities of radiation therapy involves the idea of using a small amount of high atomic number (Z) material preferentially localised within tumours in conjunction with carefully tailored x-ray radiation. The enhanced absorption of the high atomic number material results in increased dose delivery localised at the tumour mass alone.

Early studies of gold nanoparticle radiosensitisation were carried out using a mouse model, where mice with implanted tumours were treated with radiation with and without gold particles as contrast agents to enhance X ray imaging and radiotherapy The experiments showed significant improvements in overall survival, with over 70 % of mice being fully recovered from their tumours after a combination treatment of gold nanoparticles and radiotherapy. This research demonstrated a clear potential for the application of gold nanoparticles as a radio-sensitiser [91]. When using gold nanoparticles as radiosensitizers, it is important to keep in mind the amount of gold required to yield significant
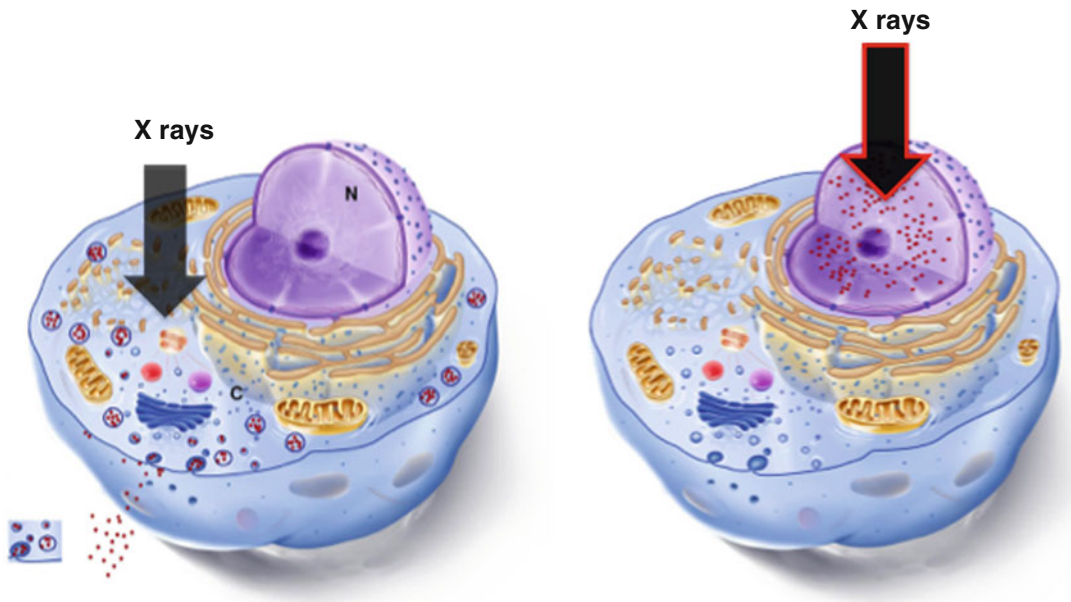
Fig. 8.6 X-ray dose enhancement of intracellular gold nanoparticles. Maximised effects are observed when gold nanoparticles are located in close proximity (*left*) of the cell nucleus or in the cell nuclei (*right*)

sensitisation, and the energy dependence of this sensitisation.

Another important aspect for this therapy application to work efficiently is that the particles designed for this application need to be of very small size (below 15 nm) and need to be targeted to the cells' nuclei or in their close proximity (Fig. 8.6). When gold nanoparticles interact with radiation, they compress the distance over which the dose is deposited in the neighbouring biological environment from centimeters to 10s of nanometers [6]. Effectively they act to replace a single long-range photon with several shorter-range electrons. Associated with this process is a massive increase in the local dose (e.g. from a few Gy to 100,000 Gy) [7].

Since most cancer patients, particularly in the case of glioblastoma, die within 2 years after diagnosis, novel therapeutic strategies for the treatment of therapy-refractory astrocytomas are desperately needed. The response to radiation is highly non-linear, therefore the local dose escalation produces a large enhancement to the cell killing in the case of cells that have taken up nanoparticles. The enhancement manifests itself as an increase in the relative biological effectiveness (RBE) of radiation and is underpinned by the mechanism which increases the RBE in ion beam therapy [92]. The means of targeting proposed by use of gold nanoparticles is thus different from that in ion beam therapy, *i.e.* drug delivery approaches can be used alongside the traditional means of targeting in radiotherapy through the use of multiple collimated radiation fields. Compared to common mechanisms of drug action, in this model, toxicity is less pronounced, *i.e.* the nanoparticle remains inert until triggered by the radiation. This approach offers the benefits of ion beam therapy, associated with the advantages of reduced cost and direct compatibility with many existing radiotherapy centres.

Thus, in combination with ionising radiation, gold nanoparticles offer great potential for therapeutic benefit in treatments of cancer.

Conclusions

Nanotechnology holds great potential in many different applications – ranging from industrial devices, sensor and microchip technology, consumer products, food additives and food packaging and biomedical

devices, diagnostics and therapeutics. The appropriate design and engineering of particle surface functionalities is the key to controlling the cellular and sub-cellular transport of nanoparticles as well as their biodistribution.

Understanding how nanoparticles interact with (complex) biological systems is paramount to ensure their safe use associated with the environment and human health. Moreover, for biomedical applications, it is necessary to understand the particle interactions with the biological machinery in order to optimise their design and efficacy.

The interactions that result from nanomaterials contacting biological matrices and living organisms are governed by complex and dynamic physical, chemical, biochemical and molecular processes. By investigating the interactions of nanoparticles with biological fluids we gain important information that are useful in further understanding of the even more complex inter-relationships with simple biological systems e.g. cells cultured *in vitro*. These findings are the foundation to study of nanoparticle interactions with more complex systems, such as tissue or animal models, adding the complex relationships between cells within a tissue, among tissues in the same organ, and among different organs in the organism, to the bio-nano interactions equation.

One of the ways forward certainly includes modelling and system biology approaches to predict bio-nano interactions and biological outcomes and develop a paradigm of nanoparticles "safer by design". By combining the knowledge on the molecular mechanisms responsible for many diseases, with the opportunities offered by the tuneability of the surface of nanomaterials and the knowledge on their interactions with target cells we are aiming to exploit the cell machinery to carry diagnostic, therapeutic or theranostic nanoparticles to the desired sub-cellular compartments and thus achieving successful targeting, maximised efficacy and minimal side effects for the future patient.

References

1. Willson R (2008) The use of gold nanoparticles in diagnostics and detection. Chem Soc Rev 37:2028–2045
2. Vigderman L, Zubarev ER (2013) Therapeutic platforms based on gold nanoparticles and their covalent conjugates with drug molecules. Adv Drug Deliv Rev 65:663–676
3. Sanhai WR, Sakamoto JH, Canady R, Ferrari M (2008) Seven challenges for nanomedicine. Nat Nanotechnol 3:242–244
4. Valentini P, Pompa PP (2013) Gold nanoparticles for naked-eye DNA detection: smart designs for sensitive assays. RSC Adv 3:19181–19190
5. Ghosh P, Han G, De M, Kim CK, Rotello VM (2008) Gold nanoparticles in delivery applications. Adv Drug Deliv Rev 60:1307–1315
6. Butterworth KT, Mcmahon SJ, Currell FJ, Prise KM (2012) Physical basis and biological mechanisms of gold nanoparticle radiosensitization. Nanoscale 4:4830–4838
7. Mcmahon SJ, Hyland WB, Brun E, Butterworth KT, Coulter JA, Douki T, Hirst DG, Jain S, Kavanagh AP, Krpetic Z, Mendenhall MH, Muir MF, Prise KM, Requardt H, Sanche L, Schettino G, Currell FJ, Sicard-Roselli C (2011) Energy dependence of gold nanoparticle radiosensitization in plasmid DNA. J Phys Chem C 115:20160–20167
8. Laromaine A, Koh L, Murugesan M, Ulijn RV, Stevens MM (2007) Protease-triggered dispersion of nanoparticle assemblies. J Am Chem Soc 129:4156–4157
9. Lin M, Pei H, Yang F, Fan C, Zuo X (2013) Applications of gold nanoparticles in the detection and identification of infectious diseases and biothreats. Adv Mater 25:3490–3496
10. Kneipp J, Kneipp H, Mclaughlin M, Brown B, Kneipp K (2006) In vivo molecular probing of cellular compartments with gold nanoparticles and nanoaggregates. Nano Lett 6:2225–2231
11. Colvin VL (2003) The potential environmental impact of engineered nanomaterials. Nat Biotechnol 21:1166–1170
12. Donaldson K, Stone V, Tran CL, Kreyling W, Borm PJ (2004) Nanotoxicology. Occup Environ Med 61:727–728

13. Monopoli MP, Aberg C, Salvati A, Dawson KA (2012) Biomolecular coronas provide the biological identity of nanosized materials. Nat Nanotechnol 7:779–786

14. Walczyk D, Bombelli FB, Monopoli MP, Lynch I, Dawson KA (2010) What the cell "sees" in bionanoscience. J Am Chem Soc 132:5761–5768

15. Gratton SEA, Ropp PA, Pohlhaus PD, Luft JC, Madden VJ, Napier ME, Desimone JM (2008) The effect of particle design on cellular internalization pathways. Proc Natl Acad Sci U S A 105:11613–11618

16. Roebben G, Ramirez-Garcia S, Hackley VA, Hackley VA, Roesslein M, Klaessig F, Kestens V, Lynch I, Garner CM, RAWLE A, Elder A, Colvin VL, Kreyling W, Krug HF, Lewicka ZA, Mcneil S, Nel A, Patri A, Wick P, Wiesner M, Xia T, Oberdorster G, Dawson KA (2011) Interlaboratory comparison of size and surface charge measurements on nanoparticles prior to biological impact assessment. J Nanoparticle Res 13:2675–2687

17. Cedervall T, Lynch I, Lindman S, Berggard T, THULIN E, Nilsson H, Dawson KA, Linse S (2007) Understanding the nanoparticle-protein corona using methods to quantify exchange rates and affinities of proteins for nanoparticles. Proc Natl Acad Sci USA 104:2050–2055

18. Lundqvist M, Stigler J, Elia G, Lynch I, Cedervall T, Dawson KA (2008) Nanoparticle size and surface properties determine the protein corona with possible implications for biological impacts. Proc Natl Acad Sci USA 105:14265–14270

19. Lynch I, Salvati A, Dawson KA (2009) Protein-nanoparticle interactions what does the cell see? Nat Nanotechnol 4:546–547

20. Dagastine RR, Manica R, Carnie SL, CHAN DYC, Stevens GW, Grieser F (2006) Dynamic forces between two deformable oil droplets in water. Science 313:210–213

21. Conner SD, Schmid SL (2003) Regulated portals of entry into the cell. Nature 422:37–44

22. Van Meer G, Voelker DR, Feigenson GW (2008) Membrane lipids: where they are and how they behave. Nat Rev Mol Cell Biol 9:112–124

23. Ikonen E (2008) Cellular cholesterol trafficking and compartmentalization. Nat Rev Mol Cell Biol 9:125–138

24. Bethani I, Skanland SS, Dikic I, Acker-Palmer A (2010) Spatial organization of transmembrane receptor signalling. EMBO J 29:2677–2688

25. Mcmahon HT, Boucrot E (2011) Molecular mechanism and physiological functions of clathrin-mediated endocytosis. Nat Rev Mol Cell Biol 12:517–533

26. Feick JD, Chukwumah N, Noel AE, Velegol D (2004) Altering surface charge nonuniformity on individual colloidal particles. Langmuir 20:3090–3095

27. Cioran AM, Musteti AD, Teixidor F, Krpetic Z, Prior IA, He Q, Kiely CJ, Brust M, Vinas C (2012) Mercaptocarborane-capped gold nanoparticles: electron pools and ion traps with switchable hydrophilicity. J Am Chem Soc 134:212–221

28. Lesniak A, Salvati A, Santos-Martinez MJ, Radomski MW, Dawson KA, Aberg C (2013) Nanoparticle adhesion to the cell membrane and its effect on

29. Varela JA, Bexiga MG, ABERG C, Simpson JC, Dawson KA (2012) Quantifying size-dependent interactions between fluorescently labeled polystyrene nanoparticles and mammalian cells. J Nanobiotechnol 10

30. Hillaireau H, Couvreur P (2009) Nanocarriers' entry into the cell: relevance to drug delivery. Cell Mol Life Sci 66:2873–2896

31. Sahay G, Alakhova DY, Kabanov AV (2010) Endocytosis of nanomedicines. J Control Release 145:182–195

32. Nel AE, Madler L, Velegol D, Xia T, Hoek EM, Somasundaran P, Klaessig F, Castranova V, Thompson M (2009) Understanding biophysicochemical interactions at the nano-bio interface. Nat Mater 8:543–557

33. Gao H, Shi W, Freund LB (2005) Mechanics of receptor-mediated endocytosis. Proc Natl Acad Sci U S A 102:9469–9474

34. Chen HM, Langer R, Edwards DA (1997) A film tension theory of phagocytosis. J Colloid Interface Sci 190:118–133

35. Rejman J, Oberle V, Zuhorn IS, Hoekstra D (2004) Size-dependent internalization of particles via the pathways of clathrin- and caveolae-mediated endocytosis. Biochem J 377:159–169

36. Salvati A, Pitek AS, Monopoli MP, Prapainop K, Bombelli FB, Hristov DR, Kelly PM, Aberg C, Mahon E, Dawson KA (2013) Transferrin-functionalized nanoparticles lose their targeting capabilities when a biomolecule corona adsorbs on the surface. Nat Nanotechnol 8:137–143

37. Yue ZG, Wei W, Lv PP, Yue H, Wang LY, Su ZG, Ma GH (2011) Surface charge affects cellular uptake and intracellular trafficking of chitosan-based nanoparticles. Biomacromolecules 12:2440–2446

38. Saha K, Kim ST, Yan B, Miranda OR, Alfonso FS, Shlosman D, Rotello VM (2013) Surface functionality of nanoparticles determines cellular uptake mechanisms in mammalian cells. Small 9:300–305

39. Xia T, Kovochich M, Liong M, Zink JI, Nel AE (2008) Cationic polystyrene nanosphere toxicity depends on cell-specific endocytic and mitochondrial injury pathways. ACS Nano 2:85–96

40. Sperling RA, Parak WJ (2010) Surface modification, functionalization and bioconjugation of colloidal inorganic nanoparticles. Philos Transact A Math Phys Eng Sci 368:1333–1383

41. Aaseth J, Haugen M, Forre O (1998) Rheumatoid arthritis and metal compounds–perspectives on the role of oxygen radical detoxification. Analyst 123:3–6

42. Duchesne L, gentili D, Comes-Franchini M, Fernig DG (2008) Robust ligand shells for biological applications of gold nanoparticles. Langmuir 24:13572–13580

43. Kanaras A G, Kamounah FS, Schaumburg K, Kiely CJ, Brust M (2002) Thioalkylated tetraethylene glycol: a new ligand for water soluble monolayer protected gold clusters. Chem Commun 2294–2295

44. Levy R, Thanh NTK, Doty RC, Hussain I, Nichols RJ, Schiffrin DJ, Brust M, Fernig DG (2004) Rational and combinatorial design of peptide capping ligands for gold nanoparticles. J Am Chem Soc 126: 10076–10084

45. Strong L, Whitesides GM (1988) Structures of self-assembled monolayer films of organosulfur compounds adsorbed on gold single crystals: electron diffraction studies. Langmuir 4:546–558

46. Templeton AC, Wuelfing WP, Murray RW (2000) Monolayer-protected cluster molecules. Acc Chem Res 33:27–36

47. Wilson R (2003) Haptenylated mercaptodextran-coated gold nanoparticles for biomolecular assays. Cheml Commun 1:108–109

48. Krpetic Z, Guerrini L, Larmour IA, Reglinski J, Faulds K, Graham D (2012) Importance of nanoparticle size in colorimetric and SERS-based multimodal trace detection of Ni(II) ions with functional gold nanoparticles. Small 8:707–714

49. Krpetic Z, Singh I, Su W, Guerrini L, Faulds K, Burley GA, Graham D (2012) Directed assembly of DNA-functionalized gold nanoparticles using pyrrole-imidazole polyamides. J Am Chem Soc 134: 8356–8359

50. Doty RC, Tshikhudo TR, Brust M, Fernig DG (2005) Extremely stable water-soluble Ag nanoparticles. Chem Mater 17:4630–4635

51. Krpetic Z, Saleemi S, Prior IA, See V, Qureshi R, Brust M (2011) Negotiation of intracellular membrane barriers by TAT-modified gold nanoparticles. ACS Nano 5:5195–5201

52. Levy R, Wang ZX, Duchesne L, Doty RC, Cooper AI, Brust M, Fernig DG (2006) A generic approach to monofunctionalized protein-like gold nanoparticles based on immobilized metal ion affinity chromatography. Chembiochem 7:592–594

53. Levy R (2006) Peptide-capped gold nanoparticles: towards artificial proteins. Chembiochem 7: 1141–1145

54. Bastús NG, Comenge J, Puntes V (2011) Kinetically controlled seeded growth synthesis of citrate-stabilized gold nanoparticles of up to 200 nm: size focusing versus Ostwald ripening. Langmuir 27:11098–11105

55. Grzelczak M, Perez-Juste J, Mulvaney P, Liz-Marzan LM (2008) Shape control in gold nanoparticle synthesis. Chem Soc Rev 37:1783–1791

56. Anderson NL, Anderson NG (2002) The human plasma proteome: history, character, and diagnostic prospects. Mol Cell Proteomics 1:845–867

57. Tenzer S, Docter D, Rosfa S, Wlodarski A, Kuharev J, Rekik A, Knauer SK, Bantz C, Nawroth T, Bier C, Sirirattanapan J, Mann W, Treuel L, Zellner R, Maskos M, Schild H, Stauber RH (2011) Nanoparticle size is a critical physicochemical determinant of the human blood plasma corona: a comprehensive quantitative proteomic analysis. ACS Nano 5:7155–7167

58. Roach P, Farrar D, Perry CC (2006) Surface tailoring for controlled protein adsorption: effect of topography at the nanometer scale and chemistry. J Am Chem Soc 128:3939–3945

59. Dobrovolskaia MA, Patri AK, Zheng JW, Clogston JD, Ayub N, Aggarwal P, Neun BW, Hall JB, Mcneil SE (2009) Interaction of colloidal gold nanoparticles with human blood: effects on particle size and analysis of plasma protein binding profiles. Nanomedicine 5:106–117

60. Casals E, Pfaller T, Duschl A, Oostingh GJ, Puntes V (2010) Time evolution of the nanoparticle protein corona. ACS Nano 4:3623–3632

61. Dell'Orco D, Lundqvist M, Oslakovic C, Cedervall T, Linse S (2010) Modeling the time evolution of the nanoparticle-protein corona in a body fluid. PLoS One 5

62. Hu WB, Peng C, Lv M, Li XM, Zhang YJ, CHEN N, Fan CH, Huang Q (2011) Protein corona-mediated mitigation of cytotoxicity of graphene oxide. ACS Nano 5:3693–3700

63. Lesniak A, Fenaroli F, Monopoli MR, Aberg C, Dawson KA, Salvati A (2012) Effects of the presence or absence of a protein corona on silica nanoparticle uptake and impact on cells. ACS Nano 6:5845–5857

64. Otsuka H, Nagasaki Y, Kataoka K (2003) PEGylated nanoparticles for biological and pharmaceutical applications. Adv Drug Deliv Rev 55:403–419

65. Tokumitsu S, Liebich A, Herrwerth S, Eck W, Himmelhaus M, Grunze M (2002) Grafting of alkanethiol-terminated poly(ethylene glycol) on gold. Langmuir 18:8862–8870

66. Gref R, Luck M, Quellec P, Marchand M, Dellacherie E, Harnisch S, Blunk T, Muller RH (2000) 'Stealth' corona-core nanoparticles surface modified by polyethylene glycol (PEG): influences of the corona (PEG chain length and surface density) and of the core composition on phagocytic uptake and plasma protein adsorption. Colloids Surf B Biointerfaces 18:301–313

67. Knop K, Hoogenboom R, Fischer D, Schubert US (2010) Poly(ethylene glycol) in drug delivery: pros and cons as well as potential alternatives. Angew Chem Int Ed 49:6288–6308

68. Maeda H, Wua J, Sawaa T, Matsumurab Y, Horic K (2000) Tumor vascular permeability and the EPR effect in macromolecular therapeutics: a review. J Control Release 65:271–284

69. Deng ZJ, Liang MT, Monteiro M, Toth I, Minchin RF (2011) Nanoparticle-induced unfolding of fibrinogen promotes Mac-1 receptor activation and inflammation. Nat Nanotechnol 6:39–44

70. Kah JCY, Chen J, Zubieta A, Hamad-Schifferli K (2012) Exploiting the protein corona around gold nanorods for loading and triggered release. ACS Nano 6:6730–6740

71. Iversen TG, Skotland T, Sandvig K (2011) Endocytosis and intracellular transport of nanoparticles: present knowledge and need for future studies. Nano Today 6:176–185

72. Mayor S, Pagano RE (2007) Pathways of clathrin-independent endocytosis. Nat Rev Mol Cell Biol 8:603–612

73. Kim JA, Aberg C, Salvati A, Dawson KA (2012) Role of cell cycle on the cellular uptake and dilution of nanoparticles in a cell population. Nat Nanotechnol 7:62–68

74. Sandin P, Fitzpatrick LW, Simpson JC, Dawson KA (2012) High-speed imaging of Rab family small GTPases reveals rare events in nanoparticle trafficking in living cells. ACS Nano 6:1513–1521

75. Lai SK, Hida K, Man ST, Chen C, Machamer C, Schroer TA, Hanes J (2007) Privileged delivery of polymer nanoparticles to the perinuclear region of live cells via a non-clathrin, non-degradative pathway. Biomaterials 28:2876–2884

76. Wang F, Yu L, Monopoli MP, Sandin P, Mahon E, Salvati A, Dawson KA (2013) The biomolecular corona is retained during nanoparticle uptake and protects the cells from the damage induced by cationic nanoparticles until degraded in the lysosomes. Nanomedicine 9:1159–1168

77. Bexiga MG, Varela JA, Wang F, Fenaroli F, Salvati A, Lynch I, Simpson JC, Dawson KA (2011) Cationic nanoparticles induce caspase 3-, 7- and 9-mediated cytotoxicity in a human astrocytoma cell line. Nanotoxicology 5:557–567

78. Wang F, Bexiga MG, Anguissola S, Boya P, Simpson JC, Salvati A, Dawson KA (2013) Time resolved study of cell death mechanisms induced by amine-modified polystyrene nanoparticles. Nanoscale 5:10868–10876

79. Torchilin VP (2006) Recent approaches to intracellular delivery of drugs and DNA and organelle targeting. Annu Rev Biomed Eng 8:343–375

80. Dam DHM, Lee JH, Sisco PN, Co DT, Zhang M, Wasielewski MR, Odom TW (2012) Direct observation of nanoparticle-cancer cell nucleus interactions. ACS Nano 6:3318–3326

81. Marrache S, Dhar S (2012) Engineering of blended nanoparticle platform for delivery of mitochondria-acting therapeutics. Proc Natl Acad Sci USA 109:16288–16293

82. Kroemer G, Reed JC (2000) Mitochondrial control of cell death. Nat Med 6:513–519

83. Bartczak D, Nitti S, Millar TM, Kanaras AG (2012) Exocytosis of peptide functionalized gold nanoparticles in endothelial cells. Nanoscale 4:4470–4472

84. Zhang Y, Yu LC (2008) Single-cell microinjection technology in cell biology. Bioessays 30:606–610

85. Tsong TY (1991) Electroporation of cell-membranes. Biophys J 60:297–306

86. Lang KS, Lang PA, Bauer C, Duranton C, Wieder T, Huber SM, Lang F (2005) Mechanisms of suicidal erythrocyte death. Cell Physiol Biochem 15:195–202

87. Nativo P, Prior IA, Brust M (2008) Uptake and intracellular fate of surface-modified gold nanoparticles. ACS Nano 2:1639–1644

88. Jackson AM, Myerson JW, Stellacci F (2004) Spontaneous assembly of subnanometre-ordered domains in the ligand shell of monolayer-protected nanoparticles. Nat Mater 3:330–336

89. Javier AM, Del Pino P, Bedard MF, Skirtach AG, Sukhorukov GB, Plank C, Parak WJ (2008) Photoactivated release of cargo from the cavity of polyelectrolyte capsules to the cytosol of cells. Langmuir 24:12517–12520

90. Krpetic Z, Nativo P, See V, Prior IA, Brust M, Volk M (2010) Inflicting controlled nonthermal damage to subcellular structures by laser-activated gold nanoparticles. Nano Lett 10:4549–4554

91. Hainfeld JF, Slatkin DN, Smilowitz HM (2004) The use of gold nanoparticles to enhance radiotherapy in mice. Phys Med Biol 49:N309–N315

92. Mcmahon SJ, Hyland WB, Muir MF, Coulter JA, Jain S, Butterworth KT, Schettino G, Dickson GR, Hounsell AR, O'sullivan JM, Prise KM, Hirst DG, Currell FJ (2011) Biological consequences of nanoscale energy deposition near irradiated heavy atom nanoparticles. Sci Rep 1:18

Design, Synthesis, and Functionalization of Nanomaterials for Therapeutic Drug Delivery

Taraka Sai Pavan Grandhi and Kaushal Rege

Contents

T.S.P. Grandhi
Biomedical Engineering, School of Biological and Health Systems Engineering, Arizona State University, Tempe, AZ, USA

K. Rege (✉)
Biomedical Engineering, School of Biological and Health Systems Engineering, Tempe, AZ, USA

Chemical Engineering, School of Engineering of Matter, Transport and Energy, Arizona State University, Tempe, AZ 85287, USA
e-mail: kaushal.rege@asu.edu

Abstract

Nanomaterials have the potential to solve some of the toughest challenges facing modern medicine. Their unique optical, magnetic and chemical properties at the nanoscale make them different from their macroscale counterparts. Successful application of nanomaterials can revolutionize therapeutics, diagnostics and imaging in several biomedical applications. Self-assembled amphiphilic polymeric nanoparticles have been employed to carry poorly soluble chemotherapeutic drugs. Loading of anticancer chemotherapeutic drugs into self assembled polymeric nanoparticles have shown to increase their circulation time, tumor localization and therapeutic potential. This book chapter provides an introductory discussion to organic nanotechnologies for drug delivery. Promising advances in the field of nanomedicine will be discussed and an outlook to the future will be provided.

Keywords

Drug-delivery • Micelles • Liposomes • PLGA-nanoparticles • FDA • Multifunctional nanomedicine • Cancer

Abbreviations

mL   Milliliters
nm   Nanometer

NP   Nanoparticle
PEG   Poly (ethyleneglycol)
QD   Quantum Dots
µL   Microliters
µm   Micrometer

9.1   Introduction

Biological processes at molecular and nanoscale levels give rise to complex cellular and organ functions which constitute the life we see around us. Alteration in molecular and nanoscale-level processes often leads to disease. Molecular and nanoscale-level interactions play a central role in the activity of disease-causing agents including viruses or bacteria, mutated cells, and altered gene or amino acid sequences. For example, mutation of one 0.24 nm nucleotide in codon sequence G$\underline{A}$G to G$\underline{T}$G, can result in exchange of the resultant amino acid from glutamic acid to valine in the heamoglobin beta protein chain, causing sickle cell anaemia [1].

The National Nanotechnology Initiative (NNI), a U.S. Government research and development (R&D) initiative, defines nanotechnology as the science, engineering and technology conducted at the nanoscale, a scale from 1 to 100 nm (1 nm = 10^{-9} m) [2]. Engineering at the nanoscale is ~10,000 times smaller than what a human eye can see. Initial concepts of nanotechnology were first described in the visionary talk of Professor Richard Feynman entitled "There is plenty of Room at the Bottom" on December 29, 1959, in which he envisioned how scientists could manipulate matter at the molecular and atomic level one day [3]. The visionary talk came a decade before the term nanotechnology was coined by Professor Norio Taniguchi [2]. New developments are aimed at harnessing the powers of nanotechnology in therapeutic applications for betterment of the human condition [4].

9.1.1   Nanomaterial Properties

At the nanoscale, materials have multiple distinctive and rather unexpected properties when compared to observations at the macroscale [5].

Important material properties including color of the particles in dispersions [6], fluorescence [7], electrical conductivity [8], magnetic permeability [9], chemical reactivity [10], and melting point [11] are drastically different at the nanoscale. For example, gold nanoparticles absorb different wavelengths of light depending on their size and generate differently colored dispersions [6]. Nanoscale characteristics that give rise to such important material properties can be broadly divided into three groups (1) increase in surface area to volume ratio of these materials as they approach the nanoscale [12], (2) quantum confinement of electrons at the nanoscale, and (3) propensity of some molecules to self-assemble into different structures and shape, including emulsions, polymeric micelles and liposomes [13–16]. This book chapter focusses on the self-assembly property of polymeric nanomaterials, and describes the preparation, functionalization and delivery of self-assembled organic nanomaterials for therapeutic drug delivery. Information on inorganic nanomaterials for drug delivery can be found elsewhere [17, 18].

9.1.2   Nanomaterials in Therapeutics

Successful translation of new therapeutic drugs from the laboratory to the clinic faces daunting challenges including the need to target the disease and reduce any systemic side-effects, without compromising function and/or stability. Drugs injected intravenously are often eliminated by the liver, spleen and kidneys. Studies have shown that <5 % of the delivered chemotherapeutic drug reaches the tumor site when injected intravenously in tumor-bearing mice [19–21].

Nanomaterials have generated significant interest as possible solutions to some of these pressing challenges. Concepts from nanotechnology have been investigated for improving targeted drug delivery [22], enhancing the stability of poorly soluble drugs in the blood [22], *in vitro* antigen detection [23], highly sensitive diagnostics kits [24], enhanced contrast agents for biomedical imaging [25, 26], and dual delivery of contrast agents and therapeutic molecules [27]. One key goal of nanomaterial-based drug delivery

Table 9.1 Various nanoparticles currently used in nanomedicine

Nanosystem	Type	Application	Advantages	Disadvantages
Liposomes	Long circulating liposomes	Drug, gene and protein delivery	PEGylation improves circulation and half life in blood, ability to load high amounts of drug via gradient generation.	Larger size might inhibit deeper penetration into the tumors
	Immunoliposomes	Drug, gene and protein delivery	Improved targeting	
	Long circulating immunoliposomes	Drug, gene and protein delivery	Long circulation with improved targeting	
Micelles	PEGylated micelles (passive accumulation)	Drug/gene delivery	Long circulation of cargo and tumor accumulation. Deeper penetration of micelles below 30 nm possible in poorly vascularized tumors.	Targeted drug delivery
	Antibody grafted drug loaded micelles (active delivery)	Drug/gene delivery	Targeted drug delivery	Amount of drug loaded/micelle
PLGA nanoparticles	Drug loaded and PEGylated	Drug/gene delivery	Biocompatibility and biodegradability	
Multifunctional nanomedicine	Gold nanorods + drug loaded immunoliposomes	Cooperative and communicating nanomedicine	Synergistic response between gold nanorods and drug loaded immunoliposomes in tumor ablation	Limited tissue penetration of NIR light.

systems is to modulate the pharmacokinetic profile of therapeutic drugs so as to achieve targeted accumulation of the drug mainly in the diseased tissue. Nanomaterials have also been utilized in many emerging fields of medicine including tissue engineering [28, 29], regenerative medicine [30], and theranostics [31, 32]. Table 9.1 lists the advantages and disadvantages of different organic and inorganic nanoparticles currently in use for therapeutic drug delivery.

9.2 Self-Assembled Organic Nanoparticles for Drug Delivery

Organic nanomaterials broadly consist of liposomes, micelles, nanoemulsions, nanocombs, polymeric nanofibres and hydrogel nanoparticles (nanogels). Formation of organic nanoparticles depends on self-assembly of the constituent molecules in aqueous media; for example, formation of polymeric micelles [33], poly-ion micelles [34], nanoemulsions [35] is governed largely by the

hydrophobic effect, electrostatic attraction, and reduction in interfacial tension in surfactant stabilized water-in-oil (W/O) systems, respectively.

Loading of anticancer drugs into organic nanoparticles results in significant improvement of their *in vivo* activity [36]. Organic nanoparticles protect their drug cargo from the host reticulo-endothelial system (RES), which consists of macrophages and monocytes in liver, spleen and in the blood stream [37]. Their hydrophilic polyethylene glycol (PEG) shell acts as a non-adhesive barrier preventing adsorption of serum proteins such as opsonins [38]. Upon adsorption by serum proteins, nanoparticles can be removed from the blood stream [39]. Premature release of loaded drugs from nanoparticles has also been reported upon serum protein adsorption [40]. The PEG shell protects and inhibits this RES mediated removal of drug loaded nanoparticles.

Most solid tumors often contain leaky vasculature, and delivery of drugs using liposomes and micelles has been shown to increase their retention at the tumor site [41]. This retention has been arttributed to the enhanced permeation and retention
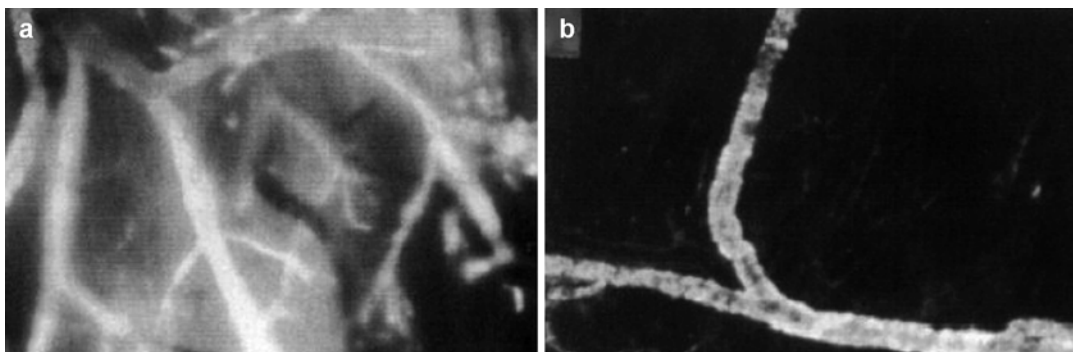
effect (EPR effect) [42]. Leaky vasculature and reduced lymphatic drainage frequently occurs due to rapid and random growth of solid tumors due to demands of high amounts of nutrients, metabolites and oxygen [43]. These leaky vasculature sites contain large gaps (>400 nm [44]) between endothelial cells lining blood vessels. These large gaps allow nanoparticles to escape the bloodstream and accumulate in the tumor tissue (Fig. 9.1) [45, 47]. Drugs loaded within organic nanoparticles demonstrate retarted renal clearance due to increase in the overall size and macromolecular weight of the delivered therapeutic formulation. Taken together, organic nanoparticles improve the half-life of hydrophobic chemotherapeutic drugs [41], which can lead to higher theeapeutic efficacies.

9.2.1 Liposomes

Liposomes are membrane-enclosed vesicles which contain aqueous core surrounded by bilayered lipid shells [48]. The lipid bilayer usually consists of amphiphilic phospholipids containing hydrophobic lipid tails attached to hydrophilic head groups. In aqueous solutions, these amphiphilic phospholipids self-assemble to form bilayered structures consisting of an aqueous core and a phospholipid shell. Phospholipid arrangement in these bilayer structures is similar to the lipid bilayer membrane surrounding mammalian cells. Liposomes can be classified based on

their size (nm) and the number of bilayered lipid shells surrounding the aqueous interior. Single Unilamellar Vesicles (SUVs) are small 25–50 nm vesicles containing an aqueous core surrounded by a single lipid bilayer shell, whereas Large Unilamellar Vesicles (LUVs) contain larger vesicles of size 100–1,000 nm [49] with a single lipid bilayer coat. Multilamellar vesicles (MLVs) consist of multiple concentric lipid bilayers (analogous to an onion) separated from each other by aqueous solution. The most commonly used phospholipids for liposomal formulation include phosphatidylcholine, phosphatidylenolamine and phosphatidylserine [50–52].

In aqueous solutions, single hydrocarbon chain amphiphiles (e.g. detergents) usually form micelles whereas double hydrocarbon chain amphiphiles form bilayers. The single hydrocarbon chains cannot stabilize the bilayer structure and hence produce micellar structure, whereas double hydrocarbon chain containing lipids can self-assemble to form stable bilayer structure in water. The choice of phospholipids can govern the fluidity of the resulting bilayer within the liposomes. Phospholipids with fully saturated hydrocarbon lipid chains such as distearolylphosphatidylcholine (DSPC) usually produce bilayers with high rigidity. Presence of unsaturation such as double bonds within the lipid hydrocarbon chains produces a kink in the structure of the bilayer, leading to an increase in overall fluidity of the liposome. Increased fluidity of liposomes

can modulate its transition temperature (T_c), which is the temperature required to induce physical change in the state of lipids from ordered gel to disordered state [53]. Presence of unsaturation can also reduce the transition temperature of the overall lipid bilayer, whereas addition of cholesterol is known to improve it [54, 55]. Thus, liposome fluidity can be controlled by the ratio of saturated: unsaturated lipids added to generate the liposome.

Although single phospholipid species can spontaneously form liposomes, several additional compounds are added to enhance the overall stability of liposomes. Single phospholipid liposomes have been shown to be unstable in the blood stream due to their interaction with high density lipoprotein [56]. Hence, various stabilizing agents are added in order to avoid disintegration of the liposomal structure during delivery through the blood stream. For example, cholesterol has been shown to greatly improve the liposome stability *in vitro* and *in vivo*. Kirby et al. [57] reported that the retention of fluorescent dye 6-carboxyfluorescein within neutral, negatively and positively charged SUVs composed of egg phosphatidylcholine, cholesterol and, when appropriate, phosphatidic acid (negative charge) or stearylamine (positive charge) was added as a function of the amount of cholesterol added. Cholesterol rich liposomal formulations (egg phosphatidylcholine/cholesterol, 7:7 molar ratio) remained stable in the blood for up to 400 min irrespective of the surface charge of liposomes whereas cholesterol-poor (egg phosphatidylcholine/cholesterol, 7:2 molar ratio) and cholesterol-free SUVs were lost in 2 min [57]. Cholesterol has also been shown to stabilize liposomes by preventing penetration of water into the bilayer structure [58, 59]. Other biomolecules such as carbohydrates have also been used to stabilize the phospholipid bilayers of the liposomes [60].

Due to their unique structure, liposomes can simultaneously load hydrophilic cargoes such as DNA/peptides/drugs in their aqueous core and lipophilic drugs in the lipid bilayer [61]. Liposomes have been used for delivery of multiple therapeutically important biomolecules such as genes [62, 63], proteins, peptides [64], fluorescent imaging agents [65], drugs [66], contrast agents for MRI [67] and quantum dots [68]. Chemotherapeutic drugs encapsulated within liposomes have longer circulation times in the blood, reduced systemic toxicity and enhanced delivery to the target site. In addition, polyethylene glycol (PEG) grafting on the bilayer of drug-loaded liposomes has shown to greatly extend its circulation times in the blood by preventing its removal by the reticuloendothelial system (RES) of the liver and spleen, resulting in 'stealth' liposomes [69]. Further, antibody grafting on liposomes ('immunoliposomes') have improved targeting potential to the desired diseased cells of interest [70]. The relatively large size of liposomes also allows their retention in solid tumors due to the EPR effect, thus improving the overall profile of drug delivered through the blood [71].

9.2.1.1 Preparation of Drug Loaded Liposomes for Delivery

Monodispersed, stable liposomal systems which can support high drug loading capacities are most desired for drug delivery. One method of liposomal preparation involves sonicating multilamellar vesicles (MLVs) in order to generate single unilamellar vesicles (SUVs). Hydrated solution of phospholipids containing multilamellar vesicles (MLVs) is sonicated using a bath or a probe sonicator to generate single unilamellar vesicles (SUVs). Although cheap and quick, this technique suffers from incomplete conversion of MLVs to SUVs, metal contaminants from the sonicator tip and possible degradation of the lipids. Another technique of generating monodispersed SUVs from multilamellar vesicles is by extrusion. Also called as French pressure cell press, it involves extrusion of a solution of multilamellar vesicles through a small orifice [72] to generate monodispersed SUVs. The resulting solution can be repeatedly passed through the orifice, if necessary. This technique, although laborious is very useful for handling sonication sensitive biomolecules such as proteins loading into liposomes.

Other methods of liposome preparation include ether vaporization method [73], thin film hydration method and ethanol injection method [74].

Ether vaporization method involves gradual injection of lipids dissolved in diethyl ether-methanol mixture into aqueous solution at high temperature or reduced pressure leading to formation of liposomes [73]. To generate liposomes using thin film hydration method, lipids are first solubilized in organic phase which is removed using a rotary evaporator. The resulting thin lipid film left behind, is hydrated with appropriate buffer to generate liposomes. Ethanol injection method involves rapid injection of lipid solution in ethanol into appropriate aqueous solution in order to obtain multilamellar vesicles [74]. The disadvantages of these systems include poor control over the size of liposomes formed and the need of an organic phase, which may not be suitable for all biomolecules.

Generation of large aqueous space within the liposome for LUVs (large unilamellar vesicles) preparation was first proposed by Szoka and Papahadjopoulos [75] in 1978 using reverse phase evaporation method. Large aqueous cavity could allow higher loading of desired cargo in the hydrophilic core. The method involves generation of reverse micelles using phospholipids surrounding an aqueous solution in an organic solvent. Gradual removal of organic solvent leads to conversion of inverted micelles to viscous gels. In the process, some of the inverted micelles break and contribute to the completion of the lipid bilayer forming large unilamellar vesicles. This technique was found to have very high cargo encapsulation efficiency (~65 %) [75] and reduced the exposure of biomolecules to the organic phase. These formulation techniques are often combined to achieve high loading of desired biomolecules into monodispersed liposomes.

Drug loading into liposomes can be broadly classified into two categories, namely active and passive, based on the mode of loading. Passive loading of drug involves random entrapment of aqueous drug solution into the hydrophilic cavity of the liposomes. The amount of drug inside the liposome generated via passive loading cannot be changed after their formation in the solution. Aqueous drug solutions, when used to hydrate lipid films, can give rise to passive drug loaded liposomes. Passive drug loading can be carried

out in all cases of liposome preparation methods described above. In a different method of passive drug loading into liposomes, phopsholipids, cholesterol and the drug of interest were dissolved in an organic solvent or a mixture of organic solvents, removed under reduced pressure to leave a thin crust/lipid cake which was further hydrated with an appropriate buffer to yield passively drug loaded liposomes [76]. Crosasso et al. [77] used a combination of sonication and extrusion techniques to load paclitaxel in sterically stabilized liposomes. Chloroformic solution of paclitaxel was mixed with egg yolk phosphatidylcholine, phosphatidylglycerol, cholesterol and polyethyleneglycol- dipalmitoylphosphatidylethanolamine (DPPE) (ePC/PG/CHOL/PEG5000–DPPE) in a molar ratio of 9:1:2:0.7, respectively, and dried under vacuum (1 mol drug: 30 mol lipid). The lipid film was hydrated using TES buffer (140 mM NaCl and 0.1 mM EDTA, pH 7.4) to produce multilamellar vesicles (MLVs). To obtain SUVs of ~100 nm, the MLVs were first sonicated for 2 min using bath type sonicator followed by 12 cycles of extrusion through a 100 nm pore polycarbonate filters [77]. The technique resulted in ~78 % encapsulation efficiency of paclitaxel into the sterically stabilized liposomes.

Active or remote mode of drug loading has been proposed over passive loading in order to improve drug loading capacity within the liposomes and to retain more drugs within the vehicle. Active mode of drug loading takes advantage of the amphiphilic nature of certain hydrophobic amine containing anticancer chemotherapeutic drugs (e.g. doxorubicin, daunorubicin, adriamycin, and mitoxantrone), and forces higher amounts of loading by creating an artificial ion or pH gradient across the lipid bilayer of the liposome. These amphiphilic anticancer chemotherapeutic drugs are highly membrane permeable when neutral, but become impermeable when charged. Maintenance of lower pH inside the liposome, compared to the solution outside, allows free entry of the drugs into the liposome, but inhibits their escape by converting them into charged species within the liposome. This method allows for higher drug/lipid ratios in the liposome than the theoretically predicted drug aqueous

solubility. Mayer and co-workers [78] reported the uptake of adriamycin into LUVs composed of egg-yolk phosphatidylcholine (egg PC) and egg PC-cholesterol (1:1) in response to a pH gradient. A pH gradient of 2.9 units (pH 4.6 interior) was generated by forming LUVs in 150 mM KOH/175 mM glutamic acid (pH 4.6) and subsequently exchanging the interliposomal buffer for 150 mM KOH/125 mM glutamic acid/30 mM NaCI (pH 7.5) using Sephadex G-50 desalting columns. This method resulted in drug loading of up to 100 mM and trapping efficiencies of ~98 % within liposomes. Using this technique, Mayer et al. [79] reported the active loading of doxorubicin (~98 % trapping efficiency, Drug/Lipid ~0.3 w/w) into egg phosphatidylcholine/cholesterol liposomes when a proton gradient was generated by transferring 300 mM citrate buffer (pH 4.0) liposomes to 20 mM Hepes buffer (pH 7.5). The trapped anthracyclines formed citrate salts and precipitated inside the liposome thus inhibiting their escape/release [80].

The ammonium sulphate method of pH gradient generation is another technique for loading drugs (e.g. doxorubicin) within phospholipid liposomes, and was first proposed by Haran et al. [81]. This technique provides a much more stable gradient when compared to others and thus increases the stability of the anthracyclines accumulated inside the liposome for a prolonged period of time [82]. The increased stability is provided by the low permeability of the sulphate counter-ion which helps to maintain the gradient for longer periods of time. In a typical experiment, liposomes are usually preparaed in a solution of 300 mM ammonium sulphate (pH 5.5), and transferred to a buffer (pH 7.4), therefore generating a pH gradient. The higher concentration of ammonium ions inside the liposome causes the diffusion of neutral ammonia into the bulk liquid (permeability coefficient 1.3×10^{-1} cm/s), which leaves behind one proton for every ammonia molecule left. The proton gradient generated causes a drop in the pH of solution inside the liposome. The permeability of the sulphate counterion across the membrane is very low (~10^{-13} cm/s) [52], indicating that the lipid bilayer is almost impermeable to the sulphate ion. Doxorubicin enters

the liposome due to the proton gradient, gels and flocculates inside due to its poor solubility in presence of sulphate. For example, solubility of doxorubicin sulphate in the pH range 4.0–7.5 is ~1.7–2.3 mg/mL, which is approximately three times lower when compared to the solubility of doxorubicin citrate at the same pH [83]. This lower solubility of doxorubicin sulphate also affects its release and leakage rates *in vivo* at the site of the disease. Although poor drug-liposome stability and fast leakage of drugs from the liposome in the blood can be addressed by creating very stable pH gradients, low drug leakage can also cause decreased availability of the drug at the target site. To resolve this, stimuli-sensitive smart chemistries have been incorporated within the architecture of liposomes in order to trigger the release of drugs loaded via ammonium sulphate gradient method at the site of disease.

9.2.1.2 Stimuli-Responsive 'Smart' Drug Loaded Liposomal Formulations for Targeted Drug Delivery

Smart stimuli sensitive immunoliposomes have been synthesized in order to improve liposomal drug delivery to the tumor site. Liposomes responsive to stimuli, e.g. low pH within the endosomes and near the site of tumors [84], temperature increase associated with inflammation and hyperthermia [85], proteases [86], magnetic fields and ultrasound [87], have been generated to ensure release of the drug at the site of disease. These smart chemistries have been coupled with targeting agents such as antibody/peptide/aptamer [88–90] and stealth polyethylene glycol (PEG) coatings to create long circulating, targeted and stimuli sensitive liposomal drug nanocarriers. These long circulating, targeted and stimuli sensitive liposomes have been used to carry multiple different types of cargoes within their compartments [91–94]. Saul et al. [95] enhanced the targeting selectivity of liposomal doxorubicin by utilizing a dual targeting approach in which, liposomal nanocarriers were loaded with doxorubicin via the ammonium sulfate gradient and surface conjugated with ligands targeted to both folate and epidermal growth factor (EGF) receptors.

Dual-targeting of the liposome allowed ~10 fold and ~4 fold reduction in off-target effects of the formulation when compared to folate and epidermal growth factor receptor (EGFR) single-ligand formulations respectively. Yang et al. [96] used a dual approach of combining high-intensity focused ultrasound trigger with interleukin-4 receptor-targeted liposomal doxorubicin to enhance the delivery and antitumor effect of doxorubicin in intracranial brain-tumor model in NOD-scid mice. Application of focused sonication allowed a two-fold increase in the amount of doxorubicin accumulated inside the brain when compared to controls without the targeting and ultrasound application. Meng et al. [97] showed enhanced antitumor effect of paclitaxel loaded PC/CHOL/mPEG2000-DSPE (90:10:5) liposomes targeted towards both, alpha V integrins and neuropilin-1 markers for angiogenesis and new vessel growth. Paclitaxel in these formulations significantly suppressed the growth of HUVEC and A549 cells, when compared to controls of untargeted liposomes and free drug. The IC_{50} value of the drug in these dual targeted liposomes reduced to almost half from ~6–7 mg/mL for the free drug to ~1–2 mg/mL for A549 cell line, indicating increased efficacy. (IC_{50}, or inhibitory concentration 50, is the concentration of drug required to achieve 50 % inhibition of cell viability).

In addition to targeted delivery to cancer cells at tumor, it is often necessary for drugs to avoid/bypass the degradative endolysozomal compartments inside cells. Drugs and biomolecules released in the endosomal space during internalization encounter low pH values (pH 4.5–5.5), which can adversely affect their stability [98]. Hence, endosomal escape of such pH sensitive cargoes becomes essential in order for the drug to maintain its intracellular therapeutic action [99]. Fusogenic liposomes fuse with the lipid bilayer of cells or intracellular endosomes, and subsequently releases their cargo into the cell [100, 101]. This activity facilitates direct delivery of therapeutic cargo to the cytoplasm of a cell, thereby avoiding the exposure to low endosomal pH altogether. Kunisawa et al. [102] reported direct delivery of nanoparticles to cytoplasm

when encapsulated within fusogenic liposomes. This activity was not seen in case of conventional liposomes, which were prepared by dissolving phosphatidylcholine, l-α-dimyristoyl phosphatidic acid, and cholesterol (4:5:1 mol ratio) in a solution containing chloroform, methanol and water (65:25:4). Conventional liposomes were mixed with UV-inactivated Sendai virus and incubated with vigorous shaking for 2 h at 37 °C and purified by centrifugation (77,000 × g, 2 h, 4 °C) in order to generate fusogenic liposomes; hemagglutinating virus of Japan (HVJ) or Sendai virus imparted the fusogenic activity to the liposomes. LLCMK2 cells were incubated with conventional liposomes and fusogenic liposomes loaded with (Fluorescein isothiocyanate) FITC-labelled-nanoparticles in presence of endocytosis inhibitor cytochalasin B or cytochalasin D (Cytochalasin D has been shown to inhibit actin dependent endocytosis pathways [103]). Nanoparticle uptake efficiency was measured using flow cytometry. Under endocytosis inhibition, fusogenic liposomes delivered equal amounts of nanoparticle cargo as the control whereas conventional liposomes delivered only 30–40 % of the nanoparticles delivered in case of the control. In these cases, control experiments involved liposomal delivery of nanoparticle cargo under no endocytosis inhibition. Similar results were obtained when cells were treated with other inhibitors such as 2,4-dinitrophenol, nocodazole or colchicines. These results clearly indicated the benefits of fusogenic liposomes in delivering sensitive cargo to the cell cytoplasm.

Simoes et al. [104] showed that addition of stealth PEG coating on pH sensitive phosphatidylethanolamine (PE)-containing liposomes, intended for enhancing circulation time and stability, may also inhibit its pH sensitivity. However, the PEG coating did not affect its ability to deliver cargo to the cytoplasm, indicating that intracellular delivery is not dictated by destabilization of the liposomes alone. Although addition of the stealth PEG coating can increase stability and circulation time of liposomes, it might inhibit the interaction between the stealth liposome and target of interest. In order to circumvent this issue, research has focused on the

preparation of stimuli-responsive, sheddable PEG coatings [105]. These pH-responsive liposomes work by shedding their stealth PEG coat below a specific pH, therefore exposing bare liposome for further delivery. pH sensitive linkers such as hydrazone and diorthoester linkages have been used to shed PEG coating at low pH [105]. Guo and Skoza [106] used diorthoester linkages to selectively shed PEG coating at a pH range of 5–6, resembling the pH region within the endosomes. Liposomes prepared from 10 % pH-sensitive poly(ethylene glycol)-diortho esterdistearoyl glycerol conjugate (POD) and 90 % of a fusogenic lipid, dioleoyl phosphatidylethanolamine (DOPE) and loaded with 8-Aminonaphthalene-1,2,3-trisulfonic acid (ANTS) and p-Xylenebis(pyridinium) bromide (DPX) were used to study pH dependent leakage of cargo. POD/DOPE liposomes were stable for over 2 weeks under conditions of alkaline pH (pH 8.5). However, significant loss in stability was observed within 10–100 min under conditions of acidic pH (pH 5–6), resembling extensive aggregation and content leakage at the endosomal pH range. In addition to pH-sensitive stimuli, matrix metalloproteinase (MMP) sensitive cleavage of PEG shell has also been investigated [107, 108].

9.2.1.3 FDA-Approved Liposomal Formulations

Extensive advances in the field of liposomal drug delivery over the last five to six decades have contributed to noticeable benefits in the clinic. Multiple liposomal drug formulations have been approved by the FDA for therapeutic interventions in the clinic. Doxil®, a liposomal formulation of anticancer drug doxorubicin, was the first nano-drug approved by the FDA in 1995 for AIDS-related Kaposi's sarcoma. Since then, its use has been approved for recurrent ovarian cancer, metastatic breast cancer and multiple myeloma [109, 110]. Liposomal formulation of doxorubicin was created in order to overcome the extreme side effects, including chronic cardiotoxicity, caused by free doxorubicin [111, 112]. In addition, the liposomal drug formulation Doxil® resulted in increased circulation times of the drug in the bloodstream.

In order to prepare Doxil®, doxorubicin is loaded via ammonium sulfate gradient into the liposomal formulation of phospholipids N-(carbonyl-methoxypolyethylene glycol 2000)-1,2-distearoyl-sn-glycero-3-phosphoethanolamine (DSPE-mPEG 2000), fully hydrogenated soy phosphatidylcholine (HSPC), and cholesterol (39:56:5 molar ratio). The presence of PEG as the outer coating helps in long circulation of the liposome in the blood stream. Long circulation in the blood stream allows Doxil® to extravasate to the tumor sites for therapeutic action [113]. Encapsulation of doxorubicin in the liposomal formulation Doxil has shown to significantly alter its pharmacokinetic distribution, confer longer plasma half-life and reduce its cardiotoxic impact in patients [110]. Since its approval, Doxil has benefitted hundreds of patients worldwide and generated global revenues upwards of ~600 million dollars.

Other liposomal formulations that have been approved by the FDA include AmBisome for intravenous injections of amphotericin B targeted towards severe fungal infections (visceral leishmaniasis) [114], DaunoXome a intravenous liposomal formulation of Daunorubicin for treatment of blood tumors [115], Depocyt a liposomal formulation of cytarbine for the treatment of Neoplastic meningitis and lymphomatous meningitis [116] etc. Till date, approximately 12 liposome-based drugs have been approved for clinical use, and more than 20 others are in various stages of clinical trials [117].

9.2.2   Micelles

A typical micelle is a supramolecular nanoparticle (10–200 nm) containing a water-loving shell/corona protecting a core [118], which may or may not be hydrophobic. Micelles can be spherical, cylindrical or hexagonal in shape [119]. Micelles form via the self-assembly of multiple individual units. These units can be amphiphilic block co-polymers, oppositely charged ionic polymers linked to a hydrophilic shell [34] or hydrophobic tethers linked to a hydrophilic polymer [120].

Amphiphilic block copolymers are made up of a core-forming hydrophobic segment attached to a shell forming hydrophilic tail in a single monomer unit [121]. In aqueous solutions, these monomers self-assemble into nanosized supramolecular structures with hydrophobic cores which remain protected by a hydrophilic shell. The driving force for the formation of such micelles is usually the hydrophobic effect [122]. In aqueous solutions, hydrophobic segments of these amphiphilic block copolymers cannot establish hydrogen bonding with adjacent water molecules. Hence, their addition into aqueous solutions results in aggregation of these segments into supramolecular structures. The resultant decrease in free energy of the system drives this self-assembly process [123]. The minimum concentration required for attaining micellization or aggregation into micelles is called critical micelle concentration (CMC), which is an indicator of stability of micelles upon dilution [124]. Lower values of CMC, indicate better stability of micelles, particularly upon dilution.

Availability of a hydrophobic core region within these micelles allows for stable loading of poorly soluble hydrophobic drugs during micellization. In aqueous solutions, mutual repulsion of hydrophobic cores and hydrophobic drugs towards water molecules allow them to aggregate together into assemblies of drug loaded micelles. Once formed, the stability of the aggregate also depends on the compatibility between the hydrophobic core and hydrophobic drug (which is given by the Flory-Huggins and Hansen solubility parameters) [125]. Apart from stability within the hydrophobic core, these drugs are further stabilized by the hydrophilic corona of the shell region. Improving solubility of poorly soluble drugs using excipients such as amphiphilic block polymers prolongs their half life in the blood and significantly enhances their bioavailability [126–128].

Commonly used hydrophobic core forming segments are polypropylene oxide (PPO) [129], polycaprolactone (PCL) [130], poly lactic acid (PLA) [131], long hydrocarbon chains such as distearoyl, dioleyl, dipalmitate groups [132] and polyamino acid groups including poly-(l-lysine).

Most common hydrophilic shells used are polyethylene oxide or polyethylene glycol groups. Apart from PEG, poly acrylic acid (PAA), poly (N-vinyl-2-pyrrolidone) (PVP),poly[N-(2-hydroxypropyl) methacrylamide] (pHPMA), thermosensitive poly (N-isopropylacrylamide) (pNIPAAm), oligonucleotides and oligopeptides have also been used as hydrophilic shells in micelles [133, 134].

9.2.2.1 Preparation of Drug Loaded Micelles for Delivery

Loading of hydrophobic chemotherapeutic drugs in the core of the micelles allows them to be stably encapsulated and transported to their target organ in the blood stream. Multiple techniques have been used for loading hydrophobic drugs into micelles. Solvent casting/solution casting involves solubilizing the drug and the polymer in an organic solvent or a mixture of solvents which can dissolve both the components [135]. Once mixed well, the solvent mixture is evaporated using a rotary evaporator leaving behind a thin polymer-drug crust. Once the organic solvent is completely removed, the film is hydrated with an appropriate buffer resulting in the formation of the micelles in solution. Upon hydration, the hydrophobic drug molecules associate with the hydrophobic core of the micelles giving rise to drug-loaded micelles. Chemotherapeutic drugs including doxorubicin [136, 137], paclitaxel [138], docetaxel [139], and camptothecin [140] have been successfully loaded into micelles using this technique. Recently, our group has used this technique to load anticancer anthracenedione drug mitoxantrone into PEG-DSPE micelles in order to exploit its synergy with TNF-alpha Related Apoptosis Inducing Ligand (TRAIL) in inducing enhanced cancer cell death [141]. Although the technique of solvent casting provides a versatile tool for drug loading into the micelles, compatible organic solvent mixtures are required to solubilize both, the drug as well as the polymer.

Dialysis-based methods have been investigated in order to overcome the above challenges with micelle loading. These involve solubilizing the drug and polymer in a water miscible solvent such as dimethyl sulfoxide (DMSO) followed

by its slow injection into buffer solution [142]. Upon dialysis of the mixture against the aqueous solvent, the gradual removal of DMSO triggers micellization. Another similar approach known as solvent displacement method [143] involves slow addition of a mixture of organic solvent such as chloroform and the drug into aqueous solution of the polymer under constant stirring. The resulting solution forms an oil-in-water emulsion. The drug is incorporated into the micelles as the organic solvent evaporates or is dialyzed out [144]. The choice of micelle preparation can impact the loading capacity of the drug into the micelles. La et al. [145] studied the impact of micelle preparation on the loading of the drug indomethacin into poly(ethylene oxide) − poly(β-benzyl l-aspartate) (PEO-b-PBLA) block copolymer micelles. Dialysis and oil-in-water emulsion methods of drug loading were compared. Higher loading of drug was recorded when oil-in-water emulsion method of drug loading was used [145].

Core-drug compatibility is another important factor that determines stable loading of drug into the core of micelles [146]. Hydrotropy involves solubilizing a lipophilic organic compound of interest by addition of large amounts of a second organic compound, the hydrotrope [125]. These hydrotropes can drastically increase the aqueous solubility of the organic compounds of interest. Lee et al. [147] identified hydrotropic agents for solubilizing anticancer drug paclitaxel. Two hydrotropes, N,N-Diethylnicotinamide (DENA) and N-Picolylnicotinamide (PNA) were identified to enhance the solubility of paclitaxel to ~39 and ~29 mg/mL respectively when compared to its native solubility in water of 0.30 ± 0.02 μg/mL. Lee et al. [148] further used DENA and PNA as hydrophobic cores in micelles to load paclitaxel. They synthesized a hydrotropic polymer micelle containing a PEG shell and a 2-(4-(vinylbenzyloxy)-N,N-diethylnicotinamide) (VBODENA) core to solubilize paclitaxel in aqueous solutions to a concentration of 38.9 mg/mL. Interestingly, the formation of drug-loaded micelles occurred by mere addition of paclitaxel to the PEG-b-VBODENA hydrotropic polymer solution, indicating its ease of preparation.

Chemical conjugation and crosslinking of the drug into the micelle is another popular method of loading drugs into the micelles. Physical encapsulation of drug into micelles may be destabilized upon dilution below CMC of the micelle unimers. Chemical cross-linking of drug-loaded micelle cores has been investigated as an alternative to circumvent the issue. Such chemically cross-linked cores do not dissociate even upon extensive dilution and thus enhance stability of the particle [149, 150]. Xu et al. [143] developed a core-surface cross-linked amphiphilic copolymer system containing poly (ε-caprolactone) (PCL) hydrophobic cores and poly(ethylene glycol) (PEG) or poly(2-(N,N-dimethylamino)ethyl methacrylate) (PDMA) shells. The resultant crosslinked micelle was ~100 times more stable than micelles generated from corresponding amphiphilic block copolymers. Further, micelle-encapsulated cisplatin demonstrated enhanced anti cancer activity (approximately four-fold) against SKOV-3 ovarian cancer cells in vitro, when compared to free cisplatin.

Yokoyama and colleagues undertook an elaborate study on the impact of drug conjugation to micelle cores [151]. The anticancer drug adriamycin was conjugated to the core of micelle formed using poly(ethylene oxide)-poly(aspartic acid) block copolymers (PEG-PAsp). Adriamycin-conjugated PEG-PAsp micelles (PEG-P(Asp(ADR) micelles) demonstrated a significant increase in *in vivo* anticancer activity of the drug against murine leukemia [152] and adenocarcinoma tumors [153], when compared to the free drug. PEG-P(Asp(ADR) micelles prolonged the median survival of murine leukemia inflicted mice from 2.7 days (drug administered with micelles without conjugation) to more than 47 days at equal doses of 200 mg equivalent ADR/kg weight. However, the PEG-P(Asp(ADR) micelles required a greater load of drug molecules to achieve therapeutic effect as the drug cross-linked micelles had very slow degradation and release. Although the slow release of the drug meant more drug molecules were needed, side effects such as loss of body weight associated with the drug were significantly reduced with the use of these

drug-conjugated micelles [152]. Another study by the same group [154] compared the performance of the same adriamycin drug when it was physically entrapped vs. chemically conjugated to the PEG-PAA micelles. Both drug formulations were studied for their *in vivo* therapeutic activity against mouse colon adenocarcinoma C 26 tumors. Micelles with physically entrapped drug showed significantly higher *in vivo* activity due to the slow release of drug from the drug-complexed micelles. Although chemical conjugation of drug to the core of micelles may lock the drug in the core and reduce its unwanted side effects, it is important that the drug be released at the site of action. Thus, it is important to trigger release the drug at the site of action while keeping it encapsulated during transport through the blood stream.

9.2.2.2 'Smart' Micelles for Targeted Drug Delivery

Passive targeting of drug-loaded nanoparticles to tumors is based on their enhanced accumulation at the tumor site due to the EPR effect (Fig. 9.2). Although passive targeting can significantly increase tumor localization of the drug, some limitations exist [155]. Drug targeting via passive accumulation is highly dependent on the extent of vascularization in tumors [156]. Cabral et al. [157] showed that particle size dictates the accumulation of sub-100 nm micelles in poorly vascularized tumor sites of pancreatic cancer. Tumoricidal agent 1,2-diaminocyclohexane-platinum(II) (DACHPt) loaded PEG–b-poly(glutamic acid) (PEG–b-P(Glu)) micelles were prepared. PEG–b-poly(glutamic acid) (PEG–b-P(Glu)) micelles were prepared by mixing PEG–b-poly(glutamic acid) copolymer and the poly(glutamic acid) (P(Glu)) homopolymer in water. The size of micelles increased with increasing ratio of (P(Glu)) in the homopolymer: copolymer resulting in micelles with diameters of 30, 50, 70 and 100 nm. Significant reduction in passive accumulation was observed for micelles above 30 nm in the poorly vascularized BxPC3 pancreatic cancer cells nests (shown in Fig. 9.3). Elevated interstitial fluid pressure in tumors also prevents homogenous distribution and uptake of

the nanoparticles within the tumor [158, 159]. The polyethylene glycol (PEG) shell can also prevent interactions between cell surface and the nanoparticles [160].

Active targeting of drug-loaded nanoparticles to the tumor site has been proposed to overcome the shortcomings of passive accumulation [161]. Active targeting involves conjugation of specific targeting molecules such as monoclonal antibodies, aptamers, or peptides, to the surface of nanoparticles. These molecules can specifically bind to tumor associated surface receptors/antigens, and interfere with their signal transduction pathways [46]. Upon binding, they usually induce receptor-mediated endocytosis and allow targeted intracellular delivery of conjugated drug. For example, overexpression of folic acid receptor (FR) in ovarian, cervical and breast cancer has been utilized to target drug loaded, folic acid conjugated micelles to those tumors [162, 163]. Overexpression of epidermal growth factor receptor (EGFR) on the surface of breast and lung cancers has also been utilized for similar purposes [164]. Han et al. [165] used folic acid conjugated PEG-DSPE micelles in order to deliver 9-nitro-camptothecin (9-NC) to cancer cells *in vitro*. A significant reduction in the IC_{50} value of the drug was observed in folate-expressing HeLa cells, 48 h after administration of the drug-loaded micelles. The lethality of the drug in folic acid-conjugated micelles was enhanced by ~304 fold, when compared to the free drug indicating the advantages to targeted drug delivery. Wei et al. [166] targeted drug-loaded nanoparticles to neuropilin-1, a transmembrane receptor glycoprotein that specifically binds to peptides carrying a C-terminal R/KXXR/K motif (CendR motif). Overexpression of neuropilin-1 receptor has been found in tumor vessels, carcinoma cells and has been targeted via tumor penetrating peptides. Wei et al. [166] conjugated a novel CendR peptide ligand, CysArg-Gly-Asp-Lys (CRGDK) in order to target doxorubicin loaded PEG-DSPE nanomicelles (TPFM-Dox) to tumor vasculature. A 15-fold improvement in penetration distance into the tumor tissue from the tumor vasculature was seen in case of TPFM-Dox micelles, when compared

Fig. 9.2 (**a**) Passive and (**b**) active targeting and delivery of chemotherapeutic drug-loaded vectors (Reprinted (adapted) with permission from Danhier et al. [46])
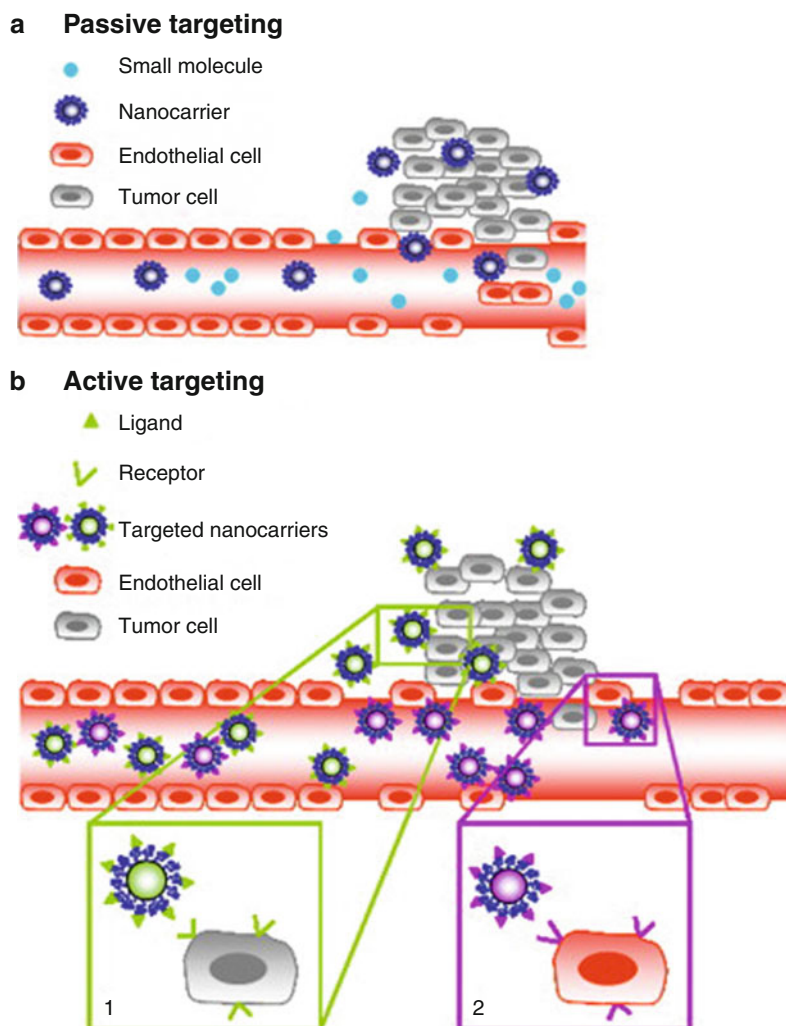
to the untargeted micelles. The targeted micelles also showed significant improvement in the amount of drug delivered to the tumor when compared to untargeted micelles.

In addition to active antibody/aptamer/peptide based targeting, smart and stimuli sensitive micelles have been employed to selectively target drug loaded cargo to tumors. Specific stimuli such as lower pH in the endosomes of the targeted cancer cells [167], elevated temperatures due to inflammation [168], and increased concentration of matrix metalloproteinases (MMP) [169] have been investigated. Bae et al. [170] conjugated adriamycin to the core of folate-poly(ethylene glycol)-poly(aspartate) (FA-PEG-PAA) micelles via a pH degradable hydrazone linker to generate folate-poly(ethylene glycol)-poly(aspartate-hydrazone-adriamycin) or FA-PEG-PA-AD micelles. Folate-conjugated drug-micelles showed lower systemic toxicity and higher antitumor activity when compared to the free drug in CD-1 nude mice bearing human pharyngeal cancer. Almost 5 times the effective dose (ED_{50}) (dose that can induce 50 % of tumor volume suppression without reducing body weight less than 20 % during the treatment) was possible when the drug was delivered in the specific micellar formulation. Safe dose of free adriamycin was 3.96 mg/kg body weight in contrast to 20.03 mg/kg body weight for drug-in-micelles (~5 times increase). Gao et al. [171] showed anti-metastatic activity of doxorubicin when loaded in a pH-sensitive micelle prepared by
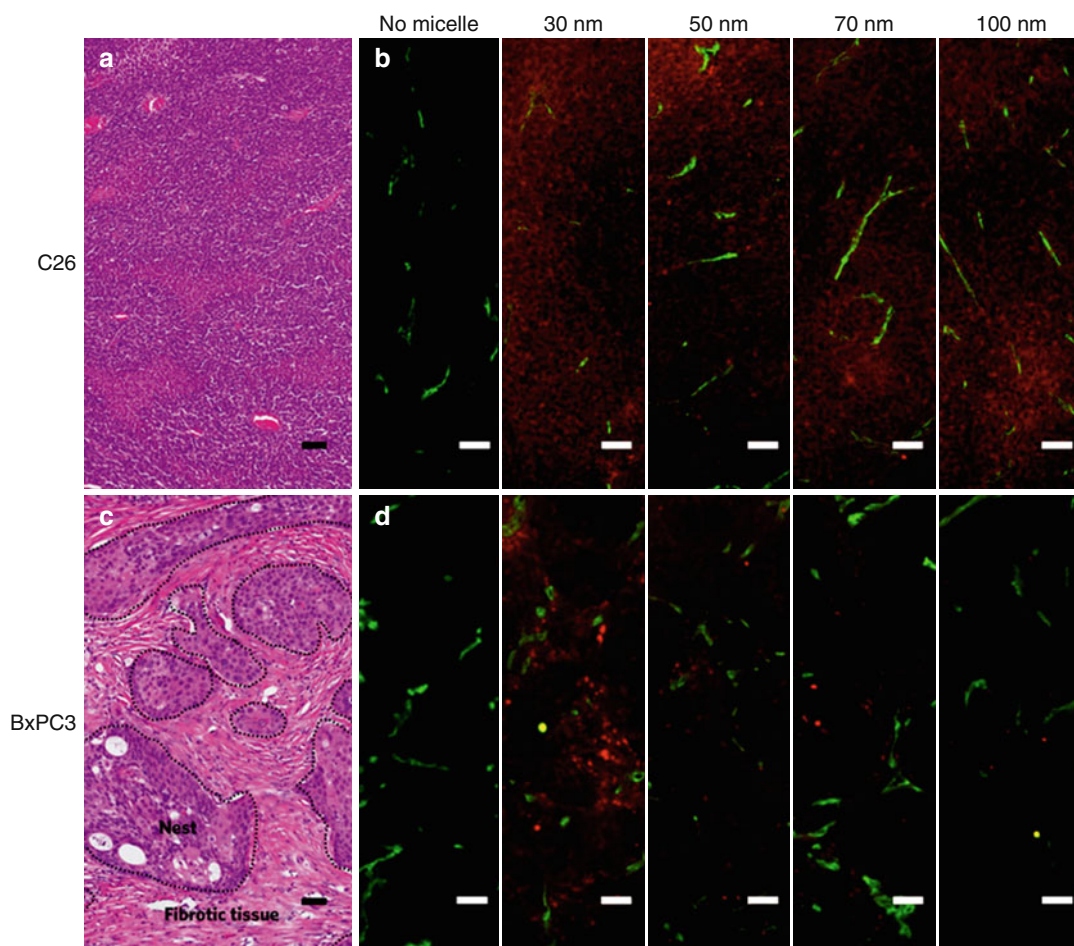
| | No micelle | 30 nm | 50 nm | 70 nm | 100 nm |

Fig. 9.3 Microdistribution of fluorescently labeled drug loaded micelles of different sizes in vascularized (C26) and poorly vascularized (BxPC3) tumors is shown. Hematoxylin and Eosin (H&E) staining of (**a**) C26 and (**c**) BxPC3 tumors is shown. *Dashed area* in (c) represents the cancer cells nests in BxPC3 tumors. (**b**, **d**) Show the fluorescent microscopic image sections of (**b**) C26 and (**d**) BxPC3 tumors 24 h after intravenous administration of

fluorescent-micelles (*red*) of different sizes. Blood vessels were labeled with PECAM-1 and Alexa 488 secondary antibody (*green*). Scale bar: 50 μm. Minimal amount of *red color* was observed in poorly vascularized BxPC3 tumor sections when mice were injected with micelles above 30 nm diameter. C26 tumor sections showed no such changes (Reprinted (adapted) with permission from Cabral et al. [157]; only (a–d) of the original image are shown)

mixing poly(l-lactide) (PLLA)-b-poly(ethylene glycol) (PEG)-folate and poly(l-histidine) (PHis)-b-PEG. Prevention of metastasis was shown in subcutaneously implanted 4 T1 murine breast cancer cell model, one of the most aggressive metastasis cancer cell lines. Metastasis to lung, heart, liver, kidney and spleen was not seen in a single mouse (0 in 5), when the group was treated with doxorubicin-loaded mixed micelles; the free doxorubicin in PBS control showed metastasis to lungs, heart and kidney.

9.2.2.3 Micellar Formulations in Clinical Trials

Multiple micellar formulations are currently under different stages of clinical trials after successfully completing pre-clinical studies. These include NK012, NK105 [172], SP1049C [173], Nanoplatin, and Genexol-PM. Genexol PM is a micellar formulation of hydrophilic PEG shell and hydrophobic poly(d,l-lactic acid) (PDLLA) core loaded with paclitaxel, and is currently undergoing phase IV clinical trials for patients

with taxane-pretreated recurrent breast cancer. Genexol-PM was well tolerated by patients suffering from advanced pancreatic cancer and metastatic breast cancer in Phase II clinical trials [174, 175]. Phase II clinical trials of Genexol-PM have recently been completed in patients with advanced urothelial cancers previously treated with gemcetabine and platinum, and in patients with advanced non-small-cell lung cancer. The results for these trials are still awaited.

A phase III clinical trial of NK105 in patients with breast cancer is currently underway. NK105, a micellar formulation of paclitaxel loaded in PEG-Poly aspartate polymer, was developed as an alternative to overcome the adverse side-effects produced by Cremophor EL and ethanol additives in commercial paclitaxel formulations. Presence of solubilizers such as Cremophor EL and ethanol caused hypersensitivity reaction in 2–4 % of its users [176], which motivated the investigated of a micellar formulation. In addition, free paclitaxel is also known to produce multiple serious side effects including neutropenia and peripheral neuropathy [177]. In a phase I clinical trial, patients suffering from pancreatic and colon cancers showed less hypersensitivity reactions to NK105 compared to commercial formulation [172].

In summary, micellar drug formulations provide a promising tool in accelerating advances towards targeted drug delivery. Although significant strides have been made, concerns regarding limited drug loading capacity in micelles, premature drug release before reaching the target tissue, and the need for compatible cores for new hydrophobic drugs need to be addressed.

9.3 PLGA Nanoparticles

Poly (lactide-co-glycolide) (PLGA) is a co-polymer made by polymerization of lactic acid and glycolic acid. Biodegradability due to hydrolysis of ester linkages, and biocompatibility has resulted in wide acceptance, FDA approval, and use of the polymer in multiple areas of drug and gene delivery. PLGA is usually prepared by random ring-opening copolymerization between cyclic dimers of glycolic acid and lactic acid in presence of tin (II) alkoxides or aluminum isopropoxide catalysts [178].

PLGA nanoparticles are most often prepared using single or double-emulsion-solvent evaporation method. The single emulsion method involves generation of stable oil/water (O/W) emulsion, widely used to encapsulate hydrophobic drugs and steroids. Double-emulsion-solvent evaporation method requires stable generation of water/oil/water (w/o/w) emulsion loaded with hydrophilic drugs. Polyvinyl alcohol is the most commonly used emulsifier to stabilize the emulsion as it produces particles of small size (~100 nm) with uniform distribution [179]. Biodegradable ester linkages in PLGA allow degradation of the nanoparticles in the body. Stealth polyethylene glycol (PEG) coatings have been employed for extending circulation of PLGA nanoparticles in the blood [180].

Yoo et al. [181] used folate-conjugated, doxorubicin-PLGA-PEG micelles (Dox-PLGA-PEG-Fol micelles) to deliver the chemotherapeutic drug to folate-expressing KB carcinoma cells. Dox-PLGA-PEG-Fol micelle formulation (110 nm) was more effective when compared to free doxorubicin, suggesting that folate mediated-endocytosis was likely responsible for increase in doxorubicin uptake and cytotoxicity. A significant reduction volume in KB cell tumor xenografts were observed in a nude mouse model when Dox-PLGA-PEG-Fol micelles were used, and this activity was greater than that observed with free doxorubicin. Antibody/aptamer-based targeting of drug-loaded PLGA nanoparticles has also been shown [182]. In a study by Dhar et al. [183], targeted delivery of Cisplatin Pt(IV) prodrug (intracellularly reducible) was shown using PSMA-targeted aptamer functionalized prodrug-PLGA–PEG nanoparticles. The biodegradable nanoparticle formulation was able to reduce the IC_{50} value of free drug from 0.13 to 0.03 μM in PSMA-expressing LNCaP prostate cancer cells.

Possibility of drug delivery via FDA approved biodegradable polymers is promising and is likely to accelerate translation of therapeutics from the bench to the bedside [178].

9.4   Multifunctional Nanomedicine: Nanomaterials of the Future for Drug Delivery

Multifunctional nanomaterials utilize properties of both, organic as well as inorganic nanoparticles, and can lead to improved loading capacities, targeting efficacies and delivery of therapeutically active drugs. Huang et al. [184] reported a novel drug loaded gold nanorod based plasmonic matrix to synergistically administer photothermal therapy and chemotherapy to cancer cells. Crosslinked elastin-like polypeptide-gold nanorod (ELP-GNR) matrix was passively loaded with the heat shock protein inhibitor 17-AAG. 17-AAG inhibited heat shock protein mediated cell death resistance in cancer cells when exposed to laser induced gold nanorod (GNR) phototherapy. Significant reduction in cell viability was reported (~80 %) when cancer cells were exposed to laser irradiation in presence of the plasmonic nanocomposites loaded with 17-AAG [184].

Park et al. [185] reported a novel cooperative nanosystem in which, hyperthermia induced by PEGylated gold nanorods (GNRs) augmented higher doxorubicin liposomal delivery to MDA-MB-435 human melanoma tumors in mice. Thermally responsive sterically stabilized liposomal formulation of doxorubicin was prepared using a mixture of dipalmitoylphosphatidylcholine/hydrogenated soy phosphatidylcholine/cholesterol and polyethylene glycol derivatized distearoylphosphatidylethanolamine at 100:50:30:6 mol ratio. To perform the synergistic treatment, PEGylated GNRs (10 mg Au kg^{-1}) were first injected followed by liposomal doxorubicin formulation (3 mg Au kg^{-1}) after 72 h. Tumors were then irradiated with a (near infrared laser) NIR laser (810 nm, 0.75 W/cm^2) for 30 min, while maintaining an average tumor surface temperature of 45 °C. As shown in Fig. 9.4, irradiated tumors treated with thermally sensitive liposomes, showed significant reduction in tumor sizes when compared to all the other formulations. Gold nanorods accumulated within the tumor raised the temperature to ~45 °C, which caused blood vessel dialation and triggered drug release from the heat sensitive liposomal carriers, leading to significant cell death and tumor shrinkage.

Maltzahn et al. [186] showed for the first time the possibility of using communicating nanoparticles in vivo to amplify tumor targeting and drug release from doxorubicin loaded liposomes. PEGylated gold nanorods (PEG-GNRs) (10 mg Au kg^{-1}) accumulated at the tumor site were irradiated with NIR light (1 W/cm^2). Irradiation with NIR light generated a focal tumor surface temperature of ~49 °C and locally disrupted MDA-MB-435 tumor vessels to initiate extravascular coagulation in mice. Local coagulation induced by hyperthermia was then used as a tool to specifically target drug loaded liposomes to the site of tumor. Doxorubicin loaded liposomes were conjugated with peptide (thiol-maleimide conjugation chemistry) substrate for the coagulation transglutaminase Factor XIII, to allow their accumulation and incorporation into the regions of active coagulation in the tumor. This technology resulted in ~40 times higher accumulation of the chemotherapeutic drug at the tumor site, when compared to non-communicating controls (doxorubicin loaded liposomes without the peptide) (Fig. 9.5).

Ashley et al. [187] reported a novel protocell that synergistically combines high surface area and liposomal lipid bilayers to target human hepatocellular carcinoma with an efficacy of ~10,000 more than hepatocytes, endothelial cells or immune cells. The protocell, owing to its extensive surface area of the nanoporous structure, could simultaneously carry a combination of multiple therapeutic drugs including doxorubicin, 5-fluorouracil and cisplatin. The resulting protocell, when targeted to human hepatocellular carcinoma was effective for cancer cell ablation, with minimal damage seen in normal hepatocytes.

Multistage nanoparticle delivery for deep tumor penetration was proposed by Wong et al. [188] for delivering drugs to the tumor site away from the leaky vasculature. Rigid ~100 nm drug liposomes effectively accumulate at the site of tumor due to EPR effect, but fail to go deeper due to diffusional limitations. To overcome this limitation, Wang et al. proposed a drug delivery system which can shrink from 100 to ~10 nm after extravasation from the leaky vasculature in presence of cues from the tumor microenvironment. The reduced size was hypothesized to facilitate diffusion into the deeper regions of the tumor. The nanoparticle contained a
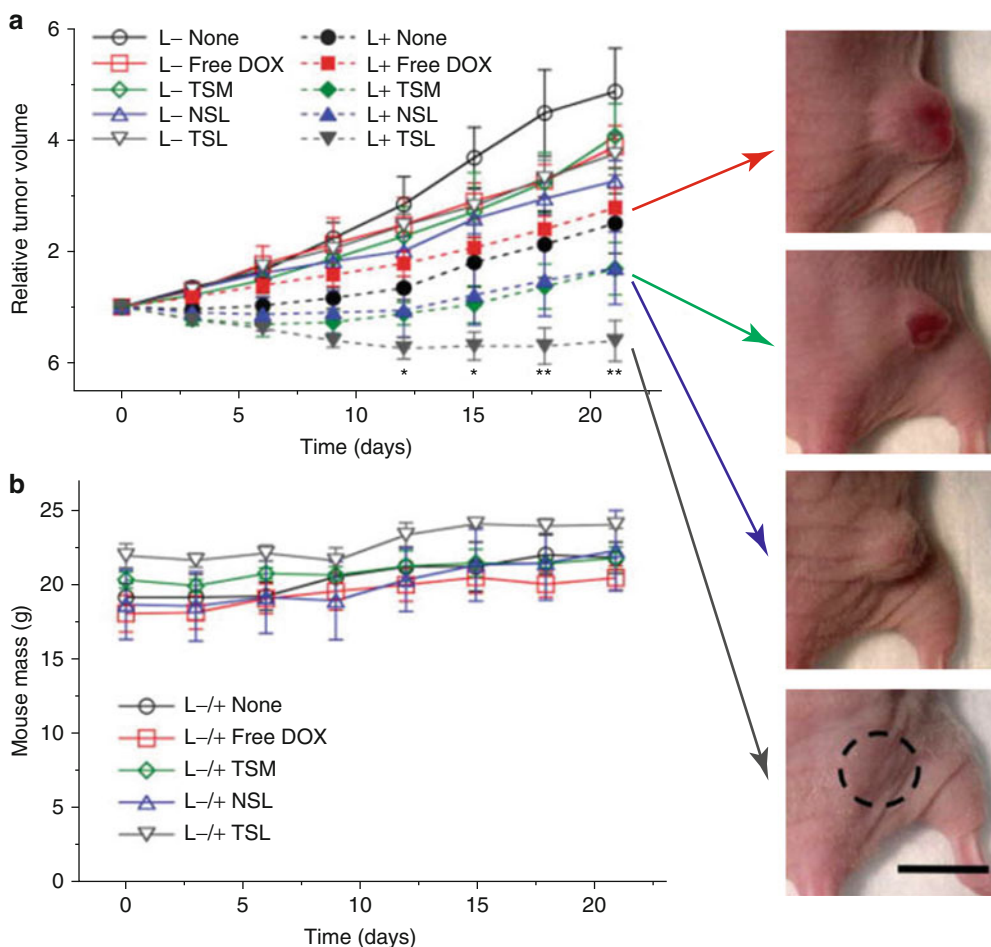
Fig. 9.4 Tumor therapy using cooperative nanosystems of gold nanorods and doxorubicin loaded thermally sensitive nanomaterials is shown. (**a**) Relative tumor volume in mice bearing bilateral MDA-MB-435 human melanoma tumors after different treatments is being measured. Tumor-bearing mice were injected with PEGylated GNRs at a concentration of 10 mg Au kg^{-1}. After 72 h of the injection, a single dose of the saline, free DOX, or other therapeutic experimental formulations (3 mg DOX kg^{-1}) was administered via tail vein injection. One tumor was irradiated with a NIR laser (810 nm, ~0.75 W cm^{-2}) for 30 min, while maintaining an average tumor surface temperature of ~45 °C. Results show maximum efficacy when the PEGylated gold nanorods loaded tumors were irradiated with laser in presence of thermosensitive liposomes. (**b**) Mouse mass (in grams) as a function of days post-treatment is being shown for the indicated treatment groups. L+ and L- indicate NIR irradiation or no irradiation after 72 hours of GNR delivery. Normal growth was observed among all groups after 21 days post-treatment. *TSL* doxorubicin loaded thermosensitive liposome, *NSL* doxorubicin loaded non-thermally sensitive liposome, *TSM* doxorubicin loaded thermosensitive micelles, *L* laser, *GNR* Gold nanorods. Scale bar: 1 cm (Reprinted (adapted) with permission from Park et al. [185])

gelatin core and shell loaded with ~10 nm (9.7±0.3 nm) neutral quantum dots. The gelatin was cleaved by matrix metalloproteinases (MMP2 and MMP9) at the tumor site, which released the quantum dots deep into the tumor tissue. QDGelNPs (~100 nm) were compared to 105.6±0.8 nm SilicaQDs to understand the impact of this multistage delivery on diffusional profiles. QDGelNPs

and SilicaQDs were coinjected intratumorally into dorsally implanted HT-1080 (MMP2 rich) tumor in severe combined immunodeficiency (SCID) mice. Six hours after the injection, nanoparticles from QDGelNPs had penetrated up to 300 μm from the site of injection, whereas SilicaQDs control did not disseminate. In addition, QDGelNPs had a longer blood half life of ~22±3.4 h when compared to
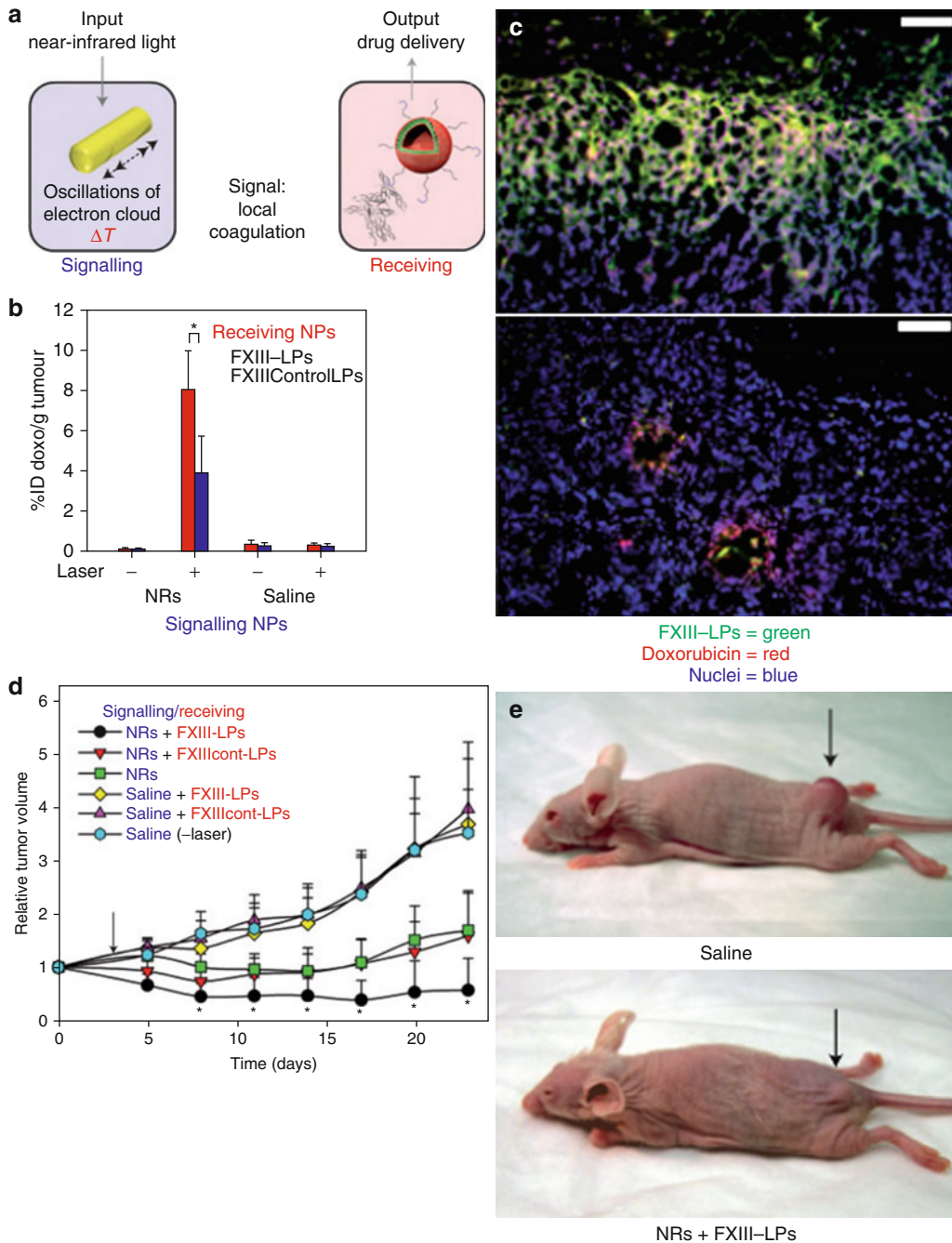
Fig. 9.5 Amplified tumor therapy via communicating nanoparticles is shown. (**a**) PEGylated gold nanorods (*NRs*) initiate local coagulation signal after photothermal response, which is detected by receiver molecules-doxorubicin-loaded liposomes conjugated with substrate for the coagulation transglutaminase Factor XIII (*FXIII-LPs*). (**b**) Quantification of FXIII-doxorubicin-loaded liposomes homing to the irradiated vs. contralateral non-irradiated tumors. Over 40-fold amplification in drug loading at tumor site was noticed when PEGylated gold nanorods in tumors were irradiated followed by the delivery of FXIII-doxorubicin-loaded liposomes. (**c**) Histopathological analysis of tumor sections after drug delivery through FXIII-LPs. FXII-LPs were observed to form a broad interstitial mesh in GNR-heated tumors (*green*), with released doxorubicin fluorescence (*red*) emanating from the nuclei of surrounded tumor cells, indicating the delivery and release of active doxorubicin within mice tumor tissues. Scale bar: 100 μm. Increased tumor ablation using communicating nanoparticles can be seen in (**d**, **e**) (*Black dots*) (Reprinted (adapted) with permission from Von Maltzahn et al. [186])

SilicaQDs, which had a blood half life of ~12.9±2.4 h. This proof-of-concept study showed the importance of bigger size of nanoparticles for successful accumulation via EPR effect, and subsequent reduction in size for deeper penetration.

Mitragotri and Barua [189] recently reported synergistic targeting of cell membrane, cytoplasm and nucleus of BT-474 breast cancer cells by using pure camptothecin (CPT) drug nanorods coated with monoclonal antibody against HER2/neu receptor trastuzumab (TTZ), and DNA intercalating doxorubicin (DOX). The CPT-TTZ-DOX nanoparticle was able to lower the IC_{50} 10–10,000 fold when compared to the individual drugs alone. Pure drug nanoparticles provide an attractive alternative for the delivery and improved bioavailablilty of hydrophobic drugs in cases when other excipients may demonstrate undesirable toxicity [190].

Schroeder et al. [191] reported remotely activated production of proteins from nanoparticles on demand in mice, thus mitigating the trouble of protein delivery. Therapeutic protein production near the site of disease can be highly beneficial if efficient delivery options do not exist. 1,2-dimyristoyl-sn-glycero-3-phosphocholine (DMPC) phospholipid vesicles were loaded with minimal E. coli S30 extract and luciferase encoding plasmid DNA caged with 1-(4,5-dimethoxy-2-nitrophenyl) diazoethane (DMNPE) to block transcription. Uncaging of DNA was prompt following irradiation with 365 nm UV rays. The resulting vesicle was highly tunable in size based on the filter used for extrusion. Mice, locally injected with particles encoding luciferase, were irradiated with UV (400 mW/cm^2), followed by whole body bioluminescent imaging showed a significant presence of luminescent signal at the site of injection compared to the rest of the body.

9.5 Summary

Nanotechnology has the potential to treat diseases and overcome multiple barriers that reduce the efficacy of drug/biomolecule delivery. Advances in polymeric, liposomal and micelle based drug delivery systems have resulted in numerous advances and breakthroughs resulting in FDA approval of nanoformulations such as Doxil and DaunoXome. These carriers can effectively modulate drug pharmacokinetics and biodistribution in the body, and help selective accumulation at the site of the disease. The next decade in nanomedicine is likely to see continued and sustained growth in targeted drug and biomolecule delivery via application of interdisciplinary knowledge from inorganic nanomaterials, biology, chemistry and engineering, leading to translation of these systems from the lab bench to bedside.

9.6 Detailed Experimental Protocols for Preparation of Nanomaterials for Drug/Gene Delivery

9.6.1 Micelles: Preparation of Mitoxantrone Loaded PEG-DSPE Micelles via Solvent Casting

(a) In a 20 mL scintillation vial weigh 10 mg of PEG-DSPE polymer (Avanti Polar Lipids) add 5 mL of methanol to the polymer and shake it thoroughly to dissolve it completely.

(b) In another 20 mL scintillation vial, weigh 1 mg of mitoxantrone (free base form) and dissolve it completely in 15 mL of methanol.

(c) Mix the methanolic solutions of mitoxantrone and PEG-DSPE in one single scintillation vial.

(d) After mixing it thoroughly for 5–10 min, carefully remove the methanol using rotary evaporator at a temperature of around 30 °C.

(e) Continue the process until methanol is removed under pressure. Once the methanol is removed, continue the rotary evaporation for another 5 min to remove all traces of methanol leaving behind a blue lipid crust/cake.

(f) Cover the blue lipid cake with aluminium foil and keep it in vacuum desiccator for 12 h.

(g) After 12 h of vacuum desiccation, add 1 mL of 10 mM HEPES buffer (pH 7.4) to the blue lipid cake and stir at 200 rpm for 20 min.

(h) Following the stir, sonicate the liquid for 20 min.

(i) Prepare a PD-10 column (GE healthcare) to perform size exclusion chromatography to

purify the drug loaded micelles from the free drug.

(j) Wash the PD-10 column with 25 mL of nanopure water followed by 25 mL of 10 mM HEPES buffer (pH 7.4) and introduce 1 mL of mitoxantrone loaded PEG-DSPE micelle solution carefully at the top of the column.

(k) Elute the drug-loaded micelles using additional HEPES buffer (pH 7.4) from the PD-10 column. Drug-loaded micelles being bigger in size elute much faster than the free unincorporated drug.

(l) The amount of drug incorporated can be measured by checking the absorbance of mitoxantrone-loaded micelles in DMSO at 680 nm.

9.6.2 Poly(lactide-co-glycolide) (PLGA) Nanoparticles: Preparation of Drug-Loaded Poly(lactide-co-glycolide) (PLGA) Nanoparticles

(a) In a 20 ml scintillation vial, prepare a 3 % poly(lactide-co-glycolide) (PLGA) solution in dichloromethane (DCM), by dissolving 90 mg PLGA in 3 ml DCM.

(b) In another 20 ml scintillation vial, prepare the model drug solution by dissolving 5 mg of a model drug in 0.5 ml of 2 % PVA solution.

(c) Mix the PLGA and drug solution into one of the 20 ml scintillation vials, and sonicate in an ice bath using a probe sonicator. Sonicate at 65 W for 90 s to form primary (W1/O) emulsion.

(d) Split the primary emulsion into two parts, mix each with 10 ml of 2 % PVA solution and sonicate over ice at 75 W for 90 s to form secondary (W1/O/W2) emulsions.

(e) Pour the two secondary emulsions together in one 250 ml glass beaker. Evaporate DCM by stirring overnight at 4 °C to form nanoparticles (NP).

(f) Pour the NP into a centrifuge tube. Centrifuge at 15,000 rpm for 30 min. After pellet has been formed, remove the supernatant and dispose it into a waste container. In order to remove

residual PVA, resuspend pellet in nanopure water by vigorous vortexing. Centrifuge at 15,000 rpm for 30 min. Repeat twice.

(g) Resuspend the NP in water and lyophilize in 10 % sucrose if required.

Notes:

(h) For preparing control NPs simply repeat above procedure without the drug.

(i) For preparing dye-loaded NPs add <0.5 mg of dye (e.g. Nile red) to the PLGA solution.

(j) Use a 3 mm probe for preparing the primary emulsion and 6 mm probe for secondary emulsion.

(k) Lyophilize particles at a concentration of 10–20 mg/ml. Lyophilized NPs can be stored at 20 °C for long-term storage. NPs in suspension should be stored 4C.

(l) Model drug – (water soluble) mitoxantrone.2HCl, doxorubicin. HCl etc.

9.6.3 Preparation of Liposomes for Drug Delivery

(a) Prepare solutions of 5 mg/mL of the lipid and co-lipid (DOPE and DOPC) using chloroform as the solvent.

(b) From these solutions place the volumes corresponding to 1:1 molar ratios of the cationic lipid and the colipid (DOPC or DOPE) in a glass vial.

(c) Remove the solvent by bubbling moisture free nitrogen gas through the organic solution, and keep the dried lipid film under high vacuum overnight.

(d) Add deionized water (1 mL) to the vacuum-dried lipid film, and allow the mixture to swell overnight.

(e) Vortex the vial for 2–3 min at room temperature and sonicate in a bath sonicator in order to generate multilamellar vesicles (MLVs). Sonicate the MLVs in an ice bath until clarity using a Branson 450 sonifier at 100 % duty cycle and 25 W output power.

(f) The resulting clear aqueous liposomes can now be used in multiple delivery applications.

(g) Note: Compatible drugs can be added in the chloroform step of the preparation.

References

1. Ingram VM (1957) Gene mutations in human haemoglobin: the chemical difference between normal and sickle cell haemoglobin. Nature 180:326–328
2. Initiative NN (2000) http://www.nano.gov/nanotech-101/what/definition
3. Feynman RP (1960) There's plenty of room at the bottom. Eng Sci 23:22–36
4. Hoffman AS, Stayton PS, Ei-Sayed MEH, Murthy N, Bulmus V, Lackey C et al (2007) Design of "Smart" nano-scale delivery systems for biomolecular therapeutics. J Biomed Nanotechnol 3:213–217
5. Mody VV, Siwale R, Singh A, Mody HR (2010) Introduction to metallic nanoparticles. J Pharm Bioallied Sci 2:282
6. Kelly KL, Coronado E, Zhao LL, Schatz GC (2003) The optical properties of metal nanoparticles: the influence of size, shape, and dielectric environment. J Phys Chem B 107:668–677
7. Zhong W (2009) Nanomaterials in fluorescence-based biosensing. Anal Bioanal Chem 394:47–59
8. Alshehri AH, Jakubowska M, Młożniak A, Horaczek M, Rudka D, Free C et al (2012) Enhanced electrical conductivity of silver nanoparticles for high frequency electronic applications. ACS Appl Mater Interfaces 4:7007–7010
9. Ortega RA (2010) A new model of iron oxide nanoparticle magnetic properties to guide design of novel nanomaterials. Vanderbilt University, Nashville
10. Buzea C, Pacheco II, Robbie K (2007) Nanomaterials and nanoparticles: sources and toxicity. Biointerphases 2:MR17–MR71
11. Roduner E (2006) Size matters: why nanomaterials are different. Chem Soc Rev 35:583–592
12. Bielecki S, Kalinowska H (2008) Biotechnological nanomaterials. Postepy Mikrobiologii 47:163–169
13. Torchilin VP, Trubetskoy VS, Whiteman KR, Caliceti P, Ferruti P, Veronese FM (1995) New synthetic amphiphilic polymers for steric protection of liposomes in vivo. J Pharm Sci 84:1049–1053
14. Weissig V, Whiteman KR, Torchilin VP (1998) Accumulation of protein-loaded long-circulating micelles and liposomes in subcutaneous Lewis lung carcinoma in mice. Pharm Res 15:1552–1556
15. Cervantes F, Cazin B, Simonnet J-T (1999) Nanoemulsion based on nonionic amphiphilic lipids and aminated silicones and uses. Google Patents: AU1998056451
16. Quina FH, Nassar PM, Bonilha JBS, Bales BL (1995) Growth of sodium dodecyl sulfate micelles with detergent concentration. J Phys Chem 99:17028–17031
17. Huang H-C, Barua S, Sharma G, Dey SK, Rege K (2011) Inorganic nanoparticles for cancer imaging and therapy. J Control Release 155:344–357
18. Huang H-C, Ramos J, Grandhi TSP, Potta T, Rege K (2010) Gold nanoparticles in cancer imaging and therapeutics. Nano LIFE (NL) 01:289–307
19. Park K (2013) Facing the truth about nanotechnology in drug delivery. ACS Nano 7:7442–7447
20. Bae YH, Park K (2011) Targeted drug delivery to tumors: myths, reality and possibility. J Control Release 153:198–205
21. Kwon G, Suwa S, Yokoyama M, Okano T, Sakurai Y, Kataoka K (1994) Enhanced tumor accumulation and prolonged circulation times of micelle-forming poly (ethylene oxide-aspartate) block copolymer-adriamycin conjugates. J Control Release 29:17–23
22. Torchilin VP (2004) Targeted polymeric micelles for delivery of poorly soluble drugs. Cell Mol Life Sci 61:2549–2559
23. Ma Z, Sui SF (2002) Naked-Eye sensitive detection of immunoglubulin G by enlargement of Au nanoparticles in vitro. Angew Chem Int Ed 41:2176–2179
24. Azzazy HME, Mansour MMH (2009) In vitro diagnostic prospects of nanoparticles. Clin Chim Acta 403:1–8
25. Kobayashi H, Brechbiel MW (2005) Nano-sized MRI contrast agents with dendrimer cores. Adv Drug Deliv Rev 57:2271–2286
26. Wang Y-XJ, Hussain SM, Krestin GP (2001) Superparamagnetic iron oxide contrast agents: physicochemical characteristics and applications in MR imaging. Eur Radiol 11:2319–2331
27. Jain TK, Richey J, Strand M, Leslie-Pelecky DL, Flask CA, Labhasetwar V (2008) Magnetic nanoparticles with dual functional properties: drug delivery and magnetic resonance imaging. Biomaterials 29:4012–4021
28. Stephens-Altus JS, West JL (2008) Nanotechnology for tissue engineering. In: Advances in tissue engineering. Imperial College Press, London, p 333
29. Anseth K. Nanotechnology in tissue engineering. American Institute of Chemical Engineers National Meeting, Cincinnati, November 2005
30. Khang D, Carpenter J, Chun YW, Pareta R, Webster TJ (2010) Nanotechnology for regenerative medicine. Biomed Microdevices 12:575–587
31. Sumer B, Gao J (2008) Theranostic nanomedicine for cancer. Nanomedicine 3:137–140
32. Park JH, von Maltzahn G, Ruoslahti E, Bhatia SN, Sailor MJ (2008) Micellar hybrid nanoparticles for simultaneous magnetofluorescent imaging and drug delivery. Angew Chem Int Ed Engl 120:7394–7398
33. Chandler D (2005) Interfaces and the driving force of hydrophobic assembly. Nature 437:640–647
34. Harada A, Kataoka K (1995) Formation of polyion complex micelles in an aqueous milieu from a

pair of oppositely-charged block copolymers with poly (ethylene glycol) segments. Macromolecules 28:5294–5299

35. Zhang J (2011) Novel emulsion-based delivery systems

36. Duncan R (2006) Polymer conjugates as anticancer nanomedicines. Nat Rev Cancer 6:688–701

37. Hu X, Jing X (2009) Biodegradable amphiphilic polymer-drug conjugate micelles

38. Lu J, Owen SC, Shoichet MS (2011) Stability of self-assembled polymeric micelles in serum. Macromolecules 44:6002–6008

39. Moghimi SM, Patel HM (1998) Serum-mediated recognition of liposomes by phagocytic cells of the reticuloendothelial system–the concept of tissue specificity. Adv Drug Deliv Rev 32:45–60

40. Liu J, Zeng F, Allen C (2005) Influence of serum protein on polycarbonate-based copolymer micelles as a delivery system for a hydrophobic anti-cancer agent. J Control Release 103:481–497

41. Greish K (2010) Enhanced permeability and retention (EPR) effect for anticancer nanomedicine drug targeting. Methods Mol Biol 624 25–37

42. Maeda H, Wu J, Sawa T, Matsumura Y, Hori K (2000) Tumor vascular permeability and the EPR effect in macromolecular therapeutics: a review. J Control Release 65:271–284

43. Maeda H, Fang J, Inutsuka T, Kitamoto Y (2003) Vascular permeability enhancement in solid tumor: various factors, mechanisms involved and its implications. Int Immunopharmacol 3:319–328

44. Li S-D, Huang L (2010) Stealth nanoparticles: high density but sheddable PEG is a key for tumor targeting. J Control Release 145:178

45. Unezaki S, Maruyama K, Hosoda J-I, Nagae I, Koyanagi Y, Nakata M et al (1996) Direct measurement of the extravasation of polyethyleneglycol-coated liposomes into solid tumor tissue by in vivo fluorescence microscopy. Int J Pharm 144:11–17

46. Danhier F, Feron O, Préat V (2010) To exploit the tumor microenvironment: passive and active tumor targeting of nanocarriers for anti-cancer drug delivery. J Control Release 148:135–146

47. Torchilin V (2011) Tumor delivery of macromolecular drugs based on the EPR effect. Adv Drug Deliv Rev 63:131–135

48. Torchilin VP (2005) Recent advances with liposomes as pharmaceutical Carriers. Nat Rev Drug Discov 4:145–160

49. Peters H (2001) Das Photoreaktionszentrum aus Rhodobacter sphaeroides als Modellmembranprotein zur Reinigung, Rekonstitution in Liposomen aus ungewöhnlichen Phospholipiden, Charakterisierung und heterologen Expression

50. Gregoriadis G (2006) Liposome technology, volume III: interactions of liposomes with the biological milieu: CRC press

51. Gregoriadis G (1984) Liposome technology. In: Incorporation of drugs, proteins and genetic material, 2nd edn. CRC Press, Boca Raton

52. Lasic DD (1993) Liposomes: from physics to applications. Elsevier, Amsterdam/New York

53. Small DM (1986) The physical chemistry of lipids. From alkanes to phospholipids, Handbook of lipid research. Plenum Press, New York

54. Szoka F Jr, Papahadjopoulos D (1980) Comparative properties and methods of preparation of lipid vesicles (liposomes). Annu Rev Biophys Bioeng 9:467–508

55. Redondo-Morata L, Giannotti MI, Sanz F (2012) Influence of cholesterol on the phase transition of lipid bilayers: a temperature-controlled force spectroscopy study. Langmuir 28:12851–12860

56. Mayer LD, Bally MB, Hope MJ, Cullis PR (1986) Techniques for encapsulating bioactive agents into liposomes. Chem Phys Lipids 40:333–345

57. Kirby C, Clarke J, Gregoriadis G (1980) Effect of the cholesterol content of small unilamellar liposomes on their stability >*in vivo* and *in vitro*. Biochem 186:591–598

58. Simon SA, McIntosh TJ, Latorre R (1982) Influence of cholesterol on water penetration into bilayers. Science 216:65–67

59. Simon SA, McIntosh TJ (1986) Depth of water penetration into lipid bilayers. Methods Enzymol 127:511–521

60. Crowe JH, Crowe LM, Carpenter JF, Wistrom CA (1987) Stabilization of dry phospholipid bilayers and proteins by sugars. Biochem J 242:1

61. Hu C-MJ, Aryal S, Zhang L (2010) Nanoparticle-assisted combination therapies for effective cancer treatment. Ther Deliv 1:323–334

62. Xu Y-M, Zhang S-B, Hu J-J, Liu D-L, Qiao W-H, Li Z-S (2004–2005) Liposomes for gene delivery. J Dalian Natl Univ

63. Lasic DD (1997) Liposomes in gene delivery. CRC Press, Boca Raton

64. Martins S, Sarmento B, Ferreira DC, Souto EB (2007) Lipid-based colloidal carriers for peptide and protein delivery–liposomes versus lipid nanoparticles. Int J Nanomedicine 2:595

65. Deissler V, Rüger R, Frank W, Fahr A, Kaiser WA, Hilger I (2008) Fluorescent liposomes as contrast agents for in vivo optical imaging of edemas in mice. Small 4:1240–1246

66. Safra T, Muggia F, Jeffers S, Tsao-Wei DD, Groshen S, Lyass O et al (2000) Pegylated liposomal doxorubicin (doxil): reduced clinical cardiotoxicity in patients reaching or exceeding cumulative doses of 500 mg/m^2. Ann Oncol 11:1029–1033

67. Mulder WJM, Strijkers GJ, Griffioen AW, van Bloois L, Molema G, Storm G et al (2004) A liposomal system for contrast-enhanced magnetic resonance imaging of molecular targets. Bioconjug Chem 15:799–806

68. Chen C-S, Yao J, Durst RA (2006) Liposome encapsulation of fluorescent nanoparticles: quantum dots and silica nanoparticles. J Nanopart Res 8:1033–1038

69. Woodle MC (1993) [67]Gallium-labeled liposomes with prolonged circulation: preparation and potential as nuclear imaging agents. Nucl Med Biol 20:149–155

70. Park JW, Hong K, Kirpotin DB, Colbern G, Shalaby R, Baselga J et al (2002) Anti-HER2 immunoliposomes enhanced efficacy attributable to targeted delivery. Clin Cancer Res 8:1172–1181

71. Maruyama K (2011) Intracellular targeting delivery of liposomal drugs to solid tumors based on EPR effects. Adv Drug Deliv Rev 63:161–169

72. Riaz M (1996) Liposomes preparation methods. Pak J Pharm Sci 19:65–77

73. Deamer D, Bangham AD (1976) Large volume liposomes by an ether vaporization method. Biochim Biophys Acta 443:629–634

74. Batzri S, Korn ED (1973) Single bilayer liposomes prepared without sonication. Biochim Biophys Acta 298:1015–1019

75. Szoka F, Papahadjopoulos D (1978) Procedure for preparation of liposomes with large internal aqueous space and high capture by reverse-phase evaporation. Proc Natl Acad Sci 75:4194–4198

76. Dua JS, Rana AC, Bhandari AK (2012) Liposomes methods of preparation and applications. Int J Pharm Stud Res 3:14–20

77. Crosasso P, Ceruti M, Brusa P, Arpicco S, Dosio F, Cattel L (2000) Preparation, characterization and properties of sterically stabilized paclitaxel-containing liposomes. J Control Release 63:19–30

78. Mayer LD, Bally MB, Cullis PR (1986) Uptake of adriamycin into large unilamellar vesicles in response to a pH gradient. Biochim Biophys Acta 857:123–126

79. Mayer LD, Tai LCL, Bally MB, Mitilenes GN, Ginsberg RS, Cullis PR (1990) Characterization of liposomal systems containing doxorubicin entrapped in response to pH gradients. Biochim Biophys Acta 1025:143–151

80. Li X, Hirsh DJ, Cabral-Lilly D, Zirkel A, Gruner SM, Janoff AS et al (1998) Doxorubicin physical state in solution and inside liposomes loaded via a pH gradient. Biochim Biophys Acta 1415:23–40

81. Haran G, Cohen R, Bar LK, Barenholz Y (1993) Transmembrane ammonium sulfate gradients in liposomes produce efficient and stable entrapment of amphipathic weak bases. Biochim Biophys Acta 1151:201–215

82. Gubernator J (2011) Active methods of drug loading into liposomes: recent strategies for stable drug entrapment and increased in vivo activity. Expert Opin Drug Deliv 8:565–580

83. Fritze A, Hens F, Kimpfler A, Schubert R, Peschka-Süss R (2006) Remote loading of doxorubicin into liposomes driven by a transmembrane phosphate gradient. Biochim Biophys Acta 1758:1633–1640

84. Drummond DC, Zignani M, Leroux J-C (2000) Current status of pH-sensitive liposomes in drug delivery. Prog Lipid Res 39:409–460

85. Al-Ahmady ZS, Al-Jamal WT, Bossche JV, Bui TT, Drake AF, Mason AJ et al (2012) Lipid–peptide vesicle nanoscale hybrids for triggered drug release by mild hyperthermia in vitro and in vivo. ACS Nano 6:9335–9346

86. Basel MT, Shrestha TB, Troyer DL, Bossmann SH (2011) Protease-sensitive, polymer-caged liposomes: a method for making highly targeted liposomes using triggered release. ACS Nano 5:2162–2175

87. Schroeder A, Kost J, Barenholz Y (2009) Ultrasound, liposomes, and drug delivery: principles for using ultrasound to control the release of drugs from liposomes. Chem Phys Lipids 162:1–16

88. Brody EN, Gold L (2000) Aptamers as therapeutic and diagnostic agents. Rev Mol Biotechnol 74:5–13

89. Janssen A, Schiffelers RM, Ten Hagen TLM, Koning GA, Schraa AJ, Kok RJ et al (2003) Peptide-targeted PEG-liposomes in anti-angiogenic therapy. Int J Pharm 254:55–58

90. Huang A, Huang L, Kennel SJ (1980) Monoclonal antibody covalently coupled with fatty acid. A reagent for in vitro liposome targeting. J Biol Chem 255:8015–8018

91. Dattagupta N, Das AR, Sridhar CN, Patel JR (1998) Method for the intracellular delivery of biomolecules using liposomes containing cationic lipids and vitamin D. Google Patents: US 5711964 A

92. Dass CR (2008) Drug delivery in cancer using liposomes. Methods Mol Biol 437:177–182

93. Balazs DA, Godbey WT (2010) Liposomes for use in gene delivery. J Drug Deliv 2011:326497

94. Weiner AL (1994) Liposomes for protein delivery: selecting manufacture and development processes. Immunomethods 4:201–209

95. Saul JM, Annapragada AV, Bellamkonda RV (2006) A dual-ligand approach for enhancing targeting selectivity of therapeutic nanocarriers. J Control Release 114:277–287

96. Yang F-Y, Wong T-T, Teng M-C, Liu R-S, Lu M, Liang H-F et al (2012) Focused ultrasound and interleukin-4 receptor-targeted liposomal doxorubicin for enhanced targeted drug delivery and antitumor effect in glioblastoma multiforme. J Control Release 160:652–658

97. Meng S, Su B, Li W, Ding Y, Tang L, Zhou W et al (2010) Enhanced antitumor effect of novel dual-targeted paclitaxel liposomes. Nanotechnology 21:415103

98. Straubinger RM, Hong K, Friend DS, Papahadjopoulos D (1983) Endocytosis of liposomes and intracellular fate of encapsulated molecules: encounter with a low pH compartment after internalization in coated vesicles. Cell 32:1069–1079

99. Torchilin V (2008) Intracellular delivery of protein and peptide therapeutics. Drug Discov Today Technol 5:e95–e103

100. Mizuguchi H, Nakanishi M, Nakanishi T, Nakagawa T, Nakagawa S, Mayumi T (1996) Application of fusogenic liposomes containing fragment A of diphtheria toxin to cancer therapy. Br J Cancer 73:472

101. Kunisawa J, Nakagawa S, Mayumi T (2001) Pharmacotherapy by intracellular delivery of drugs using fusogenic liposomes: application to vaccine development. Adv Drug Deliv Rev 52:177–186

102. Kunisawa J, Masuda T, Katayama K, Yoshikawa T, Tsutsumi Y, Akashi M et al (2005) Fusogenic liposome delivers encapsulated nanoparticles for cytosolic controlled gene release. J Control Release 105:344–353

103. Rückert P, Bates SR, Fisher AB (2003) Role of clathrin-and actin-dependent endocytotic pathways in lung phospholipid uptake. Am J Physiol Lung Cell Mol Physiol 284:L981–L989

104. Simões S, Moreira JN, Fonseca C, Düzgüneş N, Pedroso de Lima MC (2004) On the formulation of pH-sensitive liposomes with long circulation times. Adv Drug Deliv Rev 56:947–965

105. Romberg B, Hennink WE, Storm G (2008) Sheddable coatings for long-circulating nanoparticles. Pharm Res 25:55–71

106. Guo X, Szoka FC (2001) Steric stabilization of fusogenic liposomes by a low-pH sensitive PEG-diortho ester-lipid conjugate. Bioconjug Chem 12:291–300

107. Metalloprotease M (2012) 2-Responsive multifunctional liposomal nanocarrier for enhanced tumor targeting Zhu, Lin; Kate, Pooja; Torchilin, Vladimir P. ACS Nano 6:3491–3498

108. Zhu L, Kate P, Torchilin VP (2012) Matrix metalloprotease 2-responsive multifunctional liposomal nanocarrier for enhanced tumor targeting. ACS Nano 6:3491–3498

109. O'Brien MER, Wigler N, Inbar M, Rosso R, Grischke E, Santoro A et al (2004) Reduced cardiotoxicity and comparable efficacy in a phase III trial of pegylated liposomal doxorubicin HCl (CAELYX (TM)/Doxil (R)) versus conventional doxorubicin for first-line treatment of metastatic breast cancer. Ann Oncol 15:440–449

110. Barenholz YC (2012) Doxil®—the first fda-approved nano-drug: lessons learned. J Control Release 160:117–134

111. Lipshultz SE, Colan SD, Gelber RD, Perez-Atayde AR, Sallan SE, Sanders SP (1991) Late cardiac effects of doxorubicin therapy for acute lymphoblastic leukemia in childhood. N Engl J Med 324:808–815

112. Rahman A, More N, Schein PS (1982) Doxorubicin-induced chronic cardiotoxicity and its protection by liposomal administration. Cancer Res 42:1817–1825

113. Working PK, Newman MS, Huang SK, Mayhew E, Vaage J, Lasic DD (1994) Pharmacokinetics, Biodistribution and therapeutic efficacy of doxorubicin encapsulated in Stealth® liposomes (Doxil®). J Liposome Res 4:667–687

114. Meyerhoff A (1999) US Food and Drug Administration approval of Am Bisome (liposomal amphotericin B) for treatment of visceral leishmaniasis. Clin Infect Dis 28:42–48

115. Forssen EA, Ross ME (1994) Daunoxome® treatment of solid tumors: preclinical and clinical investigations. J Liposome Res 4:481–512

116. Burgess DJ, Hussain AS, Ingallinera TS, Chen M-L (2002) Assuring quality and performance of sustained and controlled release parenterals: AAPS workshop report, co-sponsored by FDA and USP. Pharm Res 19:1761–1768

117. Chang H-I, Yeh M-K (2012) Clinical development of liposome-based drugs: formulation, characterization, and therapeutic efficacy. Int J Nanomedicine 7:49

118. Kim S, Shi YZ, Kim JY, Park K, Cheng JX (2010) Overcoming the barriers in micellar drug delivery: loading efficiency, in vivo stability, and micelle-cell interaction. Expert Opin Drug Deliv 7:49–62

119. Förster S, Konrad M (2003) From self-organizing polymers to nano-and biomaterials. J Mater Chem 13:2671–2688

120. Zhang N, Wardwell PR, Bader RA (2013) Polysaccharide-based micelles for drug delivery. Pharmaceutics 5:329–352

121. Kataoka K, Harada A, Nagasaki Y (2012) Block copolymer micelles for drug delivery: design, characterization and biological significance. Adv Drug Deliv Rev 47(1):113–131

122. Tanford C (1978) Hydrophobic effect and organization of living matter. Science 200:1012–1018

123. Corkill JM, Goodman JF, Harrold SP (1964) Thermodynamics of micellization of non-ionic detergents. Trans Faraday Soc 60:202–207

124. Bae YH, Yin H (2008) Stability issues of polymeric micelles. J Control Release 131:2–4

125. Kim S, Park K (2010) 19 Polymer micelles for drug delivery. Targeted delivery of small and macromolecular drugs. CRC Press

126. Xu W, Ling P, Zhang T (2013) Polymeric micelles, a promising drug delivery system to enhance bioavailability of poorly water-soluble drugs. J Drug Deliv 2013:340315

127. Torchilin VP (2001) Structure and design of polymeric surfactant-based drug delivery systems. J Control Release 73:137–172

128. van Vlerken LE, Vyas TK, Amiji MM (2007) Poly (ethylene glycol)-modified nanocarriers for tumor-targeted and intracellular delivery. Pharm Res 24:1405–1414

129. Chiappetta DA, Sosnik A (2007) Poly (ethylene oxide)–poly (propylene oxide) block copolymer micelles as drug delivery agents: improved hydro-solubility, stability and bioavailability of drugs. Eur J Pharm Biopharm 66:303–317

130. Letchford K, Liggins R, Burt H (2008) Solubilization of hydrophobic drugs by methoxy poly(ethylene glycol)-block-polycaprolactone diblock copolymer micelles: theoretical and experimental data and correlations. J Pharm Sci 97:1179–1190

131. Deng LD, Li AG, Yao CM, Sun DX, Dong AJ (2005) Methoxy poly(ethylene glycol)-b-poly(L-lactic acid) copolymer nanoparticles as delivery vehicles for paclitaxel. J Appl Polym Sci 98:2116–2122

132. Gill KK, Nazzal S, Kaddoumi A (2011) Paclitaxel loaded PEG(5000)-DSPE micelles as pulmonary delivery platform: formulation characterization, tissue distribution, plasma pharmacokinetics, and toxicological evaluation. Eur J Pharm Biopharm 79:276–284

133. Knop K, Hoogenboom R, Fischer D, Schubert US (2010) Poly (ethylene glycol) in drug delivery: pros and cons as well as potential alternatives. Angew Chem Int Ed 49:6288–6308

134. Jeong JH, Kim SW, Park TG (2003) Novel intracellular delivery system of antisense oligonucleotide by self-assembled hybrid micelles composed of DNA/PEG conjugate and cationic fusogenic peptide. Bioconjug Chem 14:473–479

135. Gaucher G, Dufresne MH, Sant VP, Kang N, Maysinger D, Leroux JC (2005) Block copolymer

micelles: preparation, characterization and application in drug delivery. J Control Release 109: 169–188

136. Ko J, Park K, Kim Y-S, Kim MS, Han JK, Kim K et al (2007) Tumoral acidic extracellular pH targeting of pH-responsive MPEG-poly (β-amino ester) block copolymer micelles for cancer therapy. J Control Release 123:109–115

137. Wu XL, Kim JH, Koo H, Bae SM, Shin H, Kim MS et al (2010) Tumor-targeting peptide conjugated pH-responsive micelles as a potential drug carrier for cancer therapy. Bioconjug Chem 21:208–213

138. Zhang X, Jackson JK, Burt HM (1996) Development of amphiphilic diblock copolymers as micellar carriers of taxol. Int J Pharm 132:195–206

139. Elsabahy M, Perron M-È, Bertrand N, Yu GE, Leroux J-C (2007) Solubilization of docetaxel in poly (ethylene oxide)-block-poly (butylene/styrene oxide) micelles. Biomacromolecules 8:2250–2257

140. Thambi T, Yoon HY, Kim K, Kwon IC, Yoo CK, Park JH (2011) Bioreducible block copolymers based on poly (ethylene glycol) and poly (γ-benzyl L-glutamate) for intracellular delivery of camptothecin. Bioconjug Chem 22:1924–1931

141. Taylor DJ, Parsons CE, Han HY, Jayaraman A, Rege K (2011) Parallel screening of FDA-approved antineoplastic drugs for identifying sensitizers of TRAIL-induced apoptosis in cancer cells. BMC Cancer 11:470

142. Zhao X, Poon Z, Engler AC, Bonner DK, Hammond PT (2012) Enhanced stability of polymeric micelles based on postfunctionalized poly (ethylene glycol)-b-poly (γ-propargyl l-glutamate): the substituent effect. Biomacromolecules 13:1315–1322

143. Xu P, Tang H, Li S, Ren J, Van Kirk E, Murdoch WJ et al (2004) Enhanced stability of core-surface cross-linked micelles fabricated from amphiphilic brush copolymers. Biomacromolecules 5:1736–1744

144. Kataoka K, Matsumoto T, Yokoyama M, Okano T, Sakurai Y, Fukushima S et al (2000) Doxorubicin-loaded poly (ethylene glycol)–poly (β-benzyl-l-aspartate) copolymer micelles: their pharmaceutical characteristics and biological significance. J Control Release 64:143–153

145. La SB, Okano T, Kataoka K (1996) Preparation and characterization of the micelle-forming polymeric drug indomethacin-incorporated poly (ethylene oxide)–poly (β-benzyl L-aspartate) block copolymer micelles. J Pharm Sci 85:85–90

146. Huh KM, Lee SC, Cho YW, Lee J, Jeong JH, Park K (2005) Hydrotropic polymer micelle system for delivery of paclitaxel. J Control Release 101: 59–68

147. Lee J, Lee SC, Acharya G, Chang CJ, Park K (2003) Hydrotropic solubilization of paclitaxel: analysis of chemical structures for hydrotropic property. Pharm Res 20:1022–1030

148. Lee SC, Huh KM, Lee J, Cho YW, Galinsky RE, Park K (2007) Hydrotropic polymeric micelles for enhanced paclitaxel solubility: in vitro and in vivo characterization. Biomacromolecules 8:202–208

149. Shuai XT, Merdan T, Schaper AK, Xi F, Kissel T (2004) Core-cross-linked polymeric micelles as paclitaxel carriers. Bioconjug Chem 15:441–448

150. Tian L, Yam L, Wang J, Tat H, Uhrich KE (2004) Core crosslinkable polymeric micelles from PEG–lipid amphiphiles as drug carriers. J Mater Chem 14:2317–2324

151. Yokoyama M, Kwon GS, Okano T, Sakurai Y, Seto T, Kataoka K (1992) Preparation of micelle-forming polymer-drug conjugates. Bioconjug Chem 3:295–301

152. Masayuki Y, Mizue M, Noriko Y, Teruo O, Yasuhisa S, Kazunori K et al (1990) Polymer micelles as novel drug carrier: adriamycin-conjugated poly (ethylene glycol)-poly (aspartic acid) block copolymer. J Control Release 11:269–278

153. Yokoyama M, Miyauchi M, Yamada N, Okano T, Sakurai Y, Kataoka K et al (1990) Characterization and anticancer activity of the micelle-forming polymeric anticancer drug adriamycin-conjugated poly(ethylene glycol)-poly(aspartic acid) block copolymer. Cancer Res 50:1693–1700

154. Yokoyama M, Fukushima S, Uehara R, Okamoto K, Sakurai Y, Okano T (1998) Characterization of physical entrapment and chemical conjugation of adriamycin in polymeric micelles and their design for in vivo delivery to a solid tumor. J Control Release 50:79–92

155. Gullotti E, Yeo Y (2009) Extracellularly activated nanocarriers: a new paradigm of tumor targeted drug delivery. Mol Pharm 6:1041–1051

156. Bae YH (2009) Drug targeting and tumor heterogeneity. J Control Release 133:2

157. Cabral H, Matsumoto Y, Mizuno K, Chen Q, Murakami M, Kimura M et al (2011) Accumulation of sub-100 nm polymeric micelles in poorly permeable tumours depends on size. Nat Nanotechnol 6:815–823

158. Netti PA, Roberge S, Boucher Y, Baxter LT, Jain RK (1996) Effect of transvascular fluid exchange on pressure–flow relationship in tumors: a proposed mechanism for tumor blood flow heterogeneity. Microvasc Res 52:27–46

159. Heldin C-H, Rubin K, Pietras K, Östman A (2004) High interstitial fluid pressure—an obstacle in cancer therapy. Nat Rev Cancer 4:806–813

160. Hong R-L, Huang C-J, Tseng Y-L, Pang VF, Chen S-T, Liu J-J et al (1999) Direct comparison of liposomal doxorubicin with or without polyethylene glycol coating in C-26 tumor-bearing mice is surface coating with polyethylene glycol beneficial? Clin Cancer Res 5:3645–3652

161. Torchilin VP (2010) Passive and active drug targeting: drug delivery to tumors as an example. Handb Exp Pharmacol 197:3–53

162. Zwicke GL, Mansoori GA, Jeffery CJ (2012) Utilizing the folate receptor for active targeting of cancer nanotherapeutics. Nano Rev 3

163. Sudimack J, Lee RJ (2000) Targeted drug delivery via the folate receptor. Adv Drug Deliv Rev 41:147–162

164. Noh T, Kook YH, Park C, Youn H, Kim H, Oh ET et al (2008) Block copolymer micelles conjugated with anti-EGFR antibody for targeted delivery of anticancer drug. J Polym Sci Part A Polym Chem 46:7321–7331

165. Han X, Liu J, Liu M, Xie C, Zhan C, Gu B et al (2009) 9-NC-loaded folate-conjugated polymer micelles as tumor targeted drug delivery system: preparation and evaluation in vitro. Int J Pharm 372:125–131

166. Liang X-J, Wei T, Liu J, Ma H, Cheng Q, Huang Y et al (2013) Functionalized nanoscale micelles improve the drug delivery for cancer in vitro and in vivo. Nano Lett 13(6):2528–2534

167. Wu YL, Chen W, Meng FH, Wang ZJ, Cheng R, Deng C et al (2012) Core-crosslinked pH-sensitive degradable micelles: a promising approach to resolve the extracellular stability versus intracellular drug release dilemma. J Control Release 164:338–345

168. Yang M, Ding Y, Zhang L, Qian X, Jiang X, Liu B (2007) Novel thermosensitive polymeric micelles for docetaxel delivery. J Biomed Mater Res A 81:847–857

169. Lee GY, Park K, Kim SY, Byun Y (2007) MMPs-specific PEGylated peptide–DOX conjugate micelles that can contain free doxorubicin. Eur J Pharm Biopharm 67:646–654

170. Bae Y, Nishiyama N, Kataoka K (2007) In vivo anti-tumor activity of the folate-conjugated pH-sensitive polymeric micelle selectively releasing adriamycin in the intracellular acidic compartments. Bioconjug Chem 18:1131–1139

171. Gao Z-G, Tian L, Hu J, Park I-S, Bae YH (2011) Prevention of metastasis in a 4T1 murine breast cancer model by doxorubicin carried by folate conjugated pH sensitive polymeric micelles. J Control Release 152:84–89

172. Hamaguchi T, Kato K, Yasui H, Morizane C, Ikeda M, Ueno H et al (2007) A phase I and pharmacokinetic study of NK105, a paclitaxel-incorporating micellar nanoparticle formulation. Br J Cancer 97:170–176

173. Danson S, Ferry D, Alakhov V, Margison J, Kerr D, Jowle D et al (2004) Phase I dose escalation and pharmacokinetic study of pluronic polymer-bound doxorubicin (SP1049C) in patients with advanced cancer. Br J Cancer 90:2085–2091

174. Lee KS, Chung HC, Im SA, Park YH, Kim CS, Kim S-B et al (2008) Multicenter phase II trial of Genexol-PM, a Cremophor-free, polymeric micelle formulation of paclitaxel, in patients with metastatic breast cancer. Breast Cancer Res Treat 108:241–250

175. Saif MW, Podoltsev NA, Rubin MS, Figueroa JA, Lee MY, Kwon J et al (2010) Phase II clinical trial of paclitaxel loaded polymeric micelle in patients with advanced pancreatic cancer. Cancer Invest 28:186–194

176. Weiss RB, Donehower RC, Wiernik PH, Ohnuma T, Gralla RJ, Trump DL et al (1990) Hypersensitivity reactions from taxol. J Clin Oncol 8:1263–1268

177. Sissung TM, Mross K, Steinberg SM, Behringer D, Figg WD, Sparreboom A et al (2006) Association of ABCB1 genotypes with paclitaxel-mediated peripheral neuropathy and neutropenia. Eur J Cancer 42:2893–2896

178. Lü J-M, Wang X, Marin-Muller C, Wang H, Lin PH, Yao Q et al (2009) Current advances in research and clinical applications of PLGA-based nanotechnology. 2009. Expert Rev Mol Diagn 9(4):325–41

179. Zambaux MF, Bonneaux F, Gref R, Maincent P, Dellacherie E, Alonso MJ et al (1998) Influence of experimental parameters on the characteristics of poly (lactic acid) nanoparticles prepared by a double emulsion method. J Control Release 50:31–40

180. Avgoustakis K (2004) Pegylated poly (lactide) and poly (lactide-co-glycolide) nanoparticles: preparation, properties and possible applications in drug delivery. Curr Drug Deliv 1:321–333

181. Yoo HS, Park TG (2004) Folate receptor targeted biodegradable polymeric doxorubicin micelles. J Control Release 96:273–283

182. Panyam J, Labhasetwar V (2003) Biodegradable nanoparticles for drug and gene delivery to cells and tissue. Adv Drug Deliv Rev 55(3):329–347

183. Dhar S, Gu FX, Langer R, Farokhzad OC, Lippard SJ (2008) Targeted delivery of cisplatin to prostate cancer cells by aptamer functionalized Pt (IV) prodrug-PLGA–PEG nanoparticles. Proc Natl Acad Sci 105:17356–17361

184. Huang H-C, Yang Y, Nanda A, Koria P, Rege K (2011) Synergistic administration of photothermal therapy and chemotherapy to cancer cells using polypeptide-based degradable plasmonic matrices. Nanomedicine 6:459–473

185. Park JH, von Maltzahn G, Ong LL, Centrone A, Hatton TA, Ruoslahti E et al (2010) Cooperative nanoparticles for tumor detection and photothermally triggered drug delivery. Adv Mater 22:880–885

186. Von Maltzahn G, Park J-H, Lin KY, Singh N, Schwöppe C, Mesters R et al (2011) Nanoparticles that communicate in vivo to amplify tumour targeting. Nat Mater 10:545–552

187. Ashley CE, Carnes EC, Phillips GK, Padilla D, Durfee PN, Brown PA et al (2011) The targeted delivery of multicomponent cargos to cancer cells by nanoporous particle-supported lipid bilayers. Nat Mater 10:389–397

188. Wong C, Stylianopoulos T, Cui J, Martin J, Chauhan VP, Jiang W et al (2011) Multistage nanoparticle delivery system for deep penetration into tumor tissue. Proc Natl Acad Sci 108:2426–2431

189. Mitragotri S, Barua S (2013) Synergistic targeting of cell membrane, cytoplasm and nucleus of cancer cells using rod-shaped nanoparticles. ACS Nano 7(11):9558–9570

190. Kipp JE (2004) The role of solid nanoparticle technology in the parenteral delivery of poorly water-soluble drugs. Int J Pharm 284:109–122

191. Schroeder A, Goldberg MS, Kastrup C, Wang Y, Jiang S, Joseph BJ et al (2012) Remotely activated protein-producing nanoparticles. Nano Lett 12:2685–2689

Preparation of Nanoscale Pulmonary Drug Delivery Formulations by Spray Drying

10

Adam Bohr, Christian A. Ruge, and Moritz Beck-Broichsitter

Contents

Adam Bohr and Christian A. Ruge are contributed equally to this work.

A. Bohr, PhD • C.A. Ruge, PhD
M. Beck-Broichsitter, PhD (✉)
Faculté de Pharmacie,
Institut Galien, Université Paris-Sud,
5 rue J.B. Clément,
Châtenay-Malabry F-92296, France
e-mail: moritz.beck-broichsitter@u-psud.fr

Abstract

Advances in preparation technologies for nanomedicines have provided novel formulations for pulmonary drug delivery. Application of drugs via the lungs can be considered as one of the most attractive implementations of nanoparticles for therapeutic use due to the unique anatomy and physiology of the lungs. The colloidal nature of nanoparticles provides important advantages to the formulation of drugs, which are normally difficult to administer due to poor stability or uptake, partly because nanoparticles protect the drug from the physiological milieu, facilitate transport across biological barriers and can offer controlled drug release. There are numerous methods for producing therapeutic nanoparticles, each with their own advantages and suitable application. Liquid atomization techniques such as spray drying can produce nanoparticle formulations in a dry powder form suitable for pulmonary administration in a direct one-step process. This chapter describes the different state-of-the-art techniques used to prepare drug nanoparticles (with special emphasize on spray drying techniques) and the strategies for administering such unique formulations to the pulmonary environment.

10.1　Introduction

Recent progress in nanomedicine and nanotechnology has re-established an interest in the lungs as an attractive route for both local and systemic delivery of drugs. The lungs provide an excellent portal of entry for drugs to the body, as they bear a large (~100 m^2) but also thin (down to 0.1 μm) absorptive surface area, allowing for both efficient and fast mass transport from the air to the blood side, and consequently rapid onset of the desired pharmacological effect [1, 2]. Pulmonary drug administration is particularly attractive for local treatment of pathophysiological conditions affecting the lungs, such as chronic obstructive pulmonary disease (COPD), asthma and cystic fibrosis. These diseases lack effective treatment with high specificity to the lungs. By going directly via the airways one avoids first-pass metabolism by the hepatic system presumably achieving higher bioavailability and avoiding side effects that may result from systemic drug administration. Even for systemic drug administration the pulmonary route presents a rapid pathway in comparison with oral administration with fewer barriers for drug uptake and possibly higher bioavailability for drugs with low permeability such as biomacromolecules [3].

The lungs can be accessed using a variety of formulations in liquid or solid state in combination with administration devices including nebulizers, metered dose and dry powder inhalers. Here, nanoparticles and other nano-sized carriers can provide certain advantages compared to conventional milled powders at the micro-scale [4]. Many drugs are poorly water-soluble and may not dissolve well once deposited on the lung lining fluid (LLF). Nanoparticles dissolve much faster due to their higher surface area-to-volume ratio. Some drugs also benefit from being protected from the external environment and from being transported into or through the cells via nanocarriers to perform their intended effect in the lung tissue or elsewhere in the body. This typically necessitates that the vehicles are as small as possible, as the cellular internalization of particulate matter is inversely related to its diameter [5]. An overview of therapeutic nanoparticles for

systemic and local application is given in comprehensive reviews by Sung et al. [4] and Yang et al. [6].

Many preparation techniques have been suggested and investigated for the preparation of pure drug and drug-loaded nanoparticles. Furthermore, pulmonary administration of dry powder formulations is considered advantageous as dry powder inhaler devices can be used, but especially due to the higher stability of the solid state form. In order to produce a dry powder formulation of the nanoparticles, they must be either dried via lyophilization or produced in dry conditions. Production of dry nanoparticle powder can be achieved via different atomization processes including the spray drying process [7].

This chapter will elucidate the key points in pulmonary delivery of drug nanoparticles by introduction to the lung physiology and resulting biopharmaceutical challenges, describe various techniques for preparing drug nanoparticles and drug loaded nanoparticles, the deposition pattern of inhaled particulate matter and the production of aerosols comprising both individual and embedded nanoparticles. Moreover, common preclinical models (i.e. cell culture and organ models) to evaluate the potential lung-delivered nanoparticulate formulations will be briefly discussed.

10.2　Morphology of the Human Lungs

An illustrative approach to understand the macroscopic anatomy and structure of the lungs is to compare this organ to an inverted tree: where the trachea and bronchi can be compared to the trunk and branches, and the sac-like structures at the end of the airways, i.e. the alveoli, represent the leaves. The main functions of the lungs are the exchange of oxygen against carbon dioxide, and the regulation of the systemic pH. To fulfill this pivotal role, the lungs can be divided into two functional parts: a conducting and a respiratory zone (Fig. 10.1).

The conducting zone – also referred to as the airways – comprises the tubular trachea, the bronchi, and the bronchioles, which consist of
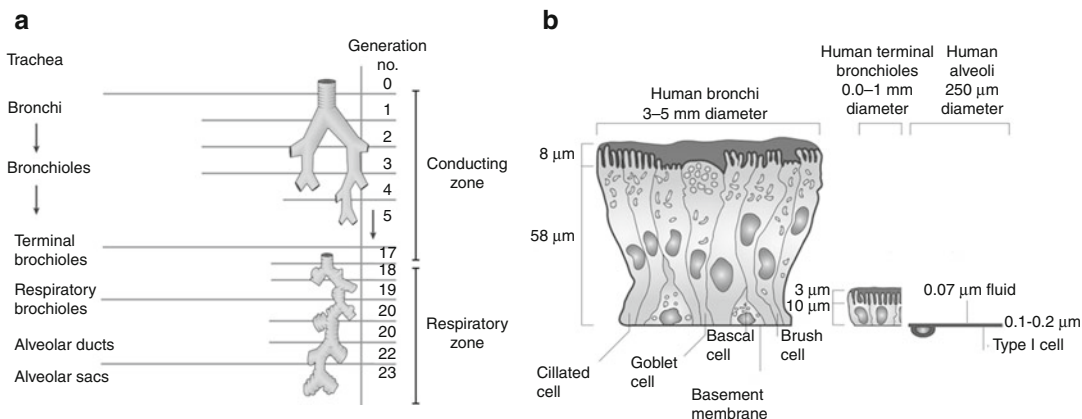
Fig. 10.1 Airway structures and morphology of the human lung. (**a**) From trachea to the alveoli, the bronchi and bronchioles bifurcate approximately 23 times, resulting in an increase of the surface area from 2–3 m^2 to ~100 m^2. This surface enlargement causes the previously accelerated inspired air (conducting zone) to slow down until diffusion only (respiratory zone) in order to facilitate the gas exchange. (**b**) From the central (i.e. airways) to the peripheral lung (i.e. alveoli), the lung epithelium changes not only in the type of cells that form the air-blood-barrier, but also becomes ultra-thin. Due to the large surface area and the ultra-thin epithelial barrier, the alveoli are the main region to target in pulmonary drug delivery (Reproduced with permission from Patton and Byron [1])

many generations of bifurcations. The main functions of this region are acceleration, heating, humidification, and filtration of the inspired air, in which the nose contributes importantly to the latter function. The trachea (generation 0) bifurcates into two main bronchi, which enter the right and left lung lobe. The main bronchi then bi- and also trifurcate into smaller bronchi and bronchioles, until the terminal bronchioles appear to show sac-like structures (approximately generation 16–17). With these so-called respiratory bronchioles begins the gas-exchanging respiratory zone (generation 17–23), which mainly comprises the alveolar ducts and alveolar sacs (i.e. alveoli; approximately 500 million per adult lung).

Whereas the cross-sectional surface of the airways (generation 0–16) is only a few square meters, the surface area increases exponentially in the alveolar region (generation 17–23) to about 75–140 m^2 [8]. Via the conducting zone, the inspired air is rapidly transported from the central to the peripheral lung by turbulent and laminar flow, while it is decelerated to diffusive movement in the transition to the respiratory zone to facilitate the gas exchange [9]. The 23 bifurcations from the trachea down to the alveoli,

combined with the changing air velocities, represent a very efficient system to filter out inhaled particulate matter. These barriers need to be overcome in order to efficiently administer particulate drug formulations to the respiratory tract.

Along the bronchial tree, the morphology of the epithelial barrier that lines the pulmonary surfaces changes significantly. In the airways, the lung epithelium represents a pseudostratified columnar epithelium, mainly consisting of ciliated epithelial cells, but also goblet cells and other secretory cells, as well as basal cells, which are considered as progenitor cells of the afore mentioned cell types. Further down towards the deep lung, the epithelium gradually becomes thinner. In the small airways (bronchioles, and terminal bronchioles), the cell layer has a thickness of about 2–10 μm, while the epithelial is less often ciliated and more of a cuboidal shape. Furthermore, club cells (formerly known as Clara-cells) are present in the region of the lungs, which can be considered as non-ciliated secretory cells, whose function is secretion of protective proteins, detoxification as well as regeneration of the airways epithelium [1, 10–12].

In the alveolar region, the pulmonary epithelium becomes as thin as 0.1 μm, and is mainly

formed by alveolar type I cells. Although these ultra-thin cells cover more than 90 % of the alveolar surface area, they account for less than 10 % of the alveolar cell population. Besides type I there are also type II cells, which resemble only about 7 % of the surface area, but are almost twice as numerous, compared to type I cells (approximately 16 % of the cell population) [11, 13]. Although type II cells can be considered the progenitor of type I cells and can replace them, their main function is the secretion of pulmonary surfactant, a complex lipo-protein mixture, whose main function is to reduce the surface tension at the air-liquid interface in order to prevent the alveoli from collapsing [14].

Besides immobilized epithelial cells, there are also mobile cells such as macrophages present, which patrol the pulmonary surfaces and phagocytize foreign materials that are deposited. The alveolar macrophage is probably the most important surface macrophage in the lungs and approximately 12–14 alveolar macrophages can be found per alveolus. These highly active phagocytic cells can efficiently sequester biological or non-biological foreign (particulate) matter that deposits in the alveolar region of the lungs. Hereby, they represent the most important clearance mechanism of the deep lungs, and contribute to the sterility of the respiratory zone [15, 16].

10.2.1 Biopharmaceutical Challenges for Inhaled Therapeutics

The air-blood-barrier does not only consist of cellular elements, but features also non-cellular elements, which especially play an important role for the fate of inhaled particulate matter. Overall, the pulmonary surfaces are covered with a liquid layer (the LLF), which however, differs significantly depending on the lung region.

Nevertheless, the components of the LLF are the first biological matter an inhaled particle interacts with after deposition, and can therefore, tremendously influence its biological fate in the lungs. It could be shown that particles that deposit on the LLF will be immersed into the liquid

phase due to surface forces, regardless of their surface chemistry [17, 18]. There is no way for deposited particles to circumvent the interaction with the LLF and its components, for which reason this system will be discussed here in more detail.

In the airways, the bronchial epithelium is covered by pulmonary mucus, a several micrometer thick viscoelastic complex fluid, which is produced and secreted by goblet cells and mainly consists of water and hydrated glycoproteins (mucins). According to current models and opinions, the mucus layer rests on a less viscous periciliary layer [3, 19]. The ciliated cells underneath the mucus blanket beat in a coordinated manner with a frequency of 3–12 Hz, resulting in a directed and ascending transport of the mucus [1, 20]. This mucociliary clearance (also referred to as the mucociliary escalator) is a very efficient system to transport most of the particulate matter that deposits in the airways out of the respiratory tract, and therefore, represents the second important clearance mechanism (besides macrophage clearance) that plays an important role in the fate of inhaled particles.

In this regard, the available liquid volume plays an important role: as LLF only has a total volume of about 15–70 ml, the dissolution kinetics of a particle affect whether it can be absorbed by the epithelium, or is cleared as a non-dissolved particle. If a particle dissolves immediately upon deposition, the molecules can of course diffuse along the water pores towards the epithelial surface following a concentration gradient [5, 21, 22]. If trapped on the mucus layer, the particles will be transported out of the lungs within 24–48 h, and eventually swallowed and processed in the gastro-intestinal tract [6, 22]. Hence, one of the challenges in particle engineering is the design of mucus-penetrating systems that can at least partially circumvent this clearance mechanism. In this respect, nanoparticles are a most promising technological approach, as they can be produced in a size-range smaller than the aqueous pores of mucus, allowing them to penetrate this barrier towards the epithelial surfaces. However, recent studies demonstrated that the

success of mucus-penetration significantly depends on the surface properties of the used nanoparticles, in order to assure minimal interaction with the mucin network [23–25].

In the alveolar region of the lungs, the epithelium is covered by the alveolar lining layer, which is profoundly different from mucus, as it is continuous (different from mucus, which has a rather patch-like appearance) and much thinner (average thickness of 0.02–0.08 μm) [26]. The major component of the alveolar lining layer is pulmonary surfactant, which consists of about 90 % lipids (mainly phospholipids), and 10 % protein of which four specific surfactant proteins (SP) are known (SP-A, -B, -C, and -D) [14, 27]. Due to its localization at the air-liquid interface, the pulmonary surfactant system reduces the surface tension and essentially contributes to the maintenance of the alveolar architecture, and is therefore essential for proper lung function. However, besides this biophysical function, some pulmonary surfactant components – namely SP-A and SP-D – act as opsonins and help alveolar macrophages to phagocytize foreign materials.

As mentioned before, alveolar macrophages account for the main clearance pathway of particles from the alveolar region of the lungs. Undissolved particles are efficiently sequestered in alveolar macrophages and phagocytosis takes place for particles in the size range between 0.2 and 5–6 μm [6, 15]. A fact that is often neglected is the complex interplay between pulmonary surfactant and alveolar macrophages. While some SP enhance the uptake of particulate matter by alveolar macrophages, phospholipids (the major constituent of surfactant) are able to counterbalance these effects [28]. As recent studies have demonstrated, the immunological functions of SP appear to play a key role also in the clearance of nanoparticles by alveolar macrophages [29, 30]. Nevertheless, nanoparticles (below 200 nm) are internalized by alveolar macrophages in a rather non-specific manner compared to larger particles in the micron range [15]. Therefore, nanoparticles are an attractive strategy to circumvent macrophage clearance by size exclusion.

10.3 Atomization Techniques for Producing Nanoparticles

There are generally two routes for preparing nanoparticles, a top-down and bottom-up approach. In the top-down route the nanoparticles are formed from fractioning of larger structures such as with the milling process [31]. With bottom-up approaches the nanoparticles are formed from the molecular level of the compounds such as in a solution, where small droplets can be formed and dried to produce nanoparticles. Further, among the bottom-up approaches nanoparticles can either be formed in the liquid phase or in the gas phase. Approaches employing the liquid route include nanoprecipitation, emulsification-solvent evaporation, polyelectrolyte complexation and sol-gel formation, which all generally require a large amount of solvent, are labor intensive and can result in introduction of impurities. Preparation of particles in the gas phase, also known as aerosol formation, typically takes place via atomization of a liquid in a gas [32]. These methods may allow the production of nanoparticles in a one-step process, with medium to high yield and enable a scalable, continuously operated manufacturing process. Further, they directly result in particles in the solid state in powder form, which are physically more stable compared to liquid state formulations. This eliminates the need for lyophilization and other post processing of the formulations, which would typically be necessary with liquid nanosuspensions.

10.3.1 Principles of Spray Drying

Spray drying represents a platform technology for the transformation of liquid samples into a dry particulate form [33–36]. This technique is well-established in many relevant branches such as the chemical, food and pharmaceutical industry. Spray drying is a continuous, one-step process, which consists of four separate phases, namely (1) sample atomization, (2) mixing of the generated droplets with the drying gas, (3) solvent evaporation from the droplets, and (4) separation of the dried product (Fig. 10.2).
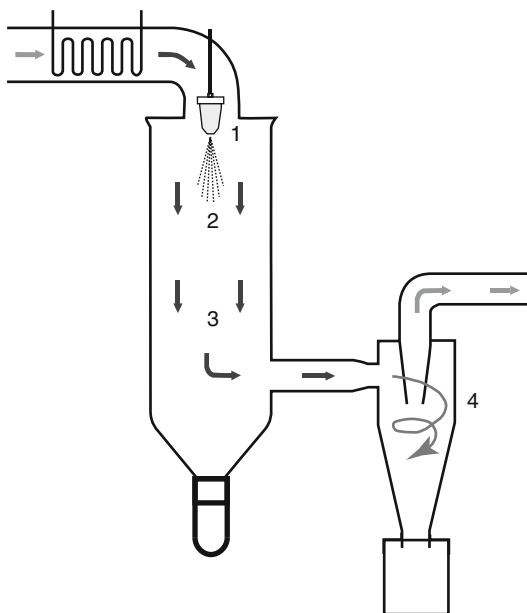
Fig. 10.2 Schematic of a conventional spray-dryer operating in co-current manner (*1* sample atomization, *2* mixing of the generated droplets with the drying gas, *3* solvent evaporation from the droplets, and *4* separation of the dried product within a cyclone)

The main goal of the atomization step is to create a maximal surface area between the drying gas and the fluidic sample in order to favor an efficient and rapid solvent evaporation. Therefore, the fluidic sample is transported to an atomization system, which breaks-up the liquid feed into a fine aerosol consisting of small droplets by applying a force. The atomization step may be conducted by means of centrifugal, pressure, kinetic or ultrasonic energy. Frequently employed devices include rotary wheel or disc configurations, pressure, pneumatic, and ultrasonic nozzles. Naturally, the choice of suitable atomizer device depends on the physicochemical characteristics of the fluidic feed and the desired properties of the final product.

Subsequently, the atomized feed is mixed with a conditioned drying gas, which initiates the drying phase. Atomizer emplacement and flow direction of the drying gas determine whether the atomized droplets are dried in co-current or counter-current manner. Mostly established co-current design indicates that the spray and gas

flow pass the instrument in the same direction, where the emerged droplets contact the highest temperature drying gas. Consequently, solvent evaporation occurs immediately and dried particles will be exposed to moderate temperatures while passing the spray dryer. During counter-current drying the spray and drying gas enter at opposite ends of the instrument. Counter-current spray drying results in dried product exposure to high temperatures, an application, which is preferred for processing of polymeric products, which are often of "sticky" nature.

Upon droplet contact with the conditioned drying gas thermal energy is transferred from the heated gas to the atomized droplets, whereas solvent transfer is initiated in the opposite direction. Just after the contact, the temperature of droplets increases to a constant value, which advances solvent evaporation and an accompanied droplet shrinkage. Finally, when the concentration of dissolved materials inside the droplet reaches a critical value, the suspended droplets form a continuous network, which rapidly decreases the drying rate. The solvent evaporation process is theoretically finished when the particle temperature rises to that of the surrounding drying gas. Usually, droplet drying is finished within 10–50 ms.

The final step of the spray drying process comprises the separation of the dried product from the stream of the drying gas. Particle collection from the carrier gas phase is often conducted using inertial phenomena. Therefore, cyclones are installed after the drying chamber, which allow for a very efficient particle separation. As the gaseous phase containing the dried particles enters the cyclone, the mixture is subjected to an accelerating flow field (rotating vortex), which forces the particles to impact on the walls of the cyclone.

A number of process and formulation parameters determine the final characteristics of the spray-dried product (e.g. particle size and morphology) (Fig. 10.3). Understanding the interplay of the diverse factors is crucial for the reproducible preparation of specified materials.

Process parameters which need to be considered during spray drying include the method of

Fig. 10.3 Potential particle morphologies prepared by spray-drying. τ_{sv} solvent evaporation characteristic time, τ_{sl} solute diffusion characteristic time (Reproduced with permission from Okuyama and Lenggoro [37])
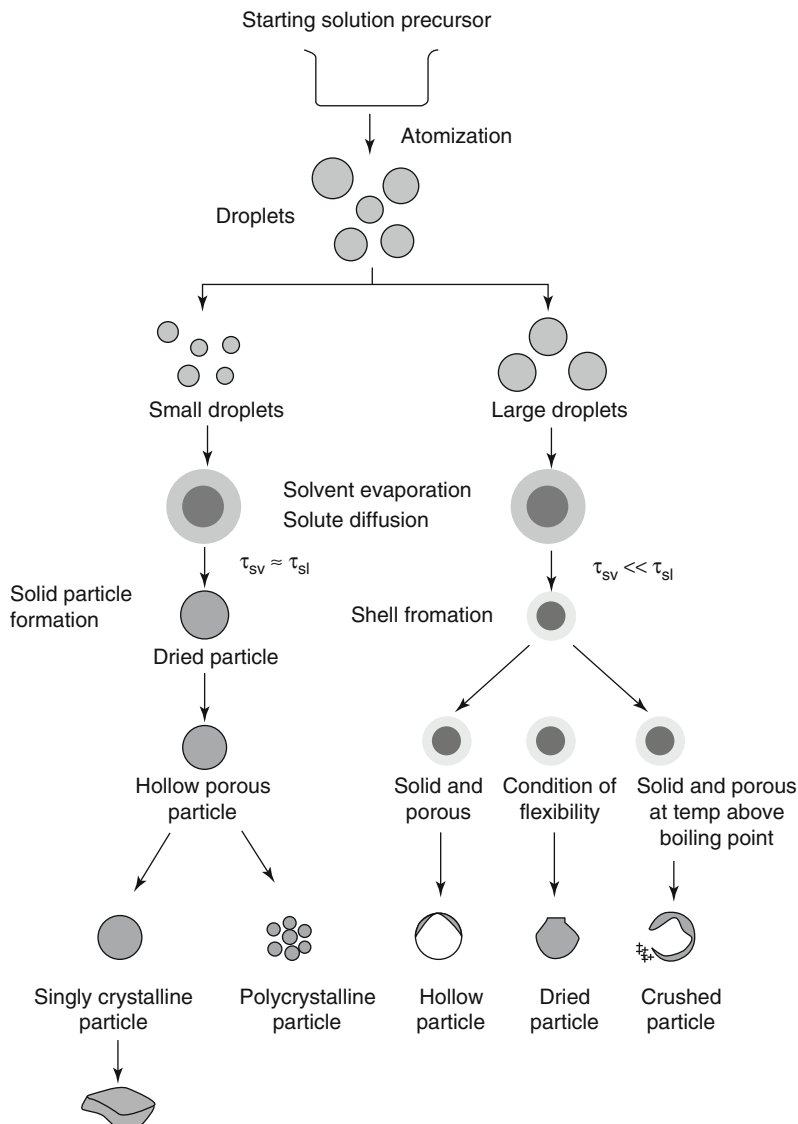
atomization (rotary wheel or disc configurations result in final particle diameters up to 200 μm, while two-fluid nozzles lead to final particle sizes below 10 μm), feed rate (final particle size is directly proportional to the feed rate), inlet drying gas temperature and flow (slow/fast solvent evaporation leads to the formation of smaller/larger particles) and type of employed particle collector. Formulation parameters with impact of the final product quality comprise the feed composition (solvent type and solids content, which impact dynamic viscosity and surface tension of the drying formulation; the size of particles increases upon elevation of dynamic viscosity and surface tension). Morphological modifications of the spray-dried particles (i.e. compact or hollow in nature) are related to the drying conditions of the atomized droplets. Here, solvent evaporation rate, as well as diffusivity of the dissolved solids are the most prominent parameters which account for the final particle morphology. It is well-known, that the particle morphology is qualified by the ratio between the convection time required for droplet drying and the diffusion coefficient of the employed solids, known as the Peclet number. In general, fast drying (Peclet

number <1, "rush hour effect") of atomized droplets causes the formation of large hollow particles with a thin solid shell, whereas slow droplet drying (Peclet number >1, "Tetris effect") leads to denser particles (with deformed character).

Overall, modeling of the final product properties during the spray-drying process remains a considerable challenge due to a large number of parameters which intervene during drying, such as droplet break-up and droplet/particle collision and coagulation/aggregation. Thus, spray-drying processes are still largely based on experience and trial & error. Moreover, to expand the spray-drying process to the nanoscale, efficient atomization systems (e.g. "vibrating-membrane nozzles") combined with highly efficient particle collectors (e.g. "electrostatic precipitators") need to be utilized [7, 38].

10.3.1.1 Büchi B-90

Spray drying is known to be a convenient one-step process for the continuous conversion of fluidic samples into dry powder formulations. Moreover, a tailored manipulation of particle properties (e.g. size and morphology) is technically feasible by an adjustment of the formulation and spray drying process parameters. Unfortunately, conventional spray-dryers lack sufficient fluid atomization and particle collection to reach sub-micrometer particle sizes.

As a strategy to extend the spray drying technique down to the nanoscale, a new generation of spray-dryers (Nano Spray Dryer B-90, Büchi) was recently made commercially available [39]. The unique construction of the instrument conquers the main shortcomings associated with conventional spray-dryers. Here, the fluidic feed breakdown is accomplished by vibrating-membrane technology, while an electrostatic particle collector ensures highly efficient precipitation of dried particles on a collecting electrode (Fig. 10.4).

Vibrating-membrane nozzles have become the focus of increasing interest for the generation of droplets of ~1–10 μm. The principle of droplet generation is accomplished by liquid flow through a piezoelectric-actuated (~60 kHz) aperture containing micro-scale perforation (Fig. 10.5).
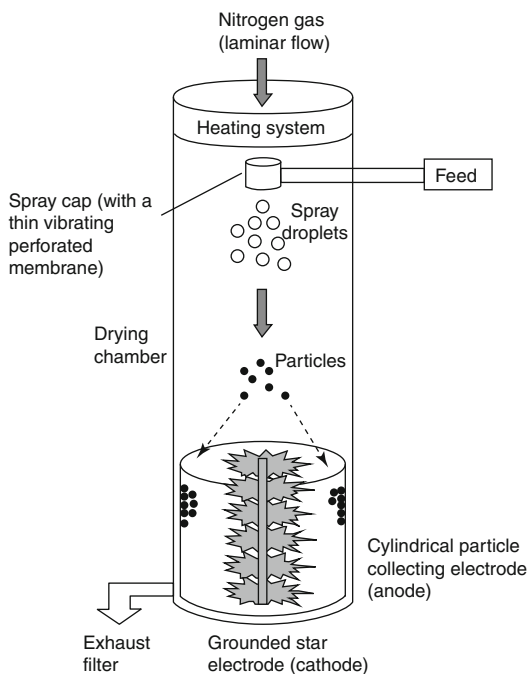

Fig. 10.4 Schematic of the Nano Spray Dryer B-90 (Reproduced with permission from Lee et al. [40])

The membranes used for fluid atomization feature an array of precise micro-scale tapered holes with large cross-sections on the reservoir side (Fig. 10.6a) and narrow cross-sections on the droplet delivery side (Fig. 10.6b). The membranes are most likely fabricated by a laser-drilling technique.

Naturally, for an accurate function of vibrating-membrane nozzles, it is essential to attenuate the operating principle (e.g. vibrating amplitude and frequency) to its technical construction (e.g. nozzle morphology and dimension).

Following sample atomization the drying step is carried out in a laminar flow of heated gas (co-current sample drying) (Fig. 10.4). The final step of particle separation within the Nano Spray Dryer B-90 is accomplished by an electrostatic particle collector, where the collection efficiency is independent of the inertial behavior of the particles. The electrostatic particle collector consists of a grounded star-shaped electrode (cathode) and a cylindrical particle collecting electrode (anode) (Fig. 10.7).

Fig. 10.5 Schematic of the piezoelectric-driven vibrating-membrane nozzle implemented inside the spray head of the Nano Spray Dryer B-90 (Reproduced with permission from Lee et al. [40])
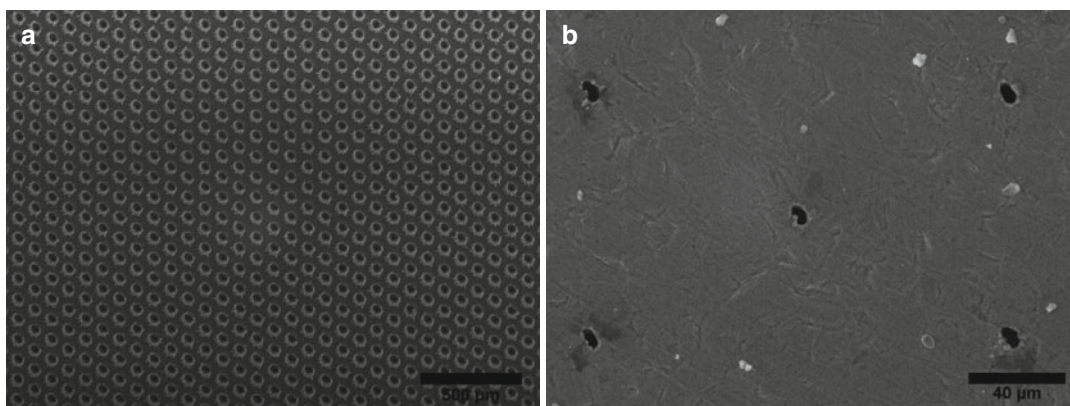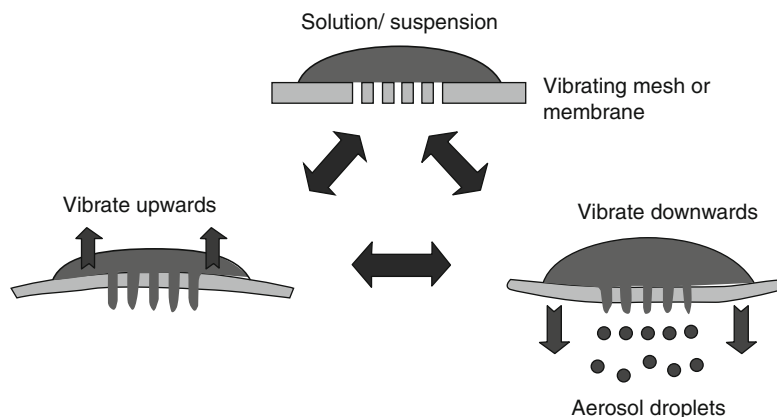

Solution/ suspension

Vibrating mesh or membrane

Vibrate upwards

Vibrate downwards

Aerosol droplets

Fig. 10.6 Representative scanning electron microscopy images of membranes implemented inside the spray head of the Nano Spray Dryer B-90 (reservoir side: (**a**), droplet delivery side: (**b**))

The high voltage (kV) applied between the two electrodes charges the dried sub-micrometer particles, which accelerates their movement and deposition on the inner wall of the cylindrical particle collecting electrode.

Besides the choice of specified hole dimension, a number of formulation parameters affect the final characteristics of collected powder (e.g. particle size). A lower surface tension (Tate's law) and higher dynamic viscosity (Hagen-Poiseuille's law) of the employed formulation would favor detachment of smaller droplets from the aperture. Moreover, the applied feed concentration is another important variable which determines the final particle size of the spray-dried product.

10.3.2 Alternative Methods for Producing Nanoparticles

Although spray drying is the most widely studied method for solid particle production, there are other liquid atomization methods available, which have demonstrated potential for preparation of nanoparticles and nano-embedded microparticles (NEM).

10.3.2.1 Spray Freeze Drying

Spray freeze drying is a modified spray drying process, and as the name suggests, it is a combination of the spray drying and freeze drying processes. In freeze drying the drug and carrier are dissolved and the solution is first frozen,
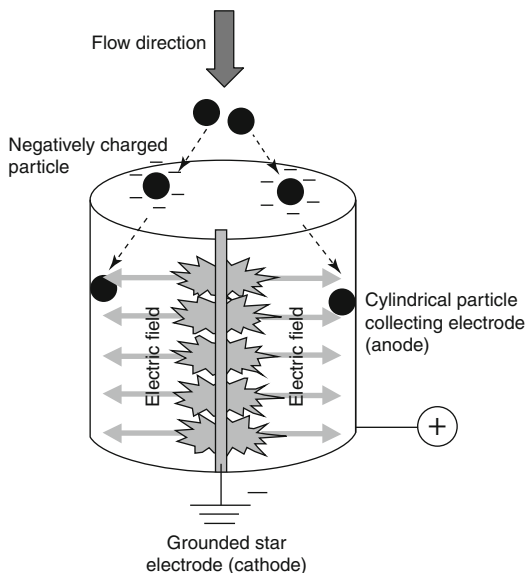
Fig. 10.7 Schematic of the electrostatic particle collector implemented inside the Nano Spray Dryer B-90 (Reproduced with permission from Lee et al. [40])

and the solvent is subsequently removed through sublimation by applying a vacuum in the given compartment (Fig. 10.8a). A dry, porous mass with approximately the original size and shape would result from this drying process and it has proven a good method for drying nanoparticles produced in the liquid phase. With spray freeze drying the solution containing the drug molecules is atomized from a nozzle into a stream of cold air (around −60°C) at atmospheric pressure. The small droplets produced quickly freeze and then their solvent sublimates in the cold air stream resulting in dry particles in the collection chamber [44]. Spray freeze drying is mainly used to produce microparticles but similar to the conventional spray drying process it can be modified to produce nanoparticles. Cheow et al. [45] have used spray freeze drying to atomize nanosuspensions into dry powders.

10.3.2.2 Spray Pyrolysis
Spray pyrolysis is a mechanical atomization process similar to spray drying but in which the droplets are dried at higher temperature using a furnace or a flame resulting in fast evaporation. Compared to spray drying and spray

freeze drying, spray pyrolysis allows reactions to take place within the particles as well as aiding the fragmentation of particles into small droplets that are rapidly evaporated. Particles below 100 nm have been produced using spray pyrolysis. Additionally, the process can be done under low pressure conditions at which higher solvent evaporation rates are achieved and small particles can be produced. This technology is, however, limited to materials that can tolerate very high heat without chemical degradation [32].

10.3.2.3 Ultrasonic Atomization
With ultrasonic atomization small droplets are formed from the break-up of a liquid using ultrasonic vibration at the air-liquid interface (Fig. 10.8b). The size of the droplets produced is partly controlled by the frequency of the vibration as well as the properties of the liquid atomized. Droplets produced with ultrasonic atomization typically have a narrow size distribution due to the controlled break-up process but it is difficult to achieve particles of sizes below 2 μm, even with dilute solutions [32]. However, there are studies that have demonstrated the direct production of nanoparticles using ultrasonic atomization and a study by Forde et al. [46] showed that a 1.65 MHz piston could be used to prepare poly(caprolactone) nanoparticles with a mean size of 186 nm and a narrow size distribution. In addition to its application in the direct preparation of nanoparticles it has been used in numerous studies in combination with a pneumatic atomization process to achieve smaller and more monodisperse particles [47].

10.3.2.4 Supercritical Fluids Technology
Supercritical fluids are liquids and gases at temperatures and pressures above their critical point, a phase area in the liquid/gas pressure curve. These fluids have lower viscosities and higher diffusivities of solutes than general liquids [48]. The drug compound is filled into a vessel either alone or together with a carrier material and a gas is added into the system. The gas is pressurized via a compressor before entering the vessel and
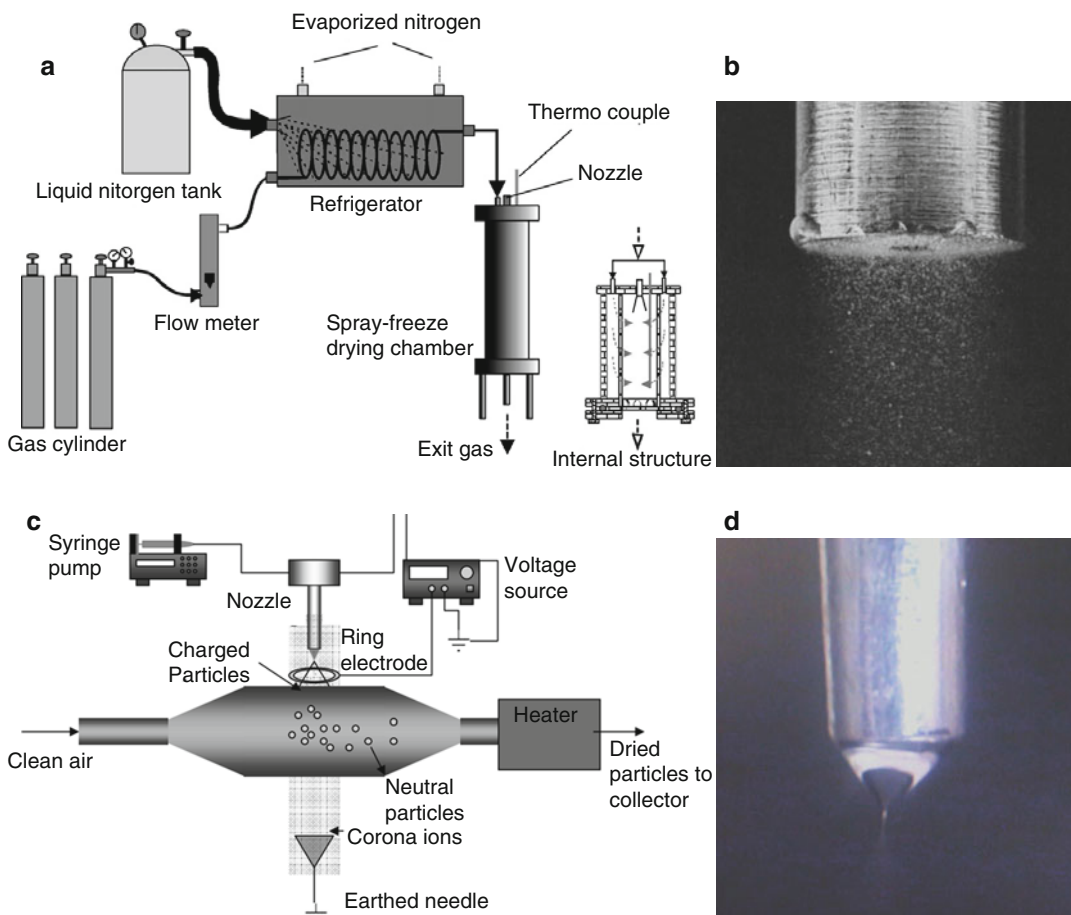
Fig. 10.8 Principles of the spray freeze drying process (**a**), ultrasonic atomization (**b**), schematic overview of electrospraying process (**c**) and image of electrospraying in cone-jet mode (**d**) (Reproduced with permission from Wang et al. [41], Topp [42] and Yurteri et al. [43])

becomes a supercritical fluid, which dissolves the drug and carrier within the vessel. Particles are then formed from the dissolved mixtures and are collected on a filter at the outlet of the vessel until the system is de-pressurized and the powder can be collected. With supercritical fluids technology nonvolatile solvents can also be dissolved. Carbon dioxide (CO_2) is the most widely used supercritical fluid, due to its low critical temperature and pressure ($T_{critical} = 31.1\,°C$, $P_{critical} = 73.8$ bar) [49]. Furthermore, CO_2 is inexpensive, non-toxic and non-flammable and is well suited for pharmaceutical processing. Supercritical fluids technology typically results in particles that are relatively small (0.5–10 μm) depending on the setup used but several recent

setups have been shown to produce even smaller particles. Griseofulvin nanocrystals of 130 nm have been prepared as well as lysozyme particles of around 190 nm and it is predicted that the supercritical fluids technology will draw more attention for nanoparticle preparation in the coming years [50].

10.3.2.5 Electrospraying

Electrohydrodynamic atomization is another technology that allows the formation of small droplets down to the nanoscale. Essentially, a liquid is passed through a concentric nozzle at a continuous flow rate and a high voltage is applied on the nozzle, thereby charging the flowing liquid. When the liquid passing through is exposed to a

sufficiently strong electric force, it can cancel out the surface tension at the liquid to air interface. This then creates instability of the drop at the tip of the nozzle, resulting in a thin jet propagating from a cone-shaped meniscus (Fig. 10.8d), which breaks up into small, charged droplets [51]. As with other atomization methods solvent evaporation takes place and the droplets become solid particles.

Different spraying modes exist depending on the voltage applied, the geometry of the electric field and the properties of the liquid atomized, but in order to achieve small particles with the lowest polydispersity the cone-jet mode is used. Certain scaling laws may also be used to determine the operational conditions required to achieve nanoparticles of a certain size [52]. Advantages of electrospraying over some of the other atomization methods include the near-monodisperse size distribution of particles produced and the self-dispersing property of the charged droplets, which prevents agglomeration of particles. Further, it allows control over the movement of droplets via the electric fields making particle deposition more efficient [53]. The main challenge with electrospraying is the scale-up and commercialization of the process due to low flow rates required to maintain a stable cone-jet, although effort is being made in this area [7].

Several studies have demonstrated that it is possible to produce nanoparticles down to a size of 10 nm with a narrow size distribution using electrospraying although this has mainly been shown using metal nanoparticles [43]. It is more difficult to produce nanoparticles using polymers or drugs despite several studies showing it can be done. Marijnissen and Gradon [54] have shown that particles of paclitaxel and poly(vinyl pyrrolidone) of around 200 nm could be formed, Enayati et al. [55] demonstrated that poly(lactide-*co*-glycolide) (PLGA) nanoparticles loaded with estradiol and polymethylsilsequioxane particles of 120 and 400 nm could be prepared using a co-axial electrospraying setup with additional control over particle shape, and Valo et al. [56] have shown that PLGA particles loaded with beclomethasone-dipropionate and salbutamol

sulfate of 200 nm could be prepared using at very low flow rates and polymer concentrations.

10.3.3 Nano-embedded Microparticles

Nanoparticles alone are not in the optimal size range for inhalation from an aerodynamic viewpoint [57]. Further, when particles are reduced in size the total surface area increases and hence, increases the free energy of the particles. This results in increased interaction between particles causing particle agglomeration or drug crystal growth [4]. In order to achieve a formulation with a long shelf life it is necessary to ensure that the nanoparticles remain physically stable under elevated temperature and humidity conditions. Generally, nanoparticles are less stable as a liquid suspension than in a dry powder form. Further, many nanoparticles would dissolve or release their drug over time. Hence, dry powder formulations prepared via atomization techniques result in some stabilization, but their small size still provides a large surface–to–volume ratio for interactions to take place and also make them more fragile [4].

One approach, which can limit the interaction between particles and at the same time protect the nanoparticles, is by entrapping them in a solid matrix, which limits their mobility and thus, prevents particle-particle interactions. They may additionally be entrapped inside micro-scale particles, which improve aerosolization properties and hence, pulmonary administration. The idea with such NEM is that the microparticles act as intermediate delivery vehicles during storage and administration until they reach their target site. With pulmonary delivery the aim is typically microparticle deposition on the pulmonary mucus lining, where the highly soluble matrix of the microparticles rapidly dissolves to release the less soluble or – depending on the proposed application – practically insoluble nanoparticles. Several studies have investigated the preparation and performance of such NEM and can generally be divided into cases where drug nanocrystals or drug-loaded nanoparticles were embedded in the microparticles (Table 10.1).

Table 10.1 Formulation of NEM intended for pulmonary drug delivery

	Preparation method	Nanoparticle material	Drug	NP size [nm]	Matrix materials	MMAD of NEM [µm]	Ref.
Drug nanocrystals	Spray drying	Terbutaline sulfate, sorbitan monostearate	Terbutaline sulfate	238	DPPC, glyceryl behenate, palm oil	4	Cook et al. [58]
	Spray drying	Pranlukast	Pranlukast	100–430	Mannitol	2	Mizoe et al. [59]
Polymeric NP	Spray drying	Polybutylcyanoacrylate	Ciprofloxacin	177	Lactose, leucine, PEG 6000	2	Ely et al. [60]
	Spray drying	PLGA	Coumarin-6	259	Mannitol	1–10	Yamamoto et al. [61]
	Spray freeze drying	Polybutylcyanoacrylate, polysorbate 80, dextran	Doxorubicin	173	Lactose	10	Azarmi et al. [62]
	Spray drying	Chitosan/tripolyphosphate	Insulin	300–419	Mannitol, lactose	2–3	Grenha et al. [63]
	Spray drying	Gelatin, polybutylcyanoacrylate	–	173–242	Lactose	3	Sham et al. [64]
	Spray drying	Polyacrylate	Acetyl salicylic acid, salbutamol sulfate	50–220	Phospholipid	3	Hadinoto et al. [65]
	Spray drying	PLGA	siRNA	262	Lactose, trehalose or mannitol	2–6	Jensen et al. [66]
	Spray freeze drying	Poly (caprolactone)	Levofloxacin	290	Mannitol, poly(vinyl alcohol)	4–5	Cheow et al. [45]

DPPC dipalmitoylphosphatidylcholine, *MMAD* mass median aerodynamic diameter, *NEM* nano-embedded microparticles, *NP* nanoparticles, *PLGA* poly(lactide-*co*-glycolide)

10.3.3.1 NEM Comprising Pure Drug Nanoparticles

NEM comprising drug nanocrystals have been prepared by atomizing separate solutions containing the drug and excipients simultaneously or by atomizing a suspension of drug nanocrystals. Typically, spray drying has been used for the preparation of these microparticles. Here, excipients like mannitol, lactose and leucine are frequently employed as microparticle matrix materials.

Mizoe et al. [59] demonstrated the preparation of NEM by simultaneous atomization of drug nanocrystals and microparticles. They prepared NEM with nanoparticles of pranlukast, a poorly soluble drug for asthma treatment into microparticles of mannitol using a 4-fluid spray drying nozzle setup with two liquid inlets and two gas inlets allowing two separate solutions with different solutes and solvents. Solutions of pranlukast and mannitol were passed through separate inlets and resulted in drug particles of 200 nm in diameter. Increased bioavailability was shown after pulmonary administration in rats compared with oral administration of pure drug. Thus, the authors provided a system where the insoluble nanosized drug particles were released from the microparticles and slowly dissolved to perform an effect at the local target site.

In another study, Cook et al. [58] prepared NEM by first preparing a drug nanosuspension and subsequently atomizing with excipients. They prepared a nanosuspension of Terbutaline sulfate via emulsification-solvent evaporation and then spray dried the drug nanoparticles of around 238 nm together with dipalmitoylphosphatidylcholine to form microparticles. Their NEM indicated absence of nanoparticles on the surface of the microparticles and showed sustained release of drug over several hours.

10.3.3.2 NEM Comprising Polymeric Nanoparticles

Embedding pure drug nanoparticles inside microparticles seems sensible for preparing a drug delivery system with sustained release or for administration of poorly soluble drugs, where the high dissolution rate of nanoparticles comes into good use. However, based on the literature more focus has been directed towards producing NEM using drug-loaded nanocarriers for both local and systemic delivery of the nanoparticles. The concept of such NEM for pulmonary delivery was introduced by Tsapis et al. [67], where model polystyrene nanoparticles were used to study their influence on porous microparticle formation. Studies with NEM using drug-loaded nanocarriers generally aim at achieving stable formulation with cellular uptake, long tissue retention times and sustained drug release.

Currently, most of the NEM embedded with drug-loaded nanocarriers are produced in a two steps process. First, the nanoparticles are prepared via nanoprecipitation or emulsification-solvent evaporation or another method and are subsequently spray dried together with an excipient. Most studies make use of non-water soluble or biodegradable polymers for preparing the nanoparticles, as they are compatible for atomization of an aqueous suspension. As an example, Yamamoto et al. [61] prepared PLGA nanoparticles loaded with coumarin-6 by emulsification-solvent evaporation, freeze-dried and reconstituted, and spray-dried the nanoparticles with mannitol in a fluid bed granulator. Nanoparticles around 200 nm were formed and were entrapped in microparticles of 1–10 μm. *In vivo* studies in rats indicated superior inhalation performance of the NEM compared with freeze-dried nanoparticle powder and more than 50 % of the NEM were delivered to the bronchioles and alveoli with prolonged pharmacological effect. In a study by Jensen et al. [66], PLGA nanoparticles were loaded with siRNA and embedded in mannitol, lactose and trehalose and prepared using similar methodology. The authors showed that microparticles could be formed with suitable aerodynamic properties for inhalation.

Moreover, the application of phospholipids as a matrix material has been investigated in a study by Hadinoto et al. [65]. Phospholipids are one of the main components of lung surfactant and are thus interesting to use in the formulation. Embedding of nanoparticles in the phospholipid matrix resulted in low uptake of particles by phagocytes possibly due to the natural presence of phospholipids in the lungs. Phospholipids, which are also surfactants, are also believed to

enhance the aerosol properties and solubility of the particles and thereby, increase alveolar deposition and pharmacological performance of the nanoparticles.

NEM prepared using a large amount of excipients for the microparticle matrix protect the nanoparticle inside but also adds more bulk that needs to be dissolved and cleared in the lungs. Further, particles with a large matrix fraction typically do not allow visualization of the nanoparticles within the microparticles. Below are, however, some examples where NEM have been prepared with low amounts of excipients (Fig. 10.9).

The preparation of NEM has typically been performed by atomization of nanoparticles produced via nanoprecipitation or emulsification-solvent evaporation. Although the atomization process has mainly been carried out using a conventional spray drying process, this should also be possible with a modified version of spray drying or using methods described earlier such as ultrasonic atomization, supercritical fluids technology or electrospraying. Regarding the use of nanoprecipitation and emulsification methods, these are acceptable for proof-of-concept and performance testing of NEM formulations but they are labor intensive, low output and costly production methods from a manufacturing viewpoint. This part of the process could thus be greatly optimized by developing an automated, continuous, and higher throughput process by for instance connecting two atomization processes in series, one for preparing nanoparticles and another for preparing microparticles. Alternatively, a more automated liquid-phase nanoparticle preparation technique could be connected with a subsequent atomization process.

10.4   Delivery of Nanoparticles to the Lungs

10.4.1 Deposition Mechanisms of Inhaled Particles

The site, extent and efficiency of particle deposition in the respiratory tract depend on factors coming both from the inhaled aerosol as well as the patient. Besides aerosol parameters such as the particle or droplet size, the density of the used material, the surface modifications and the shape, lung deposition also depends on the breathing pattern of the patient and individual parameters such as the anatomy and structure of the respective lung regions [6]. One of the most important factors, however, is the particle or droplet size, as this not only affects the underlying deposition mechanism and therefore the actual deposition site, but also opens the greatest room for adaption in terms of device and particle engineering.

In aerosol science, the mass median aerodynamic diameter (MMAD) is commonly used to describe the size of a particle. It is defined as the diameter of a particle with a density of 1 g/cm^3 that is settling with the same velocity as the particle of interest [4].

Depending on the forces inflicted on a particle, there are mainly three deposition mechanisms described: (i) impaction, (ii) sedimentation, and (iii) diffusion (Fig. 10.10). Which of these mechanisms applies to an inhaled particle depends first and foremost on its MMAD.

Due to inertia, particles are only able to follow the inspired air over a few bifurcations within the upper airways, although actually the majority already breaks the streamline of airflow in extrathoracic regions (mostly the oropharynx and larynx) and collides with the pulmonary surface. Therefore, impaction is relevant for particles with a MMAD larger than 5–6 μm, for which reason the desired size of respirable particles is normally below this limit from a particle engineering point of view (with large carrier particles facilitating the filling and aerosolization of dry powder formulations being an exception). Particles with a MMAD between 1 and 5 μm settle in the lower airways and alveolar region due to gravitational forces. As the alveoli are the lung region that is generally targeted with therapeutic aerosols, sedimentation is the essential driving force for efficient pulmonary drug delivery. For this reason, most of the pharmaceutical aerosols available on the market bear a MMAD of 2–5 μm, which corresponds to the deposition maximum in the deep lung. However, one has to keep in mind that impaction and sedimentation are also overlapping
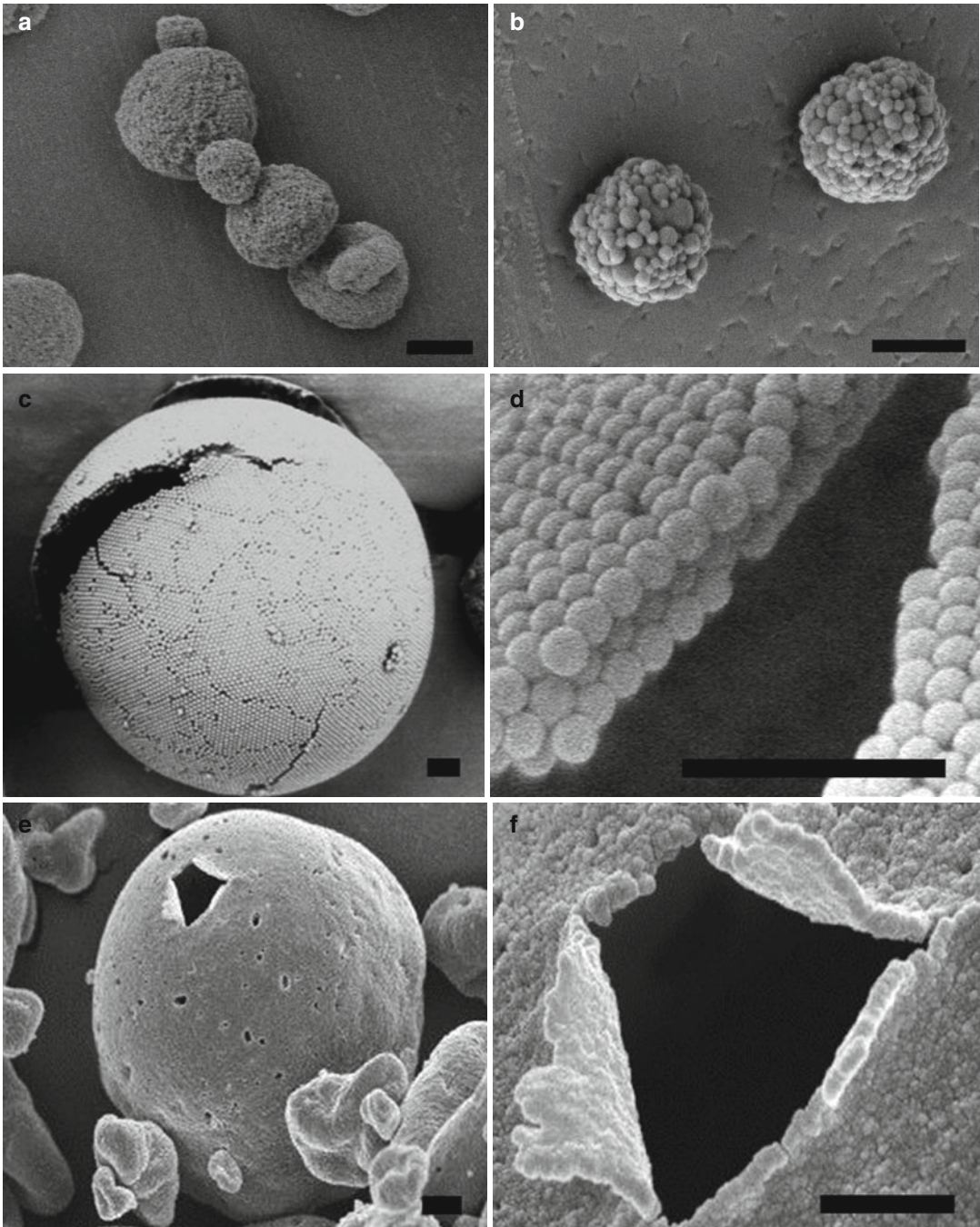
Fig. 10.9 Scanning electron microscopy images of nano-embedded microparticles prepared by spray drying from aqueous nanosuspensions containing poly(styrene) (mean size of ~100 nm) (**a**), poly(lactide-*co*-glycolide) (mean size of ~200 nm) (**b**), poly(styrene) (mean size of ~170 nm) (**c**, **d**), and polyacrylate nanoparticles (**e**, **f**). Scale bars: 1 μm (Reproduced with permission from Tsapis et al. [67] and Hadinoto et al. [65])

in the size range between 1 and 10 μm, due to which both mechanisms contribute to pulmonary deposition. Small particles with a MMAD of 0.5 μm and below (i.e. nanoparticles), underlie Brownian motion, and therefore deposit by diffusion [1, 6, 68].
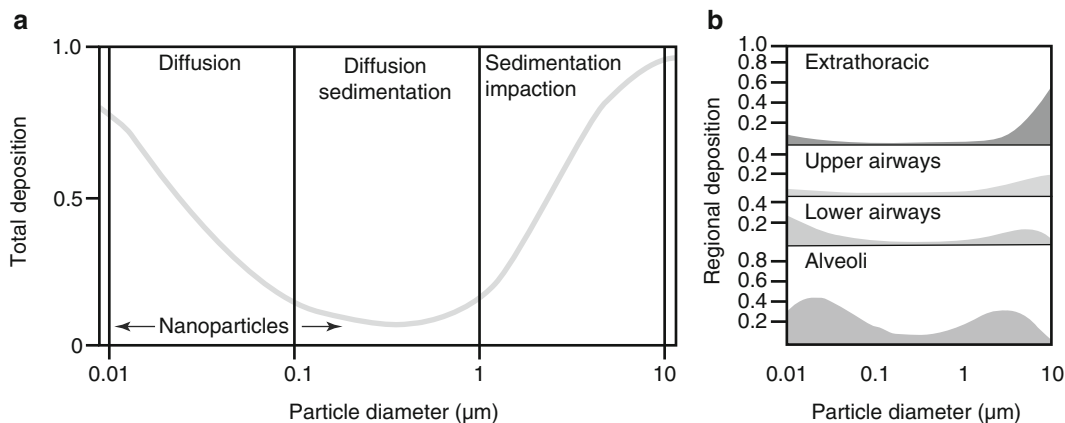
Fig. 10.10 Particle deposition in the lungs. (**a**) Total deposition of unit-density particles in the human lung. Nanoparticles are deposited by diffusion and sedimentation, but are easily exhaled again, for which reason one needs to technologically adopt such systems in order to maximize lung deposition. (**b**) Regional lung deposition of unit-density particles. While larger particles (mass median aerodynamic diameter (MMAD) >5 μm) impact in central lung (extrathoracic and upper airways), there is a first deposition maximum in the peripheral lung for particles with MMAD between 2 and 5 μm, and a second maximum for particles smaller than 0.2 μm (nanoparticles) (Reproduced with permission from Heyder [68])

It is known that nanoparticles deposit in the peripheral lung, mainly the alveolar region, but that they are easily exhaled again due their small size [6, 57]. In pulmonary drug delivery, however, a significant dose of drug needs to be deposited, and should be also retained within the lungs in order to cause a pharmacological effect. Inhalation of aerosolized nanoparticles, however, results in very poor deposition efficiencies when done over a limited time period as is usually the case with inhalation therapy. As a matter of fact, nanoparticles have disadvantageous aerodynamic properties when inhaled as such. Furthermore, production of aerosols with particle or droplet sizes in the nanometer range is difficult due to the high energies needed [4]. Therefore, technological adaptations are necessary to make them suitable to pulmonary drug delivery.

10.4.2 Application of Nanoparticles to the Lung

As described above, inhalation of drug-loaded polymeric nanoparticles might be advantageous to delay the clearance of the applied drug from the respiratory tract. Although, their small size (i.e. MMAD of 0.1–1 μm) limits pulmonary deposition [57], research has focused on developing suitable administration forms to facilitate inhalation of nanoparticles. So far, nebulization of polymeric nanosuspensions as well as dry powder aerosolization of NEM were shown to be adequate methods for the production of nanoparticle-containing aerosol particles suitable for deep lung deposition [69, 70].

10.4.2.1 Aerosolization of Nanosuspensions for Pulmonary Drug Delivery

A major advantage of nebulization processes is that regardless of the aerodynamic characteristics of the nanoparticles themselves, pulmonary deposition is achieved by supplying adequate droplet sizes. However, aerosolization of unaffected nanoparticles is a major demand to ensure their functionality after lung delivery. Pneumatic- and ultrasound-driven nebulizers failed to efficiently nebulize polymeric nanosuspensions, as these devices caused nanoparticle aggregation and concentration [71]. As an alternative to "traditional" nebulizers, aqueous formulations can be delivered to the lungs by means of vibrating-membrane technology (e.g. Aeroneb® Pro, Aerogen and eFlow®rapid, PARI) [72]. This mode of nebulization has been recommended for aerosolization of "sensitive" formulations (e.g. polymeric nanoparticles), owing to avoidance of high shear stress

and energy input during the process of droplet formation [71]. Consequently, it is emphasized that polymeric nanosuspensions should be preferentially nebulized with a vibrating-membrane device in order to achieve pulmonary deposition of unaffected nanoparticle formulations.

10.4.2.2 NEM for Pulmonary Drug Delivery

Beside nebulization, pulmonary delivery of polymeric nanoparticles is accomplished by dry powder aerosolization of NEM. The delivery of nanoparticles as part of microparticles is particularly interesting as these "Trojan" particles are thought to connect the advantages of both types of particles (i.e. aerodynamic characteristics and prolonged retention within the lungs) [67, 69, 70, 73]. However, spontaneous release of unaffected nanoparticles following pulmonary deposition remains a key requirement for this type of delivery system, which was so far only shown for NEM prepared by spray-drying.

10.4.3 Models to Evaluate the Performance of Lung-Delivered Nanoparticles

There are several models available to assess the performance of nanoparticles for lung delivery, which differ either in the degree of complexity, testing capacity and proximity to the *in vivo* situation.

10.4.3.1 *In Vitro* Models of the Air-Blood-Barrier and Exposure Set-Ups

The major advantage of cell- and tissue-based *in vitro* models is their suitability for high capacity screening and assessment of nanoparticles for pulmonary applications. Furthermore, cell culture models allow for elucidation of mechanisms, and can often cast some light into the black box of *in vivo* models. Due to the availability of cells for basically all lung regions, *in vitro* approaches are of increasing importance to the testing of pharmaceutical formulations intended for inhalation – although they can be more expensive. Cell culture models are either based on cell-lines or primary cells. Cell-lines are transformed or cancer-derived immortalized cells, and can therefore be kept in culture over a long period (several months to years). Although their ease of cultivation is advantageous as it brings flexibility in experimental design, results should be treated with caution, as observed effects might be linked to their immortalization and therefore abnormal physiology, thus deviating from healthy cell models. Therefore, the use of primary cells can be considered as a superior approach in this regard. Unfortunately, tissue from human source is often difficult to obtain and useful tissue is limited in quantity for ethical reasons. Therefore, *in vitro* studies using primary cells are often performed after extensive pre-screenings in cell-line models for comparative or control reasons. Regarding the different types of cell models, the gentle reader is referred to comprehensive reviews on this topic [11, 74].

Besides mono-cultures of certain cell types of the lungs, more complex co-culture systems have been recently published, in which lung epithelial cells are grown along with macrophages and dendritic cells. These three-dimensional cell models can be considered as artificial tissues that closely mimic the morphologic situation of the air-blood-barrier as found *in vivo* [75, 76]. However, these systems still lack complexity of a whole organ. Therefore, the conclusions that can be drawn from *in vitro* models are limited, and their value is rather complementary to other models.

Regarding the *in vitro* evaluation of nanoparticles for inhalation, it is important to consider the fact that these systems are intended for delivery as aerosols, and deposit from a gas phase when administered to the lungs. Therefore, the mode of nanoparticle application in cell culture systems would ideally be air-interface instead of submerged exposure (Fig. 10.11a). Although this approach is limited to such cell types that can be cultured under air-interface conditions, there are a few test systems published and also commercially available that support commonly used cell culture inserts and allow for such air-liquid exposure (Fig. 10.11b). Besides such exposure chambers for aerosolized nanoparticles, there are also systems described in literature to allow for controlled sedimentation of larger particles from dry powder formulations (e.g. NEM) onto air-liquid interface cultured cells [79].
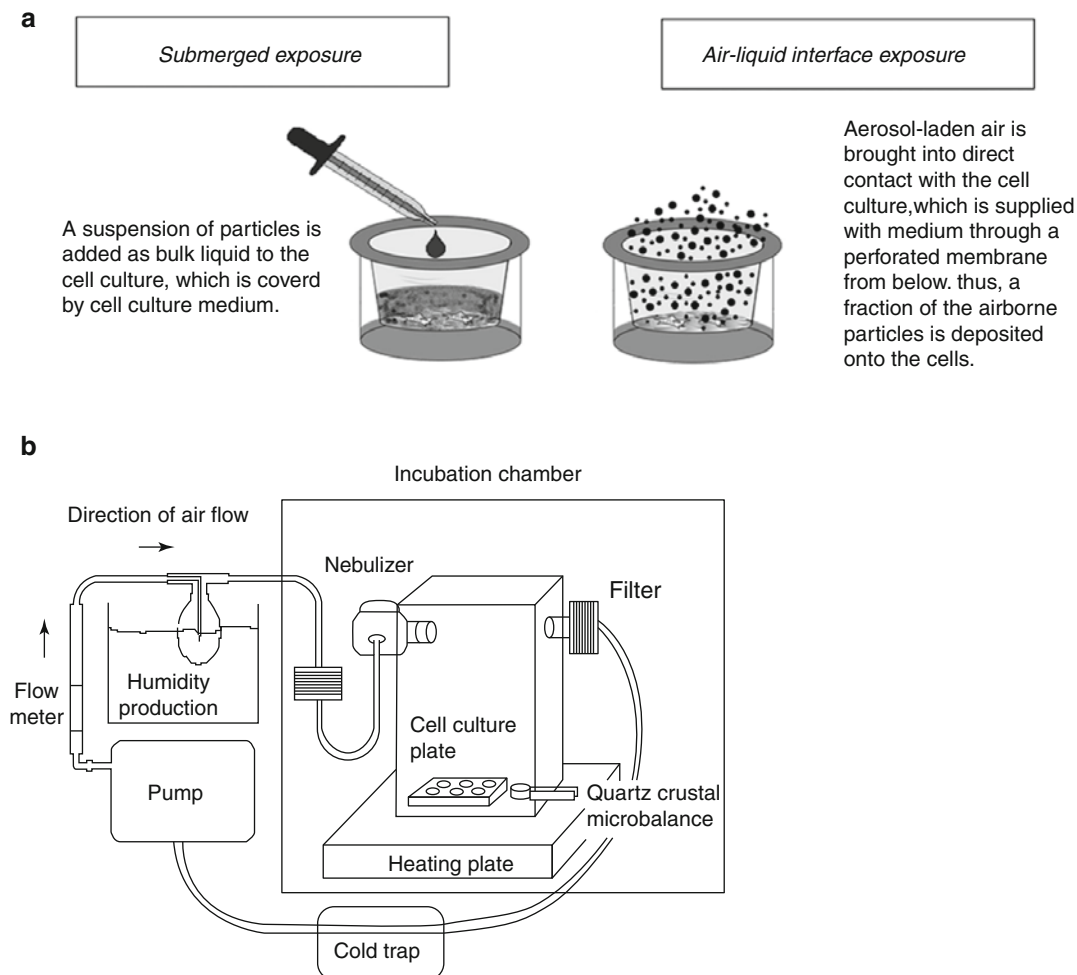
Fig. 10.11 (**a**) Submerged vs. air-liquid exposure of nanoparticles to *in vitro* cell culture models, with the latter being more realistic when studying particle-lung interactions. (**b**) A system that allows for air-interface exposure of nanoparticles. The air-liquid interface cell exposure system (ALICE) enables dose-controlled cloud settling of nebulized nanoparticle suspensions onto cells (Reproduced with permission from Paur et al. [77] and Lenz et al. [78] (BioMed Central))

10.4.3.2 Isolated Lung Models

Among the different preclinical techniques available to examine the potential of polymeric nanoparticles, isolated lung models represent a well-established approach to study the impact of lung-specific factors on the performance of inhaled therapeutics [80, 81]. Compared to *in vitro* cell culture techniques isolated lungs display the advantage of structural and functional integrity of the organ level. Hence, the isolated lung approach allows for a realistic extrapolation of pharmacokinetic profiles to the *in vivo* situation. A schematic of an isolated lung setup is depicted in Fig. 10.12.

For model installation and subsequent pharmacokinetic measurements basic steps include the isolation, perfusion, and ventilation of the lungs from a suitable organ donor, the delivery of formulations to the air-space by an appropriate method, and an adequate sample regimen and analytic. Thus, reliable formulation behavior within the target organ is obtained that adequately reflects the dynamic effects occurring *in vivo*.

As an example, the potential of novel salbutamol-loaded polymeric nanoparticles was evaluated in both an isolated lung model [83] and *in vivo* [84] (Fig. 10.13).

Fig. 10.12 Schematic of an isolated lung model useful to study the impact of lung-specific factors on the performance of pulmonary administered formulations (Reproduced with permission from Beck-Broichsitter et al. [82])
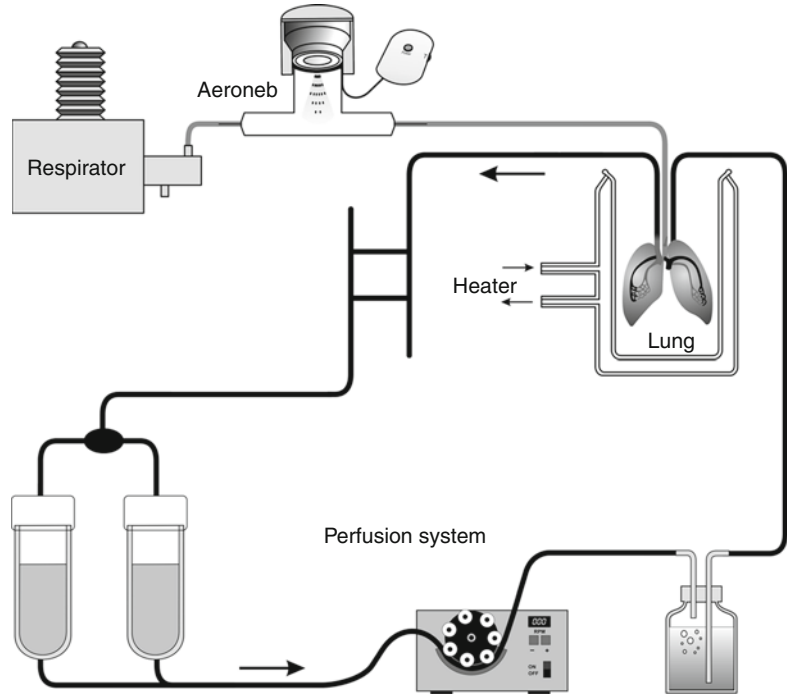

Fig. 10.13 Performance of salbutamol-loaded polymeric nanoparticles (*black triangles*) and salbutamol solution (*grey squares*) following pulmonary administration to the air-space of an isolated lung (**a**) and guinea pigs (**b**). Application of the nanoparticle formulation resulted in retarded drug absorption from the air-space into the perfusate (**a**). Likewise, bronchoprotection experiments performed *in vivo* presented a prolonged drug action for the nanoparticle formulation (**b**) (Reproduced with permission from Beck-Broichsitter et al. [69, 83] and Rytting et al. [84])
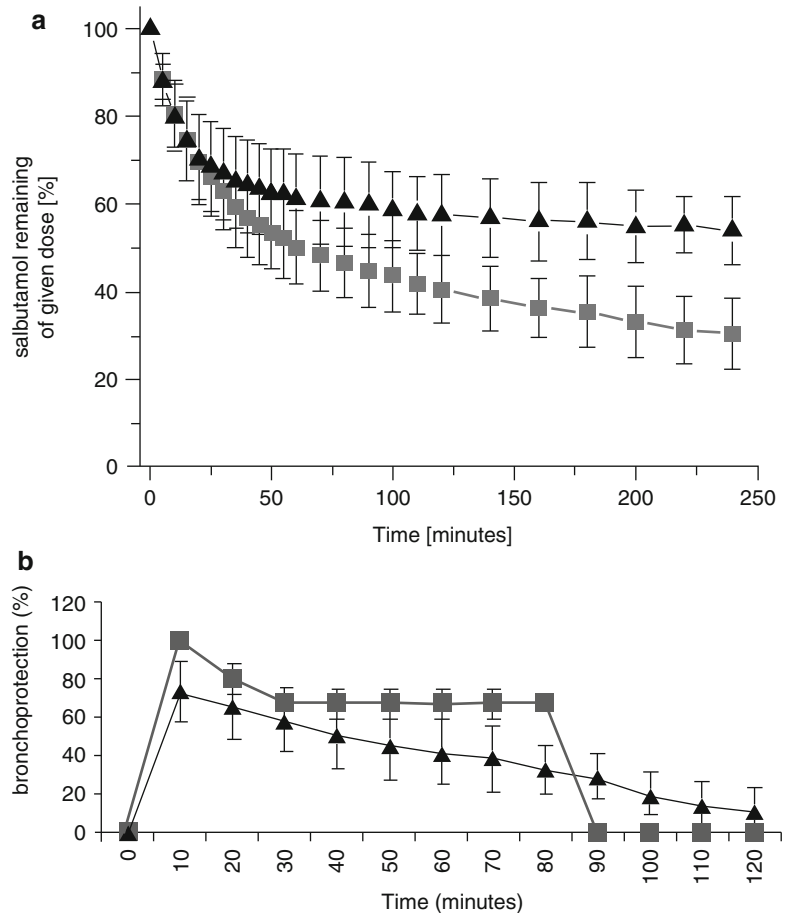
After administration of salbutamol as solution or entrapped into polymeric nanoparticles to the lung model, the drug absorption profile disclosed pulmonary retention for the nanoencapsulated salbutamol (Fig. 10.13a). This finding was confirmed by a prolonged pharmacodynamic effect (i.e. bronchoprotection) observed *in vivo* (Fig. 10.13b).

Conclusion

The application of nanoparticles for pulmonary delivery is gaining increasing interest with the current challenges in administration of numerous drug substances. Nanoparticles bear several advantages for pulmonary delivery, but some topics still remain relatively unexplored (e.g. interaction with the lung tissue, mobility, clearance and toxicity). Dry powder formulations provide higher stability, allowing for longer storage times and represent a good delivery approach for inhalation into the lungs. Furthermore, compared with the preparation of nanoparticles in the liquid phase, atomization of aerosols is attractive due to the simplicity of the process, the low cost involved and the purity of the product achieved. Moreover, it is in line with the current focus towards continuously operated manufacturing processes, which allow elimination of batches and reduction in production costs. The atomization techniques presented in this report allow continuous manufacturing with implementation of in-line process monitoring for optimization of product quality. Spray drying is currently the most employed system due to its commercial availability but it is likely that some of the other technologies described will become equally popular as their commercial demand and availability increases. NEM are most promising as a combined delivery vehicle and stabilization system for nanoparticles, and are in theory ideal for pulmonary delivery of certain drug molecules but still need more clinical validation.

With the advances in the preparation of nanoparticles and NEM it is time to place more effort in understanding the deposition of nano- and microparticles in the lungs, and

their subsequent mobility along the lung lining. This could lead to improved engineering of formulations that allow for efficient disintegration/dissolution as well as homogeneous distribution of particles within the lungs. It is still a challenge to study pulmonary drug delivery processes starting from aerosolization and particle deposition to cellular uptake and evaluation of pharmacological effect. With the progress in, and opportunities of nanomedicine, the pulmonary route is expected to regain increasing attention and lead to clinical products in the future.

References

1. Patton JS, Byron PR (2007) Inhaling medicines: delivering drugs to the body through the lungs. Nat Rev Drug Discov 6:67–74
2. Ruge CA, Kirch J, Lehr CM (2013) Pulmonary drug delivery: from generating aerosols to overcoming biological barriers – therapeutic possibilities and technological challenges. Lancet Respir Med 1:402–413
3. Sanders N, Rudolph C, Braeckmans K et al (2009) Extracellular barriers in respiratory gene therapy. Adv Drug Deliv Rev 61:115–127
4. Sung JC, Pulliam BL, Edwards DA (2007) Nanoparticles for drug delivery to the lungs. Trends Biotechnol 25:563–570
5. Patton JS, Brain JD, Davies LA et al (2010) The particle has landed – characterizing the fate of inhaled pharmaceuticals. J Aerosol Med 23:S71–S87
6. Yang W, Peters JI, Williams RO 3rd (2008) Inhaled nanoparticles – a current review. Int J Pharm 356:239–247
7. Peltonen L, Valo H, Kolakovic R et al (2010) Electrospraying, spray drying and related techniques for production and formulation of drug nanoparticles. Expert Opin Drug Deliv 7:705–719
8. Gehr P, Bachofen M, Weibel ER (1978) The normal human lung: ultrastructure and morphometric estimation of diffusion capacity. Respir Physiol 32:121–140
9. Weibel ER (1973) Morphological basis of alveolar-capillary gas exchange. Physiol Rev 53:419–495
10. Reynolds SD, Malkinson AM (2010) Clara cell: progenitor for the bronchiolar epithelium. Int J Biochem Cell Biol 42:1–4
11. Steimer A, Haltner E, Lehr CM (2005) Cell culture models of the respiratory tract relevant to pulmonary drug delivery. J Aerosol Med 18:137–182
12. Wong AP, Keating A, Waddell TK (2009) Airway regeneration: the role of the Clara cell secretory protein and the cells that express it. Cytotherapy 11:676–687
13. Crapo JD, Barry BE, Gehr P et al (1982) Cell number and cell characteristics of the normal human lung. Am Rev Respir Dis 126:332–337

14. Goerke J (1998) Pulmonary surfactant: functions and molecular composition. Biochim Biophys Acta 1408:79–89

15. Geiser M (2010) Update on macrophage clearance of inhaled micro- and nanoparticles. J Aerosol Med 23:207–217

16. Stone KC, Mercer RR, Gehr P et al (1992) Allometric relationships of cell numbers and size in the mammalian lung. Am J Respir Cell Mol Biol 6:235–243

17. Geiser M, Schuerch S, Gehr P (2003) Influence of surface chemistry and topography of particles on their immersion into the lung's surface-lining layer. J Appl Physiol 94:1793–1801

18. Schuerch S, Gehr P, Im Hof V et al (1990) Surfactant displaces particles toward the epithelium in airways and alveoli. Respir Physiol 80:17–32

19. Cone RA (2009) Barrier properties of mucus. Adv Drug Deliv Rev 61:75–85

20. Ryser M, Burn A, Wessel T et al (2007) Functional imaging of mucociliary phenomena: high-speed digital reflection contrast microscopy. Eur Biophys J 37:35–54

21. Olsson B, Bondesson E, Borgstroem L (2011) Pulmonary drug metabolism, clearance, and absorption. In: Smyth HDC, Hickey AJ (eds) Controlled pulmonary drug delivery, 1st edn. Springer, New York, pp 21–50

22. Patton JS (1996) Mechanisms of macromolecule absorption by the lungs. Adv Drug Deliv Rev 19:3–36

23. Ensign LM, Henning A, Schneider CS et al (2013) Ex vivo characterization of particle transport in mucus secretions coating freshly excised mucosal tissues. Mol Pharm 10:2176–2182

24. Kirch J, Schneider A, Abou B et al (2012) Optical tweezers reveal relationship between microstructure and nanoparticle penetration of pulmonary mucus. Proc Natl Acad Sci U S A 109:18355–18360

25. Wang YY, Lai SK, Suk JS et al (2008) Addressing the PEG mucoadhesivity paradox to engineer nanoparticles that "slip" through the human mucus barrier. Angew Chem Int Ed Engl 47:9726–9729

26. Bastacky J, Lee CY, Goerke J et al (1995) Alveolar lining layer is thin and continuous: low-temperature scanning electron microscopy of rat lung. J Appl Physiol 79:1615–1628

27. Blanco O, Perez-Gil J (2007) Biochemical and pharmacological differences between preparations of exogenous natural surfactant used to treat Respiratory Distress Syndrome: role of the different components in an efficient pulmonary surfactant. Eur J Pharmacol 568:1–15

28. Phelps DS (2001) Surfactant regulation of host defense function in the lung: a question of balance. Pediatr Pathol Mol Med 20:269–292

29. Ruge CA, Kirch J, Canadas O et al (2011) Uptake of nanoparticles by alveolar macrophages is triggered by surfactant protein A. Nanomedicine 7:690–693

30. Ruge CA, Schaefer UF, Herrmann J et al (2012) The interplay of lung surfactant proteins and lipids assimilates the macrophage clearance of nanoparticles. PLoS One 7:e40775

31. Rabinow BE (2004) Nanosuspensions in drug delivery. Nat Rev Drug Discov 3:785–796

32. Biskos G, Vons V, Yurteri CU et al (2008) Generation and sizing of particles for aerosol-based nanotechnology. KONA Powder Part J 26:13–35

33. Cal K, Sollohub K (2010) Spray drying technique. I. Hardware and process parameters. J Pharm Sci 99:575–586

34. Sollohub K, Cal K (2010) Spray drying technique: II. Current applications in pharmaceutical technology. J Pharm Sci 99:587–597

35. Vehring R, Foss WR, Lechuga-Ballesteros D (2007) Particle formation in spray drying. J Aerosol Sci 38:728–746

36. Vehring R (2008) Pharmaceutical particle engineering via spray drying. Pharm Res 25:999–1022

37. Okuyama K, Lenggoro IW (2003) Preparation of nanoparticles via spray route. Chem Eng Sci 58:537–547

38. Nandiyanto ABD, Okuyama K (2011) Progress in developing spray-drying methods for the production of controlled morphology particles: from the nanometer to submicrometer size ranges. Adv Powder Technol 22:1–19

39. Heng D, Lee SH, Ng WK et al (2011) The nano spray dryer B-90. Expert Opin Drug Deliv 8:965–972

40. Lee SH, Heng D, Ng WK et al (2011) Nano spray drying: a novel method for preparing protein nanoparticles for protein therapy. Int J Pharm 403:192–200

41. Wang Z, Finlay WH, Peppler M et al (2006) Powder formation by atmospheric spray-freeze-drying. Powder Technol 170:45–52

42. Topp MN (1973) Ultrasonic atomization-a photographic study of the mechanism of disintegration. J Aerosol Sci 4:17–25

43. Yurteri CU, Hartman RPA, Marijnissen JCM (2010) Producing pharmaceutical particles via electrospraying with an emphasis on nano and nano structured particles – a review. KONA Powder Part J 28:91–115

44. Leuenberger H (2002) Spray freeze-drying – the process of choice for low water soluble drugs? J Nanopart Res 4:111–119

45. Cheow WS, Ng ML, Kho K et al (2011) Spray-freeze-drying production of thermally sensitive polymeric nanoparticle aggregates for inhaled drug delivery: effect of freeze-drying adjuvants. Int J Pharm 404:289–300

46. Forde G, Friend J, Williamson T (2006) Straightforward biodegradable nanoparticle generation through megahertz-order ultrasonic atomization. Appl Phys Lett 89:064105–064105–3

47. Bittner B, Kissel T (1999) Ultrasonic atomization for spray drying: a versatile technique for the preparation of protein loaded biodegradable microspheres. J Microencapsul 16:325–341

48. York P (1999) Strategies for particle design using supercritical fluid technologies. Pharm Sci Technol Today 2:430–440

49. Sethia S, Squillante E (2004) Solid dispersion of carbamazepine in PVP K30 by conventional solvent evaporation and supercritical methods. Int J Pharm 272:1–10

50. Byrappa K, Ohara S, Adschiri T (2008) Nanoparticles synthesis using supercritical fluid technology – towards biomedical applications. Adv Drug Deliv Rev 60:299–327

51. Jaworek A (2007) Micro- and nanoparticle production by electrospraying. Powder Technol 176:18–35

52. Ganan-Calvo AM (1999) The surface charge in electrospraying: its nature and its universal scaling laws. J Aerosol Sci 30:863–872

53. Jaworek A, Sobczyk AT (2008) Electrospraying route to nanotechnology: an overview. J Electrostat 66:197–219

54. Marijnissen JCM, Gradon L (2010) Nanoparticles in medicine and environment: inhalation and health effects. J Aerosol Med 23:339–341

55. Enayati M, Ahmad Z, Stride E et al (2010) One-step electrohydrodynamic production of drug-loaded micro- and nanoparticles. J R Soc Interface 7:667–675

56. Valo H, Peltonen L, Vehvilaeinen S et al (2009) Electrospray encapsulation of hydrophilic and hydrophobic drugs in poly(L-lactic acid) nanoparticles. Small 5:1791–1798

57. Heyder J, Gebhardt J, Rudolf G et al (1986) Deposition of particles in the human respiratory tract in the size range 0.005–15 μm. J Aerosol Sci 17:811–825

58. Cook RO, Pannu RK, Kellaway IW (2005) Novel sustained release microspheres for pulmonary drug delivery. J Control Release 104:79–90

59. Mizoe T, Ozeki T, Okada H (2007) Preparation of drug nanoparticle-containing microparticles using a 4-fluid nozzle spray drier for oral, pulmonary, and injection dosage forms. J Control Release 122:10–15

60. Ely L, Roa W, Finlay WH et al (2007) Effervescent dry powder for respiratory drug delivery. Eur J Pharm Biopharm 65:346–353

61. Yamamoto H, Hoshina W, Kurashima H et al (2007) Engineering of poly(DL-lactic-co-glycolic acid) nanocomposite particles for dry powder inhalation dosage forms of insulin with the spray-fluidized bed granulating system. Adv Powder Technol 18:215–228

62. Azarmi S, Tao X, Chen H et al (2006) Formulation and cytotoxicity of doxorubicin nanoparticles carried by dry powder aerosol particles. Int J Pharm 319:155–161

63. Grenha A, Seijo B, Remunan-Lopez C (2005) Microencapsulated chitosan nanoparticles for lung protein delivery. Eur J Pharm Sci 25:427–437

64. Sham JOH, Zhang Y, Finlay WH et al (2004) Formulation and characterization of spray-dried powders containing nanoparticles for aerosol delivery to the lung. Int J Pharm 269:457–467

65. Hadinoto K, Zhu K, Tan RBH (2007) Drug release study of large hollow nanoparticulate aggregates carrier particles for pulmonary delivery. Int J Pharm 341:195–206

66. Jensen DMK, Cun D, Maltesen MJ et al (2010) Spray drying of siRNA-containing PLGA nanoparticles intended for inhalation. J Control Release 142:138–145

67. Tsapis N, Bennett D, Jackson B et al (2002) Trojan particles: large porous carriers of nanoparticles for drug delivery. Proc Natl Acad Sci U S A 99:12001–12005

68. Heyder J (2004) Deposition of inhaled particles in the human respiratory tract and consequences for regional targeting in respiratory drug delivery. Proc Am Thorac Soc 1:315–320

69. Beck-Broichsitter M, Merkel OM, Kissel T (2012) Controlled pulmonary drug and gene delivery using polymeric nano-carriers. J Control Release 161:214–224

70. Beck-Broichsitter M, Schweiger C, Schmehl T et al (2012) Characterization of novel spray-dried polymeric particles for controlled pulmonary drug delivery. J Control Release 158:329–335

71. Beck-Broichsitter M, Knuedeler MC, Schmehl T et al (2013) Following the concentration of polymeric nanoparticles during nebulization. Pharm Res 30:16–24

72. Watts AB, McConville JT, Williams RO III (2008) Current therapies and technological advances in aqueous aerosol drug delivery. Drug Dev Ind Pharm 34:913–922

73. Anton N, Jakhmola A, Vandamme TF (2012) Trojan microparticles for drug delivery. Pharmaceutics 4:1–25

74. Forbes B, Ehrhardt C (2005) Human respiratory epithelial cell culture for drug delivery applications. Eur J Pharm Biopharm 60:193–205

75. Lehmann A, Daum N, Bur M et al (2011) An in vitro triple cell co-culture model with primary cells mimicking the human alveolar epithelial barrier. Eur J Pharm Biopharm 77:398–406

76. Rothen-Rutishauser B, Mueller L, Blank F et al (2008) A newly developed in vitro model of the human epithelial airway barrier to study the toxic potential of nanoparticles. ALTEX 25:191–196

77. Paur HR, Cassee FR, Teeguarden JG et al (2011) In-vitro cell exposure studies for the assessment of nanoparticle toxicity in the lung – a dialog between aerosol science and biology. J Aerosol Sci 42:668–692

78. Lenz A, Karg E, Lentner B et al (2009) A dose-controlled system for air-liquid interface cell exposure and application to zinc oxide nanoparticles. Part Fibre Toxicol 6:32

79. Hein S, Bur M, Schaefer UF et al (2011) A new Pharmaceutical Aerosol Deposition Device on Cell Cultures (PADDOCC) to evaluate pulmonary drug absorption for metered dose dry powder formulations. Eur J Pharm Biopharm 77:132–138

80. Beck-Broichsitter M, Schmehl T, Seeger W et al (2011) Evaluating the controlled release properties of inhaled nanoparticles using isolated, perfused, and ventilated lung models. J Nanomaterials 2011:1–16, article ID 163791

81. Sakagami M (2006) In vivo, in vitro and ex vivo models to assess pulmonary absorption and disposition of inhaled therapeutics for systemic delivery. Adv Drug Deliv Rev 58:1030–1060

82. Beck-Broichsitter M, Gauss J, Packhaeuser CB et al (2009) Pulmonary drug delivery with aerosolizable nanoparticles in an ex vivo lung model. Int J Pharm 367:169–178

83. Beck-Broichsitter M, Gauss J, Gessler T et al (2010) Pulmonary targeting with biodegradable salbutamol-loaded nanoparticles. J Aerosol Med 23:47–57

84. Rytting E, Bur M, Cartier R et al (2010) In vitro and in vivo performance of biocompatible negatively-charged salbutamol-loaded nanoparticles. J Control Release 141:101–107

Nanomedicine: The Promise and Challenges in Cancer Chemotherapy

11

Youssef W. Naguib and Zhengrong Cui

Contents

Keywords

Nano-carrier • Tumor microenvironment •
Barriers • Anticancer • Nanomedicine • EPR
• Cancer chemoresistance • Tumor stroma •
Nanoparticles

Y.W. Naguib
Pharmaceutics Division, College of Pharmacy, The
University of Texas at Austin, Austin, TX 78712, USA

Z. Cui, PhD (✉)
Pharmaceutics Division, College of Pharmacy,
The University of Texas at Austin,
Austin, TX 78712, USA

Dell Pediatric Research Institute, The University of
Texas at Austin, 1400 Barbara Jordan Boulevard,
Austin, TX 78723, USA
e-mail: zhengrong.cui@austin.utexas.edu

Abbreviations

ABC transporter	ATP-binding cassette transporter
ADC	Antibody drug conjugate
AELs	Anticancer etherlipids
BBB	Blood brain barrier
BBTB	Blood brain tumor barrier
bFGF	basic fibroblast growth factor
CAFs	Cancer associated fibroblasts
CMC	Critical micelle concentration
CSF-1	Colony stimulating factor 1
DAR	Drug : antibody ratio
dFdCTP	difluorodeoxycytidine triphosphate
dFdU	difluorodeoxyuridine
DOPE	Dioleoyl phosphoethanolamine

DSPE	1,2-distearoyl-sn-glycero-3-phosphoethanolamine		PSMA	Prostate-specific membrane antigen
DSPG	1,2-distearoyl-glycero-3-phosphocholine		RGD	Argentine-glycine-aspartic acid
ECM	Extracellular matrix		siRNA	short-interfering RNA
EGFR	Epithelial growth factor receptor		SLN	Solid lipid nanoparticles
EPR	Enhanced permeation and retention		SMANCS	Neocarzinostatin-styrene-maleic acid conjugate
FAR	Folic acid receptor		Smo	Smoothened
GemC18	4(N)-stearoyl gemcitabine		SPARC	Specific protein, acidic and rich in cysteine
GEMM	Genetically engineered mouse model		sPLA2	secretory phospholipase A2
GLUT	d-glucose transporter protein		TAMs	Tumor-associated macrophages
HA	Hyaluronic acid		VEGF	Vascular endothelial growth factor
hENT	human equilibrative nucleoside transporter		VEGFR	Vascular endothelial growth factor receptor
HER-2	Human endothelial growth factor receptor-2		VIP	Human vasoactive intestinal peptide
Hh	Hedgehog pathway		α-SMA	α-smooth muscle actin
HIF1α	Hypoxia-inducible factor 1α			
HPMA	N-(2-hydroxypropyl) methacrylamide			
HYAL	Hyaluronidase			
IFP	Interstitial fluid pressure			
LOX	Lysyl oxidase			
mAb	monoclonal antibody			
MCP-1	Monocyte chemoattractant protein-1			
MDR	Multidrug resistance			
MIP-1 α	Macrophage inflammatory protein-1α			
MMP	Matrix metalloprotease			
MPS	Mononuclear phagocyte system			
nab	nanoparticles-albumin bound			
NO	Nitric oxide			
NSCLC	Non-small cell lung cancer			
oHA	oligo-fragments of hyaluronic acid			
PCL	Poly-ε-caprolactone			
PDAC	Pancreatic ductal adenocarcinoma			
PDGF	Platelet-derived growth factor			
PEG	Polyethylene glycol			
PEI	Polyethylene imine			
PEO	Polyethylene oxide			
P-gp	P-glycoprotein			
PLA	Poly-lactic acid			
PLGA	Poly (lactic-co-glycolic) acid			
PPO	Polypropylene oxide			
PRINT	Particle replication in non-wetting templates			
proAEL	phosphorylated prodrugs of anticancer etherlipids			

11.1 Introduction

11.1.1 Nanomedicine and Cancer

Cancer is a leading cause of death worldwide. Conventional chemotherapy has drawbacks ranging from limited effectiveness, chemoresistance, and treatment-related side-effects and damages to healthy tissues. The idea of drug targeting started to emerge as early as 1906. As outlined by Danhier et al., the challenge ahead is about how to find proper targets, to develop a drug that exploits the targets, and finally to design the proper delivery system (carrier) for the drug [1]. Cancer nanomedicine is the use of nano-sized entities (10–200 nm) to diagnose, prevent, or treat cancer. These entities can be loaded with chemotherapeutics, nucleic acids, radiosensitizers, diagnostic agents and/or probes. This chapter displays an updated review of several nano-carrier platforms, their common features, and applications, followed by a discussion of the major mechanisms by which nano-carriers are targeted to the cancer cells. Finally it discusses barriers that hinder the applications of nanomedicine in cancer chemotherapy, and how the rational

design of the nanomedicine may overcome these barriers.

11.2   General Classification of Nano-carrier Platforms

11.2.1   Liposomes

Liposomes are one of the earliest nano-scale drug carriers reported in literature, first described by Bangham et al. [2, 3]. They are spherical vesicles, composed of closed phospholipid bilayer structures that resemble the cell membrane. Their unique structure enables the encapsulation of water soluble drugs within their hydrophilic cores, while water-insoluble drugs can be entrapped within the lipid bilayer [4]. Nucleic acids (e.g., plasmids) can be non-covalently attached on the surface of cationic liposomes via electrostatic interaction [5]. Various biocompatible phospholipids, including 1,2-distearoyl-sn-glycero-3-phosphoethanolamine (DSPE) and 1,2-distearoyl-glycero-3-phosphocholine (DSPG), are in products that have been approved by the United States Food and Drug Administration (FDA) for human use [6]. Different types of liposome have different sizes. For example, multilamellar liposomes have a size range of about 500–5,000 nm, while uni-lamellar liposomes can be as small as 50–100 nm [7]. Liposome surface can be modified with polyethylene glycol (i.e., PEGylation) to prolong their blood circulation time [8–10]. In addition, liposome surface can be modified with various targeting moieties, including small molecules (e.g., anisamide as a ligand to Sigma receptors [11–13]) or macromolecules (e.g., monoclonal antibodies in immunoliposomes [14, 15]) to bind to targets that are exclusively expressed, or overexpressed, by tumor cells. Liposomal formulations of anticancer drugs currently on the market include PEGylated doxorubicin liposomes (Doxil®, about 100 nm), non-PEGylated doxorubicin liposomes (Myocet®), and non-PEGylated daunorubicin liposomes (Daunoxome®, about 35–65 nm). The advantages and disadvantages of PEGylation will be discussed in more details later.

11.2.2   Polymeric Nanoparticles

Various polymers have been used to prepare nanoparticles, including natural polymers (e.g., chitosan and albumin) and synthetic polymers (e.g., poly-lactic acid (PLA) and poly-lactic-co-glycolic acid (PLGA)). PLA and PLGA are widely used in nano- and micro-particle preparation due to their biodegradability, biocompatibility, and well-documented safety profile [16, 17]. Nanoparticles prepared by polyesters, such as PLA, PLGA, and poly-ε-caprolactone (PCL), undergo bulk erosion, where the aqueous medium penetrates inside the nano-carriers and causes hydrolysis of the core, which brings on further erosion of the bulk [18, 19]. On the contrary, nanoparticles prepared with other polymeric classes, such as poly-anhydrides and poly-orthoesters, undergo surface erosion, which provides a zero-order release pattern [19–21]. Various homopolymers (e.g., PLA), co-polymers (e.g., PLGA), and block-co-polymers (e.g., PLGA-polyethylene glycol (PLGA-PEG), and PCL-PEG) have been used to prepare nano-carriers. Block-copolymers that contain PEG chains may render the nanoparticles prepared using them 'stealthy' and 'long circulating' [22].

Emulsion-based methods can be used to prepare PLA or PLGA nanoparticles, where a single oil-in-water (O/W) emulsion method is suitable for lipophilic drugs (e.g., docetaxel [23]), whereas the double emulsion (W/O/W) method helps the encapsulation of hydrophilic drugs (e.g. siRNA [24]). The double emulsion method involves the use of two immiscible liquid phases, where a surface active agent is necessary to form the stable emulsion, and nanoparticles are solidified following solvent evaporation [25]. On the other hand, the nanoprecipitation (solvent displacement) method involves the use of two miscible liquids for the spontaneous formation of nanoparticles, without the use of surfactant, as the method does not rely on interfacial phenomenon [25, 26].

Other methods that can be used to prepare polymeric nanoparticles include spray drying [27] and supercritical fluid technology [28]. In addition, micro- and nano-fabrication methods (e.g., particle replication in non-wetting templates, PRINT) are developed to produce nano-structures with a high level of control over shapes, sizes, aspect ratios, and surface chemistry, where nano-discs, filaments, rods, cubes, cylinders, and spheres can be produced and rationally employed to tackle drug delivery hurdles. For more information on these techniques, the reader is referred to [29–31].

11.2.3 Micelles

Micelles are self-assembled nano-aggregates, composed of amphiphilic block-copolymer or lipid-based molecules, with a lipophilic core and hydrophilic shell to solubilize lipophilic drugs. Various micelles that are based on poloxamers [32], PEGylated polyesters (e.g., PLA-PEG [33], or PCL-PEG [34]) have been used to deliver anti-cancer agents. For example, Genexol-PM, which is based on PLA-PEG micelles with an average size of about 60 nm for paclitaxel delivery, has gained approval for human use in South Korea in 2006 [6]. A mixed micelle is a self-assembled nano-structure composed of a mixture of two or more block-copolymers, mixed together to impart the favorable features of each single component to the final micellar structure [35]. Poloxamers (Pluronic®, tri-block copolymers of the hydrophilic polyethylene oxide (PEO) and the lipophilic polypropylene oxide (PPO), in the form of PEO-PPO-PEO) with different grades and PEO to PPO ratios are commonly used for this purpose. Chen et al. developed a mixed micelles formulation, composed of Pluronics P105 and F127, for the delivery of docetaxel to taxol-resistant lung cancer cells [36]. Due to the high content of PPO in P105, high docetaxel content could be loaded. However, the short PEO chains were not sufficient to stabilize the micelles. The long PEO chains of Pluronic F127, when mixed with P105, successfully improved the stability of the final formulation [36].

11.2.4 Solid Lipid Nanoparticles (SLNs)

SLNs are lipid-based nano-carriers that are solid at room temperature and can successfully encapsulate lipid-soluble drugs. Materials used to prepare SLNs include mono-, di-, tri-glycerides, or a mixture of them, fatty acids (e.g., stearic acid), and phospholipids (e.g., phosphatidyl choline and lecithin). While the method of high pressure homogenization (HPH) is widely used to prepare SLNs [37, 38], other methods have also been described in literature, including emulsion-based methods [39], ultrasonication [40], and solvent injection method [41]. Advantages of SLNs include cost-effective production, even in a large-scale [42]. For more detailed information on the application of SLNs in cancer therapy, the reader is referred to [43, 44].

11.2.5 Drug-Polymer Conjugates

These are composed of a small molecule anti-cancer agent(s) covalently linked to a biocompatible polymeric chain via a bio-responsive linker. Drug-polymer conjugates may improve the pharmacokinetics profile of the drug, enhance its stability, and increase the accumulation of the drugs in tumor tissues or inside tumor cells [6, 45–48]. Various drug-polymer conjugates have been investigated since the idea was hypothesized by Ringsdorf [49]. One of the very early conjugates is the doxorubicin-(N-(2-hydroxypropyl) methacrylamide) copolymer conjugate (doxorubicin-HPMA, PK1, FCE28068), which is designed to unload the doxorubicin in tumor cells following the cleavage of the peptidyl linker by lysosomal cysteine proteinases [50]. Other drug conjugates that have been developed include HPMA-doxorubicin-gemcitabine conjugate [51], paclitaxel-polylactide conjugate [52], polyethylene glycol-camptothecin (PEG-camptothecin, Pegamotecan) [46], and paclitaxel-polyglutamic acid conjugate (paclitaxel polyglumex, PPX, Opaxio) [45]. Pegamotecan is a PEG-camptothecin conjugate that is linked via an ester bond, with a drug loading of 1.7 % (w/w). Unfortunately, Pegamotecan did not show

a promising clinical benefit compared to irinotecan in patients with gastric or gastroesophageal adenocarcinoma in a phase II trial and was subsequently discontinued by its sponsor [46]. Opaxio (PPX, formerly known as Xyotax) is a water soluble conjugate, composed of paclitaxel (37 %, w/w) conjugated in a comb-like manner to poly L-glutamic acid via a degradable linker [46, 53, 54]. Despite very promising data in preclinical and early phase clinical studies, data from several phase III clinical studies showed that PPX is not significantly more effective than standard treatments [54]. For example, the conjugate did not show any survival benefit, compared to either gemcitabine or vinorelbine single agent chemotherapeutic, in a randomized phase III trial in patients with advanced non-small cell lung cancer (NSCLC) [55]. Similarly, no survival benefit was found when PPX was used as a second line of treatment against NSCLC in a phase III trial on 849 patients, as compared to docetaxel [56]. Nonetheless, this conjugate is still under extensive clinical investigation.

11.2.6 Antibody-Drug Conjugates

Monoclonal antibody (mAb)-drug conjugates (ADC or immunoconjugates) are bifunctional molecules that benefit from the targeting capabilities of the mAb moiety and the cytotoxic activity of the drug. Candidate mAbs should be chosen to target antigens that are exclusively expressed or overexpressed on tumor cells, but not on neighboring healthy tissues [57, 58]. Advantages of ADCs include the potential to achieve a much higher concentration of the cytotoxic agent in tumor tissues (mainly due to the targeting abilities of the mAb), a lower systemic toxicity [59, 60], and an overall improved pharmacokinetic profile [61]. ADCs can benefit from the long circulatory half-life of mAbs [62]. However, the stability of the linker between the mAbs and the drug molecules should also match this long-circulation time. Modifications of the linker between the mAb and the cytotoxic agent have successfully overcome some of the major problems encountered earlier with ADCs. For example, when both

the drug and the linker were hydrophobic, the maximum drug-antibody ratio (DAR) obtained was 3–4, and further increase of the ratio resulted in aggregations and short circulation time [63]. The use of hydrophilic linkers helps improve the drug-antibody ratio (DAR) [62–64]. Clinical problems associated with ADCs include systemic toxicity, which may be attributed to immature drug release and antigen shedding from the tumor tissues into the circulation; the shed antigens can reside anywhere in the body and mislead the 'homing missile' to a false target [57, 65, 66]. Other disadvantages include unexpectedly low tumor accumulation of the cytotoxic agent, with values as low as 0.0003–0.08 % of the injected dose per gram of tumor [65]. This led to a shift from using conventional cytotoxic agents (e.g., doxorubicin) to other agents with superior toxicity profiles that previously hindered their clinical use (e.g., maytansinoids, calicheamicins, and auristatins) [58, 67]. However, systemic toxicities of these agents, even after mAb conjugation, may still prevail. For example, the FDA announced that Pfizer voluntarily withdrew Mylotarg® (gemtuzumab ozogamicin) in 2010 for safety and efficacy issues [68]. In addition, the low tumor accumulation necessitates the administration of large doses of the conjugates, which, in turn, may stir economic problems, especially for long-term therapy. For example, the estimated single dose cost of an auristatin-CD30 conjugate (Brentuximab vedotin) is about $13,500 every 3 weeks [69]. Nevertheless, ADCs are still regarded as very promising alternatives to conventional chemotherapy, with improved anticancer activity and safety profiles.

11.2.7 Inorganic Nanoparticles

These include carbon nanotubes [70], fullerenes [71], gold nanoparticles [72], silica nanoparticles [73], iron oxide nanoparticles [74], zirconium nano-platelets [75], and quantum dots [76]. These nano-structures will not be overviewed in this chapter, and comprehensive reviews on their application in cancer treatment and imaging can be found elsewhere [77–81].

11.3 Mechanisms Underlying Nano-Carrier-Based Drug Delivery to Tumors

11.3.1 Passive Targeting via Enhanced Permeation and Retention (EPR) Phenomenon

11.3.1.1 Background

The EPR phenomenon was discovered by Matsumura and Maeda in 1986 [82, 83]. Maeda and coworker(s), working on an anticancer protein-polymer conjugate called SMANCS (neocarzinostatin-styrene-maleic acid conjugate), noticed that many solid tumors exhibit enhanced vascular permeability that resembles the inflammatory state of normal non-cancerous tissues. In this context, the clearance of a macromolecule (i.e., Evans blue-albumin complex) from normal tissues was found to be much faster than that from tumor tissues [82, 84, 85].

When a tumor starts to form, the tumor cells rapidly proliferate, but the nutritional supply (mainly via diffusion) is only suitable for normally proliferating cells [86]. Thus, the tumor size is limited to what is called 'diffusion-limited size' (about 2 mm) [86, 87]. In order to satisfy their craving for nutrients, cancer cells recruit new blood vessels, and tumor angiogenesis starts to take place [86]. This phase is characterized by excessive secretion of angiogenic factors such as vascular endothelial growth factor (VEGF), platelet-derived growth factor (PDGF), basic fibroblast growth factor (bFGF), in addition to other factors (e.g., bradykinins, nitric oxide (NO), cytokines, matrix metalloproteinases (MMP)), which enhance angiogenesis and vascular permeability [87–89]. The mechanism of neo-angiogenesis in tumors is discussed in details elsewhere [86, 90].

The newly-formed blood vessels have a leaky imperfect structure and abnormal basement membrane, while pericytes and smooth muscle layer are deficient or almost absent [87, 91]. This leaves the tumor blood vessel architecture flawed with fenestrations. The size of the fenestrations is heterogeneous and can reach a maximum cut-off value of 200–800 nm [83], or 1,000–2,000 nm in some other reports [84, 91]. Blood flow within tumors is also erratic and tortuous [87]. The imperfect, and fenestrated architecture of tumor vasculature helps the extravasation of circulating macromolecules and nano-carriers into the tumor tissues (i.e., enhanced permeation), which does not happen in healthy organs with intact vasculature [83, 84, 87]. The other facet of EPR is the enhanced retention and accumulation of extravasated macromolecules and nano-carriers within tumor tissues, which is facilitated by the poor lymphatic drainage and slow venous return in tumor tissues [84, 89, 91]. Small molecules may also benefit from the enhanced permeability of the tumor vasculature, but they will fail to accumulate within the tumor tissues, as they will be 'washed out' quickly by diffusion [83, 87, 89]. The leaky tumor vasculature also gives detached cancer cells access to the circulation, causing metastasis [87, 91]. The phenomenon has been exploited in many human tumors (excluding hypovascular tumors such as pancreatic cancer) for both chemotherapeutic and imaging applications [89, 92, 93].

11.3.1.2 Challenges Associated with EPR-Mediated Delivery Systems

Tumor Heterogeneity

Heterogeneity is one of the landmarks of tumors in clinical applications. Many factors need to be studied before an EPR-based nanomedicine can move to the clinic. These factors include the differences in cancers in vasculature development and architecture, the effect of the cancer stage on the EPR features, the chances of delivering nanomedicine to the metastatic lesion vs. primary tumor sites, the effect of tumor stromal density (will be discussed later), in addition to patient-to-patient variability, and whether individualized nanomedicine is necessary. Tumor heterogeneity may also extend to pre-clinical level, as the animal tumor model selection may have a significant effect on decision-making regarding subsequent clinical trials. It is reported that subcutaneous xenografts are hastily-formed tumors that usually exhibit an exaggerated phenotype of EPR, which may not be of great value in clinical

translation [94]. Orthotopic tumor models and, more importantly, genetically engineered mouse models (GEMM) may be of greater value when studying EPR effect on nanomedicine delivery. For more information on the effect of tumor heterogeneity on the EPR effect, the reader can refer to [94–97]. In addition, in order to achieve more correlation between animal tumor models and cancer patients, factors such as the difference in treatment regimens in mice and in humans due to different metabolic rates and the huge tumor/body weight ratio in mice compared to humans should be carefully considered in translational research [98].

Augmenting the EPR Effect

Maeda and co-workers hypothesized that, since tumor vasculature lacks an intact basement membrane and smooth muscle layer, when a vasoconstrictor agent (e.g. angiotensin II) is systemically administered, the tumor blood vessels will not be affected, while other blood vessels in the body will be constricted with subsequent increased blood pressure. Thus, the tumor blood flow is expected to increase, which in turn will increase the delivery of nanomedicine to tumors via EPR effect [99]. It was noticed that the combined administration of enalapril, an angiotensin-converting enzyme inhibitor with vascular permeability enhancement effect, and angiotensin II, led to a 2-fold increase in the accumulation of a labeled mAb in human colon tumor-bearing athymic mice [91, 99]. In another report, when a nitroglycerin (NO-generating substance) ointment was applied onto tumor-bearing animal skin in an area distant from the tumor site, blood flow in tumors was significantly enhanced, but not in muscles [100]. The tumor accumulation, as well as the antitumor effect, of a ^{65}Zn-labeled macromolecular drug (PEG-Zn-protoporphyrin IX, PZP) was significantly enhanced following topical application of nitroglycerin [91, 100].

Tumor Vascular "Normalization" and Nanomedicine

While the aberrantly-formed tumor vasculature is considered to be a feature that should be taken advantage of in nanomedicine delivery, other researchers regarded it as a hurdle that should be 'normalized' in order to pave the way for the delivery of chemotherapeutic agents to tumors. Jain and co-workers were the first to introduce the idea of 'tumor vascular normalization' in response to anti-VEGF treatment [101, 102]. They proposed that the defective tumor vascular architecture may have a detrimental effect on the delivery of nanomedicines, and chemotherapy in general, to tumors [102]. According to their hypothesis, tumor vascular "normalization" is expected to alleviate tumor hypoxia, and thus enhance tumor radiation therapy outcomes, reduce metastasis and the emergence of resistance, and ultimately improve tumor chemotherapy [102–104]. In addition, the vessels themselves will have less leakiness, normal basement membrane and pericyte distribution [94, 101]. In normal state, there is a balance between pro- and anti-angiogenic factors; however, in tumor state, this balance is shifted towards pro-angiogeic activity to promote tumor neo-vasculature formation [105]. The 'cautious' use of the anti-angiogenic treatment modalities (e.g., mAb for VEGF like bevacizumab, Avastin®, and VEGF receptor tyrosine kinase inhibitors) is the most common method to shift the pro- and anti-angiogenic balance back to 'normalized' levels, not to a complete anti-angiogenicity [103, 105]. Although the latter strategy of abolishing tumor vasculature may be expected to starve the tumor, it may also harm normal tissue vasculature and adversely affect further chemotherapy delivery [101]. Unfortunately, the vascular "normalization" effect was found to be transient (about 7–10 days), and during this period (called the "normalization" window), concomitant chemotherapy or radiotherapy should start [105, 106]. However, there is an argument that this technique minimizes the benefit of EPR phenomenon in solid tumors, as the leaky tumor vasculature will be almost lost [94]. Recently, Jain and coworkers found that tumor vascular "normalization" improved the tumor uptake of 10–12 nm nanoparticles (i.e., albumin-bound paclitaxel in Abraxane®), but not 100 nm nanoparticles (i.e., Doxil®) [107]. The study highlighted the

importance of judicially adjusting the dose of the tumor vascular "normalization" treatment, as the use of a higher dose hindered the uptake of even the small nanoparticles [107].

11.3.2 Active Targeting

The term active targeting involves the exploitation of certain proteins or any other targets, exclusively expressed, or overexpressed, by tumor cells or tumor vasculature via the attachment of a specific ligand onto the surface of the nano-carriers (surface decoration); such ligand should bind with a high affinity to the tumor target. The receptor-bound nano-carriers are then internalized inside tumor cells via receptor-mediated endocytosis [108]. While tumor accumulation takes place via EPR, the role of active targeting may be thought of as a tool towards the cellular internalization of nano-carriers. Various targets have been identified in tumors, including angiogenesis targets such as vascular endothelial growth factor receptors (VEGFR), and $\alpha\nu\beta_3$ integrin, epidermal receptors such as epidermal growth factor receptor (EGFR) and human epidermal growth factor receptor 2 (HER-2), human vasoactive intestinal peptide (VIP) receptors, sigma receptors, transferrin receptors, and folic acid receptors [109, 110].

Two main EGFR tyrosine kinases are well-studied and characterized, namely, EGFR and HER-2. This family of receptor tyrosine kinases mediate cell signaling towards proliferation following the binding of growth factor ligands [109]. Cetuximab (Erbitux®, Bristol Myers Squibb, NJ) and Trastuzumab (Herceptin®, Genetech, CA) are FDA-approved mAbs against EGFR and HER-2, respectively, and have been used either as a whole mAb or a fragment of an antibody (Fab') as targeting moieties to decorate the surface of nano-carriers to improve tumor targeting [109, 111, 112]. Several methods have been adopted to conjugate mAbs onto nanoparticles, including avidin-biotin interaction and covalent conjugation between nano-carriers with thiolated surface and maleimide-modified mAbs [112, 113]. For example, Sandoval et al. designed an EGFR-targeted SLNs that contain a lipophilic gemcitabine prodrug (4(N)-stearoyl gemcitabine, GemC18) to target human breast cancer cells that overexpress EGFR [114]. Recombinant mouse epidermal growth factor (EGF) was first thiolated and purified, and then conjugated to maleimide-terminated PEG chains on the surface of GemC18-SLNs. Compared to non-targeted GemC18-SLNs, the EGFR-targeted SLNs showed enhanced antitumor activity and accumulation in tumors in mice with pre-established human breast cancer tumors (MDA-MB-468) [114]. Other tumor cell targets include transferrin receptors, sigma receptors, and folic acid receptors (FAR), which can be targeted with nano-carriers surface-decorated with transferrin [115], folic acid [116–118], and anisamide [11, 13], respectively. Currently, a prostate-specific membrane antigen (PSMA)-targeted PLGA-PEG nanoparticle formulation that contains the second generation taxane docetaxel (BIND-014, BIND Biosciences Inc., MA) is under evaluation in clinical trials [119].

11.4 Barriers to Delivering Nanomedicines to the Tumors

In this section, the major barriers that hinder the delivery of nanomedicines to tumors will be discussed. Once a nanomedicine is administered, it has to pass physiological barriers before reaching the circulation, unless it is administered by intravenous (i.v.) injection. Once injected, the nanomedicine has to travel a long way to reach its target: the cancer cell. The body starts to react the very first moment the nanomedicine is in the circulation, in a way that tends to clear the blood from the newly introduced foreign material. Even the fraction of the nanomedicines that makes its way past these clearance mechanisms and reach the tumors will encounter a totally different environment that should also be tackled in order to get to the tumor cells. Two major approaches are generally applied to tackle the tumor microenvironment; one is to breach or modify the physical barriers of the tumor microenvironment, paving

the way for subsequent doses, and the other is to take advantage of some of the unique features that characterize the tumor microenvironment to deliver more drugs to cancer cells. Unfortunately, getting to the cells will not be the end of the journey, as the cancer cells have their own set of defenses that only a nanomedicine with a 'smart' design will be able to evade. This section will discuss the barriers that nanomedicines encounters on their voyage to targets, and how nanomedicines can be designed to reach these targets.

11.4.1 Nanomedicine Circulation Time

Once in the circulation, nano-carriers are subjected to quick surface adsorption of plasma proteins, including albumin, immunoglobulins, and complement proteins (opsonins), in a process called opsonization [120]. The 'opsonin-tagged' nano-carriers are then recognized and phagocytosed by the mononuclear phagocyte system (MPS) cells (e.g., monocytes and macrophages), which carry them to the MPS organs (e.g., liver, spleen, and lymph nodes), significantly shortening the circulation half-life of the nano-carriers [121, 122]. The accumulation of non-degradable nano-carriers in MPS organs may lead to toxicity [123]. In addition, glomerular filtration of nano-carriers smaller than 5.5 nm (renal filtration cutoff size) can take place, while much larger particles (~1 μm) are quickly opsonized [120, 124]. Although the 5.5 nm cutoff size seems too small, some nano-carriers may fall within this range and are filtered in the kidney (e.g. quantum dots, and carbon nanotubes [122]). Several factors determine the rate of opsonization of nano-carriers by plasma proteins, including surface characteristics (hydrophobic vs. hydrophilic), zeta potential, particle size, and shape [120, 123]. In general, opsonization occurs more efficiently and much faster to particles with hydrophobic surfaces than to those with hydrophilic surfaces [123]. This was the basis for the surface modification of nano-carriers with a hydrophilic molecule, which is the most widely-used strategy to prolong the circulation time of nano-carriers.

PEG is the most successfully used molecule to achieve this goal, and the process is called PEGylation. The technique was first exploited by Klibanov et al. in 1990, where a PEG moiety is covalently conjugated to a phospholipid (e.g., dioleoyl phosphoethanolamine, DOPE) that was incorporated into large uni-lamellar liposomes [10]. About 85 and 49 % of PEGylated liposomes were found circulating in mouse plasma 1 and 5 h after injection, respectively, compared to about 20 and 0 % for their non-PEGylated counterparts [10]. It is thought that the protruding PEG chains sterically hinder the adsorption of plasma proteins to the nano-carrier surface [10], and the hydrophilic nature that they impart to the nano-carrier surface minimizes non-specific interaction with MPS cells [10, 125]. The term STEALTH has been used to describe such PEGylated, long-circulating nano-carriers, as PEGylation has become a solid dogma in the rational design of nano-carriers for the delivery of tumor chemotherapeutics. Various researchers studied factors that govern efficient PEGylation. Desimone and colleagues studied the effect of PEGylation density on protein binding, macrophage uptake, and circulation time of PEGylated hydrogel nanoparticles (80×80×320 nm) produced by PRINT technology, where the nanoparticles were PEG-functionalized in two different conformations, brush and mushroom [126]. The researchers found that protein binding to the surface of nanoparticles is inversely proportional to PEG density, and interestingly, efficient protein binding inhibition and prolonged circulation were achieved at a less PEG density than what was previously reported [126]. Drug release from the nano-carrier is yet another factor that should be carefully considered in nano-carrier design. Since very fast drug release can result in complete dumping of the drug in the circulation before the nano-carriers reaches their target, a prolonged circulation time should be matched with slow drug release to prevent pre-mature drug leakage [44].

PEGylation strategy is not problem-free; it was found that repeated doses of PEGylated nano-carriers (e.g., Stealth liposomes, micelles, or nanoparticles) may elicit an immune response [127].

This phenomenon, commonly known as accelerated blood clearance (ABC), may result in rapid clearance and loss of clinical benefit of subsequent doses [128]. The details of the phenomenon, in addition to methods to overcome its detrimental effects, are reviewed elsewhere [127].

Bio-mimetic particles, which are 'camouflaged' micro- or nanoparticles that resemble biological entities, such as viruses, bacteria, red blood cells (RBC's), and leukocytes, have been extensively studied for drug delivery purposes. Since these previously mentioned biological entities have tremendous capabilities to evade most biological and cellular barriers in the mammalian bodies, the 'camouflaged' nanoparticles, if properly designed, can be expected to do the same [129]. This strategy, along with the judicious control of shape and size of the nano-carriers, has been adopted to increase the circulation time of drug-loaded nano-carriers and improve overall drug delivery to tumors [124]. To mimic filamentous viruses, Discher and co-workers developed a PEGylated flexible filamentous micelle formulation (filomicelles), of at least one dimension in the nano-range and the other may extend to microns, that was able to evade MPS cell uptake and circulate longer in the plasma, and consequently, deliver more drugs to tumors via EPR [130]. The PEG-PCL filomicelles showed persistent circulation in the plasma for up to a week, while their spherical counterparts were only there for one tenth of this time [131]. The paclitaxel-loaded filomicelles showed superior proapoptotic and tumor-shrinking activities in tumor-bearing nude mice, as compared to free paclitaxel, which was completely ineffective [131]. Recently, Taciotti and co-workers synthesized leukocyte-camouflaged non-porous silicone nanoparticles (leukolike vectors, LLV) coated with a leukocyte cellular membrane to impart cell-like functions to the nano-carrier [132]. These particles exhibited significantly less opsonization and cellular uptake by murine macrophages and human phagocytic cells. These particles may be promising in delivering drugs to tumors, not only because they undergo delayed liver clearance and enhanced tumor accumulation in mice, but also because their tumoritropic accumulation is driven

by the EPR effect and is also dependent on their ability to recognize and bind to tumor endothelium in an active form [132].

11.4.1.1 Other Biological Barriers

Other biological barriers in the delivery of nanomedicines to tumors include the blood brain barrier (BBB) or blood brain-tumor barrier (BBTB) following i.v. administration. Due to the presence of BBTB, characterized by the existence of endothelial cells tight junctions and low permeability into the tumor parenchyma, with vascular pore size of about 12 nm, the EPR effect may not be useful in increasing the delivery of nanomedicines in brain tumor tissues [120]. The use of targeting ligands to enable the translocation of the nano-carriers across the endothelial cells of the tumor vasculature is becoming a very promising technique [133–135]. Among the most exploited endothelial targets in tumors are $\alpha\nu\beta_3$ and $\alpha\nu\beta_5$ integrins, and D-glucose transporter protein (GLUT), where RGD (argentine-glycine-aspartic acid) peptide motifs [134] and deoxy-D-glucose are used to modify the surface of nano-carriers to facilitate such active-targeted uptake [133].

11.4.2 Nanomedicine and Tumor Microenvironment

11.4.2.1 Background

A better understanding of the tumor microstructure is a cornerstone in the design of a successful nanomedicine. A tumor cannot be described as myriads of cancer cells, all packed together, and localized in a specific region. Tumors can be considered as organs, with both well- and ill-formed structures, and various kinds of cells, including tumor cells, tumor fibroblasts, inflammatory cells (e.g. macrophages), blood and lymphatic network of vessels, held together within a complicated cross-linked extracellular matrix (ECM) [103, 136, 137]. In this section, various features of the tumor microenvironment will be overviewed in order to make a better use of the diverse toolbox that nanomedicine may provide to potentially conquer cancer.

ECM

The ECM components include various proteins (e.g., collagens), glycosaminoglycan-containing glycoproteins (e.g., hyaluronic acid (HA) and proteoglycans), the glycoprotein SPARC (secreted protein, acidic and rich in cysteine), and polysaccharides [138–140]. ECM components are usually differentiated into basement membrane and interstitial matrix [141]. Collagen type I, in addition to fibronectin, imparts mechanical integrity of the interstitial matrix of tumors [140]. A major determinant in the heterogeneity of tumor matrix rigidity is the expression level of matrix metalloproteinases (MMPs), which are overexpressed in many tumors and are responsible for collagen fibrils proteolysis within the tumor matrix [138, 141, 142]. Overexpression of MMPs is usually associated with decreased matrix rigidity, increased potential for cancer cells migration and metastasis, and the prevention of apoptosis [143]. ECM stiffness is also attributed in part to the overexpression of lysyl oxidase (LOX), which is responsible for hyaluronic acid and collagen fibers cross-linking [141, 144]. Overexpressions of MMPs and LOX are correlated with poor cancer patient prognosis [141, 142]. The interplay between ECM components verifies the overall state of tumor heterogeneity and plays a major role in determining the outcomes of chemotherapy. Tumor cells are shielded within this matrix and connected to the blood circulation through the previously discussed aberrantly-formed vasculature.

Tumor Hypoxia, Acidity, and Increased Interstitial Fluid Pressure

Three major features characterize the nature of the tumor matrix, namely hypoxia, extracellular acidity, and increased interstitial fluid pressure (IFP). Hypoxia is a feature of many solid tumor cores, where the ill-formed vasculature become unable to deliver oxygen and nutrients to deep tumor tissues, which lie more than 100 µm from the nearest blood vessel [145, 146]. These cells can no longer depend on oxidative metabolism to produce ATP, and rather revert to glycolysis, which, along with nullified lymphatic drainage, results in the accumulation of lactate within the

deep tumor tissues, lowering the extracellular matrix pH [145]. Although hypoxic cells are viable, they are usually accompanied with necrotic tissues. Unfortunately, these untoward conditions results in the selection of 'elite' cancer cells with outstanding resistance capabilities, as hypoxia induces tumor evolution, oncogene expression, apoptosis resistance (via selection of cells with lost p53 sensitivity) [147], and metastasis [144, 148, 149].

Both hypoxia and the acidic extracellular environment contribute to cancer chemoresistance via several mechanisms. Hypoxia stabilizes hypoxia-inducible factor 1α (HIF1 α), which leads to the upregulation of drug resistance genes, including multi-drug resistance 1 (MDR1) gene and P-gp-encoding gene [145, 150]. Drugs that rely on free-radical formation will experience reduced activity (e.g., bleomycin), whereas those that are weak bases (e.g. doxorubicin) will be ionized in the extracellular matrix, and thus their internalization will be hindered [138, 151]. In addition, hypoxic conditions tend to abolish the efficacy of radiation therapy [101].

Another common feature of most solid tumors is the increased interstitial fluid pressure (IFP), which can massively hinder the efficient delivery of chemotherapeutics [152, 153]. The defective lymphatic drainage, the accumulation of metabolic products in the hypoxic environment, and the imperfect structure of the hastily-formed vasculature significantly contribute to this phenomenon [138, 153, 154]. The rapidly dividing tumor cells and the dense cross-linked ECM structure not only compress the blood and lymph vessels, but also do not expand enough to allow edema formation, which can alleviate the increased IFP [98, 154]. The fenestration that characterize the leaky tumor vasculature may not be enough to deliver nano-carriers to the tumors in such cases, as the expected extravasation into tumor tissues may also be accompanied by an intravasation into the blood vessels, which demolishes any benefit that the nano-carriers may have to reach tumors [98]. Variability of IFP contributes to the heterogeneity of tumors and complicates the predictability of clinical outcomes from chemotherapy [146].

Tumor Associated Macrophages

Tumor-associated macrophages (TAMs) are part of the inflammatory cells in the tumor microenvironment. The link between inflammation and cancer development is well-established [155, 156]. TAMs usually originate from peripheral circulating monocytes that are recruited by the tumors [157]. However, some of them may locally proliferate within the tumor environment [158]. Although macrophages may be expected to fight against the rapidly- and aberrantly-proliferating tumor cells, interestingly enough, there is strong evidence that tumor cells are not only able to block the antitumor activity of the immune cells, but also 'enslave' the TAMs to serve their cause by helping the tumor cells proliferate, nourish, and progress [157–159]. TAMs improve tumor angiogenesis, invasiveness, metastasis, and immune system suppression, and have been linked with poor prognosis [155, 160, 161]. Several chemoattractants expressed by tumor and endothelial cells are involved in TAM recruitment, which include monocyte chemoattractant protein-1 (MCP-1, CCL2), macrophage inflammatory protein-1α (MIP-1α, CCL3), vascular endothelial growth factor (VEGF), and colony stimulating factor 1 (CSF-1) [157, 160]. The evident role of TAMs in tumor progression qualifies them as a potential target for nanomedicine-based chemotherapy.

Cancer-Associated Fibroblasts

Cancer-associated fibroblasts (CAFs) are the most abundant cells within the stroma in many tumors, including breast and pancreatic cancers, and are the main source of ECM components [162–164]. Fibroblasts are mesenchymal non-inflammatory cellular components of the connective tissues, although they regulate inflammation and wound healing, and they secrete fibrillar components of the ECM (like type I, III, and IV collagens) [163]. They become activated in wound healing and fibrosis (called myofibroblasts) and start *de novo* expression of a type of filamentous actin, α-smooth muscle actin (α-SMA) [162, 164–166]. Since cancer may be regarded as 'inflammation that never heals' [167], CAFs share a lot of similarities with activated fibroblasts associated with wound healing, including α-SMA expression (commonly used to identify CAFs) [163, 165, 168] to act as a scaffold for other ECM components. However, they do not deactivate or undergo apoptosis, like activated fibroblasts, after inflammation subsides [164], mainly because tumors are persistent. Fibroblasts in tumor stroma may exist as activated or non-activated form, but the vast majority of CAFs are the activated form (e.g., 80 % of fibroblasts in mammary tumors are in the activated form) [163, 168]. CAFs are involved in tumor progression and metastasis via secretion of a panel of cytokines that stimulate the excretion of MMPs, which predispose metastasis and provide support for tumor cell proliferation [168, 169].

After this brief overview of the tumor microenvironment, it should be clear that exploiting the anticancer activity of a nanomedicine in cell culture is not sufficient. In the literature, the *in vitro* cytotoxic evaluation is usually accepted as a means to ensure that the chemotherapeutic agent still retains its activity within the formulation. In the following section, the role of nanomedicine in overcoming the tumor microenvironment barriers, including ongoing clinical trials, will be overviewed.

11.4.2.2 Application of Nanomedicines to Breach or to Take Advantage of Tumor Microenvironment Barriers to Improve Drug Delivery

A successful anticancer agent should be able to simultaneously deal with as much of these barriers as possible. Combination drug or drug/adjuvant therapy can provide a multi-target modality. However, toxicity associated with such cocktails can be expected. The versatility of nanomedicine-based approaches may help tackle multi-functional tasks with minimum toxicity. In this section, nanomedicine approaches to breach tumor stroma, or to take advantage of some of the conditions specific to tumor microenvironment will be overviewed.

Depletion or Modification of Tumor Stroma

Hyaluronic Acid

Hyaluronic acid (HA) is abundantly accumulated in almost all epithelial tumors (e.g., pancreatic

ductal adenocarcinoma, PDAC), providing a viscoelastic matrix within the collagen fibers in the tumor, and is correlated with tumor proliferation, invasiveness, and poor prognosis [170, 171]. HA also contributes to tumor progression, and its water retention capability helps increase the IFP [171]. The use of bovine hyaluronidase (HYAL) to breach the tumor ECM was evaluated in various clinical trials during the late 1990's. Although promising results ranging from low or absent recurrence to prolonged patient survival were obtained when HYAL was combined with other anticancer drugs [172, 173], the development of allergic reactions to bovine HYAL, which can be serious in many cases, hindered the widespread acceptance of this approach [170]. Researchers at Halozyme® Therapeutics developed a human recombinant HYAL (rHuPH20, Hylenex®) that was well tolerated in 100 human volunteers following intradermal injection [174] and was approved by the FDA later on. However, due to the very short half-life of this product, its use for cancer treatment was not feasible [171]. To further improve this product, the researchers, via conjugation of a 30K N-hydroxysuccinimidyl ester of methoxy-polyethylene glycol-butanoic acid to rHuPH20, designed a PEGylated form of the enzyme (PEGPH20), which exhibited a 270-fold increase of *in vivo* half-life in mice, enabling its intravenous administration [171]. The PEGylated recombinant human hyaluronidase dramatically lowered the IFP via cleavage of the HA chains, releasing the entrapped water and decompressing the previously collapsed tumor vasculature, in transgenic mice with metastatic and invasive PDAC [175, 176]. The combination of PEGPH20 with gemcitabine dramatically suppressed metastasis and significantly prolonged the survival of transgenic mice with PDAC, compared to gemcitabine alone (91.5 days vs. 55.5 days, respectively, p=0.004) [175]. The administration of PEGPH20 3 h before liposomal doxorubicin showed a 4-fold increase in doxorubicin accumulation in high HA-tumor xenografts, compared to liposomal doxorubicin alone [171]. In a different context, Yang et al. designed a lipid-based nano-carrier for the taxane drug paclitaxel. They decorated the surface of the nano-carriers with oligo-fragments of HA (oHA) that result from the breakdown of the latter by HYAL [177]. They proposed that the use of oHA, which can replace the endogenous HA on its binding sites in CD44 receptors overexpressed on cancer cells, will not only provide an efficient targeting modality for HA-rich breast tumors, but also help breach the HA coat on tumors by CD44 receptor competition [177]. This strategy successfully sensitized the tumors to paclitaxel nano-carriers, which showed a significantly stronger anticancer activity compared to the non-decorated nano-carriers [177].

Hedgehog Pathway

Stromal depletion becomes critical in dealing with deadly tumors like PDAC, where the stromal structure is tremendously dense. PDAC is one of the deadliest cancers, with a median survival of few months, which can be extended for few more weeks when the standard first line treatment gemcitabine is used [178]. The fibroblasts-rich, rock-solid, almost avascular, desmoplastic tumor stroma acts as a mechanical barrier against the intratumoral delivery of gemcitabine, which already suffers from a short circulating half-life and extensive deamination [139, 179, 180]. Olive et al. [181] described the efficient, yet transient, restoration of the diminished vasculature in a transgenic mouse model, via the co-administration of a hedgehog (Hh) pathway inhibitor IPI-926 with gemcitabine [180, 181]. Inhibition of the stromal-associated pathway depleted the stromal matrix in the mouse model, which closely resembled human PDAC, and resulted in delivering more gemcitabine to the tumors, inhibiting the tumors growth, and prolonging the median survival of mice [181]. Unfortunately the tumors reverted back to the avascular state at the end. However, the positive results may provide new hopes to defeat the malign tumors. In a commentary on that study, Olson and Hanahan highlighted two mean aspects, dealing with the hedgehog pathway paradigm; the first one being that the tumor fights back to restore the hypoxic state, instead of the opposite in order to fulfill its craving to nutrients [180, 181]. The other aspect is that this approach tends to 'vascularize' the tumor by

inhibiting an anti-angiogenic pathway, which is contrary to the commonly known dogma of tumor vascular 'normalization', proposed by Jain, via treatment with angiogenic inhibitors to balance the 'super-active' pro-angiogenic activity of tumors [103, 104, 152, 180, 181]. Although positive results have been reported in early clinical studies with GDC-0449 (vismodegib, Genentech®) plus gemcitabine, or saridegib plus gemcitabine, phase II clinical trials with the latter combination in previously untreated patients with metastatic PDAC failed to show any advantage and were stopped short [139]. This is not the end for Hh inhibitors though. Vismodegib was granted the FDA's priority review program approval in 2012 to treat advanced basal-cell carcinoma, and other Smoothened (Smo, the transmembrane protein whose reversal of repression is a major step in the Hh pathway) inhibitors (e.g., LDE 225, Novartis®) are still under clinical trials [182]. In the same regard, a nanomedicine formulation of a hedgehog inhibitor showed some promises in pre-clinical studies [183, 184]. The PEGylated polymeric nanoparticle formulation (PLGA-PEG) of a hedgehog pathway inhibitor HPI-1 could overcome the mutational resistance of orthotopic pancreatic tumors against commonly used Hh inhibitors in mice [184], and inhibited metastasis in a hepatocellular carcinoma model [183].

SPARC

Secreted protein, acidic and rich in cysteine (SPARC), also known as osteonectin, is a glycosylated 43 kDa protein that is overexpressed in the PDAC stroma and at the invasion front of the tumor. It is usually associated with poor prognosis clinically in patients with high expression in the peritumoral fibroblasts, rather than in cancer cells [185–187]. Two groups of ECM-associated proteins are known: (1) structural proteins (e.g., collagens), and (2) non-structural or matricellular proteins (e.g., SPARC) [188]. Albumin-bound paclitaxel (*nab*-paclitaxel, Abraxane®), in an active combination regimen with gemcitabine, achieved 12.2 months overall survival (OS) and 48 % 1-year survival (compared to 5.7 months and 20 %, respectively, with the standard therapy with gemcitabine) in a phase I/II clinical trial [189].

Furthermore, a phase III clinical trial in patients with metastatic PDAC revealed that the combination achieved an OS of 8.5 months (431 patients) vs. 6.7 months with gemcitabine monotherapy (430 patients), and a 1-year survival of 35 % with the combination therapy vs. 22 % with gemcitabine alone [190]. The fact that albumin-bound nano-carriers are transcytosed into the cells following binding to albumin specific receptors (e.g. gp60) [186] may not be enough to explain the improved clinical benefit achieved in the clinical trials, as the question remains: how could the 10-nm circulating albumin-paclitaxel complexes penetrate into the dense desmoplastic stroma that not only comprises a physical barrier against deep tumor penetration, but also keeps the tumor cells away from the already-poor vasculature? In a preclinical study concurrently carried out with the same phase I/II clinical study mentioned above using nab-paclitaxel with gemcitabine, Von Hoff et al. found that the use of nab-paclitaxel depleted the stroma of a pancreatic cancer xenograft tumors in nude mice, which facilitated the gemcitabine delivery to the tumors (2.8 times higher than what was achieved with gemcitabine alone). The stromal depletion effect was associated with dilated blood vessels and increased endothelial cell content in the stroma. The stromal depletion and improved vascularization are believed to improve gemcitabine penetration into the tumors and brought the tumor cells closer to vasculature [189]. The cornerstone finding in this study was that SPARC was the Achilles' heel within the dense stroma of the PDAC, as the strong affinity between the overexpressed SPARC and albumin in nab-paclitaxel brought the nano-aggregates (i.e., nab-paclitaxel) deeper into the tumors, breaching the stroma, and bringing more gemcitabine deep inside [186, 189, 191]. Similar findings were also reported with head and neck cancer tissues [187]. Another factor that contributes to the improved efficacy of gemcitabine when nab-paclitaxel was concurrently administered is that the nab-paclitaxel was found to lower the cytidine deaminase levels in a murine pancreatic cancer model [192]. Cytidine deaminase is responsible for the extensive deamination of gemcitabine (more than 90 %),

yielding the inactive compound 2′-deoxy-2′,2′-difluorouridine (dFdU) [179, 193].

α-SMA

Li and colleagues developed a PEG-docetaxel-acetylated carboxymethyl cellulose conjugate that can self-assemble and form nanoparticles of about 120 nm. This formulation (Cellax) was shown to be more efficacious than commercial solvent-based docetaxel and nab-paclitaxel in both *in vitro* and *in vivo* studies [194–197]. Docetaxel conjugation percentage was high (>30 wt %), and it was completely and slowly released following a near zero-order pattern within 3 weeks [197]. In a recent study that thoroughly investigates the tumor stroma involvement in the anticancer activity of Cellax, the authors reported that Cellax significantly depleted the stroma of orthotopically implanted mammary tumors (4T1 and MDA-MB-231), with an about 70-fold increase in tumor perfusion and about 3-fold suppression of IFP, while minimum or no effect was noticed following either solvent-based docetaxel or nab-paclitaxel, in the same tumor models [169]. In addition, and more importantly, lung metastasis was also reduced by 7- to 24-fold following Cellax treatment, whereas the solvent-based docetaxel increased the number of metastatic lesions in the lungs [169]. One day after intravenous injection of Cellax, the authors found that the vast majority of Cellax nanoparticles (85 %) co-localized with α-SMA-positive stromal cells, and the α-SMA content in tumors declined from about 30 % down to 0 % within 1 week, which indicates the stromal-depleting effect of the nanoparticles [169]. Interestingly, tumor epithelial cells population started to decline only 7 days after the initiation of the treatment (i.e., after α-SMA depletion took place). Early investigation of the mechanism of Cellax-stroma interaction revealed that the albumin adsorbed on the circulating Cellax may favor the albumin-SPARC stromal penetration pathway [169], similar to that reported for the nab-paclitaxel [189]. The fact that SPARC expression is also associated with α-SMA-positive CAFs supports this proposed mechanism [169]. However, the failure of nab-paclitaxel to outweigh the Cellax performance

in this tumor model sheds some questions on the influence of the tumor model on the stromal-depletion effect of the former.

Stimulus-Responsive Nano-carriers

This approach takes advantage of specific characteristics that are exclusively exhibited in the tumor microenvironment to improve the antitumor activity of the chemotherapeutics. Various tumor environmental stimuli are involved in this approach, including lower extracellular pH, hypoxia, and MMP overexpression. Stimuli-sensitive nano-carriers have been extensively reviewed in literature (see [198–201]). This section provides a brief overview of the most common approaches employed to increase nano-carrier penetration into tumors.

Andresen et al. developed a liposomal formulation, composed of a serum-stable prodrugs of a group of cytotoxic lipid agents (anticancer ether-lipids, AELs, also called cytotoxic lysolipids) for selective tumor site-activation and release of the active drug [202, 203]. The AELs were made into phosphorylated prodrugs (proAEL) by modification with a stable ether bond that is not hydrolysable in plasma, but is sensitive to a class of phospholipase A2 (PLA2), called secretory PLA2 (sPLA2), which is overexpressed in the tumor microenvironment. The prodrugs self-assemble into liposomes that can accumulate via EPR into tumor tissues, where the sPLA2 hydrolyzes the prodrugs, releasing the potent AELs in the tumor microenvironment [202]. Furthermore, the fatty acid by-products of the hydrolysis may also act as tumor cell permeation enhancers to improve the cellular uptake of AELs. This formulation successfully overcame the red blood cell toxicity issues encountered with the use of AELs, as the ether-based prodrugs are stable in plasma, and the liposomal nature of the prodrugs enables the encapsulation of water soluble drugs into the core of the liposomes [202, 203].

Several pH-sensitive block-copolymers have been utilized to deliver drugs in the acidic extracellular matrix, while pre-mature drug leakage is minimized. Bae and co-workers developed a novel doxorubicin-loaded mixed micelle formulation that is destabilized in acidic pH to

release doxorubicin [204]. The mixed micelle system was composed of poly (L-histidine)/PEG and poly (L-lactic acid)/PEG (polyHis/PEG and PLLA/PEG). As the polyHis moiety is protonated in the acidic condition, the critical micelle concentration (CMC) of the amphiphilic molecule increases, which disassembles the whole micelle structure [200, 204, 205]. The pH at which the formulation destabilizes can be controlled by varying the ratio between the two block-copolymers [204].

The idea of pH-dependent shedding of PEG chains has been described in literature for several purposes [206–210]. Poon et al. designed a layer-by-layer (LBL) nanoparticle platform, where the cationic poly (L-lysine), functionalized with iminobiotin (inner layer) is further decorated with biotin-functionalized PEG chains (outer layer), through a neutravidin linker (middle layer) [209]. The quantum dots-loaded nanoparticles are designed to shed PEG chains via decomposition of the acid-sensitive iminobiotin-neutravidin at the acidic pH of the hypoxic tumor microenvironment. This will bring the cationic poly (L-lysine) layer to surface, which improves the nanoparticles internalization [209], as the PEG layer, although useful for prolonged circulation, is expected to hinder efficient cellular uptake [39, 211]. A conventional biotin-avidin-based PEGylation strategy was used to prepare non-pH-sensitive nanoparticles for comparison. Although the tumor accumulations of nanoparticles in the first 8 h were not different between the pH-sensitive and non-sensitive formulations, the pH-sensitivity improved the nanoparticles accumulation after 24 and 48 h. Furthermore, histological evaluation showed that the pH-sensitive nanoparticles were associated with hypoxic regions. Early accumulation (within 8 h after injection) was assumed to be independent of the pH-sensitivity, and was rather dependent on the EPR effect, which is not expected to favor the delivery of either formulation [209].

In the same regard, Sawant et al. designed a multifunctional 'smart' nano-carrier that has a long-chain PEG-phosphoethanol amine

(PEG-PE) moiety attached to an mAb for active targeting, while shorter PEG-chains are attached to a cell penetrating peptide (e.g., Tat peptide) [210]. The design involved inserting a pH-sensitive hydrazone bond in between the long-chain PEG and PE to render this moiety pH-sheddable. After the nano-carriers reach tumors by the help of the mAb-conjugated PEG, the long PEG chains are shed due to the hydrolysis of the acid-sensitive hydrazone bond, exposing the Tat-conjugated PEG, which can then improve the internalization of the nano-carriers into tumor cells [205, 210]. In a recent study, Zhu et al. applied the idea of hydrazone-based PEG-shedding to actively target TAMs [206]. The nanoparticles are composed of PLGA core (with 5 % PLGA-FITC), stearoyl-mannose (C18-mannose), and PEG-hydrazone-stearoyl (PEG-hydrazone-C18, PHC). The stearoyl moiety in both PHC and C18-mannose are expected to be inserted into the lipophilic PLGA core, leaving the short mannose and the long PEG moieties projecting outwardly. Once the long-circulating nanoparticles accumulate in the tumor via EPR, the PEG chains are shed in the acidic tumor environment (pH 6.8), bringing the mannose moiety to the front, which enables the nanoparticles to interact with TAMs via mannose-mannose receptor interaction [206]. In contrast, nanoparticle uptake by normal macrophages at physiological pH is hindered by the shielding effect of the PEG chains [206]. This formulation provided a successful tool for the active targeting of TAMs.

Using PEG-shedding to expose another hidden surface targeting ligand can take place via other mechanisms as well. For example, Torchilin's group designed an MMP2-sensitive micellar formulation that sheds PEG chains and exposes a cell penetrating Tat-peptide once the micelles reach the MMP2-rich tumor microenvironment [212]. The shed PEG chains, which are connected to the MMP sensitive peptide, are long (2 kDa) to provide extended plasma circulation of the micelle formulation, while the Tat-peptide-conjugated PEG chains are shorter (1kDa) to keep the Tat shielded until the micelles reach tumor microenvironment. Paclitaxel, conjugated to the

MMP-sensitive PEGylated moiety, remained at the core of the Tat-peptide decorated micelle structure due to its lipophilic nature [212].

11.4.3 Cellular Barriers

11.4.3.1 Nano-carrier Internalization by Cancer Cell and Endosomal Escape

Once the nano-carrier gets past all the previously mentioned barriers, it comes in contact with the tumor cells and starts to interact with tumor cell membrane to get internalized (endocytosis). The process of endocytosis starts with invagination of the nano-carriers into the cell, forming a specific vesicle (endosome or phagosome), in which the nano-carriers are entrapped. Five major endocytic pathways for the internalization of nano-carriers have been identified, namely phagocytosis, macropinocytosis, clathrin-mediated endocytosis, caveolin-mediated endocytosis, and clathrin/caveolin-independent endocytosis [120, 213, 214]. The type of endocytosis is dependent on several factors, including nano-carrier size, surface chemistry and ligands, and the tumor cells [120]. Caveolin and clathrin are proteins assisting the endosome formation and the endocytosis process. The pH inside several internalized vesicles is usually acidic, with various values. Both clathrin-mediated and caveolin-mediated endocytosis form early endosomes (pH 6.5–6.8), which become late endosomes (pH 5.2–6.2), while phagocytosis and macropinocytosis form phagosomes and macropinosomes, respectively. All three vesicles deliver their cargos to lysosomes (pH 4.5–5.2) [213]. Both the acidic conditions and the presence of hydrolytic enzymes facilitate the digestion of the internalized cargos and destroy them. Thus, it is important that the nano-carriers find a way out of the endosomes before reaching the terminal lysosomes [215]. Among the methods adopted to enable the endosomal escape of nano-carriers from the endosomes is the proton-sponge effect method, where nano-carriers with secondary or tertiary amine groups (e.g., poly-L-histidine, polyethylene imine

(PEI), or chitosan) are protonated by the acidic pH inside, which results in the extensive flow of ions and water inside the endosomes, resulting in osmotic swelling and subsequent rupture of the lysosomes. The nano-carriers then escape into the cytosol [215, 216]. Other endosomal escape mechanisms include the use of fusogenic peptides (e.g., influenza HA2 peptide and GALA peptide) that destabilize the endosomal membrane after some acid-sensitive conformational changes of their structures take place [217, 218].

In one example, nevertheless, it seems like what comprises a 'curse' to some nano-carriers turns out to be a 'blessing' to others. Wonganan et al. found that the GemC18-SLNs are taken up by tumor cells by clathrin-mediated endocytosis, and the gemcitabine is liberated in lysosomes due to acid-sensitive hydrolysis and lysosomal enzymes such as cathepsins [219]. Free gemcitabine is then likely exported out of the lysosomes by human equilibrative nucleoside transporter-3 (hENT-3) in the lysosomal membrane. It seems that, following this pathway, the liberated gemcitabine is shuttled into a natural 'salvage' pathway that cells adopt to recycle endogenous (e.g., apoptotic bodies) or exogenous (e.g., DNA from bacteria or viruses) DNA, and is phosphorylated more efficiently into the active difluoro-deoxycytidine triphosphate (dFdCTP) to inhibit cell growth [219]. In this case, functional lysosomes are critical to efficiently generate dFdCTP, as alkalinization of lysosomes with ammonium chloride significantly inhibits the cytotoxic action of GemC18-SLNs [219]. In contrast, free GemC18 diffuses inside tumor cells very rapidly and is hydrolyzed quickly into free gemcitabine. However, it appears that the gemcitabine that reaches cell cytosol following this pathway cannot be efficiently phosphorylated into its active dFdCTP. Gemcitabine alone can be effectively taken up by cells via nucleoside transporters such as hENT-1 located in the cell membrane. However, it is extensively deactivated into its inactive dFdU derivative before being phosphorylated [219]. For a more detailed description of this example, the reader is referred to ([219]).

11.4.3.2 ATP-Binding Cassette Transporters (ABC Transporter, Efflux Transporter-Mediated Resistance)

ABC transporters are a family of proteins that include multidrug resistance protein-1 (MDR-1) and P-glycoprotein (P-gp) [138]. Human P-gp, a 170 kDa trans-membrane glycoprotein, is composed of 12 hydrophobic domains and two nucleotide domains [220], and is a major component of the blood brain barrier [221]. It can transport several small molecules, either from the cytosol or from the cell membrane, out of the cell, which significantly reduces cellular accumulation of cytotoxic molecules [138, 222]. The mere use of a nano-carrier to deliver the chemotherapeutic agents intracellularly had been shown to overcome the P-gp-mediated efflux [223], as the nano-carrier is not a substrate to the protein. Additionally, several nano-carrier based approaches, including the concomitant use of efflux inhibitors (e.g., cepharanthine [224] and tariquidar [225]), silencing the gene encoding P-gp [226, 227], and the use of certain excipients and surfactants (e.g., poloxamers and tocopheryl-polyethylene glycol succinate (TPGS) [228, 229]), are among the strategies that have been explored to reverse ABC transporter-mediated multi-drug resistance to nanomedicine.

For example, Panyam and co-workers developed a biotin-functionalized PLGA nanoparticles that encapsulate a dual drug payload of paclitaxel and the third generation P-gp inhibitor tariquidar to target the biotin receptors overexpressed by tumor cells [225]. Within a concentration range at which neither paclitaxel in solution or in nanoparticles was effective, tariquidar enhanced the cytotoxic effect of paclitaxel, both in solution and in nanoparticles, in chemoresistant cell lines that overexpress P-gp. Furthermore, the 2 h-cellular uptake of paclitaxel was the greatest when tariquidar was co-encapsulated with paclitaxel in PLGA nanoparticles. The authors attributed the lack of activity of paclitaxel nanoparticles in these cell lines to the overexpressed P-gp, as the slowly released paclitaxel is readily removed by P-gp. However, the simultaneous slow release of tariquidar inhibited P-gp and accordingly enhanced the accumulation of the slowly released paclitaxel. The dual agent encapsulation in the biotin-functionalized nanoparticles significantly enhanced the antitumor activity and survival in mice bearing resistant tumors [225]. The same group also showed that simultaneous encapsulation, and subsequent intracellular co-localization, of paclitaxel and a P-gp-silencing siRNA can successfully enhance the anticancer activity of paclitaxel in resistant cells [230]. Using a different modality, Navarro et al. showed that the pretreatment of resistant breast cancer cells with siRNA, loaded on a cationic PEI-functionalized phospholipid-based nano-carrier, can significantly enhance the cytotoxic activity of a subsequent treatment with doxorubicin solution [226]. Other cellular-mediated ABC transporter-independent resistance mechanisms to chemotherapy include apoptosis inhibition and DNA repair modification [205]. For example, survivin is an antiapoptotic protein that is overexpressed in cancer cells. and the silencing of survivin gene expression has been identified as a successful tool to overcome drug resistance in cancer cells [231, 232]. Yang et al. functionalized the polysaccharide chitosan with a cell penetrating peptide and utilized it to deliver survivin siRNA [233]. The siRNA-chitosan complexes effectively induced apoptosis in cancer cells and inhibited tumor growth in mice with orthotopic mammary tumors, while the naked siRNA was not effective [233]. For deeper insights on the use of nanomedicine to overcome cellular-mediated drug resistance mechanisms in tumors, the reader can refer to [138, 205, 221, 234, 235].

Conclusion

Nanomedicine opens a totally different horizon in cancer chemotherapy, with so many opportunities awaiting. However, as more opportunities come in the way, more challenges are also revealed. More efforts are needed to fully take advantage of its potentials.

References

1. Danhier F, Feron O, Preat V (2010) To exploit the tumor microenvironment: passive and active tumor targeting of nanocarriers for anti-cancer drug delivery. J Control Release 148:135–146
2. Bangham AD, Standish MM, Watkins JC (1965) Diffusion of univalent ions across the lamellae of swollen phospholipids. J Mol Biol 13:238–252
3. Bangham AD, Horne RW (1964) Negative staining of phospholipids and their structural modification by surface-active agents as observed in the electron microscope. J Mol Biol 8:660–668
4. Haley B, Frenkel E (2008) Nanoparticles for drug delivery in cancer treatment. Urol Oncol 26:57–64
5. Rodriguez BL, Li X, Kiguchi K, DiGiovanni J, Unger EC, Cui Z (2012) Control of solid tumor growth in mice using EGF receptor-targeted RNA replicase-based plasmid DNA. Nanomedicine (Lond) 7:475–491
6. Alexis F, Pridgen EM, Langer R, Farokhzad OC (2010) Nanoparticle technologies for cancer therapy. Handb Exp Pharmacol 197:55–86
7. Torchilin VP (2005) Recent advances with liposomes as pharmaceutical carriers. Nat Rev Drug Discov 4:145–160
8. Arias JL (2013) Liposomes in drug delivery: a patent review (2007 – present). Expert Opin Ther Pat 23:1399–1414
9. Immordino ML, Dosio F, Cattel L (2006) Stealth liposomes: review of the basic science, rationale, and clinical applications, existing and potential. Int J Nanomedicine 1:297–315
10. Klibanov AL, Maruyama K, Torchilin VP, Huang L (1990) Amphipathic polyethyleneglycols effectively prolong the circulation time of liposomes. FEBS Lett 268:235–237
11. Banerjee R, Tyagi P, Li S, Huang L (2004) Anisamide-targeted stealth liposomes: a potent carrier for targeting doxorubicin to human prostate cancer cells. Int J Cancer 112:693–700
12. Li SD, Huang L (2006) Targeted delivery of antisense oligodeoxynucleotide and small interference RNA into lung cancer cells. Mol Pharm 3:579–588
13. Rodriguez BL, Blando JM, Lansakara P, Kiguchi Y, DiGiovanni J, Cui Z (2013) Antitumor activity of tumor-targeted RNA replicase-based plasmid that expresses interleukin-2 in a murine melanoma model. Mol Pharm 10:2404–2415
14. Raju A, Muthu MS, Feng SS (2013) Trastuzumab-conjugated vitamin E TPGS liposomes for sustained and targeted delivery of docetaxel. Expert Opin Drug Deliv 10:747–760
15. Gao J, Sun J, Li H, Liu W, Zhang Y, Li B, Qian W, Wang H, Chen J, Guo Y (2010) Lyophilized HER2-specific PEGylated immunoliposomes for active siRNA gene silencing. Biomaterials 31:2655–2664
16. Wu XS, Wang N (2001) Synthesis, characterization, biodegradation, and drug delivery application of biodegradable lactic/glycolic acid polymers. Part II: biodegradation. J Biomater Sci Polym Ed 12:21–34
17. Wu XS (2004) Synthesis, characterization, biodegradation, and drug delivery application of biodegradable lactic/glycolic acid polymers: part III. Drug delivery application. Artif Cells Blood Substit Immobil Biotechnol 32:575–591
18. Nair LS, Laurencin CT (2007) Biodegradable polymers as biomaterials. Prog Polym Sci 32:762–798
19. Gopferich A (1996) Mechanisms of polymer degradation and erosion. Biomaterials 17:103–114
20. Chandra R, Rustgi R (1998) Biodegradable polymers. Prog Polym Sci 23:1273–1335
21. von Burkersroda F, Schedl L, Gopferich A (2002) Why degradable polymers undergo surface erosion or bulk erosion. Biomaterials 23:4221–4231
22. Gref R, Minamitake Y, Peracchia MT, Trubetskoy V, Torchilin V, Langer R (1994) Biodegradable long-circulating polymeric nanospheres. Science 263:1600–1603
23. Pradhan R, Poudel BK, Ramasamy T, Choi HG, Yong CS, Kim JO (2013) Docetaxel-loaded polylactic acid-co-glycolic acid nanoparticles: formulation, physicochemical characterization and cytotoxicity studies. J Nanosci Nanotechnol 13:5948–5956
24. Jagani HV, Josyula VR, Palanimuthu VR, Hariharapura RC, Gang SS (2013) Improvement of therapeutic efficacy of PLGA nanoformulation of siRNA targeting anti-apoptotic Bcl-2 through chitosan coating. Eur J Pharm Sci 48:611–618
25. Pinto RC, Neufeld RJ, Ribeiro AJ, Veiga F (2006) Nanoencapsulation I. Methods for preparation of drug-loaded polymeric nanoparticles. Nanomedicine 2:8–21
26. Beck-Broichsitter M, Rytting E, Lebhardt T, Wang X, Kissel T (2010) Preparation of nanoparticles by solvent displacement for drug delivery: a shift in the "ouzo region" upon drug loading. Eur J Pharm Sci 41:244–253
27. Jensen DM, Cun D, Maltesen MJ, Frokjaer S, Nielsen HM, Foged C (2010) Spray drying of siRNA-containing PLGA nanoparticles intended for inhalation. J Control Release 142:138–145
28. Byrappa K, Ohara S, Adschiri T (2008) Nanoparticles synthesis using supercritical fluid technology – towards biomedical applications. Adv Drug Deliv Rev 60:299–327
29. Perry JL, Herlihy KP, Napier ME, Desimone JM (2011) PRINT: a novel platform toward shape and size specific nanoparticle theranostics. Acc Chem Res 44:990–998
30. Kam KR, Desai TA (2013) Nano- and microfabrication for overcoming drug delivery challenges. J Mater Chem B Mater Biol Med 1:1878–1884
31. Yoo JW, Doshi N, Mitragotri S (2011) Adaptive micro and nanoparticles: temporal control over carrier properties to facilitate drug delivery. Adv Drug Deliv Rev 63:1247–1256
32. Saxena V, Hussain MD (2012) Poloxamer 407/TPGS mixed micelles for delivery of gambogic acid to breast

and multidrug-resistant cancer. Int J Nanomedicine 7:713–721

33. Kim SC, Kim DW, Shim YH, Bang JS, Oh HS, Wan KS, Seo MH (2001) *In vivo* evaluation of polymeric micellar paclitaxel formulation: toxicity and efficacy. J Control Release 72:191–202

34. Ostacolo L, Marra M, Ungaro F, Zappavigna S, Maglio G, Quaglia F, Abbruzzese A, Caraglia M (2010) *In vitro* anticancer activity of docetaxel-loaded micelles based on poly(ethylene oxide)-poly(epsilon-caprolactone) block copolymers: do nanocarrier properties have a role? J Control Release 148:255–263

35. Ebrahim Attia AB, Ong ZY, Hedrick JL, Lee PP, Ee PLR, Hammond PT, Yang YY (2011) Mixed micelles self-assembled from block copolymers for drug delivery. Curr Opin Colloid Interface Sci 16:182–194

36. Chen L, Sha X, Jiang X, Chen Y, Ren Q, Fang X (2013) Pluronic P105/F127 mixed micelles for the delivery of docetaxel against Taxol-resistant non-small cell lung cancer: optimization and *in vitro*, *in vivo* evaluation. Int J Nanomedicine 8: 73–84

37. Mehnert W, Mader K (2001) Solid lipid nanoparticles: production, characterization and applications. Adv Drug Deliv Rev 47:165–196

38. Xu Z, Chen L, Gu W, Gao Y, Lin L, Zhang Z, Xi Y, Li Y (2009) The performance of docetaxel-loaded solid lipid nanoparticles targeted to hepatocellular carcinoma. Biomaterials 30:226–232

39. Sloat BR, Sandoval MA, Li D, Chung WG, Lansakara P, Proteau PJ, Kiguchi K, DiGiovanni J, Cui Z (2011) *In vitro* and *in vivo* anti-tumor activities of a gemcitabine derivative carried by nanoparticles. Int J Pharm 409:278–288

40. Mosallaei N, Jaafari MR, Hanafi-Bojd MY, Golmohammadzadeh S, Malaekeh-Nikouei B (2013) Docetaxel-loaded solid lipid nanoparticles: preparation, characterization, *in vitro*, and *in vivo* evaluations. J Pharm Sci 102:1994–2004

41. Parveen R, Ahmad FJ, Iqbal Z, Samim M, Ahmad S (2013) Solid lipid nanoparticles of anticancer drug andrographolide: formulation, in vitro and in vivo studies. Drug Dev Ind Pharm. doi:10.3109/03639045.2013.810636

42. Muller RH, Mader K, Gohla S (2000) Solid lipid nanoparticles (SLN) for controlled drug delivery – a review of the state of the art. Eur J Pharm Biopharm 50:161–177

43. Wong HL, Bendayan R, Rauth AM, Li Y, Wu XY (2007) Chemotherapy with anticancer drugs encapsulated in solid lipid nanoparticles. Adv Drug Deliv Rev 59:491–504

44. Feng L, Mumper RJ (2013) A critical review of lipid-based nanoparticles for taxane delivery. Cancer Lett 334:157–175

45. Sanchis J, Canal F, Lucas R, Vicent MJ (2010) Polymer-drug conjugates for novel molecular targets. Nanomedicine (Lond) 5:915–935

46. Pasut G, Veronese FM (2009) PEG conjugates in clinical development or use as anticancer agents: an overview. Adv Drug Deliv Rev 61:1177–1188

47. Duncan R (2009) Development of HPMA copolymer-anticancer conjugates: clinical experience and lessons learnt. Adv Drug Deliv Rev 61:1131–1148

48. Li C, Wallace S (2008) Polymer-drug conjugates: recent development in clinical oncology. Adv Drug Deliv Rev 60:886–898

49. Ringsdorf H (1975) Structure and properties of pharmacologically active polymers. J Polym Sci Symp 51:135–153

50. Vasey PA, Kaye SB, Morrison R, Twelves C, Wilson P, Duncan R, Thomson AH, Murray LS, Hilditch TE, Murray T, Burtles S, Fraier D, Frigerio E, Cassidy J (1999) Phase I clinical and pharmacokinetic study of PK1 [N-(2-hydroxypropyl)methacrylamide copolymer doxorubicin]: first member of a new class of chemotherapeutic agents-drug-polymer conjugates. Cancer Research Campaign Phase I/II Committee. Clin Cancer Res 5:83–94

51. Lammers T, Subr V, Ulbrich K, Peschke P, Huber PE, Hennink WE, Storm G (2009) Simultaneous delivery of doxorubicin and gemcitabine to tumors *in vivo* using prototypic polymeric drug carriers. Biomaterials 30:3466–3475

52. Tong R, Yala L, Fan TM, Cheng J (2010) The formulation of aptamer-coated paclitaxel-polylactide nanoconjugates and their targeting to cancer cells. Biomaterials 31:3043–3053

53. Jeyapalan S, Boxerman J, Donahue S, Goldman M, Kinsella T, Dipetrillo T, Evans D, Elinzano H, Constantinou M, Stopa E, Puthawala Y, Cielo D, Santaniello A, Oyelese A, Mantripragada K, Rosati K, Isdale D, Safran H (2013) Paclitaxel poliglumex, temozolomide, and radiation for newly diagnosed high-grade glioma: a Brown University Oncology Group Study. Am J Clin Oncol. doi:10.1097/COC.0b013e31827de92b

54. Stirland DL, Nichols JW, Miura S, Bae YH (2013) Mind the gap: a survey of how cancer drug carriers are susceptible to the gap between research and practice. J Control Release 172(3):1045–1064

55. O'Brien ME, Socinski MA, Popovich AY, Bondarenko IN, Tomova A, Bilynsky BT, Hotko YS, Ganul VL, Kostinsky IY, Eisenfeld AJ, Sandalic L, Oldham FB, Bandstra B, Sandler AB, Singer JW (2008) Randomized phase III trial comparing single-agent paclitaxel Poliglumex (CT-2103, PPX) with single-agent gemcitabine or vinorelbine for the treatment of PS 2 patients with chemotherapy-naive advanced non-small cell lung cancer. J Thorac Oncol 3:728–734

56. Paz-Ares L, Ross H, O'Brien M, Riviere A, Gatzemeier U, Von PJ, Kaukel E, Freitag L, Digel W, Bischoff H, Garcia-Campelo R, Iannotti N, Reiterer P, Bover I, Prendiville J, Eisenfeld AJ, Oldham FB, Bandstra B, Singer JW, Bonomi P (2008) Phase III trial comparing paclitaxel poliglumex vs docetaxel in the second-line treatment of non-small-cell lung cancer. Br J Cancer 98:1608–1613

57. Sievers EL, Senter PD (2013) Antibody-drug conjugates in cancer therapy. Annu Rev Med 64:15–29

58. Ricart AD, Tolcher AW (2007) Technology insight: cytotoxic drug immunoconjugates for cancer therapy. Nat Clin Pract Oncol 4:245–255

59. Wu AM, Senter PD (2005) Arming antibodies: prospects and challenges for immunoconjugates. Nat Biotechnol 23:1137–1146

60. Junutula JR, Raab H, Clark S, Bhakta S, Leipold DD, Weir S, Chen Y, Simpson M, Tsai SP, Dennis MS, Lu Y, Meng YG, Ng C, Yang J, Lee CC, Duenas E, Gorrell J, Katta V, Kim A, McDorman K, Flagella K, Venook R, Ross S, Spencer SD, Lee WW, Lowman HB, Vandlen R, Sliwkowski MX, Scheller RH, Polakis P, Mallet W (2008) Site-specific conjugation of a cytotoxic drug to an antibody improves the therapeutic index. Nat Biotechnol 26:925–932

61. Mosure KW, Henderson AJ, Klunk LJ, Knipe JO (1997) Disposition of conjugate-bound and free doxorubicin in tumor-bearing mice following administration of a BR96-doxorubicin immunoconjugate (BMS 182248). Cancer Chemother Pharmacol 40:251–258

62. Gerber HP, Koehn FE, Abraham RT (2013) The antibody-drug conjugate: an enabling modality for natural product-based cancer therapeutics. Nat Prod Rep 30:625–639

63. Zhao RY, Wilhelm SD, Audette C, Jones G, Leece BA, Lazar AC, Goldmacher VS, Singh R, Kovtun Y, Widdison WC, Lambert JM, Chari RV (2011) Synthesis and evaluation of hydrophilic linkers for antibody-maytansinoid conjugates. J Med Chem 54:3606–3623

64. Kovtun YV, Audette CA, Mayo MF, Jones GE, Doherty H, Maloney EK, Erickson HK, Sun X, Wilhelm S, Ab O, Lai KC, Widdison WC, Kellogg B, Johnson H, Pinkas J, Lutz RJ, Singh R, Goldmacher VS, Chari RV (2010) Antibody-maytansinoid conjugates designed to bypass multidrug resistance. Cancer Res 70:2528–2537

65. Carter PJ, Senter PD (2008) Antibody-drug conjugates for cancer therapy. Cancer J 14:154–169

66. Chan SY, Gordon AN, Coleman RE, Hall JB, Berger MS, Sherman ML, Eten CB, Finkler NJ (2003) A phase 2 study of the cytotoxic immunoconjugate CMB-401 (hCTM01-calicheamicin) in patients with platinum-sensitive recurrent epithelial ovarian carcinoma. Cancer Immunol Immunother 52:243–248

67. Lambert JM (2005) Drug-conjugated monoclonal antibodies for the treatment of cancer. Curr Opin Pharmacol 5:543–549

68. Kharfan-Dabaja MA, Hamadani M, Reljic T, Pyngolil R, Komrokji RS, Lancet JE, Fernandez HF, Djulbegovic B, Kumar A (2013) Gemtuzumab ozogamicin for treatment of newly diagnosed acute myeloid leukaemia: a systematic review and meta-analysis. Br J Haematol 163:315–325

69. Newland AM, Li JX, Wasco LE, Aziz MT, Lowe DK (2013) Brentuximab vedotin: a CD30-directed antibody-cytotoxic drug conjugate. Pharmacotherapy 33:93–104

70. Wong BS, Yoong SL, Jagusiak A, Panczyk T, Ho HK, Ang WH, Pastorin G (2013) Carbon nanotubes for delivery of small molecule drugs. Adv Drug Deliv Rev 65(15):1964–2015

71. Liang XJ, Meng H, Wang Y, He H, Meng J, Lu J, Wang PC, Zhao Y, Gao X, Sun B, Chen C, Xing G, Shen D, Gottesman MM, Wu Y, Yin JJ, Jia L (2010) Metallofullerene nanoparticles circumvent tumor resistance to cisplatin by reactivating endocytosis. Proc Natl Acad Sci U S A 107:7449–7454

72. Dreaden EC, Austin LA, Mackey MA, El-Sayed MA (2012) Size matters: gold nanoparticles in targeted cancer drug delivery. Ther Deliv 3:457–478

73. Shen J, Song G, An M, Li X, Wu N, Ruan K, Hu J, Hu R (2013) The use of hollow mesoporous silica nanospheres to encapsulate bortezomib and improve efficacy for non-small cell lung cancer therapy. Biomaterials 35(1):316–326

74. Li X, Li H, Yi W, Chen J, Liang B (2013) Acid-triggered core cross-linked nanomicelles for targeted drug delivery and magnetic resonance imaging in liver cancer cells. Int J Nanomedicine 8:3019–3031

75. Diaz A, Saxena V, Gonzalez J, David A, Casanas B, Carpenter C, Batteas JD, Colon JL, Clearfield A, Hussain MD (2012) Zirconium phosphate nanoplatelets: a novel platform for drug delivery in cancer therapy. Chem Commun (Camb) 48:1754–1756

76. Fang M, Yuan JP, Peng CW, Pang DW, Li Y (2013) Quantum dots-based in situ molecular imaging of dynamic changes of collagen IV during cancer invasion. Biomaterials 34:8708–8717

77. Gautier J, Allard-Vannier E, Munnier E, Souce M, Chourpa I (2013) Recent advances in theranostic nanocarriers of doxorubicin based on iron oxide and gold nanoparticles. J Control Release 169:48–61

78. Chen Y, Chen H, Shi J (2013) In vivo bio-safety evaluations and diagnostic/therapeutic applications of chemically designed mesoporous silica nanoparticles. Adv Mater 25:3144–3176

79. Probst CE, Zrazhevskiy P, Bagalkot V, Gao X (2013) Quantum dots as a platform for nanoparticle drug delivery vehicle design. Adv Drug Deliv Rev 65:703–718

80. Yang F, Jin C, Subedi S, Lee CL, Wang Q, Jiang Y, Li J, Di Y, Fu D (2012) Emerging inorganic nanomaterials for pancreatic cancer diagnosis and treatment. Cancer Treat Rev 38:566–579

81. Mukerjee A, Ranjan AP, Vishwanatha JK (2012) Combinatorial nanoparticles for cancer diagnosis and therapy. Curr Med Chem 19:3714–3721

82. Matsumura Y, Maeda H (1986) A new concept for macromolecular therapeutics in cancer chemotherapy: mechanism of tumoritropic accumulation of proteins and the antitumor agent smancs. Cancer Res 46:6387–6392

83. Torchilin V (2011) Tumor delivery of macromolecular drugs based on the EPR effect. Adv Drug Deliv Rev 63:131–135

84. Maeda H (2010) Tumor-selective delivery of macromolecular drugs via the EPR effect: background and future prospects. Bioconjug Chem 21:797–802

85. Wu J, Akaike T, Maeda H (1998) Modulation of enhanced vascular permeability in tumors by a bradykinin antagonist, a cyclooxygenase inhibitor, and a nitric oxide scavenger. Cancer Res 58:159–165

86. Brannon-Peppas L, Blanchette JO (2004) Nanoparticle and targeted systems for cancer therapy. Adv Drug Deliv Rev 56:1649–1659

87. Iyer AK, Khaled G, Fang J, Maeda H (2006) Exploiting the enhanced permeability and retention effect for tumor targeting. Drug Discov Today 11:812–818

88. Alexis F, Rhee JW, Richie JP, Radovic-Moreno AF, Langer R, Farokhzad OC (2008) New frontiers in nanotechnology for cancer treatment. Urol Oncol 26:74–85

89. Maeda H, Bharate GY, Daruwalla J (2009) Polymeric drugs for efficient tumor-targeted drug delivery based on EPR-effect. Eur J Pharm Biopharm 71:409–419

90. Hobson B, Denekamp J (1984) Endothelial proliferation in tumours and normal tissues: continuous labelling studies. Br J Cancer 49:405–413

91. Fang J, Nakamura H, Maeda H (2011) The EPR effect: unique features of tumor blood vessels for drug delivery, factors involved, and limitations and augmentation of the effect. Adv Drug Deliv Rev 63:136–151

92. Maeda H, Sawa T, Konno T (2001) Mechanism of tumor-targeted delivery of macromolecular drugs, including the EPR effect in solid tumor and clinical overview of the prototype polymeric drug SMANCS. J Control Release 74:47–61

93. Maeda H (1991) SMANCS and polymer-conjugated macromolecular drugs: advantages in cancer chemotherapy. Adv Drug Deliv Rev 6:181–202

94. Prabhakar U, Maeda H, Jain RK, Sevick-Muraca EM, Zamboni W, Farokhzad OC, Barry ST, Gabizon A, Grodzinski P, Blakey DC (2013) Challenges and key considerations of the enhanced permeability and retention effect for nanomedicine drug delivery in oncology. Cancer Res 73:2412–2417

95. Bae YH, Park K (2011) Targeted drug delivery to tumors: myths, reality and possibility. J Control Release 153:198–205

96. Bae YH (2009) Drug targeting and tumor heterogeneity. J Control Release 133:2–3

97. Denison TA, Bae YH (2012) Tumor heterogeneity and its implication for drug delivery. J Control Release 164:187–191

98. Nichols JW, Bae YH (2012) Odyssey of a cancer nanoparticle: from injection site to site of action. Nano Today 7:606–618

99. Noguchi A, Takahashi T, Yamaguchi T, Kitamura K, Noguchi A, Tsurumi H, Takashina K, Maeda H (1992) Enhanced tumor localization of monoclonal antibody by treatment with kininase II inhibitor and angiotensin II. Jpn J Cancer Res 83:240–243

100. Seki T, Fang J, Maeda H (2009) Enhanced delivery of macromolecular antitumor drugs to tumors by nitroglycerin application. Cancer Sci 100:2426–2430

101. Jain RK (2005) Normalization of tumor vasculature: an emerging concept in antiangiogenic therapy. Science 307:58–62

102. Yuan F, Chen Y, Dellian M, Safabakhsh N, Ferrara N, Jain RK (1996) Time-dependent vascular regression and permeability changes in established human tumor xenografts induced by an anti-vascular endothelial growth factor/vascular permeability factor antibody. Proc Natl Acad Sci U S A 93:14765–14770

103. Goel S, Duda DG, Xu L, Munn LL, Boucher Y, Fukumura D, Jain RK (2011) Normalization of the vasculature for treatment of cancer and other diseases. Physiol Rev 91:1071–1121

104. Jain RK, Stylianopoulos T (2010) Delivering nanomedicine to solid tumors. Nat Rev Clin Oncol 7:653–664

105. Carmeliet P, Jain RK (2011) Principles and mechanisms of vessel normalization for cancer and other angiogenic diseases. Nat Rev Drug Discov 10:417–427

106. Goel S, Wong AH, Jain RK (2012) Vascular normalization as a therapeutic strategy for malignant and nonmalignant disease. Cold Spring Harb Perspect Med 2:a006486

107. Chauhan VP, Stylianopoulos T, Martin JD, Popovic Z, Chen O, Kamoun WS, Bawendi MG, Fukumura D, Jain RK (2012) Normalization of tumour blood vessels improves the delivery of nanomedicines in a size-dependent manner. Nat Nanotechnol 7:383–388

108. Huang C, Zhang Y, Yuan H, Gao H, Zhang S (2013) Role of nanoparticle geometry in endocytosis: laying down to stand up. Nano Lett 13:4546–4550

109. Byrne JD, Betancourt T, Brannon-Peppas L (2008) Active targeting schemes for nanoparticle systems in cancer therapeutics. Adv Drug Deliv Rev 60:1615–1626

110. Dagar A, Kuzmis A, Rubinstein I, Sekosan M, Onyuksel H (2012) VIP-targeted cytotoxic nanomedicine for breast cancer. Drug Deliv Transl Res 2:454–462

111. Cirstoiu-Hapca A, Buchegger F, Bossy L, Kosinski M, Gurny R, Delie F (2009) Nanomedicines for active targeting: physico-chemical characterization of paclitaxel-loaded anti-HER2 immunonanoparticles and in vitro functional studies on target cells. Eur J Pharm Sci 38:230–237

112. Nobs L, Buchegger F, Gurny R, Allemann E (2006) Biodegradable nanoparticles for direct or two-step tumor immunotargeting. Bioconjug Chem 17:139–145

113. Cirstoiu-Hapca A, Bossy-Nobs L, Buchegger F, Gurny R, Delie F (2007) Differential tumor cell targeting of anti-HER2 (Herceptin) and anti-CD20 (Mabthera) coupled nanoparticles. Int J Pharm 331:190–196

114. Sandoval MA, Sloat BR, Lansakara P, Kumar A, Rodriguez BL, Kiguchi K, DiGiovanni J, Cui Z (2012) EGFR-targeted stearoyl gemcitabine nanoparticles show enhanced anti-tumor activity. J Control Release 157:287–296

115. Yhee JY, Lee SJ, Lee S, Song S, Min HS, Kang SW, Son S, Jeong SY, Kim SH, Kim K (2013) Tumor-targeting transferrin nanoparticles for systemic polymerized siRNA delivery in tumor-bearing mice. Bioconjug Chem 24(11):1850–1860

116. Stephenson SM, Low PS, Lee RJ (2004) Folate receptor-mediated targeting of liposomal drugs to cancer cells. Methods Enzymol 387:33–50

117. Lu Y, Low PS (2002) Folate-mediated delivery of macromolecular anticancer therapeutic agents. Adv Drug Deliv Rev 54:675–693

118. Saxena V, Naguib Y, Hussain MD (2012) Folate receptor targeted 17-allylamino-17-demethoxygeldanamycin (17-AAG) loaded polymeric nanoparticles for breast cancer. Colloids Surf B Biointerfaces 94:274–280

119. Hrkach J, Von Hoff D, Mukkaram AM, Andrianova E, Auer J, Campbell T, De WD, Figa M, Figueiredo M, Horhota A, Low S, McDonnell K, Peeke E, Retnarajan B, Sabnis A, Schnipper E, Song JJ, Song YH, Summa J, Tompsett D, Troiano G, Van Geen HT, Wright J, LoRusso P, Kantoff PW, Bander NH, Sweeney C, Farokhzad OC, Langer R, Zale S (2012) Preclinical development and clinical translation of a PSMA-targeted docetaxel nanoparticle with a differentiated pharmacological profile. Sci Transl Med 4:128ra39

120. Elsabahy M, Wooley KL (2012) Design of polymeric nanoparticles for biomedical delivery applications. Chem Soc Rev 41:2545–2561

121. Huynh NT, Roger E, Lautram N, Benoit JP, Passirani C (2010) The rise and rise of stealth nanocarriers for cancer therapy: passive versus active targeting. Nanomedicine (Lond) 5:1415–1433

122. Bertrand N, Leroux JC (2012) The journey of a drug-carrier in the body: an anatomo-physiological perspective. J Control Release 161:152–163

123. Owens DE III, Peppas NA (2006) Opsonization, biodistribution, and pharmacokinetics of polymeric nanoparticles. Int J Pharm 307:93–102

124. Ernsting MJ, Murakami M, Roy A, Li SD (2013) Factors controlling the pharmacokinetics, biodistribution and intratumoral penetration of nanoparticles. J Control Release 172(3):782–794

125. Betancourt T, Byrne JD, Sunaryo N, Crowder SW, Kadapakkam M, Patel S, Casciato S, Brannon-Peppas L (2009) PEGylation strategies for active targeting of PLA/PLGA nanoparticles. J Biomed Mater Res A 91:263–276

126. Perry JL, Reuter KG, Kai MP, Herlihy KP, Jones SW, Luft JC, Napier M, Bear JE, Desimone JM (2012) PEGylated PRINT nanoparticles: the impact of PEG density on protein binding, macrophage association, biodistribution, and pharmacokinetics. Nano Lett 12:5304–5310

127. Abu Lila AS, Kiwada H, Ishida T (2013) The accelerated blood clearance (ABC) phenomenon: clinical challenge and approaches to manage. J Control Release 172:38–47

128. Alaaeldin E, Abu Lila AS, Moriyoshi N, Sarhan HA, Ishida T, Khaled KA, Kiwada H (2013) The co-delivery of Oxaliplatin abrogates the immunogenic response to PEGylated siRNA-lipoplex. Pharm Res 30:2344–2354

129. Yoo JW, Irvine DJ, Discher DE, Mitragotri S (2011) Bio-inspired, bioengineered and biomimetic drug delivery carriers. Nat Rev Drug Discov 10:521–535

130. Cai S, Vijayan K, Cheng D, Lima EM, Discher DE (2007) Micelles of different morphologies–advantages of worm-like filomicelles of PEO-PCL in paclitaxel delivery. Pharm Res 24:2099–2109

131. Geng Y, Dalhaimer P, Cai S, Tsai R, Tewari M, Minko T, Discher DE (2007) Shape effects of filaments versus spherical particles in flow and drug delivery. Nat Nanotechnol 2:249–255

132. Parodi A, Quattrocchi N, van de Ven AL, Chiappini C, Evangelopoulos M, Martinez JO, Brown BS, Khaled SZ, Yazdi IK, Enzo MV, Isenhart L, Ferrari M, Tasciotti E (2013) Synthetic nanoparticles functionalized with biomimetic leukocyte membranes possess cell-like functions. Nat Nanotechnol 8:61–68

133. Jiang X, Xin H, Ren Q, Gu J, Zhu L, Du F, Feng C, Xie Y, Sha X, Fang X (2013) Nanoparticles of 2-deoxy-d-glucose functionalized poly(ethylene glycol)-co-poly(trimethylene carbonate) for dual-targeted drug delivery in glioma treatment. Biomaterials 35(1):518–529

134. Miura Y, Takenaka T, Toh K, Wu S, Nishihara H, Kano MR, Ino Y, Nomoto T, Matsumoto Y, Koyama H, Cabral H, Nishiyama N, Kataoka K (2013) Cyclic RGD-linked polymeric micelles for targeted delivery of platinum anticancer drugs to glioblastoma through the blood-brain tumor barrier. ACS Nano 7:8583–8592

135. Gao H, Yang Z, Zhang S, Cao S, Pang Z, Yang X, Jiang X (2013) Glioma-homing peptide with a cell-penetrating effect for targeting delivery with enhanced glioma localization, penetration and suppression of glioma growth. J Control Release 172(3):921–928

136. Rasheed ZA, Matsui W, Maitra A (2012) Pathology of pancreatic stroma in PDAC. In: Grippo PJ, Munshi HG (eds) Pancreatic cancer and tumor microenvironment. Transworld Research Network, Trivandrum (India)

137. Liss AS, Thayer SP (2012) Therapeutic targeting of pancreatic stroma. In: Grippo P, Munshi HG (eds) Pancreatic cancer and tumor microenvironment. Transworld Research Network, Trivandrum (India)

138. Kirtane AR, Kalscheuer SM, Panyam J (2013) Exploiting nanotechnology to overcome tumor drug resistance: challenges and opportunities. Adv Drug Deliv Rev 65(13-14):1731–1747

139. Heinemann V, Reni M, Ychou M, Richel DJ, Macarulla T, Ducreux M (2013) Tumour-stroma interactions in pancreatic ductal adenocarcinoma: rationale and current evidence for new therapeutic strategies. Cancer Treat Rev 40(1):118–128

140. Cox TR, Erler JT (2011) Remodeling and homeostasis of the extracellular matrix: implications for fibrotic diseases and cancer. Dis Model Mech 4:165–178

141. Lu P, Weaver VM, Werb Z (2012) The extracellular matrix: a dynamic niche in cancer progression. J Cell Biol 196:395–406

142. Levental KR, Yu H, Kass L, Lakins JN, Egeblad M, Erler JT, Fong SF, Csiszar K, Giaccia A, Weninger W, Yamauchi M, Gasser DL, Weaver VM (2009)

Matrix crosslinking forces tumor progression by enhancing integrin signaling. Cell 139:891–906

143. Kessenbrock K, Plaks V, Werb Z (2010) Matrix metalloproteinases: regulators of the tumor microenvironment. Cell 141:52–67

144. Erler JT, Weaver VM (2009) Three-dimensional context regulation of metastasis. Clin Exp Metastasis 26:35–49

145. Tredan O, Galmarini CM, Patel K, Tannock IF (2007) Drug resistance and the solid tumor microenvironment. J Natl Cancer Inst 99:1441–1454

146. Minchinton AI, Tannock IF (2006) Drug penetration in solid tumours. Nat Rev Cancer 6:583–592

147. Sermeus A, Rebucci M, Fransolet M, Flamant L, Desmet D, Delaive E, Arnould T, Michiels C (2013) Differential effect of hypoxia on etoposide-induced DNA damage response and p53 regulation in different cell types. J Cell Physiol 228:2365–2376

148. Erler JT, Bennewith KL, Nicolau M, Dornhofer N, Kong C, Le QT, Chi JT, Jeffrey SS, Giaccia AJ (2006) Lysyl oxidase is essential for hypoxia-induced metastasis. Nature 440:1222–1226

149. Brown JM, Wilson WR (2004) Exploiting tumour hypoxia in cancer treatment. Nat Rev Cancer 4:437–447

150. Comerford KM, Wallace TJ, Karhausen J, Louis NA, Montalto MC, Colgan SP (2002) Hypoxia-inducible factor-1-dependent regulation of the multidrug resistance (MDR1) gene. Cancer Res 62:3387–3394

151. Gerweck LE, Vijayappa S, Kozin S (2006) Tumor pH controls the *in vivo* efficacy of weak acid and base chemotherapeutics. Mol Cancer Ther 5:1275–1279

152. Jain RK (1987) Transport of molecules in the tumor interstitium: a review. Cancer Res 47:3039–3051

153. Heldin CH, Rubin K, Pietras K, Ostman A (2004) High interstitial fluid pressure – an obstacle in cancer therapy. Nat Rev Cancer 4:806–813

154. Saggar JK, Yu M, Tan Q, Tannock IF (2013) The tumor microenvironment and strategies to improve drug distribution. Front Oncol 3:154

155. Biswas SK, Allavena P, Mantovani A (2013) Tumor-associated macrophages: functional diversity, clinical significance, and open questions. Semin Immunopathol 35:585–600

156. Balkwill F, Mantovani A (2001) Inflammation and cancer: back to Virchow? Lancet 357:539–545

157. Siveen KS, Kuttan G (2009) Role of macrophages in tumour progression. Immunol Lett 123:97–102

158. Bingle L, Brown NJ, Lewis CE (2002) The role of tumour-associated macrophages in tumour progression: implications for new anticancer therapies. J Pathol 196:254–265

159. Pollard JW (2004) Tumour-educated macrophages promote tumour progression and metastasis. Nat Rev Cancer 4:71–78

160. Coffelt SB, Hughes R, Lewis CE (2009) Tumor-associated macrophages: effectors of angiogenesis and tumor progression. Biochim Biophys Acta 1796:11–18

161. Owen JL, Mohamadzadeh M (2013) Macrophages and chemokines as mediators of angiogenesis. Front Physiol 4:159

162. Marsh T, Pietras K, McAllister SS (2013) Fibroblasts as architects of cancer pathogenesis. Biochim Biophys Acta 1832:1070–1078

163. Kalluri R, Zeisberg M (2006) Fibroblasts in cancer. Nat Rev Cancer 6:392–401

164. Cirri P, Chiarugi P (2011) Cancer associated fibroblasts: the dark side of the coin. Am J Cancer Res 1:482–497

165. Goruppi S, Dotto GP (2013) Mesenchymal stroma: primary determinant and therapeutic target for epithelial cancer. Trends Cell Biol 23(12):593–602

166. Madar S, Goldstein I, Rotter V (2013) 'Cancer associated fibroblasts'–more than meets the eye. Trends Mol Med 19:447–453

167. Dvorak HF (1986) Tumors: wounds that do not heal. Similarities between tumor stroma generation and wound healing. N Engl J Med 315:1650–1659

168. Polanska UM, Orimo A (2013) Carcinoma-associated fibroblasts: non-neoplastic tumour-promoting mesenchymal cells. J Cell Physiol 228:1651–1657

169. Murakami M, Ernsting MJ, Undzys E, Holwell N, Foltz WD, Li SD (2013) Docetaxel conjugate nanoparticles that target alpha-smooth muscle actin-expressing stromal cells suppress breast cancer metastasis. Cancer Res 73:4862–4871

170. Whatcott CJ, Han H, Posner RG, Hostetter G, Von Hoff DD (2011) Targeting the tumor microenvironment in cancer: why hyaluronidase deserves a second look. Cancer Discov 1:291–296

171. Thompson CB, Shepard HM, O'Connor PM, Kadhim S, Jiang P, Osgood RJ, Bookbinder LH, Li X, Sugarman BJ, Connor RJ, Nadjsombati S, Frost GI (2010) Enzymatic depletion of tumor hyaluronan induces antitumor responses in preclinical animal models. Mol Cancer Ther 9:3052–3064

172. Baumgartner G, Gomar-Hoss C, Sakr L, Ulsperger E, Wogritsch C (1998) The impact of extracellular matrix on the chemoresistance of solid tumors–experimental and clinical results of hyaluronidase as additive to cytostatic chemotherapy. Cancer Lett 131:85–99

173. Pillwein K, Fuiko R, Slavc I, Czech T, Hawliczek G, Bernhardt G, Nirnberger G, Koller U (1998) Hyaluronidase additional to standard chemotherapy improves outcome for children with malignant brain tumors. Cancer Lett 131:101–108

174. Yocum RC, Kennard D, Heiner LS (2007) Assessment and implication of the allergic sensitivity to a single dose of recombinant human hyaluronidase injection: a double-blind, placebo-controlled clinical trial. J Infus Nurs 30:293–299

175. Provenzano PP, Cuevas C, Chang AE, Goel VK, Von Hoff DD, Hingorani SR (2012) Enzymatic targeting of the stroma ablates physical barriers to treatment of pancreatic ductal adenocarcinoma. Cancer Cell 21:418–429

176. Provenzano PP, Hingorani SR (2013) Hyaluronan, fluid pressure, and stromal resistance in pancreas cancer. Br J Cancer 108:1–8

177. Yang C, Liu Y, He Y, Du Y, Wang W, Shi X, Gao F (2013) The use of HA oligosaccharide-loaded nanoparticles to breach the endogenous hyaluronan glycocalyx for breast cancer therapy. Biomaterials 34:6829–6838

178. Burris HA III, Moore MJ, Andersen J, Green MR, Rothenberg ML, Modiano MR, Cripps MC, Portenoy RK, Storniolo AM, Tarassoff P, Nelson R, Dorr FA, Stephens CD, Von Hoff DD (1997) Improvements in survival and clinical benefit with gemcitabine as first-line therapy for patients with advanced pancreas cancer: a randomized trial. J Clin Oncol 15:2403–2413

179. Chung WG, Sandoval MA, Sloat BR, Lansakara P, Cui Z (2012) Stearoyl gemcitabine nanoparticles overcome resistance related to the over-expression of ribonucleotide reductase subunit M1. J Control Release 157:132–140

180. Olson P, Hanahan D (2009) Cancer. Breaching the cancer fortress. Science 324:1400–1401

181. Olive KP, Jacobetz MA, Davidson CJ, Gopinathan A, McIntyre D, Honess D, Madhu B, Goldgraben MA, Caldwell ME, Allard D, Frese KK, Denicola G, Feig C, Combs C, Winter SP, Ireland-Zecchini H, Reichelt S, Howat WJ, Chang A, Dhara M, Wang L, Ruckert F, Grutzmann R, Pilarsky C, Izeradjene K, Hingorani SR, Huang P, Davies SE, Plunkett W, Egorin M, Hruban RH, Whitebread N, McGovern K, Adams J, Iacobuzio-Donahue C, Griffiths J, Tuveson DA (2009) Inhibition of Hedgehog signaling enhances delivery of chemotherapy in a mouse model of pancreatic cancer. Science 324:1457–1461

182. Sandhiya S, Melvin G, Kumar SS, Dkhar SA (2013) The dawn of hedgehog inhibitors: Vismodegib. J Pharmacol Pharmacother 4:4–7

183. Xu Y, Chenna V, Hu C, Sun HX, Khan M, Bai H, Yang XR, Zhu QF, Sun YF, Maitra A, Fan J, Anders RA (2012) Polymeric nanoparticle-encapsulated hedgehog pathway inhibitor HPI-1 (NanoHHI) inhibits systemic metastases in an orthotopic model of human hepatocellular carcinoma. Clin Cancer Res 18:1291–1302

184. Chenna V, Hu C, Pramanik D, Aftab BT, Karikari C, Campbell NR, Hong SM, Zhao M, Rudek MA, Khan SR, Rudin CM, Maitra A (2012) A polymeric nanoparticle encapsulated small-molecule inhibitor of Hedgehog signaling (NanoHHI) bypasses secondary mutational resistance to Smoothened antagonists. Mol Cancer Ther 11:165–173

185. Heinemann V, Haas M, Boeck S (2012) Systemic treatment of advanced pancreatic cancer. Cancer Treat Rev 38:843–853

186. Yardley DA (2013) nab-Paclitaxel mechanisms of action and delivery. J Control Release 170: 365–372

187. Desai N, Trieu V, Damascelli B, Soon-Shiong P (2009) SPARC expression correlates with tumor response to albumin-bound paclitaxel in head and neck cancer patients. Transl Oncol 2:59–64

188. Neuzillet C, Tijeras-Raballand A, Cros J, Faivre S, Hammel P, Raymond E (2013) Stromal expression of SPARC in pancreatic adenocarcinoma. Cancer Metastasis Rev 32(3-4):585–602

189. Von Hoff DD, Ramanathan RK, Borad MJ, Laheru DA, Smith LS, Wood TE, Korn RL, Desai N, Trieu V, Iglesias JL, Zhang H, Soon-Shiong P, Shi T, Rajeshkumar NV, Maitra A, Hidalgo M (2011) Gemcitabine plus nab-paclitaxel is an active regimen in patients with advanced pancreatic cancer: a phase I/II trial. J Clin Oncol 29:4548–4554

190. Von Hoff DD, Ervin T, Arena FP, Chiorean EG, Infante J, Moore M, Seay T, Tjulandin SA, Ma WW, Saleh MN, Harris M, Reni M, Dowden S, Laheru D, Bahary N, Ramanathan RK, Tabernero J, Hidalgo M, Goldstein D, Van CE, Wei X, Iglesias J, Renschler MF (2013) Increased survival in pancreatic cancer with nab-paclitaxel plus gemcitabine. N Engl J Med 369(18):1691–1703

191. Alvarez R, Musteanu M, Garcia-Garcia E, Lopez-Casas PP, Megias D, Guerra C, Munoz M, Quijano Y, Cubillo A, Rodriguez-Pascual J, Plaza C, de Vicente E, Prados S, Tabernero S, Barbacid M, Lopez-Rios F, Hidalgo M (2013) Stromal disrupting effects of nab-paclitaxel in pancreatic cancer. Br J Cancer 109:926–933

192. Frese KK, Neesse A, Cook N, Bapiro TE, Lolkema MP, Jodrell DI, Tuveson DA (2012) nab-Paclitaxel potentiates gemcitabine activity by reducing cytidine deaminase levels in a mouse model of pancreatic cancer. Cancer Discov 2:260–269

193. Lansakara P, Rodriguez BL, Cui Z (2012) Synthesis and in vitro evaluation of novel lipophilic monophosphorylated gemcitabine derivatives and their nanoparticles. Int J Pharm 429:123–134

194. Ernsting MJ, Murakami M, Undzys E, Aman A, Press B, Li SD (2012) A docetaxel-carboxymethylcellulose nanoparticle outperforms the approved taxane nanoformulation, Abraxane, in mouse tumor models with significant control of metastases. J Control Release 162:575–581

195. Ernsting MJ, Foltz WD, Undzys E, Tagami T, Li SD (2012) Tumor-targeted drug delivery using MR-contrasted docetaxel – carboxymethylcellulose nanoparticles. Biomaterials 33:3931–3941

196. Ernsting MJ, Tang WL, MacCallum NW, Li SD (2012) Preclinical pharmacokinetic, biodistribution, and anti-cancer efficacy studies of a docetaxel-carboxymethylcellulose nanoparticle in mouse models. Biomaterials 33:1445–1454

197. Ernsting MJ, Tang WL, MacCallum N, Li SD (2011) Synthetic modification of carboxymethylcellulose and use thereof to prepare a nanoparticle forming conjugate of docetaxel for enhanced cytotoxicity against cancer cells. Bioconjug Chem 22:2474–2486

198. Lee ES, Gao Z, Bae YH (2008) Recent progress in tumor pH targeting nanotechnology. J Control Release 132:164–170

199. Torchilin V (2009) Multifunctional and stimuli-sensitive pharmaceutical nanocarriers. Eur J Pharm Biopharm 71:431–444

200. Zhu L, Torchilin VP (2013) Stimulus-responsive nanopreparations for tumor targeting. Integr Biol (Camb) 5:96–107

201. Ganta S, Devalapally H, Shahiwala A, Amiji M (2008) A review of stimuli-responsive nanocarriers for drug and gene delivery. J Control Release 126:187–204

202. Jensen SS, Andresen TL, Davidsen J, Hoyrup P, Shnyder SD, Bibby MC, Gill JH, Jorgensen K (2004) Secretory phospholipase A2 as a tumor-specific trigger for targeted delivery of a novel class of liposomal prodrug anticancer etherlipids. Mol Cancer Ther 3:1451–1458

203. Andresen TL, Davidsen J, Begtrup M, Mouritsen OG, Jorgensen K (2004) Enzymatic release of anti-tumor ether lipids by specific phospholipase A2 activation of liposome-forming prodrugs. J Med Chem 47:1694–1703

204. Lee ES, Na K, Bae YH (2003) Polymeric micelle for tumor pH and folate-mediated targeting. J Control Release 91:103–113

205. Patel NR, Pattni BS, Abouzeid AH, Torchilin VP (2013) Nanopreparations to overcome multidrug resistance in cancer. Adv Drug Deliv Rev 65(13-14):1748–1762

206. Zhu S, Niu M, O'Mary H, Cui Z (2013) Targeting of tumor-associated macrophages made possible by PEG-sheddable, mannose-modified nanoparticles. Mol Pharm 10:3525–3530

207. Zhu S, Wonganan P, Lansakara P, O'Mary HL, Li Y, Cui Z (2013) The effect of the acid-sensitivity of 4-(N)-stearoyl gemcitabine-loaded micelles on drug resistance caused by RRM1 overexpression. Biomaterials 34:2327–2339

208. Zhu S, Lansakara P, Li X, Cui Z (2012) Lysosomal delivery of a lipophilic gemcitabine prodrug using novel acid-sensitive micelles improved its antitumor activity. Bioconjug Chem 23:966–980

209. Poon Z, Chang D, Zhao X, Hammond PT (2011) Layer-by-layer nanoparticles with a pH-sheddable layer for in vivo targeting of tumor hypoxia. ACS Nano 5:4284–4292

210. Sawant RM, Hurley JP, Salmaso S, Kale A, Tolcheva E, Levchenko TS, Torchilin VP (2006) "SMART" drug delivery systems: double-targeted pH-responsive pharmaceutical nanocarriers. Bioconjug Chem 17:943–949

211. Yanasarn N, Sloat BR, Cui Z (2009) Nanoparticles engineered from lecithin-in-water emulsions as a potential delivery system for docetaxel. Int J Pharm 379:174–180

212. Zhu L, Wang T, Perche F, Taigind A, Torchilin VP (2013) Enhanced anticancer activity of nanopreparation containing an MMP2-sensitive PEG-drug conjugate and cell-penetrating moiety. Proc Natl Acad Sci U S A 110:17047–17052

213. Xu S, Olenyuk BZ, Okamoto CT, Hamm-Alvarez SF (2013) Targeting receptor-mediated endocytotic pathways with nanoparticles: rationale and advances. Adv Drug Deliv Rev 65:121–138

214. Sahay G, Alakhova DY, Kabanov AV (2010) Endocytosis of nanomedicines. J Control Release 145:182–195

215. Varkouhi AK, Scholte M, Storm G, Haisma HJ (2011) Endosomal escape pathways for delivery of biologicals. J Control Release 151:220–228

216. Akinc A, Thomas M, Klibanov AM, Langer R (2005) Exploring polyethylenimine-mediated DNA transfection and the proton sponge hypothesis. J Gene Med 7:657–663

217. Vercauteren D, Rejman J, Martens TF, Demeester J, De Smedt SC, Braeckmans K (2012) On the cellular processing of non-viral nanomedicines for nucleic acid delivery: mechanisms and methods. J Control Release 161:566–581

218. Duncan R, Richardson SC (2012) Endocytosis and intracellular trafficking as gateways for nanomedicine delivery: opportunities and challenges. Mol Pharm 9:2380–2402

219. Wonganan P, Lansakara P, Zhu S, Holzer M, Sandoval MA, Warthaka M, Cui Z (2013) Just getting into cells is not enough: mechanisms underlying 4-(N)-stearoyl gemcitabine solid lipid nanoparticle's ability to overcome gemcitabine resistance caused by RRM1 overexpression. J Control Release 169:17–27

220. Sun YL, Patel A, Kumar P, Chen ZS (2012) Role of ABC transporters in cancer chemotherapy. Chin J Cancer 31:51–57

221. Jabr-Milane LS, van Vlerken LE, Yadav S, Amiji MM (2008) Multi-functional nanocarriers to overcome tumor drug resistance. Cancer Treat Rev 34:592–602

222. Xue X, Liang XJ (2012) Overcoming drug efflux-based multidrug resistance in cancer with nanotechnology. Chin J Cancer 31:100–109

223. Zhang P, Ling G, Sun J, Zhang T, Yuan Y, Sun Y, Wang Z, He Z (2011) Multifunctional nanoassemblies for vincristine sulfate delivery to overcome multidrug resistance by escaping P-glycoprotein mediated efflux. Biomaterials 32:5524–5533

224. Zahedi P, De SR, Huynh L, Piquette-Miller M, Allen C (2011) Combination drug delivery strategy for the treatment of multidrug resistant ovarian cancer. Mol Pharm 8:260–269

225. Patil Y, Sadhukha T, Ma L, Panyam J (2009) Nanoparticle-mediated simultaneous and targeted delivery of paclitaxel and tariquidar overcomes tumor drug resistance. J Control Release 136:21–29

226. Navarro G, Sawant RR, Biswas S, Essex S, de Tros I, Torchilin VP (2012) P-glycoprotein silencing with siRNA delivered by DOPE-modified PEI overcomes doxorubicin resistance in breast cancer cells. Nanomedicine (Lond) 7:65–78

227. Li YT, Chua MJ, Kunnath AP, Chowdhury EH (2012) Reversing multidrug resistance in breast cancer cells by silencing ABC transporter genes with nanoparticle-facilitated delivery of target siRNAs. Int J Nanomedicine 7:2473–2481

228. Wang Y, Guo M, Lu Y, Ding LY, Ron WT, Liu YQ, Song FF, Yu SQ (2012) Alpha-tocopheryl polyethylene glycol succinate-emulsified poly(lactic-co-glycolic acid) nanoparticles for reversal of multidrug resistance *in vitro*. Nanotechnology 23:495103

229. Wang J, Sun J, Chen Q, Gao Y, Li L, Li H, Leng D, Wang Y, Sun Y, Jing Y, Wang S, He Z (2012) Star-shape copolymer of lysine-linked di-tocopherol polyethylene glycol 2000 succinate for doxorubicin delivery with reversal of multidrug resistance. Biomaterials 33:6877–6888

230. Patil YB, Swaminathan SK, Sadhukha T, Ma L, Panyam J (2010) The use of nanoparticle-mediated targeted gene silencing and drug delivery to overcome tumor drug resistance. Biomaterials 31: 358–365

231. Wu H, Shi Y, Huang C, Zhang Y, Wu J, Shen H, Jia N (2013) Multifunctional nanocarrier based on clay nanotubes for efficient intracellular siRNA delivery and gene silencing. J Biomater Appl. doi: 10.1177/0885328213501215

232. Ganesh S, Iyer AK, Weiler J, Morrissey DV, Amiji MM (2013) Combination of siRNA-directed gene silencing with cisplatin reverses drug resistance in human non-small cell lung cancer. Mol Ther Nucleic Acids 2:e110

233. Yang F, Huang W, Li Y, Liu S, Jin M, Wang Y, Jia L, Gao Z (2013) Anti-tumor effects in mice induced by survivin-targeted siRNA delivered through polysaccharide nanoparticles. Biomaterials 34:5689–5699

234. Markman JL, Rekechenetskiy A, Holler E, Ljubimova JY (2013) Nanomedicine therapeutic approaches to overcome cancer drug resistance. Adv Drug Deliv Rev 65(13-14):1866–1879

235. Kunjachan S, Rychlik B, Storm G, Kiessling F, Lammers T (2013) Multidrug resistance: physiological principles and nanomedical solutions. Adv Drug Deliv Rev 65(13-14):1852–1865

Transgenerational Effects of NMs

12

Anna Poma, Sabrina Colafarina,
Gabriella Fontecchio, and Giuseppe Chichiriccò

Contents

A. Poma (✉) • S. Colafarina • G. Fontecchio
G. Chichiriccò
Department of Life, Health and Environmental
Sciences, University of L'Aquila,
Via Vetoio, Coppito, L'Aquila I-67010, Italy
e-mail: annamaria.poma@univaq.it

Abstract

Nanomaterials are present in a number of commercially available products but there are uncertainties as to whether the unique properties that support their commercial use may also pose potential health risks. Information is missing concerning the influence of nanomaterials on the overall reproductive outcome and transgenerational effects in animals and plants. To obtain this information, long-term studies would be required using animal models phylogenetically close to humans and exposure conditions that reflect realistic scenarios with regard to dosages and admission. The nanoreprotoxicology literature published to date is largely descriptive in nature regarding the effects of nanoparticles. The mechanisms, which determine particle reproduction compatibility, are mostly elusive at the moment. Thus, it is recommended that future research explore the interactions between nanomaterials and transgenerational matter on a molecular level. It would, for instance, be of major importance to understand the behaviour

of nanoparticles inside the cells but also their genotoxic and epigenetic effects. Recent studies have shown that intravenous and/or intra-abdominal administration of nanoparticles to mice results in their accumulation in the cells of many tissues, including the brain and the testis, suggesting that they easily pass through the blood–brain and blood–testis barriers. In parallel embryo development after exposure to nanoparticles should be comparatively investigated. The majority of studies on embryo toxicology have concentrated on piscine embryos, mostly derived from zebrafish. Plants for human food as an important component of the ecosystem need also to be taken into account when evaluating transgenerational effects of engineered nanomaterials in crops.

12.1   Introduction

Nanomaterial can be defined as a material having structure on a scale greater than atomic/molecular dimensions, but less than 100 nm, which exhibits physical, chemical and biological characteristics associated with its nanostructure. With recent developments in nanotechnology, various kinds of nanomaterials have been designed and produced throughout the world [1]. The small particle size and large surface area relative to volume enables nanomaterials to display a number of useful properties that are different from those of bulk materials, including high levels of electrical conductivity, tensile strength, electronic reactivity, and tissue permeability. There are many application fields for these nanomaterials such as high performance materials, energy storage and conversion, self-cleaning surface coatings and stain-resistant textiles using simple nanostructured materials such as carbon nanotubes and metal oxide

nanoparticles. Research into more complex nanomaterials will lead to applications such as cellular-level medical diagnostics and treatment [2]. Nanomaterials are present in a number of commercially available products including sunscreens, cosmetics and many industrial applications, but there are uncertainties as to whether the unique properties that support their commercial use may also pose potential occupational health risks [3]. Nanomaterials have a high surface-to-volume ratio, so surface reactivity will be high and may adopt structures that are different from the bulk form of the chemical and, therefore, may exhibit different chemical and physical properties [4]. Nanoscale materials are already becoming commercially available for industrial applications and consumer use and in the fields of biology and medicine as drug and delivery formulations, for tissue engineering, for destroying tumors by hyperthermia, for probes of DNA structure, and for biosensors [1, 5, 6]. Until recently less information was available regarding air-born levels of nanomaterials generated during production or quantities, which may be aerosolized into the environment. Ultrafine particle inhalation toxicology studies suggest that particle size can influence toxicity principally due to two factors: the large surface area and its reactivity or intrinsic toxicity [7]. The interaction of surface area and particle composition in eliciting biological responses adds an extra dimension of complexity in evaluating potential adverse events that may result from exposure to these materials [8]. There are indications to date that manufactured nanoscale materials may spread in the body in unpredictable ways, and certain nanoscale materials have been observed to preferentially accumulate in particular organelles [9]. Furthermore, the unique and diverse physico-chemical properties [10] of nanoscale materials suggest that their toxicological properties may differ from those of the corresponding bulk materials. Whole-body studies show that inhalation of nanoparticles and entry through the lungs is followed by rapid translocation to vital organs, like the kidney and liver [11]. Moreover, nanoparticles toxicity can be attributed to: release of toxic ions (for example in the case of CdSe/ZnS nanoparticles), to nonspecific interaction with biological

structures facilitated by their shape, as in the case of nanotubes and to specific interaction with bio-macromolecules through surface modifications. Particle (or aggregate) size determines whether a particle enters the cellular environment through phagocytosis, endocytosis, or some undefined mechanisms [12]. In a recent work Porter [13] showed for the first time, a bundle of single-walled carbon nanotubes (SWCNTs) within the nucleus of human macrophage-like treated cells. Uptake to these sites implies that they may interact with intracellular proteins, organelles and DNA, which would greatly enhance their toxic potential. Nanomaterials distribution to different body tissues following deposition in the respiratory tract or administered to an in vivo system can potentially affect multiple cellular functions. It will be difficult to determine with conventional assays what changes and adverse effects may have occurred. Use of genomic approach provides information about specific mechanisms at the molecular level (e.g. oxidative stress); in particular, toxicogenomics has proved to be a powerful tool for the direct monitoring of patterns of cellular pertubations in specific pathways, through identification and quantification of global shifts in gene expression resulting within treated cells [9]. Nanoparticles form a basis for many engineered nanomaterials, and are currently available in a variety of types: fullerenes (C60), carbon nanotubes (CNT), metal and metal oxide particles, polymer nanoparticles, and quantum dots are the most common.

It is rather difficult to compare studies, particularly because the information given concerning the dosage of nanoparticles is very diverse. It would be useful if common nomenclature could be developed to express nanoparticle dose. One option would be to calculate the particle surface exposed to a certain number of cells or the exact mass of an organism, as suggested by Oberdorster et al. [8] because it combines particle number and size with the amount of exposed biomass. Another weakness in the literature published so far is the almost purely descriptive nature of the toxic effects of nanoparticles. The mechanisms, which determine particle biocompatibility, are mostly elusive at the moment. Thus, it is recommended

that future research explores the interactions between nanomaterials and biological matter on a molecular level.

Furthermore, information is missing concerning the effect of nanomaterials on the overall reproductive outcome. To obtain this information, long-term studies would be required using animal models phylogenetically close to humans and exposure conditions that reflect realistic scenarios with regard to dosages and routes of admission [14]. As yet, developmental toxicity of engineered nanoparticles and transgenerational effects of nanomaterials in animals and humans have been little studied (in Table 12.1). Gametogenesis is a complex biological process that is sensitive to environmental insult, for example, from chemicals. Chemical effects on germ cells and their maturation can inhibit fertility, cause cancer, and may have negative effects on the development of offspring. Mutagens, for example, produce heritable gene mutations, and heritable structural and numerical chromosome aberrations in germ cells. The consequences of germ cell mutation for subsequent generations include genetically determined phenotypic alterations without signs of illness, reduction in fertility, embryonic or perinatal death, congenital malformations with varying degrees of severity and genetic diseases with varying degrees of health impairment. Recent studies have shown that intravenous and/or intra-abdominal administration of nanoparticles to mice results in their accumulation in the cells of many tissues, including the brain and the testis, suggesting that they easily pass through the blood–brain and blood–testis barriers [24]. In parallel embryo development after exposure to nanoparticles is comparatively well investigated. The majority of studies on embryo toxicology have concentrated on piscine embryos, mostly derived from zebrafish. Various developing organisms react to nanoparticles. Besides the chemical modalities of the tested nanoparticles, the production method and especially the test system itself seems to play a major role in the outcome of the study. Therefore, there is a pressing need for further studies of nanoreprotoxicity in animal models phylogenetically close to the human.

Table 12.1 Summary of nanomaterial transgenerational effects studies to date

Citation	Nanoparticle tested	In vitro/in vivo	Genotoxicity assay	Toxicity assay — Other analysis	Findings
Nanomaterials (Poma and Di Giorgio [9])	Fullerenes (C60), carbon nanotubes (CNT), polymer nanoparticles, and quantum dots	Fullerenes (C60) tested in larval zebrafish *Danio rerio*; mouse was exposed to multi-walled carbon nanotubes (MWCNTs), aerosolized for 7–14 days	Gene expression		Survival of larval zebrafish was reduced in nitrogen gas –C60 and nitrogen gas–water, but not in C60–water. It was that IL–6, IL–10, and NAD(P)H oxidoreductase 1 (NQO1) mRNA expression was not increased in the lungs
Carbon nanotubes (Cheng and Cheng [15])	Multi-walled carbon nanotubes (MWCNTs) of different length	Embryos zebrafish		FITC assay Double staining of F-actin and Sytox Green, TEM observation	This study suggests that length plays an important role in the in vivo toxicity of functionalized CNTs
Nanoparticulate (Kyjovska et al. [16])	Titanium dioxide (TiO₂) and carbon black (CB) nanoparticles	Sperm mice		Trypan blue assay	Prenatal exposure to nanoparticles may adversely effect male reproduction in male offspring
Zinc oxide nanoparticles (Talebi et al. [17])	Zinc oxide nanoparticles	Sperm mouse		Testicular histopathology, morphometric analysis	Zinc oxide nanoparticles act as testicular toxicant and further studies are needed to establish its mechanism of action upon spermatogenesis
Nanoparticles (Di Guglielmo et al. [18])	Cobalt ferrite and gold nanoparticles	Embryonic stem cell		MTT test ELISA test EST assay	ID(50) results permit to classify cobalt ferrite nanoparticles coated with gold and silanes as non-embryotoxic
Nanoparticles metal (Taylor et al. [19])	ZnO NP, TiO NP between 1 and 100 nm in size	Cell culture, mammalian gametes: male and female	Gene expression analysis	MTT test, LDH test Annexin assay, cell-cycle analysis, microscopy	Cellular damage caused by nanoparticle exposure includes production of reactive oxygen species and interaction with DNA. Reduced sperm density and motility, increased sperm abnormality, germ cell apoptosis

	Material	Test system	Assay/Endpoints	Results
Biomaterials (Singh et al. [20])	Metal nanoparticles, metal-oxide nanoparticles, quantum dots, fullerenes, and fibrous nanomaterials. Au NP, Ag NP, Anatase TiO_2 and ZnO (both were 40–70 nm)	Human fetal lung fibroblast cell line (MRC-5) Mouse embryonic stem cells (MES) and fibroblasts (MEF) PBL; human sperm cells	HPLC to measure 8-OHdG, expression of DNA repair proteins; H2AX phosphorylation; comet assay in dark (D), under pre-irradiation (PI) and simultaneous irradiation (SI) conditions. Cell proliferation (trypan blue), MTT assay, trypan blue staining, SEM, photon correlation spectroscopy (Zetasizer) Gene expression profiling p53 phosphorylation	The nanomaterials assessed were found to cause chromosomal fragmentation, point mutations, oxidative DNA adducts and alterations in gene expression profiles
Nanoparticles (Braydich-Stolle et al. [21])	Molybdenum trioxide (MoO_3), silver (Ag NP), aluminum Al(NP) nanoparticles	Mammalian germline stem cells in vitro	Cell proliferation (trypan blue), cytotoxicity assays (MTT), LDH assay microscopic observation apoptosis/necrosis assay	Silver nanoparticles were the most toxic while molybdenum trioxide (MoO_3) nanoparticles were the least toxic. Our results suggest that this cell line provides a valuable model with which to assess the cytotoxicity of nanoparticles in the germ line in vitro
Nanometals (Massarsky et al. [22])	Nanosilver and Ag^+	Embryos zebrafish	Production, glutathione levels ROS, antioxidant enzyme activities	AgNPs and Ag^+ are capable of inducing toxicity in zebrafish embryos including the induction of oxidative stress
Nanoparticles (Wang et al. [23])	Nanocerium oxide	Tomato plants seeds and seedlings (first and second generations)	Radicle emergence and full cotyledon expansion, chlorophyll content in leaf tissues, root electrolyte leakage status of second generation seedlings	Trans-generational impact of cerium oxide nanoparticles on tomato plants

12.2 Influence of Maternal Airway Exposure to Nanoparticulate on Mammalians Male Reproductive Function in the Two Following Generations: The Case of Titanium Dioxide (TiO₂, UV-Titan) and Carbon Black (CB, Printex90)

In mice, engineered nanoparticles have been shown to adversely affect male reproductive function after exposure in adulthood [25] as well as after maternal exposure during foetal development. Specifically, maternal subcutaneous injection of nano-sized titanium dioxide (TiO₂) particles during gestation resulted not only in TiO₂ particles aggregating in offspring testicular tissue after birth, but also in abnormal testicular morphology and lower daily sperm production in mice [26]. Also in mice, offspring seminiferous tissue and daily sperm production were adversely affected after maternal gestational exposure to nano-sized carbon black (CB) particles applied by intratracheal instillation [27]. The male reproductive function sensitivity to maternal gestational exposure to particles is supported by studies of particles generated from diesel engines. Daily sperm production (DSP) decreased in male rodents whose mothers inhaled diesel exhaust particles (DEP) or whole diesel exhaust during pregnancy [28–30]. Furthermore, maternal exposure to DEP increased the number of germline mutations in male offspring, and these mutations were transferred to the next generation in mice [31]. Observations of adverse effects on male reproductive function following prenatal exposure to particles with few associated compounds, as described above for TiO₂ and CB, indicate that prenatal exposure to particulates per se poses a threat to male reproductive function. Elucidation of the relationship between maternal exposure to engineered nanoparticles and reproductive function of the male offspring is therefore important.

Semen samples cannot easily be obtained from rodents. Assessment of DSP is therefore a suitable method for evaluation of spermatogenesis in these species. DSP is assessed by homogenization of testicular tissue, followed by counting the number of spermatids surviving homogenization. The number of counted spermatids is then divided by a time factor expressing the duration of this homogenization resistant stage. Finally, the number is recalculated taking absolute testicle weight into account [32]. The method has since been applied in several other species, e.g. humans, boars, rabbits, mouse.

The effects of maternal exposure to engineered nanoparticles on sperm production in the male offspring have only been little studied, and effects in the second generation remain to be investigated. The study reported by [16] aimed to: (1) describe and optimize the method of DSP assessment in mice and (2) examine the effects of maternal airway exposure during gestation to two types of engineered nanoparticles on DSP in the F1 and F2 generations. All assessments were made in mice of the C57BL/6J strain. When pregnant mice inhaled nanosized TiO₂, mice at a dose level corresponding to half the 8-h Danish occupational exposure limit, the male reproductive system in the F1 offspring was not affected. In [16] they also exposed pregnant female mice to CB. When male reproductive parameters were assessed in their adult F1 offspring, no differences between control and CB exposed offspring were present. The F1 males of the C57BL/6J strain were crossmated with CBA/J females to produce the F2 generation ((CBA/J)/(C57BL/6J)). When male reproductive parameters were assessed in this F2 generation, DSP tended to be lower, in F2 offspring whose grandmothers were exposed to CB, compared to offspring from the unexposed group. These observations also indicate that the effects of CB exposure during pregnancy affected male reproduction in the offspring of exposed male foetuses, but not in the offspring of exposed female foetuses. Gestational exposure to nanosized TiO₂ and CB has been found to affect male reproduction in offspring in previous studies.

Exposure of pregnant females to nanoparticles can hypothetically affect the foetus by several pathways: (1) directly, by passage of nanoparticles through the placenta followed by direct interference with foetal development; (2) due to toxic compounds associated with the particles;

(3) by change of placental function; or (4) indirectly, as e.g. maternal inflammation and oxidative stress may affect foetal development through indirect mediators (reviewed in [33, 34]). Some information may be however be obtained from particulates generated by diesel engines and observations from rodent studies with maternal inhalation of diesel particles or whole exhaust. The results indicate that gestational exposure to particles might pose a threat to reproductive function of the male offspring. The study discussed whether it is the diesel exhaust particles, the associated compounds (e.g. polyaromatic hydrocarbons, heavy metals), the exhaust gases, or the maternal lung inflammation that account for reproductive effects in the male offspring [35]. The detrimental effects of DEP on male reproductive parameters, i.e. abnormal testicular morphology and lower DSP, possibly arise due to exposure to polycyclic aromatic hydrocarbons, rather than solely due to particle exposure. In [36] nanosized surface-coated TiO_2 particles (doped with zirconium, silicon, aluminium) produced effects following prenatal exposure in mice. Inflammatory mediators and oxidative stress may therefore have interfered with foetal development through indirect pathways. The experiments reported in [16] were conducted in the inbred C57BL/6J strain, whereas the previously published studies of nanosized TiO_2 and CB were conducted in mice of the outbred ICR strain. Strain differences in foetal sensitivity to maternal particle exposure have unfortunately only been touched upon briefly in the scientific literature. When pregnant mice were exposed to whole diesel exhaust, and mRNA expression of gonadal differentiation factors was assessed in male foetuses on gestation day 14, strain differences were observed. ICR mice showed higher sensitivity to whole diesel exhaust compared to the C57BL/6J strain; and only in the ICR strain was the phenotype affected, i.e. expression of steroidogenic enzymes decreased [37, 38]. The route of exposure can also influence experimental results. In the previous developmental studies nanoparticles were administered by subcutaneous injections (TiO_2) or intratracheal instillation (CB). Whereas an injection gives a relatively

higher internal body burden of particles compared to inhalation [39], the internal body burden from instillation would be expected to compare to that of exposure by inhalation and certainly to that of instillation as used in the CB experiment. In the previous cited work, the absence of effect in the F1 generation of nanosized CB exposed males indicates that maternal exposure did not interfere directly with development of the male reproductive system, although exposure may have interfered with primordial germ cells in the male foetuses; changes in primordial germ cells might well have altered the genetic make-up of the male germ line, e.g. by introducing mutations or epigenetic changes. This could potentially affect reproductive parameters in the F2 generation.

The prenatal period of germ cell development represents a key window of epigenetic programming in the male. Testicular and germ cells have distinct methylation patterns, which might be pertinent for maintenance of the unique chromosomal structure in male germ cells. Epigenetic modifications may be influenced by environmental factors, inherited through the paternal germ line and passed onto the next generation(s). Furthermore, recent findings indicate that the prenatal environment may also interfere with DNA integrity in the offspring [40]. Since the male Y chromosome is a prerequisite for the male phenotype, it may not be surprising that only offspring from exposed F1 males exhibited decreased sperm count, whereas offspring from prenatally exposed F1 females did not. Male infertility has been observed after both paternally and maternally mediated epigenetic imprinting [41] while mutations that were induced during foetal life in males (F1) were transferred to the F2 offspring. This was not the case in the female germline, i.e. F1 females did not transfer mutations to the F2 offspring. Prenatal exposure to nanoTiO$_2$ did not affect the mutation frequency in the female germline [42].

Human fertility is considerably lower than that of rodents. This is mainly due to a rather large sperm reserve capacity in rodents, compared to the rather limited sperm reserve in humans. Thus reduction of sperm production is

of relatively greater consequence for humans than for rodents and it might have a significant impact on human fertility.

In summary, the effects of maternal airway exposure to engineered nanoparticles indicated that such exposure might interfere with male reproductive development. Human exposure to engineered nanoparticles is likely to increase considerably in the future as more engineered nanoparticles are present in the environment.

12.2.1 The Male Mice Reproductive System and the Effects of Amorphous Nanosilica Particles (nSP)

Amorphous nanosilica particles (nSP) possess a variety of unique properties, such as ease of synthesis, relatively low cost and availability of sites for surface modifications and nSP are increasingly being used for applications including cosmetics, foods, and drugs. However, several reports have shown that nSP might induce adverse effects such as pulmonary inflammation and hemolysis [43]. nSP can pass through barriers such as skin and the blood-placental barrier in mice [44]. Male infertility is for the most part caused by dysfunction of the testes. The testes are sensitive to many chemicals, such as endocrine disruptors, pesticides and anticancer agents; to insure the reproductive safety of nSP, it is important to investigate their biologic effects on the testis. The toxicity of nanomaterials to mice male reproductive functions has been investigated since [25]. However, few studies have investigated the effect of nSP on the distribution of nanomaterials in testis and male germ cells, although information about the intra-testicular distribution would greatly help to elucidate the effect of nanomaterials on male reproductive systems.

The aim of the study by [45] was to evaluate the testicular distribution and histologic effects of systemically administered nSP. Mice were injected intravenously with 100 μL (0.8 mg) nSP with diameters of 70 nm (nSP70) or conventional microsilica particles with diameters of 300 nm

(nSP300) on 2 consecutive days. The intratesticular distribution of these particles 24 h after the second injection was analyzed by transmission electron microscopy. nSP70 were detected within Sertoli cells and spermatocytes, including in the nuclei of spermatocytes. No nSP300 were observed in the testis. Next, mice were injected intravenously with 0.4 or 0.8 mg nSP70 every other day for a total of four administrations. Testes were harvested 48 h and 1 week after the last injection and stained with hematoxylin–eosin for histologic analysis. Histologic findings in the testes of nSP70-treated mice did not differ from those of control mice. Taken together, their results suggest that nSP70 can penetrate the blood–testis barrier and the nuclear membranes of spermatocytes without producing apparent testicular injury. In the above cited study they showed that nSP70, but not nSP300, were able to cross the blood–testis barrier. The limited histologic effects on the testes indicated that nSP70 may be actively transported across it without producing apparent testicular injury. By imaging fluorescently labeled nanoparticles, Kim et al. showed that 50-nm magnetic nanoparticles can also penetrate the mouse blood–testis barrier [46]. Therefore, the penetration of the blood–testis barrier is not specific to nSP. On the other hand, it is known that high-molecular-weight species(>500 Da) do not penetrate the blood-testis barrier by passive diffusion. In fact, De Jong et al. showed with inductively coupled plasma mass spectrometry that gold nanoparticles larger than 50 nm were not distributed in the testis after intravenous administration [47]. Although differences in the dose or duration of administration and in the detection method might account for the different results, these findings suggest that the testicular distribution of nanomaterials might depend on the type of material. In [45] they showed that nSP70 produced little testicular injury but the presence of nSP70 in the nuclei of spermatocytes suggests that DNA in the male germ line might be affected by nSP70. Abnormal DNA in the male germ line has been associated with an increased incidence of morbidity in the offspring [48], and paternal exposure to environmental factors has been suggested to

influence biologic functions in offspring [49, 50]. In conclusion the male mice reproductive system is influenced by nanoparticles as evidenced by the testicular and male germ cells distribution of nanomaterials in the cited studies.

12.2.2 Mouse Spermatogenesis and the Effects of Zinc Oxide Nanoparticles

Spermatogenesis is a complex process of germ cell proliferation and differentiation which leads to the production and release of spermatozoa from the testis; this elaborate process is dependent on hormonal interactions between the Sertoli cells and the germ cells [51]. Tight junctions between adjacent Sertoli cells create two separate compartments within the seminiferous epithelium: a basal compartment below the tight junction and an adluminal compartment above. Sertoli cells secrete hormonal and nutritive factors into the adluminal compartment which creates a specialized microenvironment for development and viability of germ cells. The intricate regulation and cellular interactions that occur in the testis provide multiple distinct targets by which toxicants can disrupt spermatogenesis. Many recent in vivo and in vitro studies demonstrate that most nanoparticles (NPs) show an adverse or toxic effect on male germ cells [52, 53]. Recent studies have shown that administration of NPs to mice results in their accumulation in the various tissues including the brain and the testis. This indicates that they easily pass through the blood–brain and blood– testis barriers [54]. Not all NPs will necessarily demonstrate an adverse effect leading to toxicity. For example, some NPs show a beneficial or nontoxic effect on spermatogenesis [55, 56]. It has been reported that nanoselenium diet supplementation produced positive effects on sperm quality in male goats. Thus, NPs must be investigated on a case-by-case basis to determine whether a NP will have a positive or negative effect on spermatogenesis. Among the various metal nanomaterials, zinc oxide nanoparticles (ZNP) are used in several products such as sunscreens, biosensors, food additives, pigments,

rubber manufacture and electronic materials. According to [57, 58] these nanoparticles are toxic to liver and kidneys. In [17], toxic effects of ZNP on the mouse spermatogenesis were investigated. Epididymal sperm parameters including sperm number, motility and percentage of abnormality were significantly changed in 50 and 300 mg/kg zinc oxide nanoparticles treated mice. Histopathological criteria such as epithelial vacuolization, sloughing of germ and detachment were significantly increased in 50 and 300 mg/kg zinc oxide nanoparticles treated mice. Three hundred milligram per kilogram zinc oxide nanoparticles induced formation of multinucleated giant cells in the germinal epithelium. Fifty and 300 mg/kg zinc oxide nanoparticles also caused a significant decrease in seminiferous tubule diameter, seminiferous epithelium height and maturation arrest. The just cited study [17] demonstrated that ZNPs induce testicular damage in a dose dependent manner in mice. The presence of vacuoles in the cytoplasm of Sertoli cells shows direct damage to these cells. These lesions are early morphological signs of testicular injury and are currently considered as the main Sertoli cell response to many xenobiotics. The number of testicular sperm heads, which is known as a clear index of testicular cytotoxicity, correlated well with histopathological findings. The evaluation of testicular sperm head counts seems to be a good indicator of spermatogenic damages and that the number of testicular sperm heads corresponds to the number of elongate spermatids in the testis. Gromadzka-Ostrowska [59] also showed that small amounts of silver NPs have a toxic impact on the germ cells and reduced sperm quality. Komatsu [60], have demonstrated that titanium oxide and carbon black nanoparticles were taken up by mouse Leydig TM3 cells, and affected the viability, proliferation and gene expression. It is well known that increase in seminiferous tubule diameter is indicative of fluid retention resulting from impaired emptying through the efferent ducts, whereas decrease in seminiferous diameter may indicate germ cell loss.

In summary, ZNP has cytotoxic actions on testicular germ cells in a dose dependent manner. The multinucleated giant cell formation and

sloughing of immature germ cells from the semi-niferous tubules indicates that these NPs might also affect Sertoli cell functions [17]. Alterations in the Johnsen's scoring and morphometric studies may relate to induction of apoptosis or autophagy [61] in testicular germ cells. However, to state the mechanism by which ZNP exerts its effects needs more investigations.

12.3 Impact of Metal Nanoparticles on Germ Cells and Reproductive Barriers

Compared with the corresponding bulk material, nanoscale particles are considerably more biologically active, which seems to derive mainly from their higher mass-specific surface area and is mirrored by a surface specific dose–response [8]. The reasons suggested for cellular damage caused by nanoparticle exposure include production of reactive oxygen species (ROS) and DNA damaging potential of engineered nanomaterials [20]. In somatic cells such insults cause inflammation or even malignant transformation. However, in case of germ line cells, either defect might lead to impaired fertility and/or congenital defects in the offspring. This hypothesis is supported by studies showing that male welders, especially those who work with stainless steel, have poorer sperm quality than those in other work. Consequently, it is surprising that there has been little effort on studying the effects of nanoparticles on reproduction and on other reproductively relevant cells and tissues. Mammalian gametes and the developing embryo are highly vulnerable and therefore situated in rather protected environments. However, of several studies reported, most have shown the ability of nanoparticles to effectively crossbiological barriers including the ones protecting the reproductive tissue. For example concerning the placental barrier, the results listed in the literature are less conclusive. While Wick et al. [62] showed placental crossing for polystyrene nanoparticles in a human placenta explant, Myllynen et al. [63] noted no crossing for gold nanoparticles in the same model. Several studies on rodent models investigated placental crossing of gold nanoparticles after

administration directly into the blood stream. Despite the similarity in the experimental set-up, particles were observed to have passed through the placenta in [64], whereas other groups reported the opposite effect [65]. The crossing of the placenta by titanium dioxide nanoparticles after intravenous injection of pregnant mice was proven by two authors along with embryo toxic effects [26, 44]. Chu et al. [66] showed the same for CdTe/CdS quantum dots. In summary, transplacental crossing of nanoparticles is likely, but seems to depend on currently unknown mechanisms that prevent certain particle preparations from passing through.

12.3.1 Effect of Nanoparticles on Male Gametes

Few studies have focussed on the effect of nanoparticles on germ cells. The evaluations of sperm toxic effects made so far were conducted with nanoparticles made from gold [67, 68], magnetic nanoparticles [69], zinc oxide and titanium dioxide [70]. Zakhidov et al. [68] tested very small gold nanoparticles with a diameter of 2.5 nm. Interestingly, the authors noted a disruption of nuclear chromatin decondensation. ZnONP and TiO_2NP were also found to lead to sperm DNA damage [70]. This findings show how nanoparticles, seemingly of similar material, can have widely different effects. Tests on spermatogonial stem cells [52] using silver, molybdenum trioxide and alumina nanoparticles showed a concentration-dependent cytotoxicity for all types of particles, with AgNP being the most and MoO_3NP the least toxic. In case of AgNP, the toxicity seems to be due to interactions of nanoparticles with a cell proliferation associated, intracellular kinase.In summary, despite the scarcity of experimental data, there is a clear tendency for nanoparticles to have toxic effects on male gametes.

12.3.2 Effect of Nanoparticles on Female Gametes

Nanotoxicity in female reproduction has been investigated in few studies. Huo et al. [71]

cocultured pre-antral follicles obtained from rats with titanium dioxide particles, which caused morphological changes in the follicles and lead to a reduced number of matured oocytes. A second study by Hsieh et al. [72], investigated the effect of CdSe-core QDs on oocyte maturation, fertilization, and subsequent pre- and postimplantation development of mouse oocytes/embryos in vitro. The authors reported a reduction in the rates of oocyte maturation, fertilization and in vitro embryo development along with increased resorption of post implantation embryos and decreased placental and foetal weights. The effects were obliterated when the quantum dots were ZnS-coated.

12.4 Nanoparticles Effects on Embryo Development

The types of nanoparticles tested in piscine embryos systems include metals and metal oxides such as gold [73, 74], silver [75–79], nickel [80], zinc oxide [81], titanium dioxide [82–84], aluminium trioxide [83] and copper [85]. Severe toxic effects in the form of decreased survival rates and deformations were observed after exposure to AgNP, CuNP and ZnONP, even in low concentrations. In comparison, in the case of NiNP, concentrations were tenfold higher before any toxicity was noted. AuNP, TiO_2NP and Al_2O_3NP showed hardly any detrimental effects. Extensive research on nanoreprotoxicology has also been conducted on chicken embryos. Interestingly, in chicken embryos, exposure to nanoparticles of gold [86], silver [87, 88], silver–palladium alloy [89] and silver–copper alloy [90] by in vivo injection caused no abnormal development, except a slight indication of inflammation in the embryo liver after contact with AgCu alloy nanoparticles.

Studies exploring embryo toxicology of nanoparticles in mammals are not as abundant as those for fish and chickens. However, worryingly, especially with regard to the widely used titanium dioxide nanoparticles, a considerable amount of evidence points to an effect on the development of the nervous system after prenatal and maternal exposure to injected titanium dioxide nanoparticles subcutaneously into pregnant mice [91, 92]. Hougaard et al. [36] noted that offspring prenatally exposed to titanium dioxide nanoparticles, after maternal inhalation exposure, exhibited changes in activity and in sensory-motor processes. Gao et al. [93] observed that titanium determined attenuated synaptic plasticity in the hippocampal dentate gyrus area in the foetal brain after the oral administration of titanium dioxide nanoparticles to rats during gestation. Not only the nervous system was affected, as Fedulov et al. [94] noted an increased risk of mouse pups developing respiratory disease if the mothers were exposed to titanium dioxide nanoparticles by intranasal installation. Besides titanium dioxide, only very few other nanomaterials have been explored for their developmental toxicity in mammalian species. Li et al. [95] investigated silver nanoparticles for their effect on blastocyst development after coculture in a mouse model. The authors observed increased apoptosis, decreased cell numbers and decreased implantation success rates. Contrary to these findings, Taylor et al. [19] found no detrimental effects with regard to embryo development after injecting two-cell stage mouse embryos with gold and silver nanoparticles. Interestingly, whereas the former used chemically derived nanoparticles, the latter worked with particles produced by laser ablation in liquids. This suggests a better biocompatibility of the laser-generated nanoparticles, which might be at least partially due to the complete lack of stabilizers and other potentially noxious agents used for the production of chemically derived particles. In another study, the effect of cobalt–chromium nanoparticles on human trophoblast choriocarcinoma cell lines and a layer of BeWo b30 cells was examined, and DNA damage in the fibroblast was noted despite indirect exposure [96]. Embryotoxicity of cobalt ferrite and gold nanoparticles has been considered recently by an in vitro approach. Gold nanoparticles have emerged as promising biomedical tools due to their multiple properties (stability, low inherent toxicity since the bulk gold core is basically inert and non-toxic, ease of synthesis and photo-physical properties which could promote drug release at

remote place). Cobalt ferrite ($CoFe_2O_4$) is a well-known hard magnetic material with high coercivity, moderate magnetization, and great physical and chemical stability. There are many possibilities of applications of biocompatible ferrite particles in combined cancer therapy, as for instance hyperthermia combined with chemotherapy or drug targeting. To reduce animal experimentation and predict in vivo embryotoxicity, some in vitro tests have been optimized as zebrafish embryo, rat whole embryo and cell based tests. The Embryonic Stem Cell Test (EST) is a method validated at the scientific level by ECVAM [97], whose aim is to classify chemical compounds into weak, strong or non-embryotoxic. This method is based on cardiomyocyte differentiation from murine embryonic stem cells via formation of embryoid bodies (EBs) in a way that carries similarity with the inner cell mass of embryos to develop cells of meso-, ecto-, and endodermal origin upon in vitro culture. This test is a powerful method to predict embryotoxicity of chemical compounds. The objective of the study [18] was to investigate whether gold and cobalt ferrite NPs are able to modulate cell differentiation and induce embryotoxicity, using a protocol of EST conveniently modified to be suited to this kind of substances. The ID50 results permit classification of cobalt ferrite nanoparticles coated with gold and silanes as nonembryotoxic. The remaining nanoparticles have been classified as weakly embryotoxic in this decreasing order: gold salt ($HAuCl_4 \cdot 3H_2O$) > cobalt ferrite salt ($CoFe_2O_4$) > cobalt ferrite nanoparticles coated with silanes (Si–CoFe) > gold nanoparticles coated with hyaluronic acid (HA–Au). Very few works may be found in the scientific literature, which address the embryotoxicity of nanoparticles by means of in vitro methods. Beside that, the preliminary TEM data by Di Guglielmo et al. [18] indicate that the studied NPs are internalized by cells at a very different rate according to its nature and coating. On the other hand, in [18] the standard protocol for the differentiation of embryonic stem cells has proven to be unsuccessful with NPs, embryoid bodies exposed to gold or cobalt ferrite nanoparticles are abnormal in shape and smaller in size than their control or salt-treated counterparts, and fail to adhere

after 5 days of culture. The authors in [18] addressed therefore the suitability of exposing the cells to the toxic agent only for 5 days. Actually, a parallel test with the positive control 5-FU gave them a confirmation of the validity of this solution, as the ID50 concentrations obtained were equivalent, and similar to that reported in the literature. In fact, 5-FU affects the cells mainly during the first 3 days of the protocol, at the time when proliferation is at a higher rate with respect to differentiation., NPs have shown to be less cytotoxic and less embryotoxic than their salt counterparts and the toxicity is also modulated by the kind of biocompatible coating applied to NPs. In conclusion, the experiments by Di Guglielmo et al. [18] provide a first attempt aimed at evaluating nanomaterials behaviour in the context of in vitro embryotoxicity tests, based on the ECVAM-validated protocol for EST. The results permit to classify HA–Au NPs as weakly embryotoxic. Concerning cobalt ferrite nanoparticles, they can be also classified as weakly embryotoxic if covered with silanes, but non-embryotoxic if covered with a shell of gold.

12.4.1 Carbon Nanotubes Toxicity in Zebrafish Embryos

There is currently a large difference of opinion about nanotoxicology studies of carbon nanotubes. According to [15] the length of carbon nanotubes greatly affected their toxicity in zebrafish embryos. Coupled with their nanosize, they can biophysically or biochemically act with various subcellular or molecular structures once they are introduced inside a cell. The purpose of the study by [15] was to investigate the toxicity of CNTs with different lengths by using similar preparation processes. Zebrafish embryos were loaded with CNTs by microinjection at the one-cell stage; the length of carbon nanotubes greatly affected their toxicity in early developing zebrafish embryos. Multiwalled carbon nanotubes (MWCNTs) were sonicated in a nitric acid solution for 24 and 48 h. MWCNTs prepared with the longer sonication time resulted in severe developmental toxicity; however, the shorter sonication time did not induce any obvious toxicity

in the tested developing zebrafish embryos. This study suggests that length plays an important role in the in vivo toxicity of functionalized CNTs and also highlights the importance of length information in the in vivo toxicology studies of nanomaterials. The authors have previously reported that successfully purified and functionalized MWCNTs had relatively good biocompatibility in zebrafish embryos [98]. It was found that shorter length of MWCNTs-48 h induced severe toxicity in zebrafish embryos when injected at the one-cell stage, while the FITC-BSA control showed good biocompatibility. Previous studies have reported that long and rigid MWCNTs are much more toxic than functionalized MWCNTs [99]. In [98] the embryos injected with 2 ng (equivalent weight of CNTs) of FITC-labeled BSA-MWCNTs (MWCNTs-48 h) exhibited adverse toxic effects. These affected embryos were developmentally arrested until death at 8–10 hpf. Epiboly did not initiate in these embryos. The fluorescent images showed that the BSA-MWCNTs are evenly distributed among the blastoderm cells and do not enter the yolk cell during epiboly arrest. When the dosage of loaded BSA-MWCNTs (MWCNTs-48 h) was less than 5 pg (equivalent weight of CNTs), the treated embryos passed the epiboly stage and went on to further embryonic development. The malformation percentages are 36.4 and 27.9 % for embryos loaded with 4 pg and 0.4 pg of BSA-MWCNTs (MWCNTs-48 h) (equivalent weight of CNTs), respectively. The affected embryos have severe edema, distorted notochords, dissociated muscles, flattened midbrain–hindbrain boundaries, small eyes, delayed yolk sac and yolk extension resorption, and shortened body length. The defective embryos also have impaired swimming patterns. The cardiovascular system is not the only component that the shorter BSA-MWCNTs (MWCNTs-48 h) attacked. Most of the affected embryos have more than one type of defect, and this might indicate that the influence is multiorgan targeted. TEM observation of the blastoderm cells of the affected embryos demonstrated that the membranes of the enveloping cells are disrupted, and the deep-layer cells detach and have irregular nuclei with condensed chromatins. The morphology changes of the embryonic cells, suggest an apoptosis process, chromatin fragmentation, and nuclear blebbing, which result in the formation of micronuclei.

12.4.2 AgNPs Exposure of Fish Embryos

In 2010 more than 1,300 reported consumer products contained NMs, with silver nanoparticles (AgNPs) representing the most prevalent NM (Nanoproject, 2012). Silver is known to have antiseptic properties and nanotechnology enables the incorporation of AgNPs into various products including wound dressings clothing, kitchenware, children toys, and many more. Moreover, AgNPs can attach to cell membranes, disturbing permeability and respiration and generate reactive oxygen species (ROS) which damage lipids, proteins, and DNA. Increased usage of AgNPs will lead to their emergence in the aquatic environment; e.g. AgNP-impregnated socks can release Ag after washings [100]. However, the fate and behavior of AgNPs in the aquatic environment are largely unknown. Furthermore, multiple effects are reported in fish exposed to silver. In Japanese medaka (*Oryzias latipes*) embryos exposure to AgNPs induced cardiovascular defects, ischemia, underdeveloped central nervous system, and expression of oxidative stress-, embryogenesis-, and morphogenesis-related genes [101]. The study by [22] characterizes the effects of AgNPs on zebrafish (*Danio rerio*) development. The Ag^+ was more toxic than AgNPs but both lead to death and delayed hatching in surviving embryos. Both silver types depleted glutathione levels but generally did not affect antioxidant enzymes activities. In addition to silver some of the embryos were also exposed to cysteine which generally reduced the toxicity of both silver types. Cys, a non-essential amino acid contains a reactive thiol group; silver ions have a high affinity for thiol containing molecules including Cys so Cys can protect from silver ions, possibly due to the formation of Cys–Ag complexes This study demonstrates that AgNPs and Ag^+ are capable of inducing toxicity in zebrafish embryos including the induction of oxidative stress and that Ag^+ had

greater effects than AgNP on ZF embryos. The amount of leached Ag^+ from AgNPs was low and estimated at less than 0.5 %. Nonetheless, the cited study [22] suggests that the effects seen for AgNPs are not simply due to Ag^+ dissolution. This may explain why Ag^+ was a more potent form of silver at the lower concentrations. However, at the higher concentrations the toxicity of AgNP was similar to that of Ag^+, suggesting that AgNPs are also toxic and that AgNPs toxicity is not solely due Ag^+ dissolution. Moreover, several physical deformities were observed at all concentrations of both Ag^+ and AgNPs, but without a consistent trend. Physical deformities in zebrafish embryos, including bent and twisted notochord, pericardial edema, and degeneration of body parts, were noted in a previous work [102]. Delay in hatching in response to AgNPs exposure was documented in [103]. Furthermore, the adsorption of AgNPs noted above was prevented by Cys treatment as the embryos exposed concurrently to AgNPs and Cys had chorions similar in color to the control embryos. The cited effects of Cys on AgNP toxicity contrast with those of Navarro et al. [104] and Yin et al. [105]: in [104] it is suggested that the toxicity of AgNPs in algae (*Chlamydomonas reinhardtii*) is due to Ag^+ dissolution since Cys reduced AgNP toxicity; whereas in [105] they reported that Cys did not affect the toxicity of AgNPs in grass (*Lolium multiflorum*). These discrepancies suggest that the effect of Cys on AgNPs should be examined more closely in future studies. In conclusion, AgNP and Ag^+ were both toxic to ZF embryos. Toxicity responses observed include mortality, delayed hatching, physical deformities, and depressed heart rate. Co-treatments with the chelator Cys seem overcame these effects; in both cases Ag^+ was more potent than AgNPs.

12.5 In Vitro Cytotoxicity of Nanoparticles in Mammalian Adult/Germline Stem Cells

Because nanoparticles can pass through biological membranes, they can affect the physiology of any cell in an animal body. This consideration is of importance for stem cells, where the effects of nanoparticles on their potential for self-renewal and differentiation is unknown. Data available from toxicity studies of nanoparticles, in particular in adult stem cells, are limited. The purpose of the study by [21] was to assess the suitability of a spermatogonial stem cell line as a model for the assessment of nanotoxicity in the male germ line in vitro. The effects of different types of nanoparticles on these cells was evaluated using light microscopy, cell proliferation and standard cytotoxicity assays. Their results suggest that this cell line provides a sensitive model with which to assess the cytotoxicity of nanoparticles in the germline. The results demonstrate a concentration-dependent toxicity for all types of particles tested, whereas the corresponding soluble salts had no significant effect. Silver nanoparticles were the most toxic while molybdenum trioxide (MoO_3) nanoparticles were the least toxic. Toxicants that impair normal reproductive functions are an important public health issue. A decrease in semen quality of approximately 2 % per year over the preceding 50 years has been reported for industrialized countries [106]. Nevertheless, studies have shown that high exposure of men to various chemicals in certain occupational settings resulted in lower semen quality. Several in vivo animal models have been used to assess the testicular toxicity of many compounds. In vitro model alternatives have been established, and some of them have tried to reproduce in the petri dish the complex cell–cell interactions that take place between the different germ cells and Sertoli cells [107]. However, these models are limited by the poor viability of the freshly isolated germ cells. In the study by [21] they used a cell line with spermatogonial stem cell characteristics to evaluate the toxicity of different types of nanoparticles on the germline. The authors used three parameters widely used in toxicological studies, such as the ability of mitochondria to reduce MTS, the integrity of the plasma membrane, and the activation of apoptotic pathways. The results indicate that the C18–4 cells provide a suitable test system for cytotoxicity in the germline. In male rats subcutaneously injected with 0.6 mg cadmium chloride/kg body weight,

histological examination of the testes revealed an accumulation of cadmium only in spermatogonia and spermatocytes, but not in somatic cells [108]. Subsequently, a decrease in the number of spermatogonia in relation to the time of exposure was observed, followed by a decrease in the number of spermatocytes and, ultimately, sperm cells. In the spermatogonial stem cell line studied in [21] exposure of the cells to cadmium chloride induced a significant decrease in their metabolic activity. Because oxidative stress and lipid peroxidation have been reported after exposure to both cadmium chloride and cadmium oxide, the higher toxicity of cadmium oxide might be related to the size of the particles entering into contact with the plasma membrane. Furthermore, the sensitivity of the C18–4 cells to cadmium oxide is comparable to the sensitivity of the BRL 3A liver cells and the membrane integrity of the C18–4 cells is less affected. Because the C18–4 cells showed an increased sensitivity to the particulate form of cadmium rather than the soluble form, in [21] the authors next studied the effects of others metal nanoparticles on these germline stem cells. Silver nanoparticles (15 nm) reduced mitochondrial function drastically and increased membrane leakage. Although molybdenum in soluble form is considered to be a mildly toxic substance, it did not significantly affect the metabolic activity or the membrane integrity of the C18–4 cells. Molybdenum as a nanoparticulate did not affect metabolic activity either, at least up to a concentration of 40 μg/ml (EC50 = 90 μg/ml). At higher concentrations (over 50 μg/ml), the molybdenum nanoparticles become significantly toxic. The same pattern of toxicity is shown for aluminum nanoparticles; however, the morphology of the cells did not change, indicating that at these concentrations apoptosis still occurs. In conclusion, it was demonstrated that the C18–4 germline stem cells are a valuable tool with which to study in vitro toxicity in the germline. The sensitivity of these cells to Ag nanoparticles is greater than that of BRL 3A liver cells, which are widely used in toxicity studies. However, in the case of cadmium and the other nanoparticles tested, the sensitivities of the two cell lines are comparable. The molecular mechanisms of nanoparticles toxicity

are still poorly understood, and the availability of a cell line with which to gain an understanding of these processes in the germline is of paramount importance.

12.6 Transgenerational Effects of Nanomaterials in Edible Plants

Plants are a basic component of the terrestrial ecosystem and the chief ring that links the food chain. By absorbing NPs, the plants other than running the risk to be damaged, can accumulate pollutants and generate polluted descendents becoming vehicle to introduce toxic material in unpolluted environments and in its living components [109]. Despite the absorption and the phytoxicity of NPs have been investigated in some edible plants [109], no report are available on the risk to pollute the food chain. Future experiments should give more attention to the vulnerability of the plants reproductive systems and in particular to the transgenerational effects of nanomaterials, a little known matter to date. Recent studies [23] investigated whether the treatment of tomato plants with relatively low concentrations of CeO_2-NPs (10 mg L^{-1}) during stages of their life cycle would affect the seed quality either at the first and the second generations. The results indicated that seedlings of the second generation from parent plants treated with CeO_2-NPs were generally smaller, weaker and producing smaller biomass with higher concentration of reactive oxygen species. At the same time, they developed more extensive root hairs as compared with the controls, and accumulated a higher amount of ceria than the first generation. These observations are useful for further studies on the transgenerational effects of NPs.

Conclusion

As yet, developmental toxicity of engineered nanoparticles and transgenerational effects of nanomaterials in animals and humans have been little studied and information is not

exhaustive concerning the effect of nanomaterials on the overall reproductive outcome [14, 16, 17, 21, 24, 25, 53, 67, 68]. To obtain this information, long-term studies would be required using humans and/or animal models phylogenetically close to humans and environmental and occupational exposure conditions.

References

1. Salata O (2004) Applications of nanoparticles in biology and medicine. J Nanobiotechnol 2:3
2. Oberdorster G, Maynard A, Donaldson K, Castranova V, Fitzpatrick J, Ausman K, Cartet J, Karn B, Kreyling W, Lai D, Olin S, Monteiro-Riviere N, Warheit D, Yang H (2005) Principles for characterizing the potential human health effects from exposure: elements of screening strategy. Part Fibre Toxicol 6:2–8
3. Hoet PHM, Brüske-Hohlfeld I, Salata OV (2004) Nanoparticles: known and unknown health risks. J Nanobiotechnol 8:1–12
4. Borm PJA, Robbins D, Haubold S, Kuhlbusch T, Fissan H, Donaldson K, Schins V, Stone W, Kreyling J, Lademann R, Krutmann J, Warheit D, Oberdorster E (2006) The potential risks for nanomaterials: a review carried out for ECETOC. Part Fibre Toxicol 14:3–11
5. Wang K, Xu JJ, Chen HY (2005) A novel glucose biosensor based on the nanoscaled cobalt phthalocyanine-glucose oxidase biocomposite. Biosens Bioelectron 20:1388–1396
6. Yang MH, Jiang JH, Yang YH, Chen XH, Shen GL, Yu RQ (2006) Carbon nanotube/cobalt hexacyanoferrate nanoparticle biopolymer system for the fabrication of biosensors. Biosens Bioelectron 21:1791–1797
7. Tran CL, Buchanan D, Cullen RT, Searl A, Jones AD, Donaldson K (2000) Inhalation of poorly soluble particles. II. Influence of particle surface area on inflammation and clearance. Inhal Toxicol 12:1113–1126
8. Oberdorster G, Oberdorster E, Oberdorster J (2005) Nanotoxicology: an emerging discipline evolving from studies of ultrafine particles. Environ Health Perspect 113:823–839
9. Poma A, Di Giorgio ML (2008) Toxicogenomics to improve comprehension of the mechanisms underlying responses of in vitro and in vivo systems to nanomaterials. A review. Curr Genomics 9:571–585
10. Mishra SR, Dubenko I, Losby J, Marasinghe K, Ali M, Ali N (2005) Magnetic properties of magnetically soft nanocomposite Co-SiO$_2$ prepared via mechanical milling. J Nanosci Nanotechnol 5: 2082–2087
11. Oberdorster G, Sharp Z, Atudorei V, Elder A, Gelein R, Lunts A, Kreyling W, Cox C (2002) Extrapulmonary translocation of ultrafine carbon particles following whole-body inhalation exposure of rats. J Toxicol Environ Health A 65(20):1531–1543
12. Champion JA, Mitragotri S (2006) Role of target geometry in phagocytosis. Proc Natl Acad Sci U S A 103:4930–4934
13. Porter AE, Gass M, Muller K, Snepper JN, Midgley P, Wellandi M (2007) Direct imaging of single-walled carbon nanotubes in cells. Nat Nanotechnol 2(11):713–717. doi:10.1038/nnano.2007.347
14. Taylor U, Barchanski A, Kues W, Barcikowski S, Rath D (2012) Impact of metal nanoparticles on germ cell viability and functionality. Reprod Domest Anim 47(Suppl 4):359–368
15. Cheng J, Cheng SH (2012) Influence of carbon nanotube length on toxicity to zebrafish embryos. Int J Nanomedicine 7:3731–3739
16. Kyjovska ZO, Boisen AM, Jackson P, Wallin H, Vogel U, Hougaard KS (2013) Daily sperm production: application in studies of prenatal exposure to nanoparticles in mice. Reprod Toxicol 36: 88–89
17. Talebi AR, Khorsandi L, Moridian M (2013) The effect of zinc oxide nanoparticles on mouse spermatogenesis. J Assist Reprod Genet. doi:10.1007/s10815-013-0078-y
18. Di Guglielmo C, López DR, De Lapuente J, Mallafre JM, Suàrez MB (2010) Embryotoxicity of cobalt ferrite and gold nanoparticles: a first in vitro approach. Reprod Toxicol 30:271–276
19. Taylor U, Klein S, Petersen S, Kues W, Barcikowski S, Rath D (2010) Nonendosomal cellular uptake of ligand-free, positively charged gold nanoparticles. Cytometry A 77:439–446
20. Singh N, Manshian B, Jenkins GJS, Griffiths SM, Williams PM, Maffeis TGG, Wright CJ, Doak SH (2009) NanoGenotoxicology: the DNA damaging potential of engineered nanomaterials. Biomaterials 30:3891–3914
21. Braydich-Stolle L, Hussain S, Schlager JJ, Hofmann MC (2005) In vitro cytotoxicity of nanoparticles in mammalian germline stem cells. Toxicol Sci 88(2):412–419. doi:10.1093/toxsci/kfi256
22. Massarsky A, Dupuis L, Taylor J, Eisa-Beygi S, Strek L, Vance L. Trudeau, Thomas W (2013) Moon assessment of nanosilver toxicity during zebrafish (Danio rerio) development. Chemosphere. http://dx.doi.org/10.1016/j.chemosphere.2013.02.060
23. Wang Q, Ebbs SD, Chen Y, Ma X (2013) Transgenerational impact of cerium oxide nanoparticles on tomato plants. Metallomics 5:753–759
24. Bai Y, Zhang Y, Zhang J, Mu Q, Zhang W, Butch ER, Snyder SE, Yan B (2010) Repeated administrations of carbon nanotubes in male mice cause reversible testis damage without affecting fertility. Nat Nanotechnol 5:683–689
25. Yoshida S, Hiyoshi K, Ichinose T, Takano H, Oshio S, Sugawara I, Takeda K, Shibamoto T (2009) Effect of nanoparticles on the male reproductive system of mice. Int J Androl 32:337–342

26. Takeda K, Suzuki K-I, Ishihara A, Kubo-Irie M, Fujimoto R, Tabata M, Oshio S, Nihei Y, Ihara T, Sugamata M (2009) Nanoparticles transferred from pregnant mice to their offspring can damage the genital and cranial nerve systems. J Health Sci 55:95–102

27. Yoshida S, Hiyoshi K, Oshio S, Takano H, Takeda K, Ichinose T (2010) Effects of fetal exposure to carbon nanoparticles on reproductive function in male offspring. Fertil Steril 93:1695–1699

28. Hemmingsen JG, Hougaard KS, Talsness C, Wellejus A, Loft S, Wallin H, Møller P (2009) Prenatal exposure to diesel exhaust particles and effect on the male reproductive system in mice. Toxicology 264:61–68

29. Ono N, Oshio S, Niwata Y, Yoshida S, Tsukue N, Sugawara I, Takano H, Takeda K (2007) Prenatal exposure to diesel exhaust impairs mouse spermatogenesis. Inhal Toxicol 19:275–281

30. Watanabe N (2005) Decreased number of sperms and Sertoli cells in mature rats exposed to diesel exhaust as fetuses. Toxicol Lett 155:51–58

31. Ritz C, Ruminski W, Hougaard KS, Wallin H, Vogel U, Yauk CL (2011) Germline mutation rates in mice following in utero exposure to diesel exhaust particles by maternal inhalation. Mutat Res 712:55–58

32. Swierstra EE (1968) A comparison of spermatozoa production and spermatozoa output of Yorkshire and Lacombe boars. J Reprod Fertil 17:459–469

33. Hougaard KS, Fadeel B, Gulumian M, Kagan VE, Savolainen K (2011) Developmental toxicity of engineered nanoparticles. In: Gupta RC (ed) Reproductive and developmental toxicology. Academic, Amsterdam, pp 269–290

34. Menezes V, Malek A, Keelan JA (2011) Nanoparticulate drug delivery in pregnancy: placental passage and fetal exposure. Curr Pharm Biotechnol 12:731–742

35. Hougaard KS, Jensen KA, Nordly P, Taxvig C, Vogel U, Saber AT, Wallin H (2008) Effects of prenatal exposure to diesel exhaust particles on postnatal development, behavior, genotoxicity, and inflammation in mice. Part Fibre Toxicol 5:3

36. Hougaard KS, Jackson P, Jensen KA, Sloth JJ, Loschner K, Larsen EH, Birkedal RK, Vibenholt A, Boisen AM, Wallin H, Vogel U (2010) Effects of prenatal exposure to surface-coated nanosized titanium dioxide (UV-Titan). A study in mice. Part Fibre Toxicol 7:16

37. Izawa H, Kohara M, Watanabe G, Taya K, Sagai M (2007) Effects of diesel exhaust particles on the male reproductive system in strains of mice with different aryl hydrocarbon receptor responsiveness. J Reprod Dev 53:1191–1197

38. Yoshida S, Yoshida M, Sugawara I, Takeda K (2006) Mice strain differences in effects of fetal exposure to diesel exhaust gas on male gonadal differentiation. Environ Sci 13(2):117–123

39. Sadauskas E, Jacobsen NR, Danscher G, Stoltenberg M, Vogel U, Larsen A, Kreyling W, Wallin H (2009) Biodistribution of gold nanoparticles in mouse lung following intratracheal instillation. Chem Cent J 3:16

40. Hakonsen LB, Spano M, Bonde JP, Olsen J, Thulstrup AM, Ernst E, Ramlau-Hansen CH (2013) Exposures that may affect sperm DNA integrity: two decades of follow-up in a pregnancy cohort. Reprod Toxicol 33(3):316–321

41. Rajender S, Avery K, Agarwal A (2011) Epigenetics, spermatogenesis and male infertility. Mutat Res 727(3):62–71

42. Boisen AM, Shipley T, Jackson P, Hougaard KS, Wallin H, Yauk CL, Vogel U (2012) Nano TiO$_2$ (UV-Titan) does not induce ESTR mutations in the germline of prenatally exposed female mice. Part Fibre Toxicol 9(1):19

43. Yu T, Malugin A, Ghandehari H (2011) Impact of silica nanoparticle design on cellular toxicity and hemolytic activity. ACS Nano 5:5717–5728

44. Yamashita K, Yoshioka Y, Higashisaka K, Mimura K, Morishita Y, Nozaki M, Yoshida T, Ogura T, Nabeshi H, Nagano K, Abe Y, Kamada H, Monobe Y, Imazawa T, Aoshima H, Shishido K, Kawai Y, Mayumi T, Tsunoda S, Itoh N, Yoshikawa T, Yanagihara I, Saito S, Tsutsumi Y (2011) Silica and titanium dioxide nanoparticles cause pregnancy complications in mice. Nat Nanotechnol 6:321–328

45. Morishita Y, Yoshioka Y, Satoh H, Nojiri N, Nagano K, Abe Y, Kamada H, Tsunoda S, Nabeshi H, Yoshikawa T, Tsutsumi Y (2012) Distribution and histologic effects of intravenously administered amorphous nanosilica particles in the testes of mice. Biochem Biophys Res Commun 420:297–301

46. Kim JS, Yoon TJ, Yu KN, Kim BG, Park SJ, Kim HW, Lee KH, Park SB, Lee JK, Cho MH (2006) Toxicity and tissue distribution of magnetic nanoparticles in mice. Toxicol Sci 89:338–347

47. De Jong WH, Hagens WI, Krystek P, Burger MC, Sips AJ, Geertsma RE (2008) Particle size-dependent organ distribution of gold nanoparticles after intravenous administration. Biomaterials 29:1912–1919

48. Aitken RJ, De Iuliis GN, McLachlan RI (2009) Biologic and clinical significance of DNA damage in the male germ line. Int J Androl 32:46–56

49. Anway MD, Cupp AS, Uzumcu M, Skinner MK (2005) Epigenetic transgenerational actions of endocrine disruptors and male fertility. Science 308:1466–1469

50. Carone BR, Fauquier L, Habib N, Shea JM, Hart CE, Li R, Bock C, Li C, Gu H, Zamore PD, Meissner A, Weng Z, Hofmann HA, Friedman N, Rando OJ (2010) Paternally induced transgenerational environmental reprogramming of metabolic gene expression in mammals. Cell 143:1084–1096

51. Boekelheide K, Fleming SL, Johnson KJ, Patel SR, Schoenfeld HA (2000) Role of Sertoli cells in injury-associated testicular germ cell apoptosis. Exp Biol Med 225(2):105–115

52. Braydich-Stolle LK, Lucas B, Schrand A, Murdock RC, Lee T, Schlager JJ, Hussain SM, Hofmann MC (2010) Silver nanoparticles disrupt GDNF/Fyn

kinase signaling in spermatogonial stem cells. Toxicol Sci 116(2):577–589

53. Braydich-Stolle L, Hussain S, Schlager JJ, Hofmann MC (2005) In vitro cytotoxicity of nanoparticles in mammalian germline stem cells. Toxicol Sci 88(2):412–419

54. Lan Z, Yang WX (2012) Nanoparticles and spermatogenesis: how do nanoparticles affect spermatogenesis and penetrate the blood–testis barrier. Nanomedicine 7(4):579–596

55. Shi L, Xun W, Yue W, Zhang C, Ren Y, Shi L, Wang Q, Yang R, Lei F (2011) Effect of sodium selenite, Se-yeast and nano-elemental selenium on growth performance, Se concentration and antioxidant status in growing male goats. Small Ruminant Res 96(1):49–52

56. Shi L, Yang R, Yue W, Xun WJ, Zhang CX, Ren YS, Shi L, Lei FL (2010) Effect of elemental nano-selenium quality, glutathione peroxidase activity, and testis ultrastructure in male Boer goats. Anim Reprod Sci 118(2,4):248–254

57. Sharma V, Singh P, Pandey AK, Dhawan A (2012) Induction of oxidative stress, DNA damage and apoptosis in mouse liver after sub-acute oral exposure to zinc oxide nanoparticles. Mutat Res 745(1–2):84–91

58. Wang L, Ding W, Zhang F (2010) Acute toxicity of ferric oxide and zinc oxide nanoparticles in rats. J Nanosci Nanotechnol 10(12):8617–8624

59. Gromadzka-Ostrowskaa J, Dziendzikowskaa K, Lankoffb A, Dobrzyńska M, Instanes C, Brunborg G, Gajowik A, Radzikowska J, Wojewódzka M, Kruszewski M (2012) Silver nanoparticles effects on epididymal spermin rats. Toxicol Lett 214(3):251–258

60. Komatsu T, Tabata M, Kubo-Irie M, Shimizu T, Suzuki K, Nihei Y, Takeda K (2008) The effects of nanoparticles on mouse testis Leydig cells in vitro. Toxicol In Vitro 22(8):1825–1831

61. Yu KN, Yoon TJ, Minai-Tehrani A, Kim JE, Park SJ, Jeong MS, Ha SW, Lee JK, Kim JS, Cho MH (2013) Zinc oxide nanoparticle induced autophagic cell death and mitochondrial damage via reactive oxygen species generation. Toxicol In Vitro 27(4):1187–1195

62. Wick P, Malek A, Manser P, Meili D, Maeder-Althaus X, Diener L, Diener PA, Zisch A, Krug HF, von Mandach U (2010) Barrier capacity of human placenta for nanosized materials. Environ Health Perspect 118:432–436

63. Myllynen PK, Loughran MJ, Howard CV, Sormunen R, Walsh AA, Vahakangas KH (2008) Kinetics of gold nanoparticles in the human placenta. Reprod Toxicol 26:130–137

64. Semmler-Behnke M, Fertsch S, Schmid G, Wenk A, Kreyling W (2007) Uptake of 1.4 nm versus 18 nm gold nanoparticles by secondary target organs is size dependent in and pregnant rats after intertracheal or intravenous application. EuroNanoForum 2007:102–104

65. Sadauskas E, Wallin H, Stoltenberg M, Vogel U, Doering P, Larsen A, Danscher G (2007) Kupffer cells are central in the removal of nanoparticles from the organism. Part Fibre Toxicol 4:10

66. Chu M, Wu Q, Yang H, Yuan R, Hou S, Yang Y, Zou Y, Xu S, Xu K, Ji A, Sheng L (2010) Transfer of quantum dots from pregnant mice to pups across the placental barrier. Small 6:670–678

67. Taylor U, Petersen S, Barchanski A, Mittag A, Barcikowski S, Rath D (2010) Influence of gold nanoparticles on vitality parameters of bovine spermatozoa. Reprod Domest Anim 45:60

68. Zakhidov ST, Marshak TL, Malolina EA, Kulibin AY, Zelenina IA, Pavluchenkova SM, Rudoy VM, Dement'eva OV, Skuridin SG, Evdokimov YM (2010) Gold nanoparticles disturb nuclear chromatin decondensation in mouse sperm in vitro. Biol Membr 4:349–353

69. Makhluf SBD, Qasem R, Rubinstein S, Gedanken A, Breitbart H (2006) Loading magnetic nanoparticles into sperm cells does not affect their functionality. Langmuir 22:9480–9482

70. Gopalan R, Osman I, de Matas M, Anderson D (2009) The effect of zinc oxide and titanium dioxide nanoparticles in the comet assay with UVA photoactivation of human sperm and lymphocytes. Environ Mol Mutagen 50:541–541

71. Hou J, Wan XY, Wang F, Xu GF, Liu Z (2009) Effects of titanium dioxide nanoparticles on development and maturation of rat preantral follicle in vitro. Acad J Second Mil Med Univ 29:869–873

72. Hsieh MS, Shiao NH, Chan WH (2009) Cytotoxic effects of CdSe quantum dots on maturation of mouse oocytes, fertilization, and fetal development. Int J Mol Sci 10:2122–2135

73. Bar-Ilan O, Albrecht RM, Fako VE, Furgeson DY (2009) Toxicity assessments of multisized gold and silver nanoparticles in zebrafish embryos. Small 5:1897–1910

74. Browning LM, Lee KJ, Huang T, Nallathamby PD, Lowman JE, Xu XHN (2009) Random walk of single gold nanoparticles in zebrafish embryos leading to stochastic toxic effects on embryonic developments. Nanoscale 1:138–152

75. Laban G, Nies LF, Turco RF, Bickham JW, Sepulveda MS (2010) The effects of silver nanoparticles on fathead minnow (Pimephales promelas) embryos. Ecotoxicology 19:185–195

76. Lee KJ, Nallathamby PD, Browning LM, Osgood CJ, Xu XH (2007) In vivo imaging of transport and biocompatibility of single silver nanoparticles in early development of zebrafish embryos. ACS Nano 1:133–143

77. Ringwood AH, McCarthy M, Bates TC, Carroll DL (2010) The effects of silver nanoparticles on oyster embryos. Mar Environ Res 69(Suppl):S49–S51

78. Wu Y, Zhou Q, Li H, Liu W, Wang T, Jiang G (2010) Effects of silver nanoparticles on the development and histopathology biomarkers of Japanese medaka (Oryzias latipes) using the partial-life test. Aquat Toxicol 100:160–167

79. Yeo MK, Yoon JW (2009) Comparison of the effects of nano-silver antibacterial coatings and silver ions on Zebrafish embryogenesis. Mol Cell Toxicol 5:23–31

80. Ispas C, Andreescu D, Patel A, Goia DV, Andreescu S, Wallace KN (2009) Toxicity and developmental defects of different sizes and shape nickel nanoparticles in Zebrafish. Environ Sci Technol 43:6349–6356

81. Bai W, Zhang ZY, Tian WJ, He X, Ma YH, Zhao YL, Chai ZF (2010) Toxicity of zinc oxide nanoparticles to zebrafish embryo: a physicochemical study of toxicity mechanism. J Nanopart Res 5:1645–1654

82. Yeo MK, Kang M (2009) Effects of Cu (x) TiO (y) nanometer particles on biological toxicity during zebrafish embryogenesis. Korean J Chem Eng 3:711–718

83. Zhu XS, Zhu L, Duan ZH, Qi RQ, Li Y, Lang YP (2008) Comparative toxicity of several metal oxide nanoparticle aqueous suspensions to Zebrafish (Danio rerio) early developmental stage. J Environ Sci Health A Tox Hazard Subst Environ Eng 43:278–284

84. Musee N, Oberholster PJ, Sikhwivhilu L, Botha AM (2010) The effects of engineered nanoparticles on survival, reproduction, and behaviour of freshwater snail, Physa acuta (Draparnaud, 1805). Chemosphere 81:1196–1203

85. Bai W, Tian W, Zhang Z, He X, Ma Y, Liu N, Chai Z (2010) Effects of copper nanoparticles on the development of zebrafish embryos. J Nanosci Nanotechnol 10:8670–8676

86. Zielinska AK, Sawosz E, Grodzik M, Chwalibog A, Kamaszewski M (2009) Influence of nanoparticles of gold on chicken embryos' development. Ann Warsaw Univ Life Sci SGGW Anim Sci 46:249–253

87. Grodzik M, Sawosz E (2006) The influence of silver nanoparticles on chicken embryo development and bursa of Fabricius morphology. J Anim Feed Sci 15:111–114

88. Sikorska J, Szmidt M, Sawosz E, Niemiec T, Grodzik M, Chwalibog A (2010) Can silver nanoparticles affect the mineral content, structure and mechanical properties of chicken embryo bones? J Anim Feed Sci 2:286–291

89. Studnicka A, Sawosz E, Grodzik M, Chwalibog A, Balcerak M (2009) Influence of nanoparticles of silver/palladium alloy on chicken embryos' development. Ann Warsaw Univ Life Sci SGGW Anim Sci 46:237–242

90. Sawosz E, Grodzik M, Zielinska M, Niemiec T, Olszanka B, Chwalibog A (2009) Nanoparticles of silver do not affect growth, development and DNA oxidative damage in chicken embryos. Arch Geflugelkd 73:208–213

91. Takahashi Y, Mizuo K, Shinkai Y, Oshio S, Takeda K (2010) Prenatal exposure to titanium dioxide nanoparticles increases dopamine levels in the prefrontal cortex and neostriatum of mice. J Toxicol Sci 35:749–756

92. Shimizu M, Tainaka H, Oba T, Mizuo K, Umezawa M, Takeda K (2009) Maternal exposure to nanoparticulate titanium dioxide during the prenatal period alters gene expression related to brain development in the mouse. Part Fibre Toxicol 6:20

93. Gao X, Yin S, Tang M, Chen J, Yang Z, Zhang W, Chen L, Yang B, Li Z, Zha Y, Ruan D, Wang M (2011) Effects of developmental exposure to TiO$_2$ nanoparticles on synaptic plasticity in hippocampal dentate gyrus area: an in vivo study in anesthetized rats. Biol Trace Elem Res 143:1616–1628

94. Fedulov AV, Leme A, Yang Z, Dahl M, Lim R, Mariani TJ, Kobzik L (2008) Pulmonary exposure to particles during pregnancy causes increased neonatal asthma susceptibility. Am J Respir Cell Mol Biol 38:57–67

95. Li PW, Kuo TH, Chang JH, Yeh JM, Chan WH (2010) Induction of cytotoxicity and apoptosis in mouse blastocysts by silver nanoparticles. Toxicol Lett 197:82–87

96. Bhabra G, Sood A, Fisher B, Cartwright L, Saunders M, Evans WH, Surprenant A, Lopez-Castejon G, Mann S, Davis SA, Hails LA, Ingham E, Verkade P, Lane J, Heesom K, Newson R, Case CP (2009) Nanoparticles can cause DNA damage across a cellular barrier. Nat Nanotechnol 4:876–883

97. Genschow E, Spielmann H, Scholz G, Pohl I, Seiler A, Seiler A, Clemann N, Bremer S, Becker K (2004) Validation of the embryonic stem cell test in the international ECVAM validation study on three in vitro embryotoxicity tests. Altern Lab Anim 32:209–244

98. Cheng JP, Chan CM, Veca LM, Poon WL, Chan PK, Qu L, Sun YP, Cheng SH (2009) Acute and long-term effects after single loading of functionalized multi-walled carbon nanotubes into zebrafish (Danio rerio). Toxicol Appl Pharmacol 235:216–225

99. Kostarelos K (2008) The long and short of carbon nanotube toxicity. Nat Biotechnol 26:774–776

100. Benn TM, Westerhoff P (2008) Nanoparticle silver released into water from commercially available sock fabrics. Environ Sci Technol 42:4133–4139

101. Kashiwada S, Ariza ME, Kawaguchi T, Nakagame Y, Jayasinghe BS, Gartner K, Nakamura H, Kagami Y, Sabo-Attwood T, Ferguson PL, Chandler GT (2012) Silver nanocolloids disrupt medaka embryogenesis through vital gen expressions. Environ Sci Technol 46:6278–6287

102. Bar-Ilan O, Albrecht R, Fako V, Furgeson D (2009) Toxicity assessments of multisized gold and silver nanoparticles in zebrafish embryos. Small 17:897–910

103. AshaRani PV, Lianwu Y, Gong Z, Valiyaveettil S (2011) Comparison of the toxicity of silver, gold, and platinum nanoparticles in developing zebrafish embryo. Nanotoxicology 5:43–54

104. Navarro E, Baun A, Behra R, Hartmann NB, Filser J, Miao AJ, Quigg A, Santschi PH, Sigg L (2008) Environmental behavior and ecotoxicity of engineered

nanoparticles to algae, plants, and fungi. Ecotoxicology 17:372–386

105. Yin L, Cheng Y, Espinasse B, Colman BP, Auffan M, Wiesner M, Rose J, Liu J, Bernhardt ES (2011) More than the ions: the effects of silver nanoparticles on Lolium multiflorum. Environ Sci Technol 45: 2360–2367

106. Carlsen E, Giwercman A, Keiding N, Skakkebaek NE (1992) Evidence for decreasing quality of semen during past 50 years. BMJ 305:609–613

107. Yu X, Sidhu JS, Hong S, Faustman EM (2005) Essential role of extracellular matrix (ECM) over-lay in establishing the functional integrity of primary neonatal rat Sertoli cell/gonocyte co-cul-tures: an improved in vitro model for assessment of male reproductive toxicity. Toxicol Sci 84: 378–393

108. Aoyagi T, Ishikawa H, Miyaji K, Hayakawa K, Hata M (2002) Cadmium-induced testicular damage in a rat model of subchronic intoxication. Reprod Med Biol 1:59–63

109. Rico CM, Majumdar S, Duarte-Gardea M, Peralta-Videa R, Gardea-Torresdey JL (2011) Interaction of nanoparticles with edible plants and their possible implications in the food chain. J Agric Food Chem 59(8):3485–3498

Stem Cells and Nanomaterials

13

Marie-Claude Hofmann

Contents

M.-C. Hofmann, PhD
Department of Endocrine Neoplasia and Hormonal
Disorders, University of Texas MD Anderson Cancer
Center, Houston, TX, USA
e-mail: mhofmann@mdanderson.org

Abstract

Because of their ability to self-renew and differentiate into many cell types, stem cells offer the potential to be used for tissue regeneration and engineering. Much progress has recently been made in our understanding of the biology of stem cells and our ability to manipulate their proliferation and differentiation to obtain functional tissues. Similarly, nanomaterials have been recently developed that will accelerate discovery of mechanisms driving stem cell fate and their utilization in medicine. Nanoparticles have been developed that allow the labeling and tracking of stem cells and their differentiated phenotype within an organism. Nanosurfaces are engineered that mimic the extracellular matrix to which stem cells adhere and migrate. Scaffolds made of functionalized nanofibers can now be used to grow stem cells and regenerate damaged tissues and organs. However, the small scale of nanomaterials induces changes in their chemical and physical properties that might modify their interactions with cells and tissues, and render them toxic to stem cells. Therefore a thorough understanding of stem cell-nanomaterial interactions is still necessary not only to accelerate the success of medical treatments but also to ensure the safety of the tools provided by these novel technologies.

13.1 Introduction

Nanotechnology involves the fabrication and use
of materials and devices on an atomic and molec-
ular scale, with at least one dimension measuring
from 1 to 100 nm [1]. Materials and tools created
using nanotechnologies have at least two advan-
tages. First, their minuscule sizes make them of
interest in bioengineering and medicine, for
example to build scaffolds for tissue engineering
and to carry drugs that target specific cells and
tissues [2–5]. Second, the fact that certain physi-
cal and chemical properties change as the size of
the system decreases renders nanomaterials par-
ticularly useful in mechanical, chemical and elec-
trical engineering, and ultimately life sciences
[6]. Indeed nanotubes, nanowires, fullerene
derivatives (buckyballs), and quantum dots are
now used for the manufacturing of novel analyti-
cal tools for biotechnology [7–12]. Because of
their novel properties, nanoscale materials can
also be exploited to modulate cell proliferation or
differentiation by influencing their attachment or
manipulating their environment [13–16]. This
feature is particularly applicable for the modula-
tion of stem cell fate in regeneration studies.

Stem cells are undifferentiated cells that have
the dual ability to self-renew to maintain their
own pool, or to differentiate into functional
mature cells. During early mammalian embryo-
genesis, the inner cell mass (ICM) of the blasto-
cyst is made of pluripotent cells, or embryonic
stem cells (ES cells) that are able to proliferate
and differentiate into all cell lineages that will
eventually generate the fetal organs [17]. As
these pluripotent stem cells continue to divide,
they start to specialize and become multipotent
stem cells. Multipotent stem cells are found in
the fetus and the adult animal; they are less plas-
tic than ES cells and are able to differentiate only
into specific lineages. For example, mesenchy-
mal stem cells (MSCs) isolated from adult bone
marrow or cord blood can generate only bone,
cartilage, adipocytes, cardiomyocytes, nerve
cells and supporting cells such as stromal fibro-
blasts (Fig. 13.1) [19]. Adipose tissue-derived
stem cells (ADSC) are similar to MSCs and are
found in the stromal-vascular fraction of fat
tissue [20]. Hematopoietic stem cells, found in
the bone marrow, produce both the lymphoid and
myeloid lineages and are responsible for
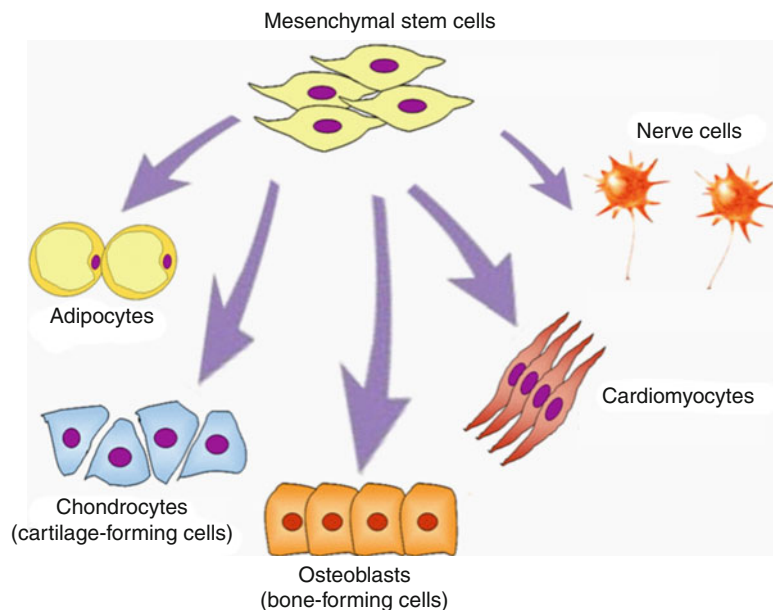
Fig. 13.1 Differentiation potential of mesenchymal stem cells (MSCs). MSC can differentiate in many tissues including bone, cartilage, adipocytes, cardiac cells and neurons (Adapted from Meregalli et al. [18])

maintaining blood cell production throughout life [21]. The intestinal crypts contain stem cells that self-renew to continuously regenerate the gut epithelium, but can also differentiate into enterocytes, enteroendocrine cells, goblet cells and Paneth cells with distinct functions [22, 23]. Similarly, skin stem cells self-renew and/or differentiate to produce keratinocytes, hair follicles, sebaceous glands and sweat glands [24]. While multipotent stem cells usually produce several, but restricted, cell types, some stem cells are unipotent and give rise to only one kind of mature cells. For example, spermatogonial stem cells (SSCs) of the testis ultimately produce only sperm cells [25]. However, SSCs have the unique property to revert to an ES cell-like state when cultured in the appropriate conditions, and might become some day a source of adult pluripotent stem cells for use in regenerative medicine [26–29]. Induced pluripotent stem cells or iPS cells, are pluripotent stem cells derived from adult somatic cells, typically fibroblasts, by forcing the expression of pluripotent genes. In mice, these genes originally were OCT4, SOX2, c-MYC and KLF4 [30–32]. However, about 16 % of chimeric mice obtained after blastocyst injection of the iPS cells died of tumors within 100 days after birth, presumably because of the oncogenic properties of c-MYC. Therefore, mouse iPS cells were later obtained by omitting c-MYC in the gene transfection cocktail [33]. In humans, efficient production of iPS cells was demonstrated by forced expression of OCT4, NANOG, SOX2 and LIN28 [34]. Expression of these genes reprograms the cells, which are then able to differentiate into tissue types of the three embryonic germline layers. Although progresses still need to be made to improve efficiency and ensure their safety, iPS cells will certainly be used in the future for tissue engineering purposes. Because stem cells constitute the building blocks for organ development and tissue repair, the past 15 years have seen growing interest in their biology and in the mechanisms that drive these cells into specialized differentiation programs. These cells are also surprisingly easy to isolate, culture and differentiate in vitro and in vivo, therefore the drive to translate findings into clinical therapeutics has

led to an increase of their applications to regenerative medicine. Stem cells hold great promises for the treatment of Parkinson disease, congenital abnormalities and spinal cord injury, as well as liver and skin regeneration. While delivering on these expectations still needs extensive work, nanotechnology will without doubt help in visualization, fate tracking, and manipulating stem cells and their environment for building and repairing tissues [35, 36]. However, there is great concern about the health consequences of using nanomaterials due to their extremely small size, their high surface area and increased surface reactivity (i.e., redox ability) as compared to larger materials. This review will describe how the combination of nanotechnology and stem cell research will dramatically advance our ability to understand and control stem cell fate decisions. This technology will lead to novel stem cell-based therapeutics for the prevention, diagnosis, and treatment of human diseases, provided that the toxicity of nanomaterials is properly assessed and understood.

13.2 Nanomaterials for Labeling and In Vivo Tracking of Stem Cells

Therapies using stem cell transplantations to regenerate tissues are currently being investigated to treat a multitude of degenerative disorders such as heart failures [37, 38], brain and spinal cord injuries [39, 40], diseases of the retina [41], liver failure [42], kidney dysfunction [43] and lower limb ischemia [44]. After transplantation, stem cells are expected to engraft, differentiate into specific cells or tissues in response to the surrounding microenvironment, and restore this tissue's functional properties. Despite these advances, the mechanisms underlying stem cell proliferation, differentiation, migration and integration within the host tissue are still poorly understood. This lack of knowledge is mainly due to our previous inability to monitor the in vivo behavior of stem cells in long-term studies because metabolic degradation and reduced photostability of cell markers such as DiI (1,1′-dioctadecyl-3,3,3′3′-tetramethylindocarbocyanine perchlorate)

or DiO (3,3-Dioctadecyloxacarbocyanine perchlorate) compromised the quality of the signal over time.

The past decade focused on discovering and improving novel approaches for labeling and tracking stem cells for tissue engineering. These methods are now increasingly replacing earlier methods and mainly utilize nanoparticles. The first attempt to label and track cells injected into mice made use of superparamagnetic iron oxide (SPIO) particles for labeling of cancer cells, as well as neural and mesenchymal stem cells (Fig. 13.2) [45–48]. While the transplanted cells could be tracked with magnetic resonance imaging (MRI), poor resolution impaired the analysis of the labeled cells at the cellular level. Subsequently, various SPIOs and SPIONs (superparamagnetic iron oxide nanoparticles) have been designed that carry specific alterations of their physical, biological and chemical properties to improve their functionality and MRI tracking [49]. In particular, sensitive, non-toxic SPIONs are now designed for future human therapeutic purposes. They can be dextran-coated to minimize aggregation [45, 50], or incubated with cathionic compounds such as poly-L-Lysine [51, 52], protamine sulfate [53] or Lipofectamine [54] to facilitate absorption by non-phagocytic cells. While the sensitivity of MRI is lower than that of single photon emission tomography (SPECT), absence of exposure to ionizing radiation and long imaging window offer an obvious advantage for human clinical studies. Indeed, the labeled stem cells should retain the marker and remain viable for months to allow their long-term follow-up, and assessment of tissue function in preclinical and clinical trials.

Tracking transplanted cells or stem cells in vivo to monitor their tissue distribution, viability and differentiation is of great importance for tissue engineering and cell therapy. Although labeling with SPIONs has become the most common procedure for longitudinal tracking of stem cells, other nanotracers have been recently developed. These include silica and titanium nanoparticles, fluorescent gold nanoclusters, nanodiamonds and

quantum dots, which all have different degrees of toxicity [55–59]. In order to improve biocompatibility, alternative strategies are being developed to provide tracers amenable to clinical translation. For example, nanomaterials with dual paramagnetic and fluorescent characteristics were recently synthetized. In 2005, Vuu and colleagues reported the construction of a dual-modality contrast agent, Gadolinium-Rhodamine nanoparticles (Gd-Rd-NPs), which they used to label and track a breast cancer cell line after injection into the hind limb of mice (Fig. 13.3) [60]. Gadolinium allowed detection of the labeled tumor cells by whole animal MRI while Rhodamine was used to visualize the cells in whole animal optical imaging or in tissue sections. More recently, fluorescent biocompatible nanoparticles were produced by polymerization of methyl methacrylate-Rhodamine complexes [61]. These nanoparticles were used to label and track human amniotic fluid cells (hAFCs), which are known to contain a significant number of stem cells with pluripotent properties [62]. Labeled hAFCs were injected into the lateral brain ventricles of mice and could be tracked for at least 14 days. Labeling was strong and reliable, indicating that these novel nanoparticles, which are highly biocompatible, are a promising tool for cell therapy.

Cancer stem cells (CSCs) comprise a small fraction of cancer cells and are believed by many to be at the origin of most tumors [63]. A number of studies suggest that CSCs are also at the origin of metastases. Identifying and tracking metastatic cancer cells is a significant task that can also be achieved using fluorescent-labeled nanoparticles. Indeed, efficacy of treatment can be radically improved through earlier detection of metastatic foci, which depends on sensitivity and specificity of the analytic tool. Soster and colleagues recently developed Rhodamine and/or Cy5 fluorescent silica-poly(ethylene glycol) nanoparticles (SPNs) coupled to two metastasis-specific peptides [64]. A poly(ethylene glycol) (PEG) shell embeds a dye-bound silica core, and presents carbonyl groups to enable covalent attachment of targeting ligands, such as
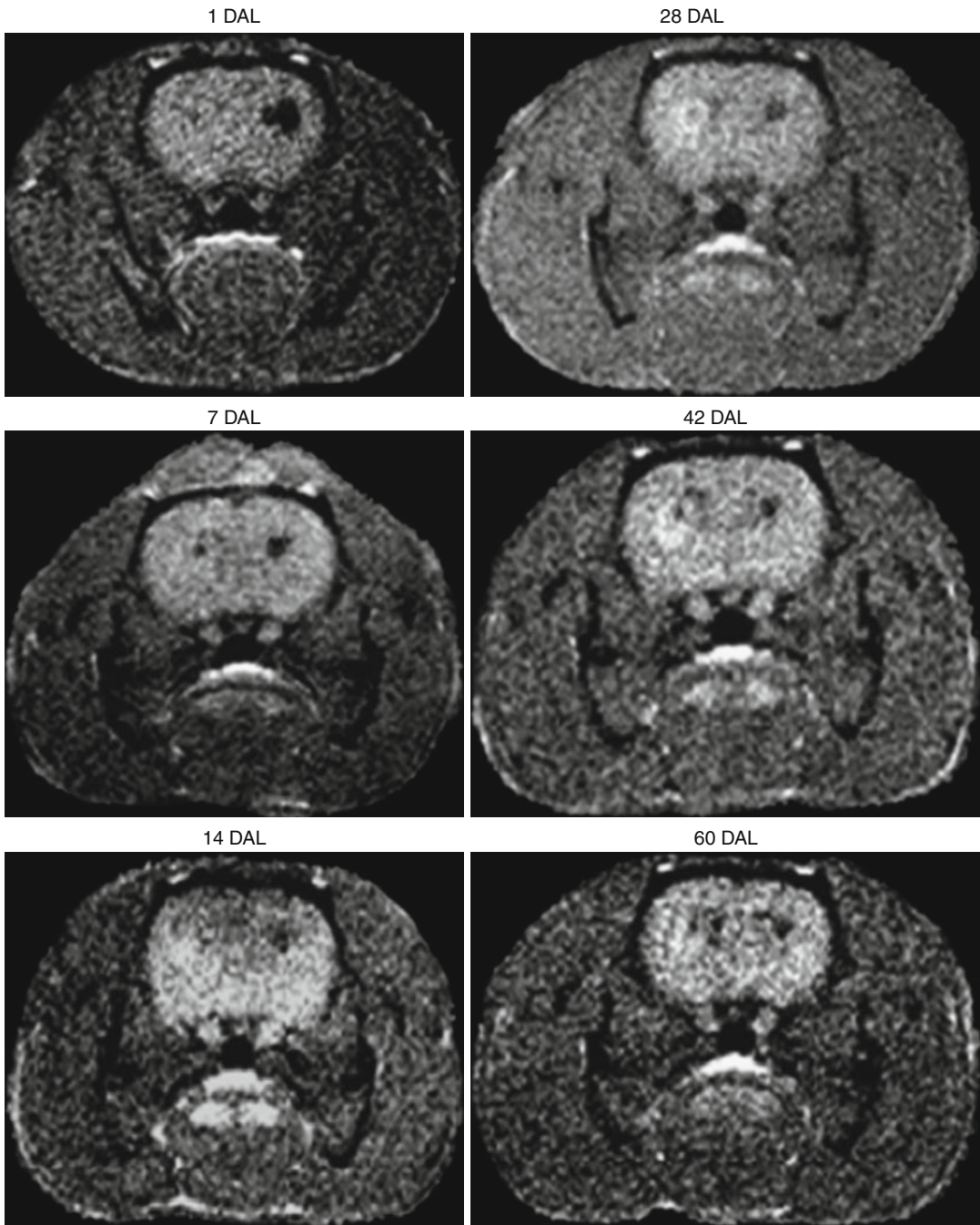
Fig. 13.2 Long-term monitoring of SPION-labeled mesenchymal stem cells (MSCs). Rat brain striata were injected bilaterally with quinolinic acid to induce neuronal death. After 1 h, SPION-labeled MSCs were injected into one side at the same location as quinolinic acid, while the other side received only saline. Hypointense signals (*black spots*) indicated the presence of MSCs in all analyzed periods. Seven days after cell injection, the black spots were also observed in the contralateral injured and non-transplanted striatum, and persisted for at least 60 days after lesion (DAL) and MSC injection (From Moraes et al. [45])

antibodies, proteins, or short peptides. These nanoparticles were coupled to the peptides CGIYRLRS and CGVYSLRS that are specific for metastatic colon carcinoma. They were intravenously injected into SCID mice bearing a spleen primary tumor (site of injection of colon cancer cells) and hepatic metastases. Whole

Fig. 13.3 In vivo optical imaging of mouse hind limb after inoculation with unlabeled tumor cells or gadolinium-rhodamine nanoparticle-labeled tumor cells. The picture shows a female mouse bearing unlabeled tumor (left limb) and Gd-Rd-NP-labeled tumor (right limb) imaged 7 days post subcutaneous inoculation (1×10^6 cells in each limb). The fluorescent signal is localized only to the labeled tumor site (From Vuu et al. [60])

organ imaging and immunohistochemistry clearly indicated that the circulating nanoparticles left the tumor capillaries and homed nearby the tumor epithelial cells. This method might therefore provide a reliable and safe way to detect small metastases before surgery.

Despite this progress, multi-imaging methods are still needed to follow the fate of different cell types simultaneously in the host tissue. For example, in tissue engineering there is the need of imaging stem cells together with endothelial cells since vascularization of reconstructed tissues is crucial for stem cell survival, which depends on oxygen and nutrient supply. Simultaneous labeling of mesenchymal stem cells (MSCs) and endothelial cells in polysaccharides-based scaffolds was recently performed by Di Corato and colleagues (Fig. 13.4) [65]. Paramagnetic gadolinium nanoparticles were used to label MSCs while SPIONs marked endothelial cells. The cells were embedded in polysaccharide-based scaffolds that were implanted subcutaneously in the flank of mice. Visualization by high-resolution MRI demonstrated that the two cell types remained distinct, with cellular level of resolution within the mouse body. Importantly, the authors

Fig. 13.4 Simultaneous imaging of endothelial cells and mesenchymal stem cells (MSCs). Two contrast agents, iron oxide nanoparticles and gadolinium oxide nanoparticles were used to label endothelial cells and MSCs respectively. No impact on cell function, including their capacity for differentiation, was detected. The labeled cells were seeded together in a polysaccharide-based scaffold and visualized simultaneously by MRI. Labeled endothelial cells appeared in black while MSCs appeared in white in vitro and in vivo (From Di Corato et al. [65])

demonstrated that the labeling of the MSCs did not alter their ability to differentiate into the osteogenic, chondrogenic or adipocytic lineages. In summary, our ability to trace stem cells in vivo using nanoparticles has remarkably improved during the past 10 years. It is evident that manufacturing of more specific and efficient nanoparticles for the visualization of these cells was concomitant to improvement of high resolution imaging techniques. In addition to their reliability and efficiency, nanoparticles with potential use in regenerative medicine have become for the most part biocompatible.

13.3 Nanomaterials for Manipulating Stem Cell Commitment

Directing the fate of stem cells in vivo is of paramount importance for the success of tissue regeneration and engineering. Extrinsic cues from the natural microenvironment of many stem cell types have been recently elucidated and include activation of the Wnt, Hedgehog and Notch pathways, binding of growth factors such as nerve growth factor (NGF) or bone morphogenetic protein (BMP) to specific membrane receptors, and composition of the extracellular matrix (ECM) [23, 66–72]. Recently, nanomaterials have been manufactured with the intention to successfully mimic or even bypass the effect of biological molecules. For example, nanofibers can increase human umbilical cord blood stem cell expansion without inducing differentiation [73]. Incorporation of growth factors such as basic fibroblast growth factor (bFGF) during scaffold preparation by electrospinning techniques stimulates skin stem cells to accelerate wound healing [74]. Fibrin nanoscaffolds with different geometry of the fibrin structure can be prepared, which are amenable to encapsulation of growth factors [75, 76]. These growth factors can then be delivered to a target site to promote stem cell growth or differentiation where tissues need to be regenerated. Indeed, Fibrin scaffolds loaded with growth factors, such as vascular endothelial growth factor (VEGF) and nerve growth factor (NGF) stimulated blood

vessel and nerve repair [77, 78]. Gene therapy using a bone morphogenetic (BMP) expression vector embedded into a Fibrin nanoscaffold allowed bone regeneration [79]. In addition to creating nanosystems able to deliver growth factors, many efforts have been directed at the construction of scaffolds mimicking the ECM for directing stem cell fate. Increasing evidence has revealed that the ECM itself through its geometry at the nanoscale level and interactions with cellular receptors such as integrins can modulate the shape and therefore gene expression and fate of stem cells [80–85]. Mechanical forces and matrix elasticity are also of great importance [86–88]. Indeed, the degree of substrate rigidity can regulate cell phenotype, which was demonstrated by the fact that an increase of matrix stiffness results in preosteoblast proliferation, while a decrease of stiffness promotes their differentiation [89]. Yet another feature of the extracellular matrix that can be mimicked using nanomaterials to direct stem cell fate is the variety of its topography, which is at the nanometer scale. Cell responses modulated by nanotopography include alignment, survival, motility, proliferation and differentiation [90–93]. For example, human induced pluripotent stem cells (iPSCs) seeded onto nanostructured silicon substrates responded by elongating and aligning along the grating axis and expressed neuronal markers, while the same cells seeded on flat substrates spread randomly and conserved their pluripotent properties [94]. The same behavior can be obtained from human MSCs [90]. Interestingly, the dimension of TiO_2 nanotubes, in particular their diameter, is instrumental in directing proliferation or differentiation of human MSCs into osteogenic lineages, although the size at which differentiation occurs seems controversial [95–97]. Arrangement of nanopits is also instrumental in determining stem cell fate. In a study using primary human osteoblastic cells, square and hexagonal nanopit arrays perturbed the formation of mature focal adhesions and the cell-spreading process, while groove/ridge arrays promoted polarised morphology and focal adhesion complexes [98]. Similarly, a square array of nanopits can support self-renewal of human MSCs, while a slightly disorganized array will promote their

osteogenic differentiation [99]. Further, the genetic profile of human primary MSCs cultured on arrays presenting nanopits and raised nano-mounds indicated that these cells differentiate into bone more efficiently than in planar surfaces with dexamethasone, a glucocorticoid commonly used to direct the differentiation of MSC into osteoblasts [100]. In another study, neural progenitors embedded into a nanofiber matrix engineered to contain the laminin-specific cell-binding domain (IKVAV) differentiated preferentially into neurons [101]. Similarly, a nanofiber scaffold that contained RGD, a binding domain for cellular integrins in many ECM proteins, significantly improved MSCs differentiation into osteoblasts [102]. Altogether, these studies clearly demonstrate that mimicking the ECM by nanotopography and engineering adhesion peptides is able to influence human adult stem cell fate, in many cases without addition of growth or differentiation factors. Therefore nanomaterials can efficiently replace the ECM and facilitate tissue regeneration and engineering protocols.

13.4 Nanomaterials Supporting Stem Cells for Regenerative Medicine

Healing and regeneration of injured or lost tissues require complex interactions between stem cells, growth factors, and extracellular matrix. Scaffolds mimicking the extracellular matrix must be constructed to establish form and structure of the organ or tissue to be regenerated. Scaffolds must be physically stable in the implanted site, allow the homing, expansion and differentiation of stem cells, and be non-toxic and biodegradable.

13.4.1 Nanofibers

Since they reproduce the morphology and structure of the natural ECM, polymeric nanofibers are among the most suitable nanomaterials for tissue engineering applications. Scaffolds made of nanofibers are three-dimensional meshes formed through the non-covalent assembly of peptides with nanometer diameters, and are commonly used in attempts of regenerating bone, skin and nerve tissue (Fig. 13.5). The most common methods for the fabrication of polymeric nanofibers are self-assembly, phase separation and electrospinning [104]. Self-assembly and phase separation allows the creation of short nanofibers with very small diameters (about 10 nm). For example, the RADA16 peptide nanofiber material self-assembles into scaffolds that were used for the growth of hippocampal neurons that subsequently produced neurites and synapses [105, 106]. This material contains the amino acids alanine, lysine, and glutamate in repeated sequences of Arg-Ala-Asp-Ala (RADA). RADA16-I nanofibers scaffold has been used for brain tissue reconstruction in mice after trauma [107], and has also been found to promote regeneration in experimental spinal cord and brain injuries [108]. Stem cell embedding into the material is feasible [109–111]. For example, Guo and colleagues embedded Schwann cells and neuro-progenitor cells (NPCs) inside a RADA16-I scaffold that integrated well within the injured spinal cord. They also demonstrated that the transplanted cells were able to survive and differentiate into neurons, astrocytes and oligodendrocytes [111]. In one of their study, Garreta and colleagues embedded embryoid bodies derived from ES cells in RADA16-I, and achieved differentiation using osteogenic medium [109]. Several functional motifs can be attached to RADA16-I, which are known to promote cell adhesion, differentiation or stem cell homing. In these conditions, neural stem cells adhered well to their matrix environment, survived and differentiated toward both the neuronal and glial phenotypes [110]. Because it is made essentially from amino acids, this type of scaffold is well tolerated and does not elicit detectable immune response or inflammation in animals. However, despite other advantages such as easiness of use and affordability, self-assembled nanofibrous scaffolds are limited in their ability to form pores wide enough to allow cell proliferation and migration since the pore size is usually between 5 and 200 nm [112]. In addition, nanofibers produced by self-assembly are very short and are often phagocytosed by the cells [113].
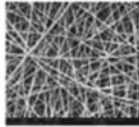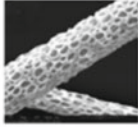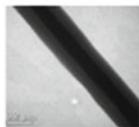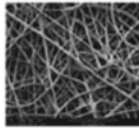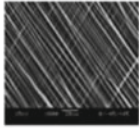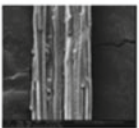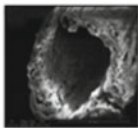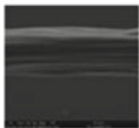
Composition	Natural	Synthetic	Blended
	• Collagen	• PCL	• Natural+Synthetic
	• Chitosan	• PLLA	• Natural+Synthetic+Coating
	• Silk	• PLGA	
	• Alginate	• PHBV	
Morphology	Solid	Porous	Core-shell
Assembly	Random	Aligned	Layered
	Yarn	Hollow yarn	Fiber bundle

Fig. 13.5 Topography of different electrospun nanofibrous structures (From Reddy et al. [103])

Electrospinning is a reliable method to fabricate long continuous strands of nanofibers with a diameter ranging from nanometers to microns (50–1,000 nm) [104]. The nanofibers form a mesh with pore sizes ranging from several to tens of micrometers, which favors cell proliferation and migration [114]. Materials used in electrospinning are natural or synthetic biopolymers or combination of both. They include poly(L-lactic acid), alginates, silicon or chitosan, sometimes in combination with collagen or gelatin [13, 115–118]. ECM proteins/peptides and growth factors can also easily be incorporated into this type of scaffold [119]. Scaffolds made of electrospun nanofibers of different types have been widely used for bone and cartilage tissue engineering using MSCs [116, 120–124]. Even adipose-derived stem cells (ADSCs) could proliferate and differentiate along the osteogenic pathway in absence of any induction medium when electrospun poly(L-lactic acid)/collagen nanofibers were engineered with a cell adhesion peptide and functionalized to retain calcium phosphate (hydroxyapatite) [123, 125]. This confirms the positive influence of cell-matrix interactions on stem cell survival and proliferation [126]. To increase the tensile strength of the scaffold, McCullen and colleagues encapsulated multiwalled carbon nanotubes (MWNTs) in poly (L-lactic acid) nanofibers [123]. Interestingly, their data indicated that addition of MWNTs significantly stimulated ADSCs proliferation. Electrospun poly(L-lactic acid)/gelatin fibers were also recently used as scaffolds to differentiate neural stem cells into motor neurons [127]. Also, poly-l-lactide (PLLA) and hybrid PLLA/collagen (PLLA/Coll) scaffolds fabricated by electrospinning were recently used to differentiate MSCs into vascular endothelial cells [128].

13.4.2 Nanotubes

Nanotubes are cylindrical structures made of a single or several layers of carbon or silicon atoms. Carbon nanotubes are known for their

electrical conductive capacity and strong mechanical properties, and they can be modified to accommodate stem cell adhesion. Single-walled or multi-walled carbon nanotubes (SWNTs or MWNTs) are used in regenerative medicine alone or as complement to poly(L-lactic acid) fibers to provide tensile or mechanical strength. As mentioned above, addition of MWNTs to poly(L-lactic acid) nanofibers seem to increase adipose stem cell proliferation [123], but they can also improve chondrogenic differentiation of MSCs [129]. When nanoscaffolds made of poly-(L-lactic acid) and MWNTs were modified with poly-L-lysine to improve cell adhesion, the MSC-derived chondrocytes produced more glycosaminoglycans than the same cells in control scaffolds without nanotubes or poly-L-lysine [129]. Combination of MSCs with the latter nanomaterial is therefore very promising for cartilage regeneration, one of the most difficult tasks in regenerative medicine since this tissue is not vascularized. MWNTs could also be combined to chitosan or hydroxyapatite to successfully mimic bone tissue with acceptable pore size amenable to periosteal stem cell proliferation [130]. Single-walled carbon nanotubes (SWNTs) were also functionalized with poly lactic-co-glycolic acid to form a biocompatible substrate allowing proliferation and differentiation of pre-osteoblasts that successfully expressed mature osteoblast markers [131]. Single-walled and multi-walled carbon nanotubes are also increasingly used as scaffolds for neural stem cell growth and differentiation. Neural stem cells (NSCs) can be isolated from the mammalian brain, propagated in culture and transplanted into damaged sites if provided with the necessary substrate. Differentiation of NSCs on single-walled carbon nanotubes layers was recently demonstrated by Jan and Kotov [132]. The stem cells were seeded onto this substrate using differentiation medium without epidermal growth factor (EGF), which is necessary for their proliferation. In these conditions, the NSCs could differentiate into neurons, astrocytes, and oligodendrocytes, with expression of neural markers such as nestin, microtubule-associated protein 2 (MAP2), glial fibrillary acidic protein (GFAP), and the

oligodendrocyte marker O4. The same authors demonstrated that thin films of single-walled carbon nanotubes mixed with laminin induced NSCs differentiation into a functional neural network with synaptic connections. In addition, the neurons were excitable [133]. Another study recently established that carbon nanotubes seeded with subventricular zone neural progenitor cells (NPCs) could effectively repair damaged neural tissue after induced stroke [134]. Further, enhanced myotube formation from myoblasts and differentiation of MSCs into cardiomyocytes were possible after seeding these cells on carbon nanotubes mixed with polyurethane or poly-(L-lactic acid), followed by electric stimulation [135, 136]. Therefore, functionalized carbon nanotubes seem to fulfill the essential requirement for the regeneration of damaged nerve and muscle tissues, which is biocompatibility, induction of stem cell differentiation and excitation of the differentiated cells.

13.4.3 Use of ES Cells on Nanoscaffolds

Because of their pluripotent properties, ES cells have also been used in nanoscaffolds to probe their biocompatibility and potential for driving stem cell fate. Since these cells reliably differentiate into cardiomyocytes, they have been seeded into nanoscaffolds predominantly to assess the influence of the material on cardiac tissue regeneration [137–139]. Nanofibers made of biodegradable polyurethane, polyethylene glycol and polycaprolactone (PCL) alone or in combination could induce the formation of cardiomyocytes from ES cells. Also, nanofiber density seemed to play an important role [138]. Other applications using ES cells include the use of electrospun PCL nanoscaffolds to enhance their differentiation into neural lineages when cultured with retinoic acid [140]. In a study by Carlberg and colleagues, human ES cells cultured on electrospun fibrous polyurethane scaffolds differentiated predominantly into dopaminergic neurons without the need of hormones or growth factors [141]. Finally, human ES cells seeded into PCL scaffolds could

be differentiated into adipocytes after induction with a hormone cocktail containing retinoic acid, insulin and triiodothyronine (T3) [142].

13.5 Stem Cell Toxicity by Nanomaterials

Because the physical and chemical properties of many compounds will change when their size is reduced to nanodimensions, nanomaterials are increasingly used for novel industrial, medical and military applications. This is particularly true for carbon- and metal-based nanotubes and nanoparticles. The small size of nanomaterials modifies their behavior to such extent that quantum physics rather than classical physics is needed to understand their properties. Characteristics of a material such as solubility, absorption, color, transparency, emission wavelength, conductivity, melting point and catalytic behavior will be drastically altered as the size is reduced [143]. It is therefore likely that these novel properties will change how the materials interact with living tissues [144]. For these reasons, there are concerns that certain nanomaterials might be harmful upon inhalation, ingestion or skin contact. Indeed, due to their very small size, nanomaterials can easily translocate across cell membranes and reach critical organelles such as mitochondria, the endoplasmic reticulum and possibly the nucleus [145–148]. It has also been demonstrated that the clearance of particles is reduced as the particle size decreases, therefore the deleterious effect of nanosized compounds, if any, will last longer [149]. Because stem cells are particularly sensitive to toxicants, the use of nanomaterials in bioengineering and medicine is a concern if their toxicity is not assessed.

13.5.1 Stem Cell Toxicity of Carbon Nanotubes

While toxicity of carbon nanotubes on cells and tissues in vitro and in vivo has been reported as early as 2003 [150–152], in 2007 the group of Y. Hong published for the first time the effects of MWNTs at the molecular level in ES cells [148]. Because stem cells are particularly sensitive to DNA damage, they have developed specialized mechanisms to preserve genomic integrity. One of these mechanisms is the expression and phosphorylation of the protein p53, which will arrest the cell cycle to allow DNA repair by the enzyme 8-oxoguanine-DNA glycosylase 1 (OGG1). The authors demonstrated that MWNTs significantly induce the expression and phosphorylation of p53, followed by an increase in expression of OGG1 in the nucleus and mitochondria, suggesting damages in the nuclear and mitochondrial DNA. Further, the authors demonstrated that DNA double-strand breaks occurred and that the frequency of mutations increased after repair. DNA alterations often happen in response to the formation of reactive oxygen species [153, 154]. A recent study testing the influence of SWNTs on myoblasts shows that these compounds also significantly alter DNA integrity [155].

Carbon nanotube manufacturing is rapidly increasing. Because of their fibrous-like shape and durability, there are concerns that their toxic properties may be similar to those of asbestosis or other fibrous materials [156]. Indeed, MWNTs induce lung inflammation and fibrosis in mice exposed to them by inhalation [157]. Therefore strict industrial hygiene measures should be taken to limit exposure during their manipulation. As mentioned above, efforts to functionalize carbon nanotubes have ensured their biocompatibility, especially when used with human NSCs or MSCs for tissue repair. Nevertheless their long-term toxicity after scaffold implantation into an animal body still needs to be assessed.

13.5.2 Stem Cell Toxicity of Metal-Based Nanoparticles

Metal and metal oxide nanoparticles (NPs) are increasingly used in medicine, consumer products, and industry. They are used for cell tracking within an animal, drug targeting, coating of medical devices, sunscreens, detergents, clothing, printer inks and fuel additives [158]. As for other nanomaterials, nanoparticles are defined as

particulate matter with at least one dimension less than 100 nm. Most NP types in current use are metal-based NPs, such as nanosilver, zinc oxide, titanium dioxide, and iron oxide. Manufactured NPs have different properties than natural NPs because of their large surface area-to-volume ratio and size that is often smaller than 20 nm. These novel physical and chemical properties imply that their interactions with cells and organelles need to be critically analyzed since many undesirable adverse effects can be triggered. Metal NPs easily penetrate tissues, epithelia and cell membranes, and pass through the blood-brain and blood-testis barriers [159–161]. Ingested nanoparticles also generate DNA alterations due to production of ROS in the bone marrow, liver and lung, which are not necessarily due to the release of free metal ions [162, 163]. Therefore these compounds are likely to interfere with the biology, viability and fate of germ line and somatic stem cells. Our group was first to assess the in vitro cytotoxicity of metal nanoparticle in germ line stem cells, or spermatogonial stem cells (SSCs) [164]. Because these cells maintain the production of sperm throughout life, preserving their viability and integrity is of paramount importance. Adverse effects on germ line stem cells maintenance, maturation and differentiation can inhibit fertility, cause cancer, and may have negative effects on the development and fertility of offspring. Our work demonstrated that nanoparticles induced production of reactive oxygen species (ROS), decrease of metabolism and apoptosis in these cells, and that the degree of toxicity depended on the metal used for nanoparticle fabrication. Silver nanoparticles were significantly more toxic than aluminum oxide nanoparticles while molybdenum nanoparticles had no deleterious effect on these stem cells (Fig. 13.6).

13.5.2.1 Toxicity of Zinc Oxide Nanoparticles

Deng and colleagues were among the first to test the effect of ZnO nanoparticles on NSCs in vitro [165]. They showed that at low concentrations (<12 ppm) ZnO nanoparticles had no effect on cell viability, but that apoptosis and necrosis increased at concentrations above 12 ppm. They also concluded that free Zn^{2+} ions were responsible for high doses effects. While scientists generally agree that ZnO nanoparticles are neither toxic to differentiated cells nor to stem cells, it was recently demonstrated that their in vitro effects depend on the number and type of cells seeded [166, 167]. For example, Taccola and colleagues provided evidence that ZnO nanoparticles selectively kill rapidly proliferating cells such as MSCs, but have no effect on the cells once they are differentiated along the osteogenic pathway [167]. Similarly ZnO nanoparticles seem to selectively kill cancer cells, possibly through ROS production leading to cell apoptosis, and is now used for certain therapies [168].

13.5.2.2 Toxicity of Aluminum Oxide Nanoparticles

Aluminum oxide nanoparticles (ANPs) are widely used, and several studies have shown that ANPs negatively affect cellular morphology and cellular components. ANPs induce oxidative stress, which leads to apoptosis, DNA damage and protein degradation in vitro, while their ingestion affects neurobehavioral patterns [169–171]. However, few studies have tested their toxicity specifically in stem cells. Only the recent investigation of Alshatwi and colleagues with MSCs indicated that ANPs might induce changes in cell morphology, decrease in cell viability and upregulation of apoptosis pathways. These effects were concentration-dependent but the physiological relevance of the doses used was not discussed [172].

13.5.2.3 Toxicity of Silver Nanoparticles

The anti-bacterial effects of silver have been known and exploited for centuries, in particular for the treatment of wounds and burns [173]. Silver is used as an antibacterial surface coating on medical devices such as stents, catheters and heart valves, and is non-toxic to human and animals in its bulk chemical form [174]. However increasing amounts of silver nanomaterials, in particular silver nanoparticles, are now finding their way into consumer products as additives to sprays, as surfactants for textiles and food con-
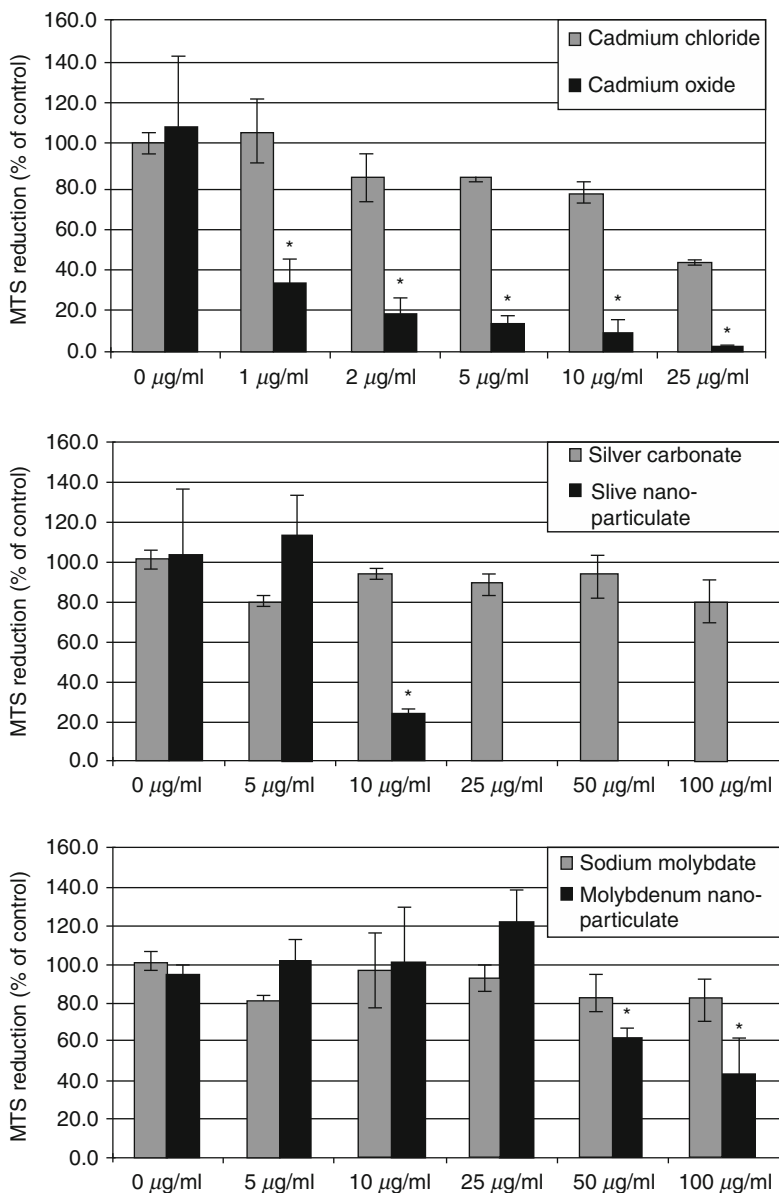
Fig. 13.6 Toxic effects of metal-based nanoparticles. The effect of silver and molybdenum nanoparticles on the metabolic activity of the C18–4 spermatogonial stem cells was evaluated after 48 h incubation. At the end of the incubation period, mitochondrial function was determined by the MTS reduction assay. (**a**) MTS reduction in presence of different concentrations of cadmium chloride and cadmium oxide. Cadmium chloride is a known toxicant and is used here as a positive control. (**b**) MTS reduction in presence of different concentrations of silver carbonate and silver nanoparticles (Ag—15 nm). (**c**) MTS reduction in presence of different concentrations of sodium molybdate and molybdenum nanoparticles. Overall silver nanoparticles were as toxic as cadmium chloride. Molybdenum nanoparticles were toxic only a high concentrations (From Braydich-Stolle et al. [164])

tainers, and as drinking water disinfectants to name a few applications. This trend is concerning because many studies have now demonstrated that the toxicity of nanosilver is much greater than that of most carbon-based and metal-based nanomaterials [143]. The cellular toxic effects of silver nanoparticles are size-dependent, and increase as the particle size decreases [175, 176].

They include reduction of mitochondrial function, increase of membrane leakage and increase of production of reactive oxygen species (ROS) [164]. They also can deplete cellular glutathione, an antioxidant [177]. As mentioned before, ROS cause DNA damages such as base oxidations, base changes or single and double-strand breaks that can lead to cell death or to mutations causing cancers. Recent studies in ES cells demonstrated that silver nanoparticles up-regulated expression and phosphorylation of the protein p53, induced DNA double-strand breaks, decreased cellular metabolism and promoted apoptosis [178]. In this work, silver nanoparticles with different surface chemistries were used: uncoated nanoparticles and particles coated with a polysaccharide to ensure biocompatibility and dispersion. Interestingly, in ES cells the coated silver nanoparticles produced more damages than the uncoated nanoparticles, but the cause remains unclear. Our group also recently investigated some of the mechanisms causing the toxic effects of silver nanoparticles in germ line stem cells [176]. Silver nanoparticles were hydrocarbon or polysaccharide-coated to study the influence of surface chemistry. We demonstrated that at low doses (<10 μg/ml), silver nanoparticles interfered with the glial cell line-derived neurotrophic factor (GDNF) signaling pathway, which is crucial for germ line stem cell self-renewal. More precisely, silver nanoparticles inhibited the phosphorylation of the membrane-associated FYN kinase downstream of the RET (REarranged during Transfection) transmembrane receptor after activation by GDNF. Silver nanoparticles did not interfere with GDNF binding to its receptor nor with receptor phosphorylation. Further, we demonstrated that silver nanoparticles reduced germ line stem cell viability and proliferation in a size- and concentration-dependent manner and that particle coating had no influence on the magnitude of the toxic effects. The effect of silver nanoparticles has since been tested on human MSCs [179]. When exposed to the dose of 10 μg/ml, these cells experienced DNA damage and their viability decreased, as shown for other stem cell types, but their ability to migrate was not impaired. However, Samberg and colleagues recently demonstrated that silver nanoparticles exert minimal toxicity to human adipose tissue-derived stem cells (ADSCs) and do not impair their differentiation [180]. Therefore, for the same sizes and concentrations, stem cell effects of silver nanoparticles might be cell type-dependent, with germ line stem cells particularly sensitive to this potential toxicant.

Conclusion

Nanomaterials have found many applications in stem cell research including tracking, delivering, and controlling the fate of these cells for tissue engineering. These applications have already started to transform several areas of cell biology and medicine. However, strategies allowing large-scale stem cell expansion before their differentiation are still lacking. In addition, the creation of complex tissues is still in infancy and will need the ability to direct the growth and differentiation of different cell types in three dimensions within biocompatible scaffolds. Furthermore, toxicity of certain nanoscaffolds such as MWNTs is still a concern since coatings that ensure their biocompatibility might not be stable within the tissue to be repaired. Finally, as the demand for nanomaterials is increasing, potential inhalation during manufacturing or packing, and their accumulation in the environment should be carefully monitored to ensure human safety.

References

1. Cui D, Gao H (2003) Advance and prospect of bionanomaterials. Biotechnol Prog 19(3):683–692
2. Rajangam T, An SS (2013) Fibrinogen and fibrin based micro and nano scaffolds incorporated with drugs, proteins, cells and genes for therapeutic biomedical applications. Int J Nanomedicine 8:3641–3662
3. Liu W, Thomopoulos S, Xia Y (2012) Electrospun nanofibers for regenerative medicine. Adv Healthc Mater 1(1):10–25
4. Ozpolat B, Sood AK, Lopez-Berestein G (2010) Nanomedicine based approaches for the delivery of siRNA in cancer. J Intern Med 267(1):44–53
5. Duncan R (2006) Polymer conjugates as anticancer nanomedicines. Nat Rev Cancer 6(9):688–701

6. Uskokovic V (2013) Entering the era of nanoscience: time to be so small. J Biomed Nanotechnol 9(9):1441–1470

7. Pandey PC, Chauhan DS, Singh V (2013) Role of nanostructured networks as analytical tools for biological systems. Front Biosci (Elite Ed) 5:622–642

8. Vilela D, Garoz J, Colina A, Gonzalez MC, Escarpa A (2012) Carbon nanotubes press-transferred on PMMA substrates as exclusive transducers for electrochemical microfluidic sensing. Anal Chem 84(24):10838–10844

9. Ramulu TS, Venu R, Sinha B, Lim B, Jeon SJ, Yoon SS, Kim CG (2013) Nanowires array modified electrode for enhanced electrochemical detection of nucleic acid. Biosens Bioelectron 40(1):258–264

10. Kruss S, Hilmer AJ, Zhang J, Reuel NF, Mu B, Strano MS (2013) Carbon nanotubes as optical biomedical sensors. Adv Drug Deliv Rev 65(15):1933–1950

11. Riegler J, Nann T (2004) Application of luminescent nanocrystals as labels for biological molecules. Anal Bioanal Chem 379(7–8):913–919

12. Lisdat F, Schafer D, Kapp A (2013) Quantum dots on electrodes – new tools for bioelectroanalysis. Anal Bioanal Chem 405(11):3739–3752

13. Premnath P, Tan B, Venkatakrishnan K (2013) Direct patterning of free standing three dimensional silicon nanofibrous network to facilitate multi-dimensional growth of fibroblasts and osteoblasts. J Biomed Nanotechnol 9(11):1875–1881

14. Martinelli V, Cellot G, Toma FM, Long CS, Caldwell JH, Zentilin L, Giacca M, Turco A, Prato M, Ballerini L, Mestroni L (2012) Carbon nanotubes promote growth and spontaneous electrical activity in cultured cardiac myocytes. Nano Lett 12(4):1831–1838

15. Solanki A, Chueng ST, Yin PT, Kappera R, Chhowalla M, Lee KB (2013) Axonal alignment and enhanced neuronal differentiation of neural stem cells on graphene-nanoparticle hybrid structures. Adv Mater 25(38):5477–5482

16. Sheets K, Wunsch S, Ng C, Nain AS (2013) Shape-dependent cell migration and focal adhesion organization on suspended and aligned nanofiber scaffolds. Acta Biomater 9(7):7169–7177

17. Pelton TA, Bettess MD, Lake J, Rathjen J, Rathjen PD (1998) Developmental complexity of early mammalian pluripotent cell populations in vivo and in vitro. Reprod Fertil Dev 10(7–8):535–549

18. Meregalli M, Farini A, Torrente Y (2011) Mesenchymal stem cells as muscle reservoir. J Stem Cell Res Ther 1:105

19. Bobis S, Jarocha D, Majka M (2006) Mesenchymal stem cells: characteristics and clinical applications. Folia Histochem Cytobiol 44(4):215–230

20. Konno M, Hamabe A, Hasegawa S, Ogawa H, Fukusumi T, Nishikawa S, Ohta K, Kano Y, Ozaki M, Noguchi Y, Sakai D, Kudoh T, Kawamoto K, Eguchi H, Satoh T, Tanemura M, Nagano H, Doki Y, Mori M, Ishii H (2013) Adipose-derived mesenchymal stem cells and regenerative medicine. Dev Growth Differ 55(3):309–318

21. Wilkinson AC, Gottgens B (2013) Transcriptional regulation of haematopoietic stem cells. Adv Exp Med Biol 786:187–212

22. Clevers H (2013) The intestinal crypt, a prototype stem cell compartment. Cell 154(2):274–284

23. Yeung TM, Chia LA, Kosinski CM, Kuo CJ (2011) Regulation of self-renewal and differentiation by the intestinal stem cell niche. Cell Mol Life Sci 68(15):2513–2523

24. Blanpain C, Fuchs E (2009) Epidermal homeostasis: a balancing act of stem cells in the skin. Nat Rev Mol Cell Biol 10(3):207–217

25. Phillips BT, Gassei K, Orwig KE (2010) Spermatogonial stem cell regulation and spermatogenesis. Philos Trans R Soc Lond B Biol Sci 365(1546):1663–1678

26. Kanatsu-Shinohara M, Inoue K, Lee J, Yoshimoto M, Ogonuki N, Miki H, Baba S, Kato T, Kazuki Y, Toyokuni S, Toyoshima M, Niwa O, Oshimura M, Heike T, Nakahata T, Ishino F, Ogura A, Shinohara T (2004) Generation of pluripotent stem cells from neonatal mouse testis. Cell 119(7):1001–1012

27. Simon L, Ekman GC, Kostereva N, Zhang Z, Hess RA, Hofmann MC, Cooke PS (2009) Direct transdifferentiation of stem/progenitor spermatogonia into reproductive and nonreproductive tissues of all germ layers. Stem Cells 27(7):1666–1675

28. Kossack N, Meneses J, Shefi S, Nguyen HN, Chavez S, Nicholas C, Gromoll J, Turek PJ, Reijo-Pera RA (2009) Isolation and characterization of pluripotent human spermatogonial stem cell-derived cells. Stem Cells 27(1):138–149

29. Golestaneh N, Kokkinaki M, Pant D, Jiang J, DeStefano D, Fernandez-Bueno C, Rone JD, Haddad BR, Gallicano GI, Dym M (2009) Pluripotent stem cells derived from adult human testes. Stem Cells Dev 18(8):1115–1126

30. Takahashi K, Yamanaka S (2006) Induction of pluripotent stem cells from mouse embryonic and adult fibroblast cultures by defined factors. Cell 126(4):663–676

31. Okita K, Ichisaka T, Yamanaka S (2007) Generation of germline-competent induced pluripotent stem cells. Nature 448(7151):313–317

32. Wernig M, Meissner A, Foreman R, Brambrink T, Ku M, Hochedlinger K, Bernstein BE, Jaenisch R (2007) In vitro reprogramming of fibroblasts into a pluripotent ES-cell-like state. Nature 448(7151):318–324

33. Nakagawa M, Koyanagi M, Tanabe K, Takahashi K, Ichisaka T, Aoi T, Okita K, Mochiduki Y, Takizawa N, Yamanaka S (2008) Generation of induced pluripotent stem cells without Myc from mouse and human fibroblasts. Nat Biotechnol 26(1):101–106

34. Yu J, Vodyanik MA, Smuga-Otto K, Antosiewicz-Bourget J, Frane JL, Tian S, Nie J, Jonsdottir GA, Ruotti V, Stewart R, Slukvin II, Thomson JA (2007) Induced pluripotent stem cell lines derived from human somatic cells. Science 318(5858):1917–1920

35. Jiang J, Papoutsakis ET (2013) Stem-cell niche based comparative analysis of chemical and nanomechanical material properties impacting ex vivo

expansion and differentiation of hematopoietic and mesenchymal stem cells. Adv Healthc Mater 2(1):25–42

36. Bressan E, Carraro A, Ferroni L, Gardin C, Sbricoli L, Guazzo R, Stellini E, Roman M, Pinton P, Sivolella S, Zavan B (2013) Nanotechnology to drive stem cell commitment. Nanomedicine (Lond) 8(3):469–486

37. Schachinger V, Assmus B, Britten MB, Honold J, Lehmann R, Teupe C, Abolmaali ND, Vogl TJ, Hofmann WK, Martin H, Dimmeler S, Zeiher AM (2004) Transplantation of progenitor cells and regeneration enhancement in acute myocardial infarction: final one-year results of the TOPCARE-AMI Trial. J Am Coll Cardiol 44(8):1690–1699

38. Sanganalmath SK, Bolli R (2013) Cell therapy for heart failure: a comprehensive overview of experimental and clinical studies, current challenges, and future directions. Circ Res 113(6):810–834

39. Tsukamoto A, Uchida N, Capela A, Gorba T, Huhn S (2013) Clinical translation of human neural stem cells. Stem Cell Res Ther 4(4):102

40. Mothe AJ, Tator CH (2013) Review of transplantation of neural stem/progenitor cells for spinal cord injury. Int J Dev Neurosci 31(7):701–713

41. Ramsden CM, Powner MB, Carr AJ, Smart MJ, da Cruz L, Coffey PJ (2013) Stem cells in retinal regeneration: past, present and future. Development 140(12):2576–2585

42. Ordovas L, Park Y, Verfaillie CM (2013) Stem cells and liver engineering. Biotechnol Adv 31(7):1094–1107

43. Yokote S, Yokoo T (2012) Stem cells in kidney regeneration. Curr Med Chem 19(35):6009–6017

44. Hart CA, Tsui J, Khanna A, Abraham DJ, Baker DM (2013) Stem cells of the lower limb: their role and potential in management of critical limb ischemia. Exp Biol Med 238(10):1118–1126

45. Moraes L, Vasconcelos-dos-Santos A, Santana FC, Godoy MA, Rosado-de-Castro PH, Jasmin, Azevedo-Pereira RL, Cintra WM, Gasparetto EL, Santiago MF, Mendez-Otero R (2012) Neuroprotective effects and magnetic resonance imaging of mesenchymal stem cells labeled with SPION in a rat model of Huntington's disease. Stem Cell Res 9(2):143–155

46. Frank JA, Zywicke H, Jordan EK, Mitchell J, Lewis BK, Miller B, Bryant LH Jr, Bulte JW (2002) Magnetic intracellular labeling of mammalian cells by combining (FDA-approved) superparamagnetic iron oxide MR contrast agents and commonly used transfection agents. Acad Radiol 9(Suppl 2):S484–S487

47. Kraitchman DL, Heldman AW, Atalar E, Amado LC, Martin BJ, Pittenger MF, Hare JM, Bulte JW (2003) In vivo magnetic resonance imaging of mesenchymal stem cells in myocardial infarction. Circulation 107(18):2290–2293

48. Bulte JW, Douglas T, Witwer B, Zhang SC, Strable E, Lewis BK, Zywicke H, Miller B, van Gelderen P, Moskowitz BM, Duncan ID, Frank JA (2001) Magnetodendrimers allow endosomal magnetic labeling and in vivo tracking of stem cells. Nat Biotechnol 19(12):1141–1147

49. Wang YX, Xuan S, Port M, Idee JM (2013) Recent advances in superparamagnetic iron oxide nanoparticles for cellular imaging and targeted therapy research. Curr Pharm Des 19(37):6575–6593

50. Molday RS, MacKenzie D (1982) Immunospecific ferromagnetic iron-dextran reagents for the labeling and magnetic separation of cells. J Immunol Methods 52(3):353–367

51. Babic M, Horak D, Trchova M, Jendelova P, Glogarova K, Lesny P, Herynek V, Hajek M, Sykova E (2008) Poly(L-lysine)-modified iron oxide nanoparticles for stem cell labeling. Bioconjug Chem 19(3):740–750

52. Arbab AS, Bashaw LA, Miller BR, Jordan EK, Bulte JW, Frank JA (2003) Intracytoplasmic tagging of cells with ferumoxides and transfection agent for cellular magnetic resonance imaging after cell transplantation: methods and techniques. Transplantation 76(7):1123–1130

53. Jasmin, Torres AL, Jelicks L, de Carvalho AC, Spray DC, Mendez-Otero R (2012) Labeling stem cells with superparamagnetic iron oxide nanoparticles: analysis of the labeling efficacy by microscopy and magnetic resonance imaging. Methods Mol Biol 906:239–252

54. Frank JA, Miller BR, Arbab AS, Zywicke HA, Jordan EK, Lewis BK, Bryant LH Jr, Bulte JW (2003) Clinically applicable labeling of mammalian and stem cells by combining superparamagnetic iron oxides and transfection agents. Radiology 228(2):480–487

55. Wang HH, Lin CA, Lee CH, Lin YC, Tseng YM, Hsieh CL, Chen CH, Tsai CH, Hsieh CT, Shen JL, Chan WH, Chang WH, Yeh HI (2011) Fluorescent gold nanoclusters as a biocompatible marker for in vitro and in vivo tracking of endothelial cells. ACS Nano 5(6):4337–4344

56. Rehor I, Vilimova V, Jendelova P, Kubicek V, Jirak D, Herynek V, Kapcalova M, Kotek J, Cerny J, Hermann P, Lukes I (2011) Phosphonate-titanium dioxide assemblies: platform for multimodal diagnostic-therapeutic nanoprobes. J Med Chem 54(14):5185–5194

57. Fang CY, Vaijayanthimala V, Cheng CA, Yeh SH, Chang CF, Li CL, Chang HC (2011) The exocytosis of fluorescent nanodiamond and its use as a long-term cell tracker. Small 7(23):3363–3370

58. Lee JK, Chun SY, Im JY, Jin HK, Kwon TG, Bae JS (2012) Specific labeling of neurogenic, endothelial, and myogenic differentiated cells derived from human amniotic fluid stem cells with silica-coated magnetic nanoparticles. J Vet Med Sci 74(8):969–975

59. Chen Y (2012) Quantum dots for labeling live cells. Methods Mol Biol 906:193–198

60. Vuu K, Xie J, McDonald MA, Bernardo M, Hunter F, Zhang Y, Li K, Bednarski M, Guccione S (2005) Gadolinium-rhodamine nanoparticles for cell labeling

and tracking via magnetic resonance and optical imaging. Bioconjug Chem 16(4):995–999

61. Cova L, Bigini P, Diana V, Sitia L, Ferrari R, Pesce RM, Khalaf R, Bossolasco P, Ubezio P, Lupi M, Tortarolo M, Colombo L, Giardino D, Silani V, Morbidelli M, Salmona M, Moscatelli D (2013) Biocompatible fluorescent nanoparticles for in vivo stem cell tracking. Nanotechnology 24(24):245603

62. Cananzi M, Atala A, De Coppi P (2009) Stem cells derived from amniotic fluid: new potentials in regenerative medicine. Reprod Biomed Online 18(Suppl 1):17–27

63. Visvader JE, Lindeman GJ (2012) Cancer stem cells: current status and evolving complexities. Cell Stem Cell 10(6):717–728

64. Soster M, Juris R, Bonacchi S, Genovese D, Montalti M, Rampazzo E, Zaccheroni N, Garagnani P, Bussolino F, Prodi L, Marchio S (2012) Targeted dual-color silica nanoparticles provide univocal identification of micrometastases in preclinical models of colorectal cancer. Int J Nanomedicine 7:4797–4807

65. Di Corato R, Gazeau F, Le Visage C, Fayol D, Levitz P, Lux F, Letourneur D, Luciani N, Tillement O, Wilhelm C (2013) High-resolution cellular MRI: gadolinium and iron oxide nanoparticles for in-depth dual-cell imaging of engineered tissue constructs. ACS Nano 7(9):7500–7512

66. Fakhry M, Hamade E, Badran B, Buchet R, Magne D (2013) Molecular mechanisms of mesenchymal stem cell differentiation towards osteoblasts. World J Stem Cells 5(4):136–148

67. Blank U, Karlsson G, Karlsson S (2008) Signaling pathways governing stem-cell fate. Blood 111(2):492–503

68. Hofmann MC (2008) Gdnf signaling pathways within the mammalian spermatogonial stem cell niche. Mol Cell Endocrinol 288(1–2):95–103

69. Garcia TX, Hofmann MC (2013) NOTCH signaling in Sertoli cells regulates gonocyte fate. Cell Cycle 12(16):2538–2545

70. Nagano MC, Yeh JR (2013) The identity and fate decision control of spermatogonial stem cells: where is the point of no return? Curr Top Dev Biol 102:61–95

71. Fuchs E (2009) Finding one's niche in the skin. Cell Stem Cell 4(6):499–502

72. Watt FM, Huck WT (2013) Role of the extracellular matrix in regulating stem cell fate. Nat Rev Mol Cell Biol 14(8):467–473

73. Das H, Abdulhameed N, Joseph M, Sakthivel R, Mao HQ, Pompili VJ (2009) Ex vivo nanofiber expansion and genetic modification of human cord blood-derived progenitor/stem cells enhances vasculogenesis. Cell Transplant 18(3):305–318

74. Yang Y, Xia T, Zhi W, Wei L, Weng J, Zhang C, Li X (2011) Promotion of skin regeneration in diabetic rats by electrospun core-sheath fibers loaded with basic fibroblast growth factor. Biomaterials 32(18):4243–4254

75. Janmey PA, Winer JP, Weisel JW (2009) Fibrin gels and their clinical and bioengineering applications. J R Soc Interface 6(30):1–10

76. Ahmed TA, Dare EV, Hincke M (2008) Fibrin: a versatile scaffold for tissue engineering applications. Tissue Eng Part B Rev 14(2):199–215

77. Ehrbar M, Metters A, Zammaretti P, Hubbell JA, Zisch AH (2005) Endothelial cell proliferation and progenitor maturation by fibrin-bound VEGF variants with differential susceptibilities to local cellular activity. J Control Release 101(1–3):93–109

78. Bhang SH, Jeon O, Choi CY, Kwon YH, Kim BS (2007) Controlled release of nerve growth factor from fibrin gel. J Biomed Mater Res A 80(4):998–1002

79. Lee TC, Ho JT, Hung KS, Chen WF, Chung YH, Yang YL (2006) Bone morphogenetic protein gene therapy using a fibrin scaffold for a rabbit spinal-fusion experiment. Neurosurgery 58(2):373–380; discussion 373–380

80. Sun Y, Chen CS, Fu J (2012) Forcing stem cells to behave: a biophysical perspective of the cellular microenvironment. Annu Rev Biophys 41:519–542

81. Guilak F, Cohen DM, Estes BT, Gimble JM, Liedtke W, Chen CS (2009) Control of stem cell fate by physical interactions with the extracellular matrix. Cell Stem Cell 5(1):17–26

82. Huebsch N, Arany PR, Mao AS, Shvartsman D, Ali OA, Bencherif SA, Rivera-Feliciano J, Mooney DJ (2010) Harnessing traction-mediated manipulation of the cell/matrix interface to control stem-cell fate. Nat Mater 9(6):518–526

83. Trappmann B, Gautrot JE, Connelly JT, Strange DG, Li Y, Oyen ML, Cohen Stuart MA, Boehm H, Li B, Vogel V, Spatz JP, Watt FM, Huck WT (2012) Extracellular-matrix tethering regulates stem-cell fate. Nat Mater 11(7):642–649

84. Kong HJ, Boontheekul T, Mooney DJ (2006) Quantifying the relation between adhesion ligand-receptor bond formation and cell phenotype. Proc Natl Acad Sci U S A 103(49):18534–18539

85. Chu C, Schmidt JJ, Carnes K, Zhang Z, Kong HJ, Hofmann MC (2009) Three-dimensional synthetic niche components to control germ cell proliferation. Tissue Eng Part A 15(2):255–262

86. Simmons CA, Matlis S, Thornton AJ, Chen S, Wang CY, Mooney DJ (2003) Cyclic strain enhances matrix mineralization by adult human mesenchymal stem cells via the extracellular signal-regulated kinase (ERK1/2) signaling pathway. J Biomech 36(8):1087–1096

87. Gwak SJ, Bhang SH, Kim IK, Kim SS, Cho SW, Jeon O, Yoo KJ, Putnam AJ, Kim BS (2008) The effect of cyclic strain on embryonic stem cell-derived cardiomyocytes. Biomaterials 29(7):844–856

88. Engler AJ, Sen S, Sweeney HL, Discher DE (2006) Matrix elasticity directs stem cell lineage specification. Cell 126(4):677–689

89. Kong HJ, Polte TR, Alsberg E, Mooney DJ (2005) FRET measurements of cell-traction forces and nano-scale clustering of adhesion ligands varied by substrate stiffness. Proc Natl Acad Sci U S A 102(12):4300–4305

90. Yim EK, Pang SW, Leong KW (2007) Synthetic nanostructures inducing differentiation of human mesenchymal stem cells into neuronal lineage. Exp Cell Res 313(9):1820–1829

91. McMurray RJ, Gadegaard N, Tsimbouri PM, Burgess KV, McNamara LE, Tare R, Murawski K, Kingham E, Oreffo RO, Dalby MJ (2011) Nanoscale surfaces for the long-term maintenance of mesenchymal stem cell phenotype and multipotency. Nat Mater 10(8):637–644

92. Lee MR, Kwon KW, Jung H, Kim HN, Suh KY, Kim K, Kim KS (2010) Direct differentiation of human embryonic stem cells into selective neurons on nanoscale ridge/groove pattern arrays. Biomaterials 31(15):4360–4366

93. Chen W, Villa-Diaz LG, Sun Y, Weng S, Kim JK, Lam RH, Han L, Fan R, Krebsbach PH, Fu J (2012) Nanotopography influences adhesion, spreading, and self-renewal of human embryonic stem cells. ACS Nano 6(5):4094–4103

94. Pan F, Zhang M, Wu G, Lai Y, Greber B, Scholer HR, Chi L (2013) Topographic effect on human induced pluripotent stem cells differentiation towards neuronal lineage. Biomaterials 34(33):8131–8139

95. Oh S, Brammer KS, Li YS, Teng D, Engler AJ, Chien S, Jin S (2009) Stem cell fate dictated solely by altered nanotube dimension. Proc Natl Acad Sci U S A 106(7):2130–2135

96. Park J, Bauer S, von der Mark K, Schmuki P (2007) Nanosize and vitality: TiO_2 nanotube diameter directs cell fate. Nano Lett 7(6):1686–1691

97. Park J, Bauer S, Schlegel KA, Neukam FW, von der Mark K, Schmuki P (2009) TiO_2 nanotube surfaces: 15 nm–an optimal length scale of surface topography for cell adhesion and differentiation. Small 5(6):666–671

98. Biggs MJ, Richards RG, Gadegaard N, Wilkinson CD, Oreffo RO, Dalby MJ (2009) The use of nanoscale topography to modulate the dynamics of adhesion formation in primary osteoblasts and ERK/MAPK signalling in STRO-1+ enriched skeletal stem cells. Biomaterials 30(28):5094–5103

99. Dalby MJ, Gadegaard N, Tare R, Andar A, Riehle MO, Herzyk P, Wilkinson CD, Oreffo RO (2007) The control of human mesenchymal cell differentiation using nanoscale symmetry and disorder. Nat Mater 6(12):997–1003

100. Dalby MJ, Andar A, Nag A, Affrossman S, Tare R, McFarlane S, Oreffo RO (2008) Genomic expression of mesenchymal stem cells to altered nanoscale topographies. J R Soc Interface 5(26):1055–1065

101. Silva GA, Czeisler C, Niece KL, Beniash E, Harrington DA, Kessler JA, Stupp SI (2004) Selective differentiation of neural progenitor cells by high-epitope density nanofibers. Science 303(5662):1352–1355

102. Hosseinkhani H, Hosseinkhani M, Tian F, Kobayashi H, Tabata Y (2006) Osteogenic differentiation of mesenchymal stem cells in self-assembled peptide-amphiphile nanofibers. Biomaterials 27(22):4079–4086

103. Jayarama Reddy V, Radhakrishnan S, Ravichandran R, Mukherjee S, Balamurugan R, Sundarrajan S, Ramakrishna S (2013) Nanofibrous structured biomimetic strategies for skin tissue regeneration. Wound Repair Regen 21(1):1–16

104. Lu T, Li Y, Chen T (2013) Techniques for fabrication and construction of three-dimensional scaffolds for tissue engineering. Int J Nanomedicine 8:337–350

105. Zhang S, Holmes T, Lockshin C, Rich A (1993) Spontaneous assembly of a self-complementary oligopeptide to form a stable macroscopic membrane. Proc Natl Acad Sci U S A 90(8):3334–3338

106. Holmes TC, de Lacalle S, Su X, Liu G, Rich A, Zhang S (2000) Extensive neurite outgrowth and active synapse formation on self-assembling peptide scaffolds. Proc Natl Acad Sci U S A 97(12):6728–6733

107. Leung GK, Wang YC, Wu W (2012) Peptide nanofiber scaffold for brain tissue reconstruction. Methods Enzymol 508:177–190

108. Ellis-Behnke RG, Liang YX, You SW, Tay DK, Zhang S, So KF, Schneider GE (2006) Nano neuro knitting: peptide nanofiber scaffold for brain repair and axon regeneration with functional return of vision. Proc Natl Acad Sci U S A 103(13):5054–5059

109. Garreta E, Genove E, Borros S, Semino CE (2006) Osteogenic differentiation of mouse embryonic stem cells and mouse embryonic fibroblasts in a three-dimensional self-assembling peptide scaffold. Tissue Eng 12(8):2215–2227

110. Gelain F, Bottai D, Vescovi A, Zhang S (2006) Designer self-assembling peptide nanofiber scaffolds for adult mouse neural stem cell 3-dimensional cultures. PLoS One 1:e119

111. Guo J, Su H, Zeng Y, Liang YX, Wong WM, Ellis-Behnke RG, So KF, Wu W (2007) Reknitting the injured spinal cord by self-assembling peptide nanofiber scaffold. Nanomedicine 3(4):311–321

112. Zhang S, Holmes TC, DiPersio CM, Hynes RO, Su X, Rich A (1995) Self-complementary oligopeptide matrices support mammalian cell attachment. Biomaterials 16(18):1385–1393

113. Beniash E, Hartgerink JD, Storrie H, Stendahl JC, Stupp SI (2005) Self-assembling peptide amphiphile nanofiber matrices for cell entrapment. Acta Biomater 1(4):387–397

114. Lao L, Wang Y, Zhu Y, Zhang Y, Gao C (2011) Poly(lactide-co-glycolide)/hydroxyapatite nanofibrous scaffolds fabricated by electrospinning for bone tissue engineering. J Mater Sci Mater Med 22(8):1873–1884

115. Leung V, Hartwell R, Elizei SS, Yang H, Ghahary A, Ko F (2013) Postelectrospinning modifications for alginate nanofiber-based wound dressings. J Biomed Mater Res Part B (in press)

116. Xin X, Hussain M, Mao JJ (2007) Continuing differentiation of human mesenchymal stem cells and induced chondrogenic and osteogenic lineages in electrospun PLGA nanofiber scaffold. Biomaterials 28(2):316–325

117. Wang W, Itoh S, Matsuda A, Aizawa T, Demura M, Ichinose S, Shinomiya K, Tanaka J (2008) Enhanced nerve regeneration through a bilayered chitosan tube: the effect of introduction of glycine spacer into the CYIGSR sequence. J Biomed Mater Res A 85(4):919–928

118. Sarkar SD, Farrugia BL, Dargaville TR, Dhara S (2013) Chitosan-collagen scaffolds with nano/microfibrous architecture for skin tissue engineering. J Biomed Mater Res A 101(12):3482–3492

119. Sun F, Zhou H, Lee J (2011) Various preparation methods of highly porous hydroxyapatite/polymer nanoscale biocomposites for bone regeneration. Acta Biomater 7(11):3813–3828

120. Li C, Vepari C, Jin HJ, Kim HJ, Kaplan DL (2006) Electrospun silk-BMP-2 scaffolds for bone tissue engineering. Biomaterials 27(16):3115–3124

121. Shih YR, Chen CN, Tsai SW, Wang YJ, Lee OK (2006) Growth of mesenchymal stem cells on electrospun type I collagen nanofibers. Stem Cells 24(11):2391–2397

122. Li WJ, Tuli R, Huang X, Laquerriere P, Tuan RS (2005) Multilineage differentiation of human mesenchymal stem cells in a three-dimensional nanofibrous scaffold. Biomaterials 26(25):5158–5166

123. McCullen SD, Stevens DR, Roberts WA, Clarke LI, Bernacki SH, Gorga RE, Loboa EG (2007) Characterization of electrospun nanocomposite scaffolds and biocompatibility with adipose-derived human mesenchymal stem cells. Int J Nanomedicine 2(2):253–263

124. Shafiee A, Soleimani M, Chamheidari GA, Seyedjafari E, Dodel M, Atashi A, Gheisari Y (2011) Electrospun nanofiber-based regeneration of cartilage enhanced by mesenchymal stem cells. J Biomed Mater Res A 99(3):467–478

125. Ravichandran R, Venugopal JR, Sundarrajan S, Mukherjee S, Ramakrishna S (2012) Precipitation of nanohydroxyapatite on PLLA/PBLG/Collagen nanofibrous structures for the differentiation of adipose derived stem cells to osteogenic lineage. Biomaterials 33(3):846–855

126. Brizzi MF, Tarone G, Defilippi P (2012) Extracellular matrix, integrins, and growth factors as tailors of the stem cell niche. Curr Opin Cell Biol 24(5):645–651

127. Binan L, Tendey C, De Crescenzo G, El Ayoubi R, Ajji A, Jolicoeur M (2014) Differentiation of neuronal stem cells into motor neurons using electrospun poly-L-lactic acid/gelatin scaffold. Biomaterials 35(2):664–674

128. Jia L, Prabhakaran MP, Qin X, Ramakrishna S (2013) Stem cell differentiation on electrospun nanofibrous substrates for vascular tissue engineering. Mater Sci Eng C Mater Biol Appl 33(8):4640–4650

129. Holmes B, Castro NJ, Li J, Keidar M, Zhang LG (2013) Enhanced human bone marrow mesenchymal stem cell functions in novel 3D cartilage scaffolds with hydrogen treated multi-walled carbon nanotubes. Nanotechnology 24(36):365102

130. Fonseca-Garcia A, Mota-Morales JD, Quintero-Ortega IA, Garcia-Carvajal ZY, Martínez-López V, Ruvalcaba E, Solis L, Ibarra C, Gutiérrez MC, Terrones M, Sanchez IC, del Monte F, Velasquillo MC, Luna-Bárcenas G (2013) Effect of doping in carbon nanotubes on the viability of biomimetic chitosan-carbon nanotubes-hydroxyapatite scaffolds. J Biomed Mater Res Part A (in press)

131. Gupta A, Woods MD, Illingworth KD, Niemeier R, Schafer I, Cady C, Filip P, El-Amin SF III (2013) Single walled carbon nanotube composites for bone tissue engineering. J Orthop Res 31(9):1374–1381

132. Jan E, Kotov NA (2007) Successful differentiation of mouse neural stem cells on layer-by-layer assembled single-walled carbon nanotube composite. Nano Lett 7(5):1123–1128

133. Kam NW, Jan E, Kotov NA (2009) Electrical stimulation of neural stem cells mediated by humanized carbon nanotube composite made with extracellular matrix protein. Nano Lett 9(1):273–278

134. Moon SU, Kim J, Bokara KK, Kim JY, Khang D, Webster TJ, Lee JE (2012) Carbon nanotubes impregnated with subventricular zone neural progenitor cells promotes recovery from stroke. Int J Nanomedicine 7:2751–2765

135. Sirivisoot S, Harrison BS (2011) Skeletal myotube formation enhanced by electrospun polyurethane carbon nanotube scaffolds. Int J Nanomedicine 6:2483–2497

136. Mooney E, Mackle JN, Blond DJ, O'Cearbhaill E, Shaw G, Blau WJ, Barry FP, Barron V, Murphy JM (2012) The electrical stimulation of carbon nanotubes to provide a cardiomimetic cue to MSCs. Biomaterials 33(26):6132–6139

137. Parrag IC, Zandstra PW, Woodhouse KA (2012) Fiber alignment and coculture with fibroblasts improves the differentiated phenotype of murine embryonic stem cell-derived cardiomyocytes for cardiac tissue engineering. Biotechnol Bioeng 109(3):813–822

138. Gupta MK, Walthall JM, Venkataraman R, Crowder SW, Jung DK, Yu SS, Feaster TK, Wang X, Giorgio TD, Hong CC, Baudenbacher FJ, Hatzopoulos AK, Sung HJ (2011) Combinatorial polymer electrospun matrices promote physiologically-relevant cardiomyogenic stem cell differentiation. PLoS One 6(12):e28935

139. Prabhakaran MP, Mobarakeh LG, Kai D, Karbalaie K, Nasr-Esfahani MH, Ramakrishna S (2013) Differentiation of embryonic stem cells to cardiomyocytes on electrospun nanofibrous substrates. J Biomed Mater Res Part B (in press)

140. Xie J, Willerth SM, Li X, Macewan MR, Rader A, Sakiyama-Elbert SE, Xia Y (2009) The differentiation of embryonic stem cells seeded on electrospun nanofibers into neural lineages. Biomaterials 30(3):354–362

141. Carlberg B, Axell MZ, Nannmark U, Liu J, Kuhn HG (2009) Electrospun polyurethane scaffolds for proliferation and neuronal differentiation of human embryonic stem cells. Biomed Mater 4(4):045004

142. Kang X, Xie Y, Powell HM, James Lee L, Belury MA, Lannutti JJ, Kniss DA (2007) Adipogenesis of murine embryonic stem cells in a three-dimensional culture system using electrospun polymer scaffolds. Biomaterials 28(3):450–458

143. Schrand AM, Dai L, Schlager JJ, Hussain SM (2012) Toxicity testing of nanomaterials. Adv Exp Med Biol 745:58–75

144. Nel A, Xia T, Madler L, Li N (2006) Toxic potential of materials at the nanolevel. Science 311(5761):622–627

145. Foley S, Crowley C, Smaihi M, Bonfils C, Erlanger BF, Seta P, Larroque C (2002) Cellular localisation of a water-soluble fullerene derivative. Biochem Biophys Res Commun 294(1):116–119

146. Christen V, Fent K (2012) Silica nanoparticles and silver-doped silica nanoparticles induce endoplasmatic reticulum stress response and alter cytochrome P4501A activity. Chemosphere 87(4):423–434

147. Zhang R, Piao MJ, Kim KC, Kim AD, Choi JY, Choi J, Hyun JW (2012) Endoplasmic reticulum stress signaling is involved in silver nanoparticles-induced apoptosis. Int J Biochem Cell Biol 44(1):224–232

148. Zhu L, Chang DW, Dai L, Hong Y (2007) DNA damage induced by multiwalled carbon nanotubes in mouse embryonic stem cells. Nano Lett 7(12):3592–3597

149. Ferin J, Oberdorster G, Penney DP (1992) Pulmonary retention of ultrafine and fine particles in rats. Am J Respir Cell Mol Biol 6(5):535–542

150. Service RF (2003) Nanomaterials show signs of toxicity. Nanomaterials show signs of toxicity. Science 300(5617):243

151. Shvedova AA, Castranova V, Kisin ER, Schwegler-Berry D, Murray AR, Gandelsman VZ, Maynard A, Baron P (2003) Exposure to carbon nanotube material: assessment of nanotube cytotoxicity using human keratinocyte cells. J Toxicol Environ Health A 66(20):1909–1926

152. Lam CW, James JT, McCluskey R, Hunter RL (2004) Pulmonary toxicity of single-wall carbon nanotubes in mice 7 and 90 days after intratracheal instillation. Toxicol Sci 77(1):126–134

153. Cheng C, Muller KH, Koziol KK, Skepper JN, Midgley PA, Welland ME, Porter AE (2009) Toxicity and imaging of multi-walled carbon nanotubes in human macrophage cells. Biomaterials 30(25):4152–4160

154. Moller P, Jacobsen NR, Folkmann JK, Danielsen PH, Mikkelsen L, Hemmingsen JG, Vesterdal LK, Forchhammer L, Wallin H, Loft S (2010) Role of oxidative damage in toxicity of particulates. Free Radic Res 44(1):1–46

155. Cancino J, Paino IM, Micocci KC, Selistre-de-Araujo HS, Zucolotto V (2013) In vitro nanotoxicity of single-walled carbon nanotube-dendrimer nanocomplexes against murine myoblast cells. Toxicol Lett 219(1):18–25

156. Pacurari M, Castranova V, Vallyathan V (2010) Single- and multi-wall carbon nanotubes versus asbestos: are the carbon nanotubes a new health risk to humans? J Toxicol Environ Health A 73(5):378–395

157. Snyder-Talkington BN, Dymacek J, Porter DW, Wolfarth MG, Mercer RR, Pacurari M, Denvir J, Castranova V, Qian Y, Guo NL (2013) System-based identification of toxicity pathways associated with multi-walled carbon nanotube-induced pathological responses. Toxicol Appl Pharmacol 272(2):476–489

158. Tourinho PS, van Gestel CA, Lofts S, Svendsen C, Soares AM, Loureiro S (2012) Metal-based nanoparticles in soil: fate, behavior, and effects on soil invertebrates. Environ Toxicol Chem 31(8):1679–1692

159. Sharma HS, Sharma A (2012) Neurotoxicity of engineered nanoparticles from metals. CNS Neurol Disord Drug Targets 11(1):65–80

160. Lan Z, Yang WX (2012) Nanoparticles and spermatogenesis: how do nanoparticles affect spermatogenesis and penetrate the blood-testis barrier. Nanomedicine (Lond) 7(4):579–596

161. Oberdorster G, Elder A, Rinderknecht A (2009) Nanoparticles and the brain: cause for concern? J Nanosci Nanotechnol 9(8):4996–5007

162. Moller P, Folkmann JK, Danielsen PH, Jantzen K, Loft S (2012) Oxidative stress generated damage to DNA by gastrointestinal exposure to insoluble particles. Curr Mol Med 12(6):732–745

163. Shaw BJ, Handy RD (2011) Physiological effects of nanoparticles on fish: a comparison of nanometals versus metal ions. Environ Int 37(6):1083–1097

164. Braydich-Stolle L, Hussain S, Schlager JJ, Hofmann MC (2005) In vitro cytotoxicity of nanoparticles in mammalian germline stem cells. Toxicol Sci 88(2):412–419

165. Deng X, Luan Q, Chen W, Wang Y, Wu M, Zhang H, Jiao Z (2009) Nanosized zinc oxide particles induce neural stem cell apoptosis. Nanotechnology 20(11):115101

166. Heng BC, Zhao X, Xiong S, Ng KW, Boey FY, Loo JS (2011) Cytotoxicity of zinc oxide (ZnO) nanoparticles is influenced by cell density and culture format. Arch Toxicol 85(6):695–704

167. Taccola L, Raffa V, Riggio C, Vittorio O, Iorio MC, Vanacore R, Pietrabissa A, Cuschieri A (2011) Zinc oxide nanoparticles as selective killers of proliferating cells. Int J Nanomedicine 6:1129–1140

168. Rasmussen JW, Martinez E, Louka P, Wingett DG (2010) Zinc oxide nanoparticles for selective destruction of tumor cells and potential for drug delivery applications. Expert Opin Drug Deliv 7(9):1063–1077

169. Choi SJ, Oh JM, Choy JH (2009) Toxicological effects of inorganic nanoparticles on human lung cancer A549 cells. J Inorg Biochem 103(3):463–471

170. Kim IS, Baek M, Choi SJ (2010) Comparative cytotoxicity of Al_2O_3, CeO_2, TiO_2 and ZnO nanoparticles to human lung cells. J Nanosci Nanotechnol 10(5):3453–3458

171. Zhang QL, Li MQ, Ji JW, Gao FP, Bai R, Chen CY, Wang ZW, Zhang C, Niu Q (2011) In vivo toxicity of

nano-alumina on mice neurobehavioral profiles and the potential mechanisms. Int J Immunopathol Pharmacol 24(1 Suppl):23S–29S

172. Alshatwi AA, Vaiyapuri Subbarayan P, Ramesh E, Al-Hazzani AA, Alsaif MA, Alwarthan AA (2012) Al_2O_3 nanoparticles induce mitochondria-mediated cell death and upregulate the expression of signaling genes in human mesenchymal stem cells. J Biochem Mol Toxicol 26(11):469–476

173. Atiyeh BS, Costagliola M, Hayek SN, Dibo SA (2007) Effect of silver on burn wound infection control and healing: review of the literature. Burns 33(2):139–148

174. Lansdown AB (2006) Silver in health care: antimicrobial effects and safety in use. Curr Probl Dermatol 33:17–34

175. Carlson C, Hussain SM, Schrand AM, Braydich-Stolle LK, Hess KL, Jones RL, Schlager JJ (2008) Unique cellular interaction of silver nanoparticles: size-dependent generation of reactive oxygen species. J Phys Chem B 112(43):13608–13619

176. Braydich-Stolle LK, Lucas B, Schrand A, Murdock RC, Lee T, Schlager JJ, Hussain SM, Hofmann MC (2010) Silver nanoparticles disrupt GDNF/Fyn kinase signaling in spermatogonial stem cells. Toxicol Sci 116(2):577–589

177. Hussain SM, Hess KL, Gearhart JM, Geiss KT, Schlager JJ (2005) In vitro toxity of nanoparticles in BRL 3A rat liver cells. Toxicol In Vitro 19(7):975–983

178. Ahamed M, Karns M, Goodson M, Rowe J, Hussain SM, Schlager JJ, Hong Y (2008) DNA damage response to different surface chemistry of silver nanoparticles in mammalian cells. Toxicol Appl Pharmacol 233(3):404–410

179. Hackenberg S, Scherzed A, Kessler M, Hummel S, Technau A, Froelich K, Ginzkey C, Koehler C, Hagen R, Kleinsasser N (2011) Silver nanoparticles: evaluation of DNA damage, toxicity and functional impairment in human mesenchymal stem cells. Toxicol Lett 201(1):27–33

180. Samberg ME, Loboa EG, Oldenburg SJ, Monteiro-Riviere NA (2012) Silver nanoparticles do not influence stem cell differentiation but cause minimal toxicity. Nanomedicine (Lond) 7(8):1197–1209

Index